INFN
LNS

LABORATORI NAZIONALI DEL SUD

Istituto Nazionale di Fisica Nucleare

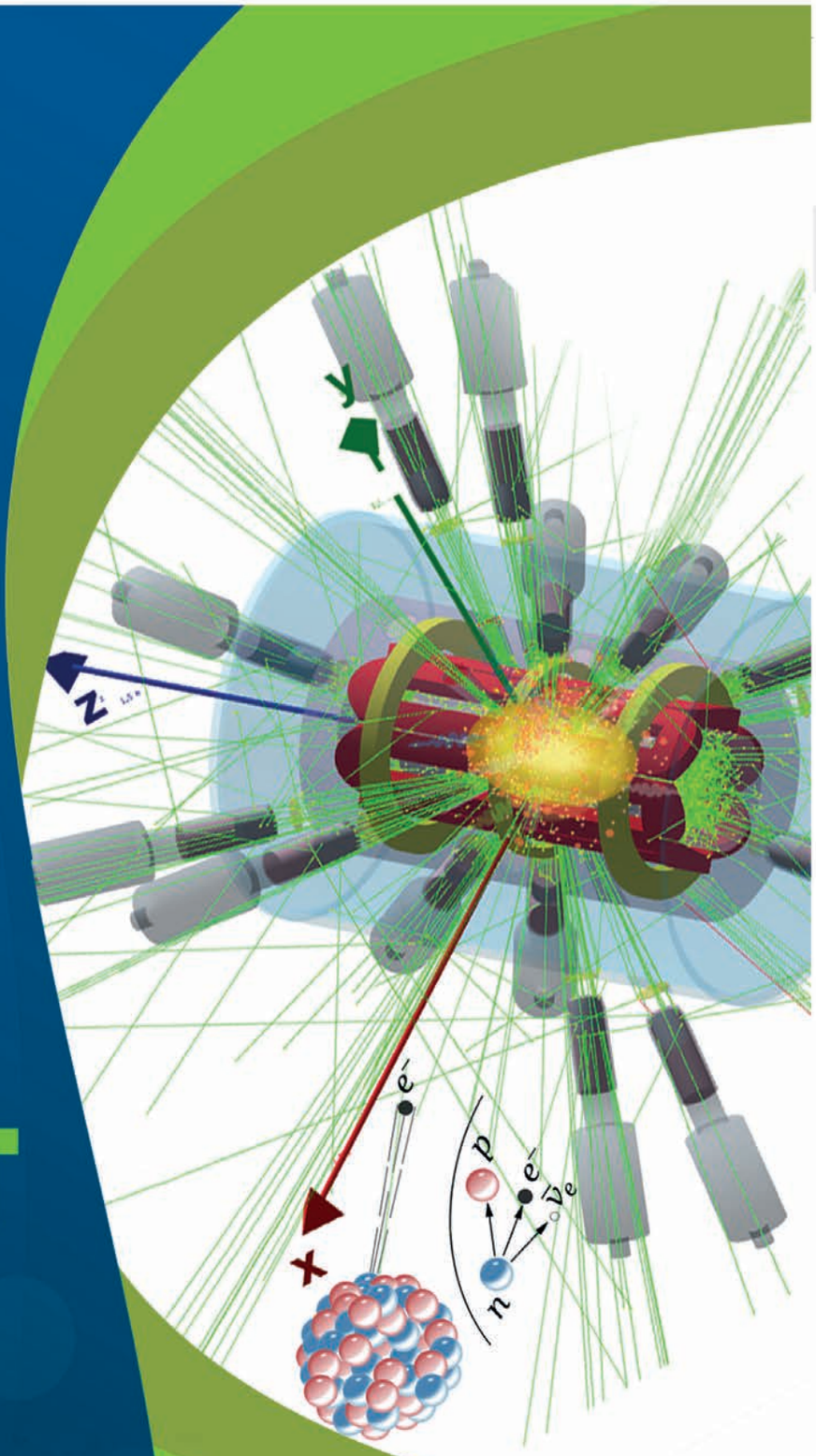

ACTIVITY REPORT 2023

The image illustrates the experimental setup and scientific objective of PANDORA, a multidisciplinary project aimed at studying, in laboratory plasmas brought to conditions similar to stellar ones, the radioactive decays that occur in stellar nucleosynthesis. The decay constant, and therefore the lifetime of various radioisotopes, is expected to vary, according to the current theoretical models, by several orders of magnitudes in stellar conditions, but direct measurements have never been made in plasma.

The measurement system consists of a superconducting magnetic trap, surrounded by an array of high-purity germanium detectors for measuring the gamma rays emitted following beta decay, and a multi-diagnostic system for monitoring the thermodynamic conditions of the plasma.

INFN LNS Activity Report 2023

INFN - LNS Director
Santo Gammino

Editorial Staff
Gaetano Agnello
Rosalia Di Mauro
Vincenzo Greco
Aurora Tumino

Cover design and layout
Grafica Uno

Istituto Nazionale di Fisica Nucleare

Laboratori Nazionali del Sud

FOREWORD 2023

The research activity carried out in 2023 has been strongly characterized by external and internal conditions and has been particularly focused on the progress of the project funded by the National Recovery and Resilience Plan (PNRR in Italian). The end of the pandemic has allowed a relevant number of experiments in different laboratories worldwide and the scientific output has been maintained high, in spite of the unavailability of beams from LNS accelerators. The progress of the construction of the magnets and cryostat of the Superconducting Cyclotron have been slower than scheduled because of the appearance of non-conformities that have been solved during the year, but that will make impossible the restart of accelerators in 2024 as scheduled. A preliminary campaign of magnetic measurements was added to the schedule in order to verify the compliance with the specifications, that was satisfactory. Meanwhile the solutions for other showstoppers, like authorizations of safety institutions, and the revamping of experimental areas have been addressed. The KM3NeT activities have been enhanced by the presence of additional personnel hired by using the additional PNRR funding and the difficulties in getting the support for marine operations have been partially overcome by a different planning of these operations. The commitment of all the LNS personnel has been praiseworthy, as it was also for the other big challenge within the PNRR, i.e. the ETIC activity consisting of setting up the valuable information to prepare the bid for the allocation of the Einstein Telescope in Italy. It is to be remarked that all the main activities within the PNRR framework, including the ones related to the construction of a laser setup in the frame of EUAPS project and those in the frame of the Sicilian ecosystem named SAMOTHRACE, mostly devoted to Applied Physics, have been completed in due time as for 2023.

A particular mention is due to the outreach and "third mission" activities, with a positive impact on the society. Young researchers have added new ideas, like the "Primavera della Scienza" and the full availability of the Visitors Center after the

pandemic have permitted to host some thousand people, mostly students. The cooperations with universities and other research institutions have continued and new links have been created. Initiatives with private institutions and companies have strengthened the footprint of INFN-LNS, that is made evident by a number of workshops and meeting that have been hosted within our premises in 2023, as the one about the opportunities for public and private companies and for regional Authorities to take profit of the new technologies for the production of energies as well the ones under development. Hundreds of experts took part to this event during a day, with the remote participation of two members of Italian government and the presence of local authorities. The capability to be involved in the big challenges of the scientific research and to operate as relevant actors of the social and economic development has been continuously increasing since the early times of the LNS, demonstrating the broad vision of those who wanted to install in Sicily such Research infrastructure and we are now in a phase that permits not only to preserve this heritage but to make it stronger and more efficient.

Finally, I wish to underline the full engagement of the LNS personnel to reach such objectives; being the personnel not much larger than 10 years ago, while the duties strongly increased, the commitment of each of us is necessary every day, and it is the main asset of LNS. It is worthwhile to remember that the most important resource, whatever is the challenge, is the human resource.

Santo Gammino
INFN-LNS Director
gammino@lns.infn.it

INDEX

Research Analyses Results

INFN LNS

01 EXPERIMENTAL NUCLEAR PHYSICS AND ASTROPHYSICS

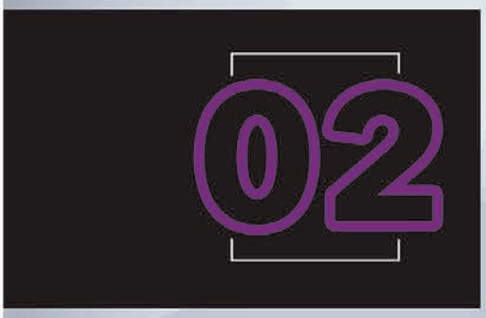

ASTROPARTICLE PHYSICS

03 THEORETICAL NUCLEAR PHYSICS

04 INSTRUMENTATION AND RELATED TECHNIQUES

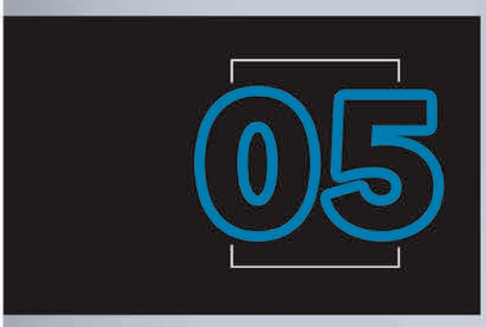

ION SOURCES AND ACCELERATOR

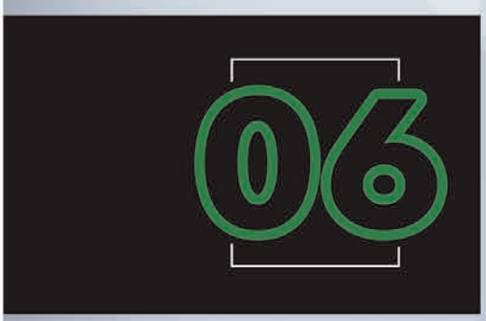

INTERDISCIPLINARY PHYSICS

07 NATIONAL RECOVERY AND RESILIENCE PLAN

08 TRAINING COURSE FOR SECONDARY SCHOOL TEACHERS

09 GENERAL INFORMATION

01

EXPERIMENTAL NUCLEAR PHYSICS AND ASTROPHYSICS

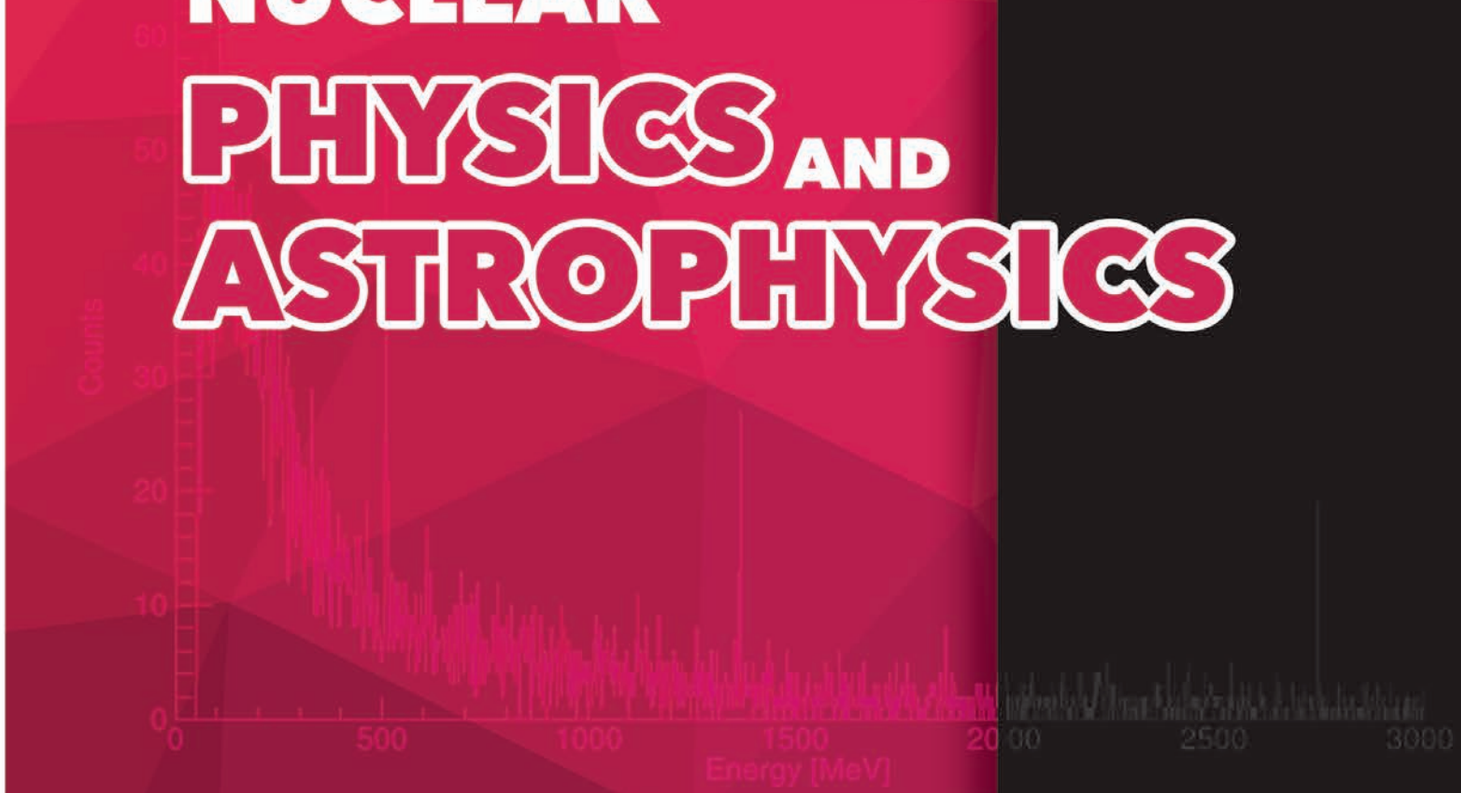

Research

Analyses

Results

INFN LNS

- The PANDORA project: status and perspectives
- Modification of ^{7}Be Electron Capture Rates in ECR Plasmas and Perspectives for PANDORA
- The Failure Mode, Effects and Criticality Analysis (FMECA) of the PANDORA project: from risk assessment to strategic decisions
- Study of the ^{48}Ti(^{18}O,^{17}O)^{49}Ti reaction at 275 MeV
- Multinucleon Transfer Studies in the ^{70}Zn (15 MeV/nucleon) +^{64}Ni System with MAGNEX
- ^{18}O + ^{48}Ti elastic and inelastic scattering at 275 MeV
- Hoyle state production and decay at forward angles in the ^{16}O+^{12}C reaction
- Coulomb-free $^{1}S_0$ p-p scattering length from the quasi-free p+d→p+p+n reaction
- Measurement of the ^{12,13}C + ^{19}F ion-ion fusion reaction at sub-barrier energies
- Direct measurement of the ^{7}Li(p, α)^{4}He reaction at astrophysical energies using ELISSA array
- Study of the ^{10}Be+^{4}He elastic excitation function by R-matrix calculation and elastic scattering ^{4}He+^{88}Sr of astrophysical interest
- Direct measurement of the ^{19}F(p,α_π)^{16}O and ^{19}F(p,α_γ)^{16}O reaction cross section
- Measurement of the ^{19}F(p,α) reaction in the astrophysical energy range of interest via Trojan Horse Method performed at INFN-LNS
- Indirect measurement of the ^{3}He(n,p)^{3}H reaction cross section at Big Bang energies
- INFN – LNS Scientific Information Service: an overview of 2023 activities
- Outreach activities @ INFN-LNS

The PANDORA project: status and perspectives

D. Mascali[1], D. Santonocito[1], for the PANDORA collaboration

1) INFN – LNS, Catania, Italy

Abstract - The PANDORA (Plasma for Astrophysics, Nuclear Decay Observation and Radiation for Archaeometry) project aims to build a compact minimum-B magnetic trap (with B_{max} = 3.0 T at the injection and extraction sides), where plasmas are heated by microwaves via Electron Cyclotron Resonance (ECR) mechanism at 18-21 GHz, up to densities $n_e \sim 10^{11}$-10^{13} cm^{-3}, and electron temperatures $T_e \sim 0.1$-30 keV. The magnetic trap will be used to confine β-radionuclides whose lifetime is expected to dramatically collapse of several order of magnitude with respect to terrestrial conditions. The predicted variation of decay rates will be measured as a function of the thermodynamic plasma properties (density and temperature), whose combination determines the Charge State Distribution (CSD) of the in-plasma ions. This report describe the overall status of the project, in particular regarding the setup including the array of 14 HPGe detectors dedicated to the measurement of the γ-rays emitted after β-decays, supported by a plasma multi-diagnostics system consisting of RF polarimeters, optical and X-ray spectroscopy, X-ray imaging and space resolved spectroscopy for the simultaneous measurements of plasma density and temperature.

INTRODUCTION

The present knowledge of the effects of the external environment on the nuclear β-decay rates is rather limited. Early attempts showed variations lower than about 0.05% (see, e. g. [1]) as a function of pressure and temperature, whilst near the end of the '60s a chemically induced change of about 3.5% in the half-life of ^{7}Be (see, e. g. [1]) was observed. An important breakthrough was achieved using storage rings. The so-called "bound-state β-decay" [2] was observed for the first time on many highly stripped isotopes. The effect induced by the opening of this decay channel was clearly observed on fully stripped $^{187}Re^{75+}$ ions which decayed by 9 orders of magnitude faster than neutral ^{187}Re atoms that have a half-life of 42 Gyr [3]. Moreover, bare $^{163}Dy^{66+}$ nuclei, being stable as neutral atoms, were observed to become radioactive, with a half-life of 33 days, thus allowing the occurrence of a branching reaction in the s-process path [4]. In order to get a deeper knowledge on the effect induced by the environment on the beta decay main features and evaluate the possible implications in s-process nucleosynthesis we are developing the PANDORA facility [5, 6].

PROGRESS IN THE PANDORA SETUP CONSTRUCTION

In 2020-2022 the PANDORA collaboration defined the main features of the experimental setup and also determined the specific details for the facility operations and the experimental runs to be undertaken. The overall picture of the experimental setup is shown in fig. 1.

A plasma trap that uses a magnetic field for plasma confinement will be employed in PANDORA [7]. It consists of a group of 3 axial solenoids and an hexapole nested inside, coaxial with the solenoids (SEXT-IN-SOL configuration). Its warm bore allows to place a cylindrical plasma chamber with inner radius R_{CH_IN} = 140 mm and a length L = 700 mm. Due to the need to place the γ-ray detection array and some diagnostic tools around the trap, 18 tapered holes has been created in the cryostat, yoke and properly positioned in the interspace of the six coils of the hexapole. The plasma will be heated using microwaves at 18 + 21 GHz via ECR. Three klystrons will generate an RF power of up to 6.5 kW, scalable up to a value of 10 kW in full-power operations. Two klystrons have been already delivered at LNS and are ready to be used.

A tender for the superconducting trap was published in Gazzetta Ufficiale on Sept. 2021 with different phases. During the pre-qualification, the INFN-LNS published the DoR, the Evaluation Criteria and the Pre-qualifications requirements. Only the suppliers able to accomplish the pre-qualification requirements could participate at the Competitive Dialogue. A total of five ''potential suppliers'' have been selected. Then, during the competitive dialogue, the selected suppliers (qualified to participate) elaborated their proposal (Technical Documentation). During this phase, the best technical solution was identified. The Competitive Dialogue ended in the second week of March 2023. Out of the initially applying five companies, three potential suppliers have presented their project in time for the next phase, whilst two of them ultimately presented the final technical and economical offer. Tender procedure has been completed in April 2024.

The γ-ray detectors array of PANDORA [8, 9] plays a fundamental role in the project as they will be used for the detection of γ-rays emitted by the daughter nuclei so allowing to tag the beta decay events. The best configuration achievable for the γ array, due to the complexity of creating the lines of sight in the cryostat, is made of 14 large volume HPGe detectors. For the initial experimental campaign, it will be possible to use the

HPGe detectors of the GALILEO experiment [10] thanks to a collaboration agreement signed in Oct. 2021 between PANDORA and GAMMA collaborations. Dedicated pre-amplifiers able to sustain high rates (>50 kHz), were developed at the LNL. In 2023 they have been procured and tested showing a limited worsening in detector energy resolution [9] and high stability so allowing for the in-plasma beta decay study.

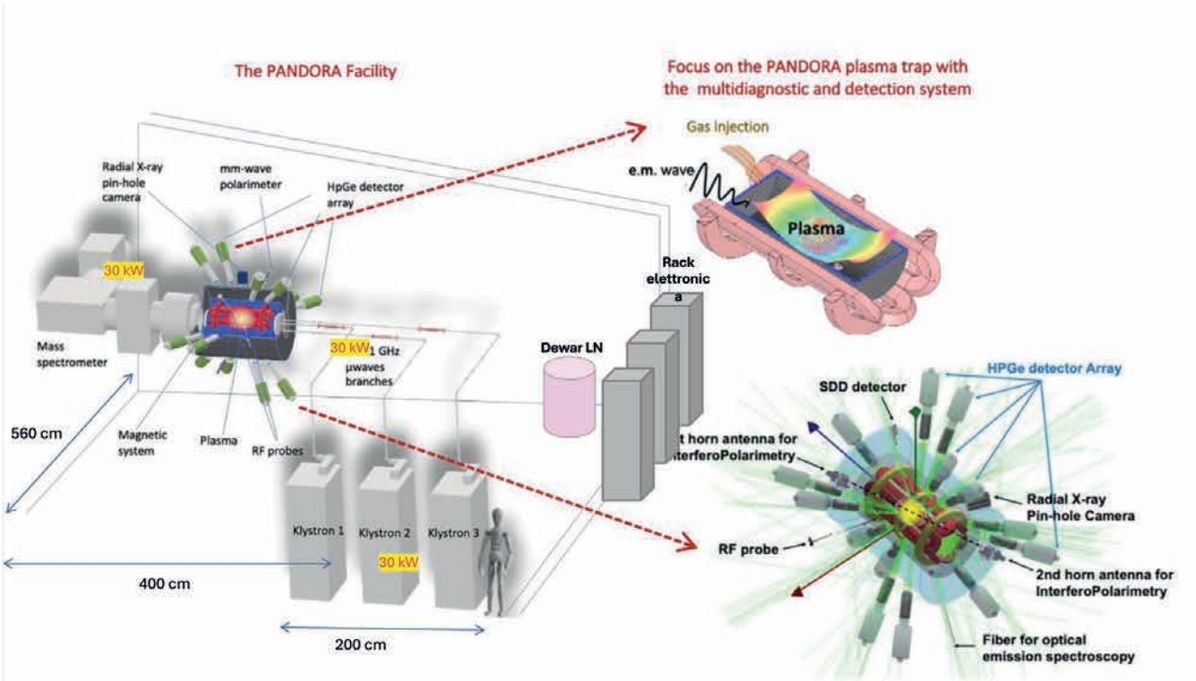

Figure 1: Rendering of the PANDORA setup, including the superconducting magnetic trap (in red) inside its cryostat (in blue) and iron yoke (on grey); the array of HPGe detectors; the main diagnostics (optical, X-ray, interfero-polarimetry); the mass spectrometer and the RF system.

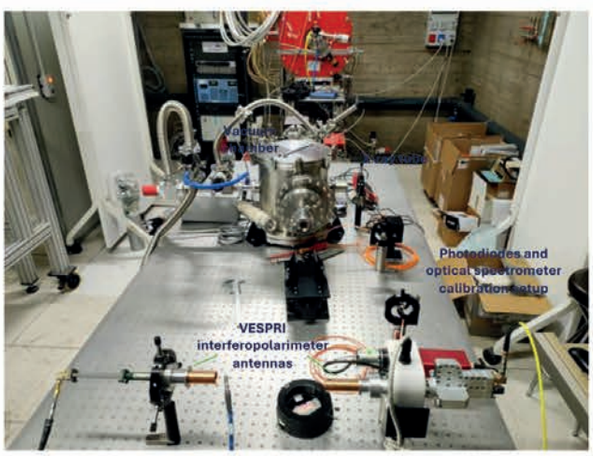

Figure 2: The new test-bench including the VESPRI 2.0, OES and PYNHO setups for simultaneous characterization of detectors, antennas and spectroscopes.

A complete characterization of ECR plasmas, which can emit radiation in a broad range of frequencies, requires a multi-diagnostic setup [11] able to measure the density and temperature of the different components. PANDORA diagnostics development was completed in 2020-2022. Thanks to the fruitful synergies with the SAMOTHRACE Innovation Ecosystem, funded by PNRR, the multi-diagnostics measurement station illustrated in figure 2 has been set-up during 2023-2024. It will allow simultaneous characterization, including calibration, noise removal, image reconstruction, etc, useful for SDD, CCD based pin-hole cameras, interferopolarimeters and optical spectrometers and photodiodes that will be used in PANDORA.

THEORY AND MODELLING

The PANDORA project aims at measuring, for the first time, nuclear β-decay rates in stellar-like conditions. However, using a plasma trap, due to the limited confinement time of the ions, the environment is neither expected to be in LTE nor uniform density conditions. Hence, starting from the relevant formulae of Takahashi-Yokoi theory, the in-plasma decay model has been extended to NLTE environment which represents the typical working conditions of a plasma trap, so allowing to infer conclusions on the effect of plasma environment in the stars using PANDORA plasma trap data.

MANAGEMENT AND SYNERGIES

From 2020 to 2022 the collaboration increased its membership up to more than 21 FTE (about 45 researchers and technologists) from 5 Italian sites: LNS, LNL, PG, BO, TIFPA. Specific agreements and collaborations are active with GSI (for the isotopes vaporization systems), GANIL/CNRS for the Thomson scattering, with ATOMKI-Debrecen about the X-ray diagnostics, with Max Planck Institute – IPP, relying to plasma optical spectroscopy. The international collaboration now accounts for around 70 members. PANDORA is also contributing, with the gained know-how, to the EUROLABS project named ERIBS, to the Innovation Ecosystem SAMOTHRACE, in the frame of the Italian PNRR program, to the partnership NQSTI. It is also synergic, at least for the plasma heating systems and diagnostics, with the DTT – Divertor Tokamak Test consortium programs.

ACKNOWLEDGEMENTS

The authors wish to thank INFN for the support through the project PANDORA_Gr3 funded by third Nat. Sci. Comm. The synergies with European Union (NextGeneration EU), through the MUR-PNRR project SAMOTHRACE (ECS00000022) and the MUR-PNRR project NQSTI (PE0000023) are gratefully acknowledged.

REFERENCES

[1] G. T. Emery, Ann. Rev. Nucl. Sci. 22 (1972) 165-202
[2] J. N. Bahcall, Phys. Rev. 124 (1961) 495
[3] M. Jung et al., Phys. Rev. Lett. 69 (1992) 2164
[4] Y. A. Litvinov et al., Phys. Rev. Lett. 99 (2007) 262501
[5] D. Mascali et al., Eur. Phys. J. A 53 (2017) 7
[6] D. Mascali et al., Universe, 80 (2022) 8
[7] G. Mauro et al., Front. Phys., 10 (2022) 931953
[8] E. Naselli et al., Front. Phys., 10 (2022) 935728
[9] A. Goasduff et al., Front. Phys., 10 (2022) 936081
[10] A. Goasduff et al., NIM A 1015 (2021) 165753
[11] E. Naselli et al., J. Instrum. 14 (2019) 10008

Modification of ^{7}Be Electron Capture Rates in ECR Plasmas and Perspectives for PANDORA

B. Mishra[1], A. Pidatella[1], A. Galatà[2], S. Taioli[3,4], S. Simonucci[5,6] and D. Mascali[1]

1) INFN – LNS, Catania, Italy
2) INFN – LNL, Legnaro, Italy
3) ECT – FBK, Trento, Italy*
4) INFN – TIFPA, Trento, Italy
5) School of Science and Technology - University of Camerino, Italy
6) INFN – Sezione di Perugia, Italy

Abstract – One of the primary objectives of the upcoming PANDORA facility at INFN – LNS is investigating the effect of a plasma on β-decay rates of radio-isotopes. However, owing to the complexity of ECR magnetoplasmas, experimental data must be complemented by simulations before use in nucleosynthesis models. We present here a brief report on plasma-induced decay rate modification, taking as example orbital electron capture (EC) in ^{7}Be. The analysis is first applied to a uniform plasma with varying density and temperature, and then extended to a realistic ECR plasma. The results demonstrate the utility of PIC-MC simulation models for predicting spatial gradients of $t_{1/2}$ in ECR plasma traps, and offer perspectives on optimising measurements.

INTRODUCTION

PANDORA (**P**lasmas for **A**strophysics, **N**uclear **D**ecay **O**bservations and **R**adiation for **A**rchaeometry) is a new facility being set up at INFN-LNS with the aim of using a high energy density electron cyclotron resonance (ECR) magnetoplasma for investigating phenomena relevant to nuclear astrophysics [1, 2], and in particular, the study of plasma-induced modification of β-decay rates for use in *s*-process nucleosynthesis models [3].

The experimental methodology will involve generating a dense (electron density $n_e \sim 10^{11\text{-}13}$ cm^{-3}), hot (electron temperature $T_e \sim 0.1$-100 keV) and stable plasma inside a magnetic trap into which radio-isotopes are injected externally. Thermalisation of the isotope atoms with the plasma will result in the formation of a charge state distribution (CSD) according to the plasma density and temperature (as in the stellar interior) which will modify the decay half-life $t_{1/2}$. The new decay rate will be measured by counting the secondary-γ emitted during the decay process, which can be used to map $t_{1/2}$ to n_e and T_e.

ECR plasmas are fertile environments to study plasma-induced effects, but there are challenges to overcome. Compared to stellar plasmas, ECR plasmas are orders of magnitude lower in density, have sharp gradients, and do not obey local theromodynamic equilibrium (LTE). As such, the comprehensive stellar plasma decay model of Takahashi and Yokoi (TY83) [4] cannot be directly applied to them without suitable modifications. Additionally, the peculiar spatial structure of the plasma and transport processes complicate the mapping between $t_{1/2}$ and (n_e, T_e) by introducing non-local effects. The nature of ECR plasma also poses technological challenges to the injection of the radio-isotope atoms which must be captured and trapped efficiently to exploit the plasma effectively.

In order to address these problems, a general model of in-plasma decay has been developed which can be applied to both stellar and laboratory magnetoplasma. The model has also been coupled with a Particle-in-Cell Monte Carlo (PIC-MC) code to calculate $t_{1/2}$ in realistic ECR plasmas. In this report, the recent results from these models are shown, using the example of orbital electron capture decay in ^{7}Be.

ORBITAL ELECTRON CAPTURE IN ^{7}BE

^{7}Be undergoes electron capture decay to ^{7}Li through two channels: $3/2^- \rightarrow 3/2^-$ ($Q = 861.815$ keV) and $3/2^- \rightarrow 5/2^-$ ($Q = 384.285$ keV) with a branching ratio of 10.44%. The accepted $t_{1/2} = 53.2 \pm 6$ days. The log *ft* of the transitions are 3.324 and 3.556 respectively. Under neutral conditions, ^{7}Be captures electrons from the atomic orbitals, with K-shells contributing the most.

The decay rate of ^{7}Be in charge state *i* and excitation level *j* can be calculated using the expression

$$\lambda^*(ij) = \ln 2 \left(\frac{f^*_{gs}(ij)}{f_{0,gs}t} + \frac{f^*_{es}(ij)}{f_{0,es}t} \right)$$

where $f_{0,gs}t$, $f_{0,es}t$ are the log *ft* values of the two transitions, and $f^*_{gs}(ij)$, $f^*_{es}(ij)$ are the lepton phase volumes which connect the nuclear decay to the i^{th} ion, where *j* refers to its excitation level. According to the formulation of TY83 [4], $f^*(ij)$ for a transition *m* associated with electron capture can be calculated as

$$f^*_m(ij) = \sum_{x(ij)} \sigma_x \frac{\pi}{2} [g_x \text{ or } f_x]^2 (Q(ij)/m_e c^2)^2 \, S_{(m)x(ij)}$$

where σ_x is the occupancy of the orbital *x*, g_x and f_x are radial charge probability densities of *x* calculated on the nuclear surface, $Q(ij)$ is the decay Q-value, and $S(m)$ is the shape factor which accounts for the spin-parity conservation in the decay.

Calculating $f^*(ij)$ requires data on the electronic configuration of the ions, which can be taken from the HULLAC database packaged into the FLYCHK population kinetics code [5]. The database contains details on ionic levels and their energies which can be used to evaluate $Q(ij)$ according to the expression

$$Q(ij) = Q_0 + \overline{\Delta}\epsilon^{ij}$$

where Q_0 is the neutral atom decay energy and the second term denotes the contribution from the ionic excitation. The radial probability densities at the nuclear surface can be calculated by solving the Dirac equation of electrons in a central Coulomb field according to the formulation of Burke and Grant [6]. The HULLAC data on electronic configuration of the ionic levels ij can also allow extracting σ_x and the shape factors $S_{(m)x(ij)}$ for ^{7}Be obtained from TY83 as

$$S_{(m)x(ij)} = \begin{cases} 1, x = 1s_{1/2}, 2s_{1/2}, 2p_{1/2} \\ 0, x = 2p_{3/2} \end{cases}$$

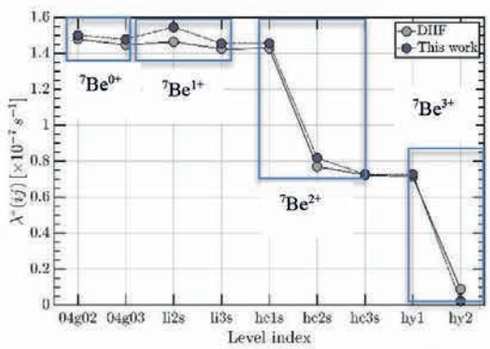

Fig 1: $\lambda^*(ij)$ as a function of ^{7}Be atomic configuration compared with DHF calculations

Fig. 1 shows the predicted $\lambda^*(ij)$ for different ^{7}Be ionic configurations calculated using the aforementioned expressions, and also compared with independent Dirac-Hartree-Fock (DHF) calculations. Both methods show a drop in decay rate on ionising the atom, which is primarily driven by loss of electrons to capture from the atomic orbitals. The model correctness is verified by calculating the neutral atom $t_{1/2}$ (corresponding to level *04g02* in Fig. 1) which comes out to be 53.44 days.

CAPTURE RATES IN UNIFORM PLASMA

The configuration-dependent decay rates $\lambda^*(ij)$ can be converted to in-plasma decay rates through the expression

$$\lambda^* = \sum_{ij} p_{ij}\,\lambda^*(ij)$$

where p_{ij} is the probability of ^{7}Be to be in configuration ij according to plasma density and temperature. p_{ij} can be calculated by providing FLYCHK with a grid of n_e and T_e of a uniform plasma, and specifying the thermodynamic nature of the system.

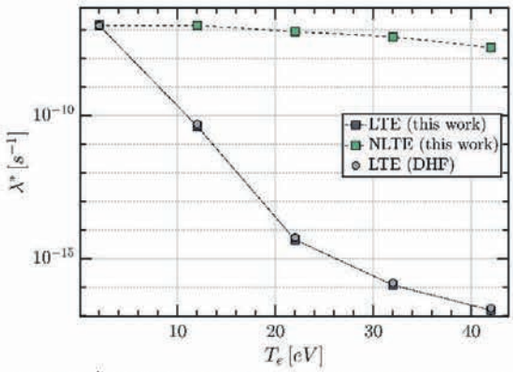

Fig 2: λ^* in LTE and NLTE plasma with uniform n_e = 10^{12} cm^{-3} as a function of T_e

Fig. 2 shows λ^* of ^{7}Be as a function of T_e for realistic n_e under LTE and NLTE conditions. The former is also compared with DHF calculations. The model predicts that decay rates fall on increasing the temperature due the loss of bound electrons to capture. However, the trends are vastly different for LTE and NLTE plasmas and therefore TY83 and DHF models cannot be applied to PANDORA which is expected to be in NLTE.

CAPTURE RATES IN ECR MAGNETOPLASMA

To predict the spatial distribution of λ^* in an ECR plasma, the general model of plasma-induced decay described above can be coupled to the PIC-MC code developed to simulate ion CSD [7]. The methodology remains the same as in the preceding section, the only difference being that the probability factors p_{ij} are now position-dependent, thus incorporating NLTE and non-local effects which are typical of laboratory magnetoplasmas.

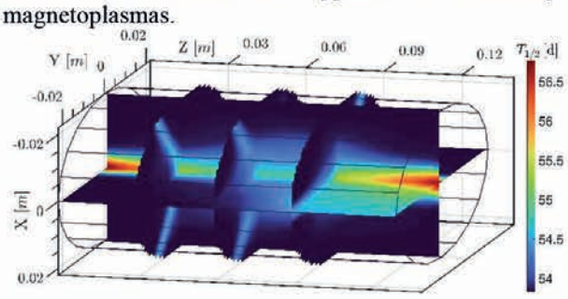

Fig 3: ^{7}Be λ^* in an ECR plasma with realistic n_e and T_e gradients. The map corresponds to the LEGIS source.

Fig. 3 shows the 3D profile of λ^* in the LEGIS ECR ion source [8] operated under conditions different from PANDORA. As in Fig. 2, there is also a decrease in λ^* here, but to a much lesser extent. The $t_{1/2}$ of ^{7}Be orbital electron capture increases in the axial region near the injection and extraction zones where the code predicts higher mean charge <Z> due to the presence of ^{7}Be^{2+} and ^{7}Be $^{3+}$ ions.

CONCLUSIONS AND PERSPECTIVES

A general model of in-plasma decay has been developed, which can predict the variation in EC and bound state β-decay rates as a function of individual ion configuration, as well as of plasma parameters in low and high density systems. In addition, the combined PIC-MC plasma-decay model allows estimating spatial gradients in $t_{1/2}$ in realistic ECR magnetoplasmas. Presently, the results predict only small changes in $t_{1/2}$, which is due to the fact that the model is applied to a low-power ECR plasma with an unoptimised isotope injection system. The model, however, is universal for all ECR plasmas, and on applying it to the actual PANDORA trap (operating at higher power with optimised injection system) larger changes in $t_{1/2}$ will be obtained. The model described in this report can help extrapolate experimentally measured in-plasma decay rates to stellar interiors, while also helping optimise ECR operating conditions for exploiting their high energy density to the fullest.

REFERENCES

[1] D. Mascali et al, Eur. Phys. J. D 69, (2015) 27.
[2] D. Mascali et al, Universe 8, (2022) 80.
[3] S. Palmerini et al, ApJ 921, (2021) 1.
[4] K. Takahashi and K. Yokoi, Nucl. Phys. A 404, (1983) 3.
[5] H.-K. Chung et al, High Energy Density Phys. 1, (2005) 1.
[6] V.M. Burke and I.P. Grant, Proc. Phys. Soc. 90, (1967).
[7] B. Mishra et al, Front. Phys. 10, (2022) 932448.
[8] A. Galatà et al, Rev. Sci. Instrum. 81, (2010)

The Failure Mode, Effects and Criticality Analysis (FMECA) of the PANDORA project: from risk assessment to strategic decisions

V. P. Bonanno, D. Santonocito, M.S. Musumeci, G. Torrisi, G.S. Mauro, E. Naselli, M. Mazzaglia, A. Pidatella, D. Mascali

1) Istituto Nazionale di Fisica Nucleare - Laboratori Nazionali del Sud, via S. Sofia 62, 95123 Catania, Italy

Abstract – Research projects like PANDORA_Gr3 (Plasmas for Astrophysics, Nuclear Decays Observation and Radiation for Archaeometry) are characterised by strong complexity and inherent uncertainty that could bring along risks. This paper exposes a tailored implementation of FMECA methodology to evaluate weaknesses/criticalities, find mitigation actions and implement strategical solutions able to help the project's leaders to make decision and to negotiate with sponsor and key suppliers.

INTRODUCTION

PANDORA_Gr3 is a research project supported by INFN with a core researchers' group at INFN-LNS that will host the facility and several international partners. The main aim of the project is to develop a totally new and complementary experimental approach to those attempted in the past to measure, for the first time, nuclear β-decay rates in a plasma simulating some stellar-like conditions. Therefore PANDORA_Gr3 is characterized by **a strong complexity** [1] due to the experimental method proposed and an **inherent uncertainty** [6] related to project method and objectives (epistemic uncertainty) [5] and organization structure, working team, activity distribution (structural uncertainty) that could bring along risks.

Accordingly with the sponsor (CSNIII) requests, in order to prevent critical events, a risk assessment by using the FMECA methodology has been implemented.

RISK ASSESSMENT METHODOLOGY

To identify and analyse the relevant risks to the PANDORA_Gr3 project, a predictive and semi-quantitative methodology has been implemented: the Failure Mode, Effects and Criticality Analysis (FMECA), who is an exhaustive and structured technique, useful for risk analysis at various levels of detail.

It highlights possible failure modes that may occur, causes and their effects that could affect the product quality or process performance. The methodology consists into break-downing the product and/or process into its base components and into identifying, for each of them, all damaging events that could bring to failure.

The FMECA analysis identifies weaknesses/criticalities relevant to project objectives (cost, time, technical and research) in order to evaluate them with expected impact and estimated probability. The Risk Priority Index considers the chance of occurrence (probability) and the severity of the damaging consequences (impact).

Input data for RA procedure

The input data used for the assessment procedure have been collected both by analysing and reviewing the PANDORA_Gr3 project documentation such as Technical Design Report, Project Schedule, Budget Analysis and also by implementing a set of brainstorming and interviewing sessions together with the researchers involved as task leaders of the five Work Packages of PANDORA_Gr3 project.

The results of these interactions are a SWOT analysis and a Risk Breakdown Structure (RBS). The first one highlights strength, weaknesses and potential opportunities and threats in relation with funders, partnership, and key suppliers, the second one identifies the main risk categories in PANDORA_Gr3.

Estimate the Risk Priority Index

In order to calculate the Risk Priority Index, the probability and impact have to be assessed for each risk identified. The Risk Probability is the likelihood that each specific risk will occur. The level of probability for each risk and its impact on each project objective have been evaluated during the brainstorm sessions and considering risk tolerance of the PANDORA_Gr3's project leaders. Due to the highly innovative nature of the project and the absence of historical data, the probability will assess as **expected probability**.

In order to assure quality and credibility of risk assessment procedure, **different types of effects on project have been defined to evaluate the Risk Impact** (RI) as potential effect on a project objective such as schedule, cost, technical, research.

The Risk Priority Index (RPI) of each risk can be calculated by using the Risk Matrix. The Risk Matrix, (Table 1), contains the risk indices obtained by multiplying all RP and RI values:

Table 1: Risk matrix resulting from the product of RP and RI

Probability scale						
	Highly likely	**5**	**10**	**15**	**20**	**25**
	Likely	4	8	12	16	20
	Moderate	3	6	9	12	15
	Less than likely	2	4	6	8	10
	Unlikely	1	2	3	4	5
		Very low	Low	Moderate	High	Very high
		Impact scale				

The Risk Matrix allows to identify risk classes in terms of tolerability and the need to implement risk mitigation measures. Referring to the previous risk matrix, is possible identify four risk levels:

Very Critical risk for $RPI \in \{15, 16, 20, 25\}$
Critical risk for $RPI \in \{9, 10, 12\}$
Tolerable risk for $RPI \in \{5, 6, 8\}$
Negligible risk for $RPI \in \{1, 2, 3, 4\}$

The risk priority index allows to define the actions priority list. If the level is negligible, interventions are not required. If the level is tolerable, it is advisable to undertake some mitigation actions. If the level is critical, it is mandatory to perform additional analysis and to provide relevant mitigation actions. If the level is very critical, some major changes in the process are required.

RESULTS

The risk assessment procedure highlights that a very critical *external risk* could be an **underfunding of 30% per year** due to budget limitation by the sponsor (in our case, as said above, the INFN management and CSN III). The procurement procedures could be critical affected on the timeline, while technical and research objectives would have moderate consequences. A similar but less likely scenario could be an initial **budget cut of 30%**. In this case, more critical effects on technical and research objectives may occur, because substantial changes/redefinition of the technical requirements (and then, of scientific goals) are needed; the effect on schedule remains the same of the precedent external risk.

To solve a potential time increase of planned activities due to an underfunding per-year, the **elaboration of a PERT (Program Evaluation Review Technique)** diagram can be considered a technique useful to highlight and monitor the tasks on the critical path, then to adequate the activities to the modulation of budget. The ab-initio budget cut case would be unacceptable because it would require a radically facility and aim upsets. In this latter case the only practicable solution is to **find other funding channels.**

An example of critical *internal risk* could be the **technical unfeasibility of some design solutions,** this due to any mismatch between the requirements proposed and the tools and methods available to transform them into features/specifications of final product. For example, for plasma diagnostic purposes, it is needed to keep up to 18 lines of sight – with a minimum of 14 – between the warm bore radius and the external iron yoke through the cryostat and the inner cold mass. The non-compliance with this fundamental requirement should entail significant effect on cost, time, and research goals. The cost of data taking activity with HPGe detectors would increase up to 30% more than the estimated value. Since also the acquisition time would increase due to a potential halving of number of lines of sight, the research goal could not be achieved on time to justify the main purpose of project. **The adoption of a specific clause of "Codice degli Appalti" – art.64 D.lgs 50/2016 – can be considered as a mitigation action able to solve both technical and manufacturing issues and to optimize the procurement procedure**. The clause is the "Dialogo Competitivo" whereby the Contracting Authority can discuss with different potential supplier in order to achieve the best solution based on a list of requirements and specifications defined in the Document of Requirements. The adoption of art. 64 could provide responses to uncertainties related to the structural complexity of the Plasma Trap, could manage the technical interaction with suppliers and could guarantee to achieve the best technical solution. Furthermore, it represents a negotiating tool with sponsor to assure the feasibility and a proper allocation of budget.

CONCLUSIONS

The FMECA analysis and its results have been submitted together with Technical Design Report to the project sponsor so as to support the soundness of the project from the management point of view. The project sponsor appreciated the solid approach and the methodology used as well as the assessment process that proves the importance to prevent risk as a guarantee for success.

Currently, in the INFN research projects context, PANDORA_Gr3 is the first project where the project leaders applied the project management techniques during the planning phase of the project. It can be considered as a sort of "proof-of-principle" of the effectiveness of Risk Management practices in the early phase of a research project.

REFERENCES

[1] Baccarini, D. (1996). The concept of project complexity - a review. *International Journal of Project Management*, 201-204.

[2] Corsi, C. (2008). Il Research Project Management. *wpcomunite.it* (44).

[3] Ernø-Kjølhede, E. (2000). Project Management Theory and the Management of Research Projects. *Department of Management, Politics and Philosophy, CBS. MPP Working Paper No. 3*.

[4] Huljenic D., D. S. (2005). Project Management in Research Projects. *Proceedings of the 8th International Conference on Telecommunications*.

[5] Turner J. R. - Cochrane, R. A. (1993). The Goals and Methods Matrix: coping with projects with ill-defined goals and/or methods of achieving them. *International Journal of Project Management*(11).

[6] William, T. (1999). The need for new paradigms for complex project. *International Journal of Project Management, Vol.17*.

Study of the ^{48}Ti(^{18}O,^{17}O)^{49}Ti reaction at 275 MeV

O. Sgouros[1,2], F. Cappuzzello[1,2], M. Cavallaro[2], D. Carbone[2], C. Agodi[2], G. A. Brischetto[1,2], D. Calvo[3], E.R. Chávez Lomelí[4], I. Ciraldo[1,2], M. Cutuli[1,2], G. De Gregorio[5,6], F. Delaunay[1,2,7], H. Djapo[8], C. Eke[9], P. Finocchiaro[2], M. Fisichella[2], A. Gargano[5], M. A. Guazzelli[10], A. Hacisalihoglu[11], R. Linares[12], J. Lubian[12], N. H. Medina[13], M. Moralles[14], J.R.B Oliveira[13], A. Pakou[15], L. Pandola[2], V. Soukeras[1,2], G. Souliotis[16], A. Spatafora[1,2], D. Torresi[2], A. Yildirim[17], V.A.B. Zagatto[12]

for the NUMEN collaboration

1) Dipartimento di Fisica e Astronomia "Ettore Majorana", Università di Catania, Catania, Italy

2) INFN – Laboratori Nazionali del Sud, Catania, Italy

3) INFN – Sezione di Torino, Torino, Italy

4) Instituto de Fisica, Universidad Nacional Autónoma de México, Mexico City, Mexico

5) INFN – Sezione di Napoli, Napoli, Italy

6) Dipartimento di Matematica e Fisica,Università della Campania "Luigi Vanvitelli", Caserta, Italy

7) LPC Caen UMR6534, Universite de CAEN Normandie, ENSICAEN, CNRS/IN2P3, Caen, France

8) Institute of Accelerator Technologies, Ankara University, Ankara, Turkey

9) Department of Mathematics and Science Education, Faculty of Education, Akdeniz University, Antalya, Turkey

10) Centro Universitario FEI, Sao Bernardo do Campo, Brazil

11) Department of Physics, Recep Tayyip Erdogan University, Rize, Turkey

12) Instituto de Fisica, Universidade Federal Fluminense, Niteroi, Brazil

13) Instituto de Fisica, Universidade de Sao Paulo, Sao Paulo, Brazil

14) Instituto de Pesquisas Energeticas e Nucleares IPEN/CNEN, Sao Paulo, Brazil

15) Department of Physics, University of Ioannina and HINP, Ioannina, Greece

16) Department of Chemistry, University of Athens and HINP, Athens, Greece

17) Department of Physics, Akdeniz University, Antalya, Turkey

Abstract – The ^{18}O+^{48}Ti collision at 275 MeV was investigated within the NUMEN and NURE experimental campaigns. The relevant experiment was carried out at the INFN-LNS in Catania employing the MAGNEX large acceptance magnetic spectrometer. In this report, an overview of the analysis and the main results obtained for the ^{48}Ti(^{18}O,^{17}O)^{49}Ti reaction will be presented.

INTRODUCTION

Single-nucleon transfer reactions induced by light ions have been extensively used in the past for studying single-particle properties in nuclei. In such a class of nuclear reactions, high yields are observed for residual states presenting a high degree of overlap with the states at the entrance channel, thus allowing for the determination of the spectroscopic factors. Then, from the comparisons between experimental and calculated values one may draw conclusions on the accuracy of the adopted nuclear structure model and improve our understanding of the nuclear structure. On the other hand, transfer reactions induced by heavy-ions are less studied than their light-ion counterparts due to the high degree of complexity in the heavy-ion dynamics. In this sense, more experimental data are necessary.

The past few years, a broad survey on heavy-ion induced transfer reactions has been undertaken by our group in the context of the NUMEN (NUclear Matrix Elements for Neutrinoless double beta decay) project [1]. NUMEN aims to provide data-driven information on the $\beta\beta$ decay Nuclear Matrix Elements (NMEs) by studying heavy-ion induced double charge exchange (DCE) reactions [2]. Precise knowledge of the NMEs may be the key for accessing the neutrino effective mass, if the neutrino-less double beta ($0\nu\beta\beta$) decay is to be observed. Considering that the nuclear structure calculations for the NMEs suffer from large uncertainties, study of single-nucleon transfer reactions in conjunction with the DCE ones can provide the necessary experimental constraints on the nuclear structure theories to be employed in the calculation of the NMEs of $0\nu\beta\beta$ decay.

In the present study, which is a part of the NURE project [3], the ^{18}O+^{48}Ti collision at 275 MeV was investigated by measuring the complete reaction network including also single-nucleon transfer reactions. In the present report, the main findings from the analysis of the ^{48}Ti(^{18}O,^{17}O)^{49}Ti reaction will be given.

EXPERIMENTAL SETUP

The experiment was carried out at the MAGNEX facility of INFN-LNS in Catania [4]. A $^{18}O^{8+}$ beam was accelerated at the energy of 275 MeV and impinged a TiO_2 target 510 μg/cm^2 thick, which was evaporated onto

a ^{27}Al backing 216 μg/cm^2 thick. Hence, auxiliary measurements with a self-supporting ^{27}Al target and a WO_3 one were performed in order to subtract the contaminant events. The different reaction products were momentum analyzed by the MAGNEX large acceptance spectrometer and were detected by its Focal Plane Detector (FPD) [5]. The particle identification (PID) of the $^{17}O^{8+}$ ions originating from the ^{48}Ti(^{18}O,^{17}O)^{49}Ti reaction was performed according to the prescription reported in Ref. [6] and representative PID spectra are reported elsewhere [7].

DATA REDUCTION

After the identification of the $^{17}O^{8+}$ ions, a high order ray reconstruction was applied to the data [4] and the momentum vector of the ions at the target position was obtained. Having known the momentum of the ions, the excitation energy E_x was determined adopting the missing mass method [4]. The reconstructed excitation energy spectrum after subtracting the background contaminations is illustrated in Fig.1. The red-filled area, marked as ROI 1, corresponds to the g.s. to g.s. transition, which is well-separated from any other transition given the achieved energy resolution which was ~450 keV FWHM. The rest of the ROIs include the contribution from transitions to various states of ^{17}O and ^{49}Ti nuclei.

The experimental yields of each ROI were integrated using an angular step $\Delta\theta_{lab.}$= (0.5°-2.0°) (depending on the statistics) and by taking into account the integrated beam charge, the solid angle and the overall efficiency of the spectrometer [8], angular distribution cross-sections were determined. As an example, the data for ROI 3 are presented in Fig.2. The complete analysis is reported in Ref. [9]. The theoretical interpretation of the data was performed in the context of the DWBA framework using FRESCO code [10]. The initial state interaction was the one determined in the analysis of the elastic and inelastic scattering data [11], while the spectroscopic amplitudes were derived from large-scale shell-model calculations. As it may be seen, the data favour the use of the KB3 [12] interaction, signalling that some modifications are needed in the case of the SDPF-MU one [13]. However, more experimental data are necessary before concluding which is the most appropriate interaction for the description of the nuclear wave functions of the DCE reaction in the ^{18}O+^{48}Ti collision.

CONCLUSIONS

The study of the ^{48}Ti(^{18}O,^{17}O)^{49}Ti reaction was performed at 275 MeV as part of the NUMEN and NURE projects. Angular distribution measurements for the $^{17}O^{8+}$ ions were performed employing the MAGNEX large acceptance magnetic spectrometer. The deduced angular distribution cross-sections were analysed under the DWBA framework and it was concluded that the KB3 interaction is more appropriate for the description of the ^{49}Ti wave functions compared to the SDPF-MU one. However, before disregard the SDPF-MU interaction from the description of the wave functions involved in the DCE reaction, more experimental data are necessary. In this sense, the analysis of the rest of the transfer reactions is of paramount importance.

Acknowledgements: This project has received funding from the European Research Council (ERC) under the European Union's Horizons 2020 research and innovation programme (NURE, Grant Agreement No 714625).

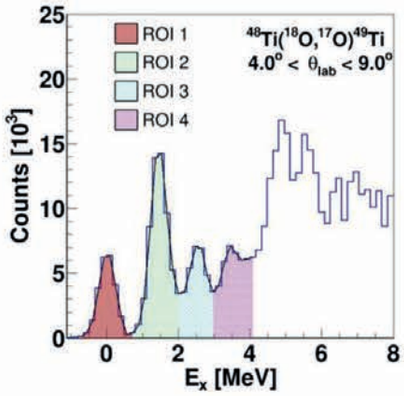

Figure 1: Excitation energy spectrum for the ^{48}Ti(^{18}O,^{17}O)^{49}Ti reaction at 275 MeV, after the background subtraction. Figure taken from Ref. [9].

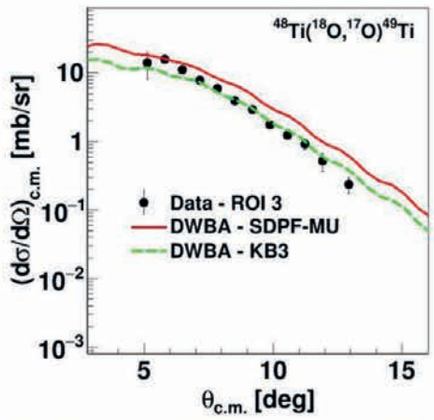

Figure 2: Comparison between experimental data and theoretical calculations for the ^{48}Ti(^{18}O,^{17}O)^{49}Ti reaction at 275 MeV. Figure taken from Ref. [9].

REFERENCES

[1] F. Cappuzzello et al., EPJA 54 (2018) 72.
[2] F. Cappuzzello et al., PPNP 128, (2023) 103999.
[3] M. Cavallaro et al., PoS (BORMIO2017) (2017) 015.
[4] F. Cappuzzello et al., EPJA 52 (2016) 167.
[5] D. Torresi et al., NIM A 989 (2021) 164918.
[6] F. Cappuzzello et al., NIM A 621 (2010) 419.
[7] O. Sgouros, Il Nuovo Cimento C 45, (2022) 70.
[8] M. Cavallaro et al., NIM A 637 (2011) 77.
[9] O. Sgouros et al., PRC 108, (2023) 044611.
[10] I. J. Thompson, Comput. Phys. Rep 7, (1988) 167.
[11] G. A. Brischetto et al., PRC 109, (2024) 014604.
[12] A. Poves and A. Zuker, Phys. Rep. 70, (1981) 235.
[13] Y. Utsuno et al., PRC 86, (2012) 051301 (R).

Multinucleon Transfer Studies in the ^{70}Zn (15 MeV/nucleon) +^{64}Ni System with MAGNEX

S. Koulouris[1], G. A. Souliotis[1], F. Cappuzzello[2,3], D. Carbone[3], A. Pakou[4], C. Agodi[3], G. A. Brischetto[2,3], S. Calabrese[3], M. Cavallaro[3], I. Ciraldo[2,3], O. Fasoula[1], J. Klimo[5], O. Sgouros[3], V. Soukeras[3], A. Spatafora[2,3], D. Torresi[3], M. Veselsky[6]

1) Laboratory of Physical Chemistry, Department of Chemistry, National and Kapodistrian University of Athens, Athens, Greece

2) Dipartimento di Fisica e Astronomia "Ettore Majorana", Università di Catania, Italy

3) Laboratori Nazionali del Sud, INFN, Catania, Italy

4) Department of Physics and HINP, The University of Ioannina, Ioannina, Greece

5) Institute of Physics, Slovak Academy of Sciences, Bratislava, Slovakia

6) Institute of Experimental and Applied Physics, Czech Technical University, Prague, Czech Republic

Abstract – In this report, we present an overview of our study of ejectile distributions of multinucleon transfer channels from the reaction of ^{70}Zn (15 MeV/nucleon) + ^{64}Ni. This project constitutes one of the few high-resolution mass spectrometric studies in the energy range of 15–25 MeV/nucleon to produce and identify neutron-rich projectile-like fragments and study the reaction mechanism. Our experimental distributions shown in this work are compared with two dynamical models, the Deep-Inelastic Transfer (DIT) model and the Constrained Molecular Dynamics (CoMD) model.

INTRODUCTION

Our research group is focused on systematic efforts to study exotic nuclei situated far away from the line of beta stability. To access these exotic nuclides with high neutron-excess, apart from the traditional approaches of projectile fragmentation, fission and spallation, it is necessary to pick up neutrons from the target [1]. Such multinucleon transfer mechanisms mainly take place in peripheral nucleon-exchange reactions at beam energies from the Coulomb barrier to the Fermi energy domain (~15-20 MeV/nucleon) [2]. For this reason, we initiated a project to produce and identify projectile-like fragments with the MAGNEX large-acceptance spectrometer at the INFN-LNS from the reaction of ^{70}Zn (15 MeV/nucleon) + ^{64}Ni. We have proceeded to a systematic approach to reconstruct the atomic number Z of the ejectiles along with their ionic charge states employing measurements of the energy loss, residual energy, and time-of-flight [3]. Subsequently, we moved on to obtain the momentum and angular distributions of the ejectiles and their production cross sections, along with comparisons with theoretical calculations. The calculations performed are mainly based on a standard two-stage Monte Carlo approach. The dynamical stage of the interaction between the projectile and the target was described by two theoretical models: the phenomenological DIT model [4] and the microscopic CoMD model [5,6]. After the dynamical stage of the reaction, the de-excitation of the primary fragments was described by the statistical deexcitation GEMINI code [7] Our findings have been extensively described in a recent article [8], providing a comprehensive presentation of the method of analysis as well as the extracted momentum distributions (p/A), production cross sections and angular distributions.

RESULTS AND DISCUSSION

To gain a greater insight of the reaction products, we have obtained two-dimensional distributions of p/A versus θ_{lab} for various reaction channels under study, as shown in Figure 1. The y-axis represents p/A (MeV/c) and the x-axis represents the reaction angle (degrees). This type of correlations is commonly utilized in the study of deep-inelastic reactions near and above the Coulomb barrier providing information on the energy dissipation of the dinuclear complex [9]. In this figure, the horizontal dashed lines represent the projectile p/A = 164.4 MeV/c, and the vertical dashed lines indicate the grazing angle θ_{gr}= 6.5° of the ejectiles of the reaction. The channels are denoted by the number of neutrons or protons added or removed from the projectile. A typical attribute in most of the channels shown is the presence of a peak (a "band") near the velocity of the beam (quasielastic peak) and an extended region of lower velocities corresponding to more dissipative events. In Figure 2, we present p/A distributions of neutron-rich products from the reaction of ^{70}Zn (15 MeV/nucleon) + ^{64}Ni, depicting the pickup of one neutron and two neutrons from the target, respectively. The vertical axis in the p/A distributions, denoted as "diff. cross section", corresponds to $d^2\sigma/d(p/A)d\Omega$ [mb/(MeV/c) msr]. The experimental data are shown by solid black circles. The DIT calculation is represented by open (blue) circles, while the CoMD calculation by open (red) squares. The green dashed line shown on each frame of the momentum distribution plot represents the momentum per nucleon of the beam, which is 164.4 MeV/c. The numbers above

some of the peaks give the total excitation energy of the quasiprojectile-quasitarget system obtained using the indicated p/A values and employing binary kinematics.

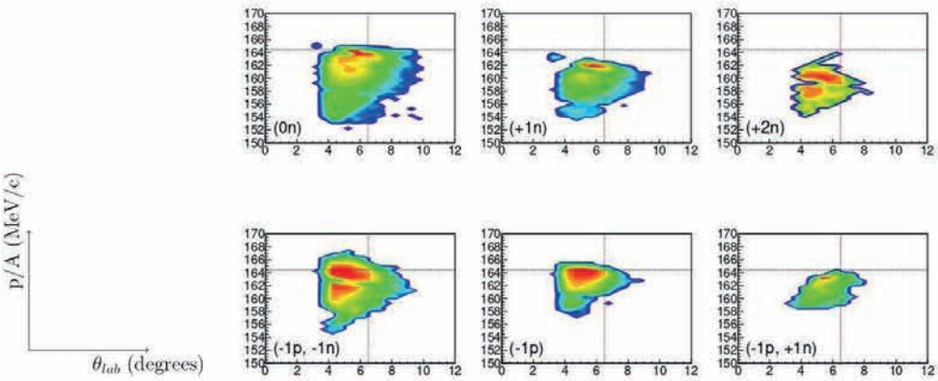

Figure 1: p/A versus θ_{lab} distributions of ejectiles from representative channels of the reaction ^{70}Zn (15 MeV/nucleon) + ^{64}Ni. The horizontal dashed lines represent the p/A of the projectile and the vertical dashed lines the grazing angle. Channels are marked by the number of neutrons or protons added or removed from the projectile.

We observe in the p/A spectra shown, that the CoMD/GEMINI calculation exhibits broad peaks at lower velocities and tends to be higher with respect to the experimental data (e.g. in the case of one neutron pickup). On the other hand, the DIT/GEMINI calculation could describe rather successfully the broad regions of the spectra in the depicted channels but cannot describe the quasielastic peak in some cases (e.g. the case of the one neutron pickup). This result is consistent with the fact that the DIT model has no inherent mechanism of inelastic excitation and direct transfer. For this reason, it cannot describe the quasielastic part of the experimental p/A spectrum.

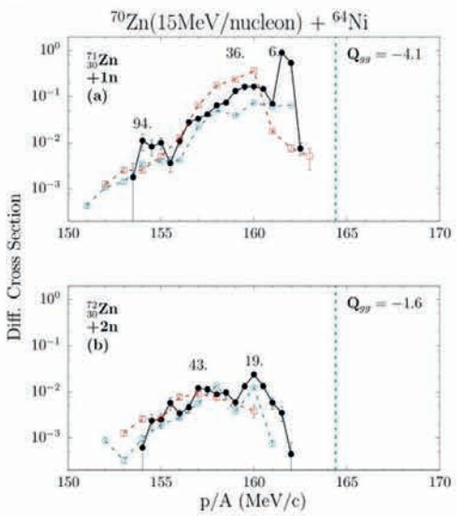

Figure 1: Momentum per nucleon distributions of ejectiles from neutron pickup channels from ^{70}Zn (15 MeV/nucleon) + ^{64}Ni. Experimental data: closed (black) circles. DIT calculation: open (blue) circles. CoMD calculation: open (red) squares.

CONCLUSIONS

The present project represents our inaugural effort to pave a path to more detailed studies of peripheral reactions of medium-mass nuclei in the Fermi energy regime with the use of the MAGNEX large acceptance spectrometer. In this first experiment, we achieved the production of several neutron-rich nuclides close to the projectile and the study of the reaction mechanism. We note that the MAGNEX facility offered the distinct advantage of the high-resolution measurement of the momentum and the reaction angle of the medium mass ejectiles in an extended region covering the quasielastic and deep-inelastic processes. We wish to mention that the ongoing upgrade of the MAGNEX focal plane detector will be of great importance in extending our efforts to study the production of more exotic neutron-rich nuclei toward the r-process path and the neutron drip line in the near future.

REFERENCES

[1] Y.X Watanabe et al., PRL 115 (2015) 172503.
[2] T. Mijatovic et al., Phys. Rev. C 94 (2016) 064616.
[3] G. A. Souliotis et al., NIMA1031 (2022) 166588.
[4] L. Tassan-Got et al., Nucl. Phys. A 524 (1991) 121.
[5] M. Papa et al., Phys. Rev. C 64 (2001) 024612.
[6] M. Papa et al., J. Comput. Phys. 208 (2005) 403.
[7] R. Charity et al., Nucl. Phys. A 483 (1988) 371.
[8] S. Koulouris et al., Phys. Rev. C 108 (2023) 044612.
[9] V. Zagrebaev et al., J. Phys. G: Nucl. Part. Phys. 31 (2005) 825.

$^{18}O + {}^{48}Ti$ elastic and inelastic scattering at 275 MeV

G. A. Brischetto[1,2], O. Sgouros[1,2], D. Carbone[2], F. Cappuzzello[1,2], M. Cavallaro[2], J. Lubian[3], G. De Gregorio[4,5], C. Agodi[2], D. Calvo[6], E. R. Chávez Lomelí[7], I. Ciraldo[1,2], F. Delaunay[1,2,8], H. Djapo[9], C. Eke[10], P. Finocchiaro[2], M. Fisichella[2], A. Gargano[4], M. A. Guazzelli[11], A. Hacisalihoglu[12], R. Linares[3], N. H. Medina[13], M. Moralles[13], J. R. B. Oliveira[14], A. Pakou[15], L. Pandola[2], V. Soukeras[1,2], G. Souliotis[16], A. Spatafora[2], D. Torresi[2], A. Yildirim[17], V. A. B. Zagatto[14]
for the NUMEN collaboration

1) Dipartimento di Fisica e Astronomia "Ettore Majorana", Università di Catania, Catania, Italy
2) Istituto Nazionale di Fisica Nucleare, Laboratori Nazionali del Sud, Catania, Italy
3) Instituto de Física, Universidade Federal Fluminense, Niterói, Brazil
4) Istituto Nazionale di Fisica Nucleare, Sezione di Napoli, Napoli, Italy
5) Dipartimento di Matematica e Fisica, Università della Campania "Luigi Vanvitelli", Caserta, Italy
6) Istituto Nazionale di Fisica Nucleare, Sezione di Torino, Torino, Italy
7) Instituto de Física, Universidad Nacional Autónoma de México, Mexico City, Mexico
8) Université de Caen Normandie, ENSICAEN, CNRS/IN2P3, LPC Caen UMR6534, Caen, France
9)Turkish Accelerator and Radiation Laboratory, Ankara, Turkey
10) Department of Mathematics and Science Education, Faculty of Education, Akdeniz University, Antalya, Turkey
11) Centro Universitario FEI, São Bernardo do Campo, Brazil
12) Department of Physics, Recep Tayyip Erdogan University, Rize, Turkey
13) Instituto de Pesquisas Energeticas e Nucleares IPEN/CNEN, São Paulo, Brazil
14) Instituto de Física, Universidade de São Paulo, São Paulo, Brazil
15) Department of Physics, University of Ioannina and Hellenic Institute of Nuclear Physics, Ioannina, Greece
16) Department of Chemistry, University of Athens and Hellenic Institute of Nuclear Physics, Athens, Greece
17) Department of Physics, Akdeniz University, Antalya, Turkey

Abstract - The $^{18}O + {}^{48}Ti$ reaction at 275 MeV incident energy was investigated at INFN-LNS in the context of the NUMEN project. The elastic and low-lying inelastic scattering channels were measured using the MAGNEX magnetic spectrometer and the corresponding angular distributions were determined. Optical model (OM), distorted wave Born approximation (DWBA), and coupled channel (CC) calculations were performed to deduce the initial state interaction (ISI) for this system.

INTRODUCTION

The NUMEN (NUclear Matrix Elements for Neutrinoless double beta decay) project at the Laboratori Nazionali del Sud of the Istituto Nazionale di Fisica Nucleare (INFN-LNS) aims at deducing data-driven information on the neutrinoless double beta decay nuclear matrix elements by measuring cross sections of heavy ion induced double charge exchange reactions [1]. To this purpose, a multi-channel description of several reaction channels is needed [2]. In this context, the analysis of the elastic and inelastic scattering channels is fundamental to determine the ISI of the system, which is a crucial ingredient for the study of all the other reaction channels.

EXPERIMENTAL APPARATUS

The experiment was held at the INFN-LNS, where a $^{18}O^{8+}$ beam of 275 MeV incident energy impinged on a 510 ± 25 μg/cm^2 thick TiO_2 target evaporated on an aluminum backing with a thickness of 216 ± 11 μg/cm^2. The background contributions due to the oxygen and aluminum target components were evaluated by performing, under the same experimental conditions, additional measurements with a WO_3 + ^{27}Al and ^{27}Al target. The flux of incident $^{18}O^{8+}$ ions was deduced by measuring in each run the total beam charge with a Faraday cup, placed 15 cm downstream the target. The ^{18}O ejectiles were analyzed in momentum by the MAGNEX large acceptance magnetic [3] spectrometer and measured by its Focal Plane Detector [4]. For the elastic and inelastic scattering channels, three different angular ranges were explored, by setting the MAGNEX optical axis (θ_{opt}) at 9°, 15°, and 21° with respect to the beam direction. At $\theta_{opt} = 9°$ MAGNEX was operated in full horizontal acceptance, but with a reduced vertical one (±2°). At θ_{opt} = 15°, 21° the solid angle was set to its maximum value (i.e. 50 msr).

DATA REDUCTION AND RESULTS

As described in Refs. [5-6], the particle identification was performed following a procedure that utilizes both the ΔE-E technique (for the atomic number identification) and a method based on the Lorentz force (for the mass number identification). A differential algebra-based algorithm was applied to the identified events to reconstruct the momentum vector at the target position,

which allows to deduce the excitation energy spectra. Such spectra were fitted with multiple-gaussian functions to derive the cross section angular distributions for the elastic scattering and two inelastic transitions. The elastic scattering angular distribution in terms of its ratio with the Rutherford one is shown in Fig. 1 as a function of the scattering angle in the center-of-mass reference frame ($\theta_{c.m.}$) [8]. In Fig. 2, the angular distributions for the ^{48}Ti(2^+_1) excitation (E_x = 0.98 MeV) and for a structure centered at 2.2 MeV, due to the superposition of the ^{18}O(2^+_1) transition (E_x = 1.98 MeV) with 3 excited states of ^{48}Ti (E_x = 2.30, 2.45, and 2.47 MeV), are shown [8].

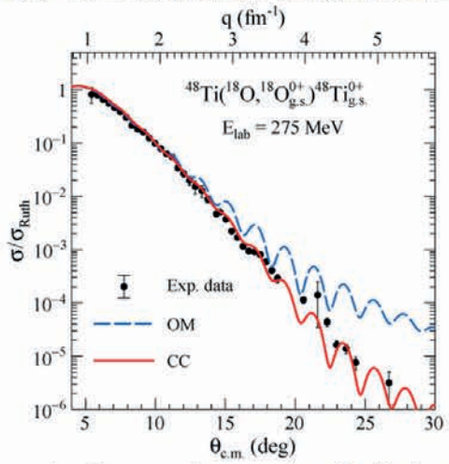

Figure 1. Cross section angular distribution of the ^{18}O + ^{48}Ti elastic scattering at 275 MeV, in terms of the ratio with the Rutherford one, compared to OM and CC calculations.

THEORETICAL ANALYSIS

Theoretical calculations were performed in OM, DWBA, and CC formalisms using the FRESCO code. The double-folding São Paulo potential (SPP) [7] was adopted to describe both the real and imaginary component of the optical potential (OP). The imaginary part of the OP was scaled by a factor of 0.78 in OM and DWBA frameworks, while it was reduced to 0.6 for CC calculations. The coupling scheme includes the first low-lying excited states of projectile (2^+_1 and 3^-_1) and target (2^+_1, 3^-_1, and 4^+_1). Such states are treated as collective excitations within the rotational model. It is worth to mention that in the DWBA approach only first-order transitions are considered, therefore neither the transition to the ^{48}Ti(4^+_1) state nor back-couplings to the elastic channel are allowed.

As can be noticed in Fig. 1, the OM calculation overestimates the elastic scattering data at large scattering angles, where the coupling effects become relevant. Analogously, by looking at Fig. 2, one can see that the DWBA predictions for the two inelastic transitions do not reproduce the experimental data, especially at large momentum transfer. The description of the data is remarkably improved when the CC method is used, as can be seen in Figs. 1 and 2 [8]. This is a clear sign of the relevance of the channel couplings for this system.

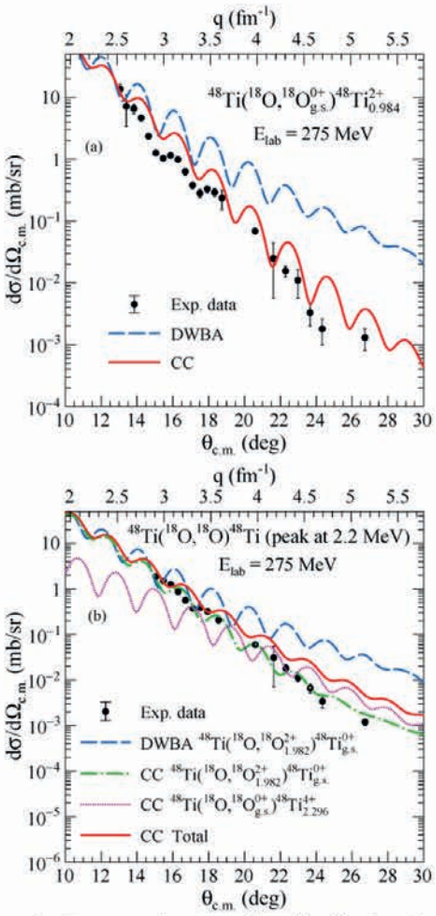

Figure 2. Cross section angular distribution for: (a) the inelastic scattering to the ^{48}Ti(2^+) excited state at 0.984 MeV, (b) a structure at 2.2 MeV (see text for details). Both angular distributions are compared to DWBA and CC calculations.

CONCLUSIONS

A satisfactory description of the ^{18}O + ^{48}Ti elastic and inelastic scattering data can be obtained adopting the SPP as OP and including the coupling effects within the CC formalism. The ISI derived in this work has been used for the analysis of the one-nucleon transfer reactions [9-10] and will be employed for the other reaction channels induced in the projectile-target collision.

REFERENCES

[1] F. Cappuzzello et al., Eur. Phys. J. A 54 (2018) 72
[2] F. Cappuzzello et al., PPNP 128 (2023) 103999
[3] F. Cappuzzello et al., Eur. Phys. J. A 52 (2016) 167
[4] D. Torresi et al., NIM A 989 (2021) 164918
[5] F. Cappuzzello et al., NIM A 621 (2010) 419
[6] G. A. Brischetto, Il Nuovo Cimento C 45 (2022) 96
[7] L. C. Chamon et al., PRC 66 (2002) 014610
[8] G. A. Brischetto et al., PRC 109 (2024) 014604
[9] O. Sgouros et al., PRC 104 (2021) 034617
[10] O. Sgouros et al., PRC 108 (2023) 044611

Hoyle state production and decay at forward angles in the $^{16}O+^{12}C$ reaction

G. Cardella[1*], L. Acosta[7,8], J. Bishop[9], N. Curtis[9], E. De Filippo[1], E. Geraci[2,1], B. Gnoffo[2,1], C. Guazzoni[6,5], Tz. Kokalova[9], N.S. Martorana[1], C. Maiolino[3], A. Pagano[1], E. V. Pagano[3,2], M. Papa[1], S. Pirrone[1], G. Politi[2,1], F. Risitano[4,1], F. Rizzo[2,3], P. Russotto[3], M. Trimarchi[4,1], C. Weldon[9], C. Zagami[2,3].

1) INFN Sezione di Catania, Italy

2) Dipartimento di Fisica e Astronomia, Università di Catania, Italy

3) INFN Laboratori Nazionali del Sud, Catania - Italy

4) Dip. di Scienze MIFT Universita' di Messina - Messina, Italy

5) INFN Sezione di Milano - Italy

6) Politecnico di Milano, Dip. Elettronica, Informazione e Bioingegneria, Italy

7) Instituto de Física, Universidad Nacional Autónoma de México, Mexico City, Mexico

8) Instituto de Estructura de la Materia, CSIC, Madrid, Spain

9) University of Birmingham, School of Philips and Astronomy, United Kingdom

** cardella@ct.infn.it*

Abstract – Data taken during the SIKO experiment with prototypes of the FARCOS telescopes have been reanalysed in order to extract the yield of population of the Hoyle state at very forward angles in the reaction $^{16}O+^{12}C$ at various beam energies. A rather good energy resolution better than 30 keV has been measured for the Hoyle resonance population and decay.

INTRODUCTION

The study of the Hoyle state [1] is one of the most popular subject in nuclear physics, due to its implications on the production of the matter in the universe. Few examples of the most recent papers published on this argument are given in references [2-7]. FARCOS [8] is one of the detectors available at INFN-LNS most suited to pursuit this study due to its excellent energy and angular resolution [9]. A reanalysis of data taken in the SIKO experiment [10] with the prototype of FARCOS telescopes was performed with the objective of a further test for the use of the pixelation method recently developed [9]. This reanalysis is still ongoing with a revision of the energy calibration of the backward side. The performed analysis allows already, to extract a beautiful spectrum of the Hoyle state in the reactions $^{16}O+^{12}C$ performed at various beam energies (160 MeV, 280MeV and 400 MeV).

THE EXPERIMENT

The SIKO experiment was performed at INFN-LNS in the 2015 campaign together with the PYGMY [11] and CLIR [12] experiments. Four prototype telescopes of the FARCOS detector were mounted inside the CHIMERA scattering chamber at small angles from 2° to about 7° covering about 70% of the azimuthal angle. The standard CHIMERA electronics was used with CAEN amplifiers and QDC to digitize the signals in this prototype phase. Each telescope of the array is composed by two stages of Double Sided Silicon Strip Detectors (DSSSDs) respectively thick 300 μm and 1500 μm. Each DSSSD is segmented in 32 strip in the front and back side with 2 mm pitch. A third stage with CsI(Tl) scintillators with photodiode readout is also present. This stage is not used in the data presented here.

Due to some incomplete treatment of the detection angle in the FARCOS telescopes the analysis of coincidence alpha particles in these telescopes was not fully included in the publication of the main results of the experiment [10]. All the prescriptions on the pixelation method developed with the analysis of FARCOS data collected during the HOYLE experiment [13] are applied to this reanalysis. The correct pixel assignment of multi-particle events was performed even if some uncertainties on the back strips energy calibration open the space to further improvements. An accurate interstrip analysis was also implemented. In fig.1 the center of mass energy

spectrum of two coincidence alpha particles detected in FARCOS telescopes in the reactions is shown. All coincidence data are shown including recovered interstrip events. Both alpha particles stopped in the first stage, and second stage are used to extract such spectrum. In red it is shown the Gaussian fit of the peak of the $^{8}Be_{gs}$ resonance at 92 keV. A RMS value around 7 keV is found.

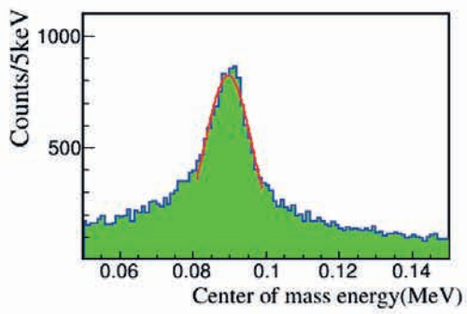

Figure 1 The center of mass energy spectrum of two alpha particles detected in the FARCOS array. The $^{8}Be_{gs}$ resonance is observed. The red line is a Gaussian fit of the resonance.

The average energy of the ^{8}Be before its decay was extracted for the different beam energies and an example it is shown in fig.2 for the lowest beam energy.

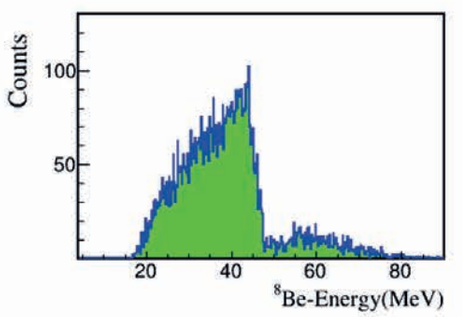

Figure 2 The reconstructed energy of $^{8}Be_{gs}$ particles detected measuring the coincidence of two alpha particles in one of the FARCOS telescopes.

Two bumps can be observed: the first one due to particles stopped in the first DSSSD and the second one due to particles identified in the telescope by the ΔE-E method. Particles stopped in the third stage are up to now not included in the analysis. The spectrum is not corrected for the efficiency. Most of the particles are stopped in the first stage, their velocity corresponds to the decay from the compound system.

THREE ALPHA PARTICLES EVENTS

The events with the detection of 3 alpha particles have been selected at all beam energies. In order to increase the statistics, the events collected at all energies were summed and plotted in fig. 3. Further improvements of the background subtraction and in the energy resolution of the resonance are expected by the on-going improvement of the energy calibration procedures. The energy resolution, 27 keV RMS, is already of the same order of magnitude as some of the most precise recent measurements [2-3].

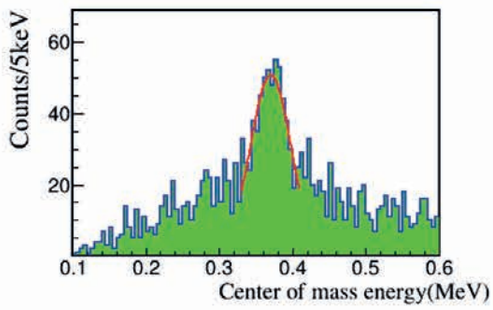

Figure 3 The Hoyle state resonance measured looking at the center of mass energy of three alpha particle events detected in FARCOS telescopes.

REFERENCES

[1] F. Hoyle, Astrophys. J. Suppl. Ser. 1, 121 (1954).
[2] R. Smith et al, Phys. Rev. Lett. 119, 132502 (2017).
[3] D. Dell'Aquila et al., Phys. Rev. Lett. 119, 132501 (2017).
[4] G. Cardella et al., Phys.Rev.C 104, 064315 (2021)
[5] M. Tsumura et al., Phys. Lett. B 817, 136283 (2021).
[6] Zifeng Luo et al., Phys. Rev C 109, 025801 (2024).
[7] T. Kibédi et al., Phys. Rev. Lett. 125, 182701 (2020).
[8] E.V. Pagano, et al., EPJ Web Conf. 117 (2016) 10008.
[9] G. Cardella et al LNS report 2021-2022 pag. 61.
[10] J. Bishop et al, Phys.rev. C 100, 034320 (2019).
[11] N.S. Martorana et al, Phys.Lett.B 782(2018)112–116.
[12] F. Risitano et al, IL NUOVO CIM. 47 C (2024) 43.
[13] G. Cardella et al, to be published NIMA.

Coulomb-free $^1S_0$ p-p scattering length from the quasi-free p+d→p+p+n reaction

Tumino[1,2], G.G. Rapisarda[1,3], M. La Cognata[1], A. Oliva[1], A. Kievsy[4], C.A. Bertulani[5], G. D'Agata[1,3], S. Gammino[1], M. Gattobigio[6], G.L. Guardo[1], L. Lamia[3], D. Lattuada[1,2], R.G. Pizzone[5], S. Romano[1,3], M.L. Sergi[1,3], R. Spartà[1,2], M. Viviani[4]

1) Laboratori Nazionali del Sud - INFN, Catania, Italy
2) Dipartimento di Ingegneria e Architettura, Università degli Studi di Enna "Kore", Enna, Italy
3) Dipartimento di Fisica e Astronomia, Università degli Studi di Catania, Catania, Italy
4)INFN-Sezione di Pisa, Pisa, Italy
5) Department of Physics and Astronomy, Texas A&M University-Commerce, Commerce, TX 75429, USA.
6) Université Côte d'Azur, CNRS, Institut de Physique de Nice, 06560, Valbonne, France

Abstract - The Coulomb-free $^1S_0$ proton-proton (p-p) scattering length relies heavily on numerous and distinct theoretical techniques to remove the Coulomb contribution. Here, it has been determined from the half-off-the-energy-shell p-p scattering cross section measured at center-of-mass energies below 1 MeV using the quasi-free $p+d\rightarrow p+p+n$ reaction. A Bayesian data-fitting approach using the expression of the s-wave nucleon-nucleon scattering cross section has been performed. A model based on universality concepts has been developed to interpret this result. It accounts for the short-range interaction as a whole, nuclear and residual electromagnetic, according to what the s-wave phase-shift δ does in the description of low-energy nucleon-nucleon scattering data. The parameters thus obtained are representative of the short-range physics and propose to assess the charge symmetry breaking of the short-range interaction instead of just the nuclear interaction. This is consistent with the current understanding that the charge dependence of nuclear forces is due to different masses of up-down quarks and their electromagnetic interactions. This achievement suggests that these properties have a lesser than expected impact in the context of the charge symmetry breaking.

The longstanding hypothesis of charge independence and charge symmetry of nuclear forces can be unveiled by fixing the low energy parameters of the strong nucleon-nucleon (NN) interaction in the spin-singlet $^1S_0$ state [1]. The n-p scattering length is the only one directly determined from experiments, since the Coulomb effects need to be theoretically removed from experimental p-p data to reveal the strong interaction contribution to the scattering length, while it is impossible to study the n-n scattering directly because of the absence of neutron targets [2]. As for the p-p scattering, the accurate and numerous experiments performed so far throughout a broad energy range, have revealed that Coulomb corrections are large. One of the latest estimates of the uncorrected p-p scattering length using available p-p scattering world data at p laboratory energies below 30 MeV is quoted as -7.8063 ± 0.0026 fm [3]. The removal of electromagnetic interactions requires sophisticated theoretical tools, which, although fairly well assessed, can introduce considerable model dependence and some uncontrolled systematic uncertainty in the nuclear p-p scattering length thus derived [4,5]. The determination of the nuclear scattering length introduces a model dependence due to the arbitrary exclusion of the short-range electromagnetic contributions. A well defined, almost model-independent quantity would be the short-range scattering length. For the pp system, this would require that only the long-range Coulomb contribution is subtracted but all the short-range contributions are taken into account. In the present work, and to our knowledge for the first time, we determine the Coulomb free p-p scattering length and effective range taking advantage of the half-off-the-energy-shell (HOES) p-p scattering obtained by measuring the ^{2}H(p, pp)n reaction in quasi-free kinematics with the Trojan Horse Method (THM) [6]. The THM is a well-known indirect technique, which has its roots in the unique properties of the quasi-free mechanism [7] that allows to study reactions between charged particles at sub-Coulomb energies free of Coulomb suppression as well as electron screening (see "THM basic features" in the Methods section). In particular, the aim of the 2H(p, pp)n measurement was to investigate the restraint of the Coulomb amplitude. A striking application of the THM where this restraint can be observed is exactly the p-p scattering at low energy, whose excitation function beautifully displays a deep minimum ($E_{pp} = 191.2$ keV, $\theta_{cm} = 90°$). This minimum is a direct signature of the interference between nuclear and Coulomb scattering amplitudes. Indeed, evidence of a vanishingly small Coulomb contribution is the lack of the interference minimum in the HOES p-p scattering excitation function. An exhaustive description of the experimental measurement as well as of data analysis performed in plane wave impulse approximation (PWIA) is given in [8,9]. The p-p scattering data free of Coulomb

interaction were fitted with the s-wave effective-range expansion, the conventional tool to analyze NN scattering data at low energies [10]. The fit was done with three free parameters: a, r_0 and a normalization coefficient C. a Bayesian approach (see Methods section "Bayesian analysis approach") was used to fit the data, in order to better sample the parameters of the cross section model according to our data. A Markov Chain Monte Carlo (MCMC) was implemented using the emcee Python library23, which is based on the algorithm described in24. A flat prior distribution was chosen for a, sampled in the interval (−25 fm, −15 fm) to account for the large historical dispersion of this model parameter. A Gaussian prior distribution was taken for r_0 with centroid at 2.80 fm corresponding to the weighted average of the current accepted values from the three NN combinations and $\sigma = 0.04$ fm. Separating the statistical uncertainties from the systematic ones, the numbers read as:

$a_{pp} = -18.17 \pm 0.055_{stat} \pm 0.01_{syst}$fm
$r_0 = 2.80 \pm 0.05_{stat} \pm 0.001_{syst}$ fm.

Numbers from our results and current accepted values for nuclear n-p, p-p and n-n scatterings (with upper case N) are reported in Table 1 for a better comparison.

Table 1 Numbers of low energy parameters.

NN	a^N(fm)	r_0^N(fm)	a^{THM}(fm)	r_0^{THM}(fm)	a^e(fm)	r_0^e(fm)	V_0(MeV)
np	−23.08 ± 0.02	2.77 ± 0.05			−23.74 ± 0.02	2.80 ± 0.08	−29.90
pp	−17.3 ± 0.4	2.85 ± 0.04	$-18.17^{+0.12}_{-0.09}$ fm	2.80 ± 0.05 fm	−17.6 ± 0.4	2.85 ± 0.09	−29.08
nn	−18.9 ± 0.4	2.75 ± 0.11			−18.6 ± 0.4	2.85 ± 0.08	−29.22

Current accepted values of a and r_0 parameters, (N superscript stands for "nuclear") for np, pp and nn scattering compared with those obtained in this work ("THM" superscript). In the last three columns, the values and the corresponding strength V_0 obtained with the Gaussian characterization are given. The e superscript stands for "short-range" (nuclear + EM).

It turns out that our extracted a_{pp} value from the quasi free p-p scattering, while disagreeing with a_{np}^N, barely agrees within experimental errors with the world accepted value, and sits closer to the estimate. This observation deserves further consideration. Despite being in a very low-energy region where the interacting protons appear as point-like, the NN s-wave phase shift δ of eq. (2) contains all short-range effects, including the electromagnetic ones. This means that the present analysis of the HOES cross section allows direct access to the short-range p-p interaction as a whole, with its peculiar a_{pp} and r_0 values. The result of the fit is shown in the upper panel of Fig. 1 as solid black line with Coulomb free THM p-p scattering data given as black solid circles. Dotted red, blue and black lines in the same figure refer to the s-wave NN scattering cross-section with current accepted values for nuclear a and r_0 parameters from n-n, p-p and n-p scatterings, respectively. In this interpretation, we have been assisted by a model based on universality concepts that we have developed to help interpret the results [6]. We conclude that this technique provides us with parameters to assess the charge symmetry breaking of the short-range interaction as a whole. This triggers the proposal of a new paradigm in the study of the charge symmetry breaking, in line with the current understanding that, at a fundamental level, the charge dependence of nuclear forces is due to a difference between the masses of the up

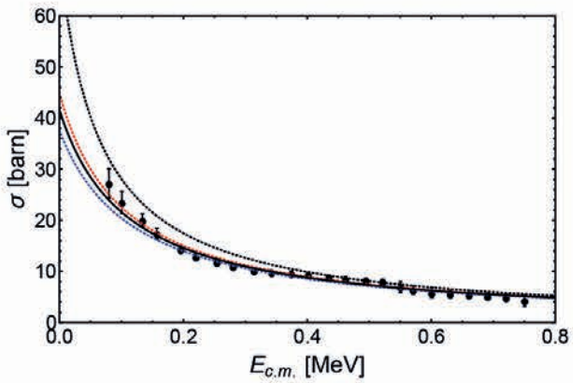

Fig. 1 Experimental quasi-free p-p scattering cross section free of Coulomb interaction (black solid circles). Error bars indicate 1σ uncertainties. The result of the fit using the s-wave NN scattering cross-section is shown as solid black line, while the dotted red, blue and black lines refer to the same cross section for n-n, p-p and n-p scatterings, respectively, using current accepted values for nuclear scattering length a^N and r_0 parameters.

and down quark and to electromagnetic interactions among the quarks. Our results indicate that the impact of the different up-down quark masses and residual electromagnetic properties has a limited effect on charge symmetry breaking. Additional experimental and theoretical studies at low energies are called for to better constrain the current existing models of charge symmetry breaking and Coulomb corrections filling up our basic understanding of low-energy NN scattering.

REFERENCES

[1] G.A. Miller, A.K. Opper & E.J. Stephenson, Annu. Rev. Nucl. Part. Sci. 56, 253 (2006).

[2] M. Goebel, et al., Phys. Rev. C 104, 024001 (2021).

[3] M. Piarulli, et al., Phys. Rev. C 91, 024003 (2015).

[4] L.P. Kok, Phys. Rev. Lett. 45, 427 (1980).

[5] S. Albeverio, et al., Phys. Rev. C 29, 680 (1984).

[6] A. Tumino et al., Commun. Phys. 6 106 (2023).

[7] A. Tumino, et al., Ann.Rev.Nucl. Part. Sci. 71, (2021).

[8] A. Tumino, et al., Phys. Rev. Lett. 98, 252502 (2007).

[9] A. Tumino, et al., Phys. Rev. C 78, 064001 (2008).

[10] G.A. Miller, et al. Phys. Rep. 194, 1 (1990).

Measurement of the $^{12,13}C + ^{19}F$ ion-ion fusion reaction at sub-barrier energies

G.L. Guardo[1], M. La Cognata[1], M. L. Sergi[1], A. Tumino[1], M. Ursino[1], A. Spiridon[2], D. Tudor[2], A. Stefanescu[2], I. Stefanescu[2], L. Trache[2], R. Andrei[2], D. Iancu[2], M. Straticiuc[2]

1) Laboratori Nazionali del Sud – INFN, Catania, Italy
2) National Institute of Physics and Nuclear Engineering (IFIN-HH), Bucharest-Magurele, Romania

Abstract – In the framework of a joint program to study reactions between light ions important for nuclear astrophysics and given the importance and difficulty of the topic, several methods gave promising results. In particular, we already used with success the indirect Trojan Horse Method (THM) in Catania and now we propose the complementary study of ion-ion fusion reactions at very low energies.

INTRODUCTION

In the stellar nuclear processes that are the source of both stellar energy and production of chemical elements, many of the important reactions are those of capture of very light particles: protons, neutrons and alphas. There are, however, a few crucial or very important reactions between light ions heavier than 4He ("metals" in the jargon of nucleosynthesis). Among them those involving ^{12}C and ^{16}O: $^{12}C + ^{12}C$, $^{12}C + ^{16}O$, $^{16}O + ^{16}O$. Even at the very high stellar temperatures occurring in explosive burning of massive stars, reaching a few GK, these reactions happen at very low energies, well below the Coulomb barriers of the respective reactions. This makes them difficult to study experimentally.

However, many attempts were and are being made, either through indirect methods or by direct measurements at energies as low as possible. Part of these are the attempts to understand the fusion reaction mechanisms at such energies, testing models that would guide the extrapolations toward the energies in the Gamow window. The indirect methods rely strongly on theoretical models. The results depend on the comparison between experiment and theory and as such, the theory must be able to accurately characterize the reaction mechanisms occurring during ion ion fusion at sub barrier energies.

Specifically, the theoretical predictions are sensitive to adopted model parameters, hindrance effects and the proved existence or the possibility of cluster or molecular resonances at relevant energies. They need to be tested widely on experimental data before their predictions are trusted.

To that end, we started joint program with the Nuclear Astrophysics Group at IFIN-HH to study ion-ion fusion reactions at sub-barrier energies. One such reaction is $^{12,13}C+^{19}F$. It was last studied in 1976 by Gaedke et al [1] who measured the fusion cross-section for an energy range of 18-27 MeV lab (Figure 1). We report here on the first experiment performed for this study, which had the goal to extend the fusion cross-section measurements below the previously known range.

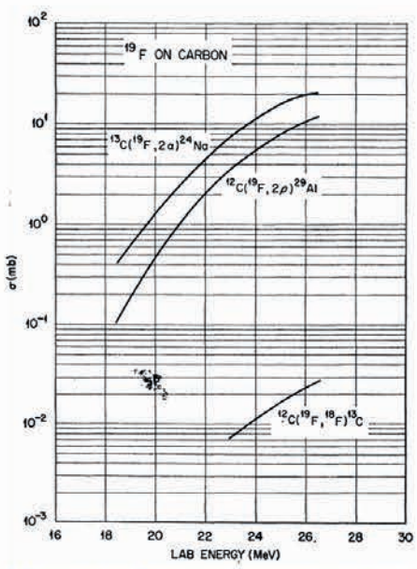

Figure 1 Excitation functions for reactions induced by ^{19}F incident on carbon obtained by Gaedke et al [1].

EXPERIMENTAL DETAILS

The experiment was performed at the National Institute of Physics and Nuclear Engineering (IFIN-HH) in Bucharest using the thick-target activation method. A beam of ^{19}F was produced with the 3 MV Tandetron and used to irradiate natural graphite targets. The beam energy was varied from 12.5 to 17.5 MeV lab (5.1 to 7.1 MeV CM), in steps of 1 MeV, with currents going from 1.25 to 4.5 μA, respectively. The length of irradiation varied from 5 h to 24 h, depending on the cross-section and estimated statistics to be expected.

Four unstable nuclei were produced: ^{29}Al ($T_{1/2}$ = 6.6 min), ^{28}Al ($T_{1/2}$ = 2.2 min), ^{27}Mg ($T_{1/2}$ = 9.5 min) and ^{24}Na ($T_{1/2}$ = 15 h). After irradiation, the graphite samples were removed from the beamline and their decay was measured with the BEGA detection system. As can be seen in

Figure 2, BEGA consists of two HPGe detectors for gamma particles and a plastic scintillator (EJ-200) for beta particles. All three sensors are surrounded by a thick lead cylindrical shield to reduce background contamination of the spectra. The irradiated sample is inserted in the centre of the system (where the yellow arrow points in Figure 2) and as such, the geometry allows for almost 4π coverage.

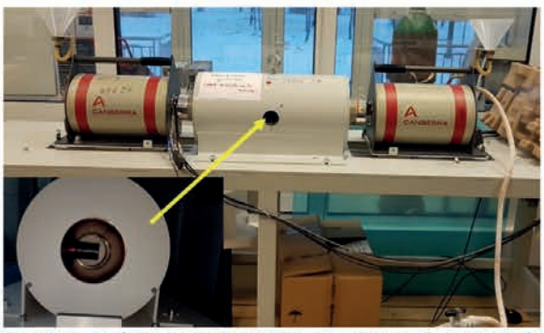

Figure 2 BEGA detection system. Picture insert to the bottom left shows a side view of the scintillator.

Since the unstable nuclei mentioned undergo beta-delayed gamma decay, the background was reduced even further using beta-gamma coincidences. The gamma energy decay spectra were recorded in 2 steps: the first 25 minutes for the shorter-lived nuclei and a longer measurement (upwards of 5 h) for ^{24}Na. In order to correct for summing issues, there were two measurements done at 17.5 MeV (where the cross-sections where higher), one in close geometry and one in far geometry (where we don't have gamma summing). The ratio of efficiencies for the energy peaks of interest gave us the corresponding correction factors to use for the remaining measurements.

Figures 3 and 4 show a pair of short-long gamma spectra at 16.5 MeV lab energy, taken with a beta-gamma coincidence gate. In Figure 3, the strongest peaks are 511 keV and 1273 keV, the decay of ^{29}Al. The other two short-lived nuclei could not be measured due to the very low cross-sections.

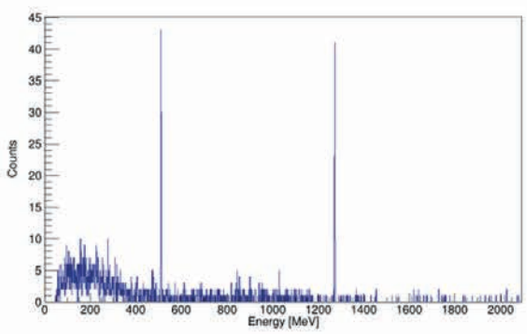

Figure 3 Gamma spectrum recorded in coincidence with beta for a measurement time of 25 minutes.

In Figure 4, the 3 strongest peaks that can be seen are again the annihilation peak, 511 keV, and then the two gamma peaks from the decay of ^{24}Na, 1368.6 keV and 2754 keV.

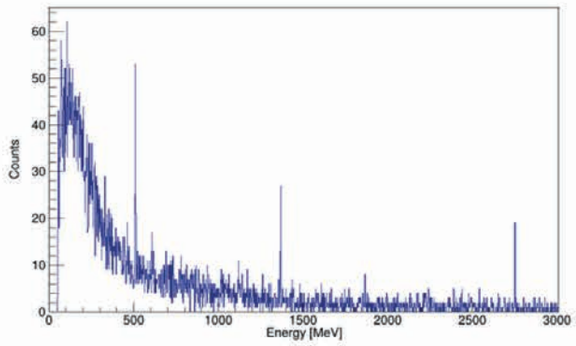

Figure 4 Gamma spectrum recorded in coincidence with beta for a measurement time of 7 hours.

A preliminary analysis of these two nuclei was done for all the energy points obtained. The resulting yields for these two channels, ^{12}C(^{19}F,2p)^{29}Al and ^{13}C(^{19}F,2α)^{24}Na, can be seen in Figure 5.

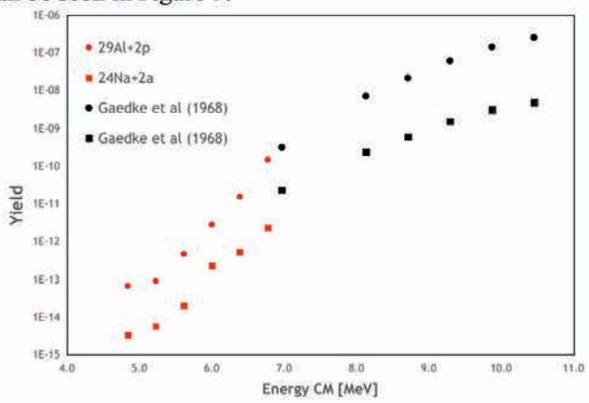

Figure 5 Yields as a function of center-of-mass energy for the 2 main activation channels produced by a 19F beam incident on carbon. Comparison with results obtained by Gaedke et al [1] (black points).

A further set of measurements is planned for this year with the goal to obtain 2-3 overlapping points with the study of Gaedke et al and then to continue going lower in energy.

REFERENCES

[1] R. M. Gaedke et al., Physical Review 167 (1968)

Direct measurement of the $^{7}Li(p, \alpha)^{4}He$ reaction at astrophysical energies using ELISSA array

H. Pai[1], Sk M. Ali[2], G. L. Guardo[3], I. Kuncser[1,4], A. Lupoae[1], T. Madgearu[1,4], C. Matei[1], Y. Xu[1], S. Aogaki[1], D. L. Balabanski[1], R. S. Ban[1], M. Brezeanu[1], A. Cassisa[5], M. La Cognata[3], A. Cvetinović[6], A. Dhal[1], P. Figuera[3], A. Kuşoğlu[1,7], L. Lamia[3,8], D. Lattuada[3,9], V. Lelasseux[1], O. Lopez[10], C.A. Marin[1], C. Nedelcu[1], A. Pappalardo[3], I.P. Parlea[1], R.G. Pizzone[3], G. Restifo[3,8], R. Roy[1,11], P.-A. Söderström[1], N. Stefan[1], N. Szegedi[3], V.A. Toma[1], A. Tumino[3,9], G. Turturica[1], T. Tozar[1], N. Vukman[12,13]

1) Extreme Light Infrastructure - Nuclear Physics/IFIN-HH, Magurele, Romania
2) Facility for Rare Isotope Beams, Michigan State University, East Lansing, Michigan 48824, USA
3) Laboratori Nazionali del Sud INFN, Catania, Italy
4) POLITEHNICA Bucureşti National University for Science and Technology, Splaiul Independenţei 313, Romania
5) Nuclear Physics Institute of the Czech Academy of Sciences, 250 68 R˘ež, Czech Republi
6) Jožef Stefan Institute, Department of Low and Medium Energy Physics (F2), 1000 Ljubljana, Slovenia
7) Department of Physics, Faculty of Science, Istanbul University, Vezneciler/Faith, 34131, Turkey
8)Dipartimento di Fisica e Astronomia "E. Majorana", Università degli Studi di Catania, Italy
9)Universitá degli Studi di Enna "Kore", Enna, Italy
10) Instituto de Física, Universidad Nacional Autónoma de México, Mexico City, Mexico
11) Department of Physics, Indian Institute of Technology Ropar (IIT-RPR), Punjab, India
12) INFN Sezione di Perugia, Italy
13) Ruder Boskovic Institute, 10000 Zagreb, Croatia

Abstract - Direct measurement of the $^{7}Li(p, \alpha)^{4}He$ reaction at astrophysical energies using the scaled-down version of the ELISSA array has been performed at IFIN-HH with the 3MV Tandem. This reaction is intimately linked with the so-called "Cosmological Lithium Problem". The measurements were successfully carried out with the ^{7}Li beam at 8.0, 7.0, 6.0, 5.0, 4.0, 3.0, 2.0, 0.9, 0.75, and 0.6 MeV energies and CH_2 target.

INTRODUCTION

The $^{7}Li(p, \alpha)^{4}He$ reaction is of significant astrophysical interest. It plays a prominent role during the Big-Bang as well as stellar nucleosynthesis. In the former case, it is intimately linked with the so-called "Cosmological Lithium Problem", because of the severe discrepancy between the observed ^{7}Li abundances from metal-poor halo stars and the predictions of standard Big-Bang Nucleosynthesis (SBBN) theory [1, 2]. Being the primary channel of lithium burning, the destruction of ^{7}Li via $^{7}Li(p, \alpha)^{4}He$ affects the ^{7}Li abundance. Thus, precise determination of its reaction rate at BBN energies is extremely important. In the context of stellar nucleosynthesis, the $^{7}Li(p, \alpha)^{4}He$ reaction is the final step in the hydrogen-to-helium burning chain [3], accounting for ~10% of the energy budget provided by the whole PP chain [3, 4]. Precision in abundance observations require an improvement in our knowledge of the low-energy astrophysical factors. The available astrophysical S-factor data [5] for the reaction $^{7}Li(p, \alpha)^{4}He$ at $10 < E < 1000$ keV exhibit an exponential increase at low energies due to the effects of electron screening. The S(0) value from various direct and indirect measurements of $^{7}Li(p, \alpha)^{4}He$ reaction varies between 40 - 60 keV b (15-40 % uncertainty in the direct measurements), while the electron screening potential estimate varies between 200 - 400 keV [4], larger if compared with the adiabatic limit. The existing low-energy angular distribution data from direct measurement of $^{7}Li(p, \alpha)^{4}He$ are limited and they suffer from large uncertainties due to normalization problems [3]. Thus, a new direct measurement of the $^{7}Li(p, \alpha)^{4}He$ reactions at low energies, from 94 keV to 1 MeV in the center-of-mass system has been carried out using the scaled-down version of the ELISSA array to reduce the uncertainty in the S(E) factor.

THE EXPERIMENT AND PRELIMINARY RESULTS

The experiment was performed using a ^{7}Li beam with an average beam intensity ~ 2 - 4 pnA and self-supported, thin polyethylene targets (CH_2, about 70 μg/cm^2 thick, placed at 90° with- respect to the beam axis) at IFIN-HH with the 3MV Tandem. This measurement was performed using a monitor detector positioned at a 27.6° angle and located 150.1 mm away from the target. Si detector having a 25 mm^2 active area was used as a monitor detector. The spot size of the ^{7}Li beam on the target was ~ 1 mm. The measurements were carried at E_{Lab} = 8.0, 7.0, 6.0, 5.0, 4.0, 3.0, 2.0, 0.9, 0.75, and 0.6 MeV. The scaled-down version of the ELISSA array [6] having 12 X3 position-sensitive strip detectors arranged in a barrel-

like configuration was used to detect the transfer alpha as shown in Fig. 1. The X3 detectors are placed at a distance of 6.1 cm from the target center. This configuration resulted in an angular coverage ranging from 36° - 58° in the laboratory system. The energy calibration has been carried out with the three-peaks α-sources (^{239}Pu, ^{241}Am, and ^{244}Cm). The ^{7}Li elastic scattering with a gold target was also used for energy calibration purposes of the detectors. The X3 detectors are position-sensitive resistive detectors. To calibrate the position, the detectors were mounted with masks having slit widths of 1 mm in front of the detectors, and three-line α-sources were used. The ballistic deficit correction of the X3 detectors has also been carried out.

The simulation of the present experimental setup was carried out using the Monte Carlo simulation code NPTool [7] which is a Geant4-based simulation. The experimental E vs θ spectrum of one of the X3 detectors with a 3 MeV beam energy is shown in Fig. 2 in blue color data points. The red points correspond to the simulated transfer α.

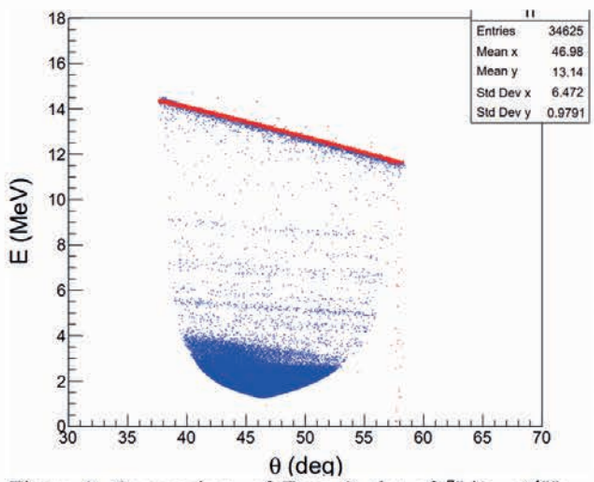

Figure 2. Comparison of E vs θ plot of ^{7}Li(p, α)^{4}He from simulations [7] (red) and experimental data (blue).

The absolute differential cross section of the ^{7}Li(p,α)^{4}He reaction has been determined by normalising to the ^{7}Li(p,p)^{7}Li Rutherford scattering cross section measured in the monitor detector. Preliminary experimental differential cross section of ^{7}Li(p, α)^{4}He reaction at E_{Lab} = 2.0 and 3.0 MeV (which in the center of mass frame corresponds to $E_{c.m.}$ = 233 and 359 keV, respectively), have been shown in Fig. 3.

A detailed analysis is in progress.

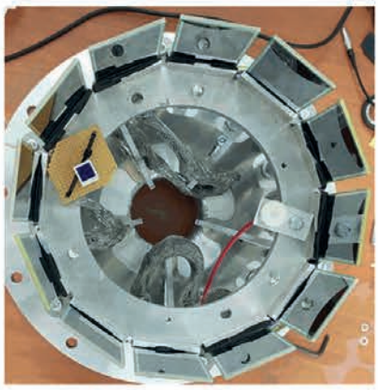

Figure 1: One ring of the ELISSA array corresponds to 12 X3 detectors.

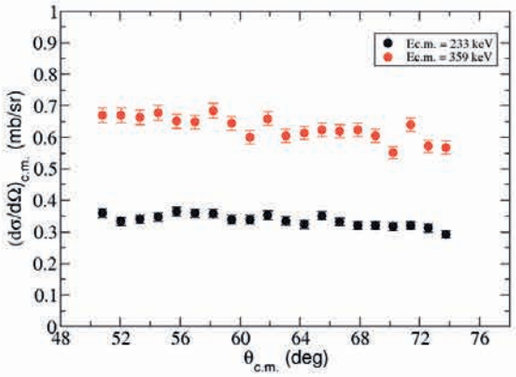

Figure 3. Differential cross-sections for ^{7}Li(p, α)^{4}He in the center of mass frame.

ACKNOWLEDGEMENTS

The authors acknowledge the staff of the 3 MV Tandetron Accelerator at IFIN-HH for providing a good-quality beam for the present experiment. This work was supported by the Romanian Ministry of Research and Innovation under research contract PN 23 21 01 06 and by the Romanian Ministry of Research, Innovation and Digitalization, Project no. PN-III-P4-PCE-2021-1014.

REFERENCES

[1] B. D. Fields Annu. Rev. Nucl. Part. Sci. 61 (2011) 47.
[2] A. Coc et al., Astrophys. J. 600 (2004) 544.
[3] H. Spinka et al., Nuclear Physics A164 1 (1971).
[4] L. Lamia et al., A&A 541, A158 (2012).
[5] Y. Xu et al., Nuclear Physics A 918 (2013) 61.
[6] S. Chesnevskaya et al., Journal of Instrumentation 13 T05006 (2018).
[7] A. Matta et al., J. Phys. G 43 045113 (2016).

Study of the ^{10}Be+^{4}He elastic excitation function by R-matrix calculation and elastic scattering ^{4}He+^{88}Sr of astrophysical interest

T.N. Szegedi, A. Di Pietro, and M. La Cognata

INFN-Laboratori Nazionali del Sud, Catania, Italy

Abstract – The α-chain cluster structure of ^{14}C was investigated by R-matrix analysis on ^{10}Be elastic α-scattering data, measured previously by the ASFIN group of LNS. Furthermore, the preparations for an upcoming elastic α-scattering measurement on ^{88}Sr related to the astrophysical weak-r process is in progress in collaboration with the Atomki institute, Hungary.

INVESTIGATING THE ALPHA CLUSTER STRUCTURE OF ^{14}C

Some nuclear properties can be explained by presuming weakly interacting clusters in the nucleus. Amongst light neutron-rich unstable nuclei, α-clusters may bond by neutrons, akin to covalent bonding. Linear α-α chain configurations in nuclei like ^{12}C or ^{16}O have been researched with no clear experimental evidence. Theoretical predictions suggest a linear chain in ^{14}C, with an associated band ($J_\pi = 0^+, 2^+, 4^+$) at a few MeV above the ^{10}Be+α threshold. Despite extensive spectroscopic studies of ^{14}C, experimental evidence remains elusive. Three experiments probing α-chain structure have yielded conflicting results [1, 2, 3], casting doubt on previous observations. Further investigation, including resonance scattering experiments, is needed to clarify discrepancies in the literature.

For this purpose, an elastic α-scattering measurement was carried out in inverse kinematics using ^{10}Be beam, produced by the tandem accelerator of LNS. The target consisted of a 2m diameter scattering chamber (CT2000) filled with isotopically pure ^{4}He gas at a pressure of 200 and 420 torr. Angular distributions have been measured by ToF method between $0° \leq \theta_{lab} \leq 17.5°$ (in the laboratory system, with respect to the centre of the chamber) separated by 2.5° steps. For the analysis of the resulted angular distributions the AZURE2 code is used. This software enables users to configure input parameters for R-matrix calculations in a user-friendly graphical interface while allowing to compute both differential and angle-integrated cross sections for resonant nuclear reactions pertinent to nuclear and nuclear astrophysical purposes.

Existing experimental data [4] was used to define the input parameters for the calculations. The Jπ and partial widths of the included levels were iteratively modified based on previous analysis, also the background of the distributions was constructed. Furthermore, the identified levels were fitted one by one and used as input parameters in the next iteration of calculations. The result of the progress above is shown by Fig.1. In order to improve the reliability of the calculation, work is in progress with the co-developer of the AZURE2 code, prof. James DeBoer.

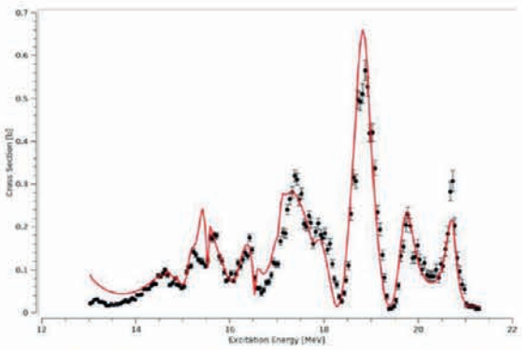

Figure 1: The results of the R-matrix calculation (p = 420 torr, η = 0 °, χ^2 = 76.5).

ELASTIC ALPHA SCATTERING ON ^{88}SR

Weak r-process

After the collapse of a massive star the neutrino-driven wind coming from the nascent neutron star can establish a slightly neutron-rich region in the ejecta, which drifts the matter to proton-deficient waiting points close to stability. From these waiting points the weak r-process nucleosynthesis proceeds by mainly (α,n) reactions [5], which may give a contribution to the abundance of light neutron-rich stable nuclei between ^{56}Fe and ^{109}Ag. The astrophysical models used to describe such processes rely on the Hauser-Feshbach statistical model, hinging on various nuclear physics parameters. The key bottleneck is the parametrization of the α-nucleus Optical Model Potential (AOMP). Accurate experimental cross-section data on influential reactions can be used to finetune the AOMP parametrizations, thereby to reduce the uncertainties of the calculated abundances.

One crucial reaction, ^{88}Sr(α,n)^{91}Zr, stands out in recent sensitivity studies among around 30 reactions. However, astrophysical S-factors calculated with different AOMP parameter sets show a significant (about one order of

magnitude) difference in the weak r-process temperature range (T ~ 2 - 4 GK) shown by Fig. 2. An experimental study of this reaction becomes essential due to its impact on the network. One method for assessing the cross-section of the (α,n) reaction involves conducting measurements on the angular distribution of elastic α-scattering. By utilizing the obtained experimental data, one can derive the parameters of the AOMP. Angular distribution of α-elastic scattering on ^{88}Sr is going to be measured. The planned experiment, combined with existing (α,α) angular distribution data on ^{92}Mo and ^{89}Y, provides an opportunity to validate global AOMP predictions. This collective effort aims to refine astrophysical models for a better understanding of the weak r-process.

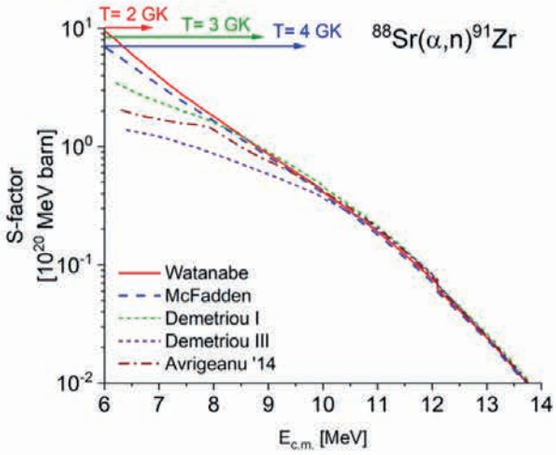

Figure 2: Astrophysical S-factors of the ^{88}Sr(α,n)^{91}Zr reaction (Q-value = -5.67 MeV) calculated by different AOMP parametrizations. The arrows represent the Gamow-window at T=2; 3; 4 GK.

The experiment is going to be performed in September 2024 at Atomki, Debrecen, Hungary with the support of ChETEC-INFRA. The target preparation has started at the target laboratory of LNS. High purity, natural isotopic composition $SrCO_3$ test targets with a nominal thickness of 150 μg/cm^2 have been prepared and transferred to Atomki for in-beam testing. The preparation of enriched $^{88}SrCO_3$ targets is in progress.

REFERENCES

[1] M. Freer et al., Phys. Rev. C **90**, 054324 (2014).
[2] A. Fritsch et al., Phys. Rev. C **93**, 014321 (2016).
[3] H. Yamaguchi et al., Phys. Lett. B **766**, 11 (2017).
[4] W. von Oertzen et al., Eur. Phys. J. A **21**, 193 (2004).
[5] A. Arcones & F. Montes, Astrophys. J. 731, 5 (2011).

Direct measurement of the $^{19}F(p,\alpha_\pi)^{16}O$ and $^{19}F(p,\alpha_\gamma)^{16}O$ reaction cross section

T. Petruse[1], G.L. Guardo[2], D. Testov[1], A. Tumino[2], D. Lattuada[2], S. Aogaki[1], J.P. Fernandez[3], H. Pai[1], I. Kuncser[1,4], N. Szegedi[5], T. Tozar[1], A. Lupoae[1,6], A. Dahl[1], R. Ban[1], G. D'Agata[2], A. Kusoglu[1], R. Corbu[1], P.A. Soederstrom[1], A. Cassisa[7], L. Lamia[2], A. Nurmukhanbetova[8], M. Gulino[2], D. Kahl[1], M. Cuciuc[1], C. Matei[1], D.L. Balabanski[1], G.R. Pizzone[2], M. LaCognata[2]

1) Extreme Light Infrastructure – Nuclear Physics
2) Instituto de Fisica Nucleare – Laboratori Nazionali del Sud
3) Universidad de Sevillia
4) Scoala Doctorala pentru Ingineria si Aplicatiile Laserilor si Acceleratorilor
5)Institute for Nuclear Research (Atomki)
6) Facultatea de Fizica, Universitatea Bucuresti
7) Nuclear Physics Institute of Academy of Sciences of Czech Republic
8) Nazarbayev University

Abstract - The $^{19}F(p,\alpha)^{16}O$ reaction is an important destruction channel in AGB stars and plays a significant role in the nucleosynthesis of heavy elements in the Universe. To better understand the astrophysical implications of this reaction, an experiment was conducted using ELISSA coupled with LHASA, forming a silicon detector array with high angular coverage and extraordinary angular and energy resolution. The results of the experiment will help to improve our understanding of the nucleosynthesis processes that take place in AGB stars and may have important implications for our understanding of the chemical evolution of the Universe. The aim of this experiment is to study the $^{19}F(p,\alpha_\pi)^{16}O$ and $^{19}F(p,\alpha_\gamma)^{16}O$ reaction channels and we are confident that this is possible due to the good performance of the experimental set-up.

INTRODUCTION

The $^{19}F(p,\alpha)^{16}O$ reaction plays a crucial role as a destruction channel for fluorine in asymptotic giant branch (AGB) stars. AGB stars are a class of low- to intermediate-mass stars that are in a late stage of their evolution, where they have exhausted their hydrogen fuel and have begun to burn helium in their cores [1]. During this phase, these stars experience thermal pulses, which drive the convective mixing of nuclear-processed material to the surface. As a result, they can undergo significant nucleosynthesis, producing a variety of elements, including carbon, nitrogen, oxygen, and fluorine [2]. Among the others, fluorine is an interesting element in AGB stars because it is thought to be produced by a combination of nucleosynthesis processes, including helium burning and proton-capture reactions. The relative abundances of different isotopes of fluorine can provide important insights into the nucleosynthesis processes that occur in AGB stars. Indeed, the observation of fluorine abundances in AGB stars have been used to test theoretical models of the nucleosynthesis processes in these stars. In particular, the observation of ^{19}F abundances in some AGB stars has been a challenge for models. The destruction of fluorine via the $^{19}F(p,\alpha)^{16}O$ reaction can provide a possible explanation for this observation. The $^{19}F(p,\alpha)^{16}O$ reaction has been the subject of extensive experimental and theoretical studies in recent years [6,7,8,9,10], since it is believed to be the dominant destruction channel for fluorine in AGB stars [3]. This reaction occurs via three types of channels, i.e., (p,α_0), (p,α_π) and (p,α_γ). The (p,α_π) channel provides less than 10% contribution at low temperatures approximately 0.05 GK [4,5]; the (p,α_γ) channel dominates at temperatures above 0.2 GK, while the (p,α_0) channel dominates at the lower temperatures below 0.15 GK. Despite its importance, the S-factors of the (p,α_π) and (p,α_γ) outgoing channels in the $^{19}F(p,\alpha)^{16}O$ reaction are still largely uncertain at astrophysical energies, pointing out the need for better measurements.

Experimental studies have been conducted using a variety of techniques, including direct measurements of the cross section or γ spectroscopy. One of the main challenges in studying the $^{19}F(p,\alpha)^{16}O$ reaction is the low cross section at the energies relevant for astrophysical environments. The cross section is highest at energies of around 200 keV, which are difficult to achieve in laboratory experiments. As a result, most experimental studies have focused on energies in the range of 0.5 to 1 MeV, which are easier to access but require extrapolation to lower energies. Despite these challenges, significant progress has been made in recent years in studying the $^{19}F(p,\alpha_0)^{16}O$ reaction, where there is experimental data in the energy

region of interest. For the $^{19}F(p,\alpha_\gamma)^{16}O$ reaction the situation is very similar [11], but there is no measurement for the $^{19}F(p,\alpha_\pi)^{16}O$ reaction in the Gamow window. One of the main uncertainties is the extrapolation of the cross section to lower energies. In this report, we will present the detailed measurement of the $^{19}F(p,\alpha_\pi)^{16}O$ and $^{19}F(p,\alpha_\gamma)^{16}O$ reactions at the 3 MV Tandetron accelerator of IFIN-HH. The astrophysical S factors will be derived in the energy region of E_{CM} = 300−700 keV. Due to the good energy resolution of the experimental set-up, we are confident that we can separate these channels.

EXPERIMENTAL SET-UP

The experiment involved bombarding the target with the fluorine beam, which resulted in the production of α particles as a result of the $^{19}F(p,\alpha)^{16}O$ reaction. The α particles were detected by the ELISSA (Extreme Light Infrastructure Silicon Strip Array) [12] and LHASA (Large High-Resolution Array of Silicon for Astrophysics) detector system, which was able to measure their energy and angle of emission with high precision. This experiment was performed at IFIN-HH, Magurele (Romania) in a close collaboration with the LNS-INFN. The 3 MV Tandetron accelerator provided a ^{19}F beam with an energy range from 7 to 15 MeV with a diameter of the spot size on target of 1 mm and intensities around 1 - 5 nA. Thin self-supported polyethylene targets (CH_2) of about 50 μg/cm^2 were placed at 90◦ with respect to the beam direction and were frequently changed to avoid degradation. The detection setup consists of one ring of ELISSA (12 Micron X3 position sensitive silicon strip detectors of 1000 μm thick) and LHASA (5 Micron YY1 silicon strip detectors of 300 μm thick). The detection system was optimized to detect the emerging α particles in a wide angular range (from 8◦ to 50◦) and was placed at 5 cm from the target. Trigger was selected to come from each strip of each detector and all the signals coming from the detectors were then delivered to electronic chain.

Detection set-up

The Micron [13] Model X3 position sensitive SSD consist of 4 front strips, 8 channels of electronics. The thickness of the detector is 1000 μm. ELISSA detector array consists of 3 rings of 12 X3 detectors. For this experiment only one ring of ELISSA was used, meaning 12 X3 detectors. The Micron [13] Model YY1 SSD is a detector that consists of 16 front strips, each of width 3 mm, arranged as a sector of a circle that covers 60 degrees. The thickness of the detector is 300 μm. LHASA detector array consists of 5 YY1 silicon strip detectors.

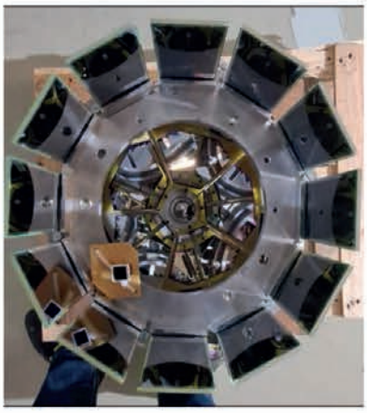

Fig. 1 – Picture of the detection set-up

CONCLUSION

The purpose of this experiment is to determine the cross section of the $^{19}F(p,\alpha_\pi)^{16}O$ and $^{19}F(p,\alpha_\gamma)^{16}O$ reaction channels. The high precision of the ELISSA and LHASA detector system will allow for a detailed study of the angular distribution of the emitted α particles, which provides insights into the reaction mechanism and the factors that determine the cross section. Overall, this experiment represents an important contribution to our understanding of the $^{19}F(p,\alpha)^{16}O$ reaction and its role in nucleosynthesis processes in AGB stars. The use of the ELISSA and LHASA detector system, coupled with the high-quality ^{19}F beam delivered by the IFIN-HH 3MV tandem accelerator and the small thickness of the CH_2 targets prepared at LNS-INFN, allowed for precise measurements of the cross section and angular distribution of the emitted α particles. The analysis is still ongoing.

REFERENCES

[1] D. Engels, Mem. S.A.It. Vol. 75 (2005), 282
[2] S. Cristallo et al., (2015) *ApJS* **219** 40
[3] S. Palmerini et al., J. Phys.: Conf. Ser. 1308, 012016 (2019)
[4] I. Indelicato et al., Astrophys. J. 845, 19 (2017)
[5] I. Lombardo et al., Phys. Rev. C 100, 044307 (2019)
[6] C. Angulo et al., NuPhA 656, (1999) 3
[7] G. Breuer et al., 154, (1959) 339
[8] A. Isoya et al., NuPhA 7, (1959) 126.
[9] R. Caracciolo et al., Lett. Nuovo Cimento 11, (1974) 33
[10] I. Lombardo et al., PhLB 748, (2015) 178
[11] JINA China experiment
[12] S. Chesnevskaya et al., 2018 *JINST* **13** T05006
[13] https://www.micron.com/
[14] https://www.mesytec.com/

Measurement of the $^{19}F(p,\alpha)$ reaction in the astrophysical energy range of interest via Trojan Horse Method performed at INFN-LNS

N. Vukman[1,2], X. D. Su[3,4], G. G. Rapisarda[5,6], M. La Cognata[5], M. Mazzocco[4,7], S. Palmerini[1,8], S. Cherubini[5,6], G. L. Guardo[5], M. Gulino[5,9], S. Hayakawa[10], I. Indelicato[5], L. Lamia[5,6], R. G. Pizzone[5,6], S. R. M. Puglia[6], S. Romano[5,6], C. Spitaleri[5], O. Trippella[1], A. Tumino[5,9]

1) INFN - Sezione di Perugia, Perugia, Italy
2) Ruđer Bošković Institute, Zagreb, Croatia
3) Beihang University, Beijing, China
4)Dipartimento di Fisica e Astronomia "Galileo Galilei," University of Padova, Padova, Italy
5) INFN - Laboratori Nazionali del Sud, Catania, Italy
6) Dipartimento di Fisica e Astronomia "E. Majorana" University of Catania, Catania, Italy
7) INFN - Sezione di Padova, Padova, Italy
8)Dipartimento di Fisica e Geologia, University of Perugia, Perugia, Italy
9) Kore University of Enna, Enna, Italy
10) CNS - University of Tokyo, Tokyo, Japan

Abstract - The complex reaction network connected to the ^{19}F stellar abundance is very sensitive to the physical condition in stars. To overcome difficulties present in the direct measurements, mainly the very low cross section in the astrophysical energy range due to the Coulomb repulsion, an indirect measurement of the $^{19}F(p,\alpha)$ reaction, with the Trojan Horse Method (THM), was performed at INFN-LNS. While the method had been successfully used to study α_0 channel, in the present analysis focus was given to the $\alpha_{1,2}$ channels, where better knowledge of the reaction rates at low energies is required, obtainable by employing the THM method.

INTRODUCTION

The complex reaction network governing the production and destruction of the ^{19}F in stars is determined by the physical condition in stars [1]. Discrepancies in the observed galactic abundance of the ^{19}F in the vicinity of Asymptotic Giant Branch (AGB) stars [2], which are believed to be the main production sites of galactic fluorine, puts a requirement for better knowledge of the reaction rates involving the main destruction channels of fluorine: (α,p) [3,4] in He-burning shell and (p,α) [5,6] in H-burning shell, both studied previously by THM. The (p,γ) channel, important for the latter was measured recently [7]. Recent direct measurements of the (p,α) reaction [8,9] suggest that large effort in the knowledge of the reaction rates still needs to be given to the α_1 [8] and α_2 [9] channels. This is particularly true in the very low energy range, where the proposed 11 keV state [9] may have significant implications for the reaction rate. For the latest results and the state of the art concerning the α_0 channel, one is referred to recently published direct measurement [10].

OVERVIEW OF THE EXPERIMENT

The indirect measurement of the $^{19}F(p,\alpha)$ reaction was performed at INFN-LNS, using the 55 MeV ^{19}F beam and CD_2 target, where the ^2H served as THM nucleus. In the data reduction phase, proper quasi-free contribution of the $^{19}F(^2H,\alpha^{16}O)$ reaction was deduced, based on the vanishing momentum of the spectator neutron (p_s=0), following the procedures described in [5,6].

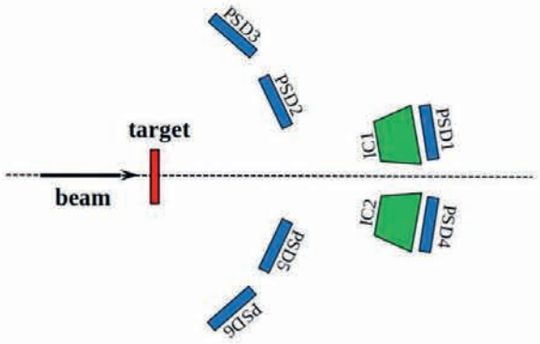

Figure 1: Experimental setup used at INFN-LNS, consisting of six Position Sensitive Detectors (PSD) and two Ionization Chambers (IC) filled with Isobutane gas.

The experimental setup (Fig.1) was optimized for the kinematically complete measurement of the aforementioned quasi-free three-body reaction, where spectator neutron was left undetected. The pressure of the gas was ≈ 52.5 mbar throughout the experiment.

ANALYSIS OVERVIEW AND RESULTS

The data collected during the experimental campaign was separated in the analysis into three independent case studies. These cases are categorized by the pairs of detected nuclei (α=a, ^{16}O=o) as follows: a2o4 (α in detector 2 and ^{16}O in detector 4, case 1), o1a5 (^{16}O in detector 1 and α in detector 5, case 2) and a1o4 + o1a4 (α in detector 1 and ^{16}O in detector 4 and vice versa, case 3), with detector numbering shown in Fig. 1. In this way a shared effort was put to collective analysis checkpoints, to speed up the calibration (Fig. 2) and quality control (QC) of the data, while keeping independent datasets as cross-check for the obtained results. For particle identification (PID) of the ^{16}O nuclei, the standard ΔE-E technique was used in all three cases, as well as for PID of detected α nuclei in the case (3), whereas for the cases (1) and (2), the exit channel of interest was identified through kinematic conditions.

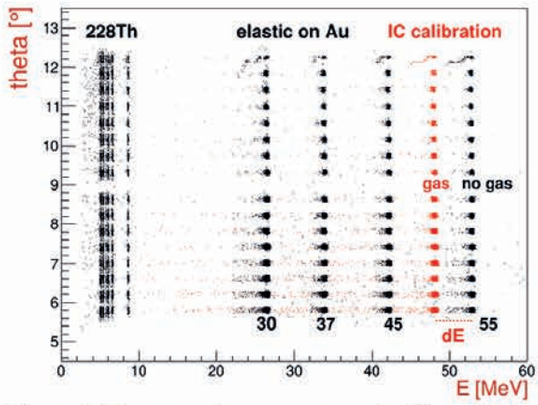

Figure 2: The exemplary spectrum of calibrated values of θ vs. E for PSD1, showing α-peaks from the ^{228}Th source and elastic scattering peaks of ^{16}O beam (E = 55, 45, 37, 30 MeV) on ^{197}Au target (^{12}C not shown here) with (red points) and without the gas (black points) in the IC1.

After multiple cross-checks performed for the quality of the calibration, needed mainly due to the low sensitivity of the IC as precise energy loss (eloss) detector, solution was found to use the calibrated value of eloss for ^{16}O and calculated (SRIM) value for α in the analysis case (3). On the other hand, for the cases (1) and (2), better precision in the calculations was found by use of the parameters of detected α (E,θ) and only the angle (θ) of ^{16}O, an approach made possible after the correct identification of the exit channel of the reaction of interest (Q-value fixed). For the quality-control of the data a detailed analysis of the two-body reaction ^{19}F(^{1}H,α)^{16}O was performed, as well as three-body one: ^{19}F(^{2}H,^{16}O)^{5}He, which proceeds

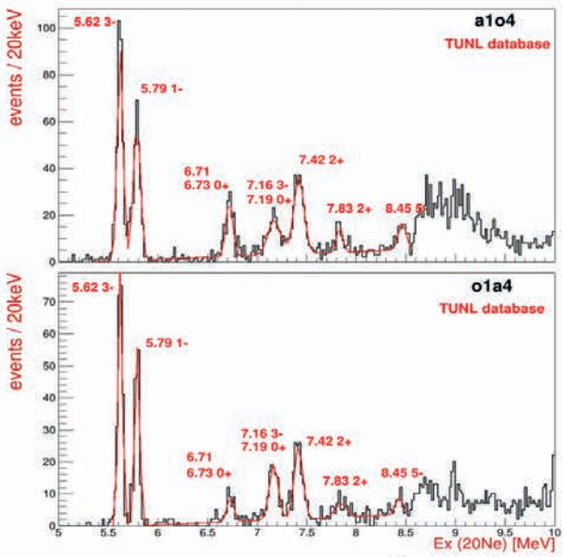

Figure 3: The excitation energy of the ^{20}Ne nucleus for the a1o4 (upper panel) and o1a4 (lower panel) datasets, used to access the quality of calibration and the analysis procedure.

through creation of the ^{5}He nucleus in the ground state, which consequently decays via emission of neutron. Likely the most important check performed was the analysis of the ^{19}F(^{2}H,α$_0$^{16}O) exit channel, where ^{16}O was in the ground state. This reaction proceeded through the creation of the compound nucleus ^{20}Ne in the excited state. The α-decaying states in 5.5 - 8.5 MeV excitation energy range were used as QC of the analysis procedure (Fig. 3) with excellent agreement of the observed values with the ones from the literature [11]. The detailed analysis of the ^{19}F(^{2}H,α$_{1,2}$) channel is in progress.

REFERENCES

[1] S. Palmerini et al. (2019) J.P.C.S. **1308**, 012016
[2] C. Abia et al. (2015) A&A **580**, A88
[3] G. D'Agata et al. (2018) ApJ **860** 61
[4] R.G. Pizzone et al. (2017) ApJ **836** 57
[5] I. Indelicato et al. (2017), ApJ **845**, 19
[6] M. La Cognata et al. (2015) ApJ **805** 128
[7] L. Zhang et al. (2022), Nature **610**, 656–660
[8] I. Lombardo et al. (2019) P.R.C **100**, 044307
[9] L. Zhang et al. (2021) P.R.L. **127**, 152702
[10] G. L. Guardo et al. (2023) E.P.J.A **59**, 65
[11] D. R. Tilley et al. (1998) Nuc.Phy. **A636**, 249-364

Indirect measurement of the $^{3}He(n,p)^{3}H$ reaction cross section at Big Bang energies

T. Zanatta-Martinez,[1, 2] R.G. Pizzone,[1, 2] M. L. Sergi,[1, 2] A.A. Oliva,[1, 2] L. Lamia, [1, 2] R. Spartá,[2, 3, 1] G.L.Guardo,[2] M. La Cognata,[2] S. Palmerini[4], S.Romano [1, 2] A. Tumino,[2, 3]

1) Dipartimento di Fisica e Astronomia "Ettore Maiorana", Universitá di Catania, Catania, Italy
2) Laboratori Nazionali del Sud - INFN, Catania, Italy
3) Facoltá di Ingegneria e Architettura, Universitá degli Studi di Enna Kore, Enna, Italy
4)University of Perugia and INFN Perugia, Perugia, Italy

The Big Bang model is supported, among others, by evidence such as Big Bang Nucleosynthesis (BBN), which produced light nuclei like ^{2}H, ^{3}He, ^{4}He, and ^{7}Li. Despite uncertainties, BBN accurately predicts primordial abundances, but discrepancies, like the "Cosmological Lithium Problem" concerning ^{7}Li, exist. BBN's accuracy relies on factors like the baryon-to-photon ratio (η), while reactions crucial for BBN occurred at low energies, posing challenges for precise measurements. Particularly the $^{3}He(n,p)^{3}H$ reaction significantly influences primordial ^{3}He and ^{7}Li production. Experiments, including theoretical predictions and indirect methods like the Trojan-Horse method (THM), contribute to understanding these reactions' cross sections. This work studied the quasi-free $^{2}H(^{3}He,pp)^{3}H$ reaction as the THM is applied in order to retrieve the cross section for the $^{3}He(n,p)^{3}H$ reaction at astrophysical energies.

The THM allows to obtain the binary reaction cross sections at astrophysical energies by studying a quasi-free (QF) three-particle reaction. Here, a particle, *a*, with a dominant cluster structure ($a = x + s$) acts as a probe, while its constituent x interacts with the target while the constituent s acts as spectator during the reaction. This method offers a way to explore the entire Gamow window of energies without performing extrapolations. However, calibration to direct measurements is necessary such as the identification of the reaction mechanism. The THM has been validated and applied in exploring various nucleosynthesis reactions beyond primordial ones over the past three decades (see References). In particular, neutron induced reactions have been studied (Gulino et al. 2010, 2013; Guardo et al. 2017, 2019) using deuterons as TH nuclei to transfer neutrons, while protons behave as spectators. The theoretical description of the three-body reaction cross-section given by the plane-wave impulse approximation (PWIA) can be factorized into three terms:

$$\frac{d^3\sigma(E)}{d\Omega_\alpha d\Omega_{^3He} dE_n} \propto KF \cdot |\phi(p_s)|^2 \cdot \left(\frac{d\sigma}{d\Omega}\right)^{HOES} \quad (1)$$

Where KF is a kinematical factor (final-state phase-space factor function of the masses, momenta, and angles of the outgoing particles); $|\varphi(p_s)|^2$ is the modulus-squared Fourier transform of the radial wave function for the p–n inter-cluster motion, given by the Hulthén function and $(d\sigma/d\Omega)^{HOES}$ is the half-off-energy-shell (HOES) differential cross section of the reaction of interest at the center-of- mass energy Ecm.

EXPERIMENT & ANALYSIS

This study analysed the coincidence between two detectors in an experimental setup described in Pizzone et al. (2020). Simulations were used to optimize angular and energy ranges, focusing on the QF reaction mechanism. A 9 MeV ^{3}He beam from the FN Tandem Accelerator at the University of Notre Dame's Nuclear Science Laboratory was employed. Detectors were positioned based on preparatory simulations, including three silicon position-sensitive detectors (PSD 1-3). Calibration runs achieved an angular resolution of 0.1°. Coincidence data between PSD1-PSD3 were analysed, exploring higher energies than PSD1-PSD2, complementing Pizzone et al. (2020).

The initial data analysis involved identification of the three-body process, in which the proton and tritium (*p* and *t*) product of the three-body reaction are detected in coincidence in 2 of the 3 detectors. Particle identification for PSD1 was conducted using the ΔE-E technique as outlined in Pizzone et al. (2020), with graphical cuts on tritium particles in the ΔE-E spectrum. A comparison of the experimental and simulated kinematical locus of the detected *t* particle in PSD1 and coincidences in PSD3 (Figure 1) shows a clear agreement across energy ranges and angular pairs confirming that particles detected on PSD3 are protons, identifying the $^{2}H(^{3}He,pt)H$ reaction. After angular and energy calibrations, the kinematics of the undetected particle was reconstructed using energy and momentum conservation, allowing extraction of the three-body reaction's Q-value. A Gaussian fit yields a value of -1.50 ±0.1 MeV, close to the expected value of Q = −1.46 MeV calculated using Qtool (MacFarlane & Moller 1997), validating the energy calibration. Further analysis focuses on events with $-1.7 \leq Q \leq -1.4$ MeV, identifying the $^{2}H(^{3}He,pt)H$ process.

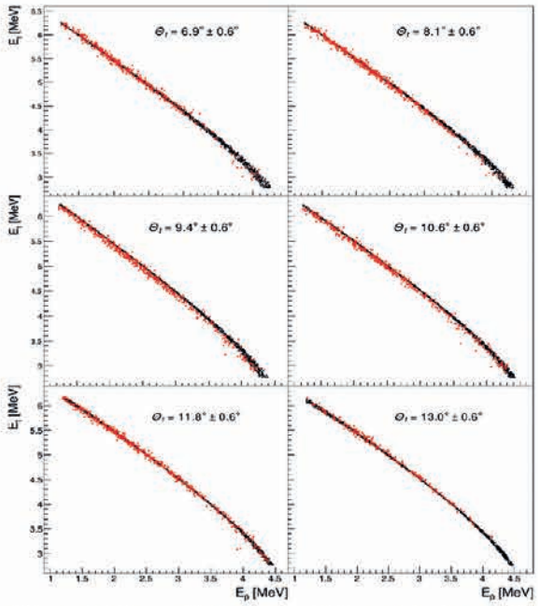

Figure 1: Kinematic locus for tritium detected in PSD1 and protons from PSD3 for $6.3° \leq \theta_t \leq 13.6°$ and $24.4° \leq \theta_p \leq 25.6°$, respectively. Experimental data (red) are compared with a Monte Carlo simulation (black) for the $^2H(^3He,pt)H$ reaction.

The subsequent stage of data analysis involved distinguishing the Quasi-Free (QF) mechanism from other processes. To ascertain its occurrence, the momentum distribution of the spectator proton within the deuteron nucleus needs to be extracted and meticulously analysed, following the methods outlined in Pizzone et al. (2020).

Given a narrow energy interval (ΔE_{cm} = 200 keV), the binary HOES cross-section remains nearly constant. By dividing the triple differential cross-section by the kinematic factor, KF, the momentum distribution $|\varphi(p_s)|^2$ in arbitrary units is derived. The obtained momentum distribution appeared distorted and narrower compared to the theoretical function, consistent with findings in Pizzone et al. (2020), indicating a transferred momentum qt = 80 MeV/c. This aligns with previous observations on deuteron break-up reported in Pizzone et al. (2020). For further analysis, only events with $p_s \leq 25$ MeV/c were considered, capturing the presence of the QF contribution in the $^2H(^3He,pt)H$ process.

RESULTS

Using the post-collision approach to define $E_{cm} = E_{12} - Q_{2b}$ (where Q_{2b} is the two-body reaction Q-value), the triple differential cross-section is divided by the KF · $|\varphi(p_s)|^2$ factor, as described in Pizzone et al. (2020), utilizing the experimentally measured distorted momentum distribution. This yields the binary cross-section for the $^3He(n,p)^3H$ reaction in arbitrary units.

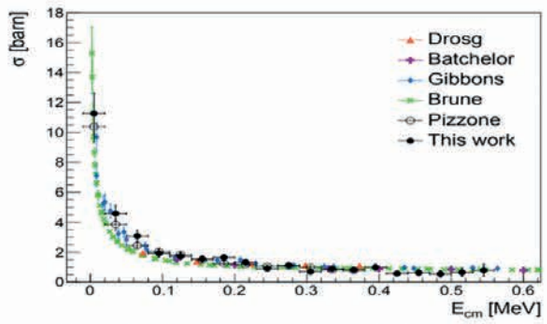

Figure 2: Binary cross section (black circles, including the penetration factor) and normalized to direct data for the $^3He(n,p)^3H$ sub-reaction extracted via the TH reaction $^2H(^3He,pt)H$. Errors from statistics and normalization are shown.

The THM data are then corrected for the penetration factor, following the procedure outlined in Gulino et al. (2010, 2013), and normalized to on-shell, direct data, as depicted in Figure 2, with normalization to data from Drosg & Otuka (2015); Batchelor et al. (2004); Gibbons & Macklin (1959) in the energy range $0.3 \leq E_{cm} \leq 0.6$ MeV. Good agreement within experimental uncertainties is observed across the examined energy range, with a maximum 10% relative error for the THM cross-section. Propagation of errors on E_p, E_t, and angular positions ($\Delta\theta p \approx \Delta\theta t \approx 0.15°$) is considered. The data confirm the expected 1/v behavior at low energies and extend the energy range explored in Pizzone et al. (2020) to higher energies. An overall average of the two datasets is compared to available direct data in Figure 6, showing satisfying agreement within experimental errors with direct and inverse reaction data from literature sources (Batchelor et al. 2004; Gibbons & Macklin 1959; Drosg & Otuka 2015; Brune et al. 1999) in the energy region $0.03 \leq E_{cm} \leq 0.6$ MeV. A slight discrepancy with data reported by Brune et al. (1999) is noted in the 60 to 200 keV range. Notably, the present data, along with those from Gibbons & Macklin (1959) and Brune et al. (1999), are the only ones available below 0.1 MeV. Lastly, the reaction rate for the $^3He(n,p)^3H$ reaction is calculated. The ultimate outcome of reaction rate calculations and primordial abundances of different isotopes resulting from this reaction rate has been formally submitted to the AP Journal.

REFERENCES

[1] Batchelor, R., et al. (2004), Rev. of Scien. Inst, 26, 1037
[2] Baur, G., et al. (1986), Nuclear Physics A, 458, 188
[3] Brune, C. R., et al. (1999), Physical Review C, 60, 015801
[4] Coon, J. H. (1950), Physical Review, 80, 488
[5] Costello, D. G., et al. (1970), Nuclear Science and Engineering, 39, 409
[6] Drosg, M., et al. (2015), INDC(AUS)-0019
[7] Gibbons, J. H., et al. (1959), Physical Review, 114, 571,
[8] Guardo, G. L., et al. (2017), Phys.Rev. C, 95, 025807,
[9] La Cognata, M., et al. (2017), APJ 846, 65
[10] Lamia, L., et al. (2019), APJ, 879, 23,
[11] Pizzone, R. G., et al. (2020), EPJA, 56, 283
[12] Pizzone, R. G., et al. (2020), EPJA, 56, 199,

INFN – LNS
Scientific Information Service: an overview of 2023 activities

G. Agnello, R.C. Di Mauro, S. Cardillo

INFN - LNS

Abstract – The Scientific Information and Dissemination Service, within the INFN-LNS Research Division, carries out its activities in various areas of the scientific research, electronic resources, outreach and dissemination of scientific culture.

SUBSCRIPTION MANAGEMENT AND ONLINE ACCESS TO SCIENTIFIC JOURNALS

The activity concerns the management of the LNS national agreement stipulated between INFN and CRUI–CARE (Conference of Italian University Rectors-Coordination for Access to Electronic Resources), aimed at acquiring access to electronic resources (magazines, databases, e-books). The Service is responsible for the use of bibliographic resources, open access resources, e-books and access to scientific databases.

PRESS AND MEDIA MANAGEMENT

The Service deals with the dissemination of the results of research activities achieved by scientific collaborations and events for the promotion and dissemination of scientific culture, through the drafting of press releases and editorials. The Service collaborates with the INFN Communication Office for the drafting of news, press releases related to the organization of events that take place at the LNS. The press review of the media products published constitute a further commitment in this area.

SOCIAL MEDIA MANAGEMENT

The Service deals with the creation and writing of posts, on the social platforms Facebook, Youtube, Instagram, Twitter, concerning the achievement of scientific results, the progress of projects and the narration of the most significant moments in the life of the LNS. In support of the written notes, images and video contributions, produced and conceived by the Scientific Information Service, are also used.

OUTREACH AND DISSEMIMATION ACTIVITIES

The scientific activity report is a very important editorial project for the whole community as it represents the finished product of the research activities and the advances of the national and international research groups that conduct their activities at the LNS. Editorial design and creation of brochures, dissemination material and videos for the promotion and dissemination of scientific culture, through the drafting of oriented educational material, are also a key point of the goal to be achieved.
Documentation and multimedia archive management of videos and images of events, meetings, institutional visits and experimental equipment are part of the activities.
The service contributes to the maintenance of the statistics of the INFN database relating to all dissemination activities, it also participates in the increase of the LNS web page in specific areas related to bibliographic resources, news, events and seminars.

VISITOR CENTRE

Inaugurated in July 2019 on an area of about 400 square meters, located in the entrance area of the LNS, in an exhibition space called the "Visitor Centre", it includes three different themes: Cosmos, Art and Health, dedicated respectively to the formation and evolution of the Universe, to the applications of physics in the field of cultural heritage and medicine. The Visitor Centre, through multimedia and the use of cutting-edge technologies, carries out educational and didactic functions of knowledge of research activities, involving a vast audience starting from primary school children up to university course students with particular attention to those of the degree course in physics and astronomy thanks to the strong link between INFN and the university. The visits are also intended for public, private, institutional subjects and associations. The service collaborates in the updating and design of multimedia contents of Visitor Centre. It is also responsible for the maintenance of the equipment and management of the rooms.

SYNERGY WITH THE "PUBLIC ENGAGEMENT" LNS GROUP

The "Public Engagement" of the LNS is a working group created in 2016, made up of young PhD students, researchers and a coordinator, appointed by the director. Alongside the Scientific Information Service, Public Engagement deals with the organization of many events and initiatives for the promotion of scientific culture in schools and society.

Outreach activities @ INFN-LNS

G. L. Guardo[1], D. Carbone[1], G. Agnello[1], M. Cavallaro[1], R. P. C. Di Mauro[1]

1) Istituto Nazionale di Fisica Nucleare, Laboratori Nazionali del Sud, Catania, Italy

Abstract – An overview of the LNS outreach activities that took place in 2023 is presented.

INTRODUCTION

Historically, there was a disconnect between the scientific community and the general public, often leading to misunderstandings and mistrust. This gap can be attributed to various factors, including the complexity of scientific jargon and the lack of effective communication channels. Public engagement efforts aim to bridge this gap by making science more accessible to non-experts. Hence, public engagement involves communication and interaction between scientists and the public, with the goal of fostering a better understanding of scientific processes, findings, and their implications and of showing how public research funding money is spent.

The benefits of public engagement in science are evident, however several challenges persist. These include limited resources, varying levels of public interest and understanding, and the need for scientists to develop effective communication skills. Nowadays, the development of new tools and platforms, such as social networks, 3D oculus, augmented reality and interactive visitor centres, helps the researchers to reach a wide range of public, from kids of primary and middle schools age to adult generic public.

In this light, in the last decade INFN-Laboratori Nazionali del Sud has put a lot of efforts in organizing many outreach events, involving undergraduate students and generic public, combining traditional and innovative methods to reach the diverse audiences.

EVENTS INVOLVING GENERAL PUBLIC

We can consider two different kinds of outreach approaches for the adult general public. There are events in which the researchers meet the population out of their work places and others in which the population is invited to visit and join the research laboratories.

One of the most important events belonging to the first category is the European Researchers' Night (ERN) that is a Europe-wide public event, which displays the diversity of science and its impact on citizens' daily lives in fun, inspiring ways. The ERN was created to enhance the figure of researchers and their role in society. To achieve this goal, the central idea of the promoters has been, since 2013, to interpret the Night as an opportunity to celebrate with the general public the passion that animate researchers in their work. The main feature of the ERN is the use of streets, squares and unusual places to talk about science and research and the collaboration between researchers and communicators to find new forms of public engagement. The ERN is an opportunity for involvement and discovery and also an example of how the communication of research is an act of responsibility.

INFN-LNS are involved in the SHARPER project [1] for ERN since 2018. The last edition took place on September 27th 2023, in which the LNS researchers met over 1000 people at Piazza Università in Catania, one of the most important squares of the city center. We organized three interactive stands showing the LNS research fields. In parallel, some activities for kids between the ages of 5 and 11 were organized at "Città della Scienza" reaching about 200 young citizens (as visible in Figure 1). These activities were promoted by the INFN-kids [2] national project of the INFN Third Mission Coordination Committee (CC3M) [3].

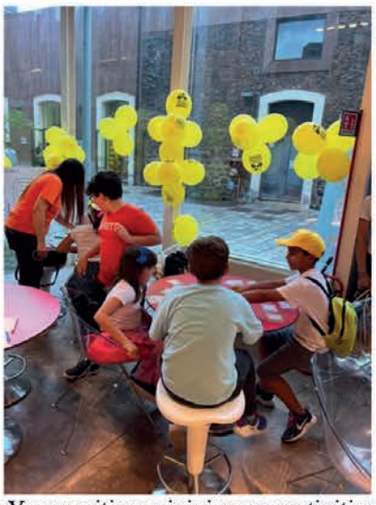

Figure 1: Young citizens joining our activities at "Città della Scienza" during the ERN2023.

During the 2023, the LNS researches met over 800 people in several other events such as public lectures in public places. In particular some of them were promoted by the Pint of Science [4] project of INFN-CC3M.

The generic public is often invited to visit our laboratories during the year. In order to make the visit more exciting and effective, in 2019 the LNS Visitor Centre was opened. The visit to the Visitor Center is aimed at all those who want to learn about nuclear physics and astrophysics, neutrino physics, the technological applications of scientific research and all the INFN-LNS activities. During the visit people immerse themselves in an engaging experience which, through interactive stations, innovative visualizations and expert

guides, reveals the heart of scientific research. Through dynamic exhibitions and practical workshops, we also discover the frontier technologies through which we try to shed light on the great mysteries of the Universe. Each stop on the tour offers a unique opportunity to better understand the world of scientific research and its impact on our daily lives. The LNS visitor center is open twice a week during all the year and in 2023 attracted about 350 adult visitors.

EVENTS INVOLVING UNDERGRADUATE STUDENTS

Outreach programs are crucial for undergraduate students as they provide valuable exposure to real-world applications of STEM (Science, Technology, Engineering and Mathematics) inspiring and guiding them towards these fields. Such initiatives help to understand complex concepts, encouraging students to pursue and persist in STEM studies.

The main event organized for students during the 2023 is the "Primavera della Scienza", which took place during the months of March, April and May. The event aims to involve and fascinate students in scientific subjects by opening the doors of the laboratories to show the research activities carried out through the brand new LNS Visitor Centre. The LNS Visitor Center welcomes schools in a dynamic and educational environment. Students explore the wonders of science through interactive tours, hands-on laboratories, and engaging demonstrations. Expert guides accompany them on a fascinating journey through nuclear physics, astrophysics and frontier technologies. Using hands-on experiences, students gain a deeper understanding of scientific concepts and their real-life applications. The Visitor Center offers a unique opportunity to inspire curiosity, stimulate creativity and promote interest in STEM disciplines. During 2023 we welcomed about 2000 students coming from all the areas of Sicily, mainly from Secondary Schools (see Figure 2).

The visit to the LNS Visitor Center is also designed for the youngest science enthusiasts. In fact, guided tours are organized for lower primary school students enriched by educational workshops which, through play and first-hand experience, will allow even the youngest children to approach the fascinating world of scientific research. These activities are managed by researchers who join the INFN-kids initiative, financed by the INFN-CC3M.

Another important initiative of INFN-kids is to create and publish for free the "Leo and Alice" Comics, designed and realized by INFN researchers, aimed at children of Primary school. The comics are organized in episodes in which ordinary and familiar situations take an imaginative twist when Leo and Alice encounter particles from the Standard Model and unravel the mysteries of various physical processes. The comics can be downloaded for free from the website of the project [2]. These educational products allowed us to expand our reachability as, thanks to these comics, we took part to the national comics festival "Etna Comics" where we presented our project and activities. During "Etna Comics 2023" about 500 children visited our stand.

Figure 2: Secondary school students visiting the LNS Visitor Centre during the "Primavera della Scienza" 2023.

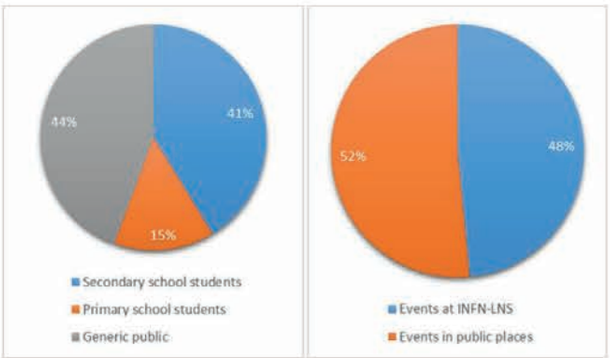

Figure 3: The distribution of the public reached and the places that hosted the LNS outreach activities in 2023.

CONCLUSIONS

In conclusion, the LNS outreach activities span a wide range of public and places, as depicted in Figure 3. The big number of people engaged during our outreach efforts underline once more that by prioritizing public engagement, the scientific community can ensure that science remains a dynamic and inclusive field that benefits all members of society.

ACKNOWLEDGMENTS

The authors are sincerely grateful to all the members of the LNS Public Engagement, the INFN-kids project, the LNS "Servizio di Informazione Scientifica" and all the CC3M initiative members. We also would like to extend our deepest gratitude to all the researchers, technologists, and technical and administrative staff that helped us in all the described initiatives.

REFERENCES

[1] SHARPER, https://www.sharper-night.it/
[2] INFN-kids, https://web.infn.it/infn-kids/
[3] INFN CC3M, https://cc3m.infn.it/
[4] INFN-Pint of Science, https://pintofscience.it/

02

ASTROPARTICLE PHYSICS

Research Analyses Results

INFN LNS

- Status of the KM3NeT project
- The IDMAR DCFO system: a major upgrade of power and data transmission capacity for the Capo Passero submarine cabled infrastructure of the Laboratori Nazionali del Sud
- The ReD experiment for the directional sensitivity of a double phase LAr TPC
- Characterization of nuclear recoils in the dual-phase Argon Time Projection Chamber of the ReD experiment
- A tool for improved monitoring of acoustic beacons and receivers of the KM3NeT neutrino telescope
- The ReD+ PRIN project: the characterization of sub-keV nuclear recoils in a dual-phase Argon Time Projection Chamber

Status of the KM3NeT project

G. Ferrara[1] on behalf of the KM3NeT collaboration

1) INFN Laboratori Nazionali del Sud, Via Santa Sofia 62, 95123 Catania, Italy

Abstract – In this brief report the most important and recent upgrades of the KM3NeT/ARCA detector and the first results achieved are shown.

INTRODUCTION

The KM3NeT [1] collaboration is constructing a multisite sub-sea infrastructure that will host two high energy neutrino detectors. The physics aims of the two KM3NeT detectors are different. The detector ARCA (Astroparticle Research with Cosmic in the Abyss), located at a depth of 3500 m 80km offshore Portopalo di Capo Passero, Italy, is optimized to study neutrino of cosmic origin in the energy range between 1TeV and 100TeV. The detector ORCA (Oscillation Research with Cosmics in the Abyss), located at about 40 km offshore Toulon, France, at a depth of 2500m, is optimised to determine the neutrino oscillation parameters, through the detection of atmospheric neutrinos in the energy range from few GeV to about 1 TeV. The two detectors share the same technology and will have a different size (ARCA about 1 km^3 and ORCA about 8Mton).

THE DETECTOR

The main elements of the detectors are the sea floor infrastructure, that provides connectivity and power to the offshore infrastructure and the Detection Units (DU) that host the optical sensors. The ARCA detector will consist of two building blocks of 115 DUs (see Fig.1 left) and the ORCA detector will consist only one building block of 115 DUs. The DUs are connected to shore via a network of submarine electro-optical cables and Junction Boxes [2].

The DU is the active part of the neutrino detector. It is a vertical structure anchored on the seabed and kept vertical by the buoyancy of its elements. In the ARCA configuration, the DU is 700 m height and hosts 18 Digital Optical Modules (DOMs) with an interspace of 36 m between them. The DU base is a mechanical structure that lies on the seafloor and is equipped with the electronics needed to power and control the DOMs. Two thin Dyneema® ropes are firmly connected to the base and are used to keep the 18 DOMs in place. A thin backbone tube equipped with optical fibres and copper wires for data and power transmission, respectively, runs along the full length of the mooring.

To allow safe transportation and deployment, the DU is folded around a dedicated spherical vehicle at the end of its integration process. Later, the DU is deployed from a boat on the seabed using this spherical structure [3]. The DU is placed on the seafloor and, with the support of a ROV, the DU is connected through the interlink to the seafloor network. Once having passed a complete system check performed from shore, the ROV triggers the unfurling mechanism of the vehicle. At the end of this process, the DU gets its final vertical position and the launcher vehicle is finally recovered on the sea surface to be reused.

The sensitive element of the telescope is the Digital Optical Module (DOM), a 0.44 m diameter pressure-resistant glass sphere which contains 31 3-inch photomultiplier tubes. The DOM also hosts calibration devices and electronic boards for power, readout, and data acquisition [4]. The implemented technology allows for sub-nanosecond timing accuracy of the PMT signal. The dynamic range spans from the single photon up to a cascade of thousands of photons, providing additional information useful for the reconstruction of the energy of the event. Given the presence of 31 PMTs, the DOM has an angular acceptance close to 4π, and can provide a better measurement of the photon direction for neutrino track reconstruction.

Typically, one sea campaigns per year is organized. The first DU was installed in December 2015; it is still in operation and taking data. Data taking was put on hold during two periods, the former related to an electrical problem with the seabed infrastructure that was fixed with a complete redesign of the Junction Boxes, and the latter

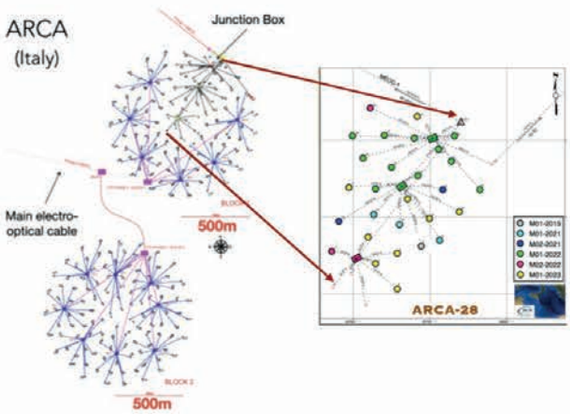

Figure 1 – Left: Layout of the completed ARCA detector. Right: A zoom of the so-called ARCA Phase-1. The installed detection units (Junction Boxes) are indicated with a coloured circle (rectangle). The colour scheme follows the sequence of marine campaigns indicated by a progressive number and the year.

due to a major upgrade of the shore station. The mass production of the detector started in 2021, once the main technical issues were addressed and solved.
At the date of September 2023, 28 (19) DUs are already in operation in the ARCA (ORCA).
The KM3net4RR project [5], of which INFN is both the proponent and leader, funds crucial actions for expanding the Italian site of Capo Passero of the KM3NeT submarine neutrino observatory. The procurement phase of the project is completed and, thanks to the PNRR funding, the KM3NeT4RR project will significantly extend the seafloor network and the onshore infrastructures, providing a significant boost toward final completion of the infrastructure.

PHYSICS RESULTS

Neutrino astronomy is nowadays a well-defined field in astroparticle physics. There are strong expectations around the neutrino experiments which are optimised to detect particles with high energies, $E_\nu > 1$ TeV. Indeed, given their neutral electrical charge, neutrinos are not deflected by interstellar magnetic fields but point back to their sources, allowing to identify and study the emitting astrophysical objects using neutrinos as a probe. The cosmic ray energy spectrum has been measured up to energies of 10^{20} eV, however the nature and position in the Universe of the cosmic ray accelerators are still unknow. Multi-messenger astronomy has started to play an emerging role in astroparticle studies. The possibility of joint detections using different mediators, like photons, gravitational waves, high energy cosmic rays, and neutrinos, has already opened new perspectives in cosmic and astronomical studies.

The first analysis [6] devoted to the search for point-like neutrino sources is performed on a data sample equivalent to 92 days of operation, taken with ARCA in a six-line configuration. The neutrino emission is searched among 40 candidate point sources plus 6 extended sources. A binned likelihood search is applied to the data set corresponding to the period between May and September 2021. Background-only and signal+background samples are built from scrambled real data and Monte Carlo simulations. The neutrino signal is generated with an E^{-2} energy spectrum in a 5° cone around the source.

The most significant source corresponding to the lowest p-value (0.02) is the radio galaxy Centaurus A (RA= 201.36, $\delta = -43.01$), for which 2.6 signal events are fitted. The p-value of ~ 2% is compatible with the expectation from the pure background hypothesis.

In Fig. 2 the final ARCA6-21 lines E^{-2} point source results are compared with the IceCube and ANTARES experiments [7–8], as well as the previous ARCA point source analyses, and with the expected sensitivity for the full ARCA detector comprising 2 building blocks [9].

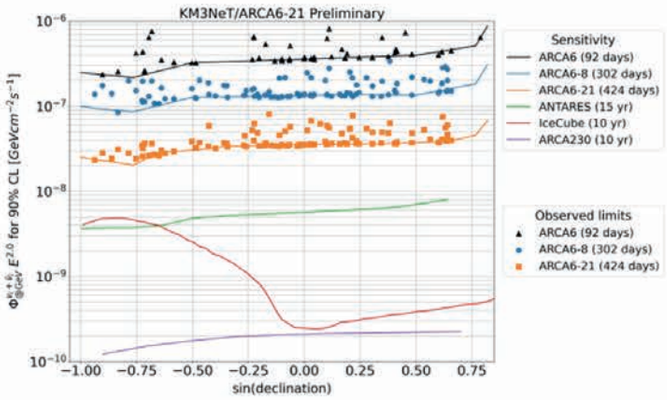

Figure 2 – Sensitivities and upper limits for a E^{-2} cosmic neutrino flux. The points are the upper limits for the candidate sources.

In the multi-messenger scenario KM3NeT has already contributed with the follow-ups of two real-time IceCube alerts of potential astrophysical neutrino sources: the IC alert IC211208A (associated with the PKS 0735+17 blazar) [10] and IC220205B (associated with the PKS 1741-03 blazar) [11]. The searches were performed using the ON-OFF method, i.e. defining a region in the sky in a cone centred on the blazar position (ON region) and sampling one or more regions far from the source position (OFF zone) in these cases a declination band centred in the source's position without the inclusion of the ON region. No excess was reported in both cases and for the IC211208A only one ν_μ candidate with E = 18TeV (p = 0.14) was identified in a time window of the search of 1 month.

REFERENCES

[1] S. Adrián-Martínez et al. (KM3NeT Collaboration), Letter of intent for KM3NeT 2.0, 207 J. Phys. G: Nucl. Part. Phys. 43, 084001 (2016).
[2] S. Biagi, The KM3NeT/ARCA seafloor infrastructure, contribution in these reports.
[3] S. Aiello et al. (KM3NeT Collaboration), JINST 15, P11027 (2020).
[4] S. Aiello et al. (KM3NeT Collaboration), JINST 17, P07038 (2022).
[5] https://km3net4rr.infn.it/project/
[6] R. Muller et al. for the KM3NeT Collaboration, Proc. Neutrino 2022. DOI: 10.5281/zenodo.6805394 (2022).
[7] Alves, S. et al. (KM3NeT Collaboration) PoS(ICRC2023)1128.
[8] Aartsen, M. G. et al. (2020). Physical review letters, 124(5), 051103.
[9] Van Eeden, T. J. et al. (KM3NeT Collaboration). PoS(ICRC2023)1075.
[10] Atel #15290 https://www.astronomerstelegram.org/?read=15290
[11] Atel #15290 https://www.astronomerstelegram.org/?read=15290

The IDMAR DCFO system: a major upgrade of power and data transmission capacity for the Capo Passero submarine cabled infrastructure of the Laboratori Nazionali del Sud

G. Riccobene[1], M. Sedita[1], R. Cocimano[1], G. Cuttone[1], A. D'Amico[2], K. Leismueller[1], C. Nicolau[3], A. Orlando[1], S. Pulvirenti[1], N. Randazzo[4], J.W. Schmelling[2], S. Viola[1]

1) INFN LNS, Via S. Sofia62 I-95123 Catania, Italy
2) Nikhef, Science Park 103 Amsterdam, The Netherlands
3) INFN sez. Roma 1, P.le A. Moro 2, I-00100 Roma, Italy
4) INFN sez. Catania, Via S. Sofia 64 I-95123 Catania, Italy

Abstract – A major upgrade of the Capo Passero deep sea cabled infrastructure of the LNS, was undertaken within the IDMAR PO-FESR project. A novel 15M€-budget installation, the so-called DCFO (Direct Current - Fiber Optic) system, designed and manufactured by Alcatel Submarine Networks (ASN) -part of Nokia- under the lead of Istituto Nazionale di Fisica Nucleare (INFN) was deployed between November 2020 and November 2022. The DCFO system is composed of: an on-shore 100 kW power feeding equipment; a "Y"-shaped electro optical cable with 48 fibers and two copper conductors; a cable termination frame equipped with four 10 kW medium voltage converters, 16 electrical and 16 optical ROV mateable connectors. The full system is designed to operate for 25 years without maintenance. Another cable termination, with identical characteristics, will be installed within 2025 to complete the Phase 2 subsea infrastructure under the PNRR KM3NeT4RR project aegis.

THE IDMAR PROJECT AND KM3NET-ARCA

IDMAR is a research project funded under the PO FESR 2014-2020 Priority Axis 1 Research, Technological Development and Innovation - Action 1.5.1 for the construction a strategic infrastructure in the Sicilian Region. IDMAR is one of the Research Infrastructures (IR) included in the National Research Infrastructure Plan (PNIR). Within the IDMAR project the Portopalo di Capo Passero cabled infrastructure of LNS has been upgraded with an enhanced submarine infrastructure capable of hosting the KM3NeT-ARCA neutrino telescope (www.km3net.org) and the Western Ionian Node of EMSO ERIC (www.emso-eu.org), the European network of seafloor and water column observatories.

DCFO: THE MAIN ELECTRO OPTICAL CABLE

The IDMAR DCFO uses a novel technology for underwater electro-optical cables, based on double coaxial conductors used to route electrical power from shore to deep sea without sea return connection. This technology improves reliability and introduces redundancy, with possibility – in case of failure-to use sea-return at cost of power reduction. The novel DCFO cable is dual coaxial conductors' cable which is composed of two copper conductors and a loose tube containing the optical fibers.

The DCFO cable copper conductors' electrical resistance inner is, for the inner conductor, less than 1.0 Ohm/km (at 10°C) and for the outer ≤0.5 Ohm/km (at 10°C)

The MEOC (main electro optical cable) holds 48 optical fibers to connect shore to deep sea. Two of them are used to control the subsea nodes, i.e. the controls that operate the subsea ROV-mateable power ports; and 46 are available for science and will used to communicate with the science observatories. Considering the distance between the shore laboratory, the presence of junction boxes and CTF, ITU-T G.654 fibre type was used to optimise the optical budget, with attenuation at 1550nm less than 0.18 dB/km and Chromatic Dispersion at 1550nm (at 20°C) less than 19.50 ps/nm/km. Light travel time on fibers as a function of frequency, has been measured following the KM3NeT protocols to take into account time delays for the White-rabbit based (https://ohwr.org/project/white-rabbit/wikis/home) time synchronization systems to be installed for the ARCA detector.

The IDMAR cable has a "Y" shape to accommodate two CTFs, designed to properly finalise the KM3NeT-ARCA detector lay-out with two building blocks.

Desktop study and cable lay

The IDAMR cable route was selected through a so called desktop study on results on bathymetry, geophysics and oceanographic parameters acquired during a cruise

onboard the Explora-INOGS ship, carried out by the Elettra, part of Orange Marine, and Geoteam. During the process, safe distance from the NEMO INFN Cable, number of crossings and recovery operations needed to install the Cable termination frames were also takein into account.

The cable, manufactured by Alcatel Submarine Networks (ASN) in the Calais plant, was then laid in October 2020 by the Pierre de Fermat (Orange Marine) ship, from the two sea-side terminations to shore (Figure 1). Three types of special double coaxial DCFO cables are used, along the route from sea to shore, to optimise endurance and lay/recovery: Light Weight, Light Weight Protected and Single Armored.

Figure 1: The NEMO (red) and the IDMAR (white) cables, starting from the harbour of Capo Passero. The Northern branch of the IDMAR cable is terminated withy CTF-02. Other telecom cables are shown in yellow.

Two cable-end boxes (CEB) were installed to protect the deep-sea cable terminations. One cable end box was removed in 2022 to install the IDMAR Cable termination Frame CTF-02, the second one remains connected till the completion and installation of CTF-03. Note that CTF-01 is the cable termination frame installed on first cable, the NEMO cable of the infrastructure.

The shore end required accurate work to dig and build a new beach man hole (about 4 times larger than the NEMO BHM to cope with the larger bending radius of the IDMAR cable with respect to the NEMO one) and protect the cable arrival at the shore. Shore protection was nicely organised minimising the impact on posidonia grass fields and on seascape rocks.

The arrival of cable at the Capo Passero shore end is show in figure 2.

Figure 2: Arrival of the IDMAR cable at the Capo Passero harbour.

A batch of several kilometres of spare DCFO cables o is stored in the MECMA warehouse of Catania in case of need for replacement.

DCFO: THE SHORE LAB INSTALLATION

The IDMAR DCFO control and power Feeding Equimpent (PFE) is hosted in a dedicated room of the shore station of Capo Passero, with controlled humidity and temperature. The main equipment installed in the room is the station joint box (SJB) wich separates fibers and the two conductors from the main cable; the Routing Cabinet; the PFE itself, manufactured by Heinzinger and divided in two power supply units: the PU-GO (0VDC to 6500 VDC, 50 kW, 8.3 A) and the PU-RETRN (-6500VDC to 0VDC, 50 kW, 8.3 A) and the Remote Control Box (RCB), that allows direct communication with the electronics stored in CTF-02 (and in future in CTF-03) to monitor the status of the Medium voltage Converters and allow open/close of electrical ports.

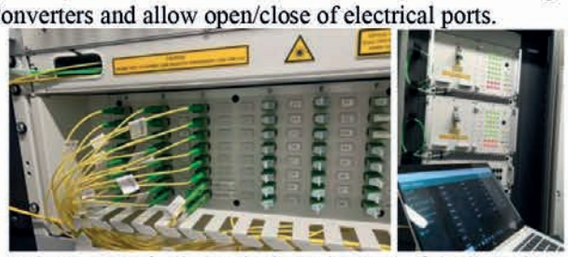

Figure 3: Left- the optical patch panel of the IDMAR RCB with 22 fibers to CTF-'2 connected together with the 2 control fibers (positions 23 and 24); Rigth- the RCB synoptic panel to control the CTF-02 and (when available) CTF-03. The system is fully redundant.

Figure 4: Left-The inner part pf the SBJ, where the MEOC is split into 2 conductors and separated by the fiber bundle. Rigth – the IDMAR DCFO room

DCFO: THE CABLE TERMINATION FRAME

The IDMAR Cable termination frame CTF-02 hosts 4 Medium voltage converters (6/12 kVDC to 363 VDC) and offers 16 off fiber-optic and 16 Off power wet-mateable connectors. Optical connectors are Teledyne ODI rolling seal series with 8 optical pins, electrical connectors are Seiemens Digitron series.
From the electrical point of view CTF-02 holds four Medium voltage converters. Each MVC provides up to 2.5 kW continuous power supply in a single port, i.e. 10 kW power in total for the 4 ports.
In order to stabilise the current and voltage variations at startup and change of load, the MVC output is connected to a so-called smoothing box equipped with an electrical "LC" circuitry to keep the voltage values within 363±10% in all power conditions.

The mechanical design of the CTF was carefully evaluated accommodate a payload of about 6 Tons (four MVCs, Smoothing Boxes, connectors and cables), the result is a 12 Ton structure, with a 1m-high mud-matrass to land on sandy seafloor, and to avoid contact of mud with the MVC vessel (Figure 5).

Figure 5: The IDMAR CTF-02.

Test and validation of all components was carried out with the target of 25-year long operation without maintenance in deep sea.

Electrical and optical tests were carried out at each phase of the construction and integration of the asset.
The CTF was completed in July 2022 at the ASN site of Calais and connected to a km-long DCFO light weight cable. Eventually the CTF was embarked aboard the Ile d'Ouessant (IOT) ASN ship in October 2022 (Figure 6) and transferred to the Capo Passero deep sea site.

Figure 6: CTF-02 aboard the Ile d'Ousseant ship of ASN.

CTF-02 deployment

One of the major constraints for the deployment of CTF-02 was the need of having the asset on the seafloor at an exact distance from CTF-01. The error on the landing point had to be less that 30 m to properly complete the KM3NeT-ARCA detector. This operation required, first, definition of landing point with a precise measurement via ROV run and deployment of a reference marker buoy. Secondly the ROV onboard IOT identified the marker buoy and referenced the field. Eventually the CEB of branch north the IDMAR cable was removed and connected to a cable trunk of about 15 km that was laid till the marker buoy, marked and recovered onboard IOT. Once the exact cable length was determined, the CTF was laid with visual assistance of ROV. The final position of the CTF was at less than 20 m from the target point.

Figure 7: Deployment of CTF-02 from the Ile d'Ousseant ship of ASN.

The operation was concluded November 16th 2022 with successful commissioning of the installation and training of INFN operators.

CONCLUSIONS

A new cabled infrastructure was deployed by INFN-LNS from the Capo Passero shores station to 3500 m water depth, about 100 km South East of Capo Passero. The system offers 40 kW power connection over 16 electrical ports that can be doubled after the installation of another CTF. The present installation quadruplicated the power capacity at the Capo Passero installation and doubled the fiber connection. This will allow the complete installation of KM3NeT ARCA building block with 115 DUs and of EMSO seafloor observatories. This installation also paves the way to the completion of the ARCA detector with a second building block of additional 100-ish Detection units.

AKNOWLEDGEMENTS

This work has been funded within the IDMAR project PO FESR 2014-2020 Asse prioritario 1 Ricerca, Sviluppo Tecnologico e Innovazione - Azione 1.5.1 "Sostegno alle infrastrutture della ricerca considerate strategiche per i Sistemi Regionali ai fini dell'attuazione della S3".

The ReD experiment for the directional sensitivity of a double phase LAr TPC

N. Pino[1,2,3], S. Albergo[1,2,3], D. Dell'Aquila[4,5], M. Gulino[4,6], L. Pandola[4], S. Sanfilippo[4]

1) Dipartimento di Fisica e Astronomia "E. Majorana", Università degli studi di Catania
2) INFN, Sezione di Catania
3)Centro Siciliano di Fisica Nucleare e Struttura della Materia (CSFNSM)
4) INFN, Laboratori Nazionali del Sud
5) Università degli studi di Sassari
6) Università degli studi di Enna Kore

Abstract – In the field of direct searches of massive particles as cold dark matter candidates (WIMPs), directionality could be a key aspect to flag a nuclear recoil event as a WIMP's one, allowing to reject isotropic background sources, like the irreducible neutrino floor. The Recoil Directionality (ReD) experiment, within the Global Argon Dark Matter Collaboration (GADMC), probed the directional sensitivity of a Liquid Argon Time Projection Chamber (LAr TPC) in the range of 20-100 keVnr energy by characterizing the charge and light response of the detector. This report describes the analysis performed in 2021 with Artificial Intelligence Algorithms to derive a data-driven prediction model as an innovative tool to investigate the columnar recombination effect.

INTRODUCTION

DarkSide-20k, the near-future experiment within the GADMC, will be a dual-phase argon-based Time Projection Chamber (TPC) with a fiducial volume of 20 t of underground Argon (UAr). In such a detector, an incoming WIMP will scatter off the Ar target nuclei thus producing a nuclear recoil (NR) event. The energy deposited in a LAr TPC produces both electron-ion pairs from ionization and scintillation light [1]. The latter is detected as a prompt light signal, referred to as S1. Electrons and ions could recombine, thus contributing to the amplitude of the S1 signal. However, the presence of an electric field, the so-called drift field E_D, allows a fraction of electrons to escape recombination since they are moved away from the ionization track. On the top part of the TPC, there is a gas layer of Ar in equilibrium with the liquid, the so-called gas pocket. Once reached the gas pocket, electrons create a delayed light signal by electroluminescence. This signal, proportional to the charge created in the liquid, is referred to as S2. Therefore, recombination effect could result in a lower S2 signal. According to the columnar recombination model [2], this effect could also depend on the angle between the nuclear recoil and E_D. Consequently, the S2-S1 correlation could in principle be used to infer information about the initial direction of the NRs. A novel model describing the electron-ion cloud, formed after thermalization, as an elongated ellipsoid was developed to catch the directional dependence in the recombination phenomenon [3]. In parallel with the likelihood statistical analysis derived according to this model, an analysis model with Machine Learning (ML) was also developed to test the S1-S2 correlation at different angles with respect to E_D, by using only patterns extracted from the data.

THE RED EXPERIMENT FOR DIRECTIONALITY

The SCENE experiment [4] was the first one to report a hint of the possible directional sensitivity coming from the correlation between the ionization and scintillation signals.

In order to investigate the hint from SCENE, the DarkSide collaboration, within the GADMC, undertook the ReD experiment: a compact, cubic-shape LAr TPC (5x5x6 cm^3) was built and characterized in order to evaluate its performance in the same energy range exploited by SCENE but with an improved energy resolution on S1 and a better granularity for the x-y identification of the S2 signals [1]. The ReD TPC was also the first one to employ new-generation cryogenic Silicon Photomultipliers (SiPMs). The detector (figure 1) was irradiated with neutrons at an energy of about 7.4 MeV for 14 days, in February 2020, at INFN Laboratori Nazionali del Sud (LNS).

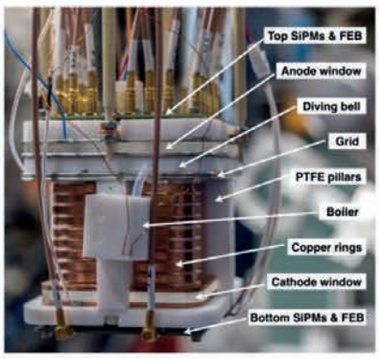

Figure 1: The ReD LAr TPC.

Neutrons directed toward the detector were produced via the $p(^7Li,^7Be)n$ reaction, and selected in energy and direction by tagging the accompanying ^7Be ions at a fixed angular position by using a $\Delta E/E$ telescope of Silicon detectors. A neutron spectrometer, made by 7 Liquid

Scintillators (LSci) detectors (EJ309), measures downstream neutrons from NR, thus closing the (n,n') kinematics and allowing to identify the direction of the recoiling Ar nucleus.

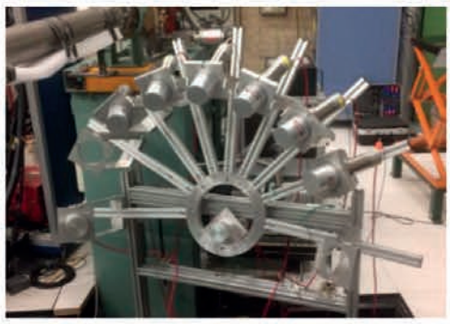

Figure 2: Structure of the neutron spectrometer.

The array that hosts the LScis (figure 2) was designed to select NRs in the TPC at the same recoil energy (about 72 keV) but with momenta at four different angles θ_r with respect to the electric drift field E_D. The investigated angles (θ_r) were 0°, 20°, 40°, and 90°, respectively. The events of interest are those passing the selection cuts of all detectors (Si-telescope, TPC, and one LSci) and these data are referred to as the triple-coincidence dataset in this report.

DATA-DRIVEN ANALYSIS WITH MACHINE LEARNING

In this work, Artificial Intelligence techniques and ML are used to extrapolate the trend of the recombination effect starting from patterns and correlations in the dataset. This approach is challenging since not all the models known in the literature [5,6] have a proper description of the ionization track that allows retrieving information about the recoil angle of the NR. This analysis procedure was performed in parallel with a statistical analysis [7] carried out with an unbinned maximum likelihood fit based on the novel model in [3].

Since the collected statistics in the triple-coincidence dataset amounts to less than 1000 events, an indirect approach was used. Firstly, a non-linear regression model was trained using numerical features extracted from NR events produced inside the TPC, thus assuming that the angle between the momentum of the recoiling Ar nucleus and the electric field is not relevant for the recombination. If any deviation from the hypothesized behaviour were found, one could in principle prove indirectly the recombination dependence on the recoil angle. The training paradigm is supervised since the model was trained on a set of input-output pairs. In this work, a vector of features related to the event (the scintillation signal S1 and the spatial coordinates) was used as input, while the corresponding measured S2 signal was the target output.

The used algorithm is Extreme Gradient Boosting (xgboost), chosen for its good performance and flexibility in multifield-possible applications [8]. At the end of the training phase, the model should be able to predict the value of the S2 corrected for TPC non-uniformity effects. The accuracy of the model was evaluated for each event with a relative error of the prediction defined as

$$\epsilon^i_{pred} = \frac{S2^i_{measured} - S2^i_{predicted}}{S2^i_{measured}} \qquad (1)$$

At a second stage, the so-called testing phase, the model was able to predict the value of the S2 signal with relative errors ϵ_{pred} approximately Gaussian-distributed, with mean 0.0043(6) and standard deviation 0.09.

Finally, the model was used on the triple-coincidence dataset divided according to four subsets of data, each related to one of the four investigated θ_r, thus obtaining four ϵ_{pred} distributions. For each distribution, the mean values and the errors on the mean were calculated. In figure 3 it can be noticed that the ϵ_{pred} value for the events with NR with parallel traces with respect to the direction of the drift field ($\theta_r = 0$) is on average lower than ϵ_{pred} errors coming from the other θ_r subsets. According to Eq. 1, this stands for a predicted S2 value greater than the experimentally measured one. Therefore, the derived model, which starts from the null hypothesis of no directional effect, tends to overestimate S2 for NR with parallel momenta with respect to E_D. According to the model [3], for parallel traces, an enhanced S1 signal, together with a reduced S2 signal, is expected. The result of the χ^2 test statistic returns a p-value for the null hypothesis of no directional effect of about 23%.

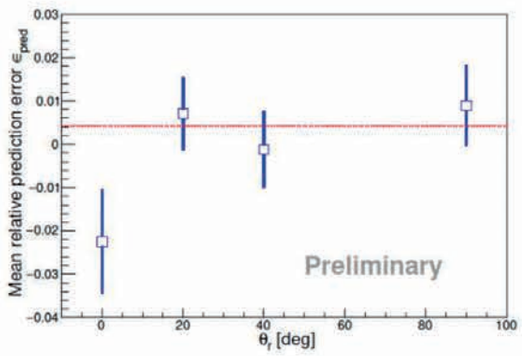

Figure 3: ϵ_{pred} distribution for triple-coincidence dataset.

REFERENCES

[1] P. Agnes et al., Eur. Phys. J. C 81 (2021) 101
[2] J.B. Birks, Proc. Phys. Soc., A64 (1951) 874
[3] V. Cataudella et al., JINST, 12 (2017) P12002
[4] H. Cao et al., Phys. Rev. D, 91 (2015) 092007
[5] J. Thomas and D.A. Imel, Phys. Rev. A, 36(2) (1987) 614
[6] G. Jaffé, Annalen Phys., 347 (1913) 303
[7] X. Li, talk at Int. Conf. on Topics in Astroparticle and Underground Physics, (2021)
[8] T. Chen et al., R package version 0.4-2 1.4, 1-4 (2015)

Characterization of nuclear recoils in the dual-phase Argon Time Projection Chamber of the ReD experiment

S. Albergo[1,2], G.A. Anastasi[1], M. Gulino[3,4], L. Pandola[3], N. Pino[1], S.M.R. Puglia[1], S. Sanfilippo[3], A. Tricomi[1,2]

1) Università di Catania and INFN, Sezione di Catania, Catania, Italy
2) Centro Siciliano di Fisica Nucleare e Struttura della Materia, Catania, Italy
3) INFN, Laboratori Nazionali del Sud, Catania, Italy
4) Università di Enna Kore, Enna, Italy

Abstract – Dark Matter in the form of Weakly Interactive Massive Particles (WIMPs) is expected to produce nuclear recoils (NRs) from elastic scattering with ordinary matter. Liquid Argon (LAr) Time Projection Chambers (TPC) operating in double-phase are able to detect these NRs via light signals from both scintillation and ionization processes.

In the scenario of a low-mass WIMP (<2 GeV/c^2), the kinetic energy of the NRs would be below 20 keV, thus making it crucial to characterize the ionization response in LAr TPCs as the lone available detection channel at such low energy.

The Recoil Directionality (ReD) project, within the Global Argon Dark Matter Collaboration, aims to measure the ionization yield of a LAr TPC down to 2 keV recoil energy.

LOW-MASS WIMP SEARCHES IN ARGON-BASED TPC

Direct searches for Dark Matter in form of WIMPs focus on detecting a signal from its interaction with ordinary matter in low-background underground detectors.

The DarkSide Collaboration within the Global Argon Dark Matter Collaboration (GADMC) is currently building DarkSide-20k, a multi-ton argon dual-phase Time Projection Chamber at the INFN Laboratori Nazionali del Gran Sasso [1]. The signal in a dual-phase TPC has two components: the prompt scintillation (S1) and the delayed electroluminescence (S2). The S2 signal is proportional to the number of electrons surviving recombination in argon, which are drifted from the interaction site by an electric field, extracted to a gas layer above and finally accelerated to produce electroluminescence. The delay between S1 and S2, which is typically of tens or hundreds of μs, is due to the time spent by the electrons to drift from the production point to the gas phase.

In the standard scenario, WIMPs have masses of O(100's) GeV and the NRs induced in Ar have kinetic energies of a few tens of keV. One scenario that recently gained wide interest in the community predicts much lighter WIMPs, with masses of O(1) GeV. Low-mass WIMPs would generate NRs with an energy of a few keV, resulting in a very low scintillation (S1) signal, often impossible to detect. Therefore, the search for low-mass WIMPs must be performed by using the S2 signal only. The DarkSide-50 Collaboration performed a dedicated S2-only analysis of the data taken with the dual-phase Ar TPC of the DarkSide-50 experiment [2], showing that Ar TPCs are potentially sensitive to S2 signals produced by a few ionization electrons, corresponding to sub-keV NRs. This measurement is strongly influenced by quenching fluctuations in the ionisation process and dedicated measurements are available in the literature only for energies above 7 keV.

THE RED PROJECT

The Recoil Directionality (ReD) project by the GADMC irradiated a miniaturized dual-phase TPC with neutrons to measure the response to Ar recoils down to 2 keV. The campaign was held at the INFN Sezione di Catania between January and March 2023.

Argon recoils of known energy were produced in the ReD TPC by elastic scattering (n,n') of neutrons emitted from an intense ^{252}Cf fission source. Neutrons elastically scattered off Ar were then detected by a neutron spectrometer made of plastic scintillator (PSci) detectors downstream. The accompanying gamma-rays of ^{252}Cf fission events were detected by two BaF_2 detectors deployed close to the source, thus providing an event-by-event fission tagging. This allows for an effective event selection based on Time of Flight (ToF) and pulse shape discrimination (PSD) in the PScis of the neutron spectrometer. The kinetic energy of Ar recoils could hence be determined on a purely kinematical basis, once the scattering angle and the neutron kinetic energy E_n are known. In this approach, the scattering angle is fixed geometrically by the layout of the neutron spectrometer. On the other hand, as the ^{252}Cf source emits neutrons over a continuous energy range up to 10 MeV, the neutron energy E_n must be evaluated event-by-event by the ToF measurement.

The dual-phase Ar TPC of ReD has a volume of 5x5x6 cm^3 [3,4] and it is readout by cryogenic Silicon PhotoMultipliers (SiPMs). In such detector electrons are collected by an electric field that drives them from the interaction site in the liquid to the gas multiplication region, where they produce the delayed S2 signal. The

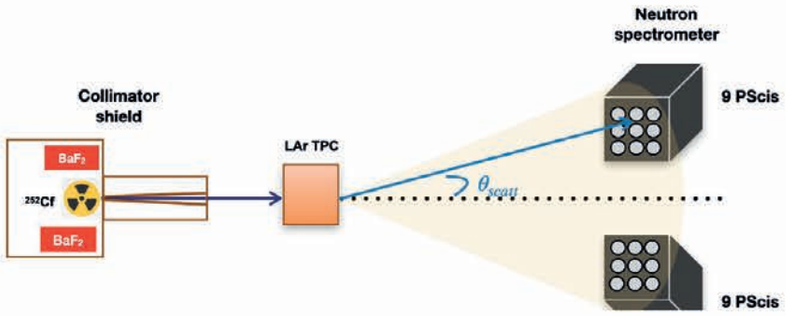

Figure 1 - Conceptual layout of the experimental setup for ReD

field was set 200 V/cm, causing the electron drift with a maximum time of 55 µs. Neutrons were emitted by a 1.0-MBq ^{252}Cf source, placed at about 90 cm distance from the TPC and collimated at 2° opening angle. The source was shielded and collimated by a custom structure made by boron-loaded polyethylene, iron and lead.

The two BaF_2 detectors were placed inside the shielding, close to the source and provided the START time for the ToF measurement. The neutron spectrometer, which provided the ToF STOP, was placed 100 cm downstream the TPC: it was made by two 3x3 arrays of 1-inch EJ-276 PScis, covering a range of scattering angles between 12° and 17°. A sketch of the experimental layout is shown in Figure 1.

PRELIMINARY RESULTS AND FUTURE PERSPECTIVES

ReD collected data for about three months. The selection of the candidate signal events primarily required the BaF_2-PSci ToF and the PSci PSD to be both compatible with neutron events: the range of ToF taken for the selection of ^{252}Cf neutrons goes from 40 to 180 ns. The resolution achieved in ToF was 0.7 ns rms, allowing an event-by-event measurement of the neutron kinetic energy at better than 5%. The candidate events were then further selected by requesting the presence of a S2-only TPC signal, with a single valid S2 signal within 55 µs from the BaF_2 signal, and estimated x-y position in the central 4x4 cm^2 region of the TPC. The final data sample, shown in Figure 2, consists in about 600 S2-only events with reconstructed Ar recoil energy below 10 keV. The corresponding S2 signals are below ~40 electrons. The design goal of ReD, i.e. to study the response of an Ar dual-phase TPC to nuclear recoils down to 2 keV, was hence successfully met [5]. Data analysis is currently in progress to finalize the measurement of the ionization yield.

Moreover, a new method involving self-supervised machine learning techniques, in particular convolutional autoencoders (CAE) [6], has been developed to improve the background rejection in S2-only events. In this analysis, the raw waveforms (averaged over the SiPMs) are compressed into 4-dimensional vectors, which have been characterized, and allow the tagging of traces without signal with a sensitivity comparable to the conventional reconstruction.

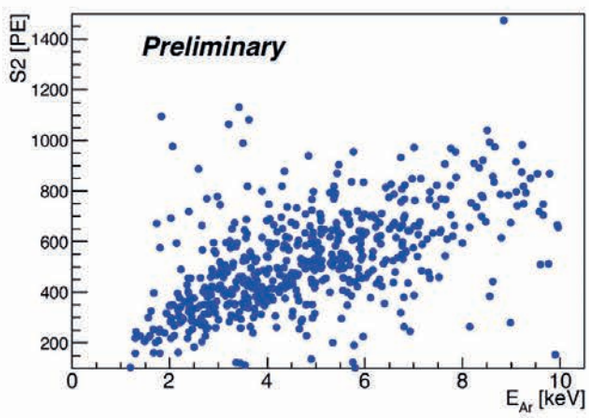

Figure 2 - (Preliminary) S2 signal vs. calculated recoil energy for events with a single neutron scattering in the TPC

This work is partially supported by ICSC – Centro Nazionale di Ricerca in High Performance Computing, Big Data and Quantum Computing, funded by European Union – NextGenerationEU

REFERENCES

[1] C. E. Aalseth et al., Eur. Phys. J. Plus **133** (2018) 131
[2] P. Agnes et al., Phys. Rev. Lett. **121** (2018) 081307
[3] P. Agnes et al., Eur. Phys. J. C **81** (2021) 1014
[4] P. Agnes et al., Eur. Phys. J. C **84** (2024) 24
[5] I. Ahmad et al., PoS(TAUP 2023) (2024) 052
[6] R. Corizzo et al., Expert Syst. Appl. **151** (2020) 113378

A tool for improved monitoring of acoustic beacons and receivers of the KM3NeT neutrino telescope

L. S. Di Mauro[1], D. Diego-Tortosa[1], G. Riccobene[1], S. Viola[1]

1) Laboratori Nazionali del Sud -INFN

Abstract - In this article we present a monitoring tool for the acoustic instrumentation of the KM3NeT neutrino detector. For effective monitoring, it is crucial to correctly associate the signal emitted by a transmitter with the correct beacon and this is achieved by leveraging the characteristic clock of each beacon. This monitoring tool has proven to be very useful in verifying the proper functioning of all acoustic devices deployed at sea, and the acoustic monitoring plot it produces will soon be included on the official ARCA monitoring page.

INTRODUCTION

For its operation, the neutrino telescope KM3NeT currently deployed in the Mediterranean sea requires an Acoustic Positioning System (APS) that allows the positions of the telescope's mechanical structures to be known within a geo-referenced coordinate system. The APS consists of acoustic emitters and acoustic receivers fixed on known locations of the sea bed. The tool presented in this article allows for monitoring the operation of these acoustic sensors.

The current Acoustic Data Filter (ADF) allows for the filtering of the Time of Arrivals (ToAs) of beacon signals to the receivers. As implemented, the ADF was a good solution for the first phase of the detector, where 3 or 4 acoustic beacons were active. Currently, with a larger number of beacons active simultaneously, the ADF sometimes confuses the emitters. Therefore, a post-analysis is necessary to identify the correct emitter. This is what this monitoring tool does by leveraging the characteristic clock of each beacon, thus understanding whether the beacon is functioning or not.

KM3NET ACOUSTIC POSITIONING SYSTEM

The KM3NeT neutrino telescope operates by detecting Cherenkov light induced by the creation of a relativistic particle from the interaction of a neutrino with a water nucleus. The detector consists of Detection Units (DUs) deployed off-shore Capo Passero, in Italy, (ARCA detector) and Toulon, in France (ORCA detector). Each DU hosts 18 Digital Optical Modules (DOMs), each one equipped with 31 Photo-Multipliers Tubes (PMTs).

To accurately reconstruct the Cherenkov track of the muon generated by the interaction of the neutrino with water, it is necessary to know the position of the DOMs with an accuracy of approximately 10 cm. This is achieved through the use of a Long Baseline (LBL) of Acoustic Beacons (ABs) and receivers (hydrophones) anchored on the seabed at known positions, and a network of acoustic piezoceramic sensors as receivers installed in each DOM. In ARCA, the acoustic beacons are located in the Junction Boxes (structures that ensure power distribution and data management between the various components of the telescope), at the base of some DUs, and some of them operate autonomously in tripods (TABs). Figure 1 shows a map of the position of the ABs and DUs for the ARCA detector.

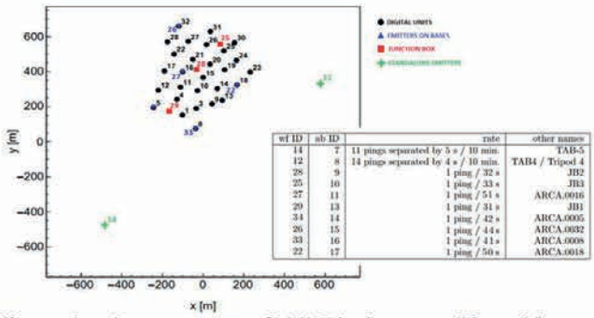

wf ID	ab ID	rate	other names
14	7	11 pings separated by 5 s / 10 min.	TAB-5
12	8	14 pings separated by 4 s / 10 min.	TAB4 / Tripod 4
28	9	1 ping / 32 s	JB2
25	10	1 ping / 33 s	JB3
27	11	1 ping / 51 s	ARCA.0016
29	13	1 ping / 31 s	JB1
34	14	1 ping / 42 s	ARCA.0005
26	15	1 ping / 44 s	ARCA.0032
33	16	1 ping / 41 s	ARCA.0008
22	17	1 ping / 50 s	ARCA.0018

Figure 1: Current map of ARCA detector. The table summarizes the parameters of the beacons.

The recorded data by the acoustic receivers are collected by on-shore computers in sessions of the usual duration of three hours, called RUNs. The ADF performs the cross-correlation between a piece of the received signal (buffer) by each receiver and each of the expected AB signals, then stores in the database each maximum peak of the correlation signal, called Quality factor (QF), and its associated ToA. Through multi-lateration techniques, it is possible to determine the positions of the single DOMs of the detector [1], but, as mentioned before, this requires a post-analysis.

Indeed, it is not guaranteed that the ToAs with the highest QF comes from the searched beacon, because the current ADF is not normalized and therefore does not take into account the distance between the beacon and the receiver, nor the intensity with which the signal is emitted. Therefore, it is not straightforward to associate a received signal with a specific beacon and determine if a beacon is functioning correctly. The method presented allows for the correct selection of ToAs for each AB, thereby enabling the monitoring of the beacons' operation.

ACOUSTIC MONITORING TOOL

The used method takes advantage of the common computational delay of AB electronic boards relative to the detector. The extent of the clock's delay is characteristic of each beacon, allowing for its identification.

Preliminary study of beacons

For a hydrophone-beacon pair, the ToAs with the highest QF are considered. The quantity of ToAs selected is regulated by the parameter n. If n=1, the expected number of ToAs based on the beacon's emission repetition rate and duty cycle is selected. If n=2, twice that number is considered, and so on. Normally, the number n is set to 1, but some beacons have lower emission intensity, so there is a risk of selecting only the ToAs from another beacon that have a higher QF (see the next paragraph). In these cases, a higher value of n is set to also select the ToAs from the correct beacon. For each beacon, We tried to consider the optimal value of n.

By plotting the Module (remainder of the division) between the selected ToAs and the Repetition Rate (RR) as a function of time, correct ToAs align along a straight line (Figure 2). Through an artificial intelligence algorithm developed in Python using the HoughLines() function of the OpenCV library, it is possible to automatically detect lines [2]. The points belonging to each line are selected, and a linear best fit is performed on them.

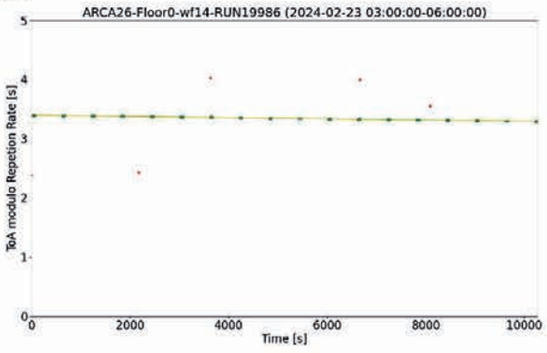

Figure 2: Module between the selected ToAs and the RR as a function of time: correct ToAs (in green) align along a straight line.

The slope of the line is related to the advance or delay of the system's clock and is therefore a characteristic feature for each beacon (Table 1).

Table 1: Characteristic slope of the line in the ToA module RR vs time plot, for each beacon in ARCA.

Beacon	**Slope (10^-5)**
WF 12 (TAB4)	-2,42
WF 14 (TAB5)	-1,02
WF 25 (JB3)	0,57
WF 28 (JB2)	1,44
WF 29 (JB1)	2,09
WF 22 (ARCA.0018)	2,11
WF 26 (ARCA.0032)	-5,59
WF 27 (ARCA.0016)	-29,5
WF 33 (ARCA.0008)	164
WF 34 (ARCA.0005)	159

Correct ToAs selection

Once the characteristic slope for each AB is known, it is possible to select the correct ToAs using a simpler algorithm that selects the points distributed along a line with the slope of the studied beacon. This allows us to distinguish the correct ToAS from spurious signals or from signals of another beacon that the ADF possibly failed to filter out (Figure 3).

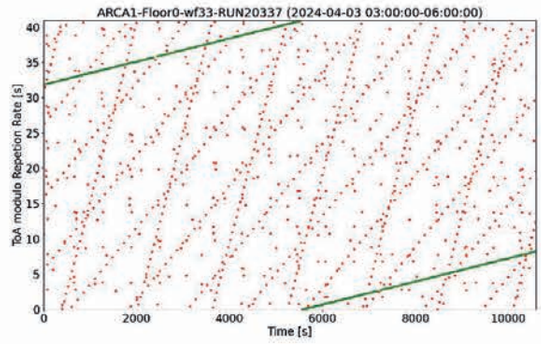

Figure 3: Module between the selected ToAs and the RR as a function of time: correct ToAs (in green) align along a straight line.

Construction of the Acoustic Monitoring Plot

Given a hydrophone-beacon pair, three scenarios can occur:

1) There are no ToAs in the database; this case is classified as MISSING, and the corresponding dot's edge in the plot will be black.

2) ToAs are present but incorrect because they do not distribute along the line with the desired slope in the module vs time plot; this case is classified as ANOMALOUS, and the corresponding dot's edge in the plot will be red.

3) ToAs are present and correct because they distribute along the line with the desired slope in the module vs time plot; this case is classified as NORMAL, and the corresponding dot's edge will be blue.

Figure 4 shows examples of the last two scenarios.

In the case of a cumulative plot over multiple runs, the border of the dot will reflect the most common state during the studied runs and the fill of the circle will have a color gradient depending on the percentage of runs in which the ToAs are present (to distinguish cases where, for example, an AB or hydrophone might only work for some runs):

- Black: ToAs missing in all of the analyzed runs
- Dark grey: ToAs missing between 50 and 99% of the analyzed runs.
- Light grey: ToAs missing in less than 50% of the analyzed runs.

Figure 5 shows an example of a cumulative acoustic monitoring plot over multiple runs. Inactive hydrophones and ABs are easily recognizable, marked by the vertical and horizontal lines of black dots.

Set the Best Value for n

Setting the optimal value for n is crucial for ensuring accurate ToA selection and effective monitoring.

As mentioned previously, for some beacons with lower emission intensity, it is necessary to consider a greater number of ToAs than the expected amount. Otherwise, only ToAs belonging to other beacons, which emit at

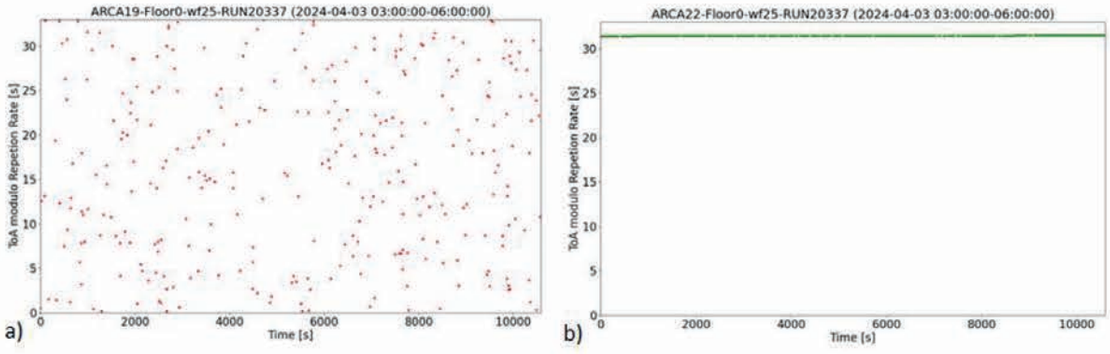

Figure 4: Module between the selected ToAs and the RR as a function of time. Two possible scenarios are shown: a) Incorrect ToAs and b) Correct ToAs. Note that the ToAs refer to the same beacon (WF 25) but are received by different hydrophones (ARCA.0019 in a and ARCA.0022 in b). Therefore, this case could indicate an anomaly in the hydrophone ARCA.0019 for which the ToAs are incorrect.

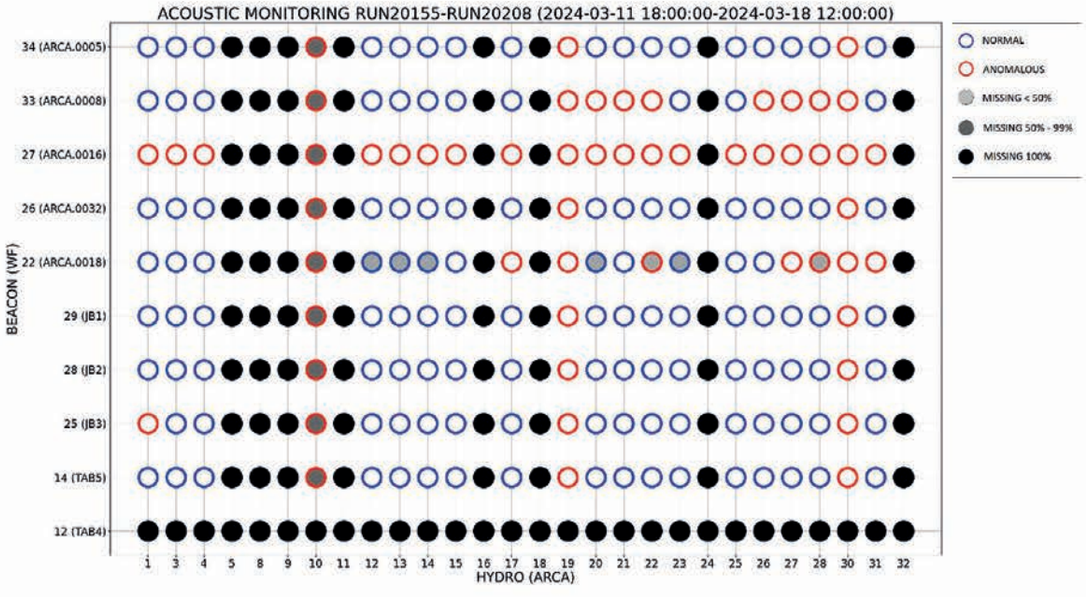

Figure 5: Example of a cumulative acoustic monitoring plot over multiple runs (20155-20208).

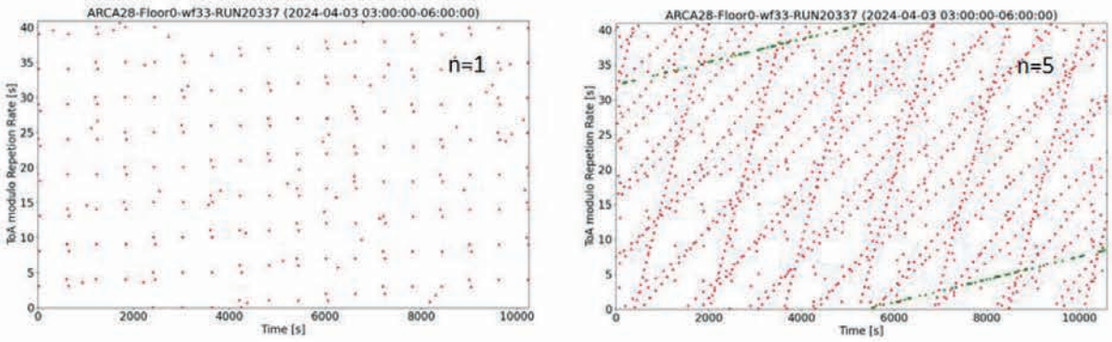

Figure 6: Module between the selected ToAs and the RR as a function of time. Choosing the correct value for n is crucial to ensure the selection of ToAs emitted by the target beacon.

higher intensities and thus have a higher QF, will be selected (see Figure 6).

Caveat and Interpretation of the Monitoring Plot

To properly understand the acoustic monitoring plot, it is essential to pay attention to the following critical points:

- Sometimes the number associated with the parameter n can be excessive, even though the best value has been used. So it may happen that the algorithm does not find this number of ToAs, and the corresponding dot in the plot is black or with shades of gray. Thus, in some cases, it may happen that there are no ToAs even if the beacon is functioning.
- If a beacon is listed as active in the run setup, ToAs will still be selected, even if they belong to other beacons, and in this case, we will have a dot with a red border instead of black.
- The ANOMALOUS state can occur in various cases: when the hydrophone is very far from the beacon and the beacon emits weak signals, when the hydrophone is in a "shadow zone" relative to a beacon, or when the hydrophone actually has an anomalous and noisy behavior (in this case, the anomalous state appears with all beacons).

For this reason, it is important to have an overall view: it can be reasonably assumed that the beacon is not functioning if it is not heard by all hydrophones. Similarly, we can assert with reasonable certainty that a hydrophone is off if it does not hear any of the beacons or assert that a hydrophone has anomalous behavior (noisy) if it does not receive the correct ToAs from all the beacons.

Taking these observations into consideration, for example, the plot in Figure 5 can be interpreted as follows:

- the beacon with WF 12 is not active;
- the beacon with WF 27 is not functioning but appears active in the run setup;
- the beacons with WF 22 and WF 33 are not recorded by some hydrophones (the farthest ones, see map in Figure 1);
- hydrophones 5, 8, 9, 11, 16, 18, 24, and 32 are not active because they are not receiving ToAs,
- hydrophone 10 is inactive for most runs, but in some runs, it was active but not functioning correctly (the border is red);
- hydrophones 19 and 30 have anomalous behavior and are noisy.

CONCLUSION

The monitoring tool described allows for monitoring the acoustic instrumentation located in the sea, which is necessary for the APS of the KM3NeT neutrino telescope structures. It enables RUN-by-RUN analysis and on more than one occasion, it has proven crucial for detecting malfunctions in beacons and hydrophones. It will soon be included in the official monitoring web page of the ARCA detector, featuring both daily cumulative plots and weekly cumulative plots.

It should also be noted that the principles applied to hydrophones can easily be extended to monitoring the internal receivers of the DOMs. Furthermore, efforts are underway to implement the same monitoring tool for the acoustic instrumentation of the ORCA detector.

REFERENCES

[1] S. Viola et al., Acoustic Positioning System for KM3NeT, Proceedings of Science (2018)

[2] OpenCV. "Hough Line Transform." *OpenCV Documentation*, OpenCV, https://docs.opencv.org/3.4/d9/db0/tutorial_hough_lines.html. Accessed 26 June 2024.

The ReD+ PRIN project: the characterization of sub-keV nuclear recoils in a dual-phase Argon Time Projection Chamber

S. Albergo[1,2], M. Gulino[3,4], L. Pandola[3], N. Pino[1], S.M.R. Puglia[1], S. Sanfilippo[3], A. Tricomi[1,2]

1) Università di Catania and INFN, Sezione di Catania, Catania, Italy
2) Centro Siciliano di Fisica Nucleare e Struttura della Materia, Catania, Italy
3) INFN, Laboratori Nazionali del Sud, Catania, Italy
4) Università di Enna Kore, Enna, Italy

Abstract - The characterization of the ionization yield for nuclear recoils in the keV range is a critical ingredient for the experiments looking for Dark Matter in the form of low-mass Weakly Interactive Massive Particles (WIMPs). The two-year project ReD+, funded by the Italian Ministry of Research through a PRIN grant, aims to improve the results obtained in the predecessor project ReD, which characterized a dual-phase Argon Time Projection Chamber (TPC) down to 2 keV nuclear recoils. ReD+ is designed to push the sensitivity down to 0.5 keV, by using the same conceptual design of ReD, with improved components, including a new optimized TPC.

THE SEARCH FOR LOW-MASS WIMP

The DarkSide program within the Global Argon Dark Matter Collaboration (GADMC) is searching for dark matter in the form of Weakly Interacting Massive Particles (WIMPs) by using argon dual-phase Time Projection Chambers (TPC) at the INFN Laboratori Nazionali del Gran Sasso. The signal in a dual-phase TPC has two components: the prompt scintillation (S1) and the delayed electroluminescence (S2). The S2 signal is proportional to the number of electrons surviving recombination in argon, which are drifted from the interaction site by an electric field, extracted to a gas layer above and finally accelerated to produce electroluminescence. The delay between S1 and S2 is due to the time spent by the electrons to drift from the production point to the gas phase.

In the standard scenario in which the WIMP mass is O(100's) GeV, the WIMP-induced nuclear recoils (NRs) in Ar have kinetic energy of a few tens of keV. Recently, interest raised on an alternative dark matter scenario, in which WIMPs are much lighter, O(1) GeV. In this case, the NR energy is as low as a few keV in Ar. As the S1 signal is often too low to be detected, the search for low-mass WIMPs must be performed by using the S2 signal only: Ar dual-phase TPCs are potentially sensitive to few-electron signals, i.e. to sub-keV Ar recoils. The S2-only analysis, as for instance the one carried out with the data of the experiment DarkSide-50 [1] is very sensitive to the knowledge of the ionization yield of Ar recoils and literature data are scarce in the energy range of interest.

THE RED PROJECT

The Recoil Directionality (ReD) project by the GADMC irradiated a miniaturized TPC with neutrons at the INFN Sezione di Catania between January and March 2023 and measured the response to Ar recoils down to 2 keV.

Argon recoils of known energy were produced in the ReD TPC by elastic scattering (n,n') of neutrons from an intense ^{252}Cf fission source. Neutrons elastically scattered off Ar were detected by a neutron spectrometer made of plastic scintillator (PSci) detectors, thus fixing the neutron scattering angle. Furthermore, two BaF_2 detectors were deployed close to the ^{252}Cf source, such to detect accompanying gamma-rays of fission events and then to provide an event-by-event fission tagging. The kinetic energy of Ar recoils could hence be determined on a purely-kinematical basis, once the scattering angle and the neutron kinetic energy E_n are known. In this layout, the scattering angle is fixed geometrically by the placement of the neutron spectrometer. On the other hand, as the ^{252}Cf source emits neutrons over a continuous energy range up to 10 MeV, the neutron energy E_n must be evaluated event-by-event by the time of flight (ToF).

The dual-phase Ar TPC used in the ReD campaign was a parallelepiped of 5x5x6 cm^3 [2,3], readout by cryogenic Silicon PhotoMultipliers. A 200 V/cm drift field collects electrons from the interaction site in the liquid and drives them to the gas multiplication region, where they produce the delayed electroluminescence signal. Neutrons were emitted by a 1.0-MBq ^{252}Cf source, placed at about 90 cm distance and collimated at 2° opening angle. The source was shielded and collimated by a structure made by boron-loaded polyethylene, iron and lead. Two BaF_2 detectors are placed inside the shielding, close to the source, in order to tag the fission products and to provide a START for the ToF measurement. The neutron spectrometer, which provides the ToF STOP, was placed 100 cm downstream the TPC: it was made by two 3x3 arrays of 1-inch EJ-276 PScis, covering a range of scattering angles between 12° and 17°. The resolution achieved in ToF was 0.7 ns rms (over a range of 40-180 ns), allowing an event-by-event measurement of the neutron kinetic energy at better than 5%.

The final event sample collected in about three months of data taking consists in about 600 S2-only events with reconstructed Ar recoil energy between 1 and 10 keV. The design goal of ReD, i.e. to study the response of an Ar dual-phase TPC to nuclear recoils down to 2 keV, was hence successfully met [4]. Data analysis is currently in progress to finalize the measurement of the ionization yield.

IMPROVING TO THE SUB-KEV SCALE: THE RED+ PROJECT

Given the interest by dark matter experiments searching for low-mass WIMPs, it is very important to further improve the characterization of the TPC response to low-energy recoils, by further extending the coverage down to the sub-keV range. ReD+ is an extension of ReD, funded by a two-year PRIN grant from the Italian Ministry of Research, designed to push the sensitivity down to 0.5 keV. The conceptual design will be the same as in ReD, i.e. employing the two-body kinematic of neutrons emitted from a source, as displayed in Fig. 1. While it is expected that a large part of the ReD set-up can be re-used, some of the components of the system will be improved in order to increase the signal rate and the signal-to-background ratio, which limited the sensitivity of ReD. In particular, a new optimized TPC is being completely re-designed and will be built and characterized within the project. The TPC will have a cylindrical shape and a special care will be taken to minimize any passive layer: in fact, multiple neutron scattering, either by non-active Ar or by any other component of the system, spoils the kinematic two-body correlation and produces an irreducible background which limits the sensitivity. The ^{252}Cf source will be deployed inside the same shielding used in ReD (boron-loaded polyethylene, iron and lead), with a minor re-design of the front face to minimize the probability of neutron leaking the shielding and hitting the TPC after one or more scattering in polyethylene. Another option under consideration is to use a commercial Deuterium-Deuterium neutron generator, which has the advantage of emitting mono-energetic 2.4-MeV neutrons. In order to push the sensitivity to sub-keV recoil energies, the neutron spectrometer has to be deployed at a smaller scattering angle with respect to ReD, but still outside the direct illumination cone from the source. For this reason, the TPC-spectrometer distance will be increased from 100 to 150 cm. In order to compensate for the loss of event rate due to the increased distance, the neutron spectrometer will be extended from 18 to 36 plastic scintillators (EJ-276, or its more recent commercial version EJ-276D) and a more active neutron source will be used (2-3 MBq, instead of 1 MBq). It is anticipated that the employment of a new optimized TPC, together with the improvement in the shielding, source activity and neutron spectrometer will allow to meet the design sensitivity of ReD+, i.e. nuclear recoils of 0.5 keV. The ReD+ project started in September 2023, involving the INFN, the University of Naples and the University of Catania. The re-design of the TPC, the procurement of the additional PScis and of the ^{252}Cf source are currently in progress. The assembly and integration of the system is expected to take place at the INFN Laboratori Nazionali del Sud in the first semester of 2025, followed by the data taking phase.

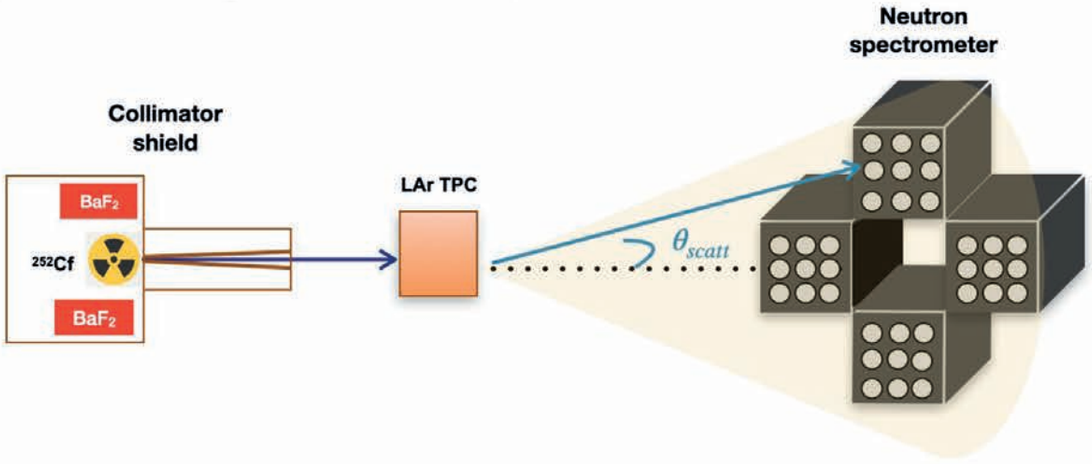

Figure 1: Conceptual layout of the experimental setup for ReD+

REFERENCES

[1] P. Agnes et al., Phys. Rev. Lett. **121** (2018) 081307
[2] P. Agnes et al., Eur. Phys. J. C **81** (2021) 1014
[3] P. Agnes et al., Eur. Phys. J. C **84** (2024) 24
[4] I. Ahmad et al., PoS(TAUP 2023) (2024) 052

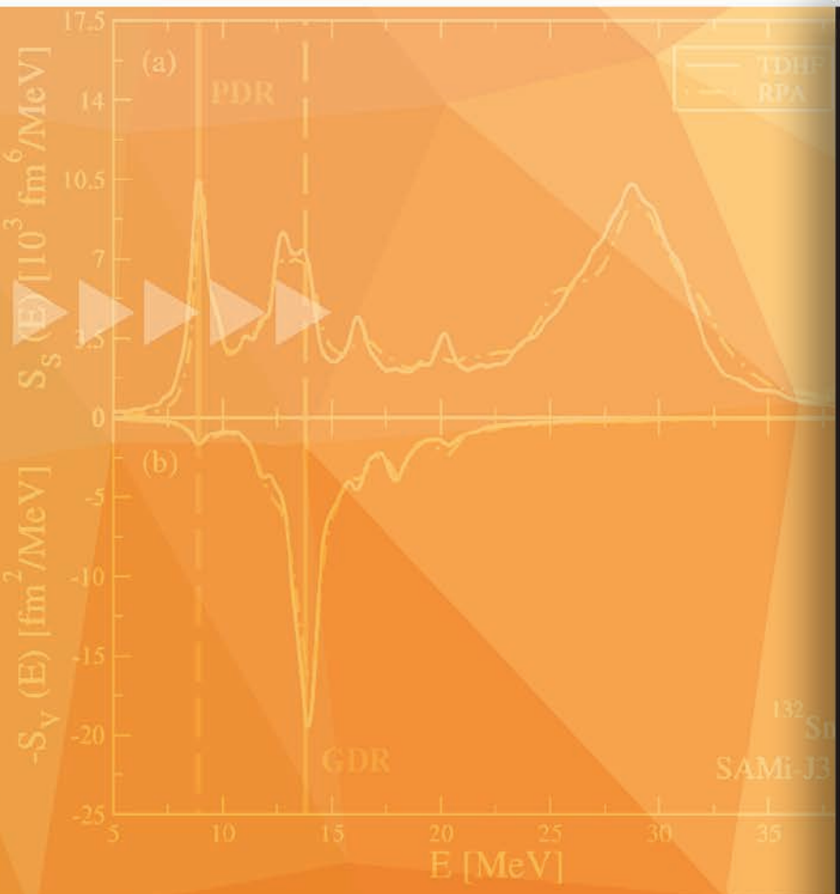

03

THEORETICAL NUCLEAR PHYSICS

Research

Analyses

Results

INFN LNS

- Beta decay half-lives within the SSRPA approach
- Inspecting two-step Nuclear Matrix Elements entering sequential Heavy Ion Double Charge Exchange reaction cross section
- Dipole modes in nuclei: exploring connections to structure and equation of state with extended energy density functional approaches
- Investigating the quarkonium suppression in strongly interacting matter via Open Quantum System Lindblad approach
- Heavy quarks dynamics in the hot QCD matter: estimating the spatial diffusion coefficient D_s from charm to the infinite mass limit
- Dynamical attractors in Full Relativistic Boltzmann approach in boost-invariant and non-boost-invariant conformal systems

Beta decay half-lives within the SSRPA approach

D. Gambacurta[1], M. Grasso[2]

1) INFN-LNS, Laboratori Nazionali del Sud, 95123 Catania, Italy

2) Université Paris-Saclay, CNRS/IN2P3, IJCLab, 91405 Orsay, France

Abstract – The charge-exchange subtracted second random-phase approximation (SSRPA) is applied for the study of the beta decay half-lives. Within this model, two-particle–two-hole configurations are included in the description of the excited states, incorporating beyond mean field effects that are usually neglected in standard studies based on the random-phase approximation (RPA). By doing so, a better agreement with the experimental data is found in SSRPA with respect to the RPA results. This result may have implications for the computation of nuclear matrix elements for neutrino-less double-beta decay and in double-charge exchange reactions within the NUMEN project.

INTRODUCTION

The nuclear beta decay is a weak interaction process where one of the protons or neutrons of a radioactive nucleus is transformed into the other in order to get more stability. This process plays thus a crucial role in the nucleosynthesis. Recently [1], we have analysed the Gamow-Teller (GT) resonances in several isotopes employing the fully self-consistent subtracted second random-phase approximation (SSRPA) which was developed and applied for the first time in Ref. [2] for charge-exchange transitions. In more detail, we have shown [2] that for ^{48}Ca the cumulative GT strength is in excellent agreement with experimental measurements as a function of the excitation energy, without any quenching factor. For heavier nuclei [1], the agreement with data obtained in SSRPA is strongly improved with respect to the RPA, though a slight remaining source of quenching might be traced back to other effects not explicitly included, such as short-range correlations and/or non-nucleonic degrees. In this work [3], we report preliminary results, where the beta decay half-lives are calculated consistently with the SSRPA model, without the use of any quenching factor.

MODELS AND RESULTS

The random phase approximation (RPA) is a well known microscopic method to describe nuclear excitations. Its main advantage, in comparison to other nuclear structure models, is that large single-particle spaces can be used, allowing for a full description of the total excitation strength and the corresponding sum rules. However, RPA excited states are approximated by a linear superposition of one particle one hole (1ph), neglecting thus high order configurations of the many particle many hole type. In the case of the beta decay half-life, the main difficulty of the RPA is indeed related to the too-low predicted strength within the so called-beta window, resulting in a too-high or even infinite half-life.

The Second RPA (SRPA) approach is a natural extension of the RPA, aimed at-overcoming this limit. In the SRPA model, the phonon operators contain explicitly the two-particle-two hole (2ph) configurations, besides the 1p1h ones already introduced in RPA. The SRPA equations of motions contain new matrices describing the full coupling between 1ph and 2ph configurations, and 2ph configurations among themselves, as they come out from the underlying two-body interaction. The subtracted SRPA (SSRPA) is a recent improvement of the SRPA, needed when effective forces are employed, for more details see Refs [1,2]. Since GT strengths are computed employing the bare GT operator, the bare value of the axial-vector coupling constant g_A=1.26 should be adopted in the expression of the half-life. However, a quenched value of g_A=1.00 is often used in the literature, to take into account missing correlations and thus to mimic a quenched GT strength.

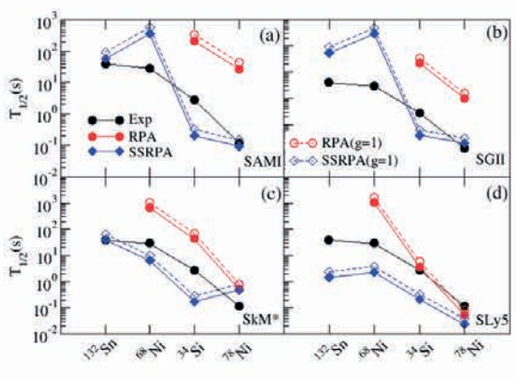

Figure 1: Experimental beta-decay half-lives for ^{132}Sn, ^{68}Ni, ^{34}Si and ^{78}Ni, compared with those obtained within the RPA and SSRPA models. Full (empty) symbols are obtained by using the bare g_A=1.26 (g_A=1.00) constant. The RPA values that are not shown correspond to infinite half-life values. See the text for more details.

In Fig. 1, the beta decay half-lives calculated within the RPA and SSRPA are compared with the experimental values. Four Skyrme parametrizations are here employed, namely SAMI [4] (panel a), SGII [5] (panel b), SkM* [6] (panel c) and SLy5 [7] (panel d). SSRPA results are obtained by using the diagonal approximation in the subtraction procedure [1], we check that this approximation is reliable for the present study. For some nuclei, the RPA does not provide any state within the beta-window, resulting in infinite half-lives. In particular, any of the adopted force is able to provide a finite beta half-life for ^{132}Sn, while for ^{68}Ni, only the SkM* force predicts a finite value. As a general feature, one can see that the RPA strongly overestimates the data, with the exception of the SLy5 force for ^{34}Si and ^{78}Ni. On the contrary, for all the Skyrme forces and nuclei, the SSRPA present excited states within the beta window, and, as a consequence, finite half-lives are provided. As a general trend, due to the inclusion of the two-particle- two-hole configurations which produces a richer and more fragmented spectrum with respect to the RPA distribution, the SSRPA half-lives are much lower, providing an overall better agreement with the experimental data. Full and dashed symbols are obtained by using g_A=1.26 and g_A=1.00, respectively, showing that a genuine quenching is introduced by the two-particle- two-hole configurations with the SSRPA, the effect being much larger that the one introduced by the use of an effective g_A=1.00 constant. In the case of the SAMI and SGII interactions, the correlations induced by the two-particle- two-hole configurations are not enough to nicely reproduce the slope of the experimental data, showing a pronounced peak for ^{68}Ni. However, considering that the RPA does not provide any strength in the beta window both for ^{132}Sn and ^{68}Ni, the improvement introduced within the SSRPA is still quite satisfactory.

CONCLUSIONS

We have shown preliminaries results on the effect of the inclusion of the two-particle- two-hole configurations within the SSRPA on the beta decay half-lives of ^{34}Si, ^{68}Ni, ^{78}Ni, and ^{132}Sn. We employ four Skyrme forces and as a general trend we observe a significant improvement of the predicted beta half-lives with respect to the RPA ones. The explicit inclusion of the two-particle- two-hole configurations producea a more fragmented and richer spectrum within the beta-window, resulting in lower beta half-lives. These results are expected to have strong implications for the computation of nuclear matrix elements for neutrino-less double-beta decay and in double-charge exchange reactions within the NUMEN project.

REFERENCES

[1] D. Gambacurta, M. Grasso, and J. Engel, Phys. Rev. Lett. 125 (2020) 212501.

[2] D. Gambacurta and M Grasso, Phys. Rev. C 105, (2022) 014321.

[3] D. Gambacurta and M. Grasso, *in preparation.*

[4] X. Roca-Maza, G. Col\`o and H. Sagawa, Phys. Rev. C 86,031306(2012)

[5] Nguyen Van Giai, H. Sagawa, Physics Letters B 106, 379 (1981)

[6] J. Bartel, P. Quentin, M. Brack, C. Guet, H.-B. , Nuclear Physics A 386, 79 (1982)

[7] E. Chabanat, P. Bonche, P. Haensel, J. Meyer, R. Schaeffer, Nuclear Physics A 635, 231 (1998)

Inspecting two-step Nuclear Matrix Elements entering sequential Heavy Ion Double Charge Exchange reaction cross section

J.I. Bellone[1,2], M. Colonna[2] , D. Gambacurta[2], S. Burrello[2], H. Lenske[3] on behalf of the NUMEN collaboration

1) Università degli Studi di Catania, via Santa Sofia 64, 95123, Catania, Italy.

2) Istituto Nazionale di Fisica Nucleare-Laboratori Nazionali del Sud (INFN-LNS), via Santa Sofia 62, 95123, Catania, Italy.

3) Institut für Theoretische Physik, Justus-Liebig-Universität Giessen, D-35392 Giessen, Germany.

Abstract - A proper treatment of the coupling of angular and linear momenta involved in Heavy Ion Double Charge Exchange reactions, described as two-step processes, allows to enuclate projectile and target two-body nuclear matrix elements from cross section expression. These nuclear matrix elements describe second order charge-changing transitions and show similarities with those involved in double beta decay observables. Investigations on these two-body nuclear matrix elements are performed for the reaction ^{76}Se(^{18}O,^{18}Ne$_{gs}$)^{76}Ge$_{gs}$, studied by the NUMEN collaboration.

INTRODUCTION

The interest on Heavy Ion Double Charge Exchange (DCE) nuclear reactions resides on their multi-purpose nature, because they allow to probe frontiers aspects of different fields of Physics: from nuclear Physics (such as the study of exotic nuclei, double Gamow-Teller giant resonance, high multipolarity transitions) to the Physics beyond the Standard Model of particle Physics.

In particular, due to several analogies between Heavy Ion DCE nuclear reactions and the 0νββ decays [1], cross section measurements for the former process could allow to get data-driven information on the nuclear matrix element (NME) of those nuclei candidate to undergo 0νββ decay. The analytical formulation of a relation between the 0νββ NME and the one describing a DCE reaction is quite tricky task and it is currently under study [1,4]. Nonetheless, the existence of a nearly linear proportionality relation between the NMEs of these two processes [5,6] supports the study of DCE reactions in the perspective outlined above. We have already proved the existence of a direct relation between the cross section for Single and two-step-Double charge changing reactions and the product of the corresponding projectile and target NMEs (a combination of these two NMEs, for the latter case), in the limit of small momentum transfer [2,3], where the "two-step-Double charge changing" (or double-single charge exchange, dSCE) reaction refers to the description of DCE reactions in terms of an incoherent sequence of two direct SCE processes. Recentely, we tried to analyze the main features of the radial transition densities (whose square modulus give the corresponding NMEs) involved in Heavy Ion dSCE transitions, because of their analogies with the corresponding quantities involved in 2νββ decays and of the similar ingredients entering the expression of 0νββ NMEs.

FORMALISM

We studied Heavy Ion dSCE reactions as two-step transitions, i.e. as a sequence of two independent direct Single Charge Exchange (SCE) reactions. As stated above, we already developed a formalism based on second order Distorted Wave Born Approximation (DWBA), which allows to express the dSCE transition matrix element (TME) as the convolution of the TMEs embedding all information on each one of the two SCE direct reactions and a Propagator describing the free propagation of the nuclear system generated by the first SCE transition, populating the so-called intermediate channel. We treated the propagator as a constant term, using the Closure approximation. A proper treatment of both linear and angular momenta involved in the whole dSCE process, and in particular in the intermediate channel, allows to get the following TME for dSCE reactions

$$M^{(DCE)}_{\alpha\beta}(\mathbf{k}_\alpha,\mathbf{k}_\beta) \simeq \int d^3\eta\, \tilde{\rho}^{2BTD}_P(\boldsymbol{\eta})\tilde{\rho}^{2BTD}_T(\boldsymbol{\eta})\tilde{V}^{dSCE}_{NN}(\boldsymbol{\eta})N_{\alpha\beta}(\boldsymbol{\eta}) \tag{1}$$

where we introduce the two-body DCE transition densities (2BTDs), defined as

$$\tilde{\rho}^{2BTD}_P(\boldsymbol{\eta}) = \sum_c \frac{(2\pi)^3}{N}\int d^3r\, e^{i\boldsymbol{\eta}\cdot\mathbf{r}}\tilde{\rho}^{(ac)}_{1P}(\mathbf{r})\tilde{\rho}^{(cb)}_{2P}(\mathbf{r}) \tag{2}$$

Eq. (2) is just the Fourier transform of the product of the two one-step transition densities accounting for the first and the second SCE transition, for example, in the projectile nucleus (same considerations hold for the target nucleus, too), summed over all nuclear states populated in the intermediate channel. These one-step transition densities are calculated within QRPA theory. The constant factor N in eq. (2) is a normalization volume, coming from the averaging procedure used to derive the 2BTD expression. The dSCE interaction potential, introduced in eq. (1), is simply defined as the Fourier transform of two nucleon-nucleon interaction potentials

$$\tilde{V}_{NN}^{dSCE}(\boldsymbol{\eta}) \equiv (2\pi)^3 \int d^3r\, e^{i\boldsymbol{\eta}\cdot\mathbf{r}} V_{S_1T_1}(\mathbf{r}) V_{S_2T_2}(\mathbf{r}) \quad (3)$$

In eq. (1), we also introduce the two-step distortion factor, $N_{\alpha\beta}(\boldsymbol{\eta})$, accounting for initial and final state interactions in the whole dSCE process [1,3]. In analogy to the procedure followed in [2], in the limit of small dSCE momentum transfer ($\eta \rightarrow 0$), the dSCE TME of eq. (1) reduces to the product of projectile and target 2BTDs, the dSCE interaction potential and the distortion term, thus allowing to directly connect the dSCE cross section to the product of projectile and target NMEs, i.e. the square moduli of the corresponding 2BTDs [9].

RESULTS

A close investigation on the 2BTDs described above is made for the nuclear reaction ^{76}Se(^{18}O,^{18}Ne$_{gs}$)^{76}Ge$_{gs}$ at 15.3 AMeV incident energy, studied within the NUMEN collaboration.

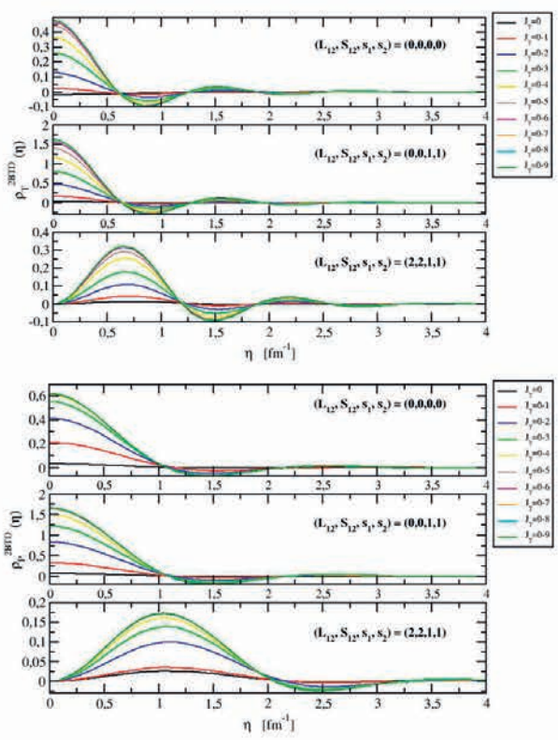

Figure 1: Target (upper panel) and Projectile (lower panel) radial two-step nuclear transition densities as a function of the two-step linear momentum transfer, for different values of the total angular momentum, J_γ, of the nuclear states in the intermediate channel.

Fig.1 illustrates the two-step radial nuclear transition densities both for projectile and target nuclei, as a function of the two-step linear momentum transfer, η; the different curves in each panel are obtained by adding different values of total angular momentum transfer, up to maximum values shown in the legenda; all these curve are obtained integrating up to 50 MeV of excitation energy of the nuclear states populating the intermediate channel; the three sub-panels refer to different combination of the the spins involved in first and second SCE reactions. The square modulus of the 2BTDs, in fig. 1, gives the NMEs of the dSCE transition in each one of the two interacting nuclei. From fig. 1, it is straightforward to note that important contributions come from several multipolarites characterizing the nuclear states in the intermediate channel and in particular from states with total angular momentum higher than J_γ=1 (e.g. J_γ =2,3,4), as expected for heavy nuclei. One can see that for projectile nucleus (^{18}O) the above contributions become neglegible from J_γ=5, while for the target nucleus (^{76}Se) convergent results are obtained from J_γ=6 onward, according to the size of the nuclei studied. The contributions coming from different nuclear states, in the intermediate channel, are coherently summed. It is worth mentioning that the NMEs, obtained from the above 2BTDs, show a structure similar to that of NMEs describing 2νββ decays. Moreover, it is interesting to note that the nuclear states involved in the (off-shell) intermediate channel are the same ones entering the NME of 0νββ decays.

CONCLUSIONS

Heavy Ion DCE reactions are described as two-step processes within second order DWBA framework allowing to get a quite simple expression for the 4-nucleon interaction potential and for the 2-body transition densities, the latter accounting for dSCE transition in each one of the two interacting nuclei. The two-body transition densities here described arise from the coherent sum of the contributions from several (and virtual) nuclear states in the intermediate channel, including those states characterized by high values of angular momentum transfer, as expected for heavy ions. We are interested in the study of these 2BTDs also because we noted that a similar peculiarity characterizes the NMEs describing 0νββ.

REFERENCES

[1] F. Cappuzzello *et al.*, Prog.Part.Nucl.Phys. 128 (2023) 103999.

[2] H. Lenske, J. I. Bellone, M. Colonna, J. A. Lay, Phys. Rev. C 98 (2018) 044620.

[3] J. I. Bellone, S. Burrello, M. Colonna, J. A. Lay and H. Lenske, Phys. Lett. B 807 (2020) 135528.

[4] H. Lenske, IOP Conf. Series: Journal of Physics: Conf. Series 1056 (2018) 012030.

[5] N. Shimizu, J. Menéndez and K. Yako, Phys. Rev. Lett. 120 (2018) 142502.

[6] E. Santopinto *et al.* , Phys. Rev. C 98 061601 (R) (2018).

[7] H. Lenske, J. I. Bellone, M. Colonna, D. Gambacurta, Universe (2021) 7(4), 98.

[8] S. Burrello, J. I. Bellone, M. Colonna, J.A. Lay Valera, and H. Lenske, Springer Proc. Phys. 225 (2019) 177.

[9] J.I. Bellone, M. Colonna, D. Gambacurta, H. Lenske, in preparation.

Dipole modes in nuclei: exploring connections to structure and equation of state with extended energy density functional approaches

S. Burrello[1], M. Colonna[1]

1) INFN, Laboratori Nazionali del Sud, Italy

Abstract - We summarize recent results on low-lying dipole modes in nuclei, investigating their connection to nuclear structure properties and their role in determining the nuclear matter equation of state (EOS). Using time-dependent mean-field calculations with standard Skyrme-like energy density functionals (EDFs), we examine dipole excitations across various nuclei. We observe how the low-energy spectrum changes with nuclear structure features such as density profile and surface properties, thus proposing a new interpretation of the Pygmy Dipole Resonance (PDR) and its relationship with neutron skin thickness in neutron-rich nuclei and reflecting important aspects of the effective interaction and EOS. Additionally, we discuss advancements in density functional theory, including the development of EDFs inspired by effective field theory and benchmarked on ab-initio calculations to better describe neutron matter and finite system surfaces.

INTRODUCTION

Collective motion offer insights into the underlying interaction among constituent particles. One prominent example in nuclei is the Giant Dipole Resonance (GDR), which provides valuable information about the isovector (IV) channel of the nuclear matter EOS, crucial for modeling compact stellar objects. Recent research has focused on low-lying dipole modes in nuclei, particularly exploring their evolution with isospin asymmetry [1-3]. In neutron-rich systems, a pronounced fragmentation of the IV response below the GDR, known as the PDR, is indeed observed. The nature of these excitations and their relation to the neutron skin, as well as their impact on the nuclear EOS, remain topics of debate. Our study aims to deepen our understanding of these features, examining the connection between low-lying dipole modes, nuclear structure properties, and the EOS. We employ phenomenological models based on EDFs, widely used for studying collective excitations. These EDFs are derived within a self-consistent mean-field approximation, providing a comprehensive description of nuclear properties across the chart, complementing ab-initio approaches. Efforts are currently underway to bridge the gap between ab-initio and EDF approaches [4] and to further extend these EDFs to account for some beyond-mean-field many-body correlations [5].

THEORETICAL FRAMEWORK

In the present work, we employ mean-field models based on the Time-Dependent-Hartree-Fock (TDHF) equation, where the evolution of the one-body density matrix ρ is determined by

$$i\hbar\partial_t\rho=[h,\rho] \qquad (1)$$

where h[ρ] is the non-relativistic single-particle Hamiltonian embedding the self-consistent mean-field potential, as derived from an EDF [2]. We restrict ourselves to the study of small amplitude fluctuations from the equilibrium (Hartree-Fock (HF) ground state), as the result of isoscalar (IS) or IV dipole excitations, determined by solving explicitly Eq. (1) or by linearizing the TDHF equation, leading to the Random Phase Approximation (RPA) approach. We then extract the corresponding strength functions at the excitation energy E

$$S_k(E)=\sum_{n>0}|\langle n|\hat{D}_k|0\rangle|\delta\left(E-\left(E_n-E_0\right)\right) \qquad (2)$$

where E_n is the excitation energy of the state $|n\rangle$ and E_0 is the energy of the ground state $|0\rangle$.

RESULTS

The energy spectrum of the dipole strength is shown in panels (a) and (b) of Fig. 1, for IS and IV excitations, respectively. It emerges that the pygmy is mostly an IS-

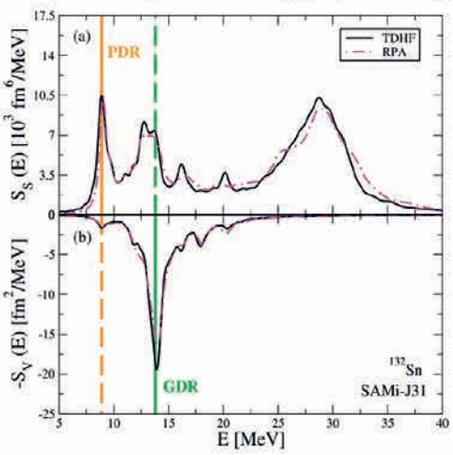

Figure 1: *Strength functions energy spectrum obtained for ^{132}Sn in TDHF or RPA calculations with SAMi-J31 EDF [2].*

like mode as its strength is mostly pronounced in the IS response. However, for asymmetric systems, some strength emerges at the same excitation energy also in the IV response, by virtue of the coupling existing between IS and IV modes in asymmetric nuclear systems and characterizing also the GDR [1-2]. The relative importance of the PDR in the IS response would be on the other hand enhanced for ^{120}Sn with respect to ^{132}Sn, at expenses of the other collective low-lying dipole modes. This is clearly evidenced in the left panel of Fig. 2.

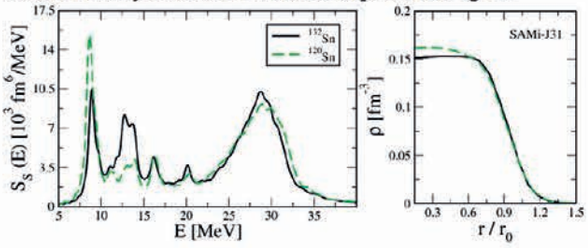

Figure 2. *Left panel: IS strength energy spectrum for ^{120}Sn and ^{132}Sn from TDHF with SAMi-J31 EDF. Right panel: Density profile in HF ground state as function of the reduced radius r/r_0* for the same tin isotopes *[3].*

The observed behavior in turn reflects the evolution of their corresponding density profiles, as one sees from the right panel of Fig. 2, where the total density profile ρ(r), obtained in the stationary HF limit of Eq. (1), is plotted as a function of the reduced radius r/r_0 where $r_0=1.2A^{1/3}$ fm and A is the mass number. The isotope ^{120}Sn has a more diffuse density profile with respect to the compact shape of closed-shell ^{132}Sn nucleus. Such a smoother behavior enhances thus surface effects leading to more robust oscillations in the low-energy region.

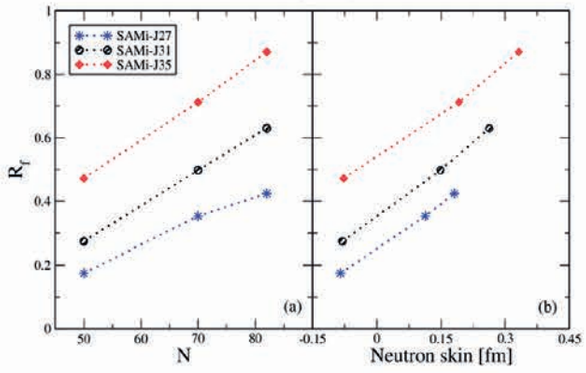

Figure 3. *Ratio between fractions of EWSR exhausted in the PDR region of IV and IS response, as function of neutron number N and neutron skin thickness of three tin isotopes with three SAMi-J EDFs [2].*

This analysis also explains why the percentage fraction of the Energy Weigthed Sum Rule (EWSR) exhausted in the PDR region of the IV response does not grow along the tin isotope chain, beyond N equal 70. The missing fraction is ascribable to the decrease observed in the IS strength. Indeed, when considering the ratio R_f between the EWSR fractions, to normalize the effect of the IS/IV mixing to the strength of the PDR that is mostly an IS-like mode, an almost linear increase versus neutron number N and neutron skin thickness is nicely recovered, as shown in Fig. 3. In the right panel of Fig. 3, also the correlation between the skin thickness and the symmetry energy J (and slope) is moreover evidenced.

OUTLOOKS AND CONCLUSIONS

We found that nuclear surface plays a crucial role in shaping the details of the low-lying dipole modes and the information on the effective interaction and EOS deduced from their study. Then, one expects that these results might be strongly affected by a more refined treatment of the low-density regime, especially when the strongly isospin-asymmetric nuclear systems are concerned. Indeed, as a common drawback, standard (phenomenological) EDFs are not able to reproduce the behavior in the very-low density region. New classes of EDFs were then recently developed [4], as inspired by systematic expansion adopted in effective field theory and benchmarked on available ab-initio calculations for pure neutron matter and neutron drops.

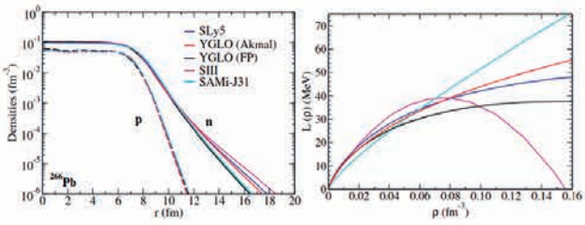

Figure 4. *Left panel: Neutron and proton density profile (in logarithmic scale) for ^{266}Pb for different EDFs considered in our study. Right panel: Density behavior of the slope L of the symmetry energy for the same EDFs (readapted from [4]).*

The analysis performed in Ref. [4] shows that these EDFs well describe ground state properties, such as binding energies and radii. Moreover, beside the correlation of the neutron skin thickness with the slope of symmetry energy L (as evidenced in Fig. 3), they highlight an interesting correlation between the tail of the density profile and the slope, as evaluated at densities much below saturation, in the regime where the new EDFs were grounded on ab-initio calculations, differently than standard phenomenological EDFS. The idea for the next future is then to implement these EDFs in dynamical mean-field models to study again the collective modes, taking advantage of their refined treatment of the surface.

REFERENCES

[1] Zheng H., Burrello S., Colonna M., Baran V., Phys. Rev. C 94 (1) (2016) 014313.
[2] Burrello S. et al., Phys. Rev. C 99 (2019) 054314.
[3] Burrello S., Colonna M., Il Nuovo Cimento C2 (2024).
[4] Burrello S., Grasso M., Yang C.-J., Phys. Lett. B 811 (2020) 13593.
[5] Burrello S., Bonnard J., Grasso M., Phys. Rev. C 103 (2021) 064317.

Investigating the quarkonium suppression in strongly interacting matter via Open Quantum System Lindblad approach

G. Coci[1,2], S. Plumari[1,2], V. Greco[1,2] and G. Falci[1]

1) Dipartimento di Fisica e Astronomia, Università di Catania, Via Santa Sofia 64 ZIP-95125 Catania, Italy
2) Istituto Nazionale di Fisica Nucleare, Laboratori Nazionali del Sud, Via Santa Sofia 62 ZIP-95123 Catania, Italy

Abstract – The search for applications of Open Quantum Systems (OQS) theory in high energy physics is growing as an important research field, in the aim for example to understand the properties of the hot and dense Quantum Chromodynamics (QCD) matter. In this work we make use of the renowned Lindblad equation to describe the dissociation of heavy quark-antiquark bound states (quarkonia) in strongly interacting hot QCD matter. We study the impact of different environment evolution with the aim to identifying the main physical parameters which enhance the decoherence of the bound states.

INTRODUCTION

The phenomenon of quarkonium suppression in QCD matter is a pivotal signature of the extreme conditions reached in heavy-ion collisions (HICs). Bound states of heavy quarks (charm and bottom) with their antiquarks (known as quarkonia), are expected to dissolve in the high-temperature, high-density environment of strongly interacting Quark Gluon Plasma (QGP) due to colour Debye-screening effects. This suppression in HICs, compared to pp collisions and quantified by the so-called nuclear modification factor R_{AA}, is observed experimentally at the CERN Large Hadron Collider (LHC) and the BNL Relativistic Heavy Ion Collider (RHIC) facilities. Its origin is still not very well understood but it certainly can provide insights into the properties of QGP and the nature of the strong force [1].

MODEL DESCRIPTION

In the theory of Open Quantum System (OQS) the quarkonium will serve as *system* and the QGP medium as *environment*. A schematic view of the physical system is depicted in Fig. (1). We consider the interaction of the system through the environment in the Markovian regime, where also the heavy quark mass M_Q, the binding energy E_B of the quarkonium states and the environment temperature T fulfil the following chain condition

$$M_Q >> M_Q v >> \pi T >> M_Q v^2 \sim E_B$$

Quarkonium states are considered to have non-relativistic velocity ($v<<1$). Hence the evolution of density matrix is described by the quantum master Lindblad equation [2][3]

$$\frac{d\rho}{dt} = -i[H,\rho] + \sum_n \left(C_n \rho C_n^\dagger - \frac{1}{2}\{C_n^\dagger C_n, \rho\} \right) \qquad (1)$$

In Eq. (1) H is the Hamiltonian of the system interacting with the environment and it is given by the sum of two terms. The first one is the vacuum Hamiltonian H_0 which represents the quarkonia as non-relativistic bound states from Coulomb potential $V = -C_F\alpha_s/r$ where r is the relative distance between the heavy quark-antiquark pair and α_s is the QCD strong coupling which is tuned to constraint the masses and widths of measured bottomonia states (Y) - the colour factor C_F=4/3. The second one is a harmonic oscillator term $H_T = \gamma\, r^2/2$ which describes the quarkonium energy loss in the medium through the coefficient γ. In potential non-relativistic pNRQCD models the coefficient γ is related to the dissipative counterpart of the diffusion coefficient κ [4].

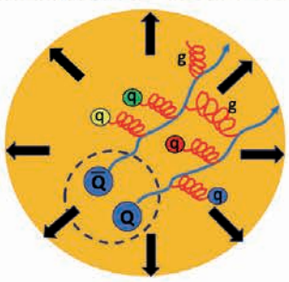

Figure 1: Schematic view of the propagation of heavy quark-antiquark bound system through the QGP environment.

In kinetic theory the role of γ and κ is hold by the so-called heavy quark transport coefficients which in Brownian motion enclose the main interaction features of heavy quarks with the QGP medium. In particular, the diffusion coefficient κ or equivalently the spatial diffusion coefficient D_s can be estimated within a relativistic Boltzmann transport approach for both bulk and heavy quark evolution by constraining the heavy quark interaction to reproduce experimental data for nuclear modification factor R_{AA}, elliptic flow v_2 and heavy-light v_n-v_n correlations [5]. The diffusion coefficient κ enters the expression of the so-called collapse operators C_n in Eq. (1) which account for the quantum transitions between different bound states as well as their dissociation into free heavy quark-antiquark pairs. In colour space bound states are represented as singlets (S) while unbound pairs belong to the octets (O). In this model there are six collapse operators, three for each colour subspace (see Ref. [6] for details). We solve Eq. (1) by means of the Montecarlo Wave Function (MCWF) method [7] employing a simulation code where the initial density matrix is represented as a projection of $|\psi(0)><\psi(0)|$ pure state. The state at any time $|\psi(t)>$ belongs to the Hilbert space constructed from the basis of first six eigenstates of the vacuum Hamiltonian H_0 and we take $|\psi(0)>$ to be the ground state wavefunction of H_0. To compute the solution of Eq. (1) we carry on a stochastic

sampling of quantum trajectories of the system state according to the following discretized time (Δt) equation

$$|\psi(t+\Delta t)\rangle\langle\psi(t+\Delta t)| = (1-\langle\Gamma(t)\rangle\Delta t)\frac{(1-iH_{eff}\Delta t)|\psi(t)\rangle\langle\psi(t)|(1+H_{eff}^{\dagger}\Delta t)}{(1-\langle\Gamma(t)\rangle\Delta t)} + \sum_n \langle\Gamma_n(t)\rangle\Delta t\ \frac{C_n|\psi(t)\rangle\langle\psi(t)|C_n^{\dagger}\Delta t}{\langle\Gamma_n(t)\rangle\Delta t} \quad (2)$$

In Eq. (2) the first term on the right-hand side describes a non-unitary deterministic evolution of the $|\psi>$ state according to the effective Hamiltonian $H_{eff} = H - i\Gamma/2$ which can be interrupted by an instantaneous transition (quantum jump) to another state with different quantum numbers. The total transition probability is controlled by the expectation value of the total width Γ which corresponds to the sum of all possible transitions $\Gamma_n=C_n^{\dagger}C_n$ depending on the collapse operators. More details of the computational framework used to perform the quantum jumps as well as to update the deterministic evolution of the $|\psi>$ state can be found in Ref. [6].

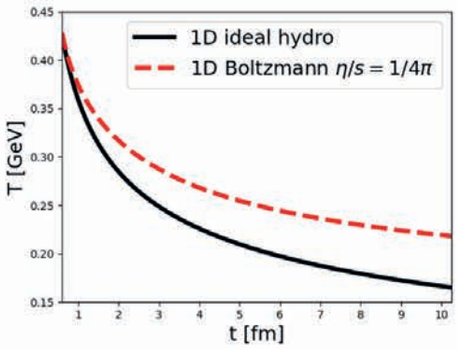

Figure 2: Temperature profile as function of time of the studied models of simplified expanding environment: black line is 1D ideal hydrodynamics, red dashed line is 1D Boltzmann evolution with $\eta/s=1/4\pi$. The initial temperature and formation time of the medium are respectively T_0=0.425 GeV and τ_0=0.6 fm.

RESULTS

Here we present our preliminary results concerning suppression of bottomonia bound states with orbital angular momentum l=0 in strongly interacting medium. We studied two different simplified models for the fireball expansion: a 1D ideal hydrodynamical profile which is characterized by a temperature dependence $T(\tau)=T_0(\tau_0/\tau)^{1/3}$ as function of proper time τ (Fig. 2 black curve) and a 1D relativistic Boltzmann evolution with collision integral tuned to viscous hydrodynamics by fixing the shear viscosity to entropy density ratio $\eta/s=1/4\pi$ (Fig. 2 red curve). In Fig. 3 the suppression of Y(nS) states up to n=3 is represented in terms of the survival probability, which we estimate by calculating for each trajectory the projections of the final and the initial wavefunction $\psi(r)$ of the system with the corresponding Y(nS) state wavefunction (each one being an eigenstate of the vacuum Hamiltonian H_0). Finally, we obtain the "overlap ratio" averaging over 10^5 quantum trajectories.

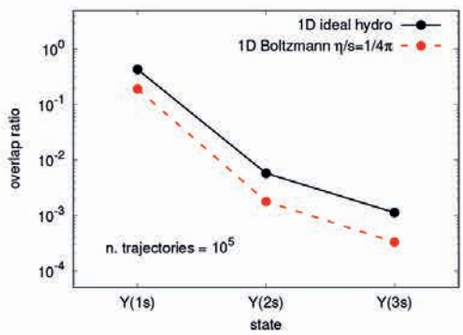

Figure 3: Survival probability of bottomonia Y(nS) states with n=1,2,3 and orbital angular momentum l=0 in two different environment scenarios: 1D ideal hydrodynamical expansion (black line) and 1D relativistic Botlzmann evolution with fixed shear viscosity to entropy ratio $\eta/s=1/4\pi$ (red dashed line).

CONCLUSIONS

In this work we described the evolution of quarkonia through the QGP within the framework of OQS by employing a simulation code for solving the Lindblad equation for the system density matrix in the quantum trajectory method. We focused on how different temperature evolutions of the QGP medium can affect the dissociation of quarkonia due to quantum decoherence effects. Our results (Fig. 3) show that the evolution of the system in a non-ideal environment, characterized by a slower decreasing temperature with time due to a finite viscosity, leads to a stronger suppression of the bound states, which can be associated to an amplified destruction of the initial quantum coherence of the system [8].
In future we plan to study the impact of heavy quark transport coefficients on quarkonium dissociation as well as to couple the Lindblad equation to a more realistic transport description of the QGP environment.

ACKNOWLEDGMENTS

This work was financially supported by the PNRR MUR project PE0000023-NQSTI.

REFERENCES

[1] A. Rothkopf, Phys. Rept. 858, 1-117 (2020)
[2] G. Lindblad, Comm. Math. Phys. 48, 119 (1976)
[3] V. Gorini et al. J. Math. Phys. (N.Y.) 17, 821 (1976)
[4] N. Brambilla et al. PRD 100 (2019), 054025
[5] S. Plumari et al. Phys. Lett. B 805, 135460 (2020)
[6] N. Brambilla et al. JHEP 05 (2021) 136
[7] H. P. Breuer and F. Petruccione "*The theory of open quantum systems*" (Oxford University Press, 2002)
[8] G. Coci, S. Plumari, V. Greco, G. Falci *in preparation*

Heavy quarks dynamics in the hot QCD matter: estimating the spatial diffusion coefficient D_s from charm to the infinite mass limit

M.L.Sambataro[1,2] , V. Minissale[2] , S. Plumari[1,2] , V. Greco[1,2]

1) Department of Physics and Astronomy "E. Majorana", University of Catania, Via S. Sofia 64, I-95123 Catania, Italy.

2) Laboratori Nazionali del Sud, INFN-LNS, Via S. Sofia 62, I-95123 Catania, Italy.

Abstract - In the last decade a Quasi-Particle Model (QPM) has been developed to study charm quark dynamics in ultra-relativistic heavy-ion collisions supplying a satisfactory description of the main observables for D meson and providing an estimate of the space-diffusion coefficient $D_s(T)$ from the phenomenology. Lately, we have extended the approach to bottom quarks dynamics describing the propagation in the quark-gluon plasma within an event-by-event full Boltzmann transport approach followed by a coalescence plus fragmentation hadronization. A significant breaking of the expected scaling of the thermalization time τ_{th} with M/T is found. Charm quark $D_s(T)$ is about 50% larger than the asymptotic value for $M \to \infty$, while the bottom one is only 20% higher. In the infinite mass limit the spatial diffusion coefficient is consistent with recent lQCD calculations with dynamical quarks.

INTRODUCTION

Heavy quarks (HQs), namely charm and bottom, are excellent probes of the system created in ultra-Relativistic Heavy Ion Collision (uRHIC). The large HQs mass value ($M_q >> T$), leads to a thermalization time comparable, at least for charm, to the mean lifetime of the Quark-Gluon Plasma (QGP) itself so that they experience the full plasma evolution. One of the main observable in HQs sector is the nuclear suppression factor R_{AA} which is defined as the ratio between the spectra of heavy flavour hadrons measured in nucleus-nucleus collisions with the same spectra in proton-proton collisions [1,2]. Another set of key observables are the anisotropic flows that are characterized by the magnitude of the coefficient v_n in the free expansion of the azimuthal particle distribution [3,4]. We have developed an event-by-event transport approach that incorporates initial state fluctuations to study the nuclear modification factor and the collective flows in Pb + Pb collisions of D and B mesons. Furthermore, we evaluate these observables also for electrons from semi-leptonic B meson decay which can be compared to the available experimental data by ALICE collaboration. A quantitative information on HQ interaction is obtained via the spatial diffusion coefficient $D_s = T/(M\gamma(p\to 0))$ where γ is the drag coefficient of the HQ being related to the thermalization time $\tau_{th} = 1/\gamma(p\to 0)$ [5]. The D_s measures the space dispersion and it can be also evaluated in lQCD in the zero momentum limit. The extension of the study to the bottom quark allows to investigate the mass dependence of the D_s in our QPM approach toward the infinite mass limit assumed in the main lQCD calculations. Indeed, in order to have a proper comparison to the lQCD calculations, we study the $D_s(T)$ coefficient for a fictitious super heavy quark staying in the limit fulfilled by lQCD data.

MODEL DESCRIPTION

In order to describe both the bulk and HQs evolution in the QGP, we solve relativistic Boltzmann equations developed to perform studies of the dynamics of heavy-ion collisions [7-9]:

$$\left\{p_k^\mu \partial_\mu + m^*(x)\partial_\mu m^*(x)\partial_p^\mu\right\} f_k(x, p_k) = C[f_{q'}, f_g](x, p_k)$$

$$p^\mu \partial_\mu f_Q(x, p) = C[f_{q'}, f_g, f_Q](x, p)$$

where $C[f_{q'}, f_g, f_Q](x, p)$ is the relativistic Boltzmann-like collision integral and $f_k(x, p)$ is the on-shell phase space one-body distribution function of the k parton. The non-perturbative effects in HQs scattering are taken into account evaluating the collision integral within a quasi-particle model (QPM) which can reproduce the lQCD equation of state [10]. In our approach, the collision integral is gauged to viscous hydrodynamics allowing to construct a relativistic transport approach at fixed $\eta/s \approx 0.1$ [11]. For what concerns the hadronization of quarks, we use an hybrid model based on the coalescence and fragmentation

processes [12] that determines the final particle spectra and, consequently, $R_{AA}(p_T)$ and $v_n(p_T)$.

RESULTS

We find that QPM approach is able to correctly predict the first available data on $R_{AA}(p_T)$ of single-electron from semi-leptonic B decays shown in Fig.1. More details can be found in Ref.[13] where we also show our results for elliptic flow $v_2(p_T)$ and $v_3(p_T)$ at top LHC energies. We have extrapolated the spatial diffusion coefficient $D_s(T)$ of HQs that we compare to lQCD calculation in Fig.2.

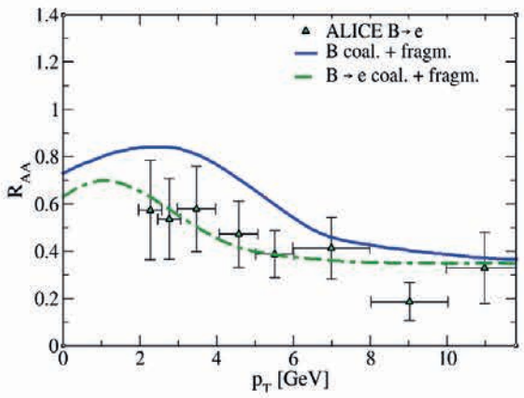

Fig1. Nuclear modification factor for B mesons and electrons from B mesons decay in PbPb collisions at top LHC energy for 0-10% centrality class. Data taken from Ref. [14].

Furthermore, we have also evaluated the spatial diffusion coefficient for a fictitious super-heavy quark ($M \approx 15\ GeV$) staying in the limit in which the thermalization time scales as M/T, a limit which is not yet reached in the charm mass scale and fulfilled in the bottom mass scale with a discrepancy of about 20%.

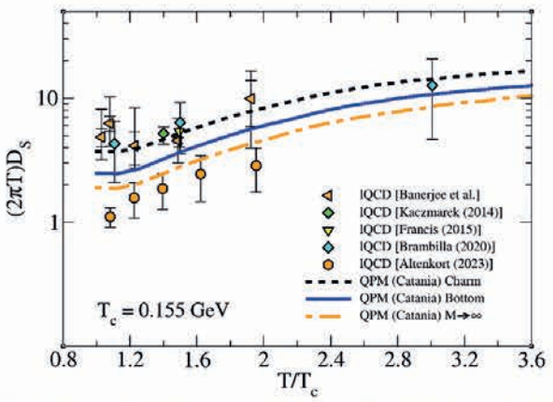

Fig2. Spatial diffusion coefficient D_s of charm, bottom and infinite mass limit for HQs.

In Fig.2, we show that the D_s in this limit (orange dot-dashed curve) is in good agreement to the new lQCD calculations which are the more pertinent one to compare to, because they include dynamical fermions differently from previous calculations (until 2020) which are for a quenched medium. For more details about the $D_s(T)$ in the infinite mass limit, see ref. [13].

CONCLUSIONS

We have discussed the HQs propagation in the QGP at top LHC energies within a relativistic event-by-event Boltzmann transport approach including non-perturbative effects of interaction by means of QPM. The extension to the bottom quark dynamics leads to a good agreement between our results of $R_{AA}(p_T)$ for electrons from B meson decay with the available experimental data by ALICE collaboration. We have also discussed the mass dependence of $D_s(T)$ in QPM in order to have a proper comparison to lQCD data evaluated in the infinite mass limit. We find that our calculation of $D_s(T)$ for a super-heavy quark staying in this limit is in agreement with the recent lQCD calculations which include dynamical fermions.

REFERENCES

[1] B.I. Abelev, et al., Phys. Rev. Lett. 98, 192301 (2007).
[2] J. Adam, et al., JHEP 03, 081 (2016).
[3] A. Adare, et al., Phys. Rev. Lett. 98, 172301 (2007).
[4] B.B. Abelev, et al., Phys. Rev. C90(3), 034904 (2014).
[5] F. Scardina, S. K. Das, V. Minissale, S. Plumari and V. Greco, Phys.Rev.C 96 (2017) 4,044905.
[6] M. L. Sambataro, Y. Sun, V. Minissale, S. Plumari, and V. Greco, Eur. Phys. J. C 82, 833 (2022),2206.03160
[7] S. K. Das, F. Scardina, S. Plumari, and V. Greco, Phys. Lett. B 747, 260 (2015).
[8] M. L. Sambataro, S. Plumari, V. Greco, Eur.Phys.J.C 80 (2020) 12, 1140.
[9] M. Ruggieri et al., Phys. Rev. C 92, 064904 (2015).
[10] S. Plumari,W. M. Alberico, V. Greco and C. Ratti, Phys. Rev. D 84, 094004 (2011).
[11] S. Plumari, G. L. Guardo, F. Scardina, V. Greco, Phys.Rev.C 92 (2015) 5, 054902.
[12] S. Plumari, V. Minissale, S.K. Das, G. Coci and V. Greco, Eur.Phys.J.C 78 (2018) 4,348.
[13]M. L. Sambataro, V. Minissale, S. Plumari and V. Greco, Phys. Lett. B 849 (2024), 138480
[14]S. Acharya et al. [ALICE], Phys. Rev. C 108 (2023) no.3, 034906

Dynamical attractors in Full Relativistic Boltzmann approach in boost-invariant and non-boost-invariant conformal systems

V. Nugara[1,2], S. Plumari[1,2], L. Oliva[1,3], V. Greco[1,2]

1) Department of Physics and Astronomy "E. Majorana", University of Catania, Via S. Sofia 64, I-95123 Catania, Italy
2) Laboratori Nazionali del Sud, INFN-LNS, Via S. Sofia 62, I-95123 Catania, Italy
3) INFN Sezione di Catania, Via S. Sofia 64, I-95123 Catania, Italy

Abstract - We study the universal behaviour associated with a Relativistic Boltzmann Transport (RBT) approach with the full collision integral in 0+1D conformal systems. We show that all momentum moments of the distribution function exhibit universal behaviour if plotted with respect to τ/τ_{eq}, with $\tau_{eq}^{-1} \propto$ collision rate. For the first time, we extend this analysis also to study the attractor behaviour under a temperature-dependent viscosity $\eta/s\,(T)$, accounting also for the rapid increase toward the hadronic phase, which a more realistic assumption with respect to the widely-used constant η/s. We find that a partial breaking of the scaling behaviour with respect to τ/τ_{eq} emerges only at $T \sim T_c$ generating a transient deviation from attractors; interestingly this in realistic finite systems may occur around the freeze-out dynamics. Finally, we investigate for the first time results beyond the boost-invariant picture, finding that also in such a case the system evolves toward the universal attractor. In particular, we present the forward and pull-back attractors at different space-time rapidities including rapidity regions where initially the distribution function is zero.

INTRODUCTION

Relativistic heavy-ion collisions (uRHICs) are a unique laboratory for probing the fundamental properties of nuclear matter under extreme conditions, studying the formation and evolution of the Quark-Gluon Plasma (QGP). The dynamics of this deconfined state of strongly interacting matter created in uRHICs can be successfully described by means of both macroscopic hydrodynamics theories and kinetic theory. This is remarkable considering that the early stage of the collision is highly anisotropic and out of equilibrium and therefore in a regime beyond the expected applicability of hydrodynamics. In recent years also small systems, such as proton-proton (pp) and proton-nucleus collisions (pA), have attracted great attention, since a collective behavior like that observed in heavy-ion collisions has been found also in high-multiplicity events of small colliding systems, rising the question of the possible formation of QGP [1]. Even more unexpectedly, the hydrodynamic model has been successful in describing collective observables in such small systems, which are thought to remain out of equilibrium throughout their dynamical evolution [2]. Therefore, the comprehension of the thermalization mechanisms and timescales of systems which are far from equilibrium is of fundamental importance in the context of uRHICs and even more in the case of small collision systems. This has led to recent advances in the theoretical framework, bringing to light a striking phenomenon: the emergence of universal behaviour in the context of relativistic hydrodynamics, kinetic theory, classical Yang-Mills equations as well as in AdS/CFT calculations [3-7]. Indeed, the far-from-equilibrium evolution of macroscopic quantities, irrespective of the initial conditions, exhibit universal scaling, denoted as non-equilibrium attractors, endowed with the noteworthy ability to capture the long-term collective behaviour of the fluid system. We have looked for attractors by means of simulations with the full Relativistic Boltzmann Transport (RBT) approach with different values of the shear viscosity over entropy density ratio η/s, as well as different initial conditions (temperature, initial proper time τ_0, pressure anisotropy). All previous studies have shown the existence of attractors in the case of longitudinal boost-invariant expansion for a system evolving with fixed η/s.

MODEL DESCRIPTION

In our approach we describe QGP matter with an on-shell one-particle distribution function $f(x,p)$, whose space-time evolution is governed by RBT equation:

$$p^\mu \partial_\mu f(x,p) = C[f(x,p)]$$

where $C[f(x,p)]$ is the full collision integral. Numerically, the RBT eq. is solved by discretizing the space-time in cells and using the so-called test particle method, while the collision integral is implemented by using the stochastic algorithm [8]. Moreover, we fix locally the cross section in order to have a fixed η/s to properly compare to hydro [9]. In our approach, we only consider elastic $2 \leftrightarrow 2$ collisions, therefore the number of particles is conserved, so that the system fugacity $\Gamma(\tau) \neq 1$. We define locally an effective temperature and fugacity via the matching conditions:

$$T = \varepsilon/3n;\ \ \Gamma = n/(T^3/\pi\text{^}2)$$

where the energy density ε is the largest eigenvalue of the energy-momentum tensor $T^{\mu\nu}$ and $n = n^\mu u_\mu$, n^μ being the four-current and u^μ the fluid flux. We look for attractors by analysing at midrapidity ($|\eta_s| < 0.1$) the distribution function moments:

$$M^{nm}(x,p) = \int dP\ (p\cdot u)^n (p\cdot z)^{2m} f(x,p).$$

In order to quantify the approach to the equilibrium distribution function $f_{eq} = \Gamma e^{-p\cdot u/T}$ we study the normalised moments $\bar{M}^{nm} = M^{nm}/M_{eq}^{nm}$, where

$$M_{eq}^{nm} = \int dP (p\cdot u)^n (p\cdot z)^{2m} \Gamma\, e^{-p\cdot u/T}$$

As a first study, we consider a one-dimensional expansion by implementing periodic boundary conditions in the transverse plane in the conformal ($m = 0$) case and choose an initial interval $[-\eta_s, \eta_s]$ for the distribution function large enough to ensure boost-invariance.

RESULTS

Our results are in very good agreement with those obtained by other models [4, 10]. When plotted with respect to the scaled time, normalised moments show attractors either if we change the initial ratio P_L/P_T (forward attractor) or the initial scaled time $\tau_0 T_0/(\eta/s)$, converging towards an universal curve, obtained by considering the limits $P_L/P_T \to 0$ and $\tau_0 T_0/(\eta/s) \to 0$. The attractor is reached at quite early times, after a strong initial longitudinal expansion, which is primarily responsible for the system to lose memory about its initial conditions.

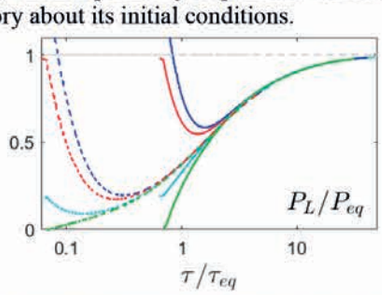

Figure 1: Different colours refer to different initial anisotropies, different line styles to different initial proper time $\tau_0 T_0/(\eta/s)$.

As far as the boost-invariance breaking is concerned, for the first time we show that attractors are not a consequence of this strong symmetric condition. We decide to break boost-invariance with a finite initial distribution in space-time rapidity η_s and look for results at finite η_s: as you can see in the figure below, the attractor is nonetheless reached, regardless of the η_s values.

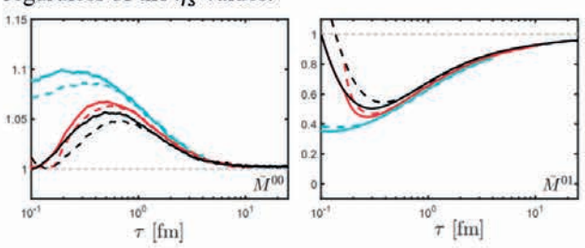

Figure 2: Different colours refer to different space-time rapidities η_s, different line styles to different initial anisotropies.

Finally, for the first time we consider a more realistic case in which the η/s is temperature dependent. We consider different cases in which, approaching the critical temperature, the system undergoes a freeze-out, with η/s suddenly rising. We see that the scaling is still present, even though at intermediate values of the scaled time, we notice an interesting departure from the universal behaviour. At $\tau/\tau_{eq} \sim 4-5$ a small loop is present in the moments calculated, with η/s that increases at lower temperatures right below the critical value. This region in scaled time corresponds to the temperature region in which η/s increases so that τ/τ_{eq} is no more a monotonic function of the proper time. This depends on the specific dependence of $T(\tau)$ and $\eta/s\ (T)$: the steeper the $\eta/s\ (T)$ curve, the more pronounced the loop. For instance in the figure below the red curve is related to a steeper $\eta/s\ (T)$.

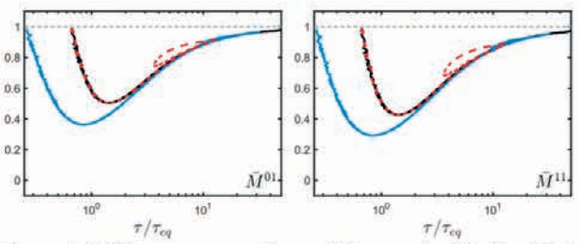

Figure 3: Different curves refer to different $\eta/s\ (T)$. The black one is for $\eta/s = 1/4\pi$, the red and blue have, respectively, a stronger and weaker temperature dependence.

CONCLUSIONS

For the first case we have demonstrated that the resulting solutions of RBT converge to a unique attractor even though the system is out of chemical equilibrium ($\Gamma \neq 1$) with two interesting extensions. On one hand, we find that a universal behaviour is observed in the momentum moments of the phase-space distribution function also when the longitudinal boost invariance is broken. On the other hand the attractor is reached nonetheless in the more realistic case of a T- dependent η/s , even though the real impact of such a dependence could be fully evaluated only in a 3+1D non-conformal ($m \neq 0$) simulation.

REFERENCES

[1] L. Yan and J.-Y. Ollitrault, Phys. Rev. Lett. 112, 082301 (2014)

[2] L. Oliva, W. Fan, P. Moreau, S. A. Bass, and E. Bratkovskaya, Phys. Rev. C 106, 044910 (2022)

[3] M. Strickland, J. Noronha, and G. Denicol, Phys. Rev. D 97, 036020 (2018)

[4] M. Strickland, JHEP 12, 128 (2018)

[5] D. Almaalol, M. Alqahtani, and M. Strickland, Phys. Rev. C 99, 014903 (2019)

[6] J.-P. Blaizot and L. Yan, Annals Phys. 412, 167993 (2020)

[7] M. P. Heller, R. Jefferson, M. Spalinski, and V. Svensson, Phys. Rev. Lett. 125, 132301 (2020)

[8] Z. Xu and C. Greiner, Phys. Rev. C 71, 064901 (2005)

[9] G. Ferini, M. Colonna, M. Di Toro, and V. Greco, Phys. Lett. B 670, 325 (2009)

[10] M. Strickland and U. Tantary, JHEP 10, 069 (2019), 1903.

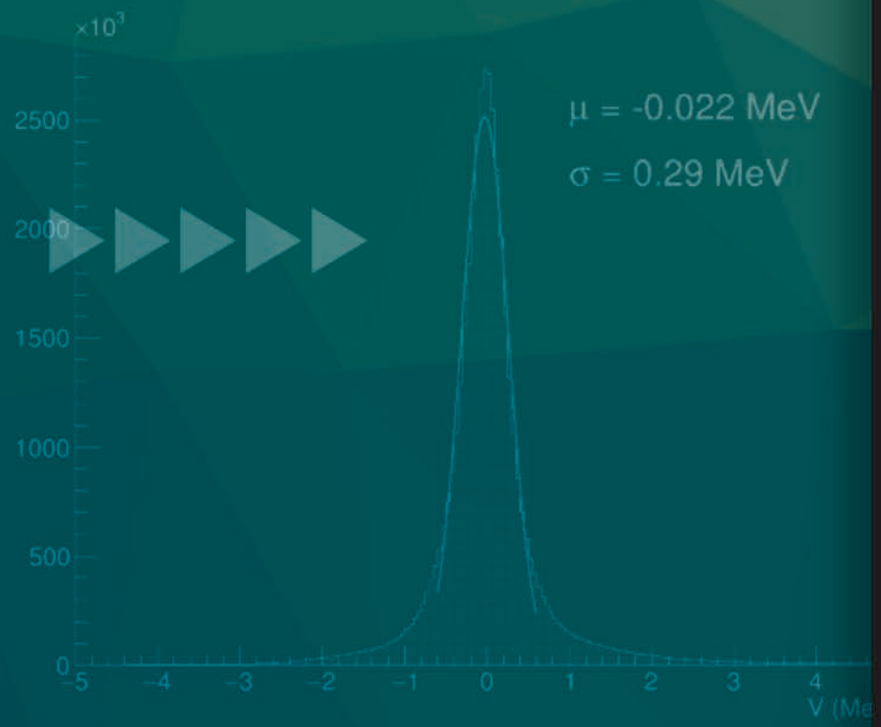

04

INSTRUMENTATION AND RELATED TECHNIQUES

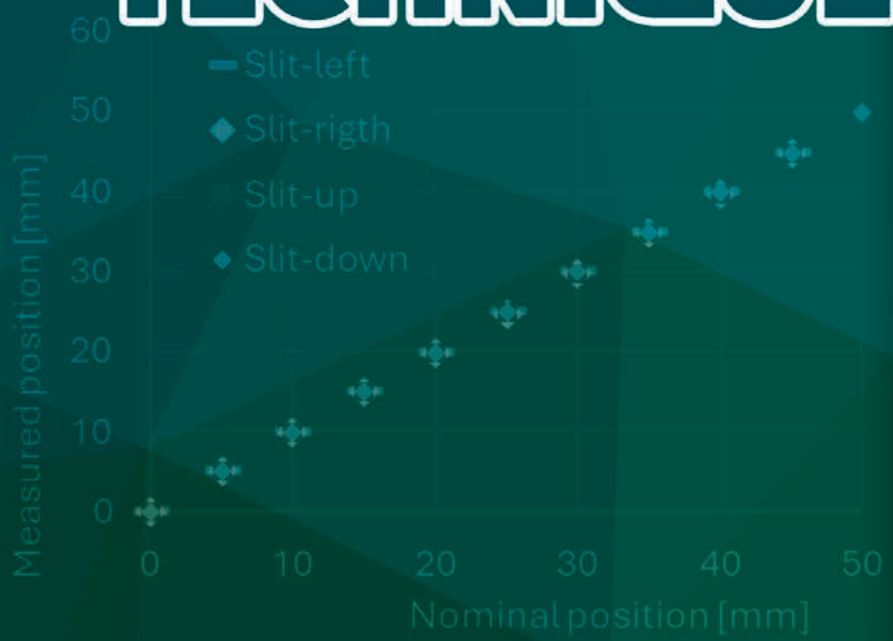

Research

Analyses

Results

INFN LNS

- Development of Silicon Carbide detectors for Radioactive Ion Beams Facilities
- The slits chamber of the NUMEN experiment
- Characterization of G-NUMEN array under high detection rates
- Prototype of the PID system for the MAGNEX spectrometer within the NUMEN project
- The new data acquisition system for the CLAD Si telescope array
- System for beam control and transport within the I-LUCE facility
- Latest results of the pixelation technique applied to the data collected by the FARCOS correlator in the CHIFAR experiment
- Data acquisition and software developments at INFN-LNS for the AsyEos-II experiment at GSI/FAIR
- News on NArCoS (Neutron Array for Correlation Studies): the new correlator for neutrons and light charged particles at LNS
- Geant4 simulations to study the cross-talk probability and efficiency for the neutron correlator NArCoS
- Calibration of FARCOS DSSSD by front and back strips comparison
- New MAGNEX digital electronics: development of on-board coincidences

Development of Silicon Carbide detectors for Radioactive Ion Beams Facilities

N.S. Martorana[1], L. Acosta[2,3], C. Altana[4], A. Barbon[1,5], G. Cardella[1], A. Castoldi[6], G. D'Agata[1,5], E. De Filippo [1], S. De Luca[4], E. Geraci [1,5,7], B. Gnoffo[1,5], N. Giudice[1], C. Guazzoni[6], L. Quattrocchi[1,8], C. Maiolino[4], C. Manna[4], E.V. Pagano[4], S. Pirrone[1], G. Politi [1,5], F. Risitano[1,8], F. Rizzo[4,5,7], P. Russotto[4], G. Sapienza[4], M. Trimarchi[1,8], S. Tudisco[4], C. Zagami [4,5,7]

1) INFN-Sezione di Catania, Catania, Italy
2) Instituto de Fìsica, Universidad Nacional Autònoma de México, Mexico City, Mexico
3) Instituto de Estructura de la Materia, CSIC, Spain
4) INFN-LNS, Catania, Italy
5) Dipartimento di Fisica e Astronomia "Ettore Majorana", Università degli Studi di Catania, Catania, Italy
6) DEIB Politecnico Milano and INFN Sez. Milano, Milano, Italy
7) CSFNSM, Catania, Italy
8) Dipartimento MIFT, Università di Messina, Messina, Italy

Abstract - Radioactive Ion Beams (RIBs) play a pivotal role in advancing nuclear physics research, as they allow for investigating nuclear matter and nuclei far from the stability valley. Furthermore, the interdisciplinary nature of RIBs research has potential impact also on medical physics, especially in the case of hadron therapy technique. This renders RIBs facilities essential drivers for enhancing our understanding in both nuclear physics and medical applications. Within this framework, there is a notable interest in employing Silicon Carbide (SiC) technology as tagging and diagnostics detection systems in facilities delivering high-intensity RIBs. SiC based detectors indeed offer numerous potential advantages over other detection systems, like those based on silicon detectors. In this framework, an array of SiC detectors is being developed, also thanks to the SAMOTHRACE (Sicilian Micro and Nano Technology Research and Innovation Center) ecosystem. This report outlines some recent results obtained in the characterization of SiC prototypes at INFN-LNS.

INTRODUCTION

Nowadays, the interest in Silicon Carbide (SiC) technology, for the detection of charged particles, neutrons and also radiations such as γ/X rays, is growing fast thanks to the important properties of this wide band gap semiconductor. SiC material presents several features that render it advantageous with respect to other semiconductors as silicon and diamonds, making it interesting for the nuclear and medical research [1,2]. The advances in SiC fabrication techniques have reached a good degree of accuracy and this decrees Silicon Carbide a very good compromise with respect to the maturity in the device fabrication of silicon detectors and the radiation hardness of diamond ones [3]. Furthermore, due to the fact that experiments with high-intensity stable and unstable beams are currently one of the most important tools for the future of nuclear physics [3], allowing the investigation of low cross section reactions and of nuclei far from the stability valley, the radiation hardness of SiC is one of the most intriguing features of this material. Another important aspect concerning Silicon Carbide detectors is the possibility to employ fast-timing techniques [1]. This possibility becomes relevant in the case of RIBs production with the in-flight method. An issue with the in-flight technique is that the beam energy resolution is ≈ 1 MeV/A for beam such as carbon ≈ 50 MeV/A. To obtain a higher energy resolution, the timing information can be used, measuring the Time of Flight (ToF) over a long base of flight. Overall, the fast timing technique in RIBs experiments involves the integration of specialized detectors and electronics front-end. In this context, a work to develop a SiC detection system has been made and it is still ongoing. This work is made possible also thanks to the SAMOTHRACE ecosystem [4,5]. The SiC detection system was mainly conceived to operate as a tagging device for the CHIMERA multidetector beamline, in conjunction with the FraISe (Fragment In-Flight Separator) facility at INFN-LNS, still under construction phase, designed to provide high-intensity RIBs [6,7]. This system will be very useful, allowing to perform studies with high-intensity RIBs for both nuclear and medical investigations [6-8]. The system will be composed by a 2D array of several SiC detectors; it needs to be: radiation hard and able to sustain several experiments per year; compact and versatile, in order to ease the transport and setting-up; able to provide the spatial distribution of the ions, the energy loss (ΔE) of ions passing through the detection system and the time of flight between two SiC detection systems or with respect to a reference time signal, in order to provide particle identification via ΔE-ToF identification technique [5]. A key feature of this detection system will be its high timing

performance (≈100 ps), offering, as mentioned above, significant advantages in experiments with RIBs. To fully satisfy this requirement, the detection system will be coupled with a fast electronics front-end, specifically designed and implemented at the Politecnico and Sezione INFN di Milano [9]. In the following, some results obtained at SICILIA laboratory of INFN-LNS are discussed.

TESTS WITH RADIOACTIVE SOURCES

The focus of the below discussed activity was the characterization and optimization of a first 2x2 pads monolithic SiC detector's (100 μm thick–1 cm^2 surface) performance in terms of energy and timing resolution, maximizing the signal-to-noise ratio. Additional work is being done to gain a thorough understanding of potential inter-pad, cross-talk and edge effects. The investigations have been performed at the SICILIA laboratory of INFN-LNS. In detail, a ^{148}Gd and a mixed nuclide α sources (Am, Pu, Cm) have been used to perform these tests. This first prototype has been glued, using a conductive glue, on a PCB in a transmission mode, in order to evaluate also the rear dead thickness, injecting the particles from the back side. For such tests, a Mesytec preamplifier, MPR 16 channels, and a CAEN digitizer 1 GHz, 14 Bit have been used. Figure 1 (left) shows the calibrated energy spectrum, obtained for one SiC pad. Performing Gaussian fits on these peaks, an energy resolution of ≈60 KeV has been obtained. Figure 1 (right) shows the energy vs. rise-time plot for the same pad: some events with a higher rise time and a lower energy, indicated as region 2 in Figure 1 (right), are present. A data analysis to characterize the origin of these events was performed, with the intent to understand if cross-talk, inter-pad or edge effects were present. 99 % of events shown in Figures 1 (left) and (right) are associated with multiplicity=1, while a lower percentage is due to events with multiplicity=2. Furthermore, plotting the energy of one pad versus the energy of another pad, and considering events with multiplicity=2, the events are not distributed in a diagonal region supporting the idea that no inter-pad effects are observed within the accumulated statistics. However, due to the poor accumulated data statistics it is not possible to draw definite conclusions about the presence or absence of inter-pad effects; consequently, further tests are ongoing.

The events in region 2 can be then due to an edge effect or a worst charge collection in the edge region of the SiC pad. Further checks improving the statistics and using collimators are ongoing to confirm these results. In the near future a comparison with another detector, preferably a silicon one, with similar capacity, will be performed. Additionally, active efforts are underway to improve the signal-to-noise ratio and digitalization, particularly through optimization of filters used to extract the energy spectrum, in order to achieve a better energy resolution. α sources will be used for extended acquisition periods to increase statistics, and a micro beam will be employed to fully scan the SiC detector in terms of both surface and thickness at the LABEC laboratory (INFN e Dipartimento di Fisica e Astronomia, Università di Firenze). This test will allow to test also the fast-electronics front end implemented at the Politecnico and Sezione INFN di Milano. Overall, some tests with beams have been already performed at INFN-LNL and at the GSI laboratory, to test the stability of the detectors coupled with two different electronics front-end. Data analysis of the two experiments is still ongoing.

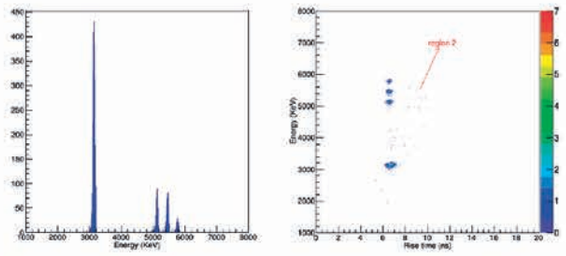

Figure 1: (left) Energy spectrum obtained for a SiC pad; (right) energy vs rise time plot obtained for one pad. No conditions on the multiplicity have been inserted in these plots.

CONCLUSIONS AND PERSPECTIVES

In this report, some results for the development of SiC detectors, specifically performed also thanks to the SAMOTHRACE ecosystem, have been discussed. The current work and next steps are focused on a deeper understanding of the first SiC prototypes, with the main aim to optimize the detectors response and to fully characterize this response when coupled with a fast-frontend electronics.

REFERENCES

[1] De Napoli M., Front. in Phys. 10:898833, (2022).
[2] Tudisco S. et al., Sensors, 18 (2018).
[3] Agodi, C. et al., Eur. Phys. J. Plus 138, 1038 (2023) and refs therein.
[4] Martorana N.S. et al, contribution to this report.
[5] https://samothrace.eu/.
[6] Martorana N. S. et al., Front. in Phys., 10 (2022) and refs therein.
[7] P. Russotto et al., J. Phys.: Conf. Ser. 1014 012016 (2018) and refs therein.
[8] M. Durante and K. Parodi, Frontiers in Physics 8:326 (2020).
[9] A. Castoldi et al., IEEE Trans. Nucl. Sci., VOL. 70, NO. 7, JULY 2023, pp. 1431-1435.

The slits chamber of the NUMEN experiment

D. Calvo[1], D. Sartirana[1], R. Panero[1], S. Brasolin[1], C. Ferraresi[2], G. Grossi[2], F. Cappuzzello[3,4], M. Cavallaro[3], M. Fisichella[3] for the NUMEN Collaboration

1) INFN - Sezione di Torino, Italy
2)DIMEAS, Politecnico di Torino, Italy
3) INFN, Laboratori Nazionali del Sud, Catania, Italy
4) Dipartimento di Fisica e Astronomia 'Ettore Majorana', Universita' di Catania, Italy

Abstract – In the NUMEN experiment [1], the upgrade of the MAGNEX to withstand the high intensity ion beams at the Laboratori Nazionali del Sud of INFN requires a new design of upstream part of the magnetic line of the spectrometer.

In particular a new slits system is set up to control the ejectiles acceptance of the spectrometer downstream the target.

INTRODUCTION

The MAGNEX spectrometer [2] is characterized by a large angular and momentum acceptance and consists of two large apertures magnets, a quadrupole and a dipole, and a focal plane detector for the ejectiles detection. The ion beam hit the target positioned inside the scattering chamber (460 mm of external diameter) and the emitted ions will enter in the spectrometer. Between the scattering chamber and the quadrupole, a slit system analyses and shapes the ejectiles cone towards the spectrometer.

Since the gamma-ray spectrometer G-NUMEN will be installed around the scattering chamber and the quadrupole shield is positioned between the chamber and the quadrupole, an extremely limited space is available for the slit chamber along the direction of the ion beam [3].

Besides the chamber houses a pepper-pot whose purpose is to select ion trajectories for calibrating the focal plane detector.

All these requests suggested studying a custom solution that will be described in the next paragraph. Some results of the characterization of the built system will follow.

THE SLITS CHAMBER

The complete system consists of a small cylindrical vacuum chamber made of stainless steel AISI 316LN installed along the beam pipe and featuring the following size: 122 mm length, 225 mm in diameter.

Four rectangular plates, the slits, and a pepper-pot can be moved individually along the direction orthogonal to the beam.

The chamber presents four rectangular holes for connecting four stainless steel pockets. Three of them allow to retract a plate each beyond the internal radius of the chamber, in a position defined as 'out of beam'. The fourth one, in the bottom position, allows to retract the remaining plate and the pepper-pot. Figure 1 shows the chamber model and the chamber surrounded by the detectors for the gamma rays, in between the scattering chamber and the quadrupole shield.

Each plate, the pepper-pot as well, is moved with a motorized linear push/pull actuator (provided by the VACGEN company) featuring a 100 mm stroke and 0.02 mm resolution. The position feedback is obtained by a magnetic absolute encoder with a closed loop control and limit switches implement the safety interval of the system. The actuator is equipped with a stepper motor (provided by the Mclennan company. Vacuum-tight feedthroughs guarantee a high vacuum level inside the chamber.

The control unit is a SIM-STEP integrated controller (from Mclennan company) equipped with a graphical interface for the user who can enter the software limits of the stroke and set the position of the slit using the conversion to the stepper motor.

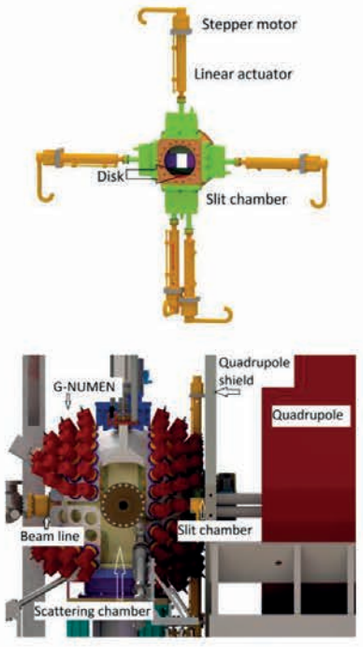

Figure 1: 3D model of the slit chamber alone and integrated in between the scattering chamber and the quadrupole shield.

Each slit and the pepper-pot move by sliding along two guides which also guarantee perpendicularity to the direction of the beam.

The two slits which move along the vertical direction feature 72 mm high and 92 mm wide. They can model the ejectiles acceptance of the spectrometer vertically up to ± 7.5°.

The horizontal slits feature 66 mm high and 96 mm wide. They can model the ejectiles acceptance of the spectrometer horizontally up to ± 6.5°.

They are made of tantalum and the thickness is 3 mm.

Each plate is electrically insulated by boron nitride spacer and plastic screw, the thermal contact is assured anyway. A wire connected to each slit allows for current measurement of the ions impinging on the plate, also useful during the beam tuning in the commissioning phase. Figure 2 shows a slit and its support system.

The pepper-pot is made of tantalum and shows a surface with a hole matrix (5 rows x 13 columns). It is 110 mm high and 92 mm wide, the diameter of each hole is 1.5 mm.

The tantalum material limits neutron production from light ion interaction and guarantees high temperature tolerance.

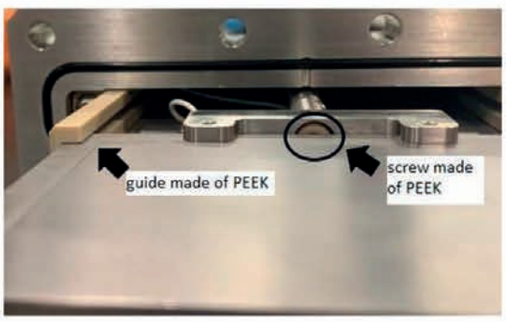

Figure 2: Picture of a tantalum slit and one of its two guides. A mechanical system grips the slit and it is connected to the stem of the linear driver with a screw made of PEEK. A spacer made of boron nitride is interposed.

Considering a $^{18}O^{7+}$ beam featuring $2.7x10^{13}$ pps at 0° angle, the expected number of particles stopped in each slit, positioned to have the maximum acceptance to the spectrometer, will not be higher than $2x10^{8}$/s. The value is obtained from simulations where the main contribution is due to the Rutherford's scattering. The corresponding generated power is less than 100 mW. Particles number more than one order of magnitude higher is expected to hit the slit system when MAGNEX is rotated of +3° with respect to the beam line, resulting in a power less than 1 W that can be dissipated with a metallic contact [1].

The slit chamber houses an additional tantalum disk positioned on the side furthest from the target and 374 mm away from it. The disk has a rectangular opening of 99 mm x 86 mm which respect the larger angular acceptance of the spectrometer helping to intercept ion trajectories that would increase the background of the detectors.

RESULTS OF CHARACTERIZATION

Dimensional measurements were done on each component of the chamber using the POLI-Galaxy Maxy measurement machine (INFN-Torino) featuring a precision of ± 6 μm.

The dimensional analysis of all the components confirms tolerances required in executive drawings.

The system has been studied in the complete assembly in working like condition and a position calibration was done for each slit. The position of the internal edge of each slit is measured with steps of 5 mm along the total working stroke of the actuator. The results are reported in Figure 3, the points are near overlapping, a linear regression returns a value of R^2 equal to 1 for each slit.

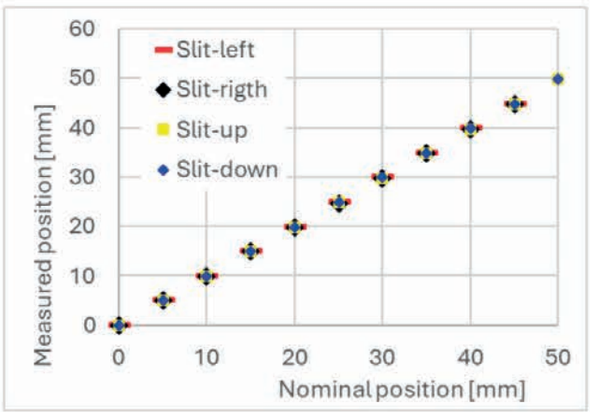

Figure 3: Position calibrations of the slits. The points of the four slits are near overlapping.

These measurements were repeated in order to evaluate repeatability of the positioning that was found within the precision of the measuring machine.

Besides for each position inside the maximum spectrometer acceptance the parallelism (and orthogonality) of each slit edge with respect a reference plane was measured to be less than 100 μm.

The pepper-pot presents a parallelism of 100 μm in its final position, when it is completely inserted into the chamber.

REFERENCES

[1] F. Cappuzzello et al., Eur. Phys. J. A 54 (2018) 72.
[2] P. Finocchiaro at al., Universe (2020), 6, 129.
[3] D. Calvo et al., Nucl. Instr. and Method in Physics Research A, 1041 (2022), 167336

Characterization of G-NUMEN array under high detection rates

E.M. Gandolfo[1], J.R.B. Oliveira[2], L. Campajola[3], D. Pierroutsakou[3], A. Boiano[3], C. Agodi[4], F. Cappuzzello[4,5], D. Carbone[4], M. Cavallaro[4], I. Ciraldo[4], D. Calvo[6], F. Delaunay[4,5,7], C. Eke[8], F. Longhitano[9], N. Medina[10], M. Moralles[10], D. Sartirana[6], V.R. Sharma[11], A. Spatafora[4], D. Toufen[12], P. Finocchiaro[4] for the NUMEN collaboration

1) GSI – Helmholtzzentrum fur Schwerionenforschung GmbH, Darmstadt, Germany;
2) Instituto de Física, Universidade de São Paulo, São Paulo 05508-070, SP, Brazil;
3) INFN—Sezione di Napoli, 80126 Napoli, Italy;
4) INFN—Laboratori Nazionali del Sud, 95123 Catania, Italy;
5)Department of Physics and Astronomy "Ettore Majorana", University of Catania, 95124 Catani, Italy;
6) INFN—Sezione di Torino, 10125 Torino, Italy;
7)LPC Caen UMR 6534, Université de Caen Normandie, ENSICAEN, CNRS/IN2P3, F-14000 Caen, France;
8)Department of Mathematics and Science Education, Faculty of Education, Akdeniz University,07058 Antalya, Turkey;
9) INFN—Sezione di Catania, 95125 Catania, Italy;
10) Instituto de Pesquisas Energéticas e Nucleares, IPEN/CNEN, São Paulo 05508-000, SP, Brazil;
11) Department of Radiation Oncology, University of Maryland, Baltimore, MD 21201, USA;
12) Federal Institute of Education, Science and Technology of São Paulo, Guarulhos 07115-000, SP, Brazil.

Abstract - G-NUMEN is the spectrometer for the NUMEN experiment, made of over 100 LaBr3:Ce scintillators, placed around the object point of the MAGNEX magnetic spectrometer. G-NUMEN aims at discriminating the Double Charge Exchange (DCE) reaction events, object of study for the NUMEN experiment, by performing a time coincidence between the gamma rays emitted in the de-excitation process of the excited states populated via DCE channel, and the ejectiles detected by the Focal Plane Detector (FPD) of MAGNEX. As the cross section of the DCE reaction is only a few nb, several order of magnitude lower than the competing channels, the G-NUMEN array is expected to operate under harsh experimental environment characterized by high detection rate up to 300 kHz. This work presents the first characterization of the gamma array performance in the extreme operational conditions foreseen.

MOTIVATIONS

The NUMEN experiment aims at obtaining information on the Nuclear Matrix Element (NME) of the neutrinoless double-beta decay using Double Charge Exchange reactions as a probe mechanism [1,2]. Typical reactions of interest for NUMEN involve isotopes which are expected to decay via neutrinoless double-beta decay as targets such as ^{76}Ge, ^{82}Se, ^{110}Pd, ^{124}Sn, ^{116}Cd, and heavy ion beams of $^{18}O^{8+}$ and $^{20}Ne^{10+}$ at energies up to 60 AMeV. In these reactions, several competing channels can be triggered, such as multi-nucleon transfer, single charge exchange, elastic and inelastic channels and so on [3-5]. All these reactions contribute to the intense background over which the DCE events need to be distinguished. In order to do so, NUMEN requires a high-performance detection apparatus with a high sensitivity and resolution and excellent discrimination capabilities [6]. The apparatus is composed by 1) the MAGNEX spectrometer and its Focal Plane Detector, and 2) the G-NUMEN array. The latter is needed in particular in studies involving high-energy beams and deformed target nuclei, for which a time coincidence between the two apparatus systems is essential to identify the nearby states of the residual nuclei of DCE channels, which would be otherwise unresolved. The demands for the G-NUMEN array are very strict: time resolution of a few ns to distinguish subsequent beam bunches (30-50 ns) and reject the intense background, high energy resolution of about 10% at 200 keV, to separate the low-excited states of the nuclei under study, resistance to harsh radiation environment. In addition to that, the array has to maintain these performances at the high counting rates expected. While ample literature is available for the characterization of $LaBr_3$(Ce) crystals at low detection rates, more studies are needed to experimentally characterize the crystal at detection rates up to 300 kHz as the ones expected in NUMEN. This work presents the test of the first prototype of the G-NUMEN scintillators, devoted to evaluating its performance and identifying the most suitable electronic system for signal acquisition. We present the results of the characterization of the scintillators using two phototube bases (active and passive) and the comparison with the simulations.

METHODS AND RESULTS

The scintillators consist of a $LaBr_3$(Ce) crystal (38 mm diameter, 50 mm length) optically coupled with a 8-dynode-stage PMT R6231 from Hamamatsu. In order to obtain a global description of the detector response, the parameters such as energy resolution, efficiency, gain and linearity have been evaluated at increasing detection rate

(up to 300 kHz) using different techniques: 1) a MBq ^{137}Ce radioactive source was placed at different distances to vary the counting rate; 2) the detector were exposed to a fusion-evaporation reaction at the ALTO facility of the IJC Laboratory in order to reach high counting rate with a radiation background similar to what expected in NUMEN. These tests were performed at different high voltages V_{PMT} and with both passive (E1198-26 Hamamatsu) and active (EPIC – Model: GW-N-N-N-1-N-0) voltage dividers. The tests showed that, as expected from literature, the passive voltage divider shows larger gain variation with respect to the active type voltage divider. The active-type detector shows an abrupt change in gain variation around 110 kHz while the response of the passive base is smoother [7]. These results are representative of the limitation in counting rate, more restrictive for the active-type voltage divider used in the test. However, within the operational range, the passive type voltage divider shows a stronger dependence of the gain on the rate: the active type is more linear and therefore preferable to the passive type. As an increase in detection rate corresponds also to an increase of anode current I_A of the PMT, it is possible to express the gain of the detectors as a function of I_A: this representation (Figure 1 - left) clearly shows that the abrupt change of the detectors corresponds to an anode current of about 33-38 μA, which can be defined as the limit current I_L i.e. the current after which there is a breakdown of the active base performances. In fact, it is possible to notice a clear degradation of the detector performances after I_L. The energy resolution of the detector can be linked as well to the detector gain: the tests show that a gain of about 0.3 pC/keV is required for a good energy resolution at all energies (Figure 1 – right).

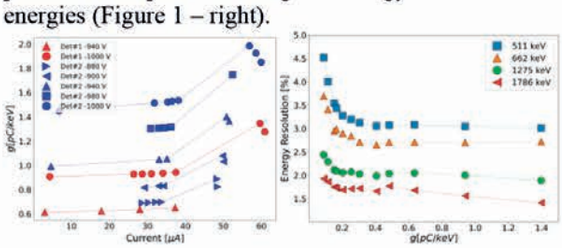

Figure 1 – Left: Active-type detector's gain as a function of the anode current for the. Right: Energy resolution as a function of the gain at different energies.

We developed a simplified modelling of the electronics for the active base voltage divider. For a given V_{PMT}, the limit in current I_L corresponds to the limit in the detection rate at which the detector can operate R_L. It is possible to calculate the approximate model limit in the detection rate as a function of V_{PMT}, the latter proportional to the detector gain. From the analysis of the active base circuit in fact, it is possible to express the limiting current I_L both in terms of V_{PMT} as $I_L \sim I_{VD}/2 = V_{PMT}/(2R_{VD})$ (where I_{VD} and R_{VD} are the equivalent current and resistance of the voltage divider) and in terms of the detection rate limit R_L as $I_L = R_L Q_{av} = R_L g E_{av}$ (where Q_{av} and E_{av} are the average charge and energy of the detector signals). Combining the two expressions for I_L and considering that the gain g and the voltage V are linked through the relation $g = p_0 V^{p1}$ (with p_0 and p_1 fit parameters) [7], it is possible to obtain the expression (1) for the limiting rate R_L of the detector:

$$R_L = \frac{g^{((1/p_1)-1)} p_0^{-(1/p_1)}}{2 E_{av} R_{VD}} \quad (1)$$

Figure 2 shows the calculated value of R_L for different value of R_{VD} according to the model, the experimental data of the active-type voltage divider (R_{VD}= 13 MΩ) and the comparison with the Pspice simulation [7,8] performed for the active-type voltage divider circuit.

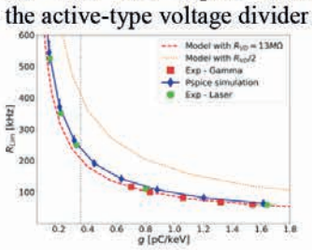

Figure 2 – Limiting rate as a function of the gain calculated with our model (red and orange dashed lines), measured with gamma background (red squared), with a laser (green circles), and simulated (blue points).

DISCUSSION AND CONCLUSIONS

The study presented in this work identify the active-type voltage divider as the best front-end electronic configuration for the G-NUMEN scintillator. However, this work underlines limitations in the anode current which translate into a restriction on the count rate sustainable by the detector R_L. Equation (1) allows for the estimation of R_L showing that a gain of 0.35 pC/keV is sufficient to reach the detection rate expected in NUMEN maintaining a good energy resolution (Figure 2, Figure 1-left), but modification of the voltage divider's resistance are required. The identified gain corresponds to a V_{PMT} in the range 750-850 V [7]. The PSpice simulation of the detector response confirms this behaviour. In conclusion, this work contributed to the global understanding of the array behaviour in the operational condition expected in the NUMEN experiment. It demonstrates that it is possible for the G-NUMEN array to meet the needs of the NUMEN experiment if some modification of the front-end electronics are implemented.

REFERENCES

[1] F. Cappuzzello et al., Front. Astron. Space Sci. (2021), 8, 668587.
[2] F. Cappuzzello et al., Eur. Phys. J. A (2018), 54, 72.
[3] D. Carbone et al., Phys. Rev. C (2020)102, 044606.
[4] M. Cavallaro et al., Front. Astron. Space Sci. (2021), 8, 659815.
[5] A. Spatafora et al., Phys. Rev. C (2019), 100, 034620.
[6] P. Finocchiaro et al., Universe (2020), 6, 129.
[7] E.M. Gandolfo et al., Instruments (2023), 7, 28.
[8] Pspice Model. Online: https://www.pspice.com/

Prototype of the PID system for the MAGNEX spectrometer within the NUMEN project

D. Carbone[1], A. Spatafora[1,2], D. Calvo[3], C. Agodi[1], G.A. Brischetto[1,2], F. Cappuzzello[1,2], M. Cavallaro[1], P. Finocchiaro[1], D. Sartirana[3], O. Sgouros[1], V. Soukeras[1], D. Torresi[1], S. Tudisco[1] for the NUMEN collaboration

1) Istituto Nazionale di Fisica Nucleare, Laboratori Nazionali del Sud, Catania, Italy
2) Dipartimento di Fisica e Astronomia "Ettore Majorana", Università di Catania, Catania, Italy
3) INFN, Sezione di Torino, Torino, Italy

Abstract – The first two towers of the new particle identification system for the focal plane detector of the MAGNEX spectrometer have been constructed. They are composed by SiC-CsI(Tl) telescopes arranged in 20 units. This will be the solution for the particle identification of the ejectiles produced in the reactions studied within the NUMEN project.

INTRODUCTION

The NUMEN project [1-2] is aiming to access experimentally driven information on Nuclear Matrix Elements (NME) involved in the neutrinoless double beta decay (0νββ) by measuring cross sections of heavy-ion induced double charge-exchange reactions. The chosen probes are the (^{18}O,^{18}Ne), (^{20}Ne,^{20}O) and (^{12}C,^{12}Be) reactions. The possibility to accurately measure such cross sections is offered by the INFN–Laboratory Nazionali del Sud (LNS) in Catania through the Superconducting Cyclotron accelerator and the MAGNEX large acceptance magnetic spectrometer. The measured cross sections are very low, limiting the past explorations to few selected isotopes of interest in the context of typically low-yield experimental runs. In order to make feasible a systematic study of all the nuclei candidate to 0νββ decay, a major upgrade of the LNS facility is ongoing, within the POTLNS project, to increase the experimental yield by more than two orders of magnitude [3]. To this purpose, frontier technologies are being developed for both the accelerator and the detection systems. In particular, a new particle identification (PID) system has been designed consisting on 720 Silicon Carbide (SiC) – Cesium Iodide (Tallium doped) CsI(Tl) telescopes arranged in towers of 20 elements each. In the present report the construction of a prototype of the final PID system is presented.

THE PARTICLE IDENTIFICATION SYSTEM

The PID for the NUMEN experiments involves ions in the mass region $10 < A < 25$ and atomic number $4 < Z < 12$. These ions emerge from the target with a distribution of different charge states (q), making the ion identification more challenging. The technique for PID implemented in MAGNEX, described in ref. [4], requires precise measurements of the energy loss (ΔE), the residual energy (E_r) and the horizontal position at the focus (X_{foc}) and guarantees a clear selection of the ions of interest in the whole range of A and Z.

In the new MAGNEX focal plane detector (FPD), the gas tracker will provide accurate measurement of the X_{foc} parameter, while ΔE and E_r are obtained from a dedicated array of two-stage telescopes of SiC and CsI(Tl) detectors. The active area of each element is 1.5 × 1.5 cm, with 0.2 mm dead space between adjacent cells. The SiC detector is 100 μm thick and measures the ΔE. The CsI(Tl) inorganic scintillator is 5 mm thick and is coupled to a Hamamatsu S3590 photodiode of 1 × 1 cm area to measure the E_r. A sketch of the single telescope is shown in Figure 1.

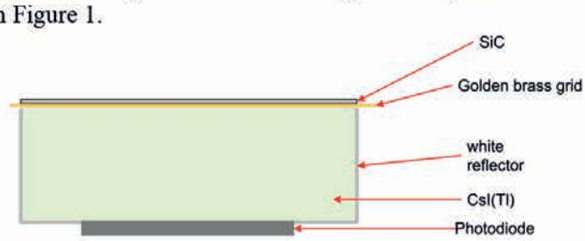

Figure 1: Sketch of the single telescope.

The telescopes are arranged in towers (10 rows and 2 columns each). They can be precisely mounted and easily attached on the top flange of the FPD chamber [2] by means of a mechanical stand, also making the mounting and maintenance procedures more comfortable.

In the design of the final PID system covering the full focal plane of MAGNEX, the towers are rotated of about 35° around the vertical axis. This choice is aimed to minimize the differences in the path length inside the detectors since the FPD is rotated around the vertical axis by 59° with respect to the plane orthogonal to the optical axis [6].

In the present geometry the full length of the FPD will be covered by 36 PID towers, placed downstream of the tracker, for a total of 720 telescopes. A 3D view of the full PID wall is visible in Figure 2.

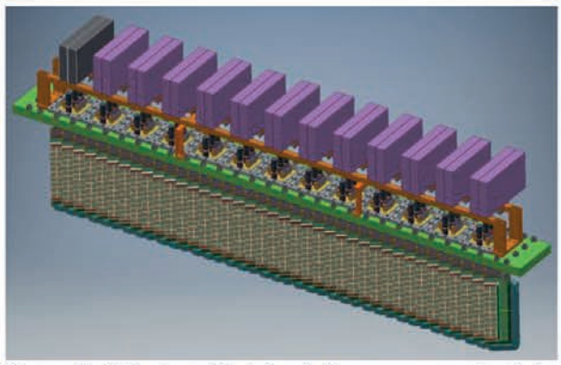

Figure 2: 3D view Sketch of the arrangement of the towers covering the full MAGNEX focal plane

THE PROTOTYPE

The first two towers of the MAGNEX PID system were recently built. They are composed by some main elements: i) a main PCB board, ii) the photodiodes, iii) the CsI(Tl) array, iv) a golden-brass grid, v) the SiC detectors, vi) the connection board, vii) the connectors. The assembled towers are shown in Figure 3.

The 20 photodiodes were soldered onto the PCB board. On top of them CsI(Tl) arrays are coupled through an optical grease. The CsI(Tl) crystals were produced in a 20 elements array with the chosen geometry ensured by the white resin. A golden brass grid, with the same planar geometry of the CsI array, is placed on the top of the crystals over which the SiC detectors were positioned using a conductive glue. In this way the ground to the SiC detectors is given by the grid itself that is connected by a cable to the main PCB board ground. The SiC negative bias, typically around 300-1000 V, is applied with a wire bonded to a dedicate pad and the detector signals are readout through the same wire, as usually done for solid state detectors. In this case the wire bonding procedure is particularly delicate, since very long wires are needed, as shown in Figure 4, in which the length of the wire bondings is about 17 mm for the left SiC detectors and 10 mm for the right ones. The wire bondings were performed at INFN-Torino from the SiC pads onto the connection board pads, which is placed about 2 mm above the SiC detectors thanks to a thickness of insulating 3D printed material. Some pins are soldered between the connection board and the main PCB board to ensure the routing of the SiC signals. Only few SiC were available, thus the towers are only partially filled by them.

The detector signals are collected and sent to the front-end electronics (Caen V1429 64-channel pre-amplifiers) by means of a 80 pins Samtec connector on the top of each tower. The bias voltage for the photodiodes (-70 V) are given through such pre-amplifiers, while the HV for the SiC is decoupled from the pre-amplifiers (that are able to manage maximum 400 V) and are given by a BNC connector on the top of the main PCB. The readout of all the signals is performed using 64-channel digitizers (Caen VX2740), as described in Ref. [5].

The commissioning of the described PID prototype was recently performed with ^{18}O beam at 270 MeV incident energy at INFN-Laboratori Nazionali di Legnaro.

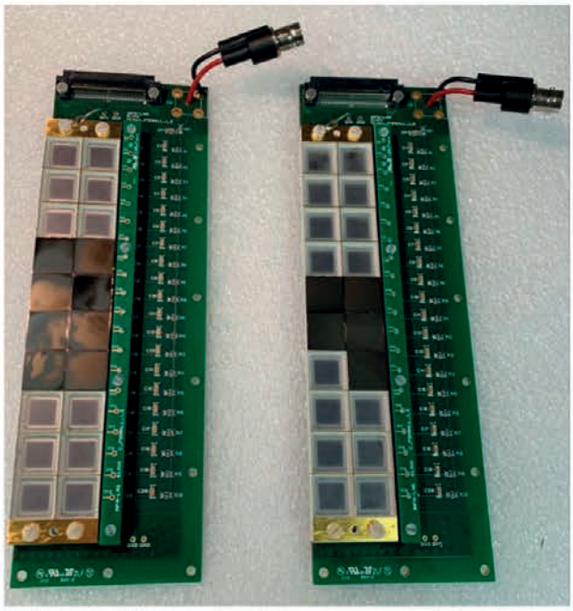

Figure 3: Picture of the first two towers of the PID prototype composed by: the main PCB board, the CsI crystals array, mounted on the top of the photodiodes, the SiC detectors glued onto the golden-brass grid.

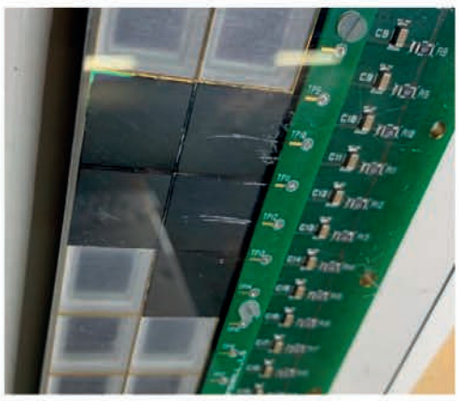

Figure 4: Picture of the long wire bondings between the SiC pads and the connection board pads.

REFERENCES

[1] F. Cappuzzello et al., Eur. Phys. J. A 54 (2018) 72
[2] F. Cappuzzello et al. Int. Jour. Mod. Phys. A 36 (2021) 2130018
[3] C. Agodi et al., Universe 7 (2021) 72
[4] F. Cappuzzello et al., Nucl. Instr. and Meth. A 621 (2011) 419
[5] P. Finocchiaro et al., Universe 6 (2020) 129
[6] A. Cunsolo et al., Nucl. Instr. Meth. A 484 (2022) 56

The new data acquisition system for the CLAD Si telescope array

P.Figuera[1], M. La Cognata[1], A. Oliva[1], D.Torresi[1]

1)INFN Laboratori Nazionali del Sud, Catania, Italy

Abstract – A new data acquisition system, based on the Mesytec MDPP32 digitizers, has been assembled and tested. This acquisition system will be used for the CLAD detection setup, an array of 8 segmented triple Si telescopes with a total of about 500 strips, normally used for reaction dynamics and nuclear astrophysics studies at LNS and abroad.

INTRODUCTION

For the study of reactions around the Coulomb barrier with stable and radioactive beams, we developed at LNS about a decade ago the CLAD detection system. This detection setup consists of up to 8 5x5 cm^2 triple Si telescopes: a 20 μm DE stage segmented into 16 strips, a 1000 μm DSSSD segmented into 16 strips each side, and a 1500 μm detector, used as last stage, not segmented. This setup was, over the years, arranged in different geometries depending on the experimental needs, and used in a variety of experiments with stable and radioactive beams, both in single and coincidence mode. The detection system was instrumented with 32 channel charge preamplifiers having differential output, coupled with 16 channel programmable amplifiers providing energy and timing outputs which, in turn, were fed into an acquisition system based on the use of CAEN 32 channel ADCs (V785) and TDCs (V775) [1].

Recently, in order to improve the angular resolution of the setup, crucial to improve the resolution when measuring relative energy of two particles in coincidence, we started to substitute the 16x16 strip DSSSDs with 32x32 strips DSSSDs. The consequent increase of electronics channels and the relatively large typical dead time of the old acquisition system (about 100 μs per event), triggered the need to move to the use of digitizers, eliminating the need of amplifiers ADCs and TDCs and decreasing the acquisition dead time. In the following, we will describe the digitizers and readout software we decided to use and the tests performed on the new system.

TEST RESULTS

At LNS we had already available the MVME data acquisition software from Mesytec with a MVLC VME controller [2]. This is a complete and very stable program allowing on-line data analysis and parallel data storage on disk for subsequent analysis. MVME supports various kinds of VME converters such Mesytec 32 channels ADCs, TDCs, and Digitizers as well as modules of other companies like the CAEN 32 channel V785 ADCs. We therefore decided to use the already available software to build a system based on the use of the Mesytec MDPP32 digitizers. In these modules a 32 channel amplifier is followed by 80 MHz sampling ADCs. The digitized data are analysed by the firmware of an FPGA, which reconstructs time and energy information for each input signal.

Instead of operating the digitizers in triggerless mode using the timestamp, in this first phase, we decided to operate the system in an event by event mode using a common gate for all the modules, storing on disk time (relative to the common gate) and energy for all input signals. Such a common gate can be built, according to the experimental needs, using the trigger outputs of the digitizers, and performing on them the needed logic operations like coincidences etc.

The dead time was managed by locking the system after each event till the end of the readout.

Dedicated tests were conducted to evaluate the possibility to improve the dead time, using the internal FIFO of the digitizers, in order to manage more than one event each readout. This possibility however, exposes to the risk of event decorrelations. In order to investigate on that, we used a CAEN DT5810 digital detector emulator [1] to send, to the preamplifiers test inputs, signals whose amplitude is changing event by event simulating a gamma source. We then correlated in a 2D spectrum two channels of two different MDPP32. If no decorrelations are there, all the events must lie on a line, whilst events outside this line are due to decorrelations. An example of such spectrum, obtained by reading 10 events at once from the FIFO, is shown in figure 1.

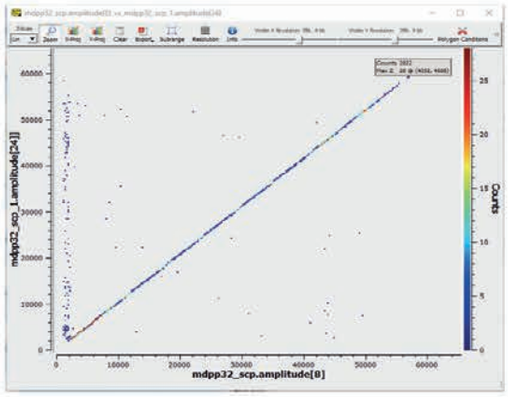

Figure 1 Correlated and decorrelated events

One can indeed see a minor fraction of decorrelated events, which disappear from the spectrum if one reads and clears the FIFO each event. We also investigated how much the average dead time per event is reduced by using the FIFO. As an example, we measured that the average dead time per event reading 1 event from the FIFO for 2 MDPP32 is about 7 μs whereas, reading 10 events at once from the FIFO, lowers the average dead time per event to 6 μs. Following the above tests, we decided to operate the system making a readout each event, avoiding the risk of decorrelations, at the price of a limited worsening of the dead time. In these conditions we obtained, for two MDPP32, the following ratio A/V of Accepted/Valid events at various rates.

Input Rate (Hz)	A/V experimental	A/V Calculated 1/ (1+R*τ)
1000	99%	99%
4000	97%	97%
10000	93%	94%
20000	88%	88%

Table 1 Experimental ratio of accepted/valid events at various input rates rates R compared with the calculated value (dead time per event $\tau = 6.7$ μs) .

Another group of tests concerned the optimisation of parameters used by the FPGA firmware for the extraction of time and energy from the digitized signals. The energy resolution was extracted using a triple alpha source and a 16x16 strip DSSSDs, looking at the FWHM of the 5.48 MeV ^{241}Am peak. After optimisation of the noise and of all other parameters (pole zero, BLR, flat top of trapezoidal shaping), we measured the resolution as a function of the shaping time, obtaining the results shown in table 2.

Shaping time (μs)	5.48 MeV peak FWHM (keV)
0.5	60
0.75	50
1.0	37
1.5	35
2	35
3	35

Table 2 Resolution as function of shaping time

Based on the above result we decided to use a shaping time of 1.5 μs.

Following the above described tests, after optimisation of pole zero, BLR and 'flat top' and using a shaping time ST=1.5 μs for the energy signal, we performed some tests at high rate, with a Poissonian time distribution of the pulses and an amplitude corresponding to an energy of 11 MeV. As an example, in figure 2, we show a spectrum obtained with a rate of 10 kHz, where pileup events are clearly visible. The fraction of pileup events measured at various rates R is shown in table 3 and compared with the corresponding expected calculated value. The possibility of suppressing pileup events is under investigation.

By using the detector emulator we generated two uncorrelated signals at high rate (1 to 10 kHz) and coincidences between the two at 10 Hz at a different energy (to separate them from the random). We then run the acquisition in coincidence mode (coincidence window 200 ns) measuring the expected calculated number of random and true coincidences at various rates.

Finally, by knowing the raw data structure of the binary output file, a software was developed which unpacks the raw data, extracting, event by event, time and energy corresponding to each strip. Such information are then written by this software into a ROOT file with a suitable structure to perform all subsequent off-line analysis.

Figure 2 Pulser spectrum with pileup events at 10 kHz

Rate R (Hz)	pileup/total experimental	pileup/total calculated P≈1-exp(-R x ST)
1000	0.13 %	0.15 %
2000	0.30 %	0.30 %
5000	0.72 %	0.75 %
7500	0.76 %	1.1 %
10000	1.5 %	1.5 %

Table 3 Pileup events measured at various rates R

In summary, the tests performed so far show a stable and reliable system with satisfactory performances for the foreseen use. We plan to use this system for the first real experiment in the second half of 2024.

REFERENCES

[1] https://www.caen.it/
[2] https://www.mesytec.com/downloads/mvme.html

System for beam control and transport within the I-LUCE facility

G. Sapienza[1], D. Bonanno[1], R. Catalano[1], G.A.P. Cirrone[1], D. Passarello[1], S. Passarello[1], G. Petringa[1], F. Schillaci[2], S. Tudisco[1]

1) Istituto Nazionale di Fisica Nucleare – Laboratori Nazionali del SUD, Catania, Italy
2) Czech Academy of Sciences, ELI–Beamlines Center, Institute of Physics, Břežany, Czech Republic

Abstract – For the I-LUCE facility we are developing a system for the transportation and the focusing of the beam, consisting of four permanent magnetic quadrupoles and a magnetic selector (currently in development).

THE MAGNETIC QUADRUPOLE

The magnetic quadrupoles system (Fig. 1) has been designed for beam focusing and will be located within the interaction chambre of the I-LUCE facility.

This device uses magnetic fields to focus the beam produced by the laser-target interaction.

The system consists of a series of 4 permanent magnet quadrupoles with known characteristics, positioned at distance from each other.

In fact, by varying the position of the quadrupoles in the system, it is possible to modify the focusing characteristics

SYSTEM OVERVIEW

The system is composed by:

- four carts with a single axis of movement (Fig. 1);
- four worm screws to which the four magnets are connected;
- four motors, each for the movement of each individual magnet;
- limit switches;

All components have been specifically designed and built for use in a vacuum chamber.

The stepper motors used (Fig. 1a), D42.1 of the Arun Microelectronics Ltd., are suitable for use in UHV (Ultra-High Vacuum), and they have the following characteristics:

Holding Torque (mNm)	Detent Torque (mNm)	Max. Axial Force (N)	Max. Radial Force (N)	Current per Phase (A)	Phase Inductance (mH)	Mass (g)
250	8	9	15	1.0	6.6	350

The motors are connected to the worm gears through flexible couplings to prevent any relative movements affecting the alignment of the motion axis.

They are controlled by drives designed by the same company (Fig.1b). The model used is "SMD3", a drive for single-axis bipolar stepper motors.

This drive is designed to maximise the performance while minimizing the temperature and also manages two limit switches (Fig. 1c).

It is possible to control it via USB and power it with an external power supply with an operating voltage ranging from 15 to 67Vdc.

The magnets have two different lengths, 40mm and 80mm and they can be swapped in position and it's possible to reverse their polarity (by rotating them 180° on the vertical axis), as they are installed on guides, to find the best configuration during calibration tests for beam focusing.

The limit switch signal transmission system, realized through sliding contacts, has been designed so as not to have cables obstructing the swapping position of the magnets. (Fig. 1d).

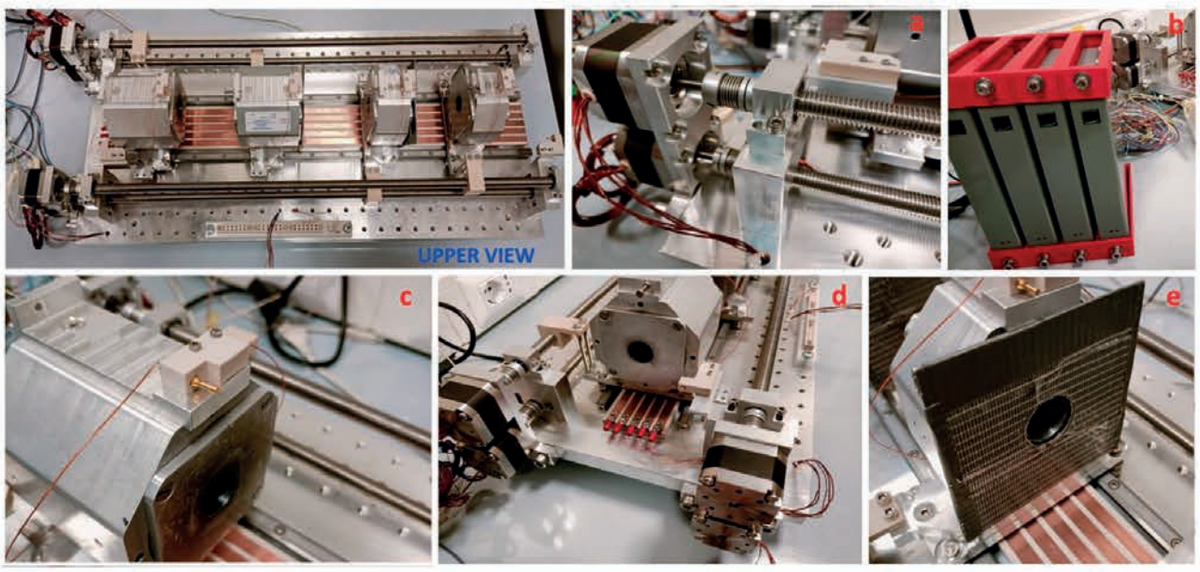

Fig. 1: Magnetic Quadrupole system

SOFTWARE

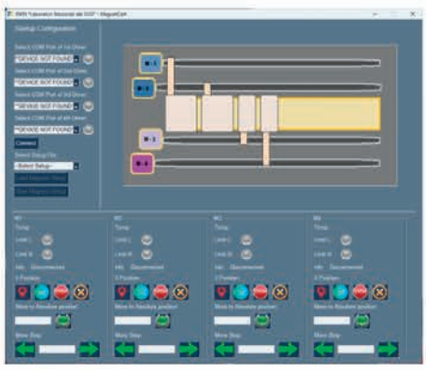

Fig. 2: Software GUI

The software (Fig. 2) used to monitor and control the system has been developed in Python.

The first release of this software uses the serial communication to interact with motor drives, but it is investigated to use digital signal instead.

It's possible to command the individual motors and, using configuration files, define the installation sequence of the magnets along their axis of movement.

The magnets can be moved individually or through a sequence of predetermined movements and the various configurations can be saved and recalled as needed.

Through the interface, it's possible to control the real-time position of the magnets and their distance from the home position.

Furthermore, the operating temperature of the stepper motors is monitored, and any errors encountered by the drivers during the movement of magnets are reported as "alerts" or "warnings" on the screen.

The choice to use python was made for its ease of implementation and its ease portability across operating systems.

The software has indeed been optimized to work under Windows, Linux, and macOS.

TESTING THE SYSTEM

The preliminary tests of movement have highlighted the need to reduce the magnetic interactions between one magnet and another.

In some particular configuration, the magnetic force exceeds the torque force provided by the motors for the movement.

To overcome these limits, it has been considered to use shielding MuMetal sheets (Fig. 1e), which do not affect the beam but reduce the interactions between one magnet and another.

Also, we have verified that the repeatability in movements is around ±50 microns.

CONCLUSIONS

The next phase will involve completing the development of the control system for the "Magnetic Selector," which is also composed of magnetic dipoles to be moved along different axes, to select the various species produced by the beam.

Latest results of the pixelation technique applied to the data collected by the FARCOS correlator in the CHIFAR experiment

C. Zagami[1,2,3*], E.V. Pagano[2], P. Russotto[2], E. De Filippo[4], L. Acosta[5,6], T. Cap[7], G. Cardella[4], F. Fichera[4], E. Geraci[1,4,3], B. Gnoffo[1,4], C. Guazzoni[8,9], G. Lanzalone[10,2], C. Maiolino[2], N.S. Martorana[4], T. Matulewicz[7], A. Pagano[4], M. Papa[4], K. Piasecki[7], S. Pirrone[4], M. Piscopo[2], R. Planeta[11], G. Politi[1,4], F. Risitano[12,4], F. Rizzo[1,2,3], G. Saccà[4], G. Santagati[4], K. Siwek-Wilczynska[7], I. Skwira-Chalot[7], M. Trimarchi[12,4]

1) Dipartimento di Fisica e Astronomia "Ettore Majorana", Università di Catania, Italy
2) INFN, Laboratori Nazionali del Sud - Catania, Italy
3) CSFNSM-Centro Siciliano di Fisica Nucleare e Struttura della Materia, Catania, Italy
4) INFN, Sezione di Catania, Italy
5) Instituto de Física. Universidad Nacional Autónoma de México, Mexico
6) Instituto de Estructura de la Materia, CSIC, Spain
7) Faculty of Physics, University of Warsaw, Warsaw, Poland
8) Dip. di Elettronica, Informazione e Bioingegneria, Politecnico di Milano, Italy
9) INFN, Sezione di Milano, Italy
10) Facoltà di Ingegneria e Architettura, Università Kore, Italy
11) M. Smoluchowski Institute of Physics, Jagiellonian University, Krakow, Poland
12) Dipartimento di Scienze MIFT, Univ. di Messina, Messina, Italy

email: zagami@lns.infn.it

Abstract – In this report the so-called "pixelation technique" applied to the data collected by the FARCOS correlator in the CHIFAR experiment is explained.

INTRODUCTION

In the CHIFAR experiment [1], carried out at INFN-LNS, the reaction mechanisms in Heavy Ion collisions and the emission probability of Intermediate Mass Fragments (IMFs), i.e. ions with atomic number $Z \geq 3$, in non-central collisions at low energy regime were investigated. The aim was the study of the features of the Equation of State of the nuclear matter. The final outcomes of the reaction strongly depend on the initial properties of the colliding nuclei: the CHIFAR experiment studied the role of the isospin degree of freedom and of the size of the colliding systems in a nuclear reaction.

In previous experiments, the CHIMERA collaboration investigated some reaction systems at 35 AMeV beam energy. The "neutron rich" system $^{124}Sn+^{64}Ni$ and the "neutron poor" system $^{112}Sn+^{58}Ni$ were studied in the REVERSE experiment [2], while in the InKiIsSy experiment [3] other two nuclear reactions were analyzed, i.e. the $^{124}Xe+^{64}Zn$, that is an isobaric combination of the neutron rich one with isospin contribution similar to the neutron poor one, and the $^{124}Xe+^{64}Ni$. Data analysis of these two experiments highlighted that the IMFs emission probability grows with the isospin content of both projectile and target, correlated to an enhancement of the dynamical emission. Thus, the mass difference of the colliding systems is irrelevant in the dynamical IMFs emission, instead the isospin content has an important role.

The CHIFAR experiment was aimed at the study of the above-mentioned physics cases, using the same colliding systems at lower energy of 20 AMeV. The experimental goals were the study of the emission mechanism (dynamical or statistical), the IMFs production and the investigation of the isospin role in HI collisions at this low energy regime.

EXPERIMENTAL SETUP

In the CHIFAR experiment, the FARCOS correlator in his final configuration was coupled with the 4π CHIMERA multi-detector. This experimental setup allows the study of nuclear reactions at Fermi energy regime with higher precision to the respect of the past. In fact, beyond the good performance of CHIMERA, FARCOS is able to give the identification of the detected fragments with higher angular and energy resolution.

The CHIMERA multi-detector [4] is made of a Si detector (300 μm thick) coupled with a CsI(Tl) scintillator detector (3-12 cm thick), with a total of 1192 telescopes.

Ten telescopes of the FARCOS (Femtoscope ARray for COrrelation and Spectrocopy) correlator [5] were used in the experimental setup. FARCOS was designed to study reaction dynamics and nuclear structure, as an array of detectors for charged particles, with high energy and angular resolution. In the CHIFAR experiment, FARCOS telescopes covered the polar angle range of 13°-30° in the laboratory frame. Each FARCOS cluster has three stages:

the first (300 μm thick) and the second (1500 μm thick) ones are Double Silicon Strip Detectors (DSSSDs), having 32 vertical strips in the front side and as many horizontal strips in the back side (6.4x6.4 cm^2 active area); the last stage consists of four CsI(Tl) crystals (6 cm thick, 3.2x3.2 cm^2 active area) and the light signal is read by photodiode. The signals were processed by the ASIC preamplifiers [6] and digitized with the GET electronics [7].

DATA ANALYSIS AND PRELIMINARY RESULTS

Energy calibration and resolution

At the beginning, data analysis is focused on the energy calibration and on the evaluation of the energy resolution of the DSSSDs.

The so-called "punching through" technique was applied to the ΔE-E identification matrices related to the two Si detectors of the FARCOS telescopes, in order to obtain the calibration. According to this method, the snap backs at the end of each hyperbolic curve are generated by the particles that are in transmission also in the second Si stage and lose completely their energy in the CsI(Tl) stage. The initial energy was reconstructed, and the energy lost in each of the two DSSSDs was evaluated by the difference.

The energy resolution of the DSSSDs front side was estimated from gaussian fits of three elastic scattering peaks. The value obtained is around 0.5% RMS (corresponding to 1.5 MeV at 300 MeV of peak). Then, also the DSSSDs back side strips were calibrated by using the front side ones; the ratio $(\Delta E_{front} - \Delta E_{back})/\Delta E_{front}$ was calculated for each front strip in coincidence with all 32 back strips. An energy resolution around 1.6% (corresponding to 4.8 MeV at 300 MeV of peak) was estimated.

The ΔE-E technique was applied to the first and second DSSSDs, for each FARCOS telescope. An automatic algorithm, based on the Bethe-Bloch formula, was developed by the CHIMERA collaboration: it has permitted to obtain an unambiguous particle identification, in charge up to Z≈16 and an isotopic identification for IMFs up to Z≈9 and A≈20.

The pixelation technique

The so-called "pixelation technique" is a method that allows to assign the correct position to each particle detected by the FARCOS correlator [8]. This means the assignment of the coordinate, the polar angle θ and the azimuthal angle ϕ from the analysis of the fired strip of the front side and the one of the back side of the DSSSDs.

The procedure works step by step. At the beginning, some experimental constraints were imposed to select the events. It was required that the particle multiplicity was equal to 1 in both sides of the first DSSSD and also in the front side of the second DSSSD; the multiplicity of the second back side must be less than 4; the particles stopped in the Si detectors, so the multiplicity of the CsI(Tl) crystals was zero. Other constraints concerned the energy because ideally the energy released in the front side must be approximately the same as that one released in the back side of the first DSSSD: it was required to be of the same range within ±15% in order to maintain a good statistic of the events. Finally, the strips hit by the particle must be the same or neighboring between the first and second DSSSDs front stage. For the events selected this way, a good assignment of the position of the particles detected without ambiguity was obtained, as shown in figure 1.

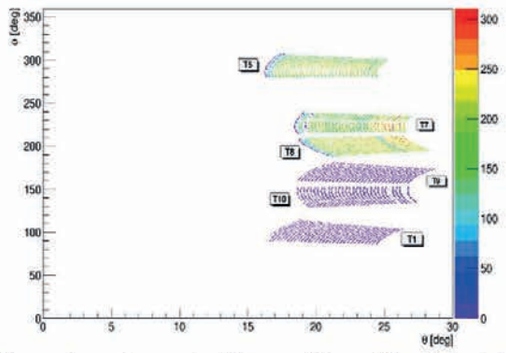

Figure 1: assignment of the position of the detected particles in the plane ϕ- θ for the six telescopes analyzed.

In the next step of the analysis, the imposed constraints will be partly modified to also include the events that have multiplicity equal to 2; the requirements concerning the energy released and the hit strips will remain the same. The comparison among only the energies released will not be enough to classify all observed events, such as interstrip, electronic induction or spurious events. The time variable will be very useful to complete the pixelation procedure [8].

REFERENCES

[1] E.V. Pagano et al., Proposal of CHIFAR experiment, approved by the 2017 LNS-PAC.

[2] E. De Filippo and A. Pagano, Eur. Phys. J. A, **50** (2014) 32 and refs. therein.

[3] P. Russotto et al., Eur. Phys. J. A. **56**, (2020) 12.

[4] A. Pagano et al., Nucl. Phys. A **734** (2004) 504-511.

[5] E.V. Pagano et al., EPJ Web of Conferences **117** (2016) 10008.

[6] A. Castoldi, C. Guazzoni, T. Parsani, on behalf of the FARCOS collaboration, IL NUOVO CIMENTO C, **41**, (2018) 168.

[7] E. C. Pollacco et al., Nucl. Instr. And Meth. A. **887**, (2018) 81.

[8] G. Cardella, N. S. Martorana et al., submitted to Nucl. Instr. And Meth. A.

Data acquisition and software developments at INFN-LNS for the AsyEos-II experiment at GSI/FAIR

E. De Filippo[1], P. Russotto[2], G. Cardella[1], E. Geraci[3,1], B. Gnoffo[3,1], C. Guazzoni[4], C. Maiolino[2], N.S. Martorana[1], A. Pagano[1], E.V. Pagano[2], M. Papa[1], S. Pirrone[1], G. Politi[3,1], F. Risitano[5,1], F. Rizzo[2], G. Saccà[1], G. Santagati[1], M. Trimarchi[5,1], C. Zagami[3,2]

1) INFN, Sezione di Catania - Catania, Italy
2) INFN, Laboratori Nazionali del Sud - Catania, Italy
3) Dip. di Fisica e Astronomia "Ettore Majorana", Università di Catania - Catania, Italy
4) Dip. di Elettronica, Informazione e Bioingegneria, Politecnico di Milano and INFN sez. di Milano, Italy
5) Dipartimento di Scienze MIFT, Università di Messina - Messina, Italy

Abstract – The AsyEos-II experiment, having the objective to study the EoS (Equation-of-State) of neutron rich matter at high baryon densities, will be realized in 2025 at GSI/FAIR within the R^{3}B collaboration, preceded by a commissioning test in 2024. In this report the development work done at INFN-LNS on data acquisition (DAQ), data analysis and simulations will be briefly described. In fact, the AsyEos-II setup will use part of the CHIMERA array together with a part of the R^{3}B detectors (NeuLAND, ToFD, LOS) and the new KRAB (Krakow Barrel) detector, especially built for this experiment.

INTRODUCTION

Heavy ion collisions offer the best way to study the EoS of nuclear matter in a large range of baryonic densities, around the saturation one ρ_0, and isospin asymmetries. The AsyEos experiment, by using as main observable the elliptic flow ratio of neutrons and charged particles [1], probed the isospin dependent component (asymmetry term) of the EoS at densities around 1-2ρ_0 in Au+Au reactions at 400 A.MeV. Constraining the asymmetry term of the EoS is important, amongst other reasons, for its strict connection with multi-messenger astrophysics, such as compact stars and core collapse supernovae phenomena [2,3]. The AsyEos-II experiment proposes [4] to extend the knowledge of the symmetry energy to higher densities near to 2ρ_0 (by using incident energies from 250 up to 1000 A.MeV) and to improve the measurement precision with respect to the previous one. This last aspect will be reached also by using innovative and powerful detectors inside the R^{3}B cave. KRAB is a new detector [2], developed at IFJ PAN, Krakow, constituted by 5 rings of 4x4 mm^2 fast scintillating fibers readout by SiPMs, placed around the target. It will provide a fast trigger based on multiplicity and charged particles azimuthal distributions for event-by-event reaction plane reconstruction. Amongst the R^{3}B collaboration devices, the NeuLAND detector [5] for high efficiency neutron and H isotopes detection and two frames of the time-of-flight ToFD, made by plastic scintillator paddles [6], will be used. The first ToFD frame in order to measure particles velocity and charge at very forward angles, and the second one acting as a charged particles *veto* for the NeuLAND detector. Finally, four rings (ring 3 to 6) of the Chimera array (mainly CsI(Tl) scintillators) will improve the determination of the impact parameter and reaction plane orientation of the events.

Figure 1: detail of the s122_2024 experimental setup. The KRAB detector is visible on the center along the beam direction. The DSSSD telescope (see text) is also visible inside the aluminium box on the right.

This complex setup requires a long preparatory work, in particular for coupling of data acquisitions, timing and trigger synchronizations amongst the R^{3}B detectors, detector simulations, data unpacking and data analysis. In this report some aspects of the activity related to DAQ development, mainly done at LNS in 2023, will be shown. The principal objective to reach in 2023 was the KRAB commissioning and Chimera DAQ test beam (GSI exp. s122_2024) performed at GSI in march 2024 by using Au parasitic beam at energies of 400 and 800 A.MeV.

RESULTS AND DAQ DEVELOPMENT

In the s122 test the Chimera detector was "emulated" by using a two stage DSSSD telescope (from FARCOS array), both 32x32 strips, 1500 μm thick, placed between 8 and 15 degrees on one side with respect to KRAB. The ToFD array was also present at forward angles. The plastic scintillator LOS start detector gives the start signal for time-of-flight measurement.

Chimera DAQ is a hybrid data acquisition [7] coupling the GET digital acquisition for CsI(Tl) in the sphere and

FARCOS device with the Silicon/CsI detectors readout of CHIMERA telescopes handled by codifiers (QDC,TDC) housed on the VME bus. In order to make easier synchronization with R^{3}B DAQ we have chosen to use in AsyEos-II experiment the VME bus and analog acquisition only.

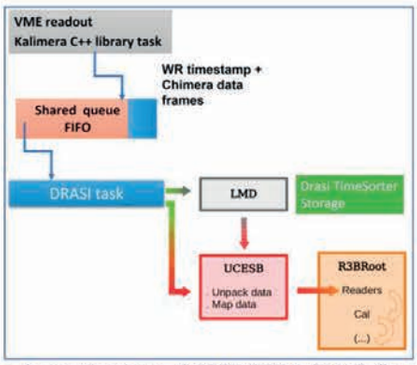

Figure 2: schematic view of CHIMERA DAQ flow within the R^{3}B DAQ framework.

The CHIMERA VME readout is done by using the KaliMera C++ library and a Caen V2718/A3818 PCIe to VME bridge as VME controller. In R^{3}B each DAQ node (related to a given detector) uses timestamp clock references, that are synchronized. The White-Rabbit (WR) protocol is generally used. In the CHIMERA node a VME WR receiver, VETAR2, operating at 125 MHz, 64 bit words length, is connected by optical fiber to a high precision subnanosecond timing WR switch and synchronized with all DAQ nodes. R^{3}B mainly uses the Drasi [8] DAQ supervisor and data transport pipeline that collect data coming from the readout of the different subsystems. A Drasi task (Drasi-reader), working in the CHIMERA node server, initializes and starts an asynchronous readout task from KaliMera library. At each valid trigger the readout task reads the timestamp from VETAR and the data buffer from codifiers; they are transferred to the Drasi task by means of a shared FIFO queue (see Fig. 2). The data in the form of a list of sub-events (LMD format), the first one containing the timestamp and trigger information, are transferred by network to the Drasi "time-sorter" together with all data coming from other subsystems for disk storage and time-sorting.

CHIMERA electronic front-end generates a trigger (in s122_2024, it was the "or" of the DSSSD front strip detectors) and a dead-time signal that are sent to the master trigger. All the DAQ subsystems share the dead-time and receive the master-trigger generated by a programmable VME module (VOLUM) with a FPGA firmware (TRLO) handling the trigger logic that is distributed to all subsystems.

In s122_2024 beam test CHIMERA WR timestamp synchronization with the master DAQ performed well with a good stability and a time jitter limited to ≈ 3 ns. Time-sorted data are grouped in the same physical event by using a time window (<4 μs) based on timestamp (time stitching). This condition is necessary but not sufficient to be sure that events data are really correlated. In order to have on-line synchronization check, the master trigger is send to all subsystems as a randomly variable width signal with 8 different values. In CHIMERA DAQ we evaluate the trigger width in a channel of a common stop TDC. The recorded TDC values, inserted in the event-header, are plotted event-by-event for stitched events with the corresponding data in master DAQ. Fig. 3 shows results of this "synch-check" procedure. The diagonal line indicates correlated events.

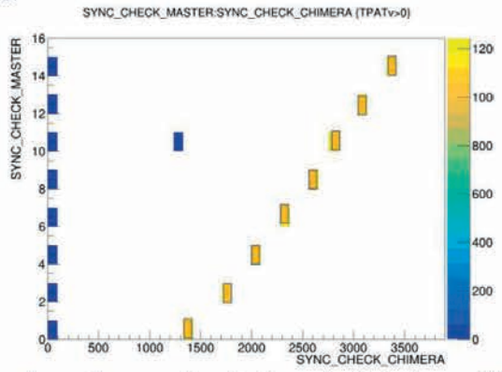

Figure 3: on-line synchronization check between CHIMERA data and master DAQ during a run of the s122 experiment.

In R^{3}B all activities as data monitoring, data analysis, calibrations, detector simulations are done within the R3BRoot software framework [9]. Great efforts were done at LNS in R3BRoot code developing for AsyEos and to reach R3BRoot compatibility. To accomplish this goal, CHIMERA data are unpacked and mapped by using the UCESB tool [10] that is the only way to stream data towards R3BRoot. Anyway, CHIMERA DAQ can stream standalone data simultaneously to its own online-offline analysis programs and to R3BRoot, transparently for the user. Online data in R3BRoot are monitored by a Root HTTP-Server. Finally, CHIMERA rings and KRAB detectors geometries were also inserted within R3BRoot for GEANT4 simulations and comparison with models.

Data analysis of the s122_2024 test is started and it will be of great help for the forthcoming experiments. In 2024 many efforts of CHIMERA group will be dedicated to preparation of rings, mechanical support and electronic front-end to be transferred at GSI/FAIR for the AsyEos-II experiment.

REFERENCES

[1] P. Russotto et al., Phys. Rev. C94 (2016) 034608.
[2] P. Russotto et al., La Riv. Nuovo Cim. 46 (2023) 1.
[3] S. Huth et al., Nature 606 (2022) 276.
[4] P. Russotto et al., arXiv:2105:09233 [nucl-ex] (2021).
[5] K. Boretzky et al. NIM A1014 (2021) 165701.
[6] M. Heil et al., Eur. Phys. J. A58 (2022) 248.
[7] E. De Filippo et al., J. Phys.: Conf. Ser. 1014 (2018) 012003.
[8] https://fy.chalmers.se/~f96hajo/drasi/doc/index.html
[9] R3BRoot: https://github.com/R3BRootGroup
[10] UCESB: https://fy.chalmers.se/~f96hajo/ucesb/

News on NArCoS (Neutron Array for Correlation Studies): the new correlator for neutrons and light charged particles at LNS

E.V. Pagano[1], C. Boiano[5], P. Russotto[1], E. De Filippo[3], G. Cardella[3], A. Castoldi[4,5], E. Geraci[2,3], B. Gnoffo[2,3], C. Guazzoni[4,5], G. Lanzalone[6,1], C. Maiolino[1], N.S. Martorana[3], F. Noto[1], A. Pagano[1], S. Pirrone[3], G. Politi[2,3], L. Quattrocchi[7,3], F. Risitano[7,3], F. Rizzo[2,1,8], G. Santagati[3], M. Trimarchi[7,3], and C. Zagami[2,1,8]

1) INFN, Laboratori Nazionali del Sud - Catania, Italy

2) Dipartimento di Fisica e Astronomia "Ettore Majorana", Università di Catania - Catania, Italy

3) INFN, Sezione di Catania - Catania, Italy

4) Dip. di Elettronica, Informazione e Bioingegneria, Politecnico di Milano - Milano, Italy

5) INFN, Sezione di Milano - Milano Italy

6) Facoltà di Ingegneria e Architettura, Università "Kore" - Enna, Italy

7) Dipartimento di Scienze MIFT, Univ. di Messina - Messina, Italy

8) CSFNSM-Centro Siciliano di Fisica Nucleare e Struttura della Materia - Catania, Italy

Abstract - An overview concerning the electronic frontend and readout system for the first version prototype of the neutron correlator NArCoS is reported. The proposed prototype of electronic was designed for the source and beam commissioning experiments like CROSSTEST performed in November 2023 at INFN-LNL.

INTRODUCTION

The effort of the international community aimed at building new facilities for Radioactive Ion beams (RIBs), such as FRAISE at LNS-INFN[1,2], SPES at LNL-INFN, FAIR at GSI, FRIB at MSU, in particular for the neutron rich ones, it will allows to study heavy ion (HI) collisions under extreme conditions of isospin asymmetry. In this perspective it is expected a more important role of neutron contribution during the collision events. The NArCoS project[3] (Neutron Array for Correlation Studies) is aimed to construct a novel detector devoted to detect neutrons and light charged particles performing high angular and energy resolutions. Conceptually the prototype is an array of 64 plastic scintillator detectors (EJ 276 family) having the dimension of 3x3x3 cm^3 arranged in a cubic geometry and individually read by SiPM. The plastic scintillator, both in the ordinary and in the green shifted versions, has proved good PSD capabilities in the neutron-gamma and neutron-alpha separation in many test, where both radioactive source at low background condition[4] and beams in high background[5] were used. Taking into account a distance of 150 cm from the interaction target the neutron angular resolution is estimated to be about 1° in the laboratory frame. The neutron energy measurement is entrusted to the time-of-flight (ToF) technique for which about 5% of energy resolution is estimated (Δt = 600 ps). The energy range of interest for neutrons is the intermediate one (2 MeV $\leq$ E $\leq$ 100 MeV) and they will be detected through the proton recoil technique. For this reason it will be mandatory to use a veto detector in order to disentangle a charged particle from a primary neutron since in the plastic scintillator both particles are seen as charged (mainly protons at the energy of interest of this project). The mission of this project is to have a second generation neutron correlator (but also light charged particles), designed to work in a stand alone mode or coupled to high granularity 4π multi-detector systems like CHIMERA[6] at INFN- LNS. Taking benefits to the large isospin asymmetry present in the next exotic beams, it will be possible to study the in-medium nuclear interaction, the equation of state of nuclear matter, the reaction mechanisms just to quote few examples. The project received a new impulse in terms of workforce and economical support thanks to the PRIN2021 ANCHISE (contract 2020H8YFRE), which will provide new studies for the three years 2022–2024, focusing on a dedicated readout digital electronic and the best mechanical configuration. One of the most important issue for the next few years will be the cross-talk study performed both with simulations and with dedicated experiments and tests. The study of cross-talk effect through simulations is already underway, through the Montecarlo based GEANT4 software. The results obtained so far are encouraging although they need to be confirmed through real experiments. In view of the CROSSTEST experiment, two configurations were studied with 9

elementary cells, one called "matrix" and one called " Three-cluster" which both give percentages of cross talk of the order of 3-4% for neutrons of energy between 1 and 10 MeV. For further details about cross talk simulation studies see ref.[7]. In the following sections the prototypal electronic readout system will be briefly described.

THE ELECTRONICS AND MECHANICAL PROTOTYPE

Each one cubic plastic scintillator is equipped with a

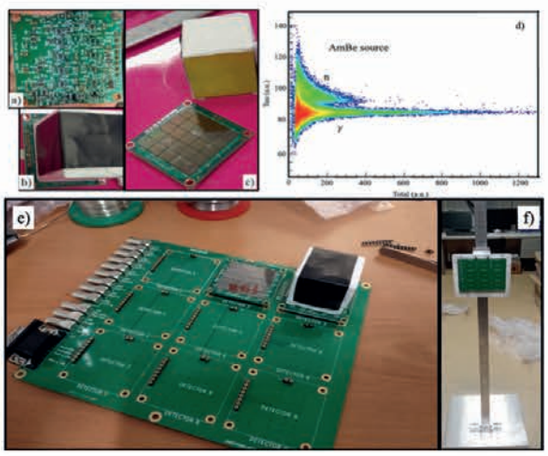

Figure 1: the read-out electronic motherboard [12] and the mechanical configuration (see text)

prototypal circuit for the readout system, performing the sum of all the signals coming from a matrix of 25 SiPMs, AFBR- S4N66C013 manufactured by BROADCOM, in order to have a fast signal, with low noise and amplitude that matches with the energy range of interest with the dynamics of the DAC acquisition. Each of the SiPMs has an active area of 6x6 mm^2 - a thickness of 0.3 mm - and contains 39384 square micro cells of 30 μm of pitch, working in avalanche mode. The readout electronics has been implemented on the bottom side, of the same PCB housing in the front side (with respect to the plastic scintillator) the SiPM matrix that is covering an active area of 30x30 mm^2. The front side of the PCB has also some pins useful for the SiPMs power supply, for the output signal, for a test input and for the temperature control as it is shown in the Fig. 1, panel a), b) and c). In the d) panel of the Fig. 1, is shown the tau as a function of the total identification matrix. The variable tau in the Y-axis, expressed in arbitrary unit, is obtained through an exponential fit procedure in the tail part of the digitalized signal. The total variable, expressed in arbitrary unit, in the X-axis, is the total energy deposited by the particle in the scintillator. Its number is obtained by an integration of the digitalized signal for all of its dynamic range (≈ 600 ns). In the identification matrix is shown the preliminary results of an acquired signal of a neutrons and gammas AmBe source for PSD tests. As it is possible to observe, a good separation between neutrons and gamma rays is achieved. Test was performed at LNS-INFN.

This electronic solution made with a compact design will allow to bring the detectors of the array closer together as maximum is possible. The circuit has a fast response time of less than 4 ns, while the intrinsic electronic noise of the readout circuit is lower by a factor of 4 than the noise due to the dark current. These characteristics are fundamental for the application of pulse shaping necessary for neutrons discrimination. For this electronics prototype good performances are achieved and in the next future a first prototype of the hodoscope will be ready to be tested with sources and beams. In the panel e) and f) of the Fig. 1 is shown the mechanical configuration manufactured for the CROSSTEST experiment and performed in November 2023 at the CN accelerator of INFN-LNL. The CROSSTEST experiment had the purpose of the experimental study of the crosstalk problem among the elementary detection cells at low neutron energy (En < 5 MeV). A PCB electronics board is shown in the panel e) of the Fig. 1 and it is able to connect the read-out SiPM boards to the acquisition system, a DT5742 CAEN digitizer. Moreover the PCB board is equipped with a test input, the High Voltage input to bias the SiPM (33V) and a temperature monitoring sensor output. In the panel f) the mechanics manufactured in order to support the completely setup (PCB board and the plastic scintillators) at the right height is shown. In conclusion the first version of the NArCoS prototype in a stand-alone configuration is under test with radioactive sources. In particular to test the PSD performances of the setup for many discrimination techniques. The good results so far achieved, both from experimental tests and simulations are encouraging to continue in this project. The data analysis of the CROSSTEST experiment is ongoing and timing response test will be made in the next future in order to compare the good timing performances of the ordinary version of the plastic with the green shifted one.

REFERENCES

[1] P. Russotto et al., Jour. of Phys. Conf. Series 1014, (2018) 012016;

[2] N.S. Martorana et al., Front. Phys. 10:1058419, (2022) and references therein;

[3] E.V. Pagano et al., Front. Phys. 10:1051058, (2023) and references therein;

[4] E.V. Pagano et al., Nuclear Instruments and Methods in Physics Research A, 889 (2018) pp. 83-88;

[5] E.V. Pagano et al., Nuclear Instruments and Methods in Physics Research A, 905 (2019) pp. 47-52;

[6] E. De Filippo and A. Pagano, Phys. Eur. Phys. J. A50, 32 (2014) and references therein;

[7] G. Santagati and E. V. Pagano et al., RAD Conf. Proc, vol. 7, (2023) to be published;

[12] E. V. Pagano et al., LNS Activity report, 144 (2021-2022) pp.144-145

Geant4 simulations to study the cross-talk probability and efficiency for the neutron correlator NArCoS

G. Santagati[1], E. V. Pagano[2], C. Boiano[3], G. Cardella[1], A. Castoldi[4,3], E. De Filippo[1], E. Geraci[5,1], B. Gnoffo[5,1], C. Guazzoni[4,3], A. Lanzalone[6,2], C. Maiolino[2], N. S. Martorana[1], F. Noto[2], A. Pagano[1], S. Pirrone[1], G. Politi[5,1], L. Quattrocchi[7,1], F, Risitano[7,1], F. Rizzo[5,2,8], P. Russotto[2], M. Trimarchi[7,1], C. Zagami[5,2,8].

1) INFN, Sezione di Catania, via Santa Sofia 62, Catania, 95123, Italy,
2) INFN, Laboratori Nazionali del Sud, via Santa Sofia 64, Catania, 95123, Italy,
3) INFN, Sezione di Milano, via Celoria 16, Milano, 20133, Italy,
4) Politecnico di Milano, Dip. Elettronica, Informazione e Bioingegneria, via Ponzio 34/5, Milano, 20133, Italy,
5) Università di Catania, Dipartimento di Fisica e Astronomia, via Santa Sofia 64, Catania, 95123, Italy,
6) Università di Enna "Kore", piazza dell'Università, Enna, 94100, Italy,
7) Università di Messina, Dipartimento di Scienze MIFT, viale F. Stagno d'Alcontres 31, Messina, 98166, Italy,
8) CSFNSM-Centro Siciliano di Fisica Nucleare e Struttura della Materia, via Santa Sofia 64, Catania, 95123, Italy.

Abstract - The target of the ANCHISE project is the development of a new detection system able to detect with high angular and energy resolution neutrons and light-charged particles at the same time. The idea is to use the new-generation of plastic scintillators EJ276-G coupled with a SiPM photosensor as the elementary detection cell of a segmented multidetector. Two geometrical configurations of the elementary cell were simulated with the GEANT4 toolkit, in order to study the detection efficiency and the cross-talk probability as a function of the incident neutron energy and of the detection threshold. The present study was preparatory for the CROSSTEST experiment, performed in November 2023 at Laboratori Nazionali di Legnaro (LNL).

INTRODUCTION

The NArCoS project [1] (Neutron Array for Correlation Studies) aims at developing a new detector able to detect neutrons and light charged particles with high angular and energy resolutions. The hodoscope will detect neutrons in nuclear reactions, from light to heavy ion collisions, in the energy range between 10 AMeV ≤ E/A ≤ 100 AMeV, it will work in a stand-alone mode or coupled to high-granularity 4π-detector systems like CHIMERA [2] or other light charged particle correlators like FARCOS [3] at Laboratori Nazionali del Sud in Catania (LNS) and it is suitable for the incoming facilities for radioactive ion beams (RIBs). such as FRAISE at LNS-INFN [4,5], SPES at LNL-INFN, FAIR at GSI, FRIB at MSU.

CROSS-TALK SIMULATION STUDY

The cross-talk effect is a predictable phenomenon in experiments aimed at neutron detection from low energy to several tens of MeV. It comes from neutrons interacting in two or more detection cells and from gammas and neutrons re-scattered from the wall and environmental structure. This background generates spurious signals that simulate unreal reaction events with a distorted neutron multiplicity.

In a recent paper [6] two different geometrical configurations of the elementary cell were investigated: the matrix configuration and the three-cluster configuration. A flux of 10^5 neutrons in air, from 1 MeV to 6 MeV (1 MeV steps) and 10 MeV, impinging on the central cell of the considered configuration was simulated, as shown in Figure 1. No detection threshold and detection thresholds of 0.5, 1.0 and 1.5 MeV were considered. Details about the simulation parameters and the detector configurations can be found in Ref [6].

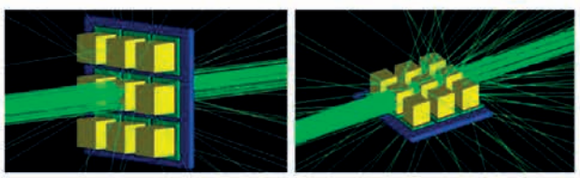

Figure 1: Simulations of the matrix configuration (left) and of the three-cluster configuration (right) with a neutron flux (green tracks). It is possible to see scattered and not scattered neutrons.

The cross-talk probability *CT* is defined by Equation 1:

$$CT = 1 - \frac{\sum_{i=1}^{9} Cell_i}{DET} \quad (1)$$

where *DET* is the integral of the number of particles detected by the whole detector configuration considered and $Cell_i$ represents the number of particles detected by the one and only cell i (i = 1, ..., 9). The overall cross-talk percentage values for both configurations are shown in Figure 2 .

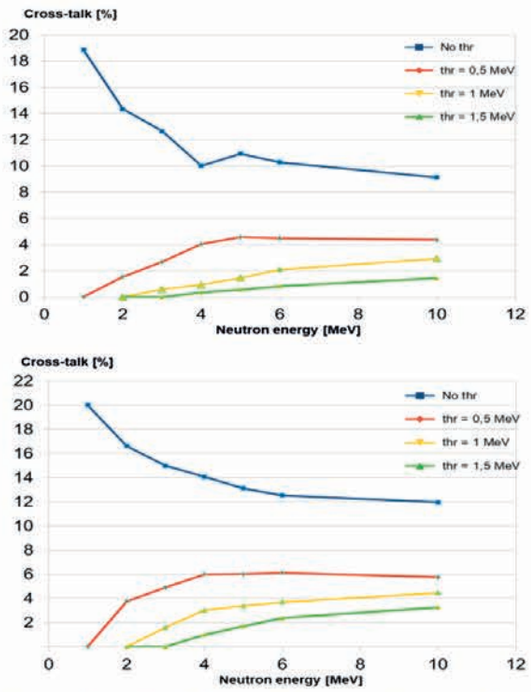

Figure 2: Overall cross-talk percentage values as a function of the neutron flux energy for the matrix (top) and the three-cluster (bottom) configuration. A different curve is plotted for each detection threshold setting in the elementary cell.

Higher cross-talk probabilities are observed for lower detection thresholds, especially for lower energy neutrons, as expected. Reasonable values of the cross-talk probability are found for both configurations with detection thresholds of 0.5, 1 and 1.5 MeV, even for higher energy neutrons [6].

EFFICIENCY SIMULATION STUDY

To estimate the efficiency values, fluxes of 10^6 neutrons impinging over the entire considered configuration surface were simulated, as shown in Figure 3.

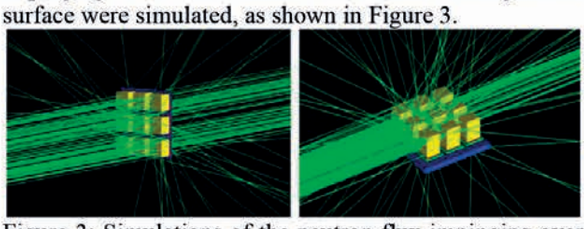

Figure 3: Simulations of the neutron flux impinging over the entire matrix configuration surface (left) and the three-cluster configuration surface (right).

The efficiency *EFF* is defined by the Equation 2:

$$EFF = \frac{DET}{TOT} \tag{2}$$

where *DET* is the number of particles detected by the whole considered configuration and *TOT* is the number of simulated neutrons impinging over the entire considered configuration surface. The number of particles detected by each cell is slightly overestimated because of the cross-talk effects. Thus, the efficiency values were corrected by the corresponding cross-talk probability values. The results are plotted in Figure 4.

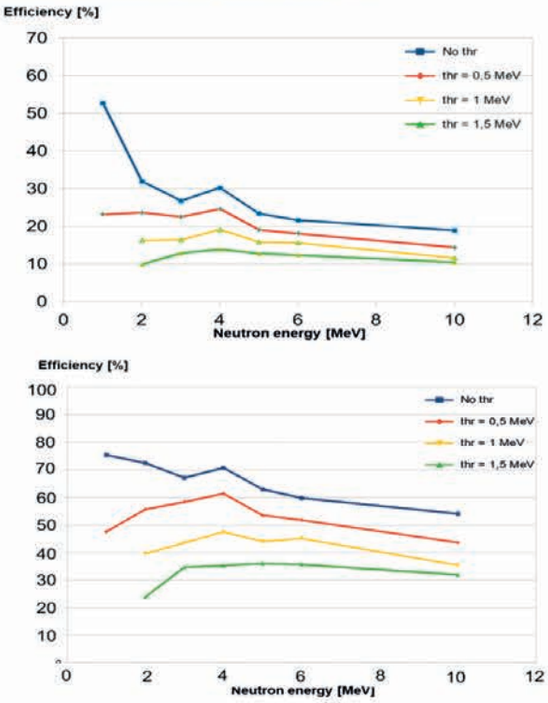

Figure 4: Corrected efficiency percentage values as a function of the neutron flux energy for the matrix configuration (top) and three-cluster configuration (bottom).

Higher values of efficiency are obtained for the three-cluster configuration, as expected. Efficiency values larger than 10% for the matrix configuration and larger than 30% for the three-cluster configuration are found even with detection thresholds of 1 and 1.5 MeV for 10 MeV neutrons [6].

The whole project, involving the INFN (LNS, CT and MI units), University of Catania and the Politecnico of Milano, recently received financial support thanks to funding of Italian Government PRIN2021 ANCHISE (contract 2020H8YFRE).

REFERENCES

[1] E.V. Pagano et al., Front. Phys. 10:1051058, (2023).
[2] A. Pagano et. al, EPJ A, 56 (2020) and refs therein.
[3] E.V. Pagano et. al., EPJ Web of Conferences, 117 (2016) 10008 and refs therein.
[4] P. Russotto et al., Jour. of Phys. Conf. Series 1014, (2018) 012016;
[5] N.S. Martorana et al., Front. Phys. 10:1058419, (2022);
[6] G. Santagati, E.V. Pagano, et. al., to be published in RAD Conference 2023 Proceedings and refs therein.

Calibration of FARCOS DSSSD by front and back strips comparison

F. Risitano[1,2], B. Gnoffo[1,3], M. Trimarchi[1,2], L. Acosta[4], G. Cardella[1], E. De Filippo[1], D. Dell'Aquila[5,6], E. Geraci[1,3], I. Lombardo[1,3], C. Maiolino[7], N.S. Martorana[3,7], A. Pagano[1], E.V Pagano[7], M. Papa[1], S. Pirrone[1], G. Politi[1,3], L. Quattrocchi[1,2], F. Rizzo[3,7,8], P. Russotto[7], C. Zagami[3,7,8]

1) INFN – Sezione di Catania, Italy
2) Dipartimento MIFT, Università degli Studi di Messina, Italy
3) Dipartimento di Fisica e Astronomia "Ettore Majorana", Università degli Studi di Catania, Italy
4) Instituto de Física, Universidad Nacional Autónoma de México, Mexico
5) INFN – Sezione di Napoli, Napoli, Italy
6) Dipartimento di Fisica "Ettore Pancini", Università degli Studi di Napoli Federico II, Italy
7) INFN – LNS, Catania, Italy
8) Centro Siciliano di Fisica Nucleare e Struttura della Materia - Catania, Italy

Abstract - The FARCOS array developed by the CHIRONE collaboration is an innovative detector which over the years has led to several accomplishments at LNS [1]. Thanks to its three different stages, it is possible to apply different detection techniques depending on the type and energy of the incident ions. Furthermore, thanks to its small size and multitude of channels it is possible to obtain high angular and energy resolutions [2]. In this activity report the results of the calibration of the FARCOS 1500 μm thick DSSSD will be discussed, also carrying out a comparison between the front and back strips, as a check on the quality of the calibration obtained.

INTRODUCTION

The FARCOS array was developed in the context of the CHIRONE collaboration in order to obtain, with a small and modular telescope, high angular and energetic resolutions that cannot be achieved by the only CHIMERA multi-detector [1]. A FARCOS array is a detection system made of three stages: two Double-Sided Silicon Strip Detectors (DSSSDs), and a third stage of our CsI(Tl) scintillators. The usage of DSSSDs in nuclear physics is becoming widely common thanks especially to the performance they can offer [2]. In particular, in the case of FARCOS, DSSSDs of 32 strips both on the front (junction side) and on the back side (ohmic side) provide a grid of 1024 "virtual" pixels for a total active surface of 64x64 mm^2.

Although DSSSDs offer numerous benefits, due to their angular and energetic resolution characteristics, they can suffer from some issues. Mainly, with fragmentation reactions with a high number of fragments detected, the correct event-by-event assignment of the particle's trace, i.e. the identification of the single pixel through which the particle passed, can be complicated. Another problem instead can arise from the possible interaction of the incident particles with oxide inter-strip regions which also considerably complicates the reconstruction of the particle track. In this report, the calibration of the front and back strips of the 1500 μm thick FARCOS DSSSDs, used during the CLIR experiment at the LNS, will be reported. Particular attention will also be paid to the analysis of interstrip events, in order to evaluate the accuracy of the reconstruction of the energy loss of the incident ion as the sum of the energy released in the two adjacent strips.

EXPERIMENTAL SETUP

The analysed data for this work belonged to the CLIR experiment, performed at INFN-LNS [3,4]. A radioactive beam was produced by the FRIBs facility fragmenting a ^{18}O (55 MeV/u) primary beam on a ^{9}Be target, 1500 μm thick. Radioactive ions of the cocktail beam were identified by means of the ΔE-ToF technique, ranging from ^{6}He to ^{17}C, also containing interesting study cases for clustering physics, like ^{10}Be, ^{13}B and ^{16}C. The main purpose of the experiment was in fact to study break-up reactions on a light target using the 4π CHIMERA multi-detector [5], coupled with four FARCOS telescopes. These arrays were placed between the sphere and the forward rings of CHIMERA, at small angles around the beam axis, covering polar angles $1.6° < \theta < 8.2°$.

FARCOS CALIBRATION

Calibration of the FARCOS 1500 μm thick stages must be done individually for each strip, both on the front and back sides. This work is important in order to identify the exact pixel (or intersection of front-back strip) of the passage of the ion through the detector, and therefore uniquely associate the θ and φ scattering angles with respect to the beam axis. Each single strip of the front side can be calibrated by simulating the energy loss of ions of the cocktail beam undergoing elastic scattering on the carbon ions of the reaction target. These values can then be correlated with their corresponding channel obtained from ΔE_{1500}-E_{CsI} plots, allowing to obtain a linear calibration, as the one shown in Fig. 1.

On the other side, calibrations of the back strips of the detector can be obtained by correlating the calibrated energy value on the front side with the channel value obtained, event-by-event, on the back side. Such a typical

calibration matrix can be observed in Fig. 2, also showing the calibration line obtained.

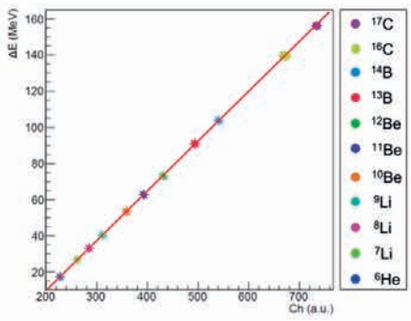

Figure 1: linear calibration for a single strip of a 1500 μm stage of FARCOS.

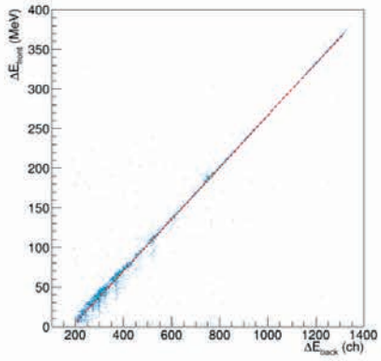

Figure 2: matrix showing the calibrated signal on the front side vs the channel values obtain on a single back strip.

The technique shown can be used regardless of the energy and type of incident ion, since, for a DSSSD, the energy detected on the front side (E_f) is the same as on the back side (E_b), both behaving linearly. Furthermore, the benefit of this technique is that it can also be applied on the front side, correlating the calibrated signal of the backs with the uncalibrated one of the fronts, as a further check of the uniformity of the calibration among all the strips. A further check of the calibration was then carried out by calculating, for each 1500 μm FARCOS stage, the difference between the energy collected, event-by-event, between front and back strips. This work was carried out initially for single multiplicity events on the front and back sides; subsequently the work was expanded by selecting interstrip events on one side of the detector, in order to verify their accuracy with the value of the energy gathered from the single multiplicity event on the opposite side. Fig. 3 shows the difference $V=E_f - E_b$ in MeV, between single multiplicity events both on the front and on the back sides: a bell shape centred at zero can be observed with FWHM ≈ 0.68 MeV.

The trend obtained, however, appears to be slightly different in the case of interstrip events. In the case of an interstrip, the energy loss attributed to event is calculated as the sum of the values obtained of the two adjacent strips.

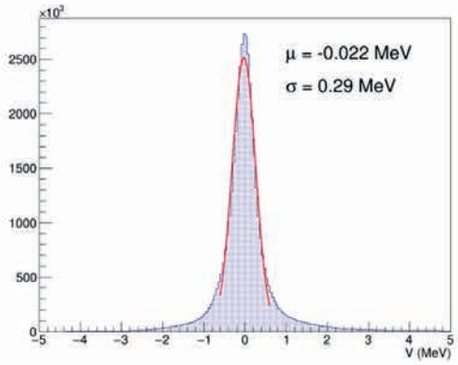

Figure 3: difference between the energy values between front and back sides obtained for single multiplicity case.

In Fig. 4 two distributions are shown: the purple distribution represents interstrip events on the front side with single multiplicity events on the back; the blue distribution refers instead to interstrip back events, with a single front.

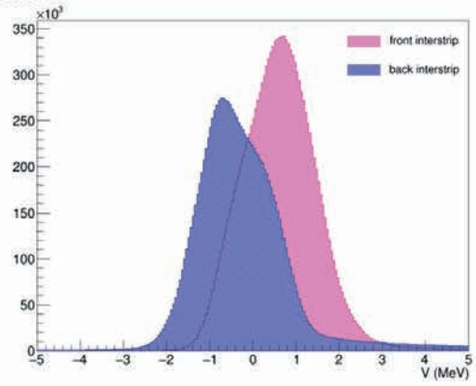

Figure 4: difference between the energy values between front and back sides obtained in the case of front-interstrips (purple) and back-interstrips (blue) (see text).

Other than a widening of the peak, it is possible to observe a shift between the two trends compared to the graph in Fig. 3: in the case of front-interstrip events, a shift to higher values is recorded, while on the back-interstrip case to lower values. This means that there appears to be an overestimation of the reconstructed energy value in the case of interstrip events of approximately ≈ 1 MeV with respect to the single multiplicity one detected on the other side. Although in the case of interstrip events there is a clear worsening of the energy resolution, it is still possible to use those events which maintain an acceptable resolution window.

REFERENCES

[1] E.V. Pagano et al., EPJ Web of Conferences 117 (2016) 10008.
[2] G. Cardella et al., to be published to NIM A;
[3] F. Risitano et al 2023 J. Phys.: Conf. Ser. 2619 012013;
[4] F. Risitano et al, Il Nuovo Cimento 47 C (2024) 43.
[5] A. Pagano et al., Nucl. Phys. A 734 (2004) 504-511.

New MAGNEX digital electronics: development of on-board coincidences

A. Spatafora[1], G. Brischetto[1], F. Cappuzzello[1,2], D. Carbone[1], M. Cavallaro[1], F. Delaunay[3], P. Finocchiaro[1], J.R.B. Oliveira[4], R. Persiani[2], V. Soukeras[1], D. Torresi[1] for the NUMEN Collaboration

1) Istituto Nazionale di Fisica Nucleare, Laboratori Nazionali del Sud, Catania, Italy
2) Dipartimento di Fisica e Astronomia "Ettore Majorana", Università di Catania, Catania, Italy)
3) LPC Caen, Normandie Univ., ENSICAEN, UNICAEN, CNRS/IN2P3, Caen, France
4) Instituto de Fisica da Universidade de São Paulo, São Paulo, Brazil

Abstract – The overall electronics system for the new MAGNEX focal plane and the gNUMEN γ-ray calorimeter detectors is presented focusing on the development of on-board coincidences, particularly relevant for the next generation NUMEN experiments.

OVERVIEW

The upgrade of the Superconducting Cyclotron and the MAGNEX facility is ongoing at the INFN-LNS within the POTLNS project [1]. The renewal of the LNS infrastructure was triggered by the NUMEN project [2], aiming to access experimentally driven information on Nuclear Matrix Elements involved in the neutrinoless double beta decay ($0\nu\beta\beta$) by measuring cross sections of heavy-ion induced double charge-exchange reactions. To make feasible a systematic study of all the nuclei candidate to $0\nu\beta\beta$ decay, the upgrade of the LNS facility is devoted to increase the experimental yield by more than two orders of magnitude.

The development of the new Focal Plane Detector (FPD) and gNUMEN γ-ray calorimeter for the MAGNEX spectrometer is requiring new digital electronics. Channel density (up to 1000 channels), rate capability (up to 500 kHz/channel), data throughput (up to 600 MB/s), time (better than 1 ns) and energy resolution, flexibility to adjust to varying experimental conditions are the main requirements for the next MAGNEX electronics [3].

The future MAGNEX experimental set-up will use 64 channels CAEN A1429 charge-sensing preamplifiers and the newly developed CAEN VX2745(B) digitizers for the front-end and read-out electronics. A sketch of the new MAGNEX electronics scheme is shown in Figure 1. Twenty VX2745 digitizers will be devoted to read-out the signals coming from the 1200 pads of the gas tracker while 24 digitizers will be used to treat the 1440 signals coming from the 720 SiC-CsI(Tl) telescopes present in the PID system. These VX2745 digitizers will have on board the Pulse Height Analysis (PHA) firmware, using a fast filter and a trapezoidal shaper to measure the timestamp and the pulse height, proportional to the energy. The A1429 preamplifier outputs and the VX2745 digitizers inputs are differential, to limit noise pickup effects. Two more VX2745B digitizers will be used for the gNUMEN γ-ray calorimeter made of 110 $LaBr_3(Ce)$ scintillators and phototubes. The VX2745B is the single-ended input version of the VX2745, required to guarantee the proper coupling to the 50 Ω single-ended phototube outputs. These 2 devices will have on board a Pulse Shape Discrimination (PSD) firmware performing a timestamp measurement with a digital discriminator and the long/short-gate energy measurement via charge integration. This second firmware is more suitable for the treatment of the fast phototube signals in which the spectroscopic information is encoded into the integral of the signal.

The parameter configuration and data readout use a Gigabit Ethernet connection (upgradable to 10 Gb with optical fiber link) and is accessible to the user via CAEN C/C++ libraries. The development of the software for the data acquisition and the parameters configuration and the construction of an appropriate 10 Gb network infrastructure are ongoing.

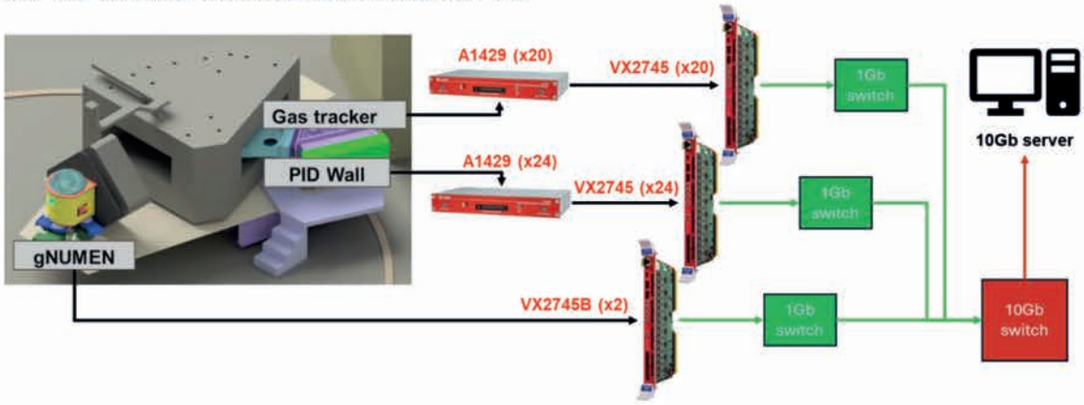

Figure 1: Sketch of the electronics and DAQ system for the MAGNEX FPD and gNUMEN γ-ray calorimeter.

ON-BOARD COINCIDENCES

Although all digitizer channels are independent and the system does not need any common trigger, the development of coincidences among different channels in the same or among different boards is a useful tool to reduce the total data throughput to manageable values and to reduce the required capacity of the storage system.

To develop the coincidences among different detectors or measure the time of flight between channels on different digitizers, the modules must be synchronised. This implies that common clock and start/stop commands must be propagated to all modules from the data acquisition program. In the tests performed so far, a daisy chain was used to distribute the clock and start/stop signals from a *master* digitizer to the others [4]. However, a long daisy chain is expected to introduce a significant time jitter and consequently a different distribution of those signals, using the VME backplane, is under study for the final system.

In the PID system, it is useful to register only the events where both the SiC and the CsI signals of the same telescope are actually detected. Let us now assume that the *i* and *j* pair of channels in a digitizer correspond to the SiC and CsI detectors of the same telescope, respectively. In this regard, it is possible to constrain the acquisition of channel *i* to the condition that a signal has also been detected on channel *j* and/or vice versa, provided that an appropriate time coincidence window is defined. This coincidence was tested using signals from a pulse generator and during the in-beam test recently performed at the Laboratori Nazionali di Legnaro (INFN-LNL) performed for the commissioning of the first two towers of the future PID system [5].

In the gas tracker, it will be useful to reject the noise due to the firing of isolated pads [6]. To this purpose, more sophisticated coincidence masks need to be implemented: the acquisition of the pad *i* is constrained to one of the *i+1* and *i-1* first-neighbour pads. This coincidence mapping has been successfully tested using the tracker prototype during the α-source tests performed in the TeBe facility at LNS. Future tests will be done for quantifying the noise suppression capability of the applied condition and to evaluate the possible extension of the selection to the second- or third-neighbour pads.

Due to the high beam intensities to be used in the DCE experiments, the target region will become a very strong source of radiation, including gamma rays, fast neutrons, electrons, light and heavy ions. The count-rate expected for the gNUMEN γ-ray calorimeter is hundreds of kHz/detector in the high intensity beam experiments. It will be mostly due to the several background sources that will be huge compared to the extremely small DCE cross-sections. This condition requires us to place more stringent constraints to the acquisition of the gNUMEN signals. The idea is to enable the data acquisition in the 110 $LaBr_3(Ce)$ digitizer channels only in case that an ejectile actually join the PID system and generate a signal in one (or both) stage of a telescope. In this framework, the OR of the 720 telescope triggers will result in a unique logic PID-OR signal used to enable the gNUMEN acquisition. This coincidence with the PID system is expected to reduce the gNUMEN throughput by a factor of about 25.

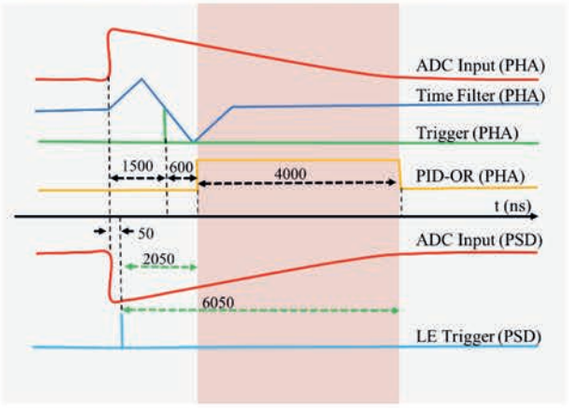

Figure 2: Analogic and logic signals processed by VX2745 digitizers using the PHA and PSD firmwares (see text).

Due to the time-of-flight inside the MAGNEX spectrometer and the time needed by the PHA algorithm to generate the trigger and by the boards to generate the PID-OR of all the detectors, it is necessary to delay the gNUMEN signals to ensure the signal coincidence. First measurements of this delay have been performed at the INFN-LNS using a pulse generator as a source of signals distributed to two different digitizers. The boards were equipped with PHA and PSD firmwares to simulate the readout of the signals coming from the PID system and gNUMEN detectors, respectively. The obtained results are shown in Figure 2 in which it is evident how the delay between the signal arrival and the PID-OR signal is due to two different components: the time needed to produce the trigger in the digitizer (1500 ns) and the time needed to make the OR of the 64 chs inside the board (600 ns). In the PSD board, where the trigger production is ≈ 50 ns, a large delay is required (from 2050 to 6050 ns, assuming a coincidence window of 4000 ns) to ensure the acquisition of the second signal.

The newly developed PSD and PHA firmwares use the FPGA memory to delay the digitized signals prior to be processed by the firmware. Being immune to noise pickup or signal distortion, such a digital delay is superior to an analog delay. Those firmware versions implementing digital delays have been recently tested at the INFN-LNS and at the IJCLab in Orsay during an in-beam test with the gNUMEN demonstrator to prove the reliability of the delayed coincidence for the purposes of NUMEN.

REFERENCES

[1] https://potlns.lns.infn.it/it/
[2] F. Cappuzzello et al., Eur. Phys. J. A (2018) 54 : 72.
[3] F. Cappuzzello et al., IJMP A 36 (2021) 2130018.
[4] F. Delaunay et al., LNS activity report 2021-2022
[5] D. Carbone et al., LNS activity report 2023
[6] D. Torresi et al., LNS activity report 2023
[7] J. R. B. de Oliveira et al., LNS activity report 2023

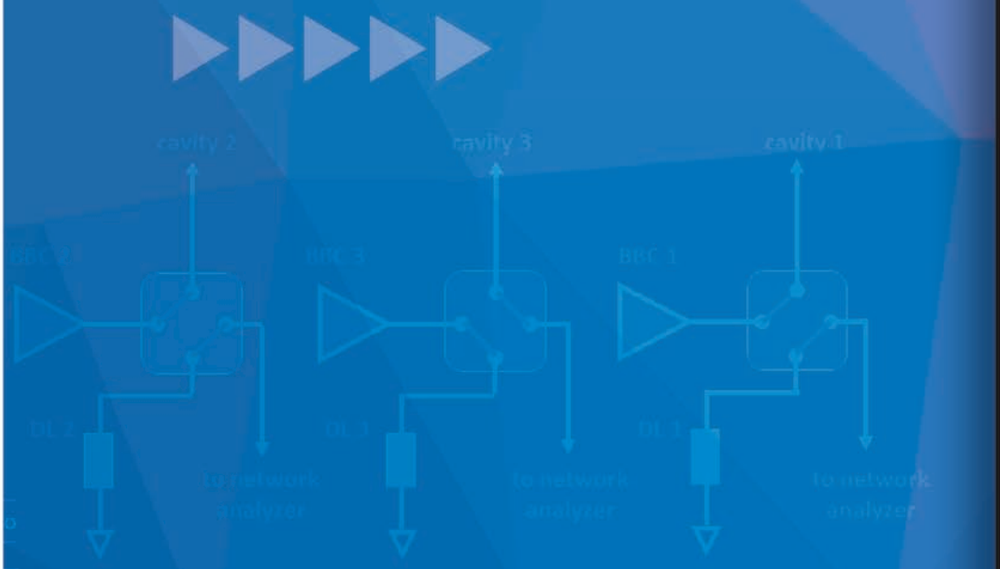

05

ION SOURCES AND ACCELERATOR

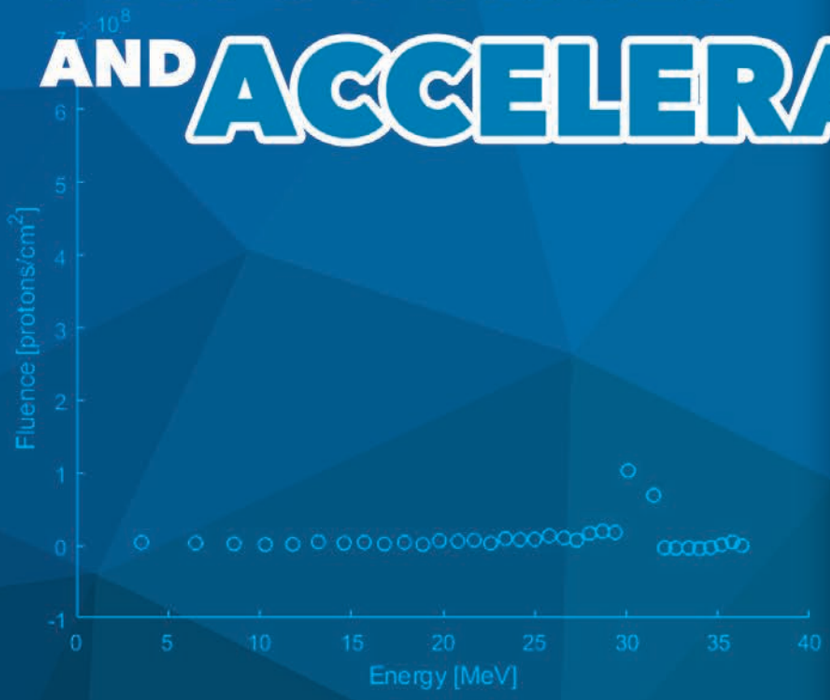

Research

Analyses

Results

INFN LNS

- Tandem, Superconducting Cyclotron, Ion Sources, Beam Lines activities
- Electron acceleration scheme for the I-LUCE facility
- LNS contribution to Divertor Tokamak Test project
- Development of a Flexible ECR Plasma Ion Source at LNS for high- intensity metal ion beams: source design and metal vaporisation modelling
- First investigation of longitudinal beam dynamics in a co-propagating Dielectric Laser-driven Accelerator
- Unfolding procedure for proton and ion spectrum reconstruction of laser-target emission
- The New Dummy Loads System for the RF Power Amplifiers of the LNS Superconducting Cyclotron (CS)

Tandem, Superconducting Cyclotron, Ion Sources, Beam Lines activities

D. Rifuggiato[1] on behalf of INFN-LNS Accelerator Division

1) Istituto Nazionale di Fisica Nucleare - Laboratori Nazionali del Sud, via S. Sofia 62, 95123 Catania, Italy

Abstract - This report briefly describes the main activities carried out in 2023 on the LNS accelerators, finalized to their restart after the stop due to the POTLNS activities [1]. The experimental activities with the ion beams accelerated by the Tandem and the Superconducting Cyclotron were stopped at the end of 2020 and have not yet restarted.

Concerning the Tandem activities, the new vacuum control system, the update of the SF6 control system, the re-organization of the injection line and the extraordinary maintenance of the 450 kV platform were carried out.

As far as the Superconducting Cyclotron, maintenance activities on the ancillary systems started. Finally, the feasibility of the cryogenic upgrade of SERSE, the superconducting source for production of high intensity and high charge state beams, started to be evaluated.

TANDEM ACTIVITIES

SF6 system upgrade

In order to upgrade some parts of the SF6 system, an updated and detailed schematics has been produced. In particular, the heart of the whole system has been replaced by a new Programmable Logic Controller (PLC) to enhance control and monitoring capabilities. This operation also allowed us to review all the gas phases already programmed.

At the same time a new remote interface was developed and all the programmed phases were revised and corrected, see Fig. 1.

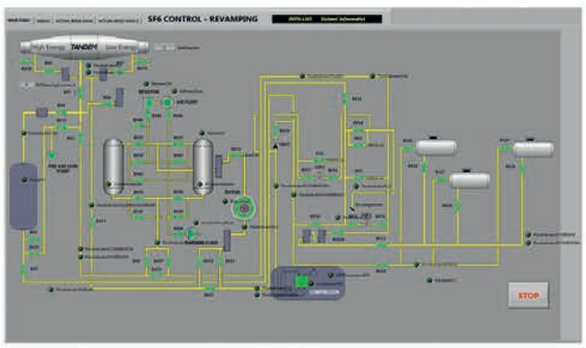

Figure 1: SF6 remote interface

New vacuum control system

A new local and remote vacuum control system for the accelerator tubes has been designed, complete with user-friendly interfaces accessible from the control console, see Fig. 2.

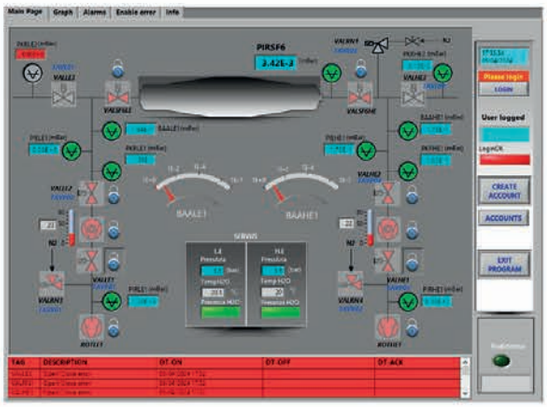

Figure 2: Vacuum control system interface

Tandem Low Energy line

The first triplet of the Tandem low energy line has been cleaned, geometrically referenced, and reinstalled in line. At the same time, the maintenance operation on the second triplet line began and is still underway.

Other activities

In addition to the activities concerning the SF6 system and the vacuum control system, the following activities have been carried out: gas recovery system testing, insulation test on the crown tips system, new Generator Volt Meter (GVM) installation for Tandem stability reasons, High-vacuum pumping tests and gas analysis using Residual Gas Analyzers (RGAs) to evaluate gas purity, server infrastructure enhancement, development of remote control of the encoders in the power supplies for steerers and magnetic quadrupoles within the TANDEM extraction line and finally the development of software for diagnostic TV cameras to be used along the beamline.

CYCLOTRON ACTIVITIES

A big effort has been devoted to follow the construction of the new superconducting magnet and to organize the Cyclotron ancillary activities at the laboratory.

New superconducting magnet

Concerning the new superconducting magnet, the room temperature mapping of the four single coils, inferior and superior alfa coils, inferior and superior beta, was carried out at the ASG Superconductors in Genova, see Fig. 3. The results are quite encouraging in terms of the first harmonic component at radii close to the extraction radius. This mapping is mandatory for the assembling of the whole new cryostat, which is able to host the new configuration of median plane penetrations.

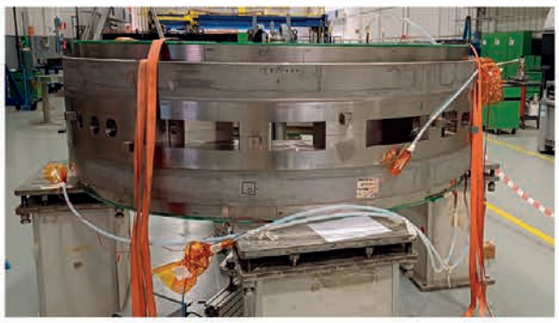

Figure 3: Assembling of the Alfa coils couple on the Helium vessel central ring

Beam dynamics study

The positioning of the coils inside the Helium vessel can be accomplished with a mechanical accuracy of about 0.1 mm, this can produce a field imperfection of the new superconducting magnet. In order to evaluate the effects of the first harmonic content on the beam quality, several beam simulations have been performed, see Fig. 4.

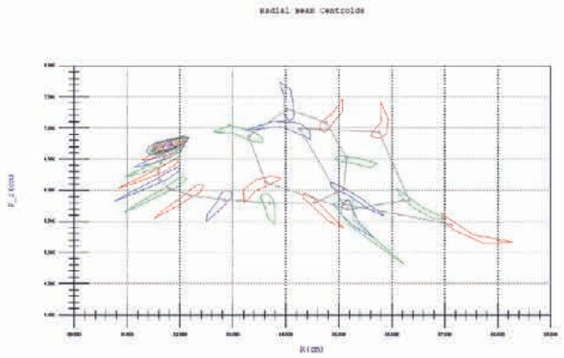

Figure 4: Effect of first harmonic content on beam dynamics

Ancillary systems: RF, cryogenics, vacuum, laser tracker use, field mapper, new beam lines

Concerning radiofrequency, the design of the new mechanical configuration of the axial buncher started, aiming at a better cooling efficiency. The first tests of the RF amplifier were accomplished in view of the Cyclotron restarting.

Concerning cryogenics, a study on several components of the helium liquefier started aiming at performing a significant upgrade of the plants in collaboration with Air Liquide.

Concerning the vacuum system, several preparatory activities on the single sub-systems, i.e. the cryostat vacuum, the liner vacuum and the acceleration chamber vacuum have been carried out.

A working group has been defined for the design and development of the new magnetic field mapper. This device will be quite similar to the one successfully used in 1993-1994 for the same scope, based on the search coil system.

The lower iron pole of the CS has been geometrically mapped using laser tracker, adding and measuring reference points: now it is possible to identify with extreme precision the median plane, the zero degree direction and the vertical axis at any time and in any condition with the machine closed, in working configuration.

The supports and some element of the Fraise line were installed, using the laser tracker system, see 5. A similar operation was carried out in the Magnex room where the two 8 tons dipoles and their supports were installed.

Figure 5: First quadrupole doublets on FRAISE room

INJECTORS ACTIVITIES

Negative Injectors

In 2023 all extraordinary maintenance activities on the High Voltage Platform aimed at the production of negative beams were completed.

While waiting to obtain the authorizations for the restart, the platform has been identified among the laboratory

facilities to be modernized and improved for enhancing safety, efficiency, and overall effectiveness. For this purpose, it was decided that the current oil-insulated transformer will be replaced with a resin-insulated one after twenty-five years of continuous operation. Figure 6 shows a possible arrangement of the new device inside the leaded structure that houses the platform.

A resin dry type transformer is more safe, fire-retardant, moisture-proof, explosion-proof and can be directly installed in the electrical terminal site, but on the other hand it has a considerable dimension, weight and exposed high voltage terminals. It must therefore be enclosed by a safety guard to provide protection to people against access to hazardous parts and to limit the access of solid foreign objects. A feasibility study is underway that will lead the best course of action to the replacement of the present 250 kV isolation transformer.

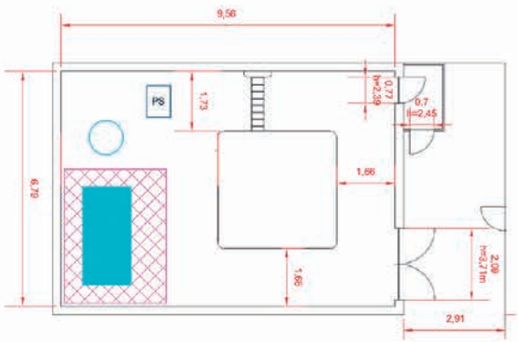

Figure 6: Possible arrangement of the resin insulation transformer inside the Tandem Injectors box

ECR Ion Source

In order to deliver the requested beams, a significant upgrading of the Superconducting Cyclotron (SC) is ongoing with the goal to increase the beam power up to 10kW for ions with mass up to 40 amu [1].

At first, a cost-benefit study on the SERSE superconducting ion source showed that the revamping of the cryogenic system was too wasteful, but at the end of the year, after an inspection together with the company Cryogenic, an alternative route was taken.

After removing the superinsulation along the cylindrical section of the radiation shield, a radiation load of 145 W was estimated, assuming emissivity equal to 0,1. In order to reduce the radiation load, the structure of the nitrogen tank used to cool the radiation shield should be removed and insulated by a new formed 10-layer blanket superinsulation. If the shield temperature is still too high, a cryocooler can be installed thermally linked to the top seam of the radiation shield.

We are currently working to implement the above tips, according to Cryogenic outline.

The next planned activities are the replacement of all o-rings, the closing of the yoke and a pressure test to verify the achievable insulation vacuum.

REFERENCES

[1] https://www.lns.infn.it/it/potlns.html

Electron acceleration scheme for the I-LUCE facility

S. Arjmand[1], A. Pappalardo[1], A. Amato[1], G. Cantone[1], D. Oliva[1], F. Vinciguerra[1], J. Suarez-Vargas[1], G. Angemi[1], E. Caruso[1], R. Catalano[1], G. Cuttone[1], F. Farokhi[1], S. Fattori[1], O. Giampiccolo[1], M. Guarrera[1], A. Kurmanova[1], G. Petringa[1], A. Pizzino[1], A. Sciuto[1], and G.A.P. Cirrone[1]

1) Istituto Nazionale di Fisica Nucleare, Laboratori Nazionali del Sud (INFN-LNS), Catania 95125, Italy

Abstract - The drive to enhance foundational laser technology, including increasing efficiency and repetition rates, has been significantly motivated by the potential to create compact, high-brightness particle and radiation sources. Technological advancements have led to the emergence of a new generation of ultrafast, high-power laser systems operating at substantially higher repetition rates. By 2026, the Istituto Nazionale di Fisica Nucleare - Laboratori Nazionali del Sud (INFN-LNS) will finalize the construction of a state-of-the-art high-power laser facility named I-LUCE (**I**NFN Laser-ind**UCE**d Radiation Acceleration), representing a significant milestone in its progress. This facility represents a European initiative focused on creating a specialized research facility for particle acceleration, employing innovative concepts in plasma acceleration and laser technology. At the core of I-LUCE, our goal is to propel electrons using laser wakefield acceleration (LWFA), representing an exciting frontier in contemporary physics. This method presents a route to achieving ultra-relativistic energies within compact systems. This paper explores the theoretical underpinnings and studies in LWFA, plasma production and focusing on the intricate interplay between laser pulses and plasma wakefields. Through a detailed examination of the underlying physics, including the ponderomotive force, electron trapping, and acceleration mechanisms, we elucidate the fundamental principles governing electron dynamics in LWFA.

LASER-PLASMA ACCELERATION

By harnessing the dynamic interplay between a robust laser pulse and plasma, laser-plasma acceleration emerges as a cutting-edge method for driving charged particles forward. The resultant electric field, significantly stronger than those generated by traditional radio-frequency accelerators, holds immense potential for revolutionizing particle acceleration technologies. Theoretically, this potent electric field could enable the development of compact accelerators capable of achieving particle energies currently beyond reach. Very high energy electron (VHEE) beams, made attainable through laser-plasma acceleration, offer promising applications in FLASH therapy and electron beam dosimetry studies. We are advancing with a novel plasma-discharge capillary waveguide design integrated into laser wakefield acceleration (LWFA). This innovative approach represents a significant advancement in electron-based therapeutic applications, enhancing precision and efficiency. The intricate configuration of the plasma-discharge capillary waveguide, serving as a VHEE source, not only departs from conventional designs but also signifies progress in LWFA contexts. The elongated length of the capillary correlates with increased output of accelerated electrons, while achieving high intensity in laser wakefield acceleration demands an exceedingly narrow internal diameter, typically about 1 millimeter. In the forthcoming I-LUCE project, our aim is to implement a plasma-discharge capillary in conjunction with electron bunches generated through LWFA.

LWFA SCHEME

Electron acceleration via LWFA stands as a promising frontier in modern physics, offering a pathway to ultra-relativistic energies in compact systems [1,2]. At the heart of LWFA lies the intricate interplay between intense laser fields and the plasma medium. When an ultrashort, high-intensity laser pulse propagates through a rarefied plasma, it rapidly ionizes the medium, creating a plasma channel. As the laser pulse traverses this channel, it displaces electrons via the ponderomotive force, leading to the formation of a wakefield behind the pulse. This wakefield, akin to a surfer riding a wave, imparts energy to electrons injected into its trough, enabling their acceleration to ultra-relativistic velocities [1,3]. The dynamics of electron acceleration in LWFA are governed by fundamental principles of plasma physics and electrodynamics. The ponderomotive force, described by the equation below:

$$F_p = -\left(\frac{1}{2m_e}\nabla\left(\frac{1}{v^2}\right) + e\nabla\phi\right), \quad (1)$$

arises from the interaction between the laser electric field and plasma electrons. Here, m_e denotes the electron mass, v represents the electron velocity, e signifies the electron charge, and ϕ stands for the electric potential. In addition to the ponderomotive force, electron trapping, and injection mechanisms play pivotal roles in LWFA. Electrons within the plasma may become trapped within the potential wells of the wakefield, experiencing acceleration phases as they ride the wake. The critical density gradient at the plasma-vacuum interface serves as a natural injector, facilitating the injection of electrons from the background plasma into the accelerating phase of the wakefield. Moreover, the quality of accelerated electron beams critically depends on various parameters, including laser intensity, pulse duration, plasma density, and waveguide geometry. Optimizing these parameters is essential to achieving high-energy electron beams with narrow energy spreads and low divergence. At this stage, we delve into the theoretical foundations of LWFA,

elucidating the complex dynamics of electron acceleration through rigorous mathematical formulations and physical principles.

PLASMA PRODUCTION

While LWFA typically involves the production of plasma, various methods exist for initiating plasma formation. Our objective is to induce plasma formation through the utilization of electrical discharge within a plasma-discharge capillary, a commonly employed technique for plasma generation [4,5,6,7]. The plasma-discharge capillary design offers several advantages for controlled plasma generation. Its confined geometry helps maintain stability and uniformity in the plasma formation process, ensuring consistent results across experimental runs. This method involves the application of electrical discharge within a specialized capillary structure designed to facilitate plasma generation. A high-voltage electrical discharge is then applied to the capillary, generating a localized electric field within the gas medium (hydrogen). This electric field ionizes the gas atoms or molecules, liberating electrons and creating positively charged ions. Figure 1 shows an example of plasma-discharge capillary waveguide for LWFA.

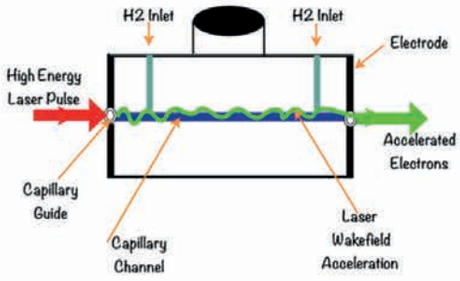

Figure 1: Design of plasma-discharge capillary waveguide for laser wakefield acceleration

Additionally, the capillary structure allows for precise control over parameters such as gas flow rate, discharge voltage, and plasma density, facilitating systematic studies of plasma properties and behavior. The plasma-discharge capillary serves as a controlled environment where the electrical discharge interacts with a suitable gas or medium, inducing ionization and the subsequent formation of plasma [8,9,10,11,12].

The process begins with the introduction of the desired gas, such as hydrogen, or gas mixture into the capillary, creating a conducive environment for plasma formation. As the electrical discharge progresses, the ionized particles within the capillary interact with each other and with the electric field, leading to the formation of a fully ionized plasma state. The plasma thus produced exhibits unique characteristics depending on factors such as gas composition, pressure, and applied voltage. Precisely, an electrical discharge is initially initiated within the capillary. This discharge serves as the energy source, ionizing particles within the capillary by stripping electrons from their atoms or molecules. As the electrical discharge progresses, the ionized particles within the capillary begin interacting with each other and with the electric field generated by the discharge. These interactions lead to the formation of a fully ionized plasma state. The resulting plasma exhibits unique characteristics that depend on several factors: gas composition, pressure, applied voltage. The type of gas used within the capillary affects the composition of the plasma and its properties. The pressure within the capillary influences the density and behavior of the plasma. The voltage applied to initiate and sustain the electrical discharge also impacts the characteristics of the plasma [13].

PLASMA CHANNEL CHARECTERIZATION

The capillary plasma channel facilitates the extended propagation of an intense laser beam, allowing for the generation of higher energy electrons. To resonantly excite the wakefield in LWFA, it is crucial for the duration of the laser pulse to synchronize with the plasma wavelength, which is determined by the density of the plasma. In this regard, comprehending the evolution of plasma density profiles over time holds pivotal importance in achieving desired experimental outcomes. For effective laser guiding at a specific plasma density, it is essential to ensure a sufficiently high-density gradient across the width of the capillary. To quantify this, the concept of plasma channel depth will be studied. This depth is defined as the difference between the maximum density and the minimum density across the cross-section of the capillary, considering its size. This parameter provides a quantitative measure of the density variation within the capillary, which is crucial for assessing the laser guiding capabilities under different plasma conditions. Given the significance of the measured characteristics of capillary discharge plasma in informing future research on laser wakefield acceleration, exploring diverse techniques to enhance result reliability becomes imperative and intriguing.

Among the array of diagnostic methods available for analyzing plasma properties, spectroscopy and interferometry emerge as prominent choices. They distinguish themselves due to their capacity to unveil essential insights into the light emitted during diverse energy transitions and to scrutinize the interference patterns of light traversing through the plasma, respectively.

Our objective is to compare spectroscopic and interferometric methods for assessing reliability. Emissive spectroscopy offers precise measurements of wavelengths and intensities of emitted light, facilitating exploration of elemental compositions, molecular structures, and energy states, including plasma properties. With its precision and versatility, emissive spectroscopy is preferred for probing high-energy particle emissions and understanding plasma properties. Thus, we will employ atomic emission

spectroscopy (AES) using visible light to study plasma properties, including density and temperature [14]. AES detects atomic spectral lines resulting from electronic transitions, aiding chemical analysis by correlating wavelength with elemental abundance. Additionally, we will utilize emissive spectroscopy techniques for low-temperature plasma analysis, investigating properties such as density and temperature through Stark broadening, which reveals plasma characteristics like temperature, density, and electric fields. In plasmas, which are ionized gases containing free electrons and ions, electric fields can arise naturally or be externally applied. These electric fields cause the energy levels of the atoms or ions to shift, resulting in broader spectral lines in the emitted light [15]:

$$n_e = 8.02 \times 10^{12} \left(\frac{\Delta\lambda_S}{\alpha_{1/2}}\right)^{3/2}. \quad (2)$$

The parameter $\Delta\lambda_S$ represents the full width at half maximum (FWHM) of the Stark-broadened spectral line, and $\alpha_{1/2}$ is the reduced wavelength, which is a function of the electron density and temperature [16]. The reduced wavelength is used to quantify the extent of Stark broadening in the spectral line, and the FWHM of the broadened line provides information about the line shape and width, which is related to the electron density and temperature of the plasma. In addition to this, we will employ an interferometry method for plasma characterization (transverse plasma density). This approach aims to deepen our understanding of how light behaves within plasma channels, a fundamental objective in our research endeavors. This understanding relies on quantifying the phase shift experienced by a probing beam during its interaction with the plasma. Mathematically, this phase shift is succinctly expressed by:

$$\Delta\phi\,(y,z) = -r_e\lambda \int_{-x/2}^{x/2} n_e(x,y,z)\,dx. \quad (3)$$

Here, r_e represents the classical electron radius, λ denotes the wavelength of the probing beam, and x signifies the width of the capillary. The variables x, y, and z denote the direction of beam propagation, the vertical position of the probe beam within the capillary, and the distance along the axis of the capillary, respectively. This equation encapsulates the intricate interplay between the probing beam and the plasma's electron density. Once the phase shift is determined, it serves as a crucial link to unveiling electron density within the plasma. The conversion from phase shift to electron density requires tailored formulas, such as the Abel inversion method, etc., depending on the experimental setup, whether it involves cylindrical symmetry or a square cross-section [17,18].

REFERENCES

[1] T. Tajima and J.M. Dawson, Phys. Rev. Lett. 43, 267 (1979).

[2] A. Modena et al., Nature (London) 377, 606 (1995).

[3] P. Chen, J. M. Dawson, Robert W. Huff, and T. Katsouleas, Phys. Rev. Lett. 54, 693 (1985).

[4] Spence, D.J.; Butler, A.; Hooker, S.M. Gas-filled capillary discharge waveguides. J. Opt. Soc. Am. B 2003, 20, 138–151.

[5] T. Hosokai, M. Kando, H. Dewa, H. Kotaki, S. Kondo, N. Hasegawa, K. Nakajima, and K. Horioka, Optical guidance of terrawatt laser pulses by the implosion phase of a fast z-pinch discharge in a gas-filled capillary, Opt. Lett. 25, 10 (2000).

[6] A. Butler, D. J. Spence, and S. M. Hooker, Guiding of High-Intensity Laser Pulses with a Hydrogen-Filled Capillary Discharge Waveguide, Phys. Rev. Lett. 89, 185003 (2002).

[7] S. Karsch, J. Osterhoff, A. Popp, T. P. Rowlands-Rees, Z. Major, M. Fuchs, B. Marx, R. Hörlein, K. Schmid, L. Veisz, S. Becker, U. Schramm, B. Hidding, G. Pretzler, D. Habs, F. Grüner, F. Krausz, and S. M. Hooker, GeV-scale electron acceleration in a gas-filled capillary discharge waveguide, New J. Phys. 9, 415 (2007).

[8] Y. Ehrlich, C. Cohen, A. Zigler, J. Krall, P. Sprangle, and E. Esarey, Guiding of High Intensity Laser Pulses in Straight and Curved Plasma Channel Experiments, Phys. Rev. Lett. 77, 4186 (1996).

[9] D. J. Spence and S. M. Hooker, Investigation of a hydrogen plasma waveguide, Phys. Rev. E 63, 015401(R) (2000).

[10] S. Arjmand et al., Characterization of plasma sources for plasma-based accelerators, 2020 JINST 15 C09055.

[11] S. Arjmand et al., Spectroscopic Measurements as Diagnostic Tool for Plasma-Filled Capillaries, JACoW IPAC2022 (2022) WEPOST035.

[12] S. Arjmand et al., Spectral line shape for plasma electron density characterization in capillary tubes, J. Phys. Conf. Ser. 2439 (2023) 012012.

[13] S. Arjmand et al., Shot-by-shot stability of the discharge produced plasmas in suitably shaped capillaries, 2023 JINST 18 C04016.

[14] S. Arjmand et al., Different elements, same results: time-resolved temperature determination by oxygen and nitrogen elements, 2023 JINST 18 P08003.

[15] D.G. Jang, M.S. Kim, I.H. Nam, H.S. Uhm and H. Suk, Density evolution measurement of hydrogen plasma in capillary discharge by spectroscopy and interferometry methods, Appl. Phys. Lett. 99 (2011) 141502.

[16] H.R. Griem, *Spectral line broadening by plasmas*, Academic Press, Amsterdam, The Netherlands (1974).

[17] I.H. Hutchinson, Principles of Plasma Diagnostics, Cambridge University Press (1987), pg. 124.

[18] A.J. Gonsalves, T.P. Rowlands-Rees, B.H.P. Broks, J.J.A.M. van der Mullen and S.M. Hooker, Transverse Interferometry of a Hydrogen-Filled Capillary Discharge Waveguide, Phys. Rev. Lett. 98 (2007) 025002.

LNS contribution to Divertor Tokamak Test project

G. S. Mauro[1], G. Torrisi[1], C. Salvia[1,2,3], V. Francalanza[1,2], A. Cardinali[1,4], A. Pidatella[1], G. Finocchiaro[1,2], S. Gammino[1], G. Castro[1], L. Celona[1], E. Naselli[1], S. Passarello[1] and D. Mascali[1]

1) Istituto Nazionale di Fisica Nucleare- Laboratori Nazionali del Sud (INFN-LNS), Via S. Sofia, 62, 95123 Catania
2) Università degli Studi di Catania - Dipartimento di Fisica e Astronomia (UNICT-DFA), Via S. Sofia, 64, 95123 Catania
3) Centro Siciliano di Fisica Nucleare e Struttura della Materia (CSFNSM), Via S. Sofia 64, 95123 Catania
4) ENEA Centro Ricerche Frascati, Via Enrico Fermi 45, 00044 Frascati

Abstract - The Italian Divertor Tokamak Test (DTT) facility is conceived to allow various magnetic configurations and reproduce edge conditions close to DEMO for a reactor-relevant exploration of alternative power exhaust solutions in an integrated scenario [1], as envisaged in the European roadmap to fusion electricity. To attain a power-over-radius ratio of around 15 MW/m crossing the separatrix, a heating power of 40-45 MW is required and will be provided by a suitable mix of electron cyclotron resonance heating (ECRH), neutral beam injection and ion cyclotron resonance frequency (ICRF) waves. INFN-LNS is contributing on ICH and ECH antennas and waveguide design respectively. Moreover INFN-LNS are involved also in the development of diagnostics tools based on reflectometry and X-ray.

3-STRAP CURVED ANTENNA FOR ICH

Main objective of this task is the definition of the most suitable antenna to start delivering Ion Cyclotron Power on DTT. Because of DTT scenario flexibility, Ion Cyclotron coupling is a difficult task. Moreover, to fulfil its mission DTT needs to be supplied reliably by 45 MW of power thus imposing sound solution in RF coupling structures. This determines a step approach strategy in defining the Ion Cyclotron system. Indeed, an initial step of limited power will demonstrate the handling capability of the chosen antenna that must reach the level of 1.5 MW, keeping the electric fields below 2.5 MV/m in the antenna and minimising spurious fields responsible for ion sputtering.
Starting from previous, 2022 flat antenna model [2, 3], 2023 LNS contribution to this task regarded the design and the optimization of a curved 3-strap antenna launcher by using the commercial RF simulation software CST Studio Suite. The curved antenna employs poloidal and toroidal curvatures suitable to better couple RF to DTT plasmas. In CST the plasma has been replaced by a standard, isotropic, dielectric layer of proper relative permittivity. The curved 3-strap antenna is shown in Figure 1. The model is composed of: a) the antenna box, composed of three minor boxes, one for each strap, separated by two septa; b) the Faraday screen, composed of a fixed number of equally spaced rods; c) the three straps: the central one is fed by two coaxial cables, operated with a phase difference of 180°, the side ones are equal and fed each by a single coaxial, connected to a strip-line. The coaxial characteristic impedance is equal to 30 Ω. The goal of the CST modelling was to optimize the antenna structure to couple a power ≥ 1.5 MW to the dielectric load with a progressive phase shift of 180° between toroidally adjacent straps. In CST model, some parameters have been fixed by the DTT standardization procedure, while the remaining others, such as strap dimension and position, have been studied and modified for the tuning purpose.

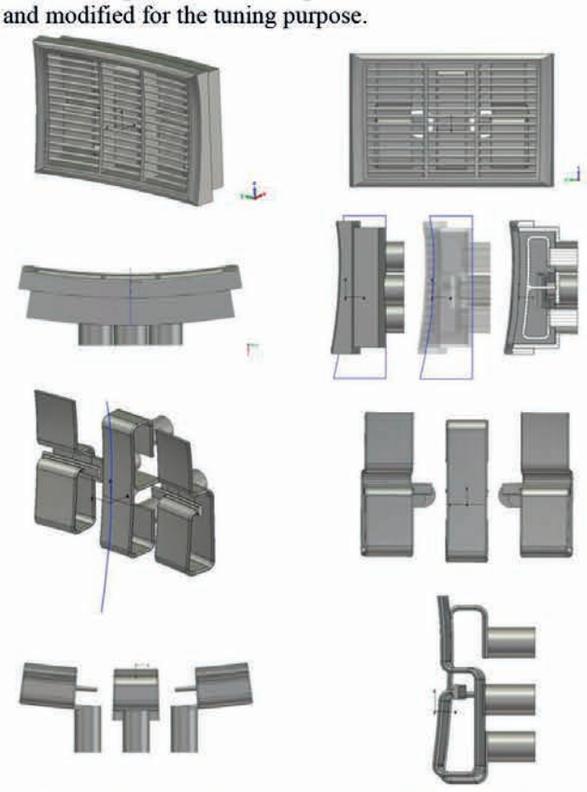

Figure 1 – curved 3-strap antenna CST model. Top, antenna exterior; bottom, antenna straps view.

In particular, starting from the 'base' structure parameter values, not reported here, an optimization procedure has been performed to maximize the structure minimum conductance, $\mathbf{G_{min,tot}}$, that is related to the maximum power delivered to the dielectric load:

$$P_{coupled} = \frac{1}{2} G_{min,tot} V_{standoff}^2$$

where $\mathbf{V_{standoff}}$ is the maximum allowable voltage in the four coaxial cables, equal to 35 kV. After a tuning campaign, performed by varying the antenna dimensions,

maximum coupled power values equal to 1.02, 1.24 and 1.27 MW at the frequencies of 60, 75 and 90 MHz have been obtained. A visual and quantitative inspection of the electric field on the whole assembly has been carried out. In the case of electric field values, everywhere inside the antenna box, $|E|$ shall be ≤ 2.5 MV/m and $|E_{\|}|$ shall be ≤ 1.5 MV/m. The electric field of the structure has been optimized by properly adjusting the antenna distance from the containing box walls and by smoothing the strap side edges. 2024 contribution will focus on the curved antenna final design, with particular emphasis on the obtainment of the coupled power values equal or higher than the DTT specifications.

DESIGN OF ECH SYSTEM

The Divertor Tokamak Test (DTT) facility [4] is under construction in Italy with focus on power and particle exhaust and it will reach the condition of 15 MW/m power flow outwards through the separatrix by coupling up to 45 MW of auxiliary heating power to the plasma. To achieve this goal, the selected heating systems are Electron Cyclotron Resonant Heating (ECRH), Ion Cyclotron Resonant Heating (ICRH) and negative Neutral Beam Injector (NBI). The final power mix (32 MW ECH, 8 MW ICH, 10 MW NBI) will be based mainly on ECH power, exploiting the great advances in the field of the last two decades. The procurement of the first bunch of 16 MW of ECH, based on 1 MW/170 GHz/100 s gyrotrons technology, has already started and will be available for the DTT first plasma. A Quasi Optical (QO) approach has been chosen for the power transmission, as solution for the long distance between Gyrotron Hall and Torus Hall Building, with multi-beam mirrors installed under vacuum to reduce the overall transmission losses below the target of 10%. The power is injected into the tokamak using single-beam independent front-steering launchers, real-time controlled, for different tasks: assisted plasma breakdown, NTM and ST control, EC current drive and main electron heating.

INFN LNS activity concerned the Conceptual Design of EC Launcher [5]. It dealt with the investigation of electromagnetic beam losses along the corrugated waveguide, that was modelled by the wave-optics module of COMSOL multiphysics. The numerical problem is tough due to the small waveguides cross-section and corrugation, and, thus, the extremely fine mesh size that is required to capture the main properties of the wave propagation and losses. First results say that we are now at the limit of computational capabilities and further studies will be carried out during 2024, with more powerful workstations. Attention has been also paid to the mechanical design of launcher structures, including the Launcher CAD design, the selection of materials and solution for vacuum and cooling, with the first drawings completed by the end of 2023.

INTERFEROMETER/POLARIMETER DESIGN

A multi-channel poloidal interferometer/polarimeter is under development for DTT facility. The aim of the diagnostics is the simultaneous measurement of the line integrated electron density, Faraday rotation and Cotton Mouton effect. The measurement of two polarimetric signals together with the interferometric one would allow for a robust electron density estimate, for the internal magnetic field measurement as well as for the magnetic equilibrium reconstruction. INFN-LNS has contributed to the advances in this diagnostics design analyzing the possibility of accommodating up to 16 lines of sight in the available space and the contribution of different chords positions in the magnetic equilibrium reconstruction and evaluating the expected interferometric/polarimetric signals [6].

X-RAY PLASMA DIAGNOSTICS IMPROVEMENTS

Soft X-ray plasma diagnostics play a crucial role in the study of magnetized plasmas. Numerous detectors and techniques have been developed in the recent past at the INFN-LNS, in collaboration with the ATOMKI laboratories (Debrecen, Hungary), to perform volumetric X-ray spectroscopy [7] and X-ray imaging by CCD pin-hole technique [8]. Within the DTT project, the INFN-LNS activities were aimed at the development and improvement of these techniques, typically used in compact traps, with respect to the state of art for application in controlled nuclear fusion plasmas. Adaptative multi-collimation systems are being designed and developed to suppress as much as possible the X-ray scattering (which hugely increases for high power heated plasmas) for both SDD, GEM and CCD detector systems. In the latter cases, X-ray shutters will be also included to reduce readout noise.

REFERENCES

[1] R. Albanese et al., 'The DTT device: role and objectives', Fusion Eng. Des. 122 (2017), 285-287

[2] G. S. Mauro et al., 32nd Symposium on Fusion Technology (SOFT 2022)

[3] G. Torrisi et al, Development/Extension of a COMSOL Full-wave Anisotropic Model for the ICRH Heating 24th Topical Conference on Radio-frequency Power in Plasmas, Annapolis, US, September 2022

[4] R. Martone et al., DTT Divertor Tokamak Test facility. Interim Design Report, ENEA (ISBN 978-88-8286-378-4), April 2019 ("Green Book")

[5] A. Romano et al; "The design of the ECRH system of DTT" 21st Joint Workshop on Electron Cyclotron Emission (ECE) and Electron Cyclotron Resonance Heating (ECRH), June 20-24, 2022, ITER Organization, France

[6] D. Fiorucci et al., J. Instrum. 17 (2022) C02023

[7] D. Mascali et al., J. Instrum. 12 (2017) C12047

[8] S. Biri et al., J. Instrum. 16 (2021) P03003

Development of a Flexible ECR Plasma Ion Source at LNS for high- intensity metal ion beams: source design and metal vaporisation modelling

A. Pidatella[1], A. Galatà[2], C. S. Gallo[2], D. Mascali[1], G. R. Mascali[2,3], G. S. Mauro[1], B. Mishra[1], S. Passarello[1], A. D. Russo[1], G. Torrisi[1]

1) INFN-LNS, Catania, Italy
2) INFN-LNL, Legnaro, Padova, Italy
3)Università La Sapienza, Roma, Italy

Abstract – We report on the design and development of a novel plasma ion source, upgrading the Flexible Plasma Trap at the LNS into an ECR-based ion source to deliver metallic beams at high-intensities (mA) and low-charge states for interdisciplinary applications, from particle acceleration to quantum technologies. The report includes studies and design of novel injection systems for metal evaporation in the plasma, along with the numerical and mechanical design of a versatile extraction system for multi-beam purposes.

INTRODUCTION

Electron cyclotron resonance ion sources (ECRIS) are largely employed to deliver multiply charged and high-intensity ion beams at several accelerator facilities. They are especially considered for producing metallic ion beams [1]. Besides, an active field of research in the quantum technologies concerns the measure of the permanent electric dipole moment (EDM) of specific molecules' electrons in a solid matrix, looking for evidence of CP violation [2]. This atomic-embedding in low-temperature solid matrix conventionally resorts to glow discharge chamber and electrostatic elements to select and transport ions to be embedded [3]. In the framework of the PNRR-NQSTI (National Quantum Science and Technology Institute) project, at INFN-LNS novel techniques to produce isotopic atomic and molecular enriched beams have been studied. These would allow to clean up the nuclear species that could be used in doping the solid matrix and overcoming the current limit in the EDM measurements. In this view, an ECRIS scheme to increase the production yield of implantation beams, to attain a higher than milliampere ionic metal beam with an extraction potential between 30 and 50 KV, has been proposed. Here, we report on the conceptual design of this metallic beam source.

DESIGN OF HIGH-INTENSITY METALLIC ION BEAMS SOURCE

The source we have scrutinized is the Flexible Plasma Trap (FPT) at INFN-LNS [4], as testbench of an ECR trap becoming an ECRIS, by which delivering enough intense isotopically pure beams onto solid targets. Several modifications will be applied to the device, most of them facing issues such as the *metallic plasma creation* and high-intensity metallic ion *beam extraction/isotopic separation*. Novel aspects with respect to the conventional ECRIS is the strong flexibility of the confining *simple-mirror* magnetic field provided by the trap, and the *radial injection* of both RF microwaves and of metallic vapors via high-temperature resistive ovens. The new strategy requires the development of an extraction system, of a magnetic system to master and control the beam, as well as for the selection of the Q/A ratio with dA/A ~ 1/200. A diagnostic box for monitoring the source and the quality of the beam will be also developed. Source's diagnostics will be based on both non-invasive (optical emission spectroscopy) and invasive (Langmuir probes) systems. Beam's diagnostics will include quadrupoles and beam viewer for the emittance monitoring, as well as the beam's current diagnostics. The design of the overall system has been based on detailed numerical simulations and mechanical constraints, imposed by the given magnetic structure of the FPT. In particular, the extraction system design has been bounded by the achievement of two main goals, to be sequentially tested, concerning the production of pure beams with the desired intensities, handling low-energy and high-intensity beams' issues, such as space-charge effects on the beam emittance and intensity. The tests will proceed in several steps. For 2024 we expect to test:

- The production of 5 mA of H^+ by creating a hydrogen plasma (preliminary).
- The production of 1 mA of Fe^+ by creating a plasma composed of a mixture of helium (80%) and iron (20%).

The iron beam is of interest for the EDM measurements of interest in the NQSTI project, as well as barium ion beams, whose latter research we remit to a second phase of tests.

From a trap to an ion source: technical design

The upgrade activity of the FPT has been pursued, starting from the design of a new plasma chamber, which size and accesses must be compatible with the maintained current magnetic system, as well as with the extraction system and the RF/metal injection systems employed. The designed preliminary system is sketched in Figure 1(a).

The conceptualized design carry on a degree of novelty, accounting for both RF and metal radial injections, leaving the extraction axis free for including source/beam diagnostics or for future development of a double extraction. To limit as much as possible the modifications on the FTP and to fulfill the previously mentioned goals, we designed, jointly with the INFN-LNL team, a flexible extraction system able to handle different beams with different intensities. Simulations have been carried out with the commercial code IBSimu [5]: the basic idea is to use the same electrodes geometry (an *accel-decel extraction system*) but to change the electrodes voltages and distances (adjustable under vacuum) to properly cope the extraction system to the desired beam properties. Simulations involving the extraction of 5 mA of H^+ and 1 mA of Fe^+ (plus 4 mA of He^+) have been independently performed, to optimize on electrodes' voltage and distances setup. Other simulations concerning the radial metal injection have been carried out. In the following we report on the main achieved results, interesting for the ion source development.

Extraction system: numerical results

We present the results from electrostatic (ES) simulations of the source extraction system. It is based on 3 electrodes, as shown in Fig. 1b: two at potentials - the plasma (source) electrode (PE) and the puller (P) - the third one at ground. We performed a systematic survey including many simulations, by sweeping on the PE-P gap, PE and P combination of potentials, fixing the electrodes shapes. The puller-ground system is thought to be a unique piece, being able to change its distance from the PE by ±6 mm. The latter is the geometrical tolerance designed, as outcome of the ES calculations, making the extraction system versatile for different goals: (1) initial test with 5 mA of protons; (2) test with mixture of He/Fe ions, for 4(He)+1(Fe) mA extracted. Optimum found are: (1) PE @ 20 kV, P @ -1KV, gap = 30 mm; (2) PE @ 35 kV, P @ -5 kV, gap= 27.5 mm. These relates to the best emittance beam conditions reconstructed, compensating for 90% of space charge effects: small beam halo, focused beam at the axis, 4 ϵ_{rms}~88% for both H and He/Fe. Extracted beams are always divergent, with maximum divergence ≤60 mrad. Normalized emittance for beam in (1) is 0.052 π mm mrad, (2) is 0.026 π mm mrad for He, and 0.0065 π mm mrad for Fe. A detailed description of the simulations and report of numerical results is available.

The calculated normalized emittance is very low, as well as the rms dimension and divergence, thus ensuring the possibility of a good isotope separation even in the case of higher mass elements expected for the second phase of the project (i.e., for Barium isotopes).

Next investigations concern the transport beam line to the dispersive/beam diagnostic system. Calculations using the simulated beam emittance at the exit of the extraction system data have been started for studying the beam optics and dispersive power/resolution. The campaign of procurement for all instrumentations to assemble the new source and start preliminary tests is ongoing.

Metal injection: first study of metal dynamics in ECR plasma

We started first-of-its-kind numerical studies of the metal diffusion dynamics via evaporation in the upcoming PANDORA plasma trap at INFN-LNS, which will make use of rare metallic radioisotopes for multidisciplinary experimental in-plasma studies. The diffusion and deposition of metal vapours at the plasma chamber's surface were explored under molecular flow regime, with stationary and time-dependent particle fluid calculations. The ionisation of vapours is then studied in the strongly energised ECR plasma. We have developed a Monte Carlo (MC) code to simulate the in-plasma metal ions' dynamics, coupled to particle-in-cell simulations of the plasma physics in the trap. The presence of strongly inhomogeneous plasmas leads to charge-exchange and electron-impact ionisations of metals, in turn affecting the deposition rate/pattern of the metal on the walls of the trap. Results showed how vapours dynamics depends both on evaporated metals and the plasma target. The ^{134}Cs, ^{176}Lu, and ^{48}Ca isotopes were investigated, the first two being radioisotopes interesting for the PANDORA project, and the third as one of the most required rare isotopes by the nuclear physics community. We refer to [6] for further details on methods and results.

A relevant outcome of this numerical study concerned the possibility to use a radial access for the metals' injection, instead of the custom (axial) one. The model predicted a relevant increase of the capture-ionisation efficiency around a factor 2. Despite this presently represents a really challenging option, since in most of the existing *B-minimum* ECRIS setups the radial access to the plasma chamber is technically almost impossible, intermediate tests could be attempted via the upgraded FPT in a *simple mirror* confinement field.

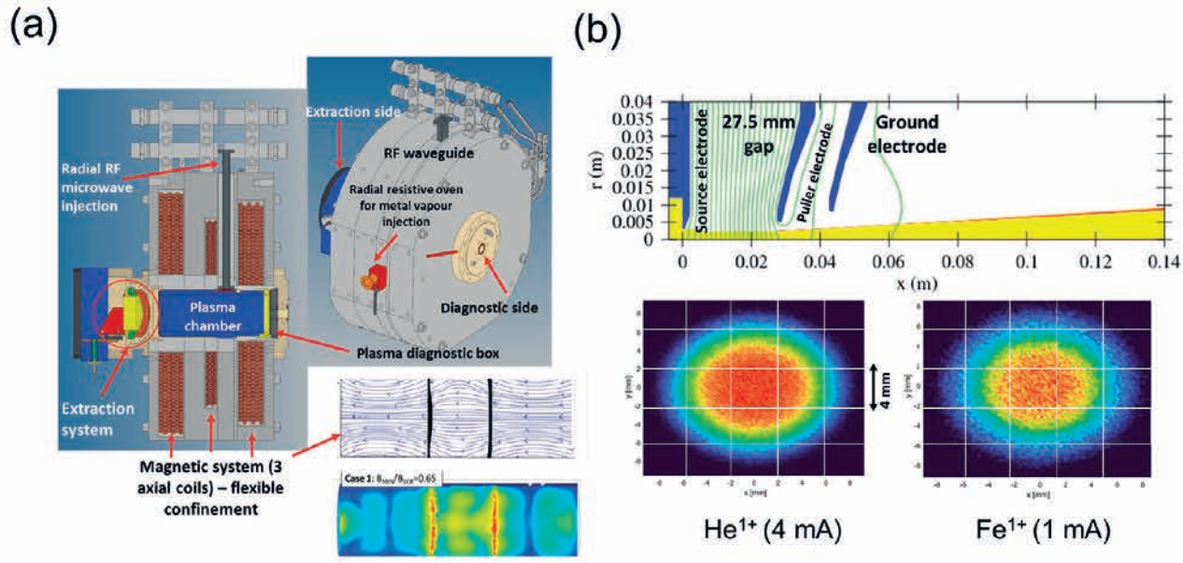

Figure 1: (a) Mechanical design of the ECRIS components: details of the plasma chamber with radial access for new RF injection and metal vapour injection, along with the designed extraction system and the diagnostic box. The simulated magnetic field lines and EM power absorbed in the FPT are also reported from [7]. (b) Extraction system simulated in IBSimu showing the ES solution for the extracted beam at the optimum condition for the 4(He) + 1(Fe) mA configuration. Rms beam sizes are also displayed.

Conclusions

The design of a novel ECRIS for high-intensity metal ion beams at LNS is almost completed. Numerical design of the extraction system has been performed, finding an optimum system for dealing with multiple kind of beams at different intensities. Radial metal injection has been investigated in an ECR trap, with promising better metal-to-plasma coupling to be tested. The source will be involved in preliminary tests in 2024, delivering proton and iron beams, as checking for the ECRIS performance, and as providing a first metal beam, as requested from the NQSTI project's goal.

ACKNOWLEDGMENTS

Authors acknowledge the financial support from the MUR-PNRR Project PE0000023-NQSTI, financed by the European Union (NextGeneration EU).

REFERENCES

[1] Maunoury L, et al., Nucl. Instrum. Methods Phys. Res. A 1040 167136 (2022).
[2] ACME Collaboration, Nature 562, 355–360 (2018).
[3] Borghesani AF, Carugno G, Messineo G, Pazzini J. J Chem Phys. 14;159(10):104501 (2023).
[4] Gammino S, et al., J. Instrum. 12, P07027 (2017).
[5] Kalvas T, et. al., Rev. Sci. Instrum. 81, 02B703, (2010).
[6] Pidatella A, et al., Plasma Phys. Control. Fusion 66 (2024) 035016.
[7] Torrisi G., et al., IEEE Trans. Antennas Propag. 67 2142–9 (2019).

First investigation of longitudinal beam dynamics in a co-propagating Dielectric Laser-driven Accelerator

A. Leiva Genre[1], D. Mascali[1], G. Mauro[1], G. Torrisi[1], G. Sorbello[1, 2]

1)INFN-LNS, Catania, Italy
2) Electric, Electronic and Informatic Engineering Department, University of Catania, Italy

Abstract - Dielectric Laser-driven Accelerators is an emerging field for more powerful, compact accelerators. It aims to provide more affordable, high-gradient accelerating structures, facilitating particle accelerator applications to small and medium-size facilities. This work is part of the project **MICRON** (Miniaturized aCceleRatOrs Network) supported and funded by INFN 5th National Scientist Committee and including the groups of LNS, LNF, INFN Milan, Bologna, and Rome. The MICRON program deals with advanced accelerator concepts and technology for the production of compact, high-gradient accelerators. Under the scope of this goal, acceleration of particles from source to high energies envisages the acceleration of sub-relativistic electrons. In this study, we analyze the capabilities of the slot waveguide for effective particle acceleration. By changing the slabs' taper profile accordingly, the synchronous condition can be fulfilled. Acceleration of particles from 80 to 85 keV has been demonstrated in PIC simulations. An accelerating gradient of 250 MV/m has been achieved, surpassing typical values of conventional RF cavities. The presented structure can potentially be included in complex accelerator system planned by the MICRON project to fulfill the needs of nowadays laboratories involving particle accelerators as a tool for their research.

THEORY – (OR INTRODUCTION)

Particle accelerators have played a fundamental role in the last century. Their extensive use has been instrumental in the development and advancement of both science and technology. However, the nowadays demands of more powerful beams has led to the construction of bigger and power-demanding accelerators. These characteristics make difficult the implement of high energy beams in small and medium size laboratories and infrastructures around the world. A considerable proportion of scientists and engineers of the particle accelerator community are working towards more compact, high-gradient accelerators. One clear candidate for this ambitious goal is the Dielectric Laser-driven Accelerator (DLA). These types of accelerators combine ultra-short, high-intensity laser pulses with the advanced manufacturing process techniques developed by the solid-state industry. The potential acceleration gradients offered by DLAs are of the order of 1 GV/m, which implies a tenfold increase in comparison with typical RF cavities [1].

SLOT WAVEGUIDE

The slot waveguide is a dielectric waveguide consisting of two high permittivity ribs (or slabs) sitting in a dielectric substrate. The propagation of EM waves along the structure is guided by total internal reflection. The high confinement of the electromagnetic field is due to the high contrast in the refraction index between the core and substrate. Figure 1 depicts a tapered slot waveguide DLA used in simulations. The slot waveguide DLA sustains a TM_{01}-like mode, suitable for sub-relativistic particle acceleration [2]. The accelerating mode can be appreciated in figure 2. Unlike DLA grating structures, the electric field co-propagates along the electron bunch, offering large interaction lengths. For effective acceleration, the phase and electron velocity must match. The synchronous condition can be satisfied by varying the rib width along the acceleration path.

SIMULATIONS

All the electromagnetic fields and PIC simulations were calculated using CST Studio Suite [3], as it offers good capabilities to solve particle acceleration problems.

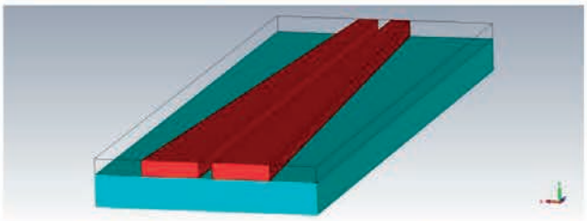

Figure 1: A schematic view of the tapered slot waveguide DLA.

The accelerator structure parameters for the simulations are rib width a = 0.45725 μm, slot width d = 0.155 μm, rib thickness b = 0.172 μm, and accelerator length L = 20 μm. The associated wavelength for the above parameters is λ = 1.55 μm. The substrate width and thickness were chosen to be 2.324 μm and 0.387 μm respectively. Silicon was the material used for the slabs, as it possesses a high index of refraction and high damage threshold at optical frequencies. Silica was the chosen substrate material.

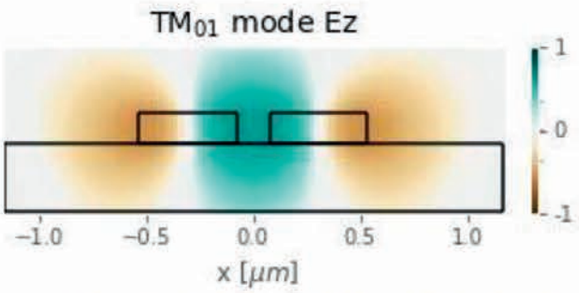

Figure 2: Longitudinal electric field profile for the slot waveguide. The excited mode was calculated using CST Microwave Studio.

The rib width profile along the accelerator is tailored such that the rib width taper profile accommodates to the accelerating electron velocity increase. The pulse propagation is obtained by employing a 1.55 μm laser with 100 fs pulse duration, and average power of 250 W.
Given the above slot waveguide parameters and condition, an energy increase of 5 keV has been attained for an 80 keV electron bunch in a 20 μm long structure, as shown in figure 1. The associated accelerating gradient falls around 250 MV/m, larger than those found in conventional RF cavities.

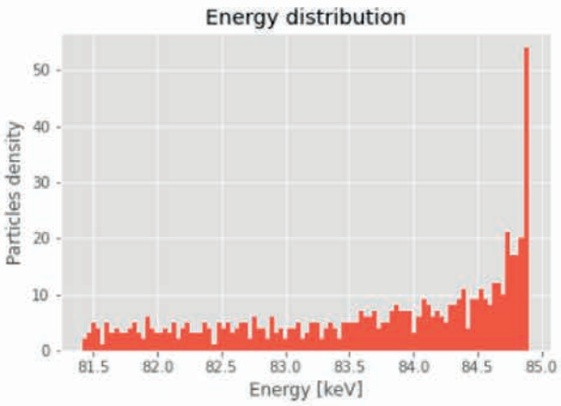

Figure 3: Electron energy distribution after the acceleration stage. A clear peak stands at energies close to 85 keV.

It is convenient to study the longitudinal beam dynamics of the slot waveguide by means of its Hamiltonian. It can be shown that the Hamiltonian in reference frame of the synchronous particle for this system can be written as [4]:

$$(1)\quad H(\delta,\varphi) = \frac{\delta^2}{2\beta_s^3\gamma_s} + \frac{eE_0\lambda}{2\pi mc^2}[\sin\varphi_s - \sin\varphi + (\varphi-\varphi_s)\cos\varphi_s]$$

where γ is the Lorenz factor, $\delta=\Delta\gamma/\gamma_s$ is the relative energy gain with respect to the synchronous particle, β is the normalized velocity, and φ correspond to the phase. The subscript "s" denotes the quantity related to the synchronous particle.

Inputting the parameters used for our structure into equation (1), phase stability can be analysed for the accelerated particles. With the correct taper profile, the slot waveguide DLA accelerated bunches exhibit longitudinal phase stability across the accelerator length. The taper is our mean to match electron and the accelerating field phase velocity. A closer look into the electrons phase space (Figure 4), it can be observed that the electrons accumulate inside the separatrix, where phase stability is achieved. The figure 3 corresponds to this exact instant after acceleration, supporting the fact that most of the particles gets "trapped" inside the phase stability condition, at the same time they get their energy increased.

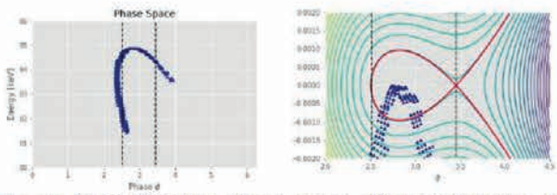

Figure 4: (a) Electron phase space after acceleration. (b) High-density of points inside the separatrix.

CONCLUSIONS

The slot waveguide as a potential DLA structure for sub-relativistic electrons have been studied within the scope of the **MICRON** project. By tailoring the ribs width according to the electron velocity energy gain, synchronization of the electron and phase velocity can be achieved. Longitudinal beam dynamics analysis of the proposed structure shows good phase stability. However, the use of a small wavelength for particle acceleration still possesses harsh conditions to the bunch parameters. Accelerating gradients larger than conventional RF cavities were obtained for all the DLA structures presented on this report. The transversal focusing of the beam remains as a continuation of this work.

REFERENCES

[1] Joel England et al. Rev. Mod. Phys. 86, 1337 (2014)
[2] Z. Zhao Opt Express Vol. 26, 22801-22815 (2018)
[3] CST studio suite. https://www.3ds.com/products-services/simulia/products/cst-studio-suite/.
[4] J. Le Duff. Dynamics and acceleration in linear structures. In CERN Accelerator School: Course on General Accelerator Physics, pages 253–288, 1992.

ACKNOWLEDGEMENT

The present work was mostly discussed and developed as a part of a Master's Thesis of the program Erasmus Mundus JMD in Nuclear Physics.

Unfolding procedure for proton and ion spectrum reconstruction of laser-target emission

A. Pizzino[1], G. Angemi[1], G. Cantone[1], E. Caruso[1], O. Giampiccolo[1], D. Oliva[1], M. Guarrera[1], S. Arjmand[1], R. Catalano[1], G. Cuttone[1], F. Farokhi[1], S. Fattori[1], A. Kurmanova[1], A. Pappalardo[1], G. Petringa[1], A. Sciuto[1], G.A.P. Cirrone[1]

1) Istituto Nazionale di Fisica Nucleare Laboratori Nazionali del Sud (INFN LNS), Catania, Italy.

Abstract - Radiochromic films (RCFs) arranged in a stack configuration can be used for the fluence and energy spectra reconstruction for proton and ion in laser – target emission. RCF response exhibits a dependence on Linear Energy Transfer (LET), which leads to an underestimation of the response in high-LET conditions. This can result in dosimetric errors if not properly taken into account. An automated analytical procedure (Unfolding) able to reconstruct the incident energy spectra in an RCF stack was developed and validated at the LNS in Catania.

INTRODUCTION

When properly calibrated, Radiochromic Films (RCFs) allow for the measurement of the proton energy spectrum by implementing the so-called unfolding (or deconvolution) procedure. The reduced water equivalent thickness (WET) of RCFs (hundreds of μm) enables the spectrum to be derived with an energy resolution of up to 200 keV (for 70 MeV protons and HD-V2 film).
The validation of the unfolding procedure applied to a stack of RCFs irradiated with a laser-driven proton beam was performed. A preliminary dose calibration of different RCF films (HD-V2 and EBT3) with beams at different LET (in water) was performed. These calibration curves were then used to estimate the energetic spectrum of a laser-driven proton beam acquired through an HD-V2 stack irradiated at the Eli Beamline laser facility [23].

MATERIALS AND METHODS

Radiochromic films

RCFs are two-dimensional self-developing devices consisting of one or more active layers containing a microcrystalline monomeric dispersion deposited on a clear plastic substrate. Upon interaction with ionizing radiation, the active layer undergoes polymerization and changes its color from nearly transparent to blue. The extent of coloring depends on the absorbed dose and is characterized in terms of Optical Density (OD) defined as:

$$OD = \log_{10} I_0/I$$

where I_0 is the light intensity detected for a non-irradiated film and I is the residual light intensity after passing through the irradiated one.
The films underwent digitization to extract quantitative data assessed in terms of pixel intensity values. The RCF were scanned at a resolution of 150 dpi and a dynamic range of 48-bit RGB. The I and I_0 measures were performed reading the signal in the red channel, following the manufacturer's recommended guidelines. The chosen region on each film for evaluating is typically referred to as the Region Of Interest (ROI). Two distinct RCF types (HD-V2, EBT3) were used.

The Unfolding procedure

An automated MATLAB-based routine was implemented for the execution of the unfolding procedure. The algorithm's performance and accuracy were also tested using experimental data collected with a Marcus Camera.
In order to perform Unfolding, it was needed to have:

- a calibration curve
- a Matrix defined by interpolation of data produced with a simulation software.
- scan of all GAFs of the stack

RCF calibrations were carried out by exposing the films to various doses in various configurations. This procedure was done for every type and for every different lot of each type of RCF (batch). Calibration curves were defined using ImageJ software and fitted (using EXCEL) as a function of the released dose using a third-order polynomial curve. The same curves were also generated using a MATLAB script. The comparison between curves and polynomial factors generated with both methods showed an optimal overlap (Fig. 1).

Figure 1

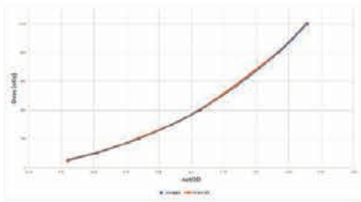

Fig.1 Calibration EBT3 60MeV FE Batch A 20 October 2019

Monte Carlo simulations using the SRIM software (*The Stopping and Range of Ions in Matter)* were performed for every specified stack, searching for the stopping power for any single RCF's WET. These simulations were performed also with and without adding an Aluminium layer at different thicknesses.

Matrices were prepared using a MATLAB script, by interpolation of SRIM data for every RCF's stacks.
Scans of all the GAF of the stacks were produced as described above.

All data produced as described before were entered in the MATLAB ambient and the routine was started. The script needs to have some input of data:

- Polynomial Factors
- GAF Type (es. EBT3)
- Images from scan

After selecting the appropriate ROI for the exposed GAF and for a background, the script could be executed. Two different graphics are produced.

- Fluence from deconvolution
- Dose Distribution of the Primary Protons in Water

Example are shown in Fig.2 and Fig.3

Figure 2

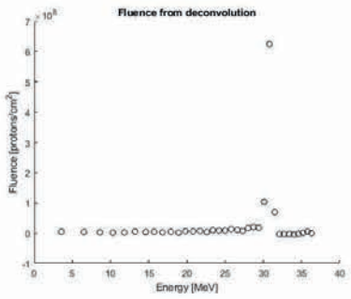

Figure 3

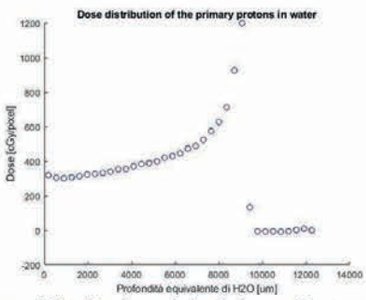

Fig.3 Dose Distribution of the Primary Protons in Water (example)

Some of the processed unfoldings were also compared with experimental data collected using a Marcus Chamber. Again a proper MATLAB script was used for this. The obtained graphics for Dose Distribution showed a good overlap of the two curves. An example is showed in Fig.4

Figure 4

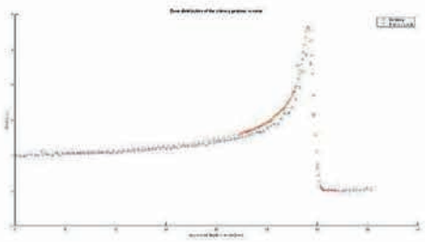

Fig.3 Comparison between Unfolding and Experimental Data (example)

REFERENCES

[1] Automated reconstruction of the initial distribution of laser accelerated ion beams from radiochromic film (RCF) stack Benedikt Schmitz; Martin Metternich; Oliver Boine-Frankenheim Rev Sci Instrum 93, 093306 (2022)

[2] Radiochromic film dosimetry: Past, present,and future Slobodan Devic (Physica Medica 2011);

[3] Use of radiochromic films for the absolute dose evaluation in high dose-rate proton beams G.A.P. Cirrone et al 2020 JINST 15 C04029;

[4] Dosimetria e spettroscopia per fasci di protoni laser-driven con film radiocromici M.C. Guarrera (Anno Accademico 2018/2019);

[5] Proton spectroscopy for 11 5 B(p,α)2α fusion reaction 6 with RCF films: calibration and unfolding procedure M. Guarrera, G. Petringa, G. Milluzzo, R. Catalano, V. Kantarelou, C. Siragusa, F. Midili, M. La Cognata, L. Guardo, D. Lattuada, D. Passarello, G. Angemi, S. Arjmand, G. Cantone, E. Caruso, G. Cuttone, F. Farokhi, S. Fattori, O. Giampiccolo, L. Giuffrida, A. Kurmanova, D. Margarone, D. Oliva, A. Pappalardo, A. Pizzino, F. Schillaci, A. Sciuto, J. Suarez, G.A.P. Cirrone (Sep 5-8, 2022).

The New Dummy Loads System for the RF Power Amplifiers of the LNS Superconducting Cyclotron (CS)

A.Longhitano#, A.Spartà, L.Platania, INFN-LNS, Catania, Italy

Abstract

A new dummy load system has been designed and installed for the three RF amplifiers that power the cavities of the K-800 superconducting cyclotron at the INFN-LNS. The new system involved the disassembly of the old and obsolete dummy load and the installation of three new dummy loads. The new system is managed by an advanced control system for reading the water flows and temperatures through sensors installed in the water-cooling circuit, moving the RF switches, and processing the interlock signals for amplifiers protection. The new system can be used both in local and in remote mode by software. This work is a part of the overall refurbishment of the RF power amplifier started three years ago.

OLD VS NEW CONFIGURATION COMPARISON

The old system used a single 100kW dummy load AK52 SWU terminated in 6-1/8 inch coaxial lines, designed and installed by Brown Boveri Corporation at the end of 1980s.

It had a complex, heavy and very bulky structure. It had a primary closed soda water cooling circuit and a secondary tap water cooling circuit. The dummy load could be switched to one of the three 75kW RF amplifiers via a complex array of 6-1/8-inch coaxial switches. This limited the connection of only one amplifier at a time while the other two remained in stand-by. Furthermore, the old dummy load needed to be calibrated periodically, in fact the soda-water mixture needed to be kept a stable concentration through a demanding procedure. The impedance depended a lot on the temperature, and 50 ohm was obtained for a range of a few degrees around 80 °C. This temperature was reached with high power values. The tests at reduced power of 10kW were incomplete as, not reaching the temperature of 80 °C, the SWR was greater than 1,8. The figure 1 show the AK52 SWU dummy load.

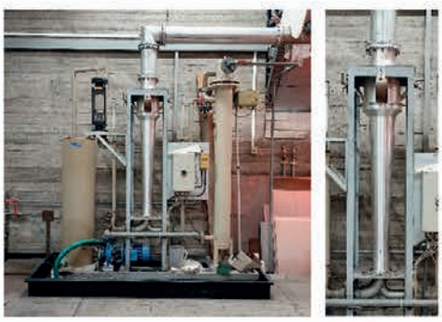

Fig.1: AK52 SWU 100kW dummy load

On the other hand, the new configuration includes three 80kW 8792 Bird dummy loads, one for each amplifier, with the following features: 80kW tap water cooling; 1kHz to 800MHz @ 1.15 SWR max; +5 to +60 °C temperature range; 864mm x 127mm dimension; 14kg weight.

The dimensions and weight are significantly lower than the old dummy load and it don't require calibration.

Furthermore, they have greater stability linked to the operating temperature, in fact already at 22 degrees the impedance is 50 ohm and remains linear for several degrees, from 5 to 60 °C. It means that the SWR is very close to 1.0 in any condition, which allows for more accurate analysis and more accurate tuning.

Fig.2: 8732 Bird 80kW dummy load

With the new configuration, each amplifier, having its own load, is completely independent from the others. The three amplifiers can be load tested simultaneously, this reducing maintenance time in the event of a fault. The figure 2 show the 8732 Bird loads installed on one of the RF power amplifier.

Figures 3 and 4 shows the different between the old and new configuration. With the new configuration only three RF switches are needed instead of the nine of the old one.

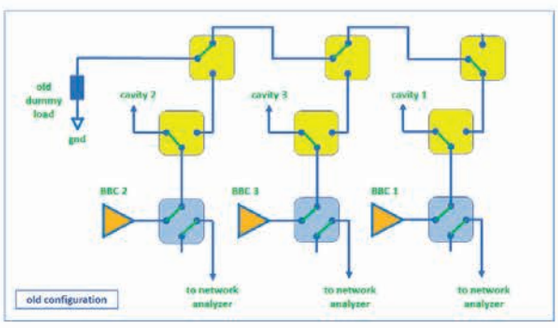

Fig.3: old configuration

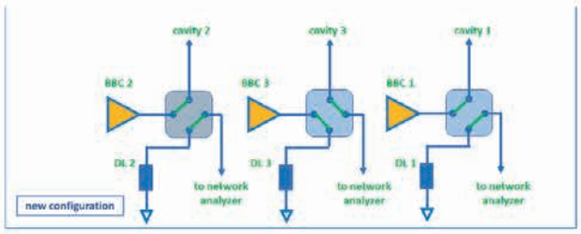

Fig.4: new configuration

Considering the figure 4, the BBC2 amplifier is switching to cavity, and the dummy load is connected to the network analyzer. In this position is also possible check the correct impedance of dummy load by network analyzer.

The BBC3 amplifier is connected to the dummy load, and, at the same time, the cavity is switched to network analyzer for the tuning procedure through the movement of sliding short, coupler and trimmer.

The figure 5 show one of the three rf power switch which are part of the new configuration.

Fig.5: 6 1/8" RF power switch

HARDWARE AND SOFTWARE

The operating parameters of the dummy load system are controlled with a completely homemade system.

The logical part that controls the water flow meters, water temperatures and interlocks is managed by a DSPIC30F4013 16bit Microchip microcontroller, while a PIC18F4585 8bit Microchip microcontroller manages the RF switches.

All the information for controlling the dummy loads system are displayed via a 4x40 LCD display, such as the reading of the flows and temperatures of the three water cooling circuits and the alarm thresholds. Using the knob, it is possible to set the parameters necessary for setting the system. Through the menu it is possible to calibrate the flow meters that use a hall effect sensor built by RS component. To avoid interactions with the magnetic field, the three flowmeters are shielded by an iron plate. At any time, it is possible to read the status of the RF switches by the led on the front panel and change the position through the three switches, one for each amplifier.

Figure 6 shows the 19-inch rack 3-unit cabinet, the three white boxes for driving the RF power switches and the box for displaying the temperatures of the three dummy loads in addition to the input and output temperatures of the main water collector. From the temperature differences between the water delivery and return it is possible to calculate the RF power dissipation from the following formula:

$$P_{[kW]} = 0.0578 \times (T_{out[°C]} - T_{in[°C]}) \times Water\_Flow_{[l/m]}$$

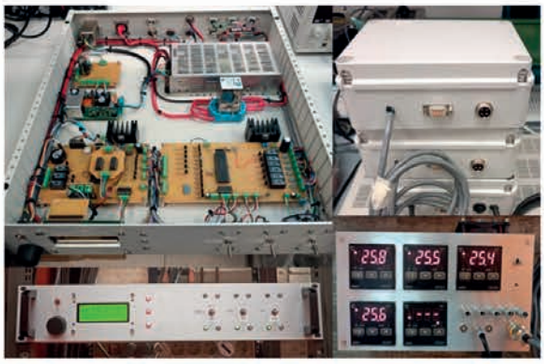

Fig.6: control system hardware

Remote control occurs via the RS422 port. The software developed in LabView is integrated into the LLRF software which manages all the RF systems. The software was developed preserving the correct functioning and reliability of the system. The screen, showed in figure 7, was designed to be both simple and complete.

The hardware and software of the control system were designed and installed entirely by the LNS RF group.

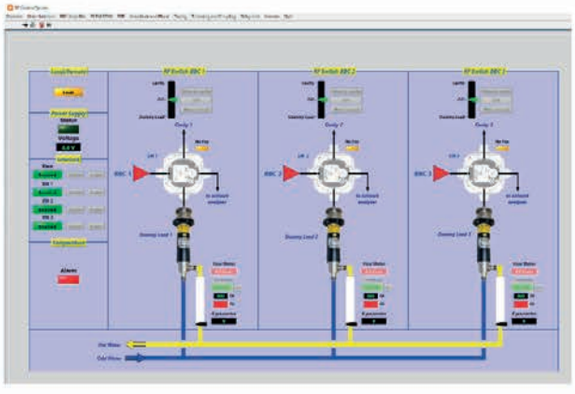

Fig.7: software LabView

REFERENCES

[1] A. Longhitano et al," The LLRF and HLRF Systems Developments, in the General Frame of the K-800 Superconducting Cyclotron Upgrade at INFN-LNS", INFN LNS Activity Report 2021-2022

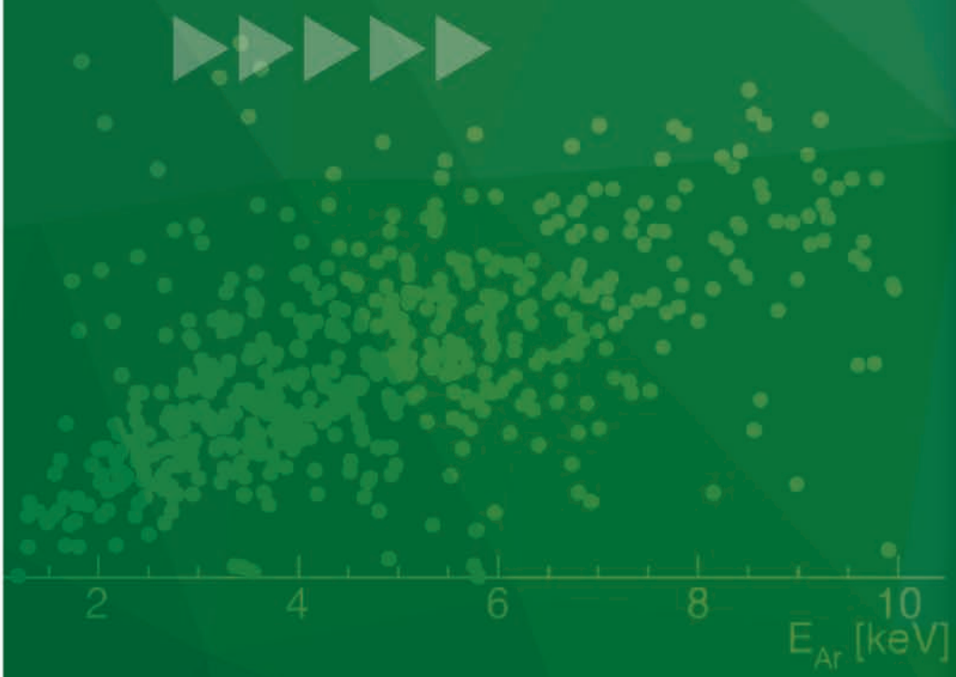

06

INTERDISCIPLINARY PHYSICS

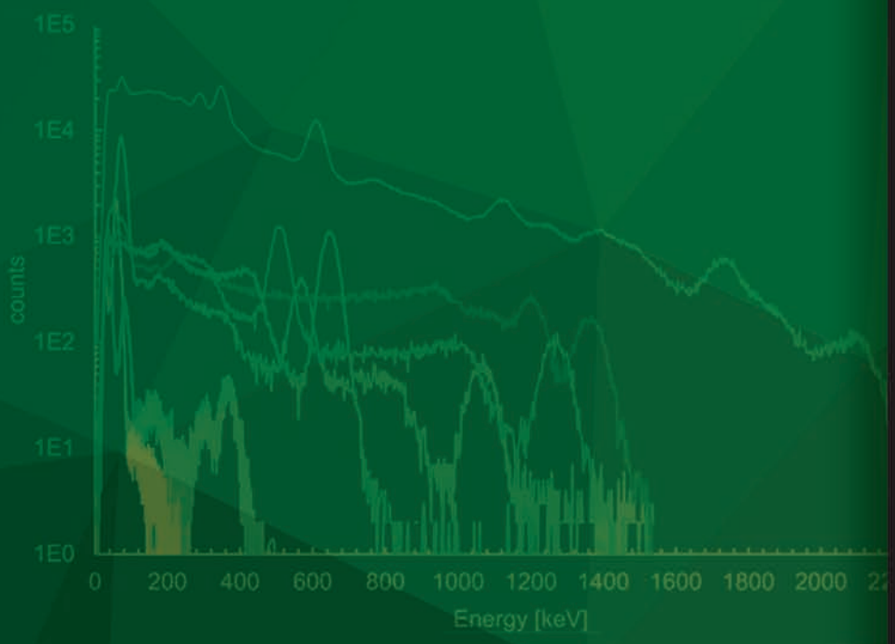

Research

Analyses

Results

INFN LNS

- MA-XRF scanning of Matthias Stomer's 'The Mocking of Christ': a reassessment of trades and use of Naples yellow
- Radiation Damage produced by Heavy Ions in Silicon Carbide Detectors
- Proton selection and acceleration for I-LUCE facility: Simulation study
- Radiobiology: A Geant4-based Application for Particle Therapy
- The MiniRadMeter gamma and neutron sensor for CLEANDEM
- New plasma diagnostics testbenches based on X-ray imaging, multi-wavelength spectroscopy and polarimetry techniques
- The MICADO radwaste monitoring system tested in a real storage site
- Cemented radwaste monitoring in PREDIS: gamma and neutron detection with WiFi electronics
- Compact radioactive wastes radwaste scanner for sort and segregate activities
- Electrical characterization of a new generation SiC detector for PRAGUE (Proton Range Measure Silicon Carbide) project
- High-power laser system for the I-LUCE facility
- Multichannel data acquisition system for external radiation therapy and its preliminary characterization
- Characterization of nuclear recoils in the dual-phase Argon Time Projection Chamber of the ReD experiment
- The ReD+ PRIN project: the characterization of sub-keV nuclear recoils in a dual-phase Argon Time Projection Chamber
- Measurements of residual radioactivity in the experimental rooms MEDEA, CICLOPE, ROOM 0°
- Modelling Radio-Frequency Waves propagation in Hot-Magnetized Plasma
- Neural Network-Based Regression for Estimating early DNA Damage Across Micro-Nano Scales

MA-XRF scanning of Matthias Stomer's 'The Mocking of Christ': a reassessment of trades and use of Naples yellow

M. Botticelli[1,2], S. Gammino[2], C. Miliani[1], E. L. Ravan[1,2], C. Caliri[1,2], F.P. Romano[1,2]

1) CNR- ISPC, Via Biblioteca, 4, 95124 Catania, Italy
2) INFN-LNS, Via Santa Sofia 62, 95123 Catania, Italy

Abstract – In a recent non-invasive analytical campaign at Museo Civico, Castello Ursino (Catania, Italy) MA-XRF imaging was used to study several paintings in the permanent collection. In this work we report the results obtained on Matthias Stomer's the *Mocking of Christ* (ca. 1640), which document his technique, including the uncommon use of Naples yellow, as well as later conservation treatments. Our findings suggest an early use of Naples yellow in South Italy, although the introduction of this pigment is usually dated to the eighteen century.

INTRODUCTION

A recent non-invasive analytical campaign at Museo Civico, Castello Ursino, in Catania, Italy, has offered the opportunity to study Matthias Stomer's production from a material perspective [1]. Among the fifteenth- and sixteenth-century paintings of the Museum permanent collection studied in this campaign, MA-XRF scanning on one of Stomer's the *Mocking of Christ* allowed identifying original paint materials - possibly constituting evidence of compositional changes (pentimenti) - and later conservation treatments. Particularly, the analysis documented the copresence of lead and antimony in some yellow areas, which suggests Stomer's use of Naples yellow for this painting.

In the early seventeenth-century, when the *Mocking of Christ* was painted, two lead-based yellows were known as potters' yellows: the first, called 'Type I', was produced from burnt lead, a mineral source of antimony and plain salt; in the second (Type II), salt was replaced by calcined wine residue and higher firing temperature was applied. A third variety (Type III) was produced using Alexandrine tutty (also mentioned as *tuccia* or *tutia allessandrina*), which has been interpreted as a tin or zinc source alternatively [2].

It is commonly accepted that three different chemical compositions exist for lead-based yellows pigments. One contains lead and tin and is more commonly mentioned as *giallolino*, one has lead and antimony and is called *Naples yellow*, and one is made of all these elements. The manufacture of *giallolino* has been linked to Venetian glass making [3], where lead and tin were common opacifiers and colorants, while Pb + Sb yellow was a common enamel pigment for colored maiolica or tin-glazed earthenware in fifteenth-century Italy. Occurrence and manufacture of antimony-based yellows in different periods and areas, at least in glass making, are proved by several historical treatises, where recipes cover a period spanning from the sixteenth to the seventeenth century. Material investigation in paintings dated to the same centuries [4] has shown that, although Pb-Sn products are still the most common in this period, the use of antimonate yellow becomes more frequent. Naples yellow reached the greatest popularity between 1750 and 1850, while *giallolino* finally disappeared from artists' palette at the beginning of the eighteenth century.

Although the widest use of Naples yellow popularity is concomitant with the introduction of its synthetic recipe, published in 1766, one might expect an earlier and less regular experimentation if painters had accessibility to potters' raw materials or were occasionally in contact with glassmakers where this technology was well developed [5]. In fact, lead antimonate yellow has been identified in Lorenzo Lotto's *A Maiden's Dream*, ca. 1505 (on panel, Samuel H. Kress Collection, National Gallery of Art, Washington) and in the *Portrait of Giovanni della Volta and his Family(?)*, probably 1547 (on canvas, National Gallery, London, NG1047), this evidence already setting the date of its introduction about a century earlier that commonly thought.

Studying paintings dated before 1766 might produce a more comprehensive chronology of lead antimonate yellow in European painting, possibly documenting its introduction in different times, depending on the technical specificity of the area where artists were operating.

MATERIALS AND METHODS

The Mocking of Christ

Stomer's *Mocking of Christ* belongs to the Finocchiaro Collection, as it is part of Giovanni Battista Finocchiaro's donation of 123 paintings to his native municipality in 1826 [1]. The painting is an oil on canvas (210×154 cm^2) dated around 1640.

All Stomer's artworks in the Finocchiaro Collection – including the *Catania Death of Cato*, the *Catania Death of Seneca* and the *Tobias healing his Father*, are attributed to his Sicilian period. All these works are set in an indoor location, possibly illustrating the painter's deliberate choice of transform the Caravaggisti concept of light, bringing more emphasis to artificial lighting. Deeper understanding of Stomer's material choices offered insights on the technical novelties of his art and their symbolic meaning.

The innovative MA-XRF imaging system developed thanks to the collaboration between the LANDIS group of the LNS-INFN and the XRAYLab of ISPC-CNR in

Catania provided real-time imaging of the *Mocking of Christ* and allowed the analysis of its large areas in fast-scanning mode.

MA-XRF scanning

The mobile MA-XRF scanner consists of a low power X-ray source – either Rh or Cr target - focused with polycapillary optics (spot size of some hundreds of microns) and two SDD detectors (50mm^2 active area and 140eV energy resolution at 5.9 keV) operated in parallel [6]. The measuring head is mounted on a three-axis system (XYZ) with 110×70×20cm^3 travel range. The head-painting distance is kept constant through dynamic correction of the Z axis using a laser sensor, while the scanning runs along the XY plane. A full area is covered in 4.3h with a pixel size of 500 µm and 5ms dwell time (100 mm/sec scanning speed). A lateral resolution down to 25µm can be achieved at the focus position, allowing the use of the scanner for high-resolution micro-XRF mapping of pigment materials. Real-time data processing is provided by an in-house software programmed under a real-time LabVIEW environment. It applies a least square fitting procedure of pixel XRF spectra and provides real-time deconvoluted elemental distribution images during each scanning. Additional functions are: RGB correlation maps, scatter plots, PCA/NNMF, integral and maximum pixel spectrum.

To analyze the whole painting, it was necessary to scan six different areas using the Rh target (High Energy mode, HE), with pixel size of 1000x1000 µm^2 and dwell time per pixel of 15 ms. Some details of the *Mocking of Christ*, for example the area around Christ's face, were scanned with the Cr target (Low Energy mode, LE) to confirm the presence of antimony.

RESULTS AND DISCUSSION

Evidence of Naples yellow

MA-XRF scanning proved that in some areas of the *Mocking of Christ* lead and antimony are both present but do not always correlate. From HE and LE results [7] Naples yellow appears to be used along with lead white to represent shadowing effects of a single light source. This technical choice creates a dramatic chiaroscuro, typical of Utrecht Caravaggisti, as it can be seen in the faces of all the left figures, but most remarkably on Christ's face. Naples yellow is also used to render artificial lighting on fabrics. As recurrently done in Western art at that time, flesh tones are illuminated through lead white in the areas where Pb and Sb do not correlate. More uncommonly, warm lighting on their clothing is given by Naples yellow over green or light brown-yellow earths.

Stomer's original materials and later interventions

MA-XRF documented the use of ochres for darker red hues and shadows. Cinnabar is also part of the palette for flesh tones and bright details in garments.

The map of lead collected on the top right area of the painting showed an important 'pentimento'. The painter's earlier sketch of Christ's face seems to show suffering and resignment, as he is looking downward. However, in the final version the figure gains more dignity and seems to look at the observer. This technological choice possibly testifies a compositional maturity, which also comes out from the comparison of this representation of Christ and earlier ones painted by Stomer in his Roman or Neapolitan period, one at Hôpital St Jean, Brussels [8] and one in the private market (www.sothebys.com/en/auctions/ecatalogue/2015/old-master-british-paintings-evening-sale-l15033/lot.10.html, accessed on 20 February 2024). Both paintings show a reversed composition, with Christ on the left looking upwards. Conversely, in the Castello Ursino *Mocking of Christ* Stomer's seems to recall the painter Van Honthorst's *Mocking of Christ* (ca. 1617) now at LACMA, Los Angeles. However, Stomer surpasses his master's lesson, playing with lights and new materials to modify the composition and give greater dignity to the main character and the whole scene.

Lead signals are also attributed to the ground, where this element correlates with calcium. In fact, grounds for seventeenth-century Italian paintings - from different regions and artists - were usually made of one or more layers with lead white and a Ca-based material like chalk, either in mixture or in different layers, usually showing light to dark color because of the addition of ochres, minimum or carbon black.

In the *Mocking of Christ* barium and titanium maps provide proof of modern conservation treatments, especially along the edges of the painting, as they are the main chemical elements in modern pigments introduced in the twentieth century as extenders, barium and titanium white respectively. A different type of intervention affects small areas of repair where the copresence of Ba and Cr suggests that here the paint formulation contains barium white and a Cr-based pigment, possibly an earth chosen to give the paint a hue similar to the original one.

Analogously, the use of a modern dark brown pigment containing zinc and titanium white is likely explained as a later intervention with a commercially available pigment.

REFERENCES

[1] F.P. Romano et al., in B. Mancuso, V. Pinto (Eds.), Messina (2018) 190–201.
[2] J. Dik et al. Archaeometry 47 (2005) 593.
[3] A. Roy et al., Stud. Conserv. 43 (1998) 160.
[4] G. Agresti et al., Color Res. Appl. 41 (2016) 226.
[5] S. Wharton, Renaiss. Stud. 19 (2005) 592.
[6] F.P. Romano et al., J. Anal. At. Spectrom. 32 (2017) 773.
[7] M. Botticelli et al., Heritage 7 (2024) 1188.
[8] B. Nicolson, Burlingt. Mag. 119 (1977) 230.

Radiation Damage produced by Heavy Ions in Silicon Carbide Detectors

S. De Luca[1], C. Altana[1], L. Calcagno[2,3], C. Ciampi[4,5], F. La Via[6], G. Lanzalone[1,7], A. Muoio[6], G. Pasquali[4,5], D. Pellegrino[3], S. Puglia[2,3], G. Rapisarda[1,3], S. Tudisco[1],

1) Laboratori Nazionali del Sud (LNS), Istituto Nazionale di Fisica Nucleare (INFN), 95123 Catania, Italy;
2) Istituto Nazionale di Fisica Nucleare (INFN)—Sezione di Catania, 95123 Catania, Italy;
3) *Physics and Astronomy Department, Catania University, 95123 Catania, Italy;*
4) Physics and Astronomy Department, Florence University, 50019 Florence, Italy;
5) Istituto Nazionale di Fisica Nucleare (INFN)—Sezione di Firenze, 50019 Florence, Italy;
6) Institute for Microelectronics and Microsystems (IMM), National Research Council (CNR), 95121 Catania, Italy;
7) Department of Engineering and Architecture, KORE University, Cittadella Universitaria, 94100 Enna, Italy.

Abstract - Silicon carbide (SiC), thanks to its high resistance to radiation damage, is one of the most promising materials to replace silicon in particle detection. In this paper, we show the radiation damage studies of recent p-n junction silicon carbide devices. We have irradiated, in two experimental conditions with different beams, several SiC detectors developed inside the SiCILIA (Silicon Carbide detectors for Intense Luminosity Investigations and Applications) project, to study for both (Si and SiC) the CCE (Charge Collection Efficiency) as a function of fluence and electrode voltage.

SILICON CARBIDE PROPERTIES

Silicon Carbide represents a new challenge for detector manufacturing [1]. SiC is extremely appealing for its expected features in terms of radiation hardness; it is a wide band gap semiconductor and exists in more than 200 different polytypes, in which it can assume a wide variety of crystallographic structures (polytypism); the 4H-SiC polytype is largely used in radiation hard applications.

Though the substrate material has recently improved both in size and purity, the present quality and uniformity of the epitaxial layers does not allow the processing of devices directly on it. Therefore, first of all, it is necessary to grow an epitaxial layer on a substrate that acts as the active region of the SiC detector. A seed substrate with very low defect concentration and the reduction of the density of defects present in the substrates by means of an epitaxial process allow a high-quality material to be obtained. The growth rate condition also has a significant influence on the defect formation or annihilation. Consequently, all these parameters are essential to obtain detectors with large area and thick active regions.

The detectors studied in this work are new large area devices developed, during the SiCILIA project, by a collaboration between INFN, IMM and ST-Microelectronic. They are produced starting from 10-100 µm and n^- epi-layers grown on 350 µm substrates. A p+ layer 0.3÷0.5 µm thick with an aluminum doping concentration of the order of 10^{18}÷10^{19}/cm^3 is grown over the n^- epi-layer with a nitrogen doping concentration in the range 5÷8 10^{13}/cm^3 (Figure 1). The activity thickness of the devices tested in this work is about 10 µm. Then the depletion bias is about 4 V. The detector area is 5x5 mm^2.

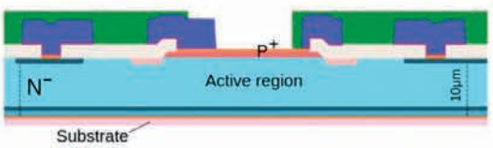

Figure 1. Schematic representation of 10 µm thick detector

CCE IN SIC AND SI WITH ^{16}O

In a first experimental campaign, the DUTs (Detector Under Test) were irradiated with ^{16}O ions at 12.5 MeV, together with a standard silicon detector, for comparison. We studied the CCE of the DUTs as a function of the ion fluence and of the anode voltage. The DUTs, collimated so that just a small portion of the device was irradiated, were placed in the CT-2000 vacuum chamber. The beam energy is 12.5 MeV. The ^{16}O beam is collimated to less than 1 mm before impinging on a ^{197}Au target. The DUTs are placed at angles ranging from 0.5° to 10° respect to the beam direction. Each DUT is irradiated at different fluence (from 8.8 10^7 to 4.2 10^{11} pp/cm^2). In the same geometrical conditions, a standard p-n junction silicon detector (a Hamamatsu S3590-06 p-i-n chip, 300 µm thick) is irradiated at a larger energy (25 MeV) with the aim to compare the damage effects in the two different

materials. At the first, the Tandem accelerator was set to deliver a high energy beam useful for the calibration of Si device. Then, the energy of the ^{16}O beam was reduced at 12.5 MeV to make the beam ions stop within the 10 µm of SiC and proceed with its investigation. The beam current is evaluated by using a pristine SiC, placed at 17° to the beam direction. Figure 2 shows the obtained CCE values as a function of the applied voltage. The CCE has been calculated only for those voltage values for which a proper peak is present. The most striking difference between the SiC and the silicon data is the behavior at the largest fluence values. The silicon detector always shows a tendency to saturate with increasing voltage. For increasing fluence, we can observe both a reduction of the CCE and an increase of the bias to obtain the saturation value: already at 10^8 cm^{-2} the saturation value stays well below 100%.

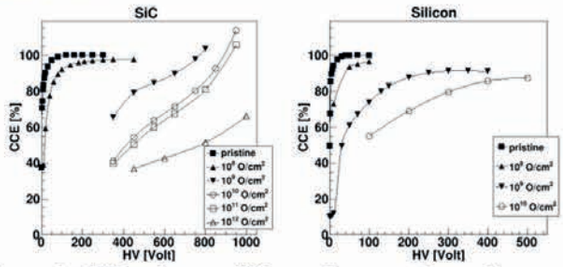

Figure 2. CCE values at different fluences. For each detector, all points are normalized to the maximum CCE obtained in pristine conditions.

The SiC detector, instead, shows an increasing CCE value, which even trespasses 100% at very high reverse bias (V > 800 V). This could be due to damage in the SiC material that produces a substantial change in the local doping concentration and, consequently, a peak of the electric field close to the electrodes and an impact ionization of the carriers in those regions. The impact ionization multiplication then gives a larger than 100% CCE as already recognized in silicon detectors [2].

CCE IN SIC AND WITH ^{27}Al

To investigate the variation of the electrical characteristics properties with irradiation fluence, a second set of measurements was performed, with only the SiC detectors (whole devices). Furthermore, due to the high radiation hardness of the SiC detectors observed in the previous experiment, it has been decided to use a heavier ion and the irradiation has been performed with ^{27}Al. Three DUTs were placed in the target position at 90° to the beam direction. At this energy, ^{27}Al has a range of 6.9 µm in SiC, and it is therefore stopped in the active region. The DUTs, nominally identical, were irradiated at different fluences (from 10^9 to 10^{11} pp/cm^2). Before and after irradiation, each device was tested in vacuum, in terms of its spectroscopic performance, using two alpha sources: a ^{148}Gd source (E = 3.183 MeV) and an ^{241}Am source (main peak E = 5.486 MeV).

In this measurement, the ion used to damage the detectors is not the same as that employed to characterize them. Moreover, the CCE was evaluated many hours after irradiation. An analysis of the CCE has been performed for both alpha sources, and data obtained with the two sources are compatible. Figure 3 shows the CCE obtained using the ^{148}Gd source, as a function of the applied voltage. All the DUTs have practically the same behavior before irradiation with the CCE reaching 100% already at 10 V bias voltage. The CCE decreases for increasing fluence. The bias voltage for which CCE saturates also tends to increase. This effect could be due to the decrease of the carrier lifetime produced by the damage in the silicon carbide epitaxial layer after the irradiation.

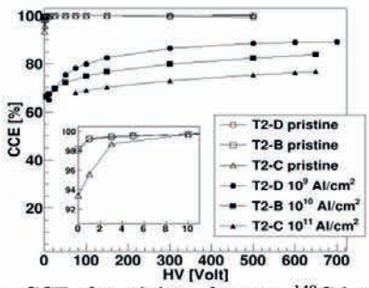

Figure 3. CCE for alphas from a ^{148}Gd source as a function of the applied bias voltage. For each DUT, CCE values before and after irradiation are shown.

CONCLUSION

In this work we reported a study on the radiation damage of SiC detectors. In a first experiment a comparison between Si and SiC detectors has been performed. The detectors have been irradiated with ^{16}O ions, and the same ions have been used for CCE evaluation (right after irradiation). The CCE is similar between the two detectors. In the second part of the experiment, a heavier ion (^{27}Al) was used to test the SiC detectors. In this case, The CCE has been evaluated many hours after irradiation by exploiting a ^{148}Gd alpha source. The CCE is always larger than 70% even for the higher fluence of 10^{11} ions/cm^2. The CCE is also always increasing with the increase of the bias of the detector, and no saturation is observed until 700 V. Finally, CCE in SiC detectors are still good, showing a much higher radiation hardness with respect to silicon.

REFERENCES

[1] F. Nava et al, "Silicon Carbide and Its Use as a Radiation Detector Material", Meas. Sci. Technol. 2008, 19, 102001.

[2] G. Kramberger et al, "Reasons for High Charge Collection Efficiency of Silicon Detectors at HL-LHC Fluences". Nucl. Instrum. Methods Phys. Res. A 2019, 924, 192–197.

Proton selection and acceleration for I-LUCE facility: Simulation study

F. Farokhi[1], S. Fattori[1], G. Petringa[1], G. Angemi[1], S. Arjmand[1], G. Cantone[1], E. Caruso[1], R. Catalano[1], G. Cuttone[1], O. Giampiccolo[1], M. Guarrera[1], A. Kurmanova[1], D. Oliva[1], A. Pappalardo[1], A. Pizzino[1], A. Sciuto[1] and G.A.P. Cirrone[1,2]

1) Istituto Nazionale di Fisica Nucleare - Laboratori Nazionali del Sud (INFN-LNS), Catania, Italy.
2) Centro Siciliano di Fisica Nucleare e Struttura della Materia (CSFNSM), Catania, Italy

Abstract - Nowadays, a major effort is being dedicated to optically accelerate charged particles, including the development of laser-driven particle accelerators. I-LUCE, which stands for INFN Laser indUCEd radiation facility, is a pioneer in the field of particle acceleration using high-powered lasers. The considerable capabilities of laser-matter interactions, such as generating diverse types of short, intense beams open doors to a wide range of multidisciplinary applications. A Geant4-Based Monte Carlo model has been developed to aid I-LUCE beam line design, ensuring optimal particle transport, precise irradiation parameters, and the ability to accurately predict clinically relevant dose distributions.

INTRODUCTION

Hadrontherapy, as one of the effective approaches in cancer treatment, faces a global adoption hurdle: the high cost of making traditional particle accelerators. A promising alternative can lie in laser-driven ion beams [1]. I-LUCE, INFN Laser indUCEd radiation, a laser-based particle acceleration facility, is pioneering research in generating various types of radiation through high-powered laser technology. High-intensity laser pulses interacting with solid surfaces trigger a sequence of events leading to the generation of fast protons. This involves rapid ionization creating plasma, hot electron generation forming a cloud near the target's front, and charge separation creating a strong electric field. This powerful field, through a process called Target Normal Sheath Acceleration, primarily accelerates protons due to their favorable charge-to-mass ratio, propelling them at high speeds from the rear surface.

After the initial acceleration, I-LUCE employs a specialized system to refine the proton beam:

- **Beam Transport**: Magnetic elements, like quadrupoles and dipoles, guide and control the trajectory of the proton beam. Quadrupoles focus the beam to a specific point or shape for experiments and dipoles which bend the beam along specific paths.
- **Energy Selection**: The energy of accelerated protons typically has a broad spectrum. To isolate protons within a specific energy range, the I-LUCE facility relies on two elements. first, dispersive elements in which magnetic elements bend protons of different energies at different angles. The second one is collimators or slits, to select and control the narrow size of the proton beam with the desired energy.

A Geant4-based application has been developed to improve beam line design, track and analyze the trajectory of accelerated proton beams as they pass through beamline in I-LUCE facility, optimize transport parameters and predict dose distributions for clinical use.

This work will present a study on how proton energy spectra, angular divergence and

transmission efficiency (within the in-vacuum section of the beamline) are interrelated.

MATERIAL AND METHODS

In order to simulate and optimize the beam transmission in the I-LUCE beamline, 'LaserDrivenBeamLine' class within the Geant4 'Hadrontherapy' example [2] has been designed. This application accurately models both geometry and magnetism of beamline elements, providing users the flexibility to design and simulate their experimental setups. The user can implement a realistic laser-driven ion source, specifying the desired energy and angular distribution of the ions.

The transport system begins with four high-gradient permanent magnet quadrupoles (PMQs). The PMQs configuration can be modified based on the particle type and energy. Following the PMQs, an in-vacuum chamber houses the Energy Selector System (ESS).

Simulations were conducted across the entire beam line to study the energy distribution (spectra) and the number of particles delivered per shot (Fig.1).

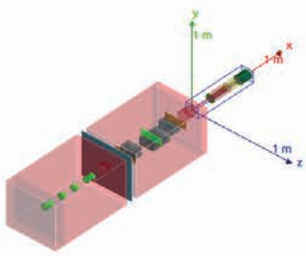

Figure 1: Laser-driven beamline simulated with Geant4 simulation toolkit.

A typical exponential proton energy spectrum with a maximum energy of 12 MeV is reproduced. We investigated the energy distribution and beam profile at different transverse planes along its propagation direction. The energy distribution at different points in the beam line are presented in Figure 2. The blue curve represents the initial proton source energy spectrum. The red one shows the energy spectrum of the beam after passing through the last PMQs. Finally, the green curve depicts the energy spectrum after the ESS has performed magnetic selection. The PMQs and ESS were configured to focus and select 1.5 MeV protons for efficient transport.

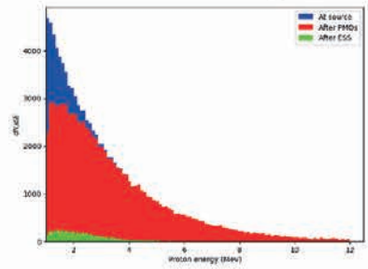

Figure 2: The energy distribution of particles at source, after PMQs and after ESS.

Another important consideration is the beamline's efficiency in transporting ions at the chosen energy level. Transport efficiency is the percentage of protons that reach the end of the ESS with the desired range of the chosen energy level which in this configuration efficiency is approximately 11%.

RESULTS AND CONCLUSION

A detailed laser-driven beamline simulation within the Geant4 toolkit, accurately modeling geometry and magnetic fields, enables analysis of beam characteristics throughout the in-vacuum transport.

In this work, transmission efficiency values at different points along the beamline were calculated. Our simulations indicate an acceptable level of transmission efficiency.

REFERENCES

[1] F. Schillaci et al., Design of the prototype of a beam transport line for handling and selection of low energy laser-driven beams, Nucl. Instrum. Meth. 837 (2016) 80.

[2] S. Agostinelli et al., Geant4—a simulation toolkit, Nucl. Instrum. Methods Phys. Res. A 506 (3) (2003) 250–303.

Radiobiology: A Geant4-based Application for Particle Therapy

S. Fattori[1], D. Chiappara[2], L. Pandola[1], G. Petringa[1], A. Sciuto[1], G. Angemi[1], S. Arjmand[1], G. Cantone[1], E. Caruso[1], R. Catalano[1], G. Cuttone[1], F. Farokhi[1], O. Giampiccolo[1], M. Guarrera[1], A. Kurmanova[1], D. Oliva[1], A. Pappalardo[1], A. Pizzino[1], and G.A.P. Cirrone[1]

1) Istituto Nazionale di Fisica Nucleare (INFN) - Laboratori Nazionali del Sud (LNS), Catania, Italy
2) University of Padova (UNIPD) · Department of Physics and Astronomy "Galileo Galilei", Padova, Italy

Abstract – "Radiobiology" is a C++ open-source application developed by our group in the framework of the Geant4 toolkit. It was released with version 11.2 of Geant4 on December 8th, 2023, within the medical section of the extended examples.

The current version of the application allows the user to simulate a particle beam interacting with a voxelized water phantom, giving in output dose, Linear Energy Transfer (LET) and survival curves.

An updated version of the application will be released by our group with a future Geant4 release. This new version will contain post-processing Python scripts obtained with the training of Machine Learning (ML) algorithms to make "radiobiology" a multiscale (micro-nano) application.

In this work, the main characteristics of the current version of "radiobiology" will be presented.

INTRODUCTION

It is well known nowadays how the Monte Carlo (MC) approach has a key role in the understanding of radiation-induced effects on biological systems. The accurate description the MC technique can provide of all the physical processes involved in radiation-matter interaction is a powerful feature playing a significant role in both clinical and research fields.

The counterpart is often given by the high degree of complexity MC modelling applications present, being often tools not versatile and hard to customize.

In response to this issue, the "radiobiology" application has been realized, being a highly customizable and handy Geant4 [1] example, that still provides very significant outcomes as the ones provided by the example from which it was derived, the Geant4 advanced example "hadrontherapy" [2], [3].

In the next section, the general description of the current version of "radiobiology" will be presented.

GENERAL DESCRIPTION OF THE RADIOBIOLOGY APPLICATION

"Radiobiology" is a C++ open-source application belonging to the medical section of the extended examples of the Geant4 toolkit. It has been publicly released by our group with version 11.2 of Geant4 on December 8th, 2023.

This application can be considered as a simplified version of the advanced example "hadrontherapy" [2], [3]. It allows the user to simulate a particle beam interacting with a water phantom, representing a typical water tank conventionally adopted in a clinical or research environment, and provides in output, through dedicated C++ classes adopted from "hadrontherapy", the depth dose distribution, the dose-weighted and the track-weighted Linear Energy Transfer (LET_{dose} and LET_{track} respectively) distributions, both of the primary and the total ones including the contribution of all the fragments, and the survival curves along with the Relative Biological Effectiveness (RBE). The algorithms implemented for LET_{dose} and LET_{track} and the RBE have been extensively validated with several publications [4], [5], [6], [7], [8].

The software interface has been developed to allow the user to easily implement his/her own algorithm to estimate the quantities of interest in radiobiological applications, without the need to develop by hand the interface with the underlying MC environment.

The geometry of the application, consisting of a voxelized phantom (see Figure 1), uses water as the default material. This geometry is fully customizable: the application provides an easy interface that allows the user to change, with simple commands in a text file, all the parameters of the phantom: the material, the dimensions, and the number and thickness of the voxels in the three axes.

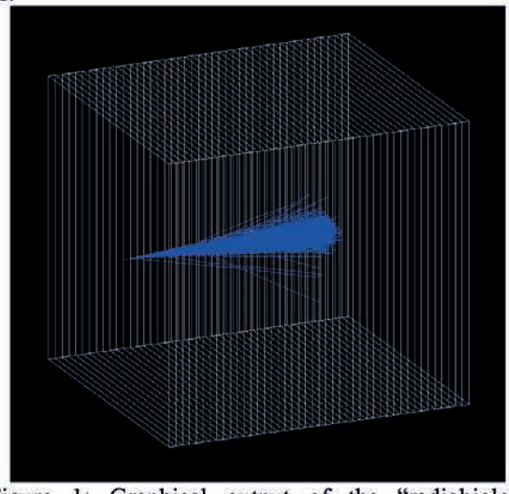

Figure 1: Graphical output of the "radiobiology" example showing the voxelized water phantom, crossed by a proton beam with 62 MeV energy.

The choice of making the geometry of the example extremely simple is given by the idea behind the development of this application, which is to create a sort of "sandbox", a code infrastructure able to produce a lot of outputs from a simple input that can easily be personalized by the user to adapt it to his/her specific needs, e.g. introduce in input a phase-space, output of a specific beamline facility.

An updated version of the application will be released by the authors with a future Geant4 release. This new version will contain post-processing Python scripts obtained with the training of Machine Learning (ML) algorithms to convert the radiation-induced effects from the micrometric scale, reachable with a standard Geant4 simulation, to the nanometric one, typical of a Geant4-DNA [9] simulation. The aim of these additional features of the "radiobiology" example is to convert a standard Geant4 output into a Geant4-DNA one without having to deal with the high CPU-time requirements of the last one. More details on this will be found in a dedicated manuscript.

RESULTS OF BENCHMARKING TESTS

The "radiobiology" application has been tested and compared for benchmarking against the results of the "hadrontherapy" application, running with the same beam configurations.

In Figure 2 we present the results of one of these comparisons, the one of dose and LET_{track} distributions, obtained with a full energy 62 MeV beam. As shown in the figure the two outputs are in full agreement with each other, and the slight difference of the LET_{track} distributions at the distal part is given by the low statistics typical of this region.

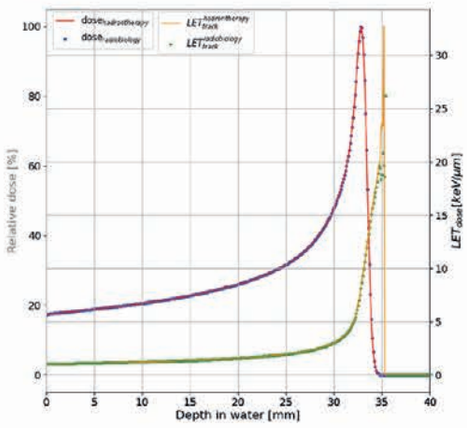

Figure 2: Comparison of dose and LET distributions obtained with the "radiobiology" application, against those obtained with the "hadrontherapy" one.

REFERENCES

[1] S. Agostinelli et al "Geant4—a simulation toolkit" Nuclear Instruments and Methods in Physics Research A 506 250–303 (2003) doi: 10.1016/S0168-9002(03)01368-8 https://www.sciencedirect.com/science/article/pii/S0168900203013688?via%3Dihub

[2] G. A. P. Cirrone et al. "Implementation of a new Monte Carlo simulation tool for the development of a proton therapy beam line and verification of the related dose distributions" 2003 IEEE Nuclear Science Symposium. Conference Record (IEEE Cat. No.03CH37515) 3 (2005), pp. 1756–1758. doi: 10.1109/NSSMIC.2003.1352218 https://ieeexplore.ieee.org/document/1352218

[3] G. A. P. Cirrone et al. "Hadrontherapy: a Geant4-Based Tool for Proton/Ion-Therapy Studies". Progress in NUCLEAR SCIENCE and TECHNOLOGY 2 (2011), pp. 207–212. https://www.aesj.net/document/pnst002/207-212.pdf

[4] F. Romano et al. "A Monte Carlo study for the calculation of the average linear energy transfer (LET) distributions for a clinical proton beam line and a radiobiological carbon ion beam line". Physics in Medicine Biology 59.12 (2014). doi: 10.1088/0031-9155/59/12/2863 https://iopscience.iop.org/article/10.1088/0031-9155/59/12/2863

[5] G. Petringa et al. "Monte Carlo implementation of new algorithms for the evaluation of averaged-dose and -track linear energy transfers in 62 MeV clinical proton beams". Physics in Medicine Biology 65.235043 (2020). doi: 10.1088/1361-6560/abaeb9 https://iopscience.iop.org/article/10.1088/1361-6560/abaeb9

[6] S. Fattori et al. "4He dose- and track-averaged linear energy transfer: Monte Carlo algorithms and experimental verification". Physics in Medicine Biology 67.165003 (2022). doi: 10.1088/1361-6560/ac776f https://iopscience.iop.org/article/10.1088/1361-6560/ac776f

[7] G. Petringa et al. "Radiobiological quantities in proton-therapy: Estimation and validation using Geant4- based Monte Carlo simulations". Physica Medica 58 (2019), pp. 72–80. doi: 10.1016/j.ejmp.2019.01.018 https://www.sciencedirect.com/science/article/abs/pii/S1120179719300183?via%3Dihub

[8] M. Dordevic et al. "Computational approaches in the estimation of radiobiological damage for human-malignant cells irradiated with clinical proton and carbon beams". Physica Medica1 117.103189 (2024). doi: 10.1016/j.ejmp.2023.103189 https://www.sciencedirect.com/science/article/pii/S1120179723012176?via%3Dihub

[9] S. Incerti THE GEANT4-DNA PROJECT. International Journal of Modeling, Simulation, and Scientific Computing, 01(02):157–178. (2010). doi: 10.1142/S1793962310000122 https://www.worldscientific.com/doi/abs/10.1142/S1793962310000122

The MiniRadMeter gamma and neutron sensor for CLEANDEM

F. Rossi [1], S. Amaducci[2], L. Cosentino[2], C. Failla[2], F. Longhitano[3], S. Minutoli[1], P. Musico[1], M. Osipenko[1], G.E. Poma[2], M. Ripani[1], G. Vecchio[2], and P. Finocchiaro[2]

1) INFN Sezione di Genova, Genova, Italy
2) INFN Laboratori Nazionali del Sud, Catania, Italy
3) INFN Sezione di Catania, Catania, Italy

Abstract - In the framework of the H2020 CLEANDEM project a small robotic vehicle was developed, equipped with a series of different sensors for high radiation contaminated areas. In this work we describe the MiniRadMeter system which is meant as a compact low-cost sensor to perform a quick gamma and neutron radiation field mapping of the environment preliminary to the possible start of human operations.

INTRODUCTION

The decommissioning of nuclear installations, as well as the possible accident remediations, requires the physical presence of human operators in potentially radiologically hostile environments. The worldwide number of active nuclear reactors is larger that 400, and most of them are 40 to 50 years old, thus implying that soon they will have to be dismantled. In the framework of the H2020 CLEANDEM project a small robotic vehicle is being developed (Unmanned Ground Vehicle, UGV, Figure 1 left), equipped with a series of different sensors for highly radiation contaminated areas. The MiniRadMeter system is meant as a compact low-cost sensor to perform a quick gamma and neutron radiation field mapping of the environment preliminary to the possible start of human operations. The miniature gamma sensor is a 1 cm^3 CsI(Tl) scintillator counter with moderate spectroscopic features read out by means of a 6×6 mm^2 SiPM. Neutrons are detected by means of two 1 cm^2 silicon diodes, arranged in a back-to-back fashion, each one coupled to a layer of ^{6}LiF neutron converter material and placed inside a 6×6×6 cm^3 polyethylene moderator box. The front-end and data acquisition electronics was developed, based on a Raspberry Pi4 microcomputer (Figure 1 right).

TESTS WITH SOURCES

The sensor was thoroughly tested with laboratory sources. In Figure 2 we show the channel-to-energy gamma ray calibration plot obtained by means of a linear fit to the positions of the peaks produced by seven sources. The corresponding spectra, in vertical logarithmic scale in order to accommodate all in one single plot, are shown in Figure 3. Remarkably, the detector has a good linear behavior up to ≈ 2 MeV and shows an excellent 5% FWHM resolution at 662 keV.

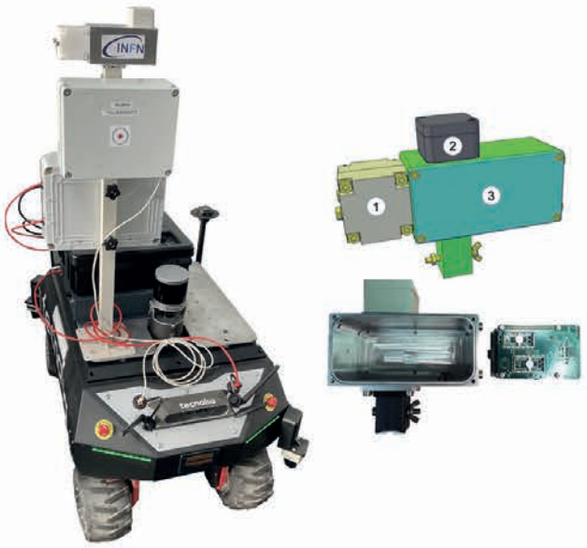

Figure 1. (Left) The CLEANDEM UGV with the MiniRadMeter installed on top. (Right) The neutron moderator and detector (1); the gamma detector (2); the front-end electronics and data acquisition microcomputer (3).

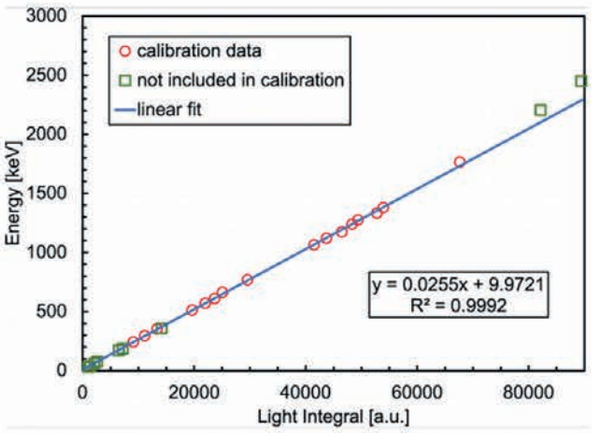

Figure 2. The channel-to-energy calibration plot for the gamma detector. The red circles refer to the gamma energies used for the calibration, the green squares refer to the energies not included in the calibration.

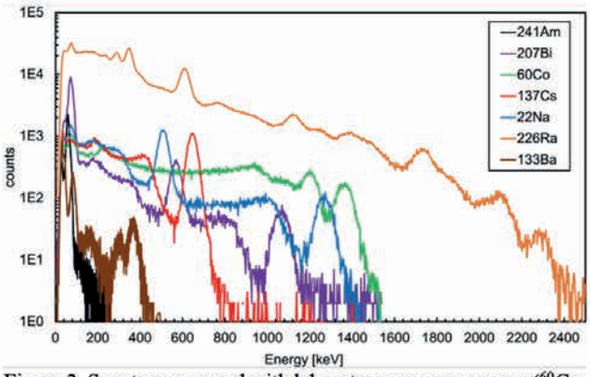

Figure 3. Spectra measured with laboratory gamma sources (^{60}Co, ^{22}Na, ^{207}Bi, ^{137}Cs, ^{241}Am, ^{226}Ra, ^{133}Ba).

The neutron detector operates by detecting alphas and/or tritons produced after thermal neutron capture in ^{6}Li. It was tested with a low intensity AmBe neutron source (≈6000 neutrons/s in 4π). Due to the non-optimal geometric setup the expected count rate during a run of several hours was 1-2 neutrons/minute. In Figure 4 we reported the spectrum of the deposited energy, that correctly shows the 2.73 MeV end point of the tritium kinetic energy. Placing a logical threshold at 1.5 MeV for neutron tagging makes it possible to achieve a $\approx 10^{-9}$ gamma/n discrimination, even though sacrificing part of the thermal neutron detection efficiency that in such a configuration is about 5%.

In Figure 5 we show a snapshot of the Graphical User Interface (GUI) that was developed to fully set up, configure and handle the MiniRadMeter sensor.

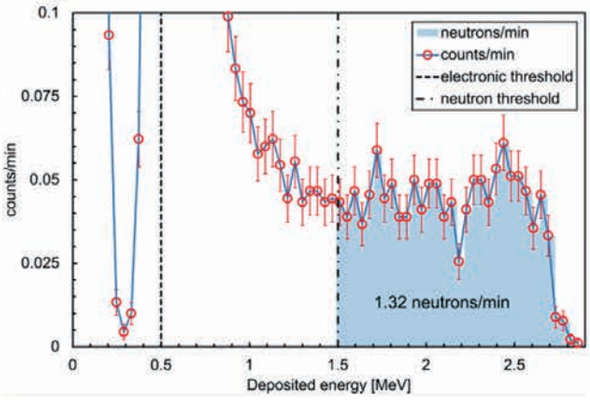

Figure 4. Deposited energy spectrum measured by the neutron detector with a low intensity AmBe neutron source.

SUMMARY

The test results of the MiniRadMeter gamma and neutron sensors indicate that it is suitable for the task it was supposed to accomplish. Indeed the small CsI(Tl) crystal behaves nicely as a dosimeter which in few seconds can provide a reasonable gamma dose rate measurement. Its additional spectroscopic features represent a useful tool for a preliminary indication of the typical emitting species possibly present in the environment.

As for the neutron detection, this is a more difficult task because a measurement of the same quality level as the gamma detection would require a complex and large equipment definitely unsuitable for the UGV. Nonetheless, the device is capable of detecting the presence of a relevant neutron field in a matter of seconds by virtue of its superior gamma/neutron discrimination. This means that even in case of a very low measured counting rate the signal is reliable and will indicate the real presence of neutrons in the environment, even though the quantitative information is poor due to the significant dependence of the detection efficiency on the neutron energy.

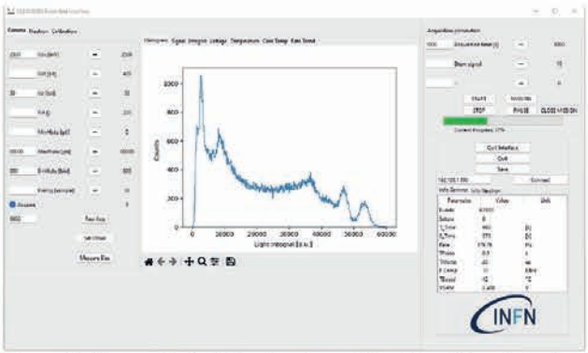

Figure 5. A snapshot of the developed Graphical User Interface (GUI).

The WiFi connection capability of the miniradmeter was successfully tested in April 2023 during an operational test done on the Tecnalia premises. The overall device weight is about 350 g, its dimensions are 20 cm × 10 cm × 7 cm but could be reduced if needed. The light weight and the compact size, along with the low cost, make it possible to update it into a deployable version. Indeed, a slim Li-ion battery could be easily incorporated inside the box, then exploiting the onboard WiFi interface for the remote control and data transfer. This could be quite useful in case of accident remediation as a number of MiniRadMeter sensors could be deployed by UGVs or flying drones on contaminated areas for a distributed mapping and monitoring of the radiation field.

The next step for the current version of MiniRadMeter will be the forthcoming test in a real environment that is planned as a final demonstration of the CLEANDEM project.

ACKNOWLEDGMENTS

The CLEANDEM project has received funding from the European Union's Horizon 2020 research and innovation programme under grant agreement No 945335.

REFERENCES

[1] CLEANDEM EU project Horizon 2020, GA 945335. https://cordis.europa.eu/project/id/945335/ (accessed on 10 March 2024).

[2] Rossi, F.; Cosentino, L.; Longhitano, F.; Minutoli, S.; Musico, P.; Osipenko, M.; Poma, G.E.; Ripani, M.; Finocchiaro, P. The Gamma and Neutron Sensor System for Rapid Dose Rate Mapping in the CLEANDEM Project. *Sensors* **2023**, *23*, 4210. https://doi.org/10.3390/ s23094210

New plasma diagnostics testbenches based on X-ray imaging, multi- wavelength spectroscopy and polarimetry techniques

G. Finocchiaro[1,2], E. Naselli[2], S. Biri[3], G. S. Mauro[2], B. Mishra[1,2], B. Peri[2,4], A. Pidatella[2], R. Rácz[3], G. Torrisi[2] and D. Mascali[2]

1) Università degli Studi di Catania ,Catania Italy
2) INFN-Laboratori Nazionali del Sud, Catania, Italy
3) ATOMKI, Debrecen, Hungary
4) Centro Siciliano di Fisica Nucleare e Struttura della Materia (CSFNSM), Catania, Italy

Abstract

Plasma diagnostics can play a crucial role in investigating laboratory magnetized plasmas. A non-invasive plasma multidiagnostics system with tens of devices has been developed at INFN-LNS in the frame of the PANDORA [1] project for fundamental nuclear and plasma physics research. Recently, within the synergistic SAMOTHRACE (SiciliAn MicronanOTecH Research And innovation CEnter) ecosystem frame, funded by the EU Next Gen Program, two new diagnostics testbenches – the spectroscopy PYN-HO prototype and the polarimetric VESPRI 2.0 setup – were designed to develop detectors and techniques beyond the state of art, making them suitable also for applications in controlled nuclear fusion.

PLASMA X-RAY IMAGING AND SPECTROSCOPY

The X-ray pinhole CCD camera setup [2] allows to perform X-ray plasma imaging and space-resolved spectroscopy [3, 4, 5] through an advanced analysis algorithm for Single Photon-Counted (SPhC) and High-Dynamic-Range (HDR) mode [6]. Recently, several improvements of the algorithm [7, 8] allowed to perform more quantitative space-resolved spectroscopic analysis, evaluating local thermodynamic plasma parameters.

Figure 1 – Left: Plasma electron density map in three circular ROIs, overlapped on the X-ray plasma image. Right: Temperature and density values.

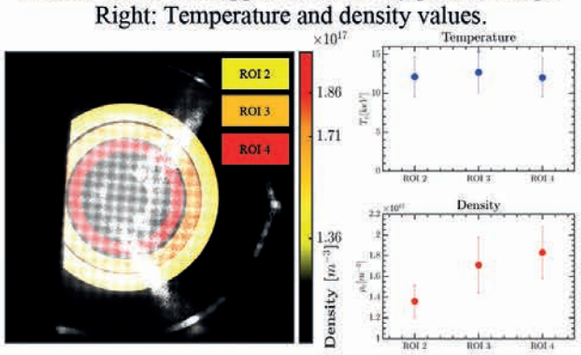

In more details, the last results [8] returned important features about the Electron Cyclotron Resonance (ECR) plasma structure and confinement, showing the clear formation of a plasmoid-halo structure inside the plasma chamber, i.e. a dense and energetic plasma confined inside the ECR magnetic iso-surface. Therein, the plasma is almost uniformly distributed in both density and temperature, whose respective values have been measured at 12.44 ± 1.84 keV and (1.66 ± 0.15) · 10^{17} m^{-3}. In the plasma halo the X-ray emission is negligible, whilst cusp structures correspond to the magnetic branches along which the deconfined electrons impinge on the plasma chamber walls and endplates. Fig. 1 (left) shows a plasma density map overlapped on an X-ray image of plasma with the respective values of density and temperature (right).

PYN-HO VISIBLE/X-RAY TESTBENCH

One of the main activities concerned the design of the new advanced X-ray diagnostic testbench PYN-HO (Probing x-raYs by imagiNg and pin-Hole spectrOscopy) conceived to operate in four different configurations. Two configurations will allow to enhance the X-ray imaging and space-resolved spectroscopy technique, with the related calibrations and characterizations in both test-benches and magnetically confined plasmas. Two other ones will be instead dedicated on high energy resolution diffractometric spectroscopy measurement in X-ray and optical domains, based on the use of gratings.

In more details, the final design (see Figure 2) includes:

A. Configuration 1.0 – X-ray calibration and characterization to perform energy and quantum efficiency calibration of the CCD detector, particularly in the low energy domain (0.5-30 keV). The system includes an X-ray source to calibrate the spectroscopic CCD system and a SDD (sensitive to low energies) to be used as a reference to normalize the CCD space-resolved spectra and correct the post-processed SPhC algorithm effects.

B. Configuration 2.0 – X-ray imaging and spectroscopy in magnetized plasma by combining different detection systems (SDD and pin-hole focused CCDs, including multi-collimators and shutters). X-ray plasma tomography can be performed by using two CCD cameras. In addition, volumetric spectroscopy on high X-ray emission plasmas will be performed by means of SDD operating at very high counting rate.

C. Configuration 3.0 – Diffractometric measurements on test-bench and in plasma. The system, based on the use of "gratings" and motorized stages, will reach resolutions of the order of $\Delta\lambda/\lambda = 10^{-3}$ at 565 eV. It will

allow to carry out XRF peak broadening measurements for the estimation of plasma ion temperature, by resolving charge-state-shifted peaks.

D. Configuration 4.0 – Optical emission spectroscopy on test-bench and in-plasma to investigate the cold electron component of plasma. The system is thought to absolutely calibrate the spectrometer by an in-lab built radiometric calibration system and calibrated focused light sources. This aiming in plasma transmission measurements for determining the plasma opacity [9].

Figure 2: Sketch of the PYNHO testbench configurations.

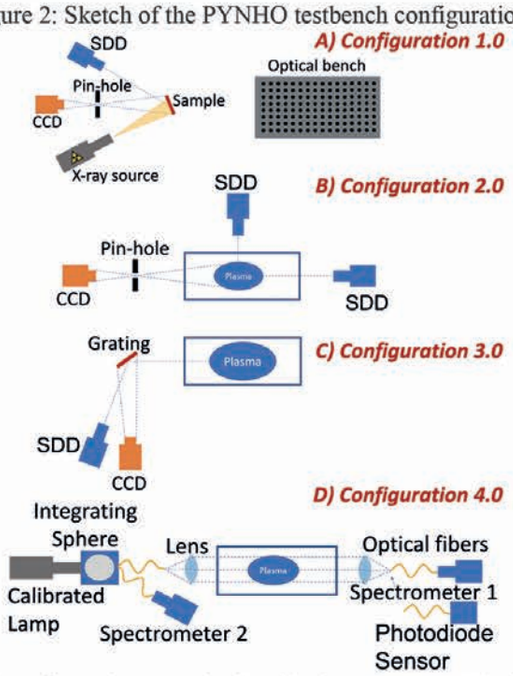

All configurations can be installed on the FPT (Flexible Plasma Trap) [9] - installed at INFN-LNS for R&D on diagnostics and detectors.

VESPRI 2.0 POLARIMETRIC SETUP

Other activities rely to the design of the polarimetric system VESPRI 2.0 for the measurement of the total electron density based on the measurement of the Faraday rotation. The new design involves the use of a THz polarimetry system based on the superheterodyne approach and on the measurement of the Lissajous figures [10]. The first experimental tests to validate the technique were conducted on the optical bench using a down-sized polarimetric system (see Fig. 3). It included a polarimeter operating in the 18-26 GHz probing frequency domain, with the following tools and devices: a signal generator for the probing wave, two high-directivity horn antennas of which the transmitting antenna was connected to the signal generator and the second rotatable receiving antenna was connected with an orthomode transducer (OMT) (a waveguide component to combine or separate two orthogonally polarized microwave signal paths).

The setup operates following the Super-Heterodyne scheme, which allows to downshift the detected frequency (1 GHz) compared to the probing one (20 or 100 GHz) to be detected in a scope. For this purpose, two mixers were installed and to each of them the output signal of the OMT and the signal coming from a second generator were connected. The measurements were carried out by interposing a wire polarizer (used to emulate magnetoplasma-induced Faraday rotation) measuring the Lissajous figures of the probing RF signal crossing the polarizer through a two channels scope (80 Gs rate) to which the two mixers outputs were connected.

Evaluations to install the testbench on the FPT at INFN-LNS for in-plasma measurements are ongoing, to test and characterize the approach directly in magnetized plasmas.

Figure 3: Pictures of the polarimetric testbench.

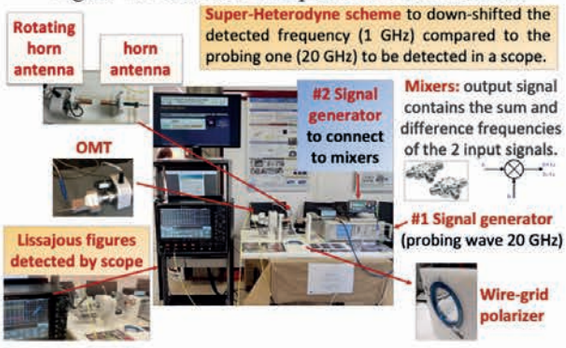

CONCLUSIONS

The design of two novel plasma diagnostic testbenches - the PYN-HO prototype for X-ray and optical spectroscopy and the VESPRI 2.0 interfero-polarimeter setup to be installed at INFN-LNS - was carried out. The X-ray analysis code was updated to investigate the response of the detectors and tools, improving also the interpretative models to estimate the plasma parameters.

ACKNOWLEDGEMENTS

The authors wish to thank INFN for the support through the project PANDORA_Gr3 funded by third Nat. Sci. Comm. This work has been partially funded by European Union (NextGeneration EU), through the MUR-PNRR project SAMOTHRACE (ECS00000022) and through the MUR-PNRR Project PE0000023-NQSTI.

REFERENCES

[1] D. Mascali et al., Universe 8(2) (2022) 80.
[2] S. Biri et al., JINST 16 (2021) P03003.
[3] R. Rácz et al., PSST 26 (2017) 075011.
[4] E. Naselli et al., J. Instrum. 17 (2022) C01009.
[5] D. Mascali et al., PPCF 64 (2022) 035020.
[6] E. Naselli et al., Condens. Matter 7 (2022) 5.
[7] B. Mishra et al., Phys. Plasmas 28 (2021) 102509.
[8] G. Finocchiaro et al., Phys. Plasmas (under review).
[9] Pidatella et al., Front. in Space Sci. and Astron. (2022)
[10] G. Torrisi et al., Front. Astron. Space Sci. 9 (2022) 949920

The MICADO radwaste monitoring system tested in a real storage site

P. Finocchiaro[1], S. Amaducci[1], L. Cosentino[1], C. Failla[1], F. Longhitano[2], G.E. Poma[1], G. Vecchio[1]

1) INFN Laboratori Nazionali del Sud, Catania, Italy
2) INFN Sezione di Catania, Catania, Italy

Abstract - We describe the installation and test of the MICADO monitoring grid around real radwaste drums in two real storage sites on the ORANO and NUCLECO premises.

INTRODUCTION

In the framework of the MICADO EU project ([1],[2]) a modular detector support structure was assembled in four units in order to accommodate four radwaste drums. Each support unit hosted four SciFi sensors (for gamma rays, [3]) and four SiLiF sensors (for neutrons, [4]). The four units were installed around four real radwaste drums also containing small quantities of actinides, and data were acquired. The system behaved as expected from previous tests and from the radiological info about the drums. The radwaste drums were tagged as A, B, C, D, and the detectors were identified by their position on the support structure as North (N), East (E), South (S) and West (W). The sensors on their support units were installed first at ORANO (High Level Waste drums) and afterwards at NUCLECO (Low Level Waste drums). The test at ORANO lasted one day, whereas at NUCLECO the monitoring system was in place during one month.

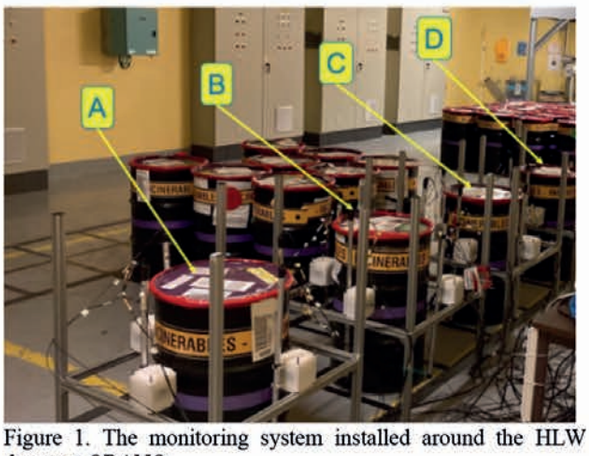

Figure 1. The monitoring system installed around the HLW drums at ORANO.

RESULTS FROM SCIFI COUNTERS

The average measured gamma counting rates are plotted in Figure 3 and Figure 4. The statistical uncertainty is so small to be invisible in the plot. The dose rate value measured near each HLW drum with a handheld device is reported on the plot as well. For the LLW the dose rates were slightly above the ambient value.

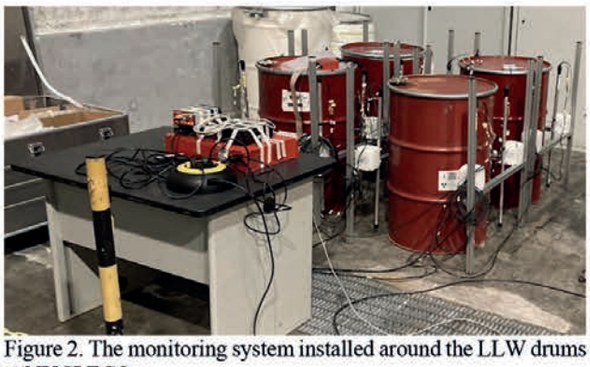

Figure 2. The monitoring system installed around the LLW drums at NUCLECO.

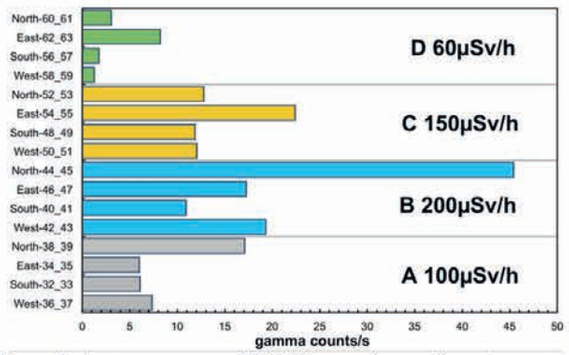

Figure 3. Average measured SciFi (gamma) counting rates around the four HLW drums at ORANO.

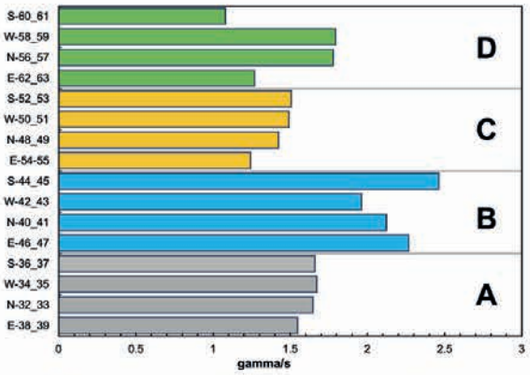

Figure 4. Average measured SciFi (gamma) counting rates around the four LLW drums at NUCLECO.

In Figure 5 we show as an example the time-stamped counting rate for the HLW drum A at ORANO and for the LLW drum C at NUCLECO.

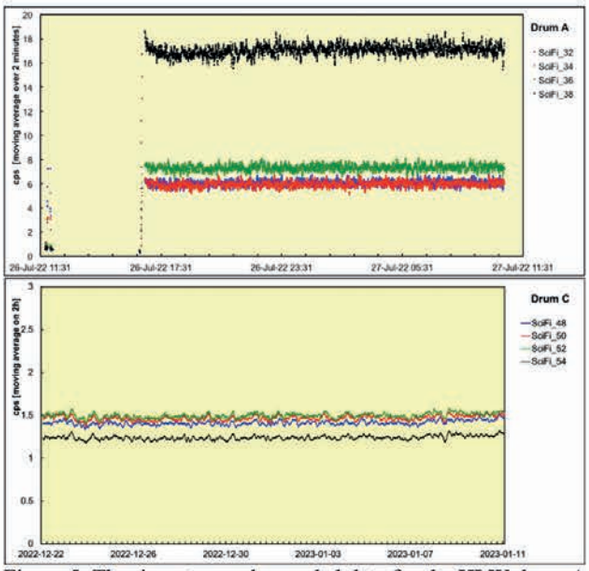

Figure 5. The time-stamped recorded data for the HLW drum A (ORANO) and LLW drum C (NUCLECO).

RESULTS FROM SILIF COUNTERS

The average neutron counting rates are reported in Figure 6 and Figure 7. We remark that the HLW drums at ORANO contained up to 20g of plutonium, versus the tiny amounts of actinides of the LLW at NUCLECO. This is why there are about two orders of magnitude between the counting rates measured in the two cases.

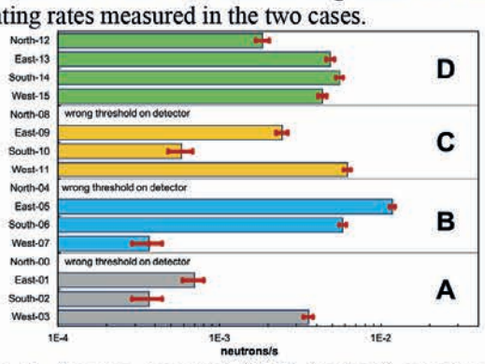

Figure 6. Average measured SiLiF (neutron) counting rates around the four HLW drums at ORANO.

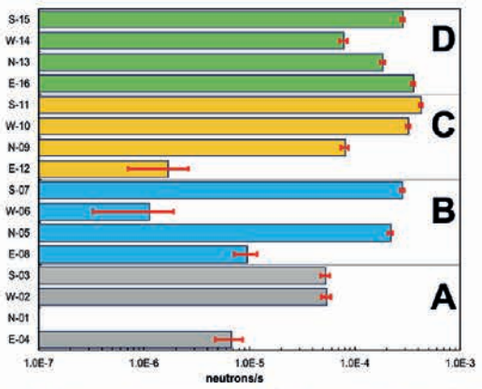

Figure 7. Average measured SiLiF (neutron) counting rates around the four LLW drums at NUCLECO.

In Figure 8 we show two examples of radar plots clearly showing the measured anisotropy of the (tiny) neutron emission from the drums. The $\approx 10^{-9}$ gamma/neutron discrimination of SiLiF makes possible to appreciate and measure the very low neutron flux coming from the drums.

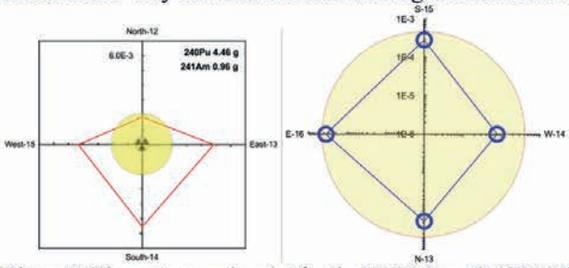

Figure 8. The neutron radar plot for the HLW drum D (ORANO, left) and LLW drum D (NUCLECO, right).

SUMMARY

16+16 SciFi and SiLiF detectors were installed on their support units and placed around real radwaste drums also containing small to tiny quantities of actinides. Two data taking runs were performed in two storage sites on HLW and LLW drums, showing the expected performance. The observed gamma count rate, mainly due to ^{241}Am, ^{60}Co and ^{137}Cs present in the drums, is in line with the expectation. The quite low observed neutron count rate is in line with the expectation as well, due to the small number of neutrons emitted by spontaneous fission and (α,n) reactions on light nuclei present in the drum matrices. The tests done at ORANO and NUCLECO have shown that the sensor system developed in the framework of MICADO WP7 can be successfully exploited to monitor radwaste drums in real storage sites.

ACKNOWLEDGMENTS

This work was funded within the framework of European Union's Horizon 2020 research and innovation program under grant agreement No 847641, project MICADO.

REFERENCES

[1] Finocchiaro, P.; Ripani, M.; Radioactive Waste Monitoring: Opportunities from New Technologies. In *Proceedings of the IAEA* 457 *International Conference on Physical Protection of Nuclear Material and Nuclear Facilities*, IAEA-CN-254/117, Vienna, Austria, 13–17 458 November 2017. 459

[2] MICADO Project. Available online: https://www.micado-project.eu/ (accessed on 12 Mar 2024).

[3] Cosentino,L.; Giuffrida, M.; Lo Meo, S.; Longhitano, F.; Pappalardo, A.; Passaro, G.; Finocchiaro, P. Gamma—Ray Counters to 460 Monitor Radioactive Waste Packages in the MICADO Project. Instruments 2021, 5, 19. https://doi.org/10.3390/ 461

[4] Cosentino, L.; Ducasse, Q.; Giuffrida, M.; Lo Meo, S.; Longhitano, F.; Marchetta, C.; Massara, A.; Pappalardo, P.; Passaro, G.; 462 Russo, S.; Finocchiaro, P. SiLiF Neutron Counters to Monitor Nuclear Materials in the MICADO Project. Sensors 2021, 21, 2630. 463 https://doi.org/10.3390/s21082630 464

Cemented radwaste monitoring in PREDIS: gamma and neutron detection with WiFi electronics

M. Romoli[1], P. Finocchiaro[2], M. Di Giovanni[1,3], P. Di Meo[1], A. Pandalone[1], C. Principe[1], A. D'Onofrio[3], C. Sabbarese[3], S. Amaducci[2], L. Cosentino[2], F. Longhitano[4], G.E. Poma[2], G. Vecchio[2]

1) INFN Sezione di Napoli, Napoli, Italy
2) INFN Laboratori Nazionali del Sud, Catania, Italy
3) Department of Mathematics and Physics - University of Campania "Luigi Vanvitelli", Caserta, Italy
4) INFN Sezione di Catania, Catania, Italy

Abstract - In the framework of the PREDIS EU project a wireless battery operated gamma ray and neutron detection system was developed in order to provide a medium-to-long term monitoring system for radioactive waste drums. It was initially proposed to monitor the gamma radioactivity outcoming from steel drums containing cemented radwaste, even though it could be usefully employed in a wider range of applications. Being gamma rays and neutrons penetrating, they convey information from the drum internal structure as the count rate measured on the surface depends on the structure of the crossed materials. A number of sensors arranged around a drum, typically four units, provide indications of the emission anisotropy, and any sensitive change in the measured count rate would hint at some anomaly thus triggering a suitable inspection by operators.

INTRODUCTION

The PREDIS (Predisposal management of radioactive waste) Euratom project is aimed at the development and implementation of activities for predisposal treatment of radioactive waste streams other than nuclear fuel and high-level radioactive waste [1]. Within its Work Package 7 the project contemplates to test and evaluate innovative tools and techniques in cemented waste handling and predisposal storage, and in particular to demostrate the feasibility of medium-to-long term monitoring by means of low-cost radiation sensors to be installed around the radwaste drums. A periodic automatic check of the radiation levels around radwaste drums could represent an added value of safety and security, with recorded streams of count-rate data providing a useful tool for an early detection of possible anomalies or tampering with the drums. SciFi [2] and SiLiF [3] radiation sensors have been developed by INFN in the past years and have been successfully tested to be used as gamma and neutron detectors. In the framework of PREDIS we built a number of detection units featuring two such detectors and a custom electronics board with some particular features: high modularity and re-configurability (to ensure fast and easy maintenance), battery operation, WiFi connection for data transfer and remote control, low power consumption, temperature measured on board (Figure 1).

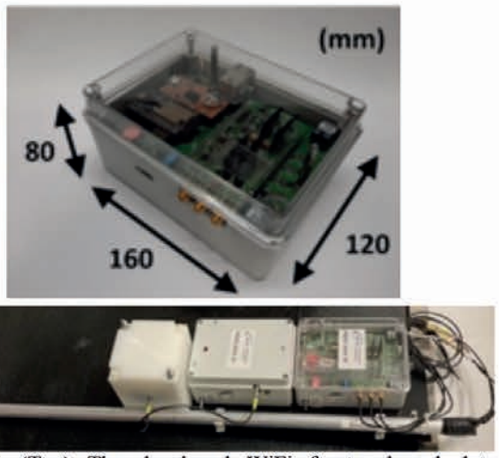

Figure 1. (Top) The developed WiFi front-end and data acquisition electronics. (Bottom) A monitoring unit consisting of one SiLiF and one SciFi detectors with their electronics.

THE DEMONSTRATION

The proposed monitoring method relies on a number of SciFi and SiLiF sensors, say four of each kind, to be hung to the cemented drums for monitoring purpose during the whole predisposal phase. The demonstration test of this technology was performed in a realistic environment, an underground radwaste storage room on the premises of UJV at Řež (Prague). A 200 liter cemented mockup (Figure 2) was built for a demonstration with a 165 MBq ^{137}Cs gamma source placed into the quasi-central hole, and the drum was equipped with four sensor units to monitor it during a two month period (Figure 3).

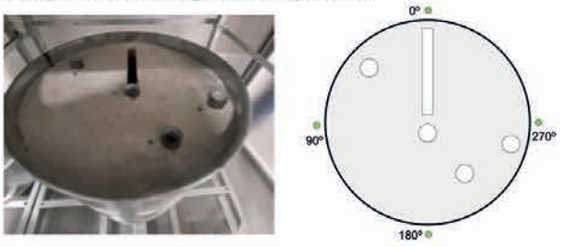

Figure 2. Top view of the mockup scheme; the four green circles (0°, 90°, 180°, 270°) indicate the position of the sensor units.

Simulations have been performed highlighting the possibility of using such detectors to hint at anomalies (cracks, displacements,...) by detecting changes in the emitted radiation counting rates. The mockup structure was reproduced in FLUKA [4], including four SciFi detectors around the drum (Figure 4). As no neutrons were expected the SiLiF sensors were not included in the simulation. However, the feasibility of neutron measurement, not shown here, was assessed in a separate test done by means of a PuBe neutron source.

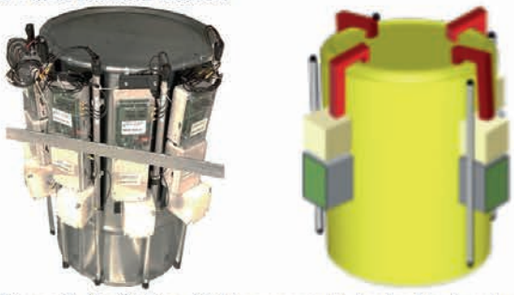

Figure 3. (Left) Four WiFi sensor units hooked to the drum before correctly positioning. (Right) The final arrangement.

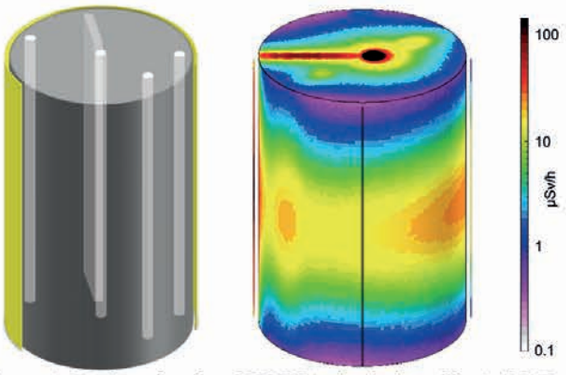

Figure 4. Mockup sketch and FLUKA simulation of the 165 MBq ^{137}Cs gamma source placed at mid-height inside the quasi-central hole, with the expected dose rate distribution on the drum surface. Three scintillating fibers (SciFi) are also visible.

The four sensor units were hooked to the mockup and several drums filled with concrete were placed all around it (Figure 5) in order to also verify the signal transmission capability through such a heavy shielding. The sensors, interfaced to a local server through a WiFi connection, were programmed to wake up every six hours and acquire data for one minute. The local server was connected to a network router with a public IP address and thus reachable remotely via a Virtual Private Network (VPN). Indeed this configuration enabled the authorized users to interact remotely with the server. An additional sensor was installed about six meters away in the same room to measure the ambient background. Since there was only a gamma source installed, no meaningful neutron counting rate was detected. The measured counting rate data for the five SciFi sensors collected between 17-Nov-2023 and 15-Jan-2024 are plotted in Figure 6. The normal sensor behavior was assumed to be when the counting rate fluctuations kept within ±5 standard deviations, to account for any possible electrical or mechanical disturbance.

Figure 5. Several drums filled with concrete placed around the mockup. Other drums, not shown, were also placed in front.

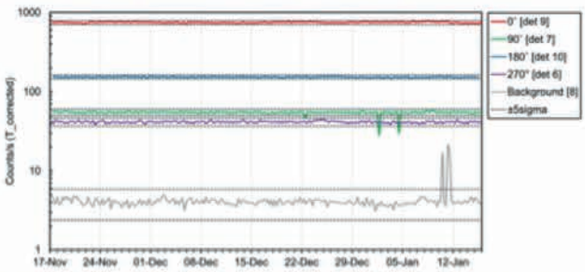

Figure 6. Measured counting rate data for the five SciFi sensors between 17-Nov-2023 and 15-Jan-2024.

SUMMARY

The feasibility of medium-to-long term monitoring by means of radiation sensors to be installed around the radwaste drums was assessed by preliminary laboratory tests, simulations, and a two-month data collection in a demonstration with a cemented mockup drum and a 165 MBq ^{137}Cs gamma source. The feasibility of neutron measurement was assessed separately by means of a PuBe neutron source. A periodic automatic check of the radiation levels around radwaste drums, as an added value with respect to safety and security, can be attained by recording streams of count-rate data from the sensors proposed within PREDIS. Such a monitoring technique, we believe, could represent in the near future a useful tool for an early detection of possible anomalies or tampering with the drums during their predisposal phase.

ACKNOWLEDGMENTS

This research was partially funded by EU Horizon 2020, project name PREDIS, Grant Agreement No. 945098.

REFERENCES

[1] PREDIS project, Euratom H2020, GA No. 945098. Available online: https://predis-h2020.eu/ (accessed on 30 Nov 2023).
[2] Cosentino, L., et al. Instruments 2021, 5, 19.
[3] Cosentino, L.; et al. Sensors 2021, 21, 2630.
[4] Fasso, A.; Ferrari, A.; Ranft, J.; Sala, P.R. *CERN Technical Report* No. SLAC-R-773; Stanford University: Stanford, CA, USA, 2005

Compact radioactive wastes radwaste scanner for sort and segregate activities

G. E. Poma[1], L. Cosentino[1], C. Failla[1], F. Longhitano[2], G. Vecchio[1] and P. Finocchiaro[1]

1) INFN Laboratori Nazionali del Sud, 95123 Catania, Italy *2) INFN Sezione di Catania, 95123 Catania, Italy*

Abstract - A scanning gamma-ray system has been developed and characterized as part of the PI3SO (Proximity Imaging System for Sort and Segregate Operations) INFN-Energy project. The primary goals involve the classification characterization of low and intermediate-level radioactive waste (radwaste) in order to sort and segregate nuclear materials.

Eight detectors are arranged in linear and sliding arrays grouped into modules, and 128 (CsI(Tl)+SiPM) elements compose two sensitive units. Positioned with one above a scanning table and the other parallel to it underneath, the two co-moving arrays detect gamma-rays emitted by sparse objects on the table, enhancing the detection of partially gamma sources and identifying hotspots.

Detectors were tested with point-like laboratory gamma-ray ^{137}Cs and ^{22}Na sources: the results are promising in view of planned tests in a real environment by using real radwaste.

INTRODUCTION

The radioactive materials have to be handled in several fields, for instance radwaste sorting and segregating operations [1,2]: the availability of an efficient and easy-to-handle tool to quickly detect gamma radiation hot-spots can be very useful.

As recommended by Innovative UK, the development of innovative solutions which sort and segregate radwaste represents a priority [3]. Each adopted solution requires a tool to monitor the waste radioactivity with the priority in recycling over its disposal, to reduce sorting and segregation process carried out by humans [4].

A few projects are currently being developed for the automatic manipulation of nuclear waste, like ROMANS [5] and VIRERO [6] projects. Based on system like these, a new compact gamma-ray scanning system named PI3SO has been proposed and funded by INFN-Energy, and successively built and characterized at LNS.

PI3SO SCANNER

Two prototype detectors have been built at LNS in the last decade as demonstrators for the quick detection of hot-spots. One of these was built as a proof-of-principle: it consists of a hundred CsI(Tl) scintillators 1 cm^3 with spectroscopic capability, arranged in a 10x10 cm^2 array and read-out by a 10x10 SiPM array [7].

Based on precursors proximity imaging, counting and spectroscopic capabilities (figure 1), PI3SO innovative system has been proposed with the aim of speed up the sorting process of the radwaste material. The technology was proved suitable to build a modular gamma detection system as part of a work desk, with counting capability and spectroscopic features.

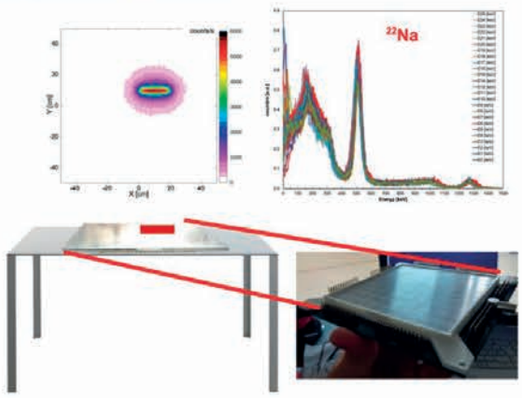

Figure 1. One PI3SO precursor: gamma-ray imaging (left, Monte Carlo simulation) and spectra (right) with ^{22}Na source (top); detector sketch and photo (bottom).

The system is equipped with a reasonable operational 84x128 cm^2 desk surface: this would imply that to make the whole surface sensitive to the radiation, a thousand of 1 cm^3 scintillators are required, which is too expensive in terms of costs, DAQ and time consuming. In order to reduce the complexity of the system and build a device that can be easily employed in real radwaste handling operation, a simplified linear array of scintillators is proposed (figure 2).

Figure 2. Top: PI3SO printed circuit board equipped with 16 SiPMs (top) and 16 CsI(Tl) crystal unit (bottom, white array) compose a module: four modules compose one linear array or detection unit. Bottom: one detection unit with four flanked modules, arranged for DAQ and characterization tests.

The system is composed of two linear arrays composed each by 1x64 channels (CsI(Tl)+SiPM) and a work table for the radwaste support: the bottom array is be placed beneath the table and will stay fixed, while the upper one hovering will be moved up and towards the materials guided by a led-based proximity sensor (figure 3). These arrays scan the total table length in 1 cm steps by means of two handling engines which provide also the vertical translation of the linear array in order to avoid possible collisions with the deposited materials.

The sensitive element of each detection unit is a CsI(Tl) 1 cm^3 crystal [8], each one is coupled to a 6x6 mm^2 S14160-6050HS Hamamatsu SiPM [9]. PI3SO feature

three different and dependent operational modalities: as an overall gamma radiation counter, where the global counting rate is the sum of the individual counting rates; as a proximity imaging system (1 cm^2 pixels); as an array of spectroscopic detectors.

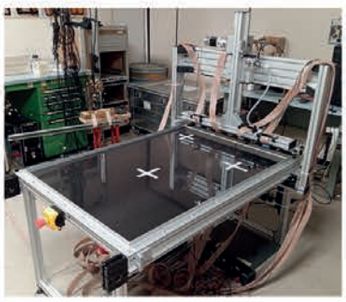

Figure 3. PI3SO radwaste scanner.

The PI3SO detection units are able to locate the gamma hot-spots, reconstruct their energy spectra and compute the isotope-related images. The need of two detectors arises from the possibility that flat metal objects could be activated on one side only or could shield other objects. In this application the two detectors would scan the objects above the table assessing their activity., driving the decision on whether an object can be released or should be repacked and stored.

PRELIMINARY RESULTS

Measurements with gamma sources have been done in order to evaluate the system performances in terms of photon detection capability, spectroscopic response, energy resolution, rate and spectral efficiency.

A test campaign with gamma-ray sources together with Monte-Carlo simulations allowed to study the performances as proximity imaging system. The aim of the tests is to characterize the detection elements in terms of energy resolution, hot-spot reconstruction and S/B ratio as a function of the channel threshold. Simulations demonstrated that a reduced source-to-detector distance is important to localize and identify the hot-spots. The contribution of few mm carbon fiber plane in terms of image degradation is negligible.

Figure 4 reports the values of the FWHM of the hot-spot as a function of the source-to-detector distance: hot-spot is well-reconstructed at small distance, which testified the importance to approach objects at each step during scanning.

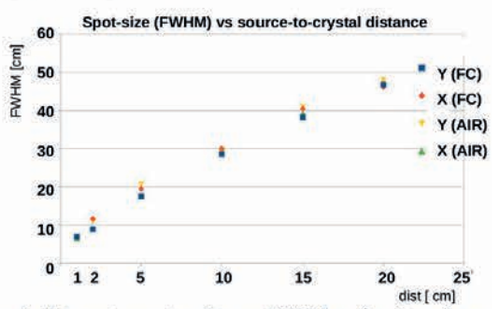

Figure 4. Hot-spot reconstruction as FWHM as function of source-to-detector distance, by varying plane (FC fiber carbon, AIR i.e. no plane).

In order to study the system performance in terms of energy calibration and S/B ratio, CsI(Tl)+SiPM characterization has been done in laboratory using two gamma-ray sources using gamma-ray source. In particular, the 662 keV (^{22}Na) average peak resolution is 6.8 % with sigma 0.71 %, in line with the expectation from existing literature.

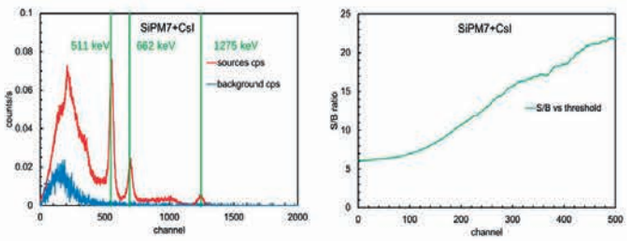

Figure 5. Energy spectrum (left) for source and background runs; S/B ratio as function of channels by varying threshold [0, 500] channels (right).

In order to evaluate detector performance, the energy spectrum quality has been studied for all the channels in terms of S/B ratio as a function of the energy threshold. In figure 5 the spectra acquired with the source and without the source (background) is reported, considering the S/B ratio from 6 to 22 as function of channel threshold. It shows the S/B ratio as a function of the channel threshold, ranging from 6 to 22. By choosing a threshold close to 200, S/B ratio is close to 10 which assures well-resolved small peaks.

CONCLUSIONS

A modular and portable gamma-ray system was described as radwaste scanner for radioactive objects characterization,. Tests of the PI3SO scanning detectors were done in order to study its ability to reconstruct hot-spots, proximity images and energy spectra. Due to the large sensitive area and related short scanning time, system can be employed in a wide radwaste range of size, shape and nature. The system could also be extended in future with complementary alpha/beta detectors, and it can be used in several ways, due to its versatility and modularity.

REFERENCES

[1] IAEA International Atomic Energy Agency: https://www.iaea.org/topics/processing

[2] Status and trends in spent fuel and radioactive waste management. IAEA, Vienna, 2022.

[3] Functions and processes of the regulatory body for safety. IAEA, Vienna, 2018.

[4] Guidance "Sort and segregate nuclear waste: specification", 27 July 2020

[5] ROMANS https://cordis.europa.eu/project/id/645582

[6] VIRERO, https://www.faps.fau.eu/curforsch/virero-virtual-remote-robotics-for-radiometric-sorting

[7] F. Longhitano et al. "A Scintillator Array Table with Spectroscopic Features" Sensors 22, no. 13: 4754.

[8] Hilger crystals, CsI(Tl)

[9] Hamamatsu, MPPC S14160-6050HS

Electrical characterization of a new generation SiC detector for PRAGUE (Proton Range Measure Silicon Carbide) project

M. Guarrera[1], G. Petringa[1], A. Amato[1], G. Angemi[1], S. Arjmand[1], G. Cantone[1], E. Caruso[1], R. Catalano[1], G. Cuttone[1], F. Farokhi[1], S. Fattori[1], O. Giampiccolo[1], A. Kurmanova[1], D. Oliva[1], A. Pappalardo[1], A. Pizzino[1], A. Sciuto[1], S. Tudisco[1], C. Verona[2], and G.A.P. Cirrone[1]

1) Istituto Nazionale di Fisica Nucleare (INFN) - Laboratori Nazionali del Sud (LNS), Catania, Italy
2) Università di Roma Tor Vergata, Macroarea di Ingegneria, Roma, Italy

Abstract - The PRAGUE (Proton RAnGe measure Using silicon carbidE) project, relying on Silicon Carbide (SiC) technology, intends to facilitate the measurement of the Percentage Depth-Dose (PDD) distribution of both clinical and high-intensity proton beams.

This contribution outlines the progress achieved toward the development of the PRAGUE project and the accomplishment of its goals. In particular, tests carried out on 80 SiC devices will be described. By assessing their performances, it is possible to select good candidates for the realization of the final PRAGUE detector.

THE PRAGUE PROJECT

The PRAGUE project consists in the realization and characterization of a real-time multilayer SiC detector, able to reconstruct the PDD distribution of a 30-150 MeV proton beam with both conventional (10^4 pps) and high (10^{12} pps) intensity. The detector is designed to include 60 SiC devices (sensitive area of 15 × 15 mm^2, active thickness of 10.3 μm, passive substrate of ≈100 μm) arranged in a stack configuration. The last 30 SiC detectors will be deprived of the passive layer through a chemical etching procedure. This peculiar configuration, combined with the physical properties of SiC material [1], will enable for more precise, accurate, and time-saving Bragg peak sampling than is now possible using clinical practice procedures [2] or innovative dosimetric approaches still under investigation [3, 4].

The electronic chain involves the use of the TERA08 chip [5] and has been designed to work properly with high and low intensity beams. It will lead to real-time and shot-to-shot acquisition of the PDD distribution also in presence of laser-driven ion beams, which are notoriously lacking in reproducibility [4].

DETECTORS CHARACTERIZATION

To develop the final device, the I-V (current vs. voltage) and C-V (capacitance vs. voltage) characterization of 80 SiC devices was performed. The stability, linearity, and charge collection efficiency (CCE) of the detectors were also evaluated. Experimental tests were conducted at the "Tor Vergata" Industrial Engineering Department of the University of Rome (Italy).

Detectors description

The 80 SiC devices object of this study were produced through the Chemical Vapor Deposition process carried out in a low-pressure regime at high temperatures (1630 °C). During this phase, a growth of 10 μm 4H-epitaxial layers on commercial four-inch (400 μm thick) wafers was obtained. The wafers were subsequently treated with several photolithographic steps to define the active area of the SiCs and supply the dopants necessary for the realization of a p^+n planar junction. Finally, through the metallization process, the realization of the ohmic contacts was performed. The 80 SiC detectors were obtained by dicing the wafers into 15 x 15 mm^2 dice (Figure 1a). Each device has a 0.3 μm thick p-layer with a doping concentration $N_A=1\cdot10^{19}$cm^{-3} and a 10 μm thick n-layer with a doping concentration $N_D = 0.5 - 1 \cdot 10^{14}$ cm^{-3}. A substrate of 110 μm thick with a doping concentration $N_D > 10^{18}$ cm^{-3} is placed close to the active layer. Each device was mounted on a PCB board with silver conductive glue. The electrical connection was realized through a thermocompression bonding process (Al wire, 50 μm diameter) between the SiC pad and the PCB at Terminal 1 (Figure 1b).

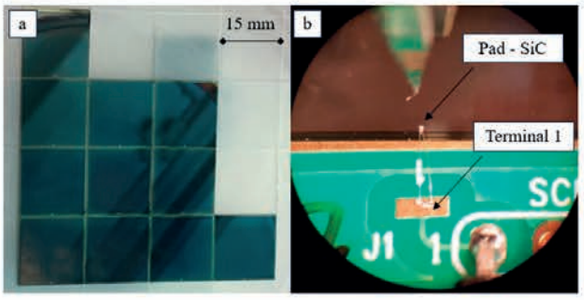

Figure 1: a) 15 x 15 mm^2 dices of a SiC wafer. b) Microscopic view of a SiC during the bonding process.

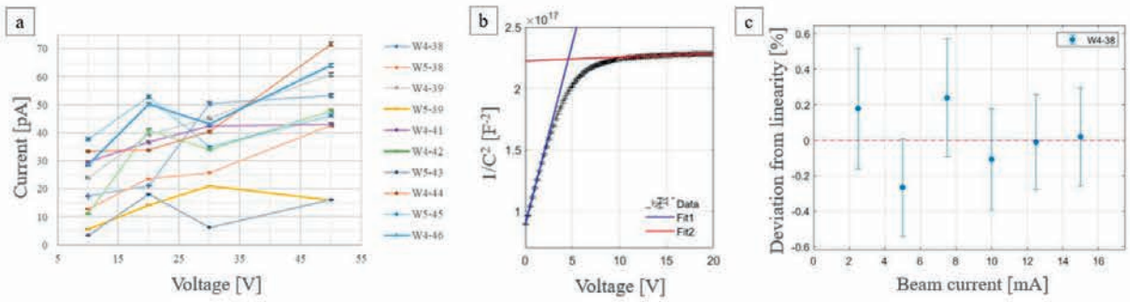

Figure 2: a) I-V curves for 10 SiC detectors in the reverse 10-50 V voltage range. b) Trend of $1/C^2$ vs. reverse applied voltage for a SiC detector. The linear fits in the low voltage range (Fit1) and in the saturation region (Fit2) are also shown. The depletion voltage V_D, obtained as the voltage value corresponding to the intersection of the two best-fit curves, was $V_D = 4.7 \pm 0.3$ V, while the saturation capacitance was $C_s = 2.096 \pm 0.005$ nF. c) Percentage deviation from linearity of W4-38 detector response plotted against the X-Ray tube current [6].

Electrical characterization

Before testing the SiC detectors as dosimeters, their electrical characterization was performed. The I-V profile is useful to establish the leakage current of the detector and its breakdown voltage, while the C-V profile allows an estimation of the detector's depletion voltage and saturation capacitance. The I-V and C-V characteristics of the detectors under investigation were measured at room temperature, in air. During I-V measurements, the current generated by the detector was measured with a KEITHLEY 6517B electrometer which was also used as detector bias source. To perform the C-V acquisition, the capacitance was measured by means of an LCR meter (Agilent, model 4263B) coupled with EXT Voltage Bias Fixture (Agilent, model 16065A), while the bias voltage was once again supplied by the 6517B electrometer.

The I-V profile was studied in the reverse bias voltage range 0 - 200 V and in the forward bias voltage range 0-2.5 V. Through this characterization, it was possible to reject 30 of the initial 80 detectors. Their leakage current reached values of the order of mA at a few Volts, highlighting the presence of structural defects. For this reason, the characterization work continued on the 50 SiC devices left. The latter exhibits a leakage current < 100 pA when reverse-biased up to 50 V (Figure 2a).

The capacitance C was measured for each SiC detector in the reverse bias voltage range of 0–20 V, with a step of 0.25 V. The interception method (Figure 2b) was used to evaluate the depletion voltage, V_D, finding V_D values ranging from 2.0 ± 0.3 V to 6.0 ± 0.3 V. The saturation capacitance C_s for the 50 SiC devices, determined as the minimum capacitance value obtained by increasing the reverse bias voltage, ranges between 2.031 ± 0.004 nF and 2.139 ± 0.005 nF.

Stability, linearity and CCE tests

Linearity and stability tests were performed by irradiating the detectors in air with an X-Ray tube photon beam. The SiC–X-ray tube distance was 15 cm, ensuring uniform irradiation of the active detector area. A plastic collimator (1 cm diameter) was used to shield the beam. During X-ray irradiation, the measurement of the current produced by the detectors and their polarization (set to 30 V) was again performed through the KEITHLEY 6517B.

The linearity of the devices was studied as the beam current varied. In particular, the X-ray tube acceleration voltage was set to 10 kV, while the X-ray tube current was varied in the 2.5-15 mA range (in steps of 2.5 mA). The maximum percentage deviation from linearity was found to be up to 1.5% (Figure 2c).

The stability was studied by subjecting the detectors to prolonged irradiation sessions (with duration comparable to clinical treatments) and evaluating the oscillations of their current response in terms of standard deviation, σ. The measurement conditions were kept similar to those described for the linearity test, setting the current and acceleration voltage of the tube at 5 mA and 10 kV, respectively. For all detectors, σ takes values less than 0.5% compared to mean value.

The investigation of the CCE of SiC devices was conducted by measuring their I-V curve during their irradiation, which were performed in the same experimental condition adopted for linearity test, but fixing the X-Ray tube parameters (X-ray tube acceleration voltage 10 kV, X-ray tube current 5 mA). The current produced by the detectors when subjected to irradiation was acquired for 20 s at voltage values between 0 and 40 V. The trend of the current signals was then studied as the applied depletion voltage varied, showing complete collection starting from 30 V.

REFERENCES

[1] M. De Napoli, Frontiers in physics 10 (2022): 898833.
[2] H. Paganetti, Phys Med Biol. 2012 June 7; 57(11): R99–R117.
[3] Durante M, Bräuer-Krisch E, Hill M. Br J Radiol. 2018; 91(1082):20170628.
[4] P. Bolton et al., Physica Medica (2014), 30: 255-270.
[5] R. Cirio et al, NIM A, Vol. 798 (2015) 107–110.
[6] M. Guarrera, PhD Thesis (2024), Unict.

High-power laser system for the I-LUCE facility

J. Suarez-Vargas[1], C. Altana[1], G. Angemi[1], S. Arjmand[1], D. Bonanno[1], G. Cantone[1], E. Caruso[1], R. Catalano[1], G. Cuttone[1], F. Farokhi[1], S. Fattori[1], O. Giampiccolo[1], M. Guarrera[1], A. Kurmanova[1], D. Oliva[1], A. Pappalardo[1], G. Petringa[1], A. Pizzino[1], A. Sciuto[1], S. Tudisco[1], G.A.P. Cirrone[1,2]

1) Laboratori Nazionali del Sud, Istituto Nazionale di Fisica Nucleare (INFN), Catania, Italy

2) Centro Siciliano di Fisica Nucleare e Struttura della Materia (CSFNSM), Catania, Italy

Abstract – The I-LUCE facility currently in development will have one of the more powerful and versatile high-intensity lasers in Italy. In this brief report we describe the characteristics, operation modes and potential usage of this powerful laser system.

INTRODUCTION

The I-LUCE high-power laser system is based on THALES LAS QUARK family [1], which are femtosecond Titanium-Sapphire (Ti:Sa) lasers made of an innovative combination of building blocks starting from the primary oscillator to the optical compressor vacuum chamber. The main laser building blocks are represented in Fig. 1. Each block can be individually upgraded and continue to operate independently, allowing for fast scaling in total power and repetition rate for future performance upgrades.

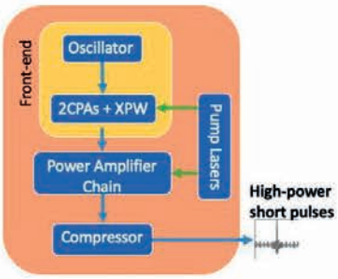

Figure 1: Block diagram of the high-power laser system of I-LUCE.

DESCRIPTION

The initial stage, called the 'front-end', is composed of an oscillator, two independent chirped pulse amplification (CPA) systems, a regenerative amplifier and a cross-polarised wave (XPW) filter.

The oscillator, based on Ti:Sa crystals, delivers Fourier-transform pulses of 20 fs with a broad bandwidth of around 40 nm. Then, the CPAs use aberration-free Öffner triplet configuration to stretch the pulses to several hundred of picoseconds. This compressed pulse is injected into an XPW filter, which using a $\chi(3)$ process allows cleaning of the front edge of the pulse and spectral bandwidth increase [2,3]. With good filtering of the polarization, an intensity contrast of 10^{-10} can be achieved at the output of the laser system. Then this XPW filter is used to enhance the temporal contrast by a factor of up to 10^4. The stretcher of the second CPA has an adjustable stretching factor implemented through motorised stages for the optics. This allows to obtain pulses with different time durations, ranging from the Fourier limit of 25 fs up to a few tens of picoseconds at the output of the compressor.

The next stage is composed of a chain of multi-pass power amplifiers. They are designed in bow-tie configuration with multiple passes (up to 5) in water-cooled Ti:Sa crystals. The first two amplifiers run at 10 Hz, while the third one runs at 1 Hz. These amplifiers have been designed to suppress amplified spontaneous emission (ASE) and transverse lasing. The last amplifier can be bypassed to enable low power mode (LPM) operation at lower peak power (see Table 1).

Table 1: Anticipated main features of both the LPM and HPM beamlines of I-LUCE laser system.

Laser Parameter	HPM	LPM
Peak Power [TW]	≥ 50	≥ 350[a]
Output Energy [J]	≥ 1	≥ 7
Pulse Duration [fs]	≤ 25[b]	≤ 25[b]
Focusing Surface [um^2]	36	36
Repetition Rate [Hz]	≥ 10	≥ 1
Intensity [W/cm2]	7.72×10^{19}	5.64 ×1020
Spectrum (FWHM) [nm]	≥ 40	≥ 40
Central Wavelength [nm]	800±10	800±10
Energy Stability [rms]	≤ 1.2%	≤ 1.5%
Contrast Ratio at 100 ps (ASE)	≥ 10^{10}	≥ 10^{10}
Strehl Ratio	> 80%[c]	> 80%[c]

a: Upgradable up to 500 TW.
b: Variable pulse width from 25 fs to a few picoseconds.
c: with deformable mirrors.

The high-energy pump lasers for the amplifier chain are designed to have optimal spatial homogeneity to avoid non-uniform beam profiles in the pulses. The pump system is based on THALES' RHEA lasers operating at

532 nm with a repetition rate of 5 or 10 Hz and an output energy of 5.5 J. The last stage involves the optical compressor, structured with conventional 'Treacy configuration' for its gratings, tailored for a 100 nm bandwidth capable of accommodating 25 fs pulses. This compressor will operate in vacuum above 10^{-6} mbar to be compatible with pulses of 500 TW of peak power. The last mirror of the compressor is used to sample the beam and send it to a diagnostics bench, which will contain a complete electro-optical setup to measure shot-to-shot several beam parameters, including energy, spatial profile at near and far fields. The flexibility of this system allows optional pulse control mechanisms to be inserted, including: A variable attenuator before the compressor to control the pulse energy with precision; An electro-mechanical shutter for single-shot and burst operation; A deformable mirror at the output of the compressor helps compensate for wavefront aberrations and is essential for maintaining the beam's Strehl ratio over 0.8.

The system, when fully amplified, is designed to produce 320 TW peak-power pulses at 2.5 Hz repetition rate. Alternatively, the final amplification stages can be bypassed to enable the production of pulses with up to 40 TW of peak power at a higher repetition rate of 10 Hz.

In Table 1 the main characteristics of the full compressed laser system in both operation modes of low power mode (LPM) and high-power mode (HPM) are reported.

The complete laser system will be installed within a controlled environment adhering to an ISO-7 cleanliness standard. A laser control system dedicated to remotely manage and oversee all laser components and subsystems (including the main oscillator, booster, amplifiers, compressor, etc.), along with diagnostic system devices, will be integrated into the personal computers (PCs) in the control room.

LASER BEAM TRANSPORT AND INTERACTION

The laser beam transport system will be collaboratively developed with the ELI-Beamlines (Extreme Light Infrastructure-Beamlines) facility, drawing from the expertise and advancements made in the ELIMAIA user beamline for laser-based ion acceleration [4].

The beam transport from the compressor to the interaction rooms is represented by the block diagram in Fig. 2.

Along the main transport line, a flipping mirror will provide the option to use a second interaction chamber at 45° angle. The path from the compressor to the interaction chambers will be enclosed in vacuum pipes and smaller vacuum chambers along the beam path to house plasma mirrors, turning mirrors, and monitoring stations. These components are crucial in aligning the laser beam with the interaction points and ensuring optimal pulse contrast is maintained. Beam diagnostic stations (BDS) will be positioned both at the output of the main laser compressor and at the interaction chambers to evaluate the quality of the beam at the interaction points.

Additionally, signal data from the BDS and target stations will be integrated into the main control system of the entire facility. This includes various parameters such as beam profiles, spectrograms, pulse duration, wavefronts, pulse contrast, and more, which will act as input signals for the control system (see Fig. 2).

The laser system, spanning from the front-end to its compressor, will undergo monitoring via multiple CCD/CMOS cameras, sensors, and actuators, all managed by its dedicated control system crafted by the laser manufacturer.

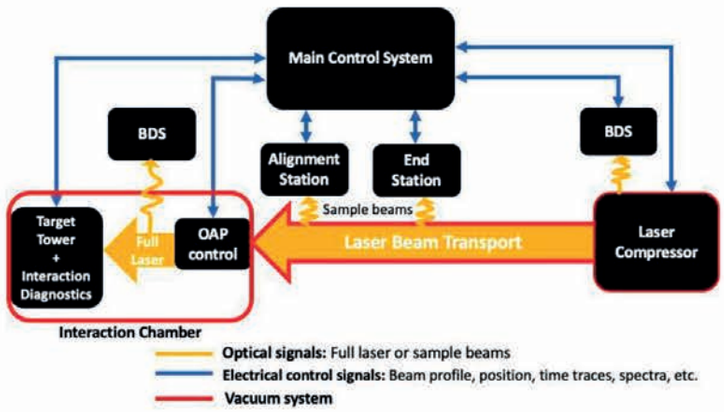

Figure 2: Laser transport, sampling and control. BDS: beam diagnostic station. OAP: off-axis parabolic mirror example of a full-width figure showing the latest LNS Activity Report cover

REFERENCES

[1] Thales LAS. QUARK – From 45 TW to multi-PW. https://www.thalesgroup.com/en/quark-45-tw-multi-pw

[2] Julien et Al. Opt. Letters 30(8) 920-922, 2005.

[3] Julien et Al. Opt. Express 14(7) 2760-2769, 2006.

[4] F. Schillaci et al., Quantum Beam Science, 6(4), 2022.

Multichannel data acquisition system for external radiation therapy and its preliminary characterization

A. Kurmanova[1,2], G. Petringa[1], M. Guarrera[1], G. Angemi[1], S. Arjmand[1], G. Cantone[1], E. Caruso[1], R. Catalano[1], G. Cuttone[1], F. Farokhi[1], S. Fattori[1], O. Giampiccolo[1], D. Oliva[1], A. Pappalardo[1], A. Pizzino[1], A. Sciuto[1] and G.A.P. Cirrone[1]

1) Istituto Nazionale di Fisica Nucleare (INFN) - Laboratori Nazionali del Sud (LNS), Catania, Italy

2) Università degli Studi di Catania, Dipartimento di Fisica e Astronomia "Ettore Majorana", Catania, Italy

Abstract - External beam radiotherapy, widely employed in cancer treatment, demands precision in Quality Assurance (QA) devices during both the planning phase and treatment verification. One crucial component ensuring precision, stability, linearity, and reproducibility is a Data Acquisition System (DAQ) relying on analog/digital front-end electronics. Within the framework of the PRAGUE project, DAQs are constructed using a TERA08 readout chipset, a Field Programmable Gate Array (FPGA) master board, and a customised graphical user interface developed with LabView software. Preliminary characterization of the DAQ has been conducted and is presented in this report.

INTRODUCTION

External radiation therapy is a localised form of treatment, necessitating the utmost precision in tumour localization and radiation transport to the clinical target volume. A Quality Assurance (QA) device is deemed essential to detect uncertainties in treatment planning and delivery, with an active detection system featuring a stack configuration being suitable for 2D dose reconstruction for both conventional and ultrafast dose delivery. Such a QA device mandates a multi-channel DAQ architecture with a wide current range and real-time measurement capabilities.

The objective of this study is to develop a customised graphical user interface using LabView software [3] to interface with the array of PRAGUE silicon carbide detectors[1], focusing on 2D dose mapping. This DAQ is based on a TERA08 readout chipset designed by INFN-Turin [2] and utilised in several laboratories [4-7], along with a Field Programmable Gate Array master board [8]. The PRAGUE detection system comprises arrays of silicon carbide detectors with an active area of 1.3 x 1.3 x 0.001 cm³. Preliminary and comprehensive characterizations of the detectors have been conducted [9, 10], yielding a relative error of 1.3%.

METHODS AND MATERIAL

The DAQs are equipped with an analog chip, TERA08, enabling simultaneous data acquisition from 64 channels by converting instantaneous current into digital pulse frequency. Each channel includes a 16-bit digital counter to tally the input charge accumulated into a capacitor, exceeding the user-set quantum charge of up to 1.115 pC. The chip is connected through an FRGA board to the PC with installed LabView software, which has been utilised to design a customised graphical user interface (GUI). Preliminary characterization has been performed with the use of a current source Keithley 2400 [11] and a custom-designed detector holder with a resistor.

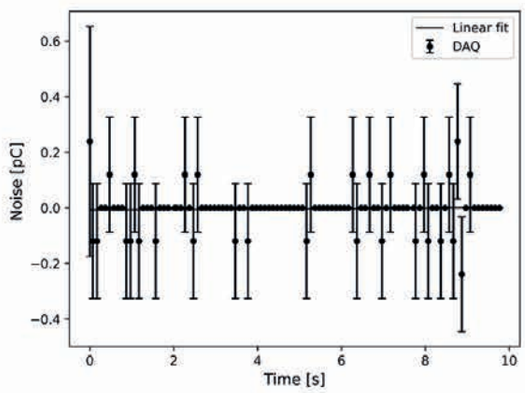

Figure 1: Background data for a single channel

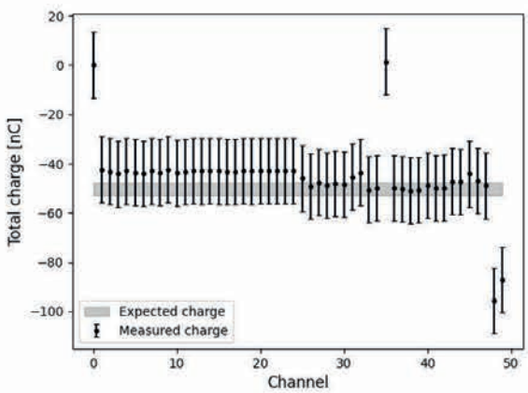

Figure 2: Current-charge linearity

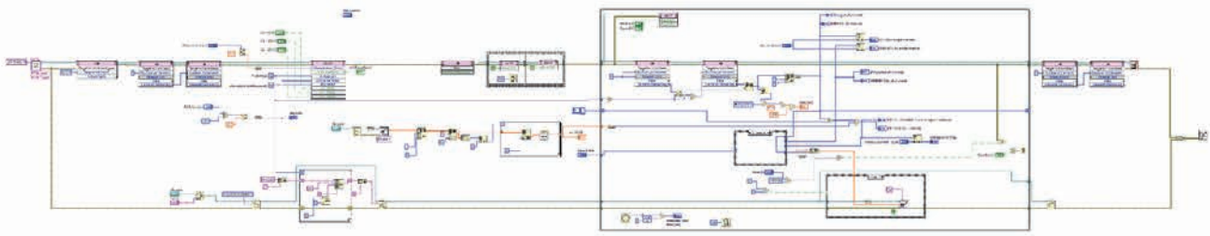

Figure 3: Block diagram for the recording data

RESULTS AND CONCLUSION

To utilise the interface, two virtual instruments (VIs) have been designed: a front panel for configuring charge quantum, acquisition time and data storage path, and a block diagram illustrating the signal processing steps. The VIs were developed to record both the background data for subtraction and the signal data acquired during irradiation. A real-time display of differential and integral data for all channels and specific channels was also implemented. An example of the signal recording block diagram is shown in Fig. 3.

A preliminary characterization was performed for the evaluation of the background and linearity of the current charge using the current source. The background evaluation of the DAQ included changing and analysing parameters such as charge quantum and acquisition time. Figure 1 shows the differential value over time for this evaluation. The value fluctuates around the axis with time, indicating that the readout chipset makes an insignificant contribution. The test then simulated the irradiation of the detector and compared it to the expected integrated charge within the acquisition time. Figure 2 shows that the measured data is within the expected value, including two channels with connectivity issues. However, the uncertainty bar is considerable, which will be further investigated to identify the sources of uncertainty. This will lead to higher precision and a detailed assessment of the uncertainty.

REFERENCES

[1] Petringa, G., Cirrone, G.A.P., Guarrera, M., Kurmanova, A., Amato, A., Catalano, R., Messina, G.E., Istokskaia, V., ELI-Bemalines, D.M. and Březany, D., PRAGUE (PROTON RANGE MEASUREMENT USING SILICON CARBIDE): A DETECTOR TO MEASURE ONLINE THE PROTON BEAM RANGE WITH LASER-DRIVEN PROTON BEAMS.

[2] La Rosa, Alessandro, et al. "Design and test of a 64-channel charge measurement ASIC developed in CMOS 0.35 μm technology." *Nuclear Instruments and Methods in Physics Research Section A: Accelerators, Spectrometers, Detectors and Associated Equipment* 583.2-3 (2007): 461-468.

[3] http://www.ni.com/labview

[4] Givehchi, Nasim, et al. "Online monitor detector for the proton therapy beam at the INFN Laboratori Nazionali del Sud-Catania." *Nuclear Instruments and Methods in Physics Research Section A: Accelerators, Spectrometers, Detectors and Associated Equipment* 572.3 (2007): 1094-1101.

[5] Giordanengo, S., et al. "Design and characterization of the beam monitor detectors of the Italian National Center of Oncological Hadron-therapy (CNAO)." *Nuclear Instruments and Methods in Physics Research Section A: Accelerators, Spectrometers, Detectors and Associated Equipment* 698 (2013): 202-207.

[6] Mazza, G., et al. "A 64-channel wide dynamic range charge measurement ASIC for strip and pixel ionization detectors." IEEE transactions on nuclear science 52.4 (2005): 847-853.

[7] Cirio, Roberto, et al. "A simple method to increase the current range of the TERA chip in charged particle therapy applications." *Nuclear Instruments and Methods in Physics Research Section A: Accelerators, Spectrometers, Detectors and Associated Equipment* 798 (2015): 107-110.

[8] http://www.ni.com/pdf/manuals/373047b.pdf

[9] Petringa, Giada, et al. "First characterization of a new Silicon Carbide detector for dosimetric applications." Journal of Instrumentation 15.05 (2020): C05023.

[10] Guarrera, M. and Petringa, G. and Tudisco, S. and Cirrone, G. A. P. (2022) *Characterization of a SiC detector for dosimetric application.* Il nuovo cimento C, 45 (4). pp. 1-9. ISSN 1826-9885

[11] ttps://www.tek.com/en/products/keithley/source-mea s ure-units/2400-standard-series-sourcemeter

Characterization of nuclear recoils in the dual-phase Argon Time Projection Chamber of the ReD experiment

S. Albergo[1,2], G.A. Anastasi[1], M. Gulino[3,4], L. Pandola[3], N. Pino[1], S.M.R. Puglia[1], S. Sanfilippo[3], A. Tricomi[1,2]

1) Università di Catania and INFN, Sezione di Catania, Catania, Italy
2) Centro Siciliano di Fisica Nucleare e Struttura della Materia, Catania, Italy
3) INFN, Laboratori Nazionali del Sud, Catania, Italy
4) Università di Enna Kore, Enna, Italy

Abstract – Dark Matter in the form of Weakly Interactive Massive Particles (WIMPs) is expected to produce nuclear recoils (NRs) from elastic scattering with ordinary matter. Liquid Argon (LAr) Time Projection Chambers (TPC) operating in double-phase are able to detect these NRs via light signals from both scintillation and ionization processes.

In the scenario of a low-mass WIMP (<2 GeV/c^2), the kinetic energy of the NRs would be below 20 keV, thus making it crucial to characterize the ionization response in LAr TPCs as the lone available detection channel at such low energy.

The Recoil Directionality (ReD) project, within the Global Argon Dark Matter Collaboration, aims to measure the ionization yield of a LAr TPC down to 2 keV recoil energy.

LOW-MASS WIMP SEARCHES IN ARGON-BASED TPC

Direct searches for Dark Matter in form of WIMPs focus on detecting a signal from its interaction with ordinary matter in low-background underground detectors.

The DarkSide Collaboration within the Global Argon Dark Matter Collaboration (GADMC) is currently building DarkSide-20k, a multi-ton argon dual-phase Time Projection Chamber at the INFN Laboratori Nazionali del Gran Sasso [1]. The signal in a dual-phase TPC has two components: the prompt scintillation (S1) and the delayed electroluminescence (S2). The S2 signal is proportional to the number of electrons surviving recombination in argon, which are drifted from the interaction site by an electric field, extracted to a gas layer above and finally accelerated to produce electroluminescence. The delay between S1 and S2, which is typically of tens or hundreds of μs, is due to the time spent by the electrons to drift from the production point to the gas phase.

In the standard scenario, WIMPs have masses of O(100's) GeV and the NRs induced in Ar have kinetic energies of a few tens of keV. One scenario that recently gained wide interest in the community predicts much lighter WIMPs, with masses of O(1) GeV. Low-mass WIMPs would generate NRs with an energy of a few keV, resulting in a very low scintillation (S1) signal, often impossible to detect. Therefore, the search for low-mass WIMPs must be performed by using the S2 signal only. The DarkSide-50 Collaboration performed a dedicated S2-only analysis of the data taken with the dual-phase Ar TPC of the DarkSide-50 experiment [2], showing that Ar TPCs are potentially sensitive to S2 signals produced by a few ionization electrons, corresponding to sub-keV NRs. This measurement is strongly influenced by quenching fluctuations in the ionisation process and dedicated measurements are available in the literature only for energies above 7 keV.

THE RED PROJECT

The Recoil Directionality (ReD) project by the GADMC irradiated a miniaturized dual-phase TPC with neutrons to measure the response to Ar recoils down to 2 keV. The campaign was held at the INFN Sezione di Catania between January and March 2023.

Argon recoils of known energy were produced in the ReD TPC by elastic scattering (n,n') of neutrons emitted from an intense ^{252}Cf fission source. Neutrons elastically scattered off Ar were then detected by a neutron spectrometer made of plastic scintillator (PSci) detectors downstream. The accompanying gamma-rays of ^{252}Cf fission events were detected by two BaF_2 detectors deployed close to the source, thus providing an event-by-event fission tagging. This allows for an effective event selection based on Time of Flight (ToF) and pulse shape discrimination (PSD) in the PScis of the neutron spectrometer. The kinetic energy of Ar recoils could hence be determined on a purely kinematical basis, once the scattering angle and the neutron kinetic energy E_n are known. In this approach, the scattering angle is fixed geometrically by the layout of the neutron spectrometer. On the other hand, as the ^{252}Cf source emits neutrons over a continuous energy range up to 10 MeV, the neutron energy E_n must be evaluated event-by-event by the ToF measurement.

The dual-phase Ar TPC of ReD has a volume of 5x5x6 cm^3 [3,4] and it is readout by cryogenic Silicon PhotoMultipliers (SiPMs). In such detector electrons are collected by an electric field that drives them from the interaction site in the liquid to the gas multiplication region, where they produce the delayed S2 signal. The

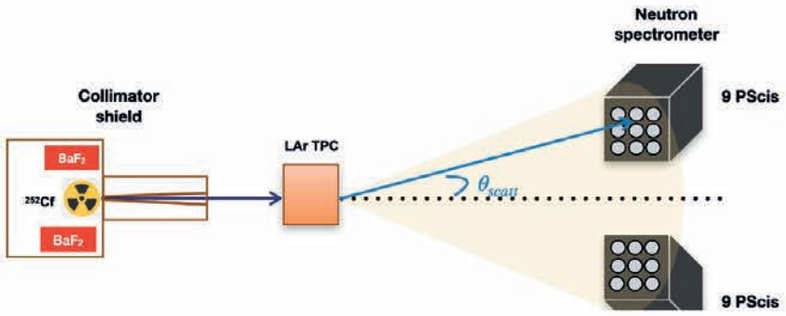

Figure 1 - Conceptual layout of the experimental setup for ReD

field was set 200 V/cm, causing the electron drift with a maximum time of 55 µs. Neutrons were emitted by a 1.0-MBq ^{252}Cf source, placed at about 90 cm distance from the TPC and collimated at 2° opening angle. The source was shielded and collimated by a custom structure made by boron-loaded polyethylene, iron and lead.

The two BaF_2 detectors were placed inside the shielding, close to the source and provided the START time for the ToF measurement. The neutron spectrometer, which provided the ToF STOP, was placed 100 cm downstream the TPC: it was made by two 3x3 arrays of 1-inch EJ-276 PScis, covering a range of scattering angles between 12° and 17°. A sketch of the experimental layout is shown in Figure 1.

PRELIMINARY RESULTS AND FUTURE PERSPECTIVES

ReD collected data for about three months. The selection of the candidate signal events primarily required the BaF_2-PSci ToF and the PSci PSD to be both compatible with neutron events: the range of ToF taken for the selection of ^{252}Cf neutrons goes from 40 to 180 ns. The resolution achieved in ToF was 0.7 ns rms, allowing an event-by-event measurement of the neutron kinetic energy at better than 5%. The candidate events were then further selected by requesting the presence of a S2-only TPC signal, with a single valid S2 signal within 55 µs from the BaF_2 signal, and estimated x-y position in the central 4x4 cm^2 region of the TPC. The final data sample, shown in Figure 2, consists in about 600 S2-only events with reconstructed Ar recoil energy below 10 keV. The corresponding S2 signals are below ~40 electrons. The design goal of ReD, i.e. to study the response of an Ar dual-phase TPC to nuclear recoils down to 2 keV, was hence successfully met [5]. Data analysis is currently in progress to finalize the measurement of the ionization yield.

Moreover, a new method involving self-supervised machine learning techniques, in particular convolutional autoencoders (CAE) [6], has been developed to improve the background rejection in S2-only events. In this analysis, the raw waveforms (averaged over the SiPMs) are compressed into 4-dimensional vectors, which have been characterized, and allow the tagging of traces without signal with a sensitivity comparable to the conventional reconstruction.

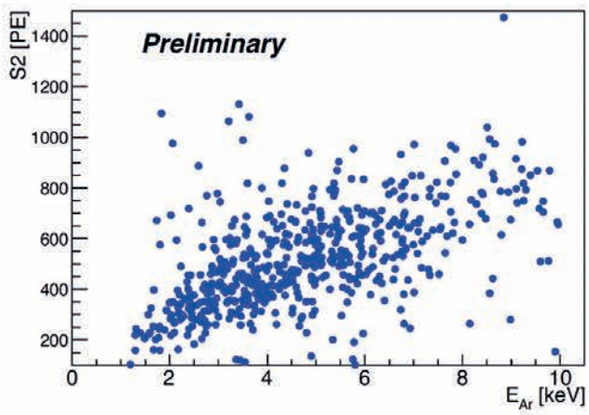

Figure 2 - (Preliminary) S2 signal vs. calculated recoil energy for events with a single neutron scattering in the TPC

This work is partially supported by ICSC – Centro Nazionale di Ricerca in High Performance Computing, Big Data and Quantum Computing, funded by European Union – NextGenerationEU

REFERENCES

[1] C. E. Aalseth et al., Eur. Phys. J. Plus **133** (2018) 131
[2] P. Agnes et al., Phys. Rev. Lett. **121** (2018) 081307
[3] P. Agnes et al., Eur. Phys. J. C **81** (2021) 1014
[4] P. Agnes et al., Eur. Phys. J. C **84** (2024) 24
[5] I. Ahmad et al., PoS(TAUP 2023) (2024) 052
[6] R. Corizzo et al., Expert Syst. Appl. **151** (2020) 113378

The ReD+ PRIN project: the characterization of sub-keV nuclear recoils in a dual-phase Argon Time Projection Chamber

S. Albergo[1,2], M. Gulino[3,4], L. Pandola[3], N. Pino[1], S.M.R. Puglia[1], S. Sanfilippo[3], A. Tricomi[1,2]

1) Università di Catania and INFN, Sezione di Catania, Catania, Italy
2) Centro Siciliano di Fisica Nucleare e Struttura della Materia, Catania, Italy
3) INFN, Laboratori Nazionali del Sud, Catania, Italy
4) Università di Enna Kore, Enna, Italy

Abstract - The characterization of the ionization yield for nuclear recoils in the keV range is a critical ingredient for the experiments looking for Dark Matter in the form of low-mass Weakly Interactive Massive Particles (WIMPs). The two-year project ReD+, funded by the Italian Ministry of Research through a PRIN grant, aims to improve the results obtained in the predecessor project ReD, which characterized a dual-phase Argon Time Projection Chamber (TPC) down to 2 keV nuclear recoils. ReD+ is designed to push the sensitivity down to 0.5 keV, by using the same conceptual design of ReD, with improved components, including a new optimized TPC.

THE SEARCH FOR LOW-MASS WIMP

The DarkSide program within the Global Argon Dark Matter Collaboration (GADMC) is searching for dark matter in the form of Weakly Interacting Massive Particles (WIMPs) by using argon dual-phase Time Projection Chambers (TPC) at the INFN Laboratori Nazionali del Gran Sasso. The signal in a dual-phase TPC has two components: the prompt scintillation (S1) and the delayed electroluminescence (S2). The S2 signal is proportional to the number of electrons surviving recombination in argon, which are drifted from the interaction site by an electric field, extracted to a gas layer above and finally accelerated to produce electroluminescence. The delay between S1 and S2 is due to the time spent by the electrons to drift from the production point to the gas phase.

In the standard scenario in which the WIMP mass is O(100's) GeV, the WIMP-induced nuclear recoils (NRs) in Ar have kinetic energy of a few tens of keV. Recently, interest raised on an alternative dark matter scenario, in which WIMPs are much lighter, O(1) GeV. In this case, the NR energy is as low as a few keV in Ar. As the S1 signal is often too low to be detected, the search for low-mass WIMPs must be performed by using the S2 signal only: Ar dual-phase TPCs are potentially sensitive to few-electron signals, i.e. to sub-keV Ar recoils. The S2-only analysis, as for instance the one carried out with the data of the experiment DarkSide-50 [1] is very sensitive to the knowledge of the ionization yield of Ar recoils and literature data are scarce in the energy range of interest.

THE RED PROJECT

The Recoil Directionality (ReD) project by the GADMC irradiated a miniaturized TPC with neutrons at the INFN Sezione di Catania between January and March 2023 and measured the response to Ar recoils down to 2 keV.

Argon recoils of known energy were produced in the ReD TPC by elastic scattering (n,n') of neutrons from an intense ^{252}Cf fission source. Neutrons elastically scattered off Ar were detected by a neutron spectrometer made of plastic scintillator (PSci) detectors, thus fixing the neutron scattering angle. Furthermore, two BaF_2 detectors were deployed close to the ^{252}Cf source, such to detect accompanying gamma-rays of fission events and then to provide an event-by-event fission tagging. The kinetic energy of Ar recoils could hence be determined on a purely-kinematical basis, once the scattering angle and the neutron kinetic energy E_n are known. In this layout, the scattering angle is fixed geometrically by the placement of the neutron spectrometer. On the other hand, as the ^{252}Cf source emits neutrons over a continuous energy range up to 10 MeV, the neutron energy E_n must be evaluated event-by-event by the time of flight (ToF).

The dual-phase Ar TPC used in the ReD campaign was a parallelepiped of 5x5x6 cm^3 [2,3], readout by cryogenic Silicon PhotoMultipliers. A 200 V/cm drift field collects electrons from the interaction site in the liquid and drives them to the gas multiplication region, where they produce the delayed electroluminescence signal. Neutrons were emitted by a 1.0-MBq ^{252}Cf source, placed at about 90 cm distance and collimated at 2° opening angle. The source was shielded and collimated by a structure made by boron-loaded polyethylene, iron and lead. Two BaF_2 detectors are placed inside the shielding, close to the source, in order to tag the fission products and to provide a START for the ToF measurement. The neutron spectrometer, which provides the ToF STOP, was placed 100 cm downstream the TPC: it was made by two 3x3 arrays of 1-inch EJ-276 PScis, covering a range of scattering angles between 12° and 17°. The resolution achieved in ToF was 0.7 ns rms (over a range of 40-180 ns), allowing an event-by-event measurement of the neutron kinetic energy at better than 5%.

The final event sample collected in about three months of data taking consists in about 600 S2-only events with reconstructed Ar recoil energy between 1 and 10 keV. The design goal of ReD, i.e. to study the response of an Ar dual-phase TPC to nuclear recoils down to 2 keV, was hence successfully met [4]. Data analysis is currently in progress to finalize the measurement of the ionization yield.

IMPROVING TO THE SUB-KEV SCALE: THE RED+ PROJECT

Given the interest by dark matter experiments searching for low-mass WIMPs, it is very important to further improve the characterization of the TPC response to low-energy recoils, by further extending the coverage down to the sub-keV range. ReD+ is an extension of ReD, funded by a two-year PRIN grant from the Italian Ministry of Research, designed to push the sensitivity down to 0.5 keV. The conceptual design will be the same as in ReD, i.e. employing the two-body kinematic of neutrons emitted from a source, as displayed in Fig. 1. While it is expected that a large part of the ReD set-up can be re-used, some of the components of the system will be improved in order to increase the signal rate and the signal-to-background ratio, which limited the sensitivity of ReD. In particular, a new optimized TPC is being completely re-designed and will be built and characterized within the project. The TPC will have a cylindrical shape and a special care will be taken to minimize any passive layer: in fact, multiple neutron scattering, either by non-active Ar or by any other component of the system, spoils the kinematic two-body correlation and produces an irreducible background which limits the sensitivity. The ^{252}Cf source will be deployed inside the same shielding used in ReD (boron-loaded polyethylene, iron and lead), with a minor re-design of the front face to minimize the probability of neutron leaking the shielding and hitting the TPC after one or more scattering in polyethylene. Another option under consideration is to use a commercial Deuterium-Deuterium neutron generator, which has the advantage of emitting mono-energetic 2.4-MeV neutrons. In order to push the sensitivity to sub-keV recoil energies, the neutron spectrometer has to be deployed at a smaller scattering angle with respect to ReD, but still outside the direct illumination cone from the source. For this reason, the TPC-spectrometer distance will be increased from 100 to 150 cm. In order to compensate for the loss of event rate due to the increased distance, the neutron spectrometer will be extended from 18 to 36 plastic scintillators (EJ-276, or its more recent commercial version EJ-276D) and a more active neutron source will be used (2-3 MBq, instead of 1 MBq). It is anticipated that the employment of a new optimized TPC, together with the improvement in the shielding, source activity and neutron spectrometer will allow to meet the design sensitivity of ReD+, i.e. nuclear recoils of 0.5 keV. The ReD+ project started in September 2023, involving the INFN, the University of Naples and the University of Catania. The re-design of the TPC, the procurement of the additional PScis and of the ^{252}Cf source are currently in progress. The assembly and integration of the system is expected to take place at the INFN Laboratori Nazionali del Sud in the first semester of 2025, followed by the data taking phase.

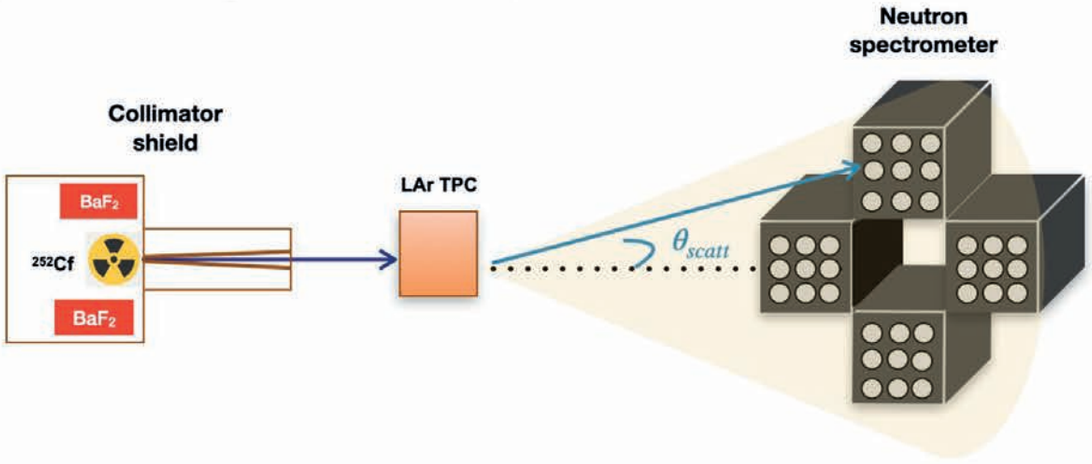

Figure 1: Conceptual layout of the experimental setup for ReD+

REFERENCES

[1] P. Agnes et al., Phys. Rev. Lett. **121** (2018) 081307
[2] P. Agnes et al., Eur. Phys. J. C **81** (2021) 1014
[3] P. Agnes et al., Eur. Phys. J. C **84** (2024) 24
[4] I. Ahmad et al., PoS(TAUP 2023) (2024) 052

Measurements of residual radioactivity in the experimental rooms MEDEA, CICLOPE, ROOM 0°

S. Russo[1], R. Leanza[1], M. Costa[1]

1) *INFN – LNS*

Abstract - This report refers to the results of the dosimetry and residual radioactivity measurements carried out before equipment and facilities disassembly inside the LNS experimental rooms.

INTRODUCTION

The LNS are carrying out modifications in the experimental rooms which are commonly called Sale Misura 1 (SM1), installing new experimental equipment (I-Luce and Pandora, figure 1b) to replace the existing ones (Medea and Ciclope, figure 1a).

As a consequence, the old equipment, the beam transport lines and the systems connected to them will be disassembled. The shielding structures will be modified, also resulting in the demolition of some concrete parts of the floor.

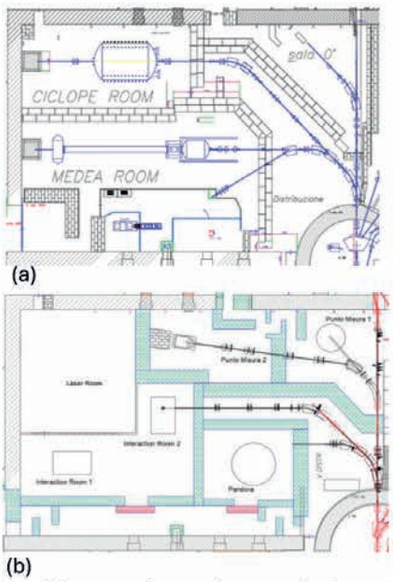

Figure 1: The experimental rooms before (a) and the future disposition (b).

The apparatus of experimental rooms could be radioactive because they have been exposed to secondary neutron fields generated by the experiments carried out during the last 40 years of LNS activity.

For this reason, before dismantling the equipment, in order to guarantee the safety of personnel and the possible disposal of objects, external exposure measurements were carried out on all objects and devices. Furthermore, other measurements, done with HPGE detectors, were carried out to reveal residual radioactivity on objects that are not expected to be reused, to predict the possibility of future disposal.

MEASUREMENTS

Three years after the beam was stopped, environmental ambient dose equivalent and spectrometric measurements were performed on each device present inside the experimental rooms which we can consider as individual parts:

- Medea, (chamber and internal steel supports, detectors (BaF3), photomultipliers, bases, cables and connectors).
- Sole, (yoke, superconducting magnet, internal and external chamber).
- Maciste (large and long beam transport tube and scattering chamber).

In the Ciclope apparatus, measurements were done only on the steel scattering chamber because the inside was already empty, figure 2.

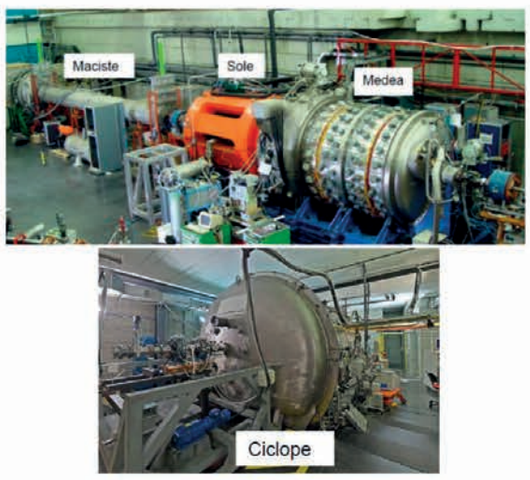

Figure 2: Experimental devices.

Ambient dose equivalent measurements

Environmental ambient dose equivalent (H*) measurements were realised at various points in contact and, if necessary, at different distances of the beam transport lines and experimental apparatus (indicated by arrows in figure 3a – 3b), using detectors sensitive to gamma and beta radiation.

From the measurements carried out, it is underlined that only the 0° transport line presented detectable activation with a maximum of 17 μSv/h at few cm from

the surface of the line, because it was affected by the frequent passage of proton beams.
No other point on the other lines or equipment had doses higher than the natural background ($f \leq 0.1$ µSv/h).

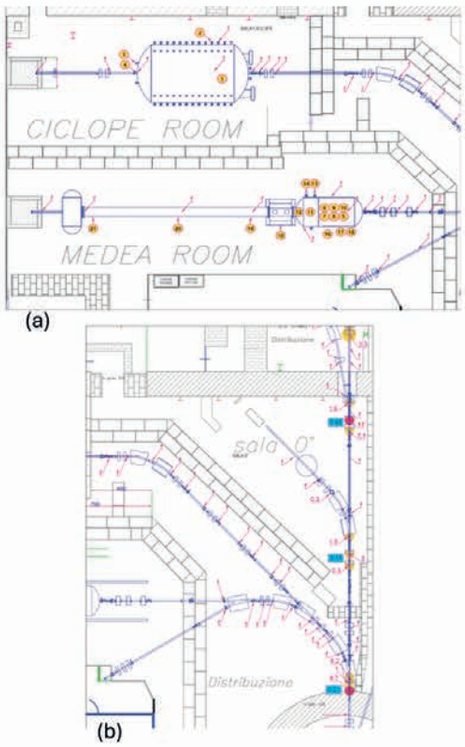

Figure 3a – 3b: scheme of measurements along the beam line and equipment.

Gamma spectrometry measurements

To search for the presence of artificial radionuclides in very low concentrations, gamma spectrometry measurements were executed with HPGE germanium detectors in a fixed shielded shell or with a portable system in all points circled in yellow in Figure 3a.

Each measurement had different times, from 1 to 7 days, and the MDA values are the follows: 5E-5 Bq/g (1 days) and 5E-6 Bq/g (7 days).

The measurements, done on the various elements of Medea, Sole and Maciste, did not reveal radionuclides higher than the MDA values.

Regarding Ciclope, the measurements carried out on the internal center of the chamber, with the detector positioned on the basis, did not reveal artificial radionuclides higher than MDA. The same for the side part measured in the fixed detector shell.

Instead, the measurement of the backside chamber, done with fixed detector, shown only the presence of Co60 with an activity which just exceeds the MDA value of 5E-5 Bq/g (figure 4a).

While the measurement of the output central flange, with both fixed and portable detectors, shown the presence of Co60, Mn54 and Na22 with an activity of approximately 2E-3 Bq/g each (figure 4b).

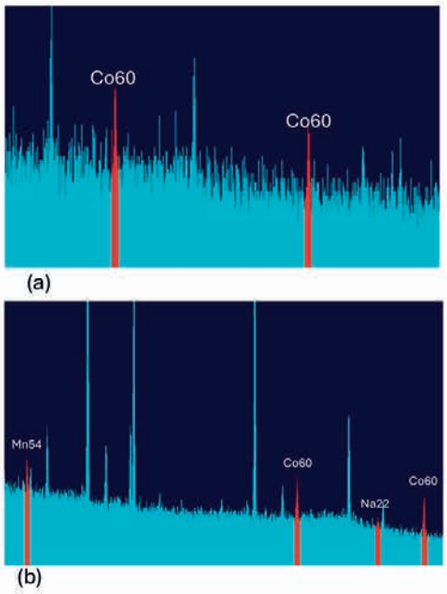

Figure 4: Gamma spectra of backside of the chamber (a) and output flange (b) of Ciclope equipment; in red ROI's of Co60, Mn54 and Na22.

CONCLUSIONS

The study of the residual radioactivity had the purpose of verifying the presence of activation deriving from the interaction of the accelerated beams and the secondary neutron field.

In our case, from the environmental ambient dose equivalent measurements conducted, it can be observed that, except on the beam transport line, after three years of cooling, we do not find a dose higher than the natural background.

Furthermore, from spectrometric measurements, despite the values found for Ciclope chamber, there is no significant residual radioactivity present on the equipment disassembled.

As in the measurements of the concrete shields demolished from the experimental rooms [1], also in this case no significant residual radioactivity was found.

This work demonstrated that in the research laboratories of the LNS, where the heavy beam accelerators had in operation for more than 40 years, the apparatus of the experimental rooms and the equipment did not present significant radioactivity.

REFERENCES

[1] R. Leanza, S. Russo, G. Russo - Measurements and Monte Carlo evaluations of shielding concrete radioactivation in a nuclear physics facility to verify the clearance levels - SATIF-15 20-23 September 2022, East Lansing MI, USA.

Modelling Radio-Frequency Waves propagation in Hot-Magnetized Plasma

C. Salvia[1,2,3], A. Cardinali[1,4,5], G. S. Mauro[1], B. Mishra[1,2], A. Pidatella[1]
G. Torrisi[1] and D. Mascali[1,2]

1) Istituto Nazionale di Fisica Nucleare - Laboratori Nazionali del Sud, Via S. Sofia 62, 95123 Catania, Italy
2) Dipartimento di Fisica e Astronomia, Università degli Studi di Catania, Via S. Sofia 64, 95123 Catania, Italy,
3) Centro Siciliano di Fisica Nucleare e Struttura della Materia (CSFNSM), Via S. Sofia 64, 95123 Catania, Italy
4) CNR, Istituto Sistemi Complessi, Politecnico di Torino, Corso Duca degli Abruzzi 24, 10129 Turin, Italy
5) Istituto Nazionale di Astrofisica (INAF), IAPS, Via del Fosso del Cavaliere 100, 00133 Rome, Italy

Abstract – This report presents analytical modelling and numerical simulations of radio-frequency (RF) wave propagation in hot magnetized (^{2}H) plasma, investigating the thermal effects' impact on wave dispersion relations. Using a realistic Ion Cyclotron Heating (ICH) antenna model from the Divertor Tokamak Test (DTT) device, simple 1D wave propagation is achieved. Antenna spectra are extracted and analyzed using CST®, while 1D wave propagation is performed via MATLAB®.

INTRODUCTION

Ion cyclotron resonance heating is a key method for heating plasma in fusion devices, achieved by inducing resonant absorption of high-frequency electromagnetic waves into plasma ions. In thermonuclear fusion research, coupling electromagnetic power to tokamak plasma via RF antennas is a significant challenge, requiring precise modelling of plasma propagation and detailed antenna geometry. In previous studies, advanced methods like the FELICE and TORIC codes ([1],[2]) have been employed for wave propagation analysis. However, these methods frequently exhibit less precision in describing antennas compared to TOPICA® or COMSOL Multiphysics®. Our study aims to simplify the plasma's electromagnetic field description, neglecting the slow wave effect and treating hot plasma as a perturbation. Additionally, we employ an advanced antenna model within the DTT scenario.

1D WAVE PROPAGATION MODEL

In a cold plasma (the kinetic velocity of particles in plasma is much smaller than the phase velocity of waves) the stationary wave equation, derived from the Maxwell-Vlasov model, yields an exact differential equation:

$$\nabla \times \nabla \times \vec{E}(\vec{r}) - \frac{\omega^2}{c^2}\bar{\bar{\epsilon}}^H(\vec{r}) \cdot \vec{E}(\vec{r}) = 0 \qquad (1)$$

where ω is the antenna frequency, c is the speed of light, and $\bar{\bar{\epsilon}}^H(\vec{r}) = \left(\bar{\bar{I}} + \frac{4\pi i}{\omega}\bar{\bar{\sigma}}^H(\vec{r})\right)$ is the Hermitian dielectric tensor. For a homogeneous, stationary and boundless thermal plasma, the dielectric tensor is typically determined from the Maxwell-Vlasov equation, which in this case is a set of algebraic equations (dispersion relation, refer to [4]). The dielectric tensor, comprised of Hermitian (H) and anti-Hermitian (A) components, governs propagation and absorption phenomena in the frequency and wave-vector domains. Our study focuses on a Cartesian slab plasma configuration (see Fig.1), with plasma characteristics varying along the slab coordinate (x). Starting from Eq. (1) within the context of a cold plasma environment and a single propagating mode, (specifically the fast mode), we set boundary condition at the antenna (vacuum)-plasma interface. Moreover, we consider the damping coefficient (the anti-Hermitian part of the dielectric tensor) as a perturbation of the Hermitian part. This methodology results in the following second-order differential equation for the $\tilde{E}_y$ component of the electric field:

$$-\frac{\partial^2 \tilde{E}_y}{\partial x^2} + \left[k_z^2 - \frac{\omega^2}{c^2}\left(\epsilon_{yy}^H + i\epsilon_{yy}^A\right) + \frac{\omega^4}{c^4}\frac{\left(\epsilon_{xy}^H + i\epsilon_{xy}^A\right)^2}{k_z^2 - \frac{\omega^2}{c^2}\left(\epsilon_{xx}^H + i\epsilon_{xx}^A\right)}\right]\tilde{E}_y = 0 \quad (2)$$

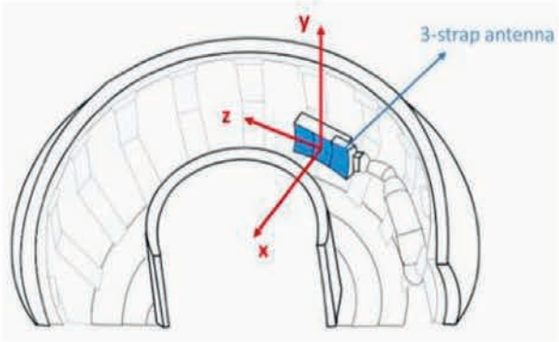

Fig. 1 – Reference frame adopted for propagation model.

Parametric Studies in Ideal Tokamak Example

Eq. (2) identifies key tensor elements in the 1D case. Parametric analyses were performed on ϵ_{xx}, ϵ_{xy}, and ϵ_{yy} concerning x and parallel wavenumber $n_z = \frac{k_z c}{\omega}$ (n_z =

[1, 10]). Using a DTT scenario (Major radius R0=219 cm, minor radius a=75 cm) (5), three dielectric tensor forms were compared: COLD (see [3], Ch.5 Par.17), Finite Larmor Radius (FLR) (see [3], Ch.6 Par.26) , and FULL (see [3], Ch.4 Par.14). The parametric studies demonstrate the effectiveness of the COLD approximation near the antenna, whereas FLR or FULL models are required for internal plasma regions to accurately represent wave behaviour.

The 3-strap antenna field extraction and k-spectra analysis.

To solve Eq. (2) and isolate $\tilde{E}y$ terms, antenna-derived fields were utilized. CST® facilitated field extraction employing a flat 3-strap antenna geometry at 60 MHz. Fourier transforms have been performed using MATLAB's FFT algorithm. Fig. 3 shows real and imaginary E_y parts extracted along z-axis (2 cm from Faraday Screen along x-axis) and their Fourier transforms.

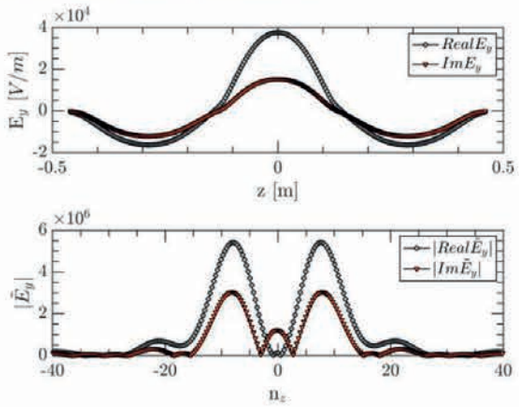

Fig. 2 - (Top) $E_y(z)$ field. (Bottom) Fourier Trasform of $E_y(z)$ as function of n_z.

Solution of the 1D Waves's Propagation Model: the Homogeneous case.

By performing some algebraic manipulations, Eq. (2) can be analytically solved. By operating a coordinate change $\xi = 1-x$ and imposing the boundary condition at the antenna-plasma interface, the solution of Eq. (2) can be expressed in terms of progressive and regressive waves with damping terms:

$$\tilde{E}_y(\xi, n_z) = C_1 e^{i\sqrt{\alpha}\xi} e^{-\frac{\beta}{2\sqrt{\alpha}}\xi} + C_2 e^{-i\sqrt{\alpha}\xi} e^{\frac{\beta}{2\sqrt{\alpha}}\xi} \quad (3)$$

where $\boldsymbol{\alpha = 1}$ and $\boldsymbol{\beta = \pi^{1/2}\omega_{ce}^2 \frac{v_{the}}{n_z \Omega_{ce}^2} e^{-\left(\frac{1}{n_z} v_{the}\right)^2}}$. Fig.3 shows a plot of the propagating field Ey in the $\hat{\boldsymbol{z}}$-ξ plane, showing the electric field in real space as a function of ξ. The propagation of the field towards the center of the Tokamak is evident, with maximum intensity originating from the antenna and a gradual decrease in electric field amplitude.

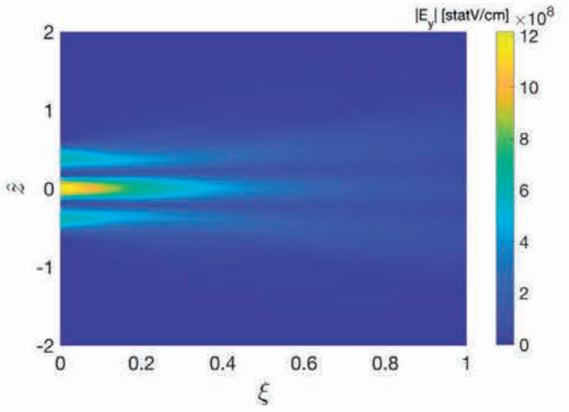

Fig. 4 - 2D plot of electric field E_y propagated by the antenna into the plasma, where $\hat{\boldsymbol{z}}$ represents the spatial coordinate normalized with respect to the minor radius of the antenna $\boldsymbol{a}$. Antenna placed at $\xi = 0$ and plasma center at $\xi = 1$.

CONCLUSIONS

A one-dimensional model was used to study electromagnetic wave propagation and absorption in plasma, focusing on the interaction between ion cyclotron antenna emissions and plasma waves. Using CST® software, the antenna's radiated field was analyzed considering its geometry, with electromagnetic field matching at the interface of antenna. MATLAB® facilitated comparison of dielectric tensors for absorption model integration. This analysis, initially applied to pure Deuterium plasma for DTT scenarios, provided valuable insights into coupling, propagation, and absorption physics, serving as groundwork for future research utilizing advanced numerical methods and realistic plasma scenarios.

BIBLIOGRAPHY

[1]. Brambilla M. et al., Nuclear Fusion, 28 (1988) 1813.
[2]. Brambilla M., Plasma Physics and Controlled Fusion, 41 (1999) 1.
[3]. Brambilla M., Kinetic theory of plasma waves: homogeneous plasmas, no. 96 (Oxford University Press) 1998.
[4]. Brambilla M. et al., A model to evaluate coupling of ion bernstein waves to tokamak plasmas, presented at europhysics confenence abstracts, Vol. 15C (EPS) 1991.
[5]. Casiraghi I. et al., Nuclear Fusion, 61 (2021) 116068.

Neural Network-Based Regression for Estimating early DNA Damage Across Micro-Nano Scales

A. Sciuto[1], S. Fattori[1], S. Arjmand[1], G. Angemi[1], G. Cantone[1], E. Caruso[1], R. Catalano[1], G. Cuttone[1], F. Farokhi[1], O. Giampiccolo[1], M. Guarrera[1], A. Kurmanova[1], D.Oliva[1], A. Pappalardo[1], G. Petringa[1], A. Pizzino[1], and G.A.P. Cirrone[1]

1) Istituto Nazionale di Fisica Nucleare Laboratori Nazionali del Sud (INFN LNS), Catania, Italy.

Abstract - The prediction of radiation-induced DNA damage, knowing the characteristics of the radiation field, is a challenging task that necessitates an understanding of the complexities presented at both microscopic and nanoscopic scales. After the release of Geant4-DNA , Geant4 appears as an optimal tool for implementing multiscale studies. While Geant4 can explore particle-matter interactions at the microscopic scale, Geant4-DNA can reach the nanoscopic one. In this study, we propose a post-processing tool to be integrated within a Geant4 application to bridge the gap between the micro and the nanoscopic scale simulations.

INTRODUCTION

Radiation therapy uses high-energy particles to damage and stop cancer cell growth. The primary challenge is to maximize cancer cell damage while minimizing injury to surrounding healthy tissues.

Understanding the biological effects of radiation on various scales is critical to achieving this equilibrium. Radiation therapy currently determines organ and tissue doses using macroscopic dosimetry. To fully understand radiation effects, a nanoscopic perspective is required. We focus on the interactions of radiation with cells and DNA. A thorough understanding is required for regulating radiation distribution near sensitive tissues. Combining macroscopic and nanoscopic methods improves radiation treatment efficacy.

Currently, multiscale radiation simulation at multiple biological levels is underexplored. Simulated interactions between radiation and biological tissues are critical for understanding complex interactions at all scales, from macro to micro.

Geant4-DNA [1, 2, 3, 4] and its "mother" toolkit, Geant4 [5, 6, 7] , are critical tools in this field, sharing a common platform but employing different models for calculations at various scales. Geant4 provides a macro-scale framework for particle-matter interactions, whereas Geant4-DNA models radiation effects at the molecular and cellular levels.

Although useful, these modeling tools require a lot of computing power and have slow processing speeds. New methodologies are required to improve simulation speed and accuracy, particularly at the nanoscopic scale, where Geant4-DNA is the primary bottleneck due to its high computational demands.

To bridge the gap between Geant4's microscopic and Geant4-DNA's nanoscopic results, a Python-based ML tool called GANDALF (Generative ANsatz for DNA Damage evALuation and Forecast) was developed.

Machine learning has advanced in a variety of scientific disciplines, including medical physics. Complex datasets are used to train algorithms that can identify patterns and make accurate predictions. Regression analysis, a key machine learning technique, can predict continuous outcomes based on input features. This is especially useful for making accurate quantitative predictions about outcomes such as radiation-induced damage.

GANDALF employs machine learning here. This neural network-based regression system analyzes Linear Energy Transfer (LET) data to predict early DNA damage, such as SSBs and DSBs.

Our Python tool set, GANDALF, employs a three-density layer architecture to generate nanoscopic DNA damage data from macroscopic LET measurements for regression purposes. The network uses an Automated Nonlinearity Encoder (ANE) to improve forecast accuracy and efficiency. This is accomplished by identifying and documenting nonlinear relationships between LET data and DNA damage.

Additionally, GANDALF's modular design allows for future modifications and extensions. Modularity is required for adapting to different radiation types and other factors such as Relative Biological Effectiveness (RBE). GANDALF adapts to new challenges and data, making it a versatile and effective tool in a constantly evolving field.

MATERIALS AND METHODS

The work begins by conducting two comprehensive Geant4 simulations with the explicit objective of doing a microscopic analysis of how radiation, particularly protons, interact with matter. The initial simulation aims to collect data on the relationship between Linear Energy Transfer (LET) and depth within a water phantom, as mentioned in [8]. Simultaneously, the

second simulation aims to gather LET data within an ellipsoid that has the same volumetric properties as the nucleus of an Escherichia coli (E. coli) cell.
In the following stage of the study, the analysis shifts from examining objects at a small scale to examining them at an even smaller scale. This transition is made easier by utilizing simulations based on the Geant4-DNA example "moleculardna" [9]. These simulations play a crucial role in creating a thorough dataset that include instances of early single-strand breaks (SSBs) and double-strand breaks (DSBs) in the DNA contained within the nucleus of an E. coli cell [10]. This dataset is essential as it accurately represents the effects of proton irradiation at different energy levels.

The analysis includes a complex regression method based on Neural Networks [11], which aims to establish connections between the microscopic LET measurements and the nanoscopic occurrences of SSBs and DSBs that were previously recorded. The initial testing of this model utilizes a three-layer architecture. This architecture includes an input layer with 14 neurons activated by the Rectified Linear Unit (ReLU) function, a middle layer with 23 neurons also activated by ReLU, and a final output layer without activation. The configuration of the output layer is specifically designed to have the same number of neurons required for regression tasks. The purpose of this model design is to enhance the predictive accuracy in determining the influence of specific linear energy transfer (LET) values on rates of DNA damage.

RESULTS

Our trained regression algorithm predicts early SSBs and DSBs in a water phantom cube using standard Geant4 simulation data. In this example, a high-density voxelized phantom was used. This method uses a simulated experiment to evaluate DNA damage in E. coli cells at various depths within a water phantom. It excludes damage induced by charged particles interacting with the cytoplasm.
Feeding the LET depth curve into the neural network model generates different output curves for each feature trained on.

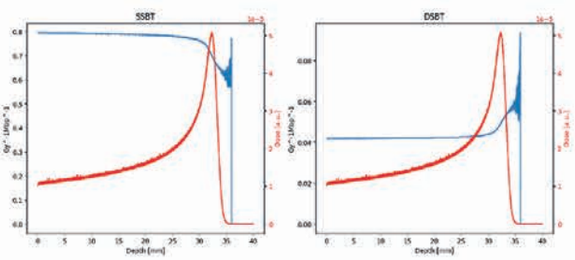

Figure 1: Total SSB and DSB (Blue) curves and Dose (Red) vs. depth. SSBT and DSBT where generated with our trained ML algorithm, while Dose was calculated with a Geant4 Simulation.

DISCUSSIONS

Future perspectives

Future work should address the Neural Network model's underestimating bias and investigate the possibility of including additional variables, such as Relative Biological Effectiveness and other radiation types, to improve the model's predictive capabilities. GANDALF's modular architecture enables various extensions to other radiation types, ensuring its relevance and adaptability to changing requirements in radiobiological research and clinical applications.

REFERENCES

[1] S. Incerti et al., "THE GEANT4-DNA PROJECT," International Journal of Modeling, Simulation, and Scientific Computing, vol.01, pp. 157-178, 2010
[2] S. Incerti et al., "Comparison of GEANT4 very low energy cross section models with experimental data in water," Medical Physics, vol. 37, pp. 4692-708, Sep 2010.
[3] M. A. Bernal et al., "Track structure modeling in liquid water: A review of the Geant4-DNA very low energy extension of the Geant4 Monte Carlo \simulation toolkit," Phys Med, vol. 31, pp. 861-874, Dec 2015.
[4] S. Incerti et al., "Geant4-DNA example applications for track structure simulations in liquid water: A report from the Geant4-DNA Project," Medical Physics, vol. 45, pp. e722-e739, 2018.
[5] S. Agostinelli et al 2003 Geant4 a simulation toolkit Nucl. Instrum. Methods Phys. Res. A 506 250–303
[6] J. Allison et al 2006 Geant4 developments and applications IEEE Trans. Nucl. Sci. 53 270–8
[7] J. Allison et al 2016 Recent developments in GEANT4 Nucl. Instrum. Methods Phys. Res. A 835 186–225
[8] David J. Thomas, ICRU report 85: fundamental quantities and units for ionizing radiation, Radiation Protection Dosimetry, Volume 150, Issue 4, July 2012, Pages 550–552,
[9] Chatzipapas et al. Simulation of DNA damage using Geant4-DNA: an overview of the "molecularDNA" example application, Prec. Radiat. Oncol. (2023) 1–11
[10] N. Lampe et al. Mechanistic DNA Damage Simulations in Geant4-DNA Part 2: Electron and Proton Damage in a Bacterial Cell, Phys. Med. 48 (2018) 146-155
[11] Charu C. Aggarwal Neural, Networks and Deep Learning, Springer Cham

07

NATIONAL RECOVERY AND RESILIENCE PLAN

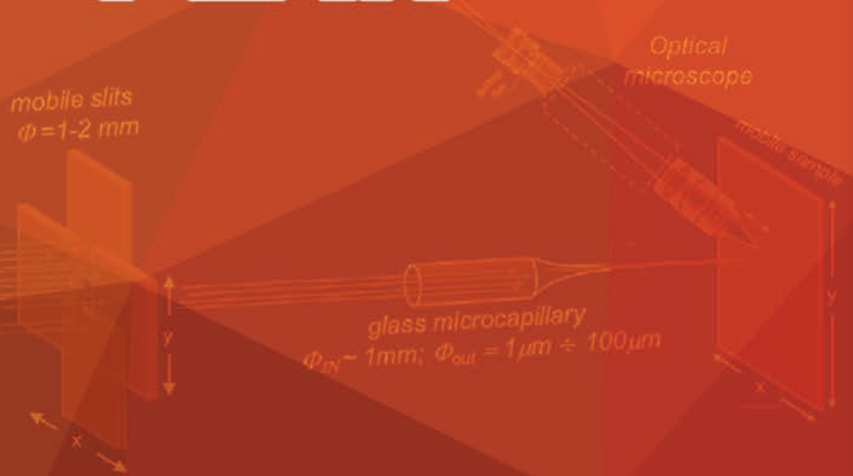

Research Analyses Results

INFN LNS

- SAMOTHRACE SiciliAn MicronanOTecH Research And Innovation CEnter
- Micro accelerators for health and energy applications within the SAMOTHRACE ecosystem
- Microbeams with glass capillaries within the SAMOTHRACE ecosystem
- Micro detectors for particle therapy, dosimetry, and micro-dosimetry within the SAMOTHRACE ecosystem
- Detectorsand technologies for fusion plasmas within the samothrace ecosystem
- NQSTI spoke-3 INFN task 3.1: atomic, molecular platform for quantum technologies
- Implementation of a smart and reliable infrastructure for underwater synchronization and acoustic data transmission in the PNRR- ITINERIS project
- Ocean Noise Subsystem for the "Italian Integrated Environmental Research Infrastructures System (ITINERIS)" project
- Preparatory studies for the Einstein Telescope engineering design
- I-LUCE. Status of the INFN Laser indUCEd radiation facility at INFN-LNS

SAMOTHRACE
SiciliAn MicronanOTecH Research And Innovation CEnter

S. Albergo[1,2], G. Cardella[1], G.A.P. Cirrone[3], G. Cosentino[3], S. Gammino[3], E. Geraci[1,2], G. Marsella[1,4], M. Marrale[1,4], D. Mascali[3], A. Tricomi[1,2] and S. Tudisco[3]

1) INFN-Sezione di Catania, Catania, Italy
2) Universita` di Catania - Catania, Italy,
3) INFN-Laboraratori Nazionali del Sud, Catania, Italy
4) Università di Palermo, Palermo Italy

Abstract - Innovation Ecosystems are "territorial leaders of research and innovation", networks of public and private universities, international research centers, local authorities, companies, and other highly qualified and international entities. The Italian National Recovery and Resilience Plan is part of the Next Generation EU programme which are funding 11 Ecosystems for a total investment of 1.3 billion euros. SAMOTHRACE, with a Hub & Spoke governance structure and overall funding of approximately 120 million euros, is the Sicilian innovation center. SAMOTHRACE has the ambition to leverage the consolidated vocation of the Sicilian territory in microelectronics e micro-and nano technologies to bring this to a higher and more diffuse level. In this framework INFN has the Spoke role.

SAMOTHRACE ORGANIZATION

SAMOTHRACE Ecosystem [1] was proposed and headed by University of Catania, has twenty-eight partners, four Universities, six Research Institutes, four Large Companies, fourteen SMEs. The whole Ecosystem Hub & Spoke governance structure is reported in figure 1.

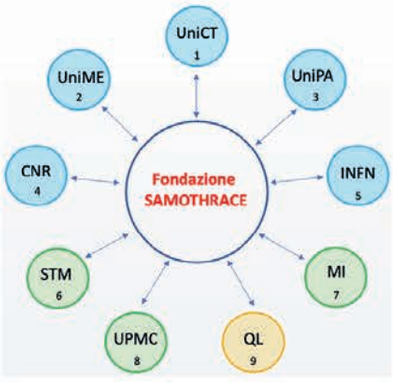

Figure 1: SAMOTHRACE Hub & Spoke governance structure.

The SAMOTHRACE Foundation manages the ecosystem with the role of Hub while each Spoke is characterized by specific activities and objectives, as outlined by Spoke titles. *Spoke1*: **ITM3**-Innovation Through Microelectronics, Microsystems and Materials (University of Catania); *Spoke2*: **AdSeS**-Advanced Sensors and Systems (University of Messina); *Spoke3*: **S2-COMMs**-Micro and Nanotechnologies for Smart & Sustainable Communities (University of Palermo): *Spoke4*: **MiSteRI**-MicroSystems based Routes to Innovation (CNR-Italian National Research Council); *Spoke5*: **MADE4IS**-Micro-Accelerator and DEtectors for Innovation and Sustainability (INFN); *Spoke6*: **MicTex**-Microelectronic based Technologies (ST-Microelectronics); *Spoke7*: **I3**-Industrial & ICT Innovation (Meridionale Impianti); *Spoke8*: **MedTex**-Medical oriented Technologies (UPMC Itay, University of Pittsburgh Medical Center); *Spoke9*: **R2I**-Route to Innovation (Quantum Leep).

THE INFN SPOKE

Spoke operates in the frame of the international network established along the years by INFN; spoke-aims will be carried out in close synergy with the two affiliated partners Catania and Palermo Universities.

The main specific goals of the INFN-Spoke (LNS plus Catania Division) can be condensed on five technological developments or work packages (WPs): *WP1*-Micro accelerators for Health and Energy applications; *WP2*-Micro and nano beams for Health and Energy; *WP3*-Photodetectors and digital ACQ for Environment, Health, Agritech; *WP4*-Micro detectors for particle therapy, dosimetry e micro-dosimetry; *WP5*-Detectors and technologies for Fusion Power.

All these proposed technological innovations would strongly impact on society, thanks also to the internationally recognized INFN expertise on radiation detection, particle accelerators, nuclear and plasma physics, and its experience in dissemination and technology transfer-oriented actions.

Work Package 1 is focused on the need of compact and miniaturized (laser-plasma or dielectric-laser) particle accelerators for: *i)* medical treatment and/or imaging systems, to be installed in Hospital; *ii)* carbon free energy production via ICF-Inertial Fusion, or by accelerator driven subcritical fission reactors. New particle acceleration concepts based on the frontiers of the Laser-Plasma (LP) and Dielectric- Laser Acceleration (DLA) will be investigated, reaching accelerating or focusing gradients orders of magnitude higher than those of

conventional accelerators. A high-power, high-intensity and ultra-short laser of appropriate repetition rate will be coupled with advanced micro and nano-structured materials to extend the frontier of electrons, ions, gamma and neutrons production on a table-top and portable scale for health and energy applications. In order to demonstrate/obtain increased acceleration length, a compact and low energy (μ/mJ class) laser will be coupled to the manufactured DLA prototypes. In particular, we will focus on the fabrication of three-dimensional photonic-crystal structures, adopting special Direct Laser Writing (DLW) - based optical lithography techniques, aiming at achieving the required spatial resolutions of tens of nanometers. This activity is entirely carried out at LNS-INFN.

Work Package 2 - The availability of proton and light ions in the keV and MeV ranges represents a breakthrough in the study of fundamental functions in living cells and sub-cellular organelles, as well as in the latest approach in radiation oncology such as Microbeam Radiation Therapy (MRT). WP2 aims to develop technologies based on micro/nano tapered glass capillaries and nanotubes fed by protons and ion beams, to be focused on a submicron scale in order to irradiate single cells; an adequate live imaging approach will follow the outcome of irradiation, even in single particle regime. In addition, bundles of capillaries or nanotubes will be manufactured to produce parallel microbeams array needed for MRT. Monte Carlo codes and Finite Elements simulations can be used to model beam transmission, implementing guiding mechanisms in nanotubes/nanocapillaries such as charge-up, charge diffusion and transport. Nano capillaries and nanotubes with different surface structure, roughness, insulating materials, geometries and clustering displacement /alignment will be designed and developed. The capillaries/nanotubes will be coupled to beams available at INFN-LNS for the characterization and fine- tuning of the software codes, through the use of dedicated micro beam diagnostics. This activity is entirely carried out at LNS-INFN.

Work Package 3 aims to develop photo-detectors and related data-acquisition systems for environment monitoring, as well as to development of sustainable technologies in agriculture and health applications. Primary attention is devoted to groundwater, both for saving and quality monitoring, such as for accidental release of pollutants, i.e. whenever real time equipment is used to raise early warning in order to prevent higher levels of contamination. Innovative photo-sensors for environment, agriculture, health and cultural heritage studies and monitoring will be studied as they will be a basic platform for innovative biosensor development; a tool for environment monitoring studies based on light absorption spectroscopy in water or air. In addition, applications for a TOF-PET can be exploited. WP3 investigations on photo-sensors will focus on some key technologies: silicon avalanche photo-diode (APD); analog and digital silicon photomultipliers; wide-bandgap semiconductor (SiC) photo-sensors; cmos image sensors; wavelength shifter couplings. A further task will be the design of SiC APD arrays. The main applications of SiC photosensors being to obtain a solar blind detector in the ultraviolet band, where several elements and materials show absorption and emission lines. This activity is entirely carried out at INFN – Catania Division.

Work Package 4 aims to develop new SiC particle detectors for dose measurements in radiation dosimetry, including radiation hardness validation, high sensitivity, small dimensions, fast response, energy and dose rate independence, and tissue equivalence. WP4 will be organized in two tasks: WP4.1 characterization and optimization of ultra-thin SiC devices, in single and 2D array configurations, for real-time beam monitoring and dosimetry (supported by dose measurements acquired through Electron Paramagnetic Resonance with alanine detectors); WP 4.2-R&D on new SiC microdosimeters (at a single event level) for measuring the random processes of energy deposition in micrometric sites: it can change the paradigm of particle therapy treatments. A quality assurance program based on LET (Linear Energy Transfer) and RBE-(Relative Biological Effectiveness) estimation to optimize the clinical treatment planning will be performed. The new detectors, able to identify the contribution from different species in local sites of the order of 2-3 um, will be able to change the paradigm of particle therapy treatments and to perform, on the same chip, both dosimetric and microdosimetric measurements. This activity is carried out in collaboration between INFN - LNS and Catania Division.

Work Package 5- Thermonuclear Fusion represents the most attractive scenario for delivering to humankind safe and sustainable low-carbon energy, aiming at in-plasma ignition of thermonuclear fuel by two approaches: a) ICF-Inertial Fusion; b) Magnetically-Confined Fusion (MCF). The availability of new technologies in the manufacture of micro and nano-materials and innovative diagnostics and detectors, plays a crucial role. R&D, hence, will deal with new materials and innovative detectors. Materials i) Nanostructured targets (nanotubes, nanowires, et.) to embed the thermonuclear fuel and maximize the efficiency of laser-matter energy transfer; ii) advanced micro-nano structures covering the plasma chamber walls for the control and optimisation of plasma-walls interaction in magneto-plasma reactors, including the tailoring of electromagnetic field structures. Detectors New devices for X-ray detection; new interferometers, polarimeters and Thomson scattering systems in sub-THz range and up to optical domain (eventually in space and time-resolved way) for plasma density and temperature monitoring. This activity is entirely carried out at LNS-INFN.

REFERENCES

[1] https://samothrace.eu

Micro accelerators for health and energy applications within the SAMOTHRACE ecosystem

C. Altana[1], G.A.P. Cirrone[1], S. Gammino[1], P. Litrico[1], G. Messina[1], M. Musumeci[1], A. Amato[1], R. Avolio[1], C. Calì[1], M. Costa[1], V. Lo Vecchio[1], A. Massara[1], S. Passarello[1], L. Pandola[1], G. Passaro[1], S. Pulvirenti[1], G. Torrisi[1], G.Vecchio[1] and S. Tudisco[1]

1) INFN-Laboraratori Nazionali del Sud, Catania, Italy

Abstract - Within the SAMOTHRACE ecosystem the INFN spoke5 on Micro-Accelerator and DEtectors for Innovation and Sustainability (MADE4IS) is subdivided into different WP. The WP1 is devoted to Micro accelerators for Health and Energy applications, which goal is the development of a two classes of micro-scale accelerators based on the interaction of high-power lasers with matter: a prototype of a Laser-Plasma (LP) accelerator and a Dielectric Laser (DL) accelerator.

This report provides a description of the WP1 activities of SAMOTHRACE Spoke5 and a first discussion of the prototypes specifications.

MICRO ACCELERATORS FOR HEALTH AND ENERGY APPLICATIONS: AIMS

The goal of the project is the design, realization and characterizations of prototypes of laser-plasma (LP) accelerators - based on the interaction of the high-power laser with solid targets for a novel particle acceleration setup and of laser dielectric accelerator to obtain dielectric guiding structures able to sustain an accelerating Transverse Magnetic $(TM)_{01}$-like field synchronous with particle velocity at accelerating gradient >200 MV/m and dielectric waveguide couplers and mode launchers able to convert the Transverse Electric (TE)-like mode from the laser to the TM accelerating field.

These setups will have implications in the accelerators, medical and energetic field connected to the fusion processes and will open potentially practical applications including radiotherapy; hadronic therapy; generation of X-ray beams for diagnostics; advanced imaging; isotope production; realization of tabletop free-electron lasers; ion implantation in semiconductor chip fabrication.

Laser-Plasma acceleration

The laser-plasma accelerator is based on the Target Normal Sheath Acceleration (TNSA) method [1-2], an innovative approach in which a high-intensity laser beam is meticulously transported to a solid target. The laser is precisely focused onto the target surface, initiating a remarkable phenomenon. As the laser strikes the solid target, it generates a plasma sheath at the target's rear surface.

The interaction between the intense laser field and the plasma sheath leads to the acceleration of charged particles, predominantly ions, to high velocities. This accelerated plasma stream, rich in energetic particles, becomes a potent source for various applications, ranging from fundamental physics research to potential applications in medical and industrial fields. In this contest, two aspects are of fundamental importance:

- the Target Station (TS), a system for the precise target positioning. It ensures that the laser beam accurately strikes the solid target, optimizing the efficiency of the acceleration process.
- the Test Bench (TB) for the laser transport and optical focusing on target. In fact, the high-intensity laser beam is transported from its point of origin, often a pulsed laser system, to the location of the target. This can be achieved using optical systems such as mirrors and lenses that guide the laser path towards the desired target. Once the laser reaches the vicinity of the target, a series of optical lenses are employed to focus the beam. Focusing is a critical process where the laser beam is concentrated on a small area on the target surface. This is essential to achieve extremely high light intensities required to initiate the plasma acceleration process.

Dielectric-Laser acceleration

The maturity of solid-state laser technology is already at (or near) the capabilities required for a laser-driven microstructure accelerator based on Dielectric Laser Acceleration [3-4]. In this case fields from lasers can be used for acceleration of charged particles up to tens of MeV in nanofabricated dielectric structures of few millimeters length based on planar symmetric gratings, hollow core fibers, photonic crystals, and plasmonic meta-surfaces. The activity is focused on the design of innovative dielectric laser particle accelerating structures/schemes based on both sub-relativistic and relativistic sections, which have been studied and simulated. The final goal will be the demonstration of an integrated multi-stage particle dielectric laser accelerator able to validate the potential to scale to energy levels (MeV) of interest for "real-world" applications.

THE MICRO-ACCELERATOR PROTOTYPES

Technical specifications for both laser-plasma and dielectric-laser accelerators are discussed.

LP accelerator prototype

The TS system for proton/ion acceleration was designed. It is composed by:

1) A Target-Tower with a 5-axis positioning system with high sensitivity and precision; it operates in high vacuum, at $1x10^{-6}$ mbar;

2) A CCD camera, also motorized, for the alignment of the target with the laser spot.

In Figure 1 a version of the target tower (representing the main part of the accelerator in the laser-plasma approach) is reported.

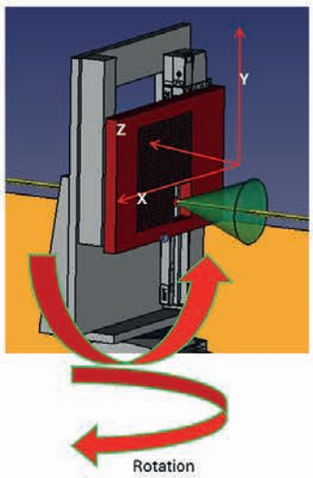

Figure 1: 3D drawing of the target system representing the main part of the micro-accelerator in the laser-plasma approach.

In particular, the target tower is equipped with five motorized axes: three axes which will allow to translate the target holder in the X, Y and Z directions, a rotation along the Y axis and a tilt motion.

Solid targets, that could be both metallic and plastic materials, will be mounted in special holders that protect adjacent targets from heat transfer and shockwave damages induced by laser–plasma interaction.

Another important aspect is the alignment system, that plays a crucial role in the target station, because allows the fine alignment of the target tower and the definition of the shooting spots. The idea is to use a needle to identify the position of the laser focal point, and images it into a CCD camera through the use of a microscope objective.

DL accelerator prototype

A tapered slot waveguide has been simulated since the waveguide rib width can be tailored for matching the wave phase velocity $v\phi$ to the electron velocity along the accelerator. Then, PIC simulations of different tapering profiles have been carried out up to the optimal one. The Hamiltonian of the waveguide system has been derived and the conditions needed for net acceleration for the slot waveguide DLA have been obtained. For practical applications, a bunched electron source has been selected for a PIC simulation. The acceleration factor (or "damage factor") of the structure has been also evaluated to find the upper limit of the accelerating gradient for the structure. Concerning the relativistic section, a woodpile crystal - that consists of a “pile” of rectangular bricks, with a cross section w × h, are stacked has been selected. Bricks in each layer of the pile are rotated by 90 deg with respect to the bricks in the previous one; thus, the resulting total structure is composed of several layers with brick axes alternatively aligned along x or z. The final executive design has been obtained for both the sub relativistic and relativistic prototypes and are shown in Fig. 2.

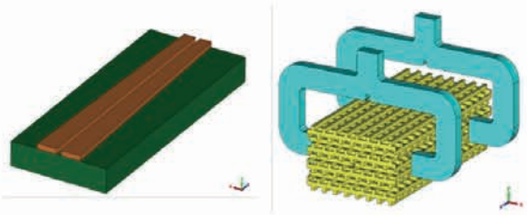

Figure 2: 3D drawing of the final versions of the (Left): sub-relativistic structure; (Right): silicon woodpile waveguide (yellow part) and input waveguides (light blue parts, only for simulating the laser excitation).

A sensitivity study has been performed for evaluating the required features and tolerances including the proposed method and processes of fabrication. In particular, the slot waveguide - formed by two high refractive index photonic wires surrounded by a low refractive index medium - will be fabricated by exploiting the Silicon-On-Insulator (SOI) technology. For the woodpile a 3D printing technique based two-photon polymerization (TPP) able to fabricate 3D nano/micro-structures with sub-100-nm resolution. The operative wavelength is $\lambda = 5$ μm for both prototypes.

CONCLUSIONS

This report has outlined the WP1 activities conducted inside MADE4IS, spoke5 of SAMOTHRACE ecosystem [5] at INFN-LNS concerning the development of Micro accelerators prototypes for Health and Energy applications. The work was focused on the definition of the specifications for the design of the target station for laser-plasma acceleration and of the dielectric laser particle accelerating structures/schemes. The next step will be the purchase, the development, and the mechanical assembly of the prototypes.

REFERENCES

[1] M. Passoni et al., New Journal of Physics, 12(4), 045012, (2010).

[2] A. Macchi, et al., Reviews of Modern Physics, 85(2), 751, (2013).

[3] E. A. Peralta et al., Nature 503, 91 (2013).

[4] J. Breuer, P. Hommelhoff, Phys. Rev. Lett. 111, 134803 (2013).

[5] https://samothrace.eu

Microbeams with glass capillaries within the SAMOTHRACE ecosystem

S. Amaducci[1], G. Calabrese[1], G. Castro[1], L. Celona[1], L. Cosentino[1], M. Costa[1], C. Manna[1], A. Massara[1], G. Mauro[1], G. Messina[1], O. Leonardi[1], S. Passarello[1], A. Pidatella[1], G. Torrisi[1], G. Vecchio[1] and S. Tudisco[1]

1) INFN-Laboratori Nazionali del Sud, Catan , Italy

Abstract – Within the SAMOTHRACE project, a research line (Spoke5 - WP2) aims to develop an experimental prototype for the production and characterization of ion microbeams, with dimensions down to a few micrometers and energy from keV to several MeV. These microbeams will be available to the scientific community working in various scientific and technological fields, such as high-resolution surface mapping and selective irradiation of internal parts of a cell. The core of this system is represented by glass microcapillaries placed at the end of a beam line, which by collimating and focusing a common ion beam coming from an ion source or a particle accelerator, can reduce its size even below one micrometer.

INTRODUCTION

Ion beams represent a powerful tool in several scientific and application fields beyond nuclear and particle physics. Materials science, as well as microbiology, electronics and medicine have profited greatly from the peculiar characteristics of fluxes of energetic ions. Although the range of applications is extremely broad, it is easy to understand that the availability of beams with micrometric dimensions can allow spatially resolved irradiation to be carried out, which in many fields can represent a real breakthrough. An example is the induction of spatially selective inactivation or destruction of arbitrary cellular structures, to investigate their functions in living cells with real-time monitoring of the irradiated region. Among the various techniques for producing microbeams in a compact way, one of the most promising is based on tapered glass microcapillaries [1,2,3], which can provide progressive collimation and focusing of the beams in the keV and MeV energy range [4,5]. The typical glass capillary has an entrance window of about 1 mm and an exit one down to one micrometer or less. Beam injection is a very crucial aspect and needs to be optimized by shaping suitably the beam to optimize the micro-injection inside the capillary. It is done by using high precision mobile slits in axis with the capillary, installed a few meters upstream. Transmission through capillary walls depends primarily on the energy range of the beam and is classified accordingly. In case of keV ions, immediately after the injection most of them implant inside the inner walls, producing patches of charge which over time produce electric potential, which gradually influences the trajectory of the incoming particles, bending their tracks and favoring transmission of the beam through the capillary. This self-lensing phenomenon is known as the self-organized charging effect. By the same principle ions can be guided through a tilted capillary, once a charge patch is formed in the bent section of the capillary. For MeV ions this effect is not effective, because the potential is not high enough to reflect their trajectory, so the guidance through the capillary is mainly due to Rutherford scattering and is not as effective as for lower energy particles.

DESCRIPTION OF THE SETUP

We started a fruitful scientific collaboration with the group operating at Riken Pelletron facility, where a microbeam line using glass capillaries is operational using beams accelerated by the 1.7 MV Tandem. Our goal is to develop an advanced equipment for the production of microbeams with a similar technique, capable of characterizing the properties of the beam in different operating conditions and different geometries of the capillary. This equipment must be easily moved and installed in a standard beam line, where KeV or MeV beams are available. The adoption of sub-micrometer translation and rotation stages, as well as suitable high sensitivity beam diagnostics, will ensure efficient remote control and real-time monitoring during all the alignment procedures. It will be also used during irradiation processes of organic and inorganic samples, in order to monitor the irradiate sample, and naturally beam operations can be performed both in air and in vacuum when needed.

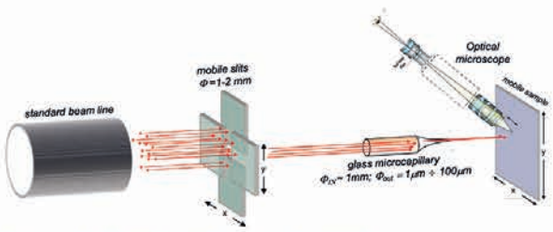

Figure 1: Sketch of the microbeam line

The whole equipment consists of two units to be installed along the beam line. One is an aluminum vacuum chamber containing two pairs of mobile slits, located a few meters upstream of the second unit which houses the capillary and beam diagnostics. This configuration should ensure the effective micro-injection inside the capillary, which represents the final element of the beam line. The capillary is fixed in a submicrometric hexapod which, allowing movements on 5 axes, allows for high precision

alignment procedures. If necessary the second chamber can work at atmospheric pressure, as in the case of cell irradiation, a capillary closed with a cap will be used. A careful characterization of the microbeam requires adequate beam imaging diagnostics, which is made up of a scintillating plate intercepting the beam and a high sensitivity CMOS camera (QE ≈ 90%), equipped with microscopic optical lenses. The magnification factor of the optical lens allows for the required sub-micrometer spatial resolution, necessary to control the beam profile with high precision and to visualize the finest details of the irradiated sample. Moreover, a particle detector for measuring beam current and energy spectra is used, to better optimize the transmission through the capillary. We are moving to use the new generation SiC detector, which by combining all the advantages of semiconductor detectors (such as compactness and energy resolution) with a high resistivity to radiation damage, should be the optimal solution, covering intensity from single particle regime to $10^5 - 10^6$ particles per second.

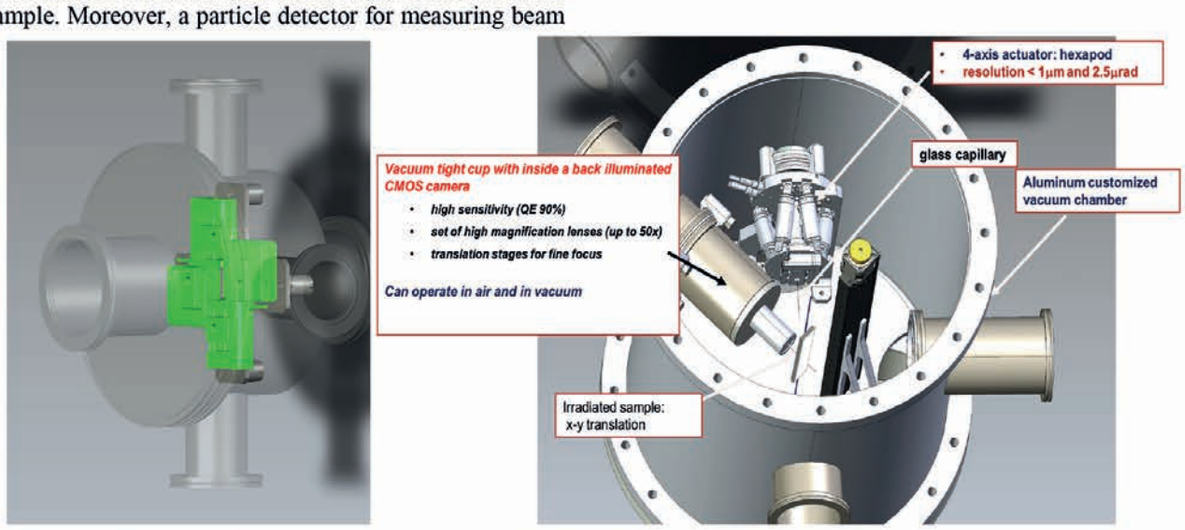

Figure 2: Sketches of the two aluminum vacuum chambers housing the slits and the microbeam equipment. They can be installed wherever a beam is available, within a few meters of each other. A dedicated pumping station equips the vacuum chambers

FINAL DESIGN

In Fig. 2 a sketch of the vacuum chambers containing the slits and the capillary with the diagnostics. Dedicated simulation codes were run to study particle transmission through the capillary, with different geometries in the keV and MeV energy ranges. These allow us to study how the length, tapering angle and size of the windows influence the beam transmission and energy resolution [6]. The ultimate goal is to produce customized capillaries for any type of microbeam, with geometry optimized to maximize beam transmission and possibly preserve energy resolution. These capillaries will be produced at LNS by using a dedicated puller and a microforge.

POSSIBLE APPLICATION

As said, one of the most interesting applications of microbeams is the study of fundamental functions in living cells, by spatially selective irradiation of cellular structures [7,8]. This activity can represent a first test bench for this technique, with the further characteristic of studying the dynamics inside the cell during and immediately after irradiation, thanks to the high-sensitivity imaging system equipped with microscopic optics.

ACKNOWLEDGEMENTS

This work has been funded by European Union (NextGeneration EU), through the MUR-PNRR Project SAMOTHRACE (ECS00000022).

REFERENCES

[1] T. Ikeda et al., NIM B470 (2020) 42-47.
[2] T. Hikeda et al., Surface & Coatings Technology 206 (2011) 859-863.
[3] T. Ikeda Quantum Beam Sci. 2020, 4, 22.
[4] G.U.L. Nagy et al., NIM B460 (2019) 216–219
[5] Marko Brajković et al., NIM B 461 (2019) 237–242
[6] M.J. Simon et al., NIM B330 (2014) 11–17
[7] V. Mäckel et al., Rev. Sci. Instrum. 85, 014302 (2014)
[8] Iwai et al. Appl. Phys. Lett. 92, 023509 (2008)

Micro detectors for particle therapy, dosimetry, and micro-dosimetry within the SAMOTHRACE ecosystem

N.S. Martorana[1], C. Altana[2], A. Barbon[1,3], P. Belluomo[1], G. Cardella[1], G. A. P. Cirrone[2], G. D'Agata[1,3], E. De Filippo[1], M.C. D'Oca[4], P. Figuera[2], E. Geraci[1,3], B. Gnoffo[1,3], A. Grimaldi[1], C. Guazzoni[5], L. Lamia[2,3], G. Lanzalone[6,2], M. Marrale[4], E.V. Pagano[2], S. Pirrone[1], G. Politi[1,3], L. Quattrocchi[1,7], F. Risitano[1,7], F. Rizzo[2,3], F. Romano[1], S. Romano[2,3], P. Russotto[2], M. G. Salemi[1], M. Trimarchi[1,7], C. Zagami[2,3] and S. Tudisco[2]

1) INFN-Sezione di Catania, Catania, Italy
2) INFN-LNS, Catania, Italy
3) Dipartimento di Fisica e Astronomia "Ettore Majorana", Università degli Studi di Catania, Catania, Italy
4) Dipartimento di Fisica e Chimica "Emilio Segrè", Università degli Studi di Palermo, Palermo, Italy
5) DEIB Politecnico Milano and INFN Sez. Milano, Milano, Italy
6) Università "Kore"di Enna-Enna, Italy
7) Dipartimento MIFT, Università di Messina, Messina, Italy

Abstract - In recent years, there has been an increasing interest in the development of detectors based on Silicon Carbide (SiC) technology. SiC is a semiconductor with significant features, among which the radiation hardness, that render this material promising in the detection of charged particles, neutrons, and ɣ/X radiation. Presently, SiC finds applications in both nuclear physics and medical research. Within the SAMOTHRACE (Sicilian Micro and Nano Technology Research and Innovation Center) ecosystem, a development of SiC detectors is ongoing with the aim to employ this technology for dosimetry, micro-dosimetry, and beam monitoring, for ɣ, electrons, and ion clinical radiation beams. This report provides a description of the WP4 activities of SAMOTHRACE Spoke5 and an overview of recent results obtained within this context at INFN-LNS.

SAMOTHRACE SPOKE 5 WP4: AIMS AND PERSPECTIVES

Silicon Carbide (SiC) detectors represent a promising technology for the detection of charged particles and radiations and they are also indicated as viable alternatives to Si detectors, for both nuclear and medical studies. There are several SiC polytypes, which differ from each other due to the variations in the stacking order of the SiC structure. The most commercially available types are 3C-SiC, 4H-SiC, and 6H-SiC. Due to its higher bandgap in comparison to 6H-SiC and 3C-SiC, 4H-SiC is typically the first choice for SiC detectors. This preference arises because most of the other characteristics are generally similar between the three polytypes. SiC detectors present numerous features that make this material advantageous also with respect to the Si one. Among them the radiation hardness, which makes them suitable for environments with high levels of radiations, the temperature resistance, and the wide band gap, which allows for a higher signal-to-noise ratio with respect to the Si detectors and makes them insensitive to visible light [1-3].

Advancements in the fabrication of SiC detectors continue today, and with it the wide interest of researchers in evaluating the potentialities of this material. Different are the drivers for such interest. First, it concerns the medical physics and the possibility to use dosimeters, micro-dosimeters and beam monitoring based on SiC technology to improve the clinical approach [4]. The second motivation concerns the nuclear field, using both high-intensity stable and unstable beams, and the development of SiC detector arrays as tagging elements for the production of high-intensity Radioactive Ion Beams (RIBs) with the in-flight method [5-6]. Concerning the first topic, it is important to underline that nowadays the interest in hadron therapy is growing fast also thanks to the latest technological advances in accelerators and delivery technologies [4]. Overall, achieving a precise assessment of the beam quality and accurately evaluating the biological effectiveness of various radiations are essential steps to fully exploit the advantages of hadron therapy with respect to the conventional methods [4]. In this framework, solid state sensors have been studied so-far for dosimetry, micro-dosimetry and beam monitoring. Among them, silicon carbide sensors are indicated as a great compromise between the good established fabrication techniques of silicon sensors and the robustness of the diamond material. Due to their radiation hardness, SiC are also important because they can be used employing new radiotherapy techniques, as the FLASH one [4].

Within the SAMOTHRACE ecosystem [7], and in detail thanks to the work of WP4, Spoke 5, a significant effort to characterize SiC detectors has been made and this effort is still ongoing. The SAMOTHRACE ecosystem aims to generate an important technological advancement thanks to the collaboration among several actors in the

area of microelectronics, microsystems, materials and micro technologies that operate in the Sicilian territory [7]. SAMOTHRACE focuses on the European Commission global challenges *Digital, Industry & Space*, *Health*, *Energy & Mobility*, *Agriculture & Environment* [7]. The goal of the pillar *Health* is the development of new technologies based on micro-nano electronics and sensors to produce a progress in several fields of healthcare [7]. In particular, the WP4 activities of SAMOTHRACE Spoke5 aim at the characterization and at the development of SiC sensors for dosimeter, micro-dosimeter and beam monitor, for ɣ, electrons and ion clinics radiation beams. This activity is made possible thanks to the collaboration and synergy of several institutions, which include researchers and technicians mainly from the INFN-Sezione di Catania, the INFN-Laboratori Nazionali del Sud, the Dipartimento di Fisica e Astronomia "Ettore Majorana", UNICT, and Dipartimento di Fisica e Chimica "Emilio Segrè", UNIPA.

EXPERIMENTAL RESULTS AT INFN-LNS

The focus of the activity so far performed at INFN-LNS has been the characterization and the optimization of thin monolithic SiC detectors performances in terms of energy and timing resolution, maximizing the signal-to-noise ratio. Additional work has been done to gain a thorough understanding of potential inter-pads, cross-talk and edge effects. The investigations have been performed at the INFN-LNS, using a ^{148}Gd radioactive α source. Figure 1 shows the detectors test point with the vacuum chamber and some electronics, used at the LNS for the preliminary prototype qualification. Furthermore, the obtained results have been compared with simulations studies performed with the GEANT4 simulation toolkit [8]. An active work is ongoing to improve the signal-to-noise ratio, particularly through optimization of dedicated electronics chains and acquisition systems. An additional work with tests and simulations is underway in order to better define the structure of new silicon carbide devices that will be produced. This work will include: a test at the LABEC (INFN e Dipartimento di Fisica e Astronomia, Università di Firenze) laboratory using a proton beam, with the main intent to test the response function of detectors, to fully explore and to understand what observed with the α source and to analyze also the linearity of the SiC response function; an experiment at the HIL laboratory in Warsaw using carbon beams in order to test a fast-electronics front end specifically implemented for fast-timing measurements [9]; a comparison with standard alanine dosimeters response function [10]; the use of X-ray facility of INFN-LNS to test the response of the dosimeter to ɣ radiation. Finally, electron beams available also using flash intensity will be used with both the new SiC prototypes and the alanine detectors to validate the SiC response function.

Figure 1: Test point with vacuum chamber and electronics at the INFN-LNS, used for the preliminary prototype qualification.

CONCLUSIONS AND PERSPECTIVES

This report has outlined the WP4 activities conducted inside the SAMOTHRACE Spoke5 ecosystem at INFN-LNS, concerning the advancement in the development of silicon carbide detectors. The aim of the WP4 activity is the development of SiC sensors for dosimetry, micro-dosimetry and beam monitoring. The current work and forthcoming steps are focused on a deeper understanding of the thin SiC detectors using both radioactive sources and beams, with the main goal to optimize the SiC detectors response and to compare it with the standard alanine detectors. Subsequently, taking advantages of these results, a production phase of new silicon carbide sensors will be started.

REFERENCES

[1] M. De Napoli, Front. in Phys. 10:898833 (2022) and refs therein.
[2] S. Tudisco et al., Sensors 18 (2018) 2289 and refs therein.
[3] C. Altana et al., Sensors 23 (2023) 6522.
[4] G. Parisi et al., Front. Phys. 10:1035956 (2022) and refs therein.
[5] Martorana N. S. et al., Front. in Phys. 10:1058419(2022) and refs therein.
[6] Martorana N.S. et al., contribution to this report (2024).
[7] https://samothrace.eu/.
[8] https://geant4.web.cern.ch/.
[9] A. Castoldi et al., IEEE Trans. Nucl. Sci. VOL. 70NO. 7 (2023) pp. 1431-1435.
[10] M. Marrale et al., NIM B 368 (2016) 96-102.

Detectorsand technologies for fusion plasmas within the samothrace ecosystem

D. Mascali[1], E. Naselli[1], A. Amato[1], D. Bonanno[1], G. Calabrese[1], C. Calì[1], P. Cirrone[1], M. Costa[1], G. Finocchiaro[1], S. Gammino[1], A. Massara[1], G. Messina[1], G. Mauro[1], L. Neri[1], G. Passaro[1], S. Passarello[1], E. Pagano[1], A. Russo[1], R. Catalano[1], G. Torrisi[1] and S. Tudisco[1]

1) INFN-Laboratori Nazionali del Sud, Catania, Italy

Abstract

Laboratory-plasmas are studied by means of diagnostics systems for plasma density and temperature monitoring. Setup and tools – at LNS typically at the service of particle accelerators, applications and fundamental nuclear physics research - are being redesigning and improving for application in controlled nuclear fusion, including new techniques and detectors schemes, in the frame of SAMOTHRACE (SiciliAn MicronanOTecH Research And innovation CEnter, EU Next Gen Program).

INTRODUCTION

Thermonuclear fusion represents the most attractive scenario for delivering to humankind safe and sustainable low-carbon energy, aiming at in-plasma ignition of thermonuclear fuel by two approaches: a) ICF-Inertial Fusion; b) Magnetically-Confined Fusion (MCF). The availability of new technologies in the manufacture of micro and nano-materials and innovative diagnostics and detectors, plays a crucial role. R&D, hence, deal with new materials and innovative detectors. The first specific aim of the WG5-activity is to design and develop advanced diagnostics testbenches for detectors and techniques development (X-ray/optical spectroscopy, X-ray imaging and tomography, mm-wave polarimetry) beyond the state of art, making them suitable for applications in controlled nuclear fusion for plasma density and temperature monitoring. INFN-LNS ensures strong expertise in ion sources and plasma traps, ion beam and plasma diagnostics, Particle-in-Cell simulations for plasma modelling, 3D Monte Carlo simulations to develop and design sensors systems. This is crucial for benchmarking the numerical toolkit with experimental data.

PLASMA DIAGNOSTICS

Plasma diagnostics, especially in the range of soft-X rays, play a crucial role in investigating laboratory magnetized plasmas. Several detectors and techniques were developed in the recent past at the INFN-LNS to perform volumetric X-ray spectroscopy (by Silicon Drift Detector-SDD [1]) and X-ray imaging (by CCD pin-hole technique [2, 3]).
The aim of the WG5-activity is to design and develop an X-ray advanced diagnostics testbench where detectors and techniques can be properly developed and improved with respect to the state of art for application in controlled nuclear fusion plasmas [4, 5] and plasma physics [6, 7], thus, tested, characterized, and used simultaneously. The X-ray pinhole CCD camera setup [8] allows to perform X-ray plasma imaging and space-resolved spectroscopy [9, 10, 11]. Innovative analysis algorithms were properly developed for obtaining Single Photon-Counted (SPhC) images providing the local plasma emitted spectrum in a High-Dynamic-Range (HDR) mode [12], also removing the readout noise. Several improvements are needed to make the space-resolved spectroscopic analysis more quantitative and overcome the criticalities intrinsically induced by the SPhC algorithm.
In the framework of SAMOTHRACE SPOKE-INFN WP5 task, the new X-ray diagnostic prototype PYN-HO (Probing x-raYs by imagiNg and pin-Hole spectrOscopy) has been developed, able to operate in four different configurations: (A) X-ray calibration and characterization; (B) X-ray imaging and spectroscopy in magnetized plasma; (C) Diffractometric measurements on test-bench and in plasma; (D) Optical emission spectroscopy on test-bench and in-plasma. As a first step, we built the test bench to perform energy and quantum efficiency calibration of the CCD, i.e. configuration (A), as shown in Figure 1.

Figure 1: Pictures of the PYN-HO prototype operating in the first configuration for testbench measurements.

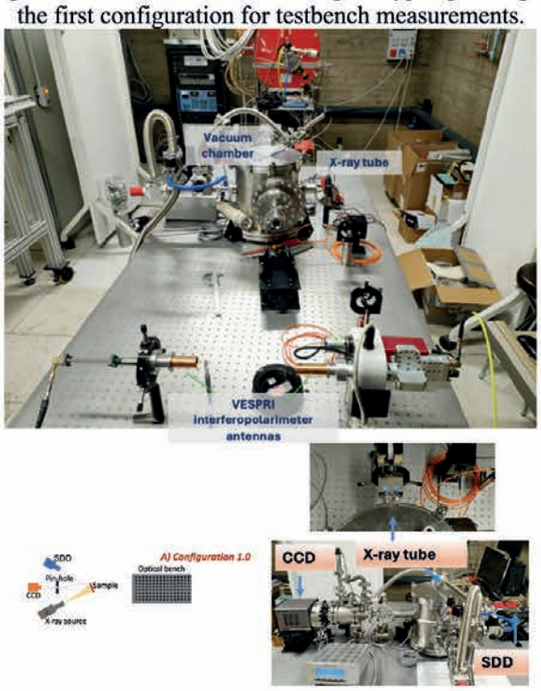

Different X-ray sources were needed to calibrate and characterize the spectroscopy CCD system, and a SDD sensitive to low energies is required as a reference to normalize the CCD space-resolved spectra and correct the post-processed algorithm effects. In addition, SDD is suitable to operate at a very high counting rate to perform volumetric spectroscopy on high X-ray emission fusion plasma. Specific multi-component targets were supplied by the chemical-physical techniques laboratory of the LNS for measurements in the vacuum scattering chamber (see Figure 2).

The activity involves the simultaneous use of an X-ray tube, used as X-ray source in a scattering chamber to irradiate the target, inducing fluorescence emissions from the multi-component material, and of a SDD detector (interchangeable with CCD at high space and energy resolution) for the characterization of the CCD detector in terms of spatial and energy resolution response in single-photon counting operating mode. First characterization has been carried out and a total of 350 X-ray frames (100 seconds of exposure time) were acquired in SPhC mode.

Figure 2: Pictures of the multi-component targets.

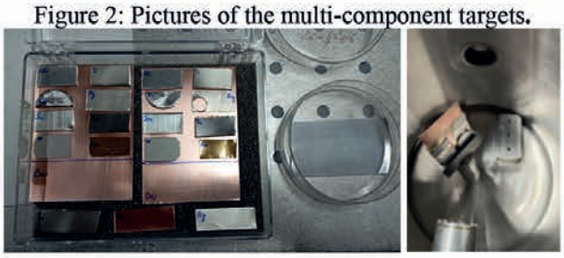

The afore-mentioned systems are compatible to be installed and used in the plasma testbenches - namely FPT (Flexible Plasma Trap) [13] - installed at INFN-LNS for R&D on diagnostics and detectors. In the recent days, the system has been installed (see Figure 3, configuration (B)) and characterization of Argon plasmas via the multi-diagnostic system (high resolution X-ray imaging and spectroscopy using CCD and SDD) is ongoing.

Figure 3: Pictures of the PYN-HO prototype operating in the second configuration for in-plasma measurements.

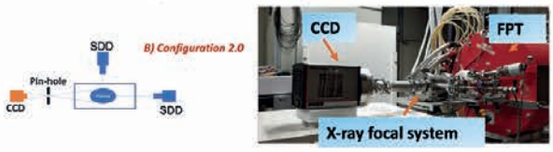

A second task of the WG5-activity aims at the design study of the VESPRI 2.0 mm-wave polarimetry based on a superheterodyne scheme for the measurement of the total electron density based on the measurement of the Faraday rotation [14]. The expected Faraday rotation angle has been evaluated and a mm-wavelength range corresponding to a frequency range of 90–110 GHz was chosen as ideal range. The super-heterodyne approach allows to downshift the detected frequency (1 GHz) compared to the probing one (20 or 100 GHz) to be detected in a 80 GS/s scope to measure the Lissajous's figures. It consists of two W-band horn antennas, the receiving one is connected to an orthomode transducer (OMT), two low-noise amplifiers and two filter. The two output signals of the wave received by the antenna are delivered to two subharmonic mixers which convert the mm-wave to intermediate frequency. The scheme based on the Detection of Lissajous figure consists of direct RF signals detection through a scope. This allows the real-time reconstruction of the State of Polarization (SOP) curve described by the electric field vector. This result can be obtained by using the two channels scope in an x-y representation.

A DEMO operating at lower frequency domain (18-26 GHz) has been developed and first measurements were performed on test-bench (see Figure 1).

The DEMO has now been installed on FPT and a complete plasma characterization is expected soon.

CONCLUSIONS

Two new plasma diagnostic testbenches for laboratory plasma investigation have been developed. The PYN-HO prototype has been conceived for X-ray spectroscopy and imaging measurement and preliminary characterization have been carried out. The VESPRI 2.0 polarimeter is based on the super-heterodyne approach to measure the total electron density through Faraday rotation estimation. A DEMO has been developed, tested at INFN-LNS.

ACKNOWLEDGEMENTS

This work has been funded by European Union (NextGeneration EU), through the MUR-PNRR project SAMOTHRACE (ECS00000022).

REFERENCES

[1] D. Mascali et al., J. Instrum. 12 (2017) C12047
[2] S. Biri et al., J Instrum., 13 (2018) C11016
[3] E. Naselli et al., J. Instrum. 14 (2019) C10008
[4] D. Pacella et al., Plasma Phys. Control. Fusion 46 (2004) 1075
[5] I. Song et al., Curr. Appl. Phys.16 (2016) 10
[6] L.A. McPherson et al., Rev. Sci. Instrum. 87 (2016) 063502
[7] T. Sasaya et al., Sci. Rep. 7 (2017) 5742
[8] S. Biri et al., Journal of Instrumentation 16 (2021) P03003
[9] R. Rácz et al., Plasma Sources Sci. Technol. 26 (2017) 075011
[10] E. Naselli et al., Journal of Instrumentation 17 (2022) C01009
[11] D. Mascali et al., Plasma Phys. Control. Fusion 64 (2022) 035020
[12] E. Naselli et al., Cond. Matter 7(1) (2022) 5
[13] S. Gammino et al., JINST 12 (2017) P07027
[14] G. Torrisi et al., Front. Astron. Space Sci. 9 (2022) 949920

NQSTI spoke-3 INFN task 3.1: atomic, molecular platform for quantum technologies

A. Pidatella[1], A. Galatà[2], C. S. Gallo[2], G. R. Mascali[2,3], G. S. Mauro[1], S. Passarello[1], A. D. Russo[1], G. Torrisi[1], D. Mascali[1]

1) INFN-LNS, Catania, Italy
2) INFN-LNL, Legnaro, Padova, Italy
3)Università La Sapienza, Roma, Italy

Abstract

There is an ongoing research field in quantum technologies which will exploit neutral atoms, molecules, and ions to quantum engineer systems from first principles, with thorough control of interactions, particle statistics, system dimensionality, and even topological or transport properties all the way to the single particle level. Within the NextGeneration EU project NQSTI (National Quantum Science and Technology Institute) novel paradigms from the upstream theoretical activities in such field are used to develop and experimentally demonstrate novel techniques and resources for preparing atomic, molecular, and ionic homogenous and hybrid systems with reduced entropy, enhanced control of external fields and optimized encoding of quantum states. Moreover, experimentally prove reliable, robust, and controllable quantum interfaces between different atomic, molecular, and optical systems to connect them with one another and with those based on solid state platforms. We report here on the activity carried out by INFN-LNS in the concern of the task 3.1, about the development of a plasma based ion source for the production and handling of continuous atomic and molecular isotopic enriched beams cooled down to a few °K level.

INTRODUCTION

Within the aims of the Task 3.1 of Spoke 3 is to develop novel atomic/molecular systems to extend coherence time in quantum system. There is an active field of research in the quantum technologies concerning the measure of the permanent electric dipole moment of specific molecules' electrons in a solid matrix, looking for evidence of CP violation [1]. This atomic-embedding in low-temperature solid matrix conventionally resorts to glow discharge chamber and electrostatic elements to select and transport ions to be embedded [2]. INFN has studied novel techniques to produce isotopic atomic and molecular enriched beams. A scheme to increase the production yield of accelerated beams, to attain a higher than milliampere ionic metallic beam (iron, barium) with an extraction potential between 30 and 50 KV, has been studied. The use of HTC SC dipolar magnet has been taken into consideration, together with the possibility to use permanent magnets with the aid of correction coils to be used in the isotopic separation chamber. The source we have investigated is the Flexible Plasma Trap (FPT) at INFN-LNS, as testbench of an ECR trap to be an ECRIS [3]. This novel strategy, which has never been used before for ion beam production, requires an HV platform, an extraction system plus a diagnostic box. INFN is working on the development of techniques for mastering and controlling the beam, as well as for the selection of the Q/A ratio, to reduce the risks of bad-beam quality.

DEVELOPMENT OF THE PLASMA ION SOURCE

The *upgrade activity* of the FPT into an ECR-based ion source has been pursued, starting from the design of a new plasma chamber, which size and accesses must be compatible with the maintained current magnetic system, as well as with the on-going design of the extraction system and the metal injection technology employed. The designed preliminary system is sketched in the following Figure 1 (a,b); the system conceptualized carry on a degree of novelty, accounting for both RF and metal radial injections, leaving the extraction axis free for including source/beam diagnostics or developing (in the near future) a double extraction scheme – see Figure 1(c). The dimensioning and procurement activity for some RF components has been started.

The design of the extraction system has been completed from the point of view of electrodes' geometry. It is based on the *"accel-decel"* principle and should allow the production of a beam with minimum divergence, to optimize the beamline transmission and the following isotopes selection. The optimization of the extraction elements' positions/voltage is presently ongoing: the idea is to define an extraction system with a fixed geometry but with modifiable relative distances and voltages, to fit with the different extracted currents expected to be produced during the evolution of the project. Results from electrostatic (ES) simulations of the designed FPT extraction system are part of another, more detailed report. The LNS magnets engineer has started the beam optics design and study based on the extraction input delivered in the previous report. The beam optics design requirements have been accounted for good beam quality (optimizing the beam's transmission) and for a good isotopic separation.

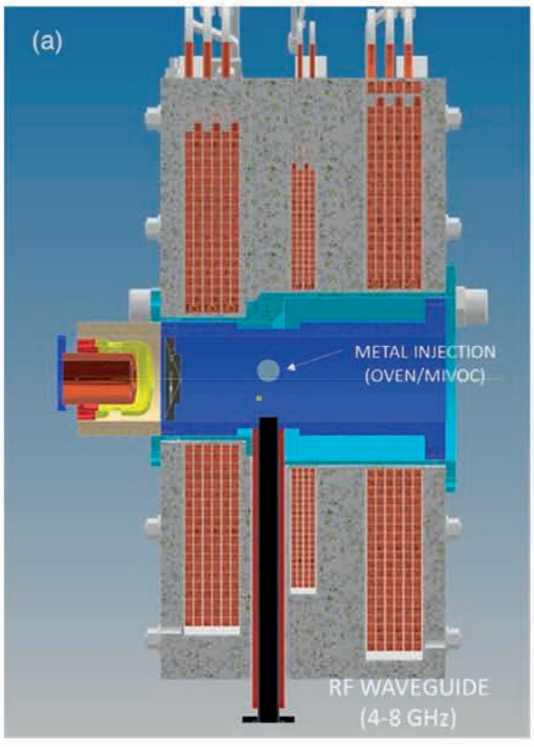

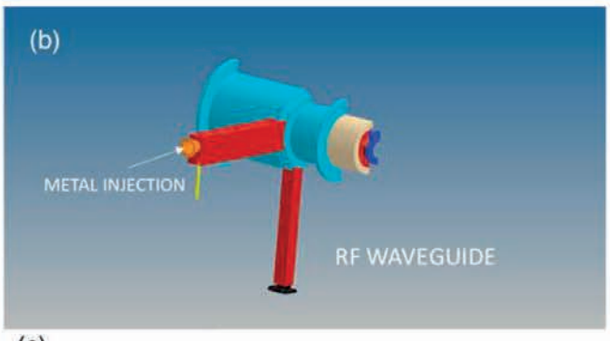

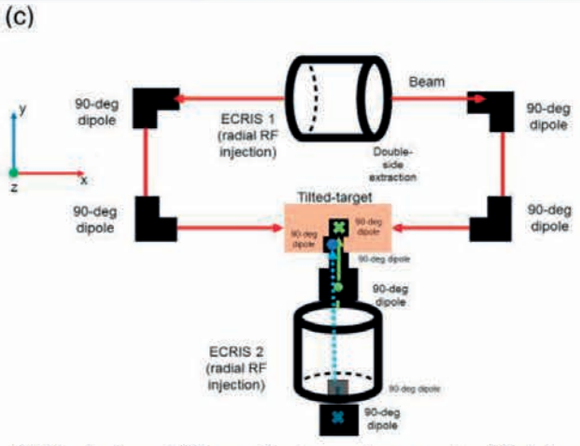

Preliminary results on the beam optics elements required, the resulting beam envelope (proton test beam), and phase-space parameters (among which the resolving power of the dipole magnet) have been obtained. It turns out that a beam transport line including a solenoid and an electrostatic quadruplet, would give a great advantage and versatility in the beam management along the dispersive element/plane. Thus, for a test proton beam and such line, the resolving power is about 1/660, against the desired 1/200 necessary for iron and barium isotopic separation. Further calculations will follow to optimize the transport line, since results so far do not account for charge compensation or space charge effects expected for the designed high-intensity beams.

We started the campaign of instrumentation procurement. We will purchase the power supplies for the extraction system, and a customized travelling wave tube (TWT) as microwave amplifier working in the 5.86-6.75 GHz, with RF power delivering up to 2 kW. The tender call for the latter one will be started within April; the direct assignment to a single supplier for the procurement of the extraction system power supply system is going to be finalized.

At the same time, we explored other possible technical solutions to fulfil the final goal of the project. A possible candidate could be the implementation of a filament ion source, presently installed at GSI: such a source is able to produce very intense beams of metallic species with an optimum beam quality. The Accelerator Division Head of GSI agreed to schedule a week of experiment at GSI in 2024, during which we plan to produce a pulsed Fe+ beam up to 10 mA with a duty cycle of 25%. Those values perfectly fit with the rate of isotopes deposition requested by the project.

CONCLUSIONS

The design of a novel ECRIS for high-intensity metal singly charged ion beams at LNS is almost completed. Numerical design of the extraction system has been performed, finding an optimum system for dealing with multiple kind of beams at different intensities. The source will be involved in preliminary tests in 2024, delivering proton and iron beams, as checking for the ECRIS performance, and as providing a first metal beam, as requested from the NQSTI project's goal.

ACKNOWLEDGEMENTS

This work has been funded by European Union (NextGeneration EU), through the MUR-PNRR project NQSTI (PE0000023).

REFERENCES

[1] ACME Collaboration, Nature 562, 355–360 (2018).
[2] Borghesani AF, Carugno G, Messineo G, Pazzini J. J Chem Phys. 14;159(10):104501 (2023).
[3] Gammino S, et al., J. Instrum. 12, P07027 (2017).

Implementation of a smart and reliable infrastructure for underwater synchronization and acoustic data transmission in the PNRR- ITINERIS project

Danilo Bonanno[1], Letizia Stella Di Mauro[1], Giorgio Riccobene[1], Simone Sanfilippo[1], Didac Diego-Tortosa[1], Salvatore Viola[1]

1) INFN – Laboratori Nazionali del Sud, Catania

Abstract - The PNRR-ITINERIS project will establish the Italian Hub of Research Infrastructures in the environmental science sector and aims to facilitate the study of environmental processes through the atmosphere, the marine domain, the terrestrial biosphere, and the geosphere. As part of the project, the Southern National Lab (LNS) are constructing a wired underwater node that will ensure robust high-speed data connections and the transmission of electrical power from the mainland to the seabed. The use of acoustic sensors within these infrastructures also requires a temporal synchronization system, currently undergoing testing, which will be able to synchronize the measurement and data acquisition devices installed on land and at sea, using the Precision Time Protocol (PTP) IEEE1588.

TIME SYNCHRONIZATION SYSTEMS IN THE UNDERWATER ENVIRONMENT

The challenge of transmitting a precise clock signal, necessary for the synchronization and positioning of underwater systems, also known as "underwater GPS," is crucial when attempting to communicate or coordinate underwater devices or systems in various contexts ranging from oceanographic research to search and rescue operations and extending to the Oil & Gas industry sector.

Several technologies are available on the market, including the use of ad hoc synchronization systems designed specifically for underwater environments and the use of communication technologies suitable for underwater conditions (such as acoustic communication instead of radio waves). Techniques based on USBL (Ultra Short Baseline) or LBL (Long Baseline) are widely used in such solutions. Another solution is the one adopted at the two underwater research infrastructures built by the Southern National Lab (LNS) of the National Institute for Nuclear Physics (INFN), based on the transmission of the GPS signal over fiber optic networks connecting the mainland to the underwater environment.

The LNS-INFN has built and operates two underwater research infrastructures off the coast of eastern Sicily: one at a depth of 2100 meters, 25 kilometers east of the port of Catania, and the other at a depth of 3500 meters, approximately 100 kilometers southeast of Capo Passero (SR).

Both are connected to onshore laboratories via electro-optical cables, allowing for the powering of abyssal

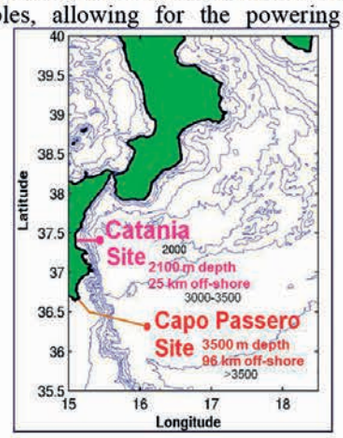

Figure 1: Localization of LNS Research Infrastructures

observatories and real-time transmission of acquired data. These abyssal observatories are equipped with acoustic, optical, and environmental sensors aimed at studying particle astrophysics and conducting research in the marine environment.

ITINERIS (Italian Integrated Environmental Research Infrastructures System)

The technologies developed by INFN for the construction of underwater infrastructures off the coast of Sicily have also enabled participation in the first long-term studies on the identification of acoustic signals in deep marine environments in the Ionian Sea, with a significant impact on various research areas: Marine biology and ecology and Oceanography.

In this context, the LNS-INFN participates in the PNRR-ITINERIS project, which aims to establish the first hub of environmental research infrastructures for the study and observation of atmospheric processes, the marine environment, the terrestrial biosphere, and the geosphere, supporting access to data and services and assisting Italy in addressing present and future climate challenges [1]. Within the project, the LNS coordinates Task 5.7, which aims for a significant expansion of connectivity for underwater scientific instrumentation through the upgrade, both in terms of power and data

transfer systems, of its own underwater infrastructures to accommodate new cabled observatories. This activity includes the design, construction, and testing of a new underwater Junction Box (JB) that will be installed at a depth of approximately 3500 meters and will allow for the distribution of power and optical links to new underwater environmental observation stations. INFN has already successfully designed, built and installed various prototypes of JB capable of interfacing with dozens of observatories simultaneously. About 100 kilometers from the coast and at a depth of 3500 meters, the main cables branch out (thanks to three JB) into a network of electro-optical cables that allow for the distribution of power and data to different instruments and sensors.

UNDERWATER SYNCHRONIZATION USING PRECISION TIME PROTOCOL (PTP)

In the onshore laboratory of Capo Passero, a microSync RX NTP (Network Time Protocol) server from Meinberg [2] is installed, which, thanks to its GPS satellite receiver, can synchronize with Coordinated Universal Time (UTC) and distribute various synchronization signals through different types of connections. In the specific configuration, in addition to serving as an NTP server through one of the four available ethernet ports on the device, the microSync provides two TTL signals (2.5 V), the pulse-per-second (PPS), and a 10 MHz clock.

Most of the sensors connected to the LNS underwater network use a specific implementation of the IEEE 1588v2 protocol (PTP), not yet standardized, called White Rabbit (WR) [3], which allows for synchronization with an accuracy of about 1 ns. In this application, GPS synchronization signals are sent to a WR switch, which acts as a Grandmaster clock and distributes timestamps, with minimal latency, to all nodes in its network. The use of this architecture ensures temporal synchronization of data even over long distances, enabling the creation of synchronous and phased arrays of optical sensors capable of reconstructing the position and/or direction of a source. The same protocol is implemented on the JB for the creation of hydrophone arrays.

IMPLEMENTATION OF A PTP-BASED TIME DISTRIBUTION SYSTEM FOR ITINERIS

The LNS is developing a data transmission and time synchronization system based on the standard IEEE 1588v2 protocol. Although less performant than the WR protocol, the standard PTP protocol easily allows for synchronization, below the microsecond level, of arrays of acoustic sensors, thus enabling the creation of underwater hydrophone phased arrays.

Within the ITINERIS Project, extensive testing is currently underway at the underwater infrastructure of the LNS in Catania on a network architecture that supports, on one hand, the NTP protocol for managing the synchronization of control and data acquisition machines, and on the other hand, a modular and scalable PTP network architecture to which sensors and various measurement devices are connected.

In this architecture, the microSync acts as the Grandmaster clock of the PTP network; two of the four Ethernet ports of the device have been configured to support the PTP protocol simultaneously, on two different network instances. The device has also been configured to provide PPS signals and a 10 MHz clock through a series of connectors of various types on the front panel.

With the addition to the microSync of hardware PTP compliant (SICOM3000A switch [4] and SyncBox/N2X

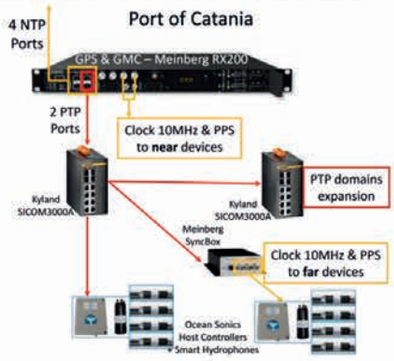

Figure 2: Scheme of the network infrastructure designed for the test site of the Port of Catania.

signal converter [2]), it was possible to create a general-purpose PTP network architecture, as shown in Figure 2, capable of simultaneously synchronizing dozens of devices on land and underwater. During the test, delays between the PPS and the 10 MHz clock signals in a chain consisting of a microSync, a SICOM3000A and a SyncBox were measured. The measurement demonstrates that the temporal synchronization of the signals, measured at both ends of the chain, is contained below 100 ns, as per the specifications of the PTP protocol.

Figure 3: Measurement of the delays.

REFERENCES

[1] Ministero dell'Università e della Ricerca, Direzione generale dell'internazionalizzazione e della comunicazione, ITINERIS proposal. Missione 4, Linea di investimento 3.1 "Fondo per la realizzazione di un sistema integrato di infrastrutture di ricerca e innovazione" finanziato dall'Unione europea–pp. 213

[2] https://www.meinbergglobal.com/

[3] https://white-rabbit.web.cern.ch/

[4] https://www.kyland.com/

Ocean Noise Subsystem for the "Italian Integrated Environmental Research Infrastructures System (ITINERIS)" project

S. Sanfilippo[1], D. Bonanno[1], L.S. Di Mauro[1], G. Riccobene[1], D. Diego-Tortosa[1], S. Viola[1]

1) INFN, Laboratori Nazionali del Sud, Catania, Italy

Abstract – LNS coordinates WP 5.7 of the PNRR - ITINERIS project by developing an underwater Junction Box to be installed at a depth of 3450 m. Within the project, LNS is also involved in developing the *Ocean Noise subsystem*, which is a part of the data collection system envisioned in the project. This contribution demonstrates the capability to collect and analyse acoustic data from the Portopalo test node.

OCEAN ACOUSTICS

The sounds produced by humans, like natural ones, propagate effectively underwater, increasing the overall noise level and overlapping with natural sounds. The seas, once relatively quiet environments where numerous species could efficiently utilize sound as a primary communication channel, have rapidly become extremely noisy. Two categories of anthropogenic sounds can directly or indirectly harm marine fauna: high-intensity impulsive sounds and persistent background noise [1]. While the former is directly linked to specific activities such as the use of sonar or underwater explosions and industrial activities, diffuse noise is due to the presence of hundreds of thousands of ships constantly navigating all the world's seas. Each of these ships produces low-frequency noise that propagates for tens of kilometres, adding to that of others [1]. Consequently, many seas, especially the Mediterranean, have become very noisy due to intense and continuous maritime traffic [2]. Continuous exposure to noise is known to cause increased stress, physiological weakening, difficulties in communication with conspecifics, and the inability to detect prey or predators. It is therefore reasonable to presume that this also applies to all marine organisms that use sound as a primary sense, but this requires further investigations at various levels. Observing the short and long-term effects of noise caused by maritime traffic, at the species, population, and ecosystem levels, requires large-scale long-term monitoring (over decades) to provide time series of data describing how ecosystems respond to this pressure [3]. At the institutional level, underwater anthropogenic noise is now considered as a source of pollution with impacts at both individual and population levels [2]. The Marine Strategy Framework Directive (MSFD) 2008/56/C includes "underwater noise produced by humans" in the definition of "pollution" and includes it in the list of variables (Descriptor 11) to be analysed and monitored for determining the ecological status of marine environments [2].

ITINERIS

To design, develop, and implement a national contribution to this need, twenty-two Research Infrastructures (RIs) have jointly agreed to present the ITINERIS project [4] to the relevant ministries. The harmonized activities of the RIs within ITINERIS will create an integrated system of Italian environmental RIs to be proposed as a reference at the European level. To build this system, ITINERIS is constructing a network of RIs all relevant to environmental studies and operational knowledge, with the main goal of establishing the Italian Hub of Research Infrastructures in the environmental science sector for observation and study of processes in all relevant subdomains. ITINERIS will sustainably develop interdisciplinary research through the use and reuse of existing (or pre-operational) data and services, providing access to data and services, supporting our country in addressing the upcoming environmental challenges expected to worsen in the coming years.

Integrated ITINERIS acoustic system

The main objective is, therefore, to develop interdisciplinary research in environmental sciences to address scientifically and socially relevant issues such as sustainable use of natural resources, implementation of nature-based solutions, green and blue economy, pollution reduction, management and restoration of critical zones and ecosystems, carbon cycle, and mitigation of downstream effects of climate and environmental changes. The focal point is to create a flexible system to collect and store, for the first time in a national integrated system, ocean acoustic data and metadata and make them available, traceable, accessible, interoperable, and reusable for the entire scientific community (FAIR principles [5]).

In this context, LNS coordinates WP 5.7 of the ITINERIS project [4], focused on the integration and testing of a new underwater Junction Box (JB) to be installed at the infrastructure of Portopalo di Capo Passero at a depth of about 3450 m. The JB will distribute power to various underwater observatories and provide an optical connection for communication and control/data transfer between the observatories and the data acquisition systems hosted on land. Qualified scientific payloads can also be permanently mounted on the JB, thanks to dedicated additional customized ports. LNS has already designed and successfully operates a prototype JB at 3450 meters, capable of interfacing with around 10 observatories. This translates into the ability to efficiently

store, collect, and analyse acoustic data from this prototype almost in real-time.

DAQ AND ANALYSIS: PRELIMINARY RESULTS

The LNS test site is located in Portopalo di Capo Passero (Sr). From here, two electro-optical cables (MEOC) depart, carrying and receiving signals from the sea, each approximately 100 km long. JBs are then connected st the terminations of these cables (CTF). In the case reported here, and for the purposes of ITINERIS, a hydrophone is connected in a dedicated housing of the JB. This sensor (DG0330 from co.l.mar.) is omnidirectional, operates in the range of 5 kHz - 90 kHz, and has two channels. The first has a gain of +26 dB, while the other has a gain of +46 dB. These gains are used to study distant/weak and close/strong sources, thus avoiding signal saturation. Their received voltage response (RVR) is approximately -156 dB (re 1 V/µPa at 1 m) in the high-gain channel. The audio signals recorded by the hydrophone (according to the AES3 standard) are amplified and sent on-shore through the use of optical fibers and control electronic boards (ICE). On land, the data are stored and distributed to analysis stations. In accordance with the MSFD, five minutes of continuous data are acquired every hour and analyzed in real-time. The analysis of the sound pressure level (SPL) in one-third octave bands is then performed, with particular attention to the bands related to the central frequencies of 63 Hz and 125 Hz, suggested in the European directive as excellent indicators for acoustic monitoring of marine environments [2]. Figure 1 shows a five-minute spectrogram in one-third octave bands recorded on February 29, 2024 (08:35 UTC). Two types of high-frequency signals can be identified: an acoustic emitter at around 6.5 kHz and a time-varying signature from acoustic emitters, positioned on the seabed of the test site, captured by the JB hydrophone, at frequencies in the range of 20 kHz - 40 kHz. At lower frequencies, the bands at 63 Hz and 125 Hz show characteristic diffuse noise from maritime traffic.

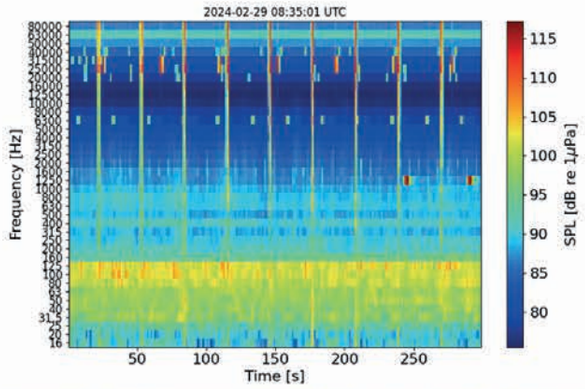

Figure 1: Spectrogram in one-third octave bands obtained from 5 minutes of acoustic recordings from the ITINERIS test site on February 29, 2024 (8:35 a.m. UTC). Details in the text.

OUTLOOK AND FUTURE STEPS

According to the European Marine Strategy Framework Directive, studying the sound pressure level in one-third octave bands is essential for monitoring the ecological status and the impact of anthropogenic noise on marine mammals and animals in oceanic environments. In this context, LNS, within the ITINERIS project, contributes to the establishment of a national database for cataloguing and validating the acoustic data recorded by the various research infrastructures partnering in the project. The quality of data, especially metadata, is of great importance as it will directly influence result management and, particularly, analyses that need to be comparable and repeatable across different RIs. For this reason, a common strategy is being developed among the involved entities to establish, at the national level and for the first time, a common standard for the type and format of result sharing. Since the analysis is primarily conducted at the local level, data management rules will ensure uniformity and universality of processing. Each recording will therefore be accompanied by a set of metadata written in a common format for all RIs, enabling analysis by all partners even years later. Currently, verification tests of analysis algorithms are being conducted using historical data from different databases.

ACKNOWLEDGEMENT

The work presented here has been funded by the European Union – NexGenerationEU and by Ministero dell'Università e della Ricerca of Italian Government in the context of Avviso pubblico per la presentazione di proposte progettuali *Decreto Direttoriale n. 3264 del 28/12/2021*, PNRR MUR, Missione 4, *"Istruzione e Ricerca"* – Componente 2, *"Dalla ricerca all'impresa"*, Linea di investimento 3.1, *"Fondo per la realizzazione di un sistema integrato di infrastrutture di ricerca e innovazione"*, con Decreto D.D. n 130 del 21/06/2022. Progetto Codice IR0000032, *"ITINERIS – Italian Integrated Environmental Research Infrastructures System"*, CUP B53C22002150006.

REFERENCES

[1] P.L. Tyack et al., International Quiet Ocean Experiment, Scientific Committee on Oceanic Research and partnership for Observation of the Global Ocean, (2023) pp. 87.
[2] N.D. Merchant et al., Ocean & Coastal Management, 228 (2022), 106299.
[3] T.A. Smith and J. Rigby, Ocean Engineering, 266 (2022), 112863.
[4] MUR, *ITINERIS proposal*, (2022), pp. 213.
[5] https://www.dtls.nl/fair-data/fair-data-knowledge-expertise/

Preparatory studies for the Einstein Telescope engineering design

D. Cittadino,[1] E. Licciardello[2], G. Schillaci[3]

1) INFN-LNS, Catania, Italy

Abstract – The area around the Sos Enattos former mine in the Province of Nuoro (Sardina, Italy), is one of the region candidates to host the European third generation of gravitational wave detector: Einstein Telescope (ET).

LNS is currently leading the procedural activities related to the ET preliminary feasibility study in Sardina, including geotechnical and engineering studies, key elements of the Italian candidacy for ET (Figure 1).

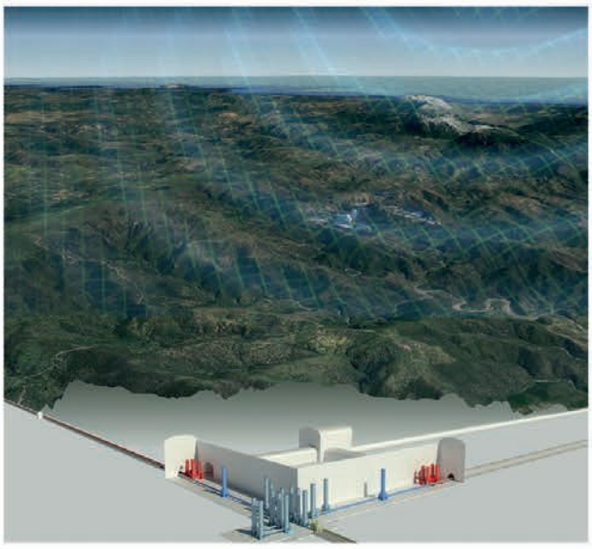

Figure 1: Rendering of the hypothetical main caver in the Sardina site.

INTRODUCTION

The Einstein Telescope is one of the leading European research projects with global scientific impact, and Italy is a candidate to host it in Sardinia around the disused Sos Enattos mine around Nuoro.

The ET project involves the construction of a large underground facility that will house a gravitational wave detector between 100 and 300 metres deep to keep it in "silent" conditions, isolating it from the vibrations produced by both seismic waves and human activities, which constitute what is called "noise", a source of disturbance for the measurements to be made by the ET [1].

Sardina, in particular the Sos Enattos area, is an ideal place for the ET activities. Seismic noise, which affects detector performance at low frequencies, is very low due to the geological characteristics of Sardinia. Sardinia is, in fact, is a stable and solid area, characterised by rock masses that are ideal for safely building the underground spaces that will constitute the ET laboratory.

Finally, in the area around Nuoro, between the municipalities of Bitti, Lula and Onanì, there are large expanses of rural areas with very low population density and, therefore, limited anthropogenic and industrial activity.

THE PNRR ETIC PROGRAM

In the aim to realize a feasibility study of the infrastructure in Sardina, including geotechnical and engineering studies, the Italian Ministry for University and Research (MUR) founded the Einstein Telescope Italian Consortium (ETIC). ETIC is lead by INFN, it involves other two national research institutions, INAF (Italian institute of Astrophysics) and ASI (Italian Space Agency) and the Department of physic, civil engineering, architecture of several Italian universities. The ETIC project is also realizing a network of research infrastructures located in the participating laboratories or universities addressing to the ET enabling technologies [2].

Figure 2: optimization of the infrastructure in the Sardina area

THE PRELIMINARY STUDIES

Preliminary studies for ET in Sardinia are founded by the European program PNRR. These multidisciplinary studies are crucial to confirm that the Sardina's site is the ideal place to host the experiment.

The ET scientific community, at the moment, is considering two hypothetical configurations of the interferometer, illustrated in Figure 3 e 4: triangular (six interferometers inserted in a system of tunnels and caverns with an equilateral triangle layout on a site about 11 km) and L shape (two interferometers

Figure 3: a 3d view of the ET civil infrastructure study in the L-shaped and Triangular-shaped configuration

inserted in a system of tunnels and caverns with an 'L' layout on a side about 16 km).

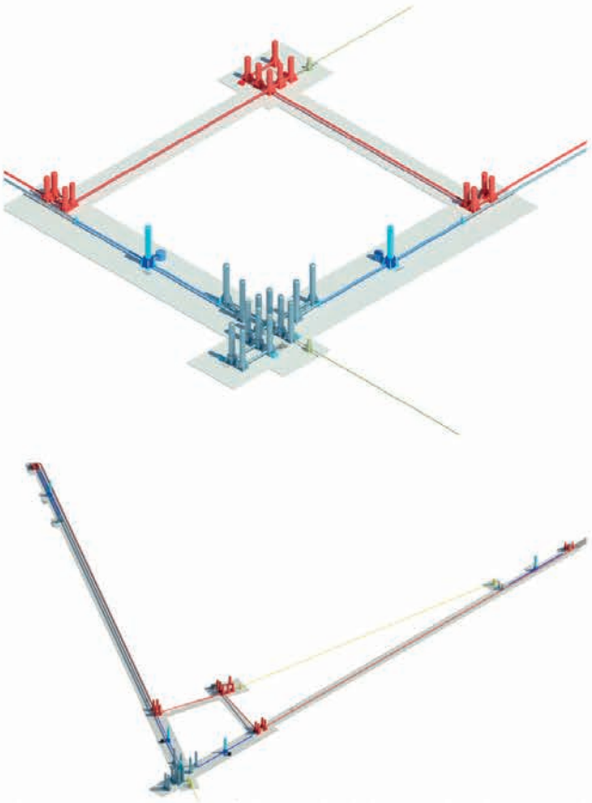

Figure 4: 3d view of the optical layout in the L and Triangular configuration

While the optical layout is in a development face, a call for tenders of the PNRR ETIC project has been published and the LNS group is leading the procedural activities and will interact with the project team, supporting the formulation of the engineering solution satisfying scientific requirements.

The multidisciplinary studies regard both the "L" and "Triangular" configuration include:

- Modelling and layout.
- Mechanical, electrical, plumbing design.
- Preliminary cost estimates, especially for the excavation.
- Evaluation of TBM configuration and tunnel monitoring.
- Preliminary strategies on the management of excavated soil and rocks.
- Multicriteria analysis for the optimization of the position
- Sustainable strategy of the project: evaluation and minimization of the carbon footprint; evaluation of landscape, environmental and societal impacts; energy efficiency.

Geology and seismic studies will start by June 2024 and will implement the ongoing INFN local team work on the site characterization. This is a crucial activity to check if the site meets the fundamental requirements, to evaluate the impact of local environmental noises on the detector performances and to prepare possible mitigation strategies. Important sources of environmental noise in the LF band: seismic and Newtonian, magnetic, acoustic [3].

Deliverables and results will be ready by the end of June 2025. These studies are fundamental for the compilation of the bid book, the formal document of the Italian candidacy.

REFERENCES

[1] einstein-telescope.it

[2] D. D'Urso, Introduction Sardina Site Characterization, Paris-Saclay University, 2nd Einstein Telescope Annual Meeting

[3] L. Naticchioni , Site Characterization in Sardinia for ET, ET Scienza e Tecnologia in Italia

I-LUCE.
Status of the INFN Laser indUCEd radiation facility at INFN-LNS

G.A.P. Cirrone[1,2], C. Altana[1], A. Amato[1], G. Angemi[1], S. Arjmand[1], D. Bandieramonte[1], D. Bonanno[1], S. De Luca[1], G. Cantone[1], E. Caruso[1], R. Catalano[1], G. Cuttone[1], F. Farokhi[1], S. Fattori[1], O. Giampiccolo[1], F. Grillo[1], M. Guarrera[1], A. Kurmanova[1], G. Maggiore[1], C. Manna[1], G. Messina[1], A. Miraglia[1], M. Musumeci[1], D. Oliva[1], A. Pappalardo[1], S. Passarello[1], G. Petringa[1], A. Pizzino[1],
G. Sapienza, A. Sciuto[1], J. Suarez-Vargas[1], M. Tringale[1], S. Tudisco[1], F. Vinciguerra[1]

1) Laboratori Nazionali del Sud, Istituto Nazionale di Fisica Nucleare (INFN), Catania, Italy

2) Centro Siciliano di Fisica Nucleare e Struttura della Materia (CSFNSM), Catania, Italy

Abstract – I-LUCE (INFN Laser indUCEd Radiation Production) facility is a novel European research infrastructure that is in its realisation phase thanks to the "Recovery Funds" European initiative. I-LUCE will focus on creating a specialised research facility for particle acceleration, employing innovative concepts in plasma acceleration and laser technology. This facility is set to pioneer advancements in particle acceleration and radiation production at INFN-LNS (Istituto Nazionale di Fisica Nucleare - Laboratori Nazionali del Sud).

This report describes the main characteristics of the upcoming I-LUCE facility.

Introduction

In the near future, research efforts at INFN-LNS (Istituto Nazionale di Fisica Nucleare - Laboratori Nazionali del Sud) will focus on a cutting-edge high-power laser facility and the unprecedented opportunity to integrate intense laser-accelerated and traditional ion beams within the same experimental domain. An upcoming high-power laser facility, named I-LUCE is scheduled for completion at LNS in 2026. The realisation of this facility is made possible through funding from three Italian programs under PNRR (Piano Nazionale Ripresa Resilienza): EUAPS (EuPRAXIA Advanced Photon Sources), SAMOTHRACE (Sicilian Micro and Nano Technology Research and Innovation Center), and ANTHEM (Advanced Technologies for Human-centered Medicine). As this facility continues to evolve, it holds immense potential to revolutionize our understanding of the cosmos and contribute to breakthroughs in plasma physics, nuclear physics, atomic physics, nuclear astrophysics, their applications, and beyond.

Utilizing high-power laser systems with capacities of up to 1 PW and ultra-short pulse durations as brief as 23 fs, I-LUCE will focus on solid, liquid, or gaseous materials to generate radiation with novel and highly compelling characteristics. Distinguished as the inaugural Italian open users facility, I-LUCE will provide researchers with the opportunity to conduct experiments involving laser-driven radiations and activities within the warm dense matter (WDM) regimes facilitated by the installed laser beam lines. I-LUCE will feature laser pulses ranging from 1 Hz to 10 Hz, pulse durations spanning from 23 fs to 20 ps, and power outputs from 45 TW to 350 TW. Considering in addition that one of the experimental areas will be dedicated to the interaction studies of the laser-generated plasma with the ions coming from the conventional accelerators, I-LUCE will become the most potent and adaptable laser facility in Italy, serving the realms of basic sciences, medical physics, and various applications.

General Description

Representing the second global facility of its kind alongside the PHELIX laser at the GSI (Darmstadt, Germany), I-LUCE will bring together high-power laser plasmas and conventional medium-energy (4–100 AMeV) proton and ion beams within a single experimental chamber. I-LUCE facility will enhance both the quantity and the quality of the radiation beams currently accessible at INFN-LNS. It will enable the investigation of physics phenomena within high-power laser-generated plasmas using methodologies not feasible in other laboratories worldwide. Its unique feature lies in its ability to house, in a single location, both a high-power laser and controlled conventional ion beams, facilitating novel avenues of research and exploration. Additionally, it will introduce a new category of radiation beams to LNS, encompassing protons and ions, with distinct temporal characteristics compared to those generated by the existing accelerators. Furthermore, it will introduce beams that have never been present at LNS, such as neutrons or electrons. I-LUCE will also enable the investigation of nuclear phenomena in plasma and of the dynamic and interaction mechanisms connected to the warm dense matter (WDM) status.

The I-LUCE facility will encompass the laser area, an ISO-7 clean zone housing the laser system, including the optical compressor.

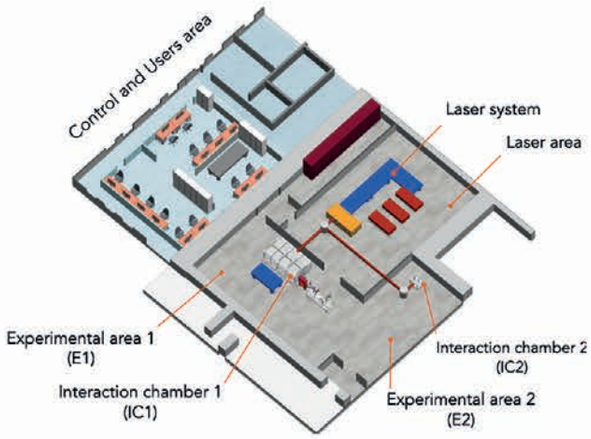

Figure 1: layout of the I-LUCE facility

The Experimental Areas

Alongside this, two experimental areas, Experimental Area 1 (E1) and Experimental Area 2 (E2), will be established, each featuring unique in-vacuum interaction chambers. Laser pulses will then be transported to both E1 and E2, where they will be precisely focused using dedicated optical parabolic lenses. The schematic layout with the laser beam characteristics expected in the two experimental areas is illustrated in Figure 2. The E1 will be specifically allocated for the production of laser-driven protons, electrons, and neutrons within the first in-vacuum interaction chamber (IC1) measuring 4m x 2m x 1m.
Moreover, all essential laser, plasma, and radiation diagnostic equipment will be installed to ensure thorough monitoring of the interaction process and the secondary radiation generated. A dedicated station will be established for electron acceleration within the laser wakefield acceleration (LWFA) scheme.

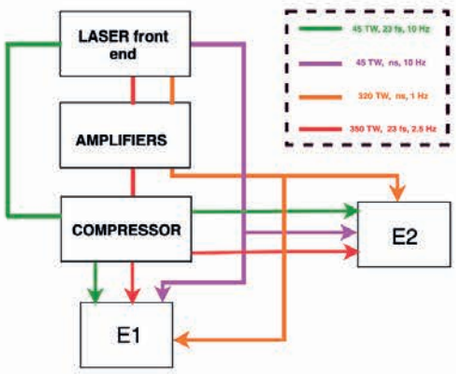

Furthermore, a utility room will be allocated for the laser amplifier power supplies and cooling systems. Additionally, a control room, a users' room, and an optical laboratory will be integral parts of I-LUCE. The overall layout of I-LUCE infrastructure is shown in Figure 1.

Figure 2: block diagram of I-LUCE experimental areas (E1 and E2).
This station will be equipped with gas-targeted plasma sources, including plasma-discharge capillaries and/or gas jets, as well as online diagnostic tools. Additionally, it will feature a transport system capable of selecting electrons with energies up to 3 GeV. A separate beamline designed for selecting, transporting, and focusing proton beams up to 50 MeV energy range will be implemented and fine-tuned for conducting in-air experiments.
Furthermore, in the same chamber, an experimental setup will be arranged to explore laser-driven neutron and X-ray or gamma-ray production up to 20 MeV and 80 MeV, respectively. Table 1 summarises the primary anticipated characteristics of electrons, proton/ion, neutron, gamma and X-ray beams.
The E2 will be equipped with a second in-vacuum interaction chamber (IC2) that will be completely dedicated to plasma and nuclear studies.

This chamber will provide an unparalleled experimental opportunity to study the interaction of conventional ion beams accelerated by the LNS accelerators such as the Superconductive Cyclotron [1] and Tandem, with laser-generated plasma. This distinctive combination will open avenues for conducting fascinating experiments in the fields of plasma physics, nuclear physics [2, 3, 4], and atomic physics. These experiments may include the investigation of stopping powers and interaction cross-sections of ions interacting with plasma, in-plasma nuclear fusion reactions, and nuclear astrophysical phenomena.
A more extensive list of the future possible physics cases of I-LUCE facility have been discussed in [5].

Characteristic	Electron Beam	Proton/ion Beam	Neutron Beam	gamma/x-ray Beams
Maximum Energy	3 GeV	50 MeV	20 MeV	80 MeV
Number of Particle Per Pulse	10^9	10^{11} MeV^{-1} Sr^{-1}	10^8	-
Beam Divergence	±20 mrad	±20°	Isotropic	Directionality in beam propagation

Table 1: expected characteristics of electron, proton/ion, neutron, gamma and X-ray beams from I-LUCE facility.

At the moment, the main elements of the E1 have been designed. In particular, the vacuum interaction chamber, the target system for proton/ion acceleration and a Thomson-like spectrometer for the plasma characterisation have been defined and their procurement is ongoing. Figure 3 show a preliminary 3D rendering of the E1 with the interaction chamber and part of the beamline for the proton/ion transport.

Figure 3: 3D rendering of the E1 area. The vacuum interaction chamber and part of the transport beamline for proton/ion beams are shown.

AKNOWLEDGMEMNT

The author would like to express gratitude to the three Technical Divisions of LNS-INS for their continuous support throughout the design process of I-LUCE. Additionally, heartfelt thanks are extended to the INFN-LNS Administration Service for their invaluable assistance in the preparation and implementation of tenders, as well as in handling all bureaucratic aspects.

REFERENCES

[1] L. Calabretta et al. Commissioning of the k800 infn 955 cyclotron. in 14th International Conference on Cyclotrons and Their Applications, 6(4):2, 1996.

[2] F. Cappuzzello, M. Cavallaro, C. Agodi, M. Bondì, D. Carbone, A. Cunsolo, and A. Foti. Heavy-ion double charge exchange reactions: a tool toward 0 $\nu\beta\beta$ nuclear matrix elements. Eur. Phys. J. A, 51, November 2015.

[3] D. Mascali et al. Ion acceleration by superintense laser-plasma interaction. Eur. Phys. J. A, 53.7:145, 2017.

[4] F. Cappuzzello et al. The numen project: nuclear matrix elements for neutrino-less double beta decay. Eur. Phys. J. A, 54(5)(72), November 2018.

[5] C. Agodi et al. Nuclear physics midterm plan at LNS. Eur. Phys. J., 138:1038, May 2023.

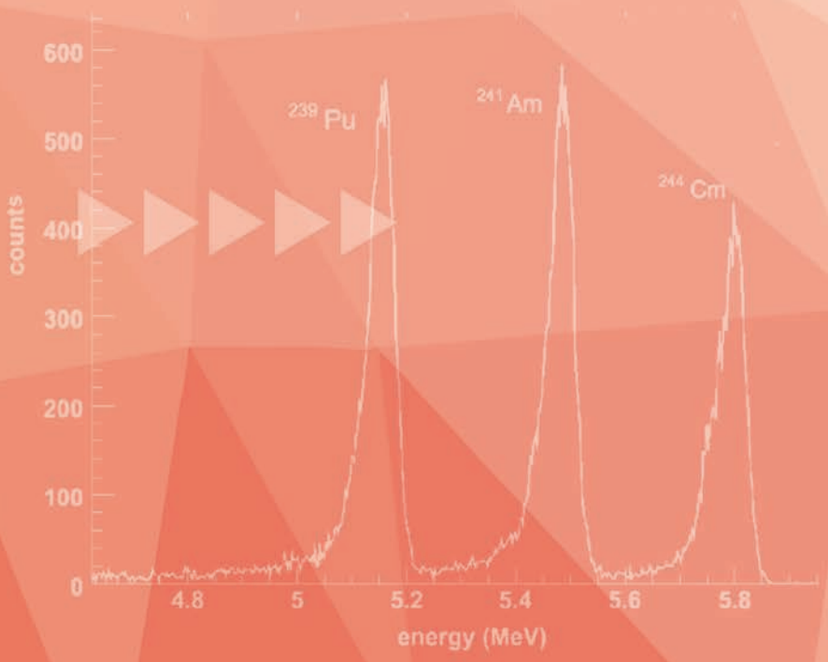

TRAINING COURSE FOR SECONDARY SCHOOL TEACHERS

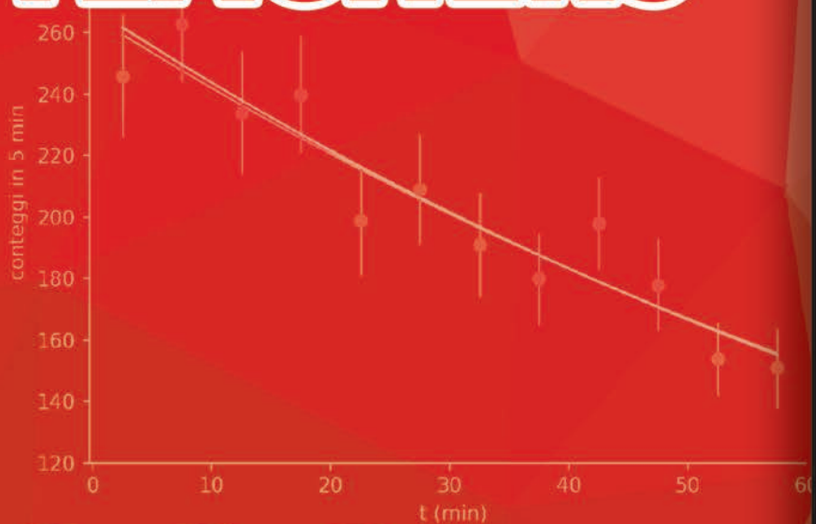

08

INFN LNS

- Analisi dello spettro di emissione di una sorgente α di Pu-239, Am-241 e Cm-244 tramite un rivelatore al Silicio
- Laboratorio di fisica dei plasmi @PID-LNS 2023
- Misura del tempo di dimezzamento e dell'attività di un campione di ^{116}In

Analisi dello spettro di emissione di una sorgente α di Pu-239, Am-241 e Cm-244 tramite un rivelatore al Silicio

G. Augello[1], F. Badaracco, M. Busca, P. Caggiano, V. Cavicchi, M. Clementi[2], D. Gambi[3]

1) Liceo Scientifico Statale S. Cannizzaro - Palermo

2) Liceo Scientifico A. Einstein - Rimini

3) Liceo Statale Ariosto - Ferrara

Riassunto – Presentiamo lo studio dello spettro di emissione di una sorgente mista di calibrazione di Pu-239, Am-241 e Cm-244 ottenuto tramite un rivelatore a PAD al Silicio.

La sorgente radioattiva e il rivelatore sono stati posti all'interno di una cameretta da vuoto. Il rivelatore era collegato alla catena elettronica, presente all'esterno della cameretta, che è stata utilizzata per la lettura dei segnali raccolti. Lo spettro di emissione è stato analizzato stimando la risoluzione energetica dei picchi delle particelle α e la figura di merito; è stata, inoltre, determinata la retta di calibrazione del rivelatore.

INTRODUZIONE

L'analisi dello spettro di emissione di particelle α riveste particolare importanza nello studio dell'attività degli elementi transuranici. Ad esempio, la presenza di Pu, Am e Cm in campioni di acqua provenienti da centrali nucleari può essere ricavata a partire dalle caratteristiche degli spettri di emissione α [1]. Lo stesso metodo può essere utilizzato per valutare gli effetti della ricaduta radioattiva sul territorio e sui sistemi biologici [2].

I rivelatori a semiconduttori sono ampiamente usati nella fisica delle alte energie e in fisica nucleare per l'analisi degli spettri di emissione, vista l'alta risoluzione in energia, la velocità di risposta, la bassa tensione di esercizio e la possibilità di realizzare dispositivi compatti con alta sensibilità [3]. In particolare, le matrici di rivelatori a PAD al Silicio presentano una struttura basata su strisce sovrapposte di giunzioni p-n ognuna con spessori dell'ordine del centinaio di micron [4].

Nell'ambito del Programma Nazionale INFN per Docenti (PID) svoltosi per la prima volta ai Laboratori Nazionali del Sud dal 6 al 10 novembre 2023, abbiamo partecipato a seminari e attività di laboratorio aggiornate alle più recenti ricerche nel campo della fisica nucleare. In particolare, abbiamo avuto l'opportunità di analizzare lo spettro di emissione α di una sorgente mista di Pu-239, Am-241 e Cm-244 che presenta tre picchi con massimi ben risolvibili corrispondenti a tre distinti valori di energia. In ciò che segue esporremo le caratteristiche dell'apparato sperimentale a nostra disposizione e i passaggi più significativi dell'esperienza svolta in laboratorio sotto la guida della Dott.ssa N. Martorana e del Dott. G. Santagati.

MISURA DELLO SPETTRO DI EMISSIONE

Per effettuare la misurazione dello spettro di emissione α ci siamo serviti di un apparato sperimentale composto da una sorgente radioattiva e da un rivelatore al Silicio, posti all'interno di una cameretta da vuoto, da una catena elettronica necessaria all'amplificazione del segnale elettrico proveniente dal rivelatore e da un sistema di acquisizione automatica preposto alla raccolta dei dati che sono stati successivamente analizzati facendo uso di un software dedicato.

Apparato Sperimentale

La sorgente radioattiva è stata posta all'interno di una cameretta nella quale è stato ottenuto un vuoto ad una pressione di circa 10^{-5} millibar. In tal modo è stato possibile eliminare gli effetti di perdita di energia subita dalle particelle α a causa della presenza dell'aria.

I rivelatori al Silicio sfruttano le proprietà delle giunzioni fra semiconduttori drogati per convertire gli effetti indotti dal passaggio di una particella carica in un impulso di corrente.

In prossimità di una giunzione p-n si istaura una condizione di equilibrio dinamico e si genera una zona di svuotamento di portatori di carica maggioritari a causa di fenomeni di diffusione e ricombinazione degli elettroni e delle lacune. Applicando una tensione di polarizzazione in modo che il semiconduttore di tipo n si trovi ad un potenziale maggiore rispetto al semiconduttore di tipo p, l'ampiezza della zona di svuotamento aumenta migliorando l'efficienza di rivelazione della giunzione.

Le particelle α che raggiungono il rivelatore generano una traccia di ionizzazione all'interno della zona di svuotamento creando coppie elettrone-lacuna che producono segnali di corrente proporzionali all'energia della particella α incidente. L'energia di ionizzazione media di un rivelatore al Silicio è circa *3.6 eV*. Le cariche prodotte nel rivelatore vengono inizialmente raccolte ed elaborate da un preamplificatore che le converte in un segnale di tensione ottimizzando l'impedenza del sistema. Successivamente, un amplificatore incrementa l'ampiezza dei segnali provenienti dal preamplificatore da un intervallo di pochi millivolt fino a valori compresi fra 0.1 e 10 V. L'amplificatore modifica la forma dei segnali in modo da ottimizzare il rapporto segnale-rumore, la

risoluzione energetica e in modo da minimizzare la sovrapposizione fra impulsi successivi. Al fine di effettuare un confronto, i segnali provenienti dal preamplificatore e dall'amplificatore sono stati analizzati attraverso l'uso di un oscilloscopio digitale. I segnali forniti dall'amplificatore presentavano una forma con un fronte in cui la tensione cresceva molto velocemente e decresceva lentamente con tempi dell'ordine dei 50 μs. Tali segnali sono stati inviati ad un convertitore analogico-digitale (ADC) che li ha trasformati in segnali in formato digitale. Gli impulsi ottenuti sono stati raccolti da un analizzatore multicanale (MCA) che ha elaborato i dati per generare l'istogramma relativo al conteggio degli impulsi.

ANALISI DATI

L'istogramma dei dati raccolti presenta tre picchi in corrispondenza delle energie di emissione della sorgente come in Fig. 1.

Figura 1: Spettro di emissione α di una sorgente mista (Pu-239, Am-241 e Cm-244) [5].

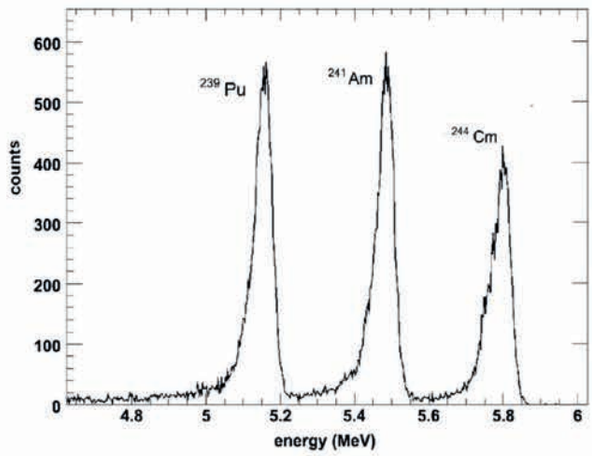

Facendo uso di un software di analisi abbiamo effettuato un fit gaussiano per determinare il centroide e l'ampiezza a mezza altezza (FWHM) dei picchi espressi in numero di conteggi per canale.

Le energie dello spettro di emissione della sorgente radioattiva, i corrispondenti canali e la risoluzione ($FWHM/n_{ch}$) in corrispondenza di ciascun picco sono riportati in Tab. 1.

Tabella 1: Energie dello Spettro α e canali corrispondenti

Sorgente	Energia (keV)	Canali	Risoluzione (%)
Pu - 239	5156.59	810 ± 7	0.86
Am - 241	5485.56	862 ± 7	0.81
Cm - 244	5804.82	913 ± 6	0.66

Abbiamo effettuato una regressione lineare per determinare i parametri caratteristici della retta di calibrazione del rivelatore ottenendo l'Eq. 1, dove E rappresenta l'energia espressa in keV e n_{ch} rappresenta il numero del canale corrispondente.

$$E = 6.2972 \frac{keV}{canale} n_{ch} + 53.947\ keV \quad (1)$$

Abbiamo stimato la figura di merito (FOM) per le coppie di picchi successivi utilizzando l'Eq. 2, dove n_{ch1} e n_{ch2} rappresentano i numeri dei canali corrispondenti a picchi successivi dell'istogramma mentre $FWHM_1$ e $FWHM_2$ rappresentano, rispettivamente, l'ampiezza a mezza altezza di ciascun picco.

$$FOM = \frac{n_{ch_2} - n_{ch_1}}{FWHM_1 + FWHM_2} \quad (2)$$

In Tab. 2 sono riportati i risultati ottenuti dal calcolo effettuato utilizzando l'Eq. 2.

Tabella 2: Figura di Merito

	FOM
^{239}Pu - ^{241}Am	3.8016
^{241}Am - ^{244}Cm	3.9426

CONCLUSIONI

Abbiamo studiato lo spettro di emissione α di una sorgente mista di Pu-239, Am-241 e Cm-244 tramite un rivelatore al Silicio in condizioni di vuoto. I segnali elettrici provenienti dal rivelatore sono stati opportunamente ottimizzati facendo uso di una catena elettronica che prevedeva stadi di amplificazione e digitalizzazione. L'istogramma ottenuto dalle misure dei conteggi per canale durante l'intervallo di misurazione è stato analizzato procedendo con un fit gaussiano dei picchi dei segnali per determinare il centroide dei picchi e la loro ampiezza a mezza altezza. Confrontando i valori ottenuti in funzione dei canali con i valori nominali di energia della sorgente attraverso un fit lineare è stato possibile ottenere la funzione di calibrazione del rivelatore. Abbiamo stimato la risoluzione in energia all'ampiezza a mezza altezza per ciascuno dei picchi ottenendo $\Delta E_{Pu} = 43.70\ KeV$, $\Delta E_{Am} = 42.63\ KeV$, $\Delta E_{Cm} = 38.98\ KeV$.

BIBLIOGRAFIA

[1] S. Salminen-Paatero et al., J. Radioanal. Nucl. Chem. (2021) 329(3) .

[2] E. Holm et al., J. Radioanal. Nucl. Chem. (1992) 156: 183–200.

[3] A. Topkar et al., Nucl. Inst. Meth. Phys. Res. Sec. A (2016) 834: 205-210.

[4] M. Jadhav et al., XXI DAE-BRNS High Energy Physics Symposium (2016): 541-546.

[5] A. Galbiati et al., IEEE Trans. Nucl. Sci. (2009) 56(4): 1863 - 1874.

Laboratorio di fisica dei plasmi @PID-LNS 2023

A.Battistoni[1], A. Forieri[2], G. Gambini[3], D. Iavarone[4], D. Mambrini[5], G. Tigano[6], F. Violini[7]

1) Liceo Scientifico Statale "Plinio Seniore", Roma
2) Liceo Scientifico Statale "Paolo Frisi", Monza
3) I.I.S. "Vanvitelli - Stracca - Angelini", Ancona
4) Liceo Statale "Sandro Pertini", Ladispoli
5) Liceo Scientifico Statale "Federigo Enriques", Livorno
6) Liceo Artistico Statale di Brera, Milano
7) Liceo Scientifico Statale "Enrico Fermi" Castel del Piano, Grosseto

Abstract - Nella seconda settimana di novembre 2023 si è tenuto a Catania il Programma INFN per Docenti (PID), che ha radunato da tutta Italia docenti di scuola secondaria superiore per un corso di aggiornamento sulle ricerche condotte oggi dai Laboratori Nazioni del Sud (LNS). Durante le giornate si sono susseguiti seminari, visite ai laboratori e sessioni di gruppo sperimentali. In questo manoscritto viene riportata una delle attività laboratoriali realizzata dal gruppo dei "Positroni" nell'ambito della fisica dei plasmi: in particolare verrà descritta la tecnica polarimetrica per la misura della densità elettronica di un plasma.

INTRODUZIONE

Uno degli ambiti di ricerca dei LNS è la fisica dei plasmi, che trova la sua ricaduta in campo energetico [1,2], nella fisica applicata [3] e nell'astrofisica nucleare [4].
Un plasma, detto quarto stato della materia, altro non è che un gas ionizzato quasi neutro che esibisce, grazie alle interazioni elettromagnetiche di lungo raggio, un comportamento collettivo. Diverse sono le tecniche utilizzate per produrre lo stato di plasma e, in alcuni casi, si rende necessario operare ad altissime temperature (10^5 - 10^8 K) e in condizioni di confinamento magnetico per aumentare la probabilità (sezione d'urto) del processo ionizzante.
Durante questi processi è importante monitorare i parametri caratteristici del plasma, tra questi sicuramente la densità elettronica n_e. A tale scopo sono state sviluppate modalità non invasive per sondare le proprietà - tra cui lo stato di carica - del gas ionizzato: spettroscopia ottica ad emissione, interferometria, polarimetria. Questo articolo è dedicato in particolare alla polarimetria, la tecnica che studia la variazione della polarizzazione di un'onda elettromagnetica di *probe* (tipicamente nel regime di microonde) che attraversa il plasma.
Il campo elettrico di un'onda elettromagnetica polarizzata linearmente (Fig. 1) che attraversa un plasma magnetizzato subisce una rotazione nel piano di polarizzazione di un angolo detto *angolo di Faraday* β tale che

$$(1)\quad \beta = \int_0^d \frac{e^3}{8\pi^2 c^3 m_e^2 \varepsilon_0} B(z) n_e(z) \lambda^2 dz$$

dove e è la carica dell'elettrone, m_e la sua massa, c la velocità della luce nel vuoto, ε_0 la costante dielettrica del vuoto, $B(z)$ il campo magnetico locale in funzione della posizione e λ la lunghezza d'onda della radiazione di probe.

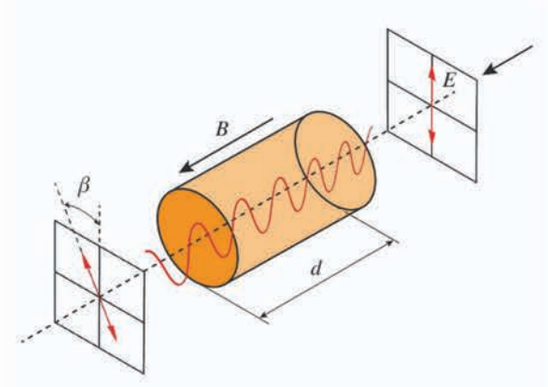

Figura 1: la rotazione di Faraday (adattata da [8])

Note dunque le proprietà locali del campo magnetico è possibile risalire dall'angolo di Faraday alla densità elettronica del plasma.

MISURE DI POLARIZZAZIONE

Nella sessione applicativa si è proceduto a simulare una misura dell'angolo di Faraday grazie ad una versione da laboratorio della strumentazione con cui sono equipaggiate le reali camere sperimentali.
In Fig. 2 viene riportato l'apparato sperimentale [6] sviluppato all'interno del progetto Pandora [10]: un'onda elettromagnetica polarizzata linearmente nel range di frequenze Ka (26-40 GHz) viene emessa dall'antenna di trasmissione (TX) e rivelata da un'altra antenna ricevente (RX) accoppiata con un trasduttore ortomodale (OMT) [5] che ha la funzione di separare in canali diversi le

componenti verticali e orizzontali del campo elettrico incidente. I due segnali così separati vengono poi visualizzati uno in funzione dell'altro grazie ad un oscilloscopio operante in modalità XY.

Figure di Lissajous

Tra le antenne TX e RX veniva montato un polarizzatore di tipo *wire-grid* per simulare l'azione del plasma nell'indurre una rotazione di polarizzazione rispetto a quella emessa dall'antenna TX.

Nel caso dell'esperimento condotto durante il PID-LNS 2023 ci si è limitati semplicemente a ruotare l'antenna RX di 45° rispetto a quella TX, così da simulare una polarizzazione incidente sul rivelatore con una inclinazione relativa di 45°.

Come è possibile osservare in Fig.2-a, l'immagine dell'oscilloscopio per i canali accoppiati, mostra una figura di Lissajous ellittica anziché lineare, come ci si sarebbe invece aspettati per il caso di una radiazione incidente polarizzata linearmente. Tale fenomeno è in realtà dovuto all'introduzione di una differenza di fase tra i due canali dell'oscilloscopio a causa della diversa lunghezza dei cavi utilizzati per la trasmissione del segnale.

Una volta introdotta, per via elettronica, una correzione sulla fase relativa tra i canali, si è ottenuta la figura di Lissajous mostrata in Fig. 2-b. Come si può notare ora l'andamento è lineare e inclinato a 45°, compatibilmente con il fatto che il campo elettrico incidente sull'antenna RX è inclinato di 45° rispetto all'asse del rivelatore.

Una volta calibrato il sistema e corretti opportunamente gli offset di fase, è possibile dunque, dalla forma e dalla inclinazione delle figure di Lissajous, avere un'informazione diretta sullo stato di polarizzazione della radiazione incidente e sull'angolo di Faraday.

Per poter estrarre informazioni circa la densità elettronica del plasma n_e, in accordo con l'eq. 1, sarebbe ora necessario misurare l'angolo di Faraday al variare della lunghezza d'onda (λ) emessa dall'antenna TX [7,8].

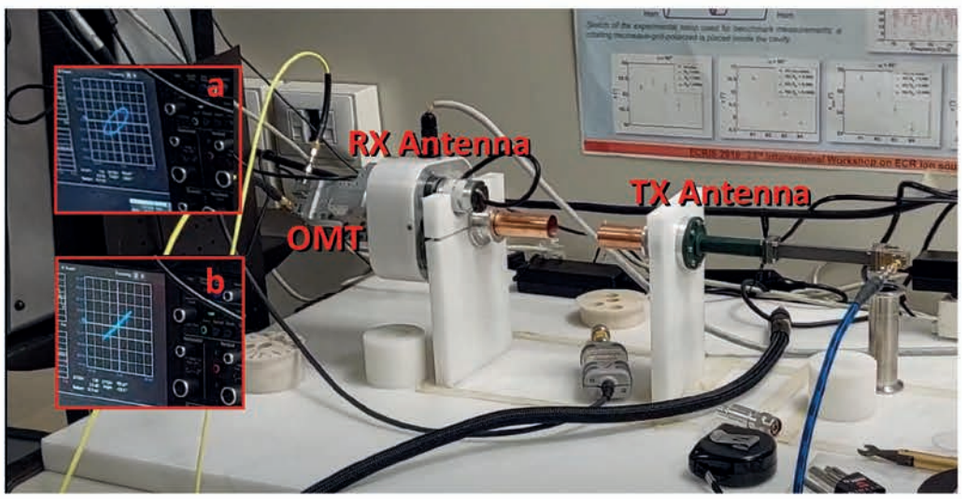

Figura 2: il setup sperimentale. Da destra verso sinistra: l'antenna trasmettitrice (TX) di microonde, l'antenna ricevente (RX) accoppiata con un trasduttore ortomodale (OMT) in grado di separare le componenti di polarizzazione della radiazione incidente. Inset a: i segnali uscenti dall'OMT vengono inviati all'oscilloscopio che permette di visualizzarne la differenza di fase grazie alle figure di Lissajous. A causa della differente lunghezza dei cavi che collegano i due canali, è possibile che si introduca uno sfasamento spurio che deve essere compensato elettronicamente. Inset b: una volta compensati eventuali effetti di ritardi di fase dovuti al cablaggio dell'esperimento, sull'oscilloscopio appare un segmento dalla cui inclinazione si ricava l'angolo di Faraday.

Legge di Malus

Il setup fin qui descritto è un setup semplificato che lavora in aria, per cui il segnale trasmesso dall'antenna TX non subisce alterazioni sensibili nel tragitto fino all'antenna RX. Ciò non si verifica sempre quando il segnale deve attraversare il plasma all'interno della camera sperimentale. E' stato osservato [7,8] infatti che a causa di riflessioni spurie all'interno della camera sperimentale, per alcune frequenze di microonde trasmesse, si possono verificare effetti di risonanza che inficiano la misura dell'angolo di Faraday con la tecnica fin qui descritta.

Per poter verificare che il segnale rivelato non contenga contributi spuri, è necessario dunque individuare per quali λ non si hanno questo tipo di distorsioni imputabili alla geometria della camera sperimentale.

Per poter essere ritenuta affidabile una determinata λ di emissione, è necessario effettuare il test della *legge di Malus*. E' noto infatti che, misurando l'intensità (I) del campo elettrico trasmesso attraverso uno solo dei canali dell'OMT, questa deve seguire un andamento di tipo

$$(2)\quad I = I_0 \cos^2\theta$$

dove θ è l'angolo di orientazione dell'antenna RX rispetto all'angolo di Faraday dell'onda che ha attraversato il plasma.
Per simulare, dunque, tale test è stata effettuata in laboratorio una misura dell'intensità di uno dei canali dell'OMT variando con continuità l'orientazione dell'antenna RX. Dal momento che la misura è stata effettuata in aria, si è ottenuto, come atteso, l'andamento descritto dall'eq. 2.

CONCLUSIONI

La misura dell'angolo di Faraday permette di misurare la densità elettronica di un plasma magnetizzato. Lo stato di plasma della materia è quello maggiormente presente nell'Universo (98%). Riuscire ad emulare in laboratorio alcune condizioni simili a quelle dei plasmi stellari potrebbe pertanto dare un enorme impulso alle ricerche in astrofisica nucleare [9]. Infatti, misure di decadimento beta nei plasmi di laboratorio – principale obiettivo del progetto PANDORA [10] - potrebbero condurre ad una maggior comprensione della nucleosintesi stellare, ovvero il processo di formazione di elementi chimici pesanti di cui è composta anche la nostra Terra.
Inoltre, misure dell'opacità del plasma consentirebbero di approfondire lo studio dei meccanismi di produzione di elementi pesanti nella fusione delle stelle di neutroni [11].

REFERENCES

[1] J. Zhang et al. Rev. Sci. Instrum. 83, 10E321 (2012).
[2] E.E. Scime, Rev. Sci. Instrum. 72, 1672 (2001).
[3] M. Laroussi, J. Appl. Phys. 122, 020901 (2017).
[4] P.S. Ramkumar, J. Astrophys. Astron. 20, 37 (1999).
[5] O. A. Peverini, IEEE Transactions on Microwave Theory and Techniques, vol. 51, no. 4, pp. 1207-1213, (2003).
[6] G. Torrisi et al., Front. Astron. Space Sci. 9:949920 (2022).
[7] G. Torrisi et al. JINST 12 C10003 (2017).
[8] E. Naselli et al. JINST 13 C12020 (2018).
[9] P.P. Kronberg, Physics Today 55 (12), 40–46 (2002)
[10] D. Mascali et al., Universe 8(2) 80 (2022)
[11] A. Pidatella et al., Front. Astron. Space Sci. 9: 931744 (2022)

Misura del tempo di dimezzamento e dell'attività di un campione di ^{116}In

L. Barberi, R. Becca, O. Boccia, V. L. Cannia, A. Di Naso, D. Drago, F. Tondini

Abstract

Il tempo di dimezzamento e l'attività di un campione di ^{116}In sono stati misurati mediante il conteggio dei raggi gamma di energie selezionate emessi dal campione. Sono stati in particolare misurati i conteggi dei gamma emessi alle energie di 416.90 keV, 1097.28 keV e 1293.56 keV. I raggi gamma sono stati misurati mediante un rivelatore al germanio ad alta purezza (HPGe) ad intervalli di 5 min ed è stata ricostruita la curva del decadimento radioattivo, mediante tecniche di best fit, e calcolato il tempo di dimezzamento e l'attività.

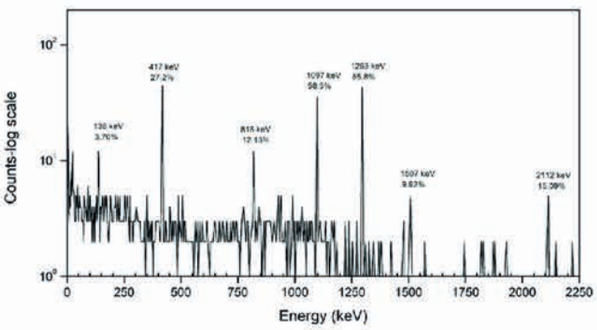

Figura 1: Spettro gamma del ^{116}In.

1 Introduzione

L'isotopo dell'indio con numero di massa 116 (^{116}In) è caratterizzato da due stati isomerici (m_1 e m_2) e dallo stato fondamentale. Questi tre stati decadono con tre differenti modalità [1]:

- lo stato isomerico ad energia più alta (m_2) decade per transizione interna nello stato isomerico a più bassa energia (m_1) con con emissione di raggi gamma ($T_{1/2}$ = 2.18 s).
- lo stato isomerico m_1 decade β^- (BR 100%) in stagno-116 (^{116}Sn) con $T_{1/2}$ = 54.29 min. Lo stagno viene prodotto in diversi stati eccitati e decade emettendo gamma di varie energie, con un tempi di decadimento trascurabili rispetto al quello dell'indio.
- lo stato fondamentale decade o β^- (BR 99.97%) o per cattura elettronica (BR 0.023%), trasformandosi rispettivamente in ^{116}Sn e ^{116}Cd ($T_{1/2}$=14.10 s)

A causa dei tempi di dimezzamento relativamente bassi, l' ^{116}In deve essere prodotto poco prima della misura. I decadimenti dello stato isomerico m_2 e dello stato fondamentale diventano trascurabili a pochi minuti di distanza dalla produzione, per cui per la nostra misura risulta importante solo il decadimento dello stato isomerico m_1. Gli stati eccitati dello ^{116}Sn sono numerosi e di conseguenza i relativi gamma emessi, i quali sono quindi distribuiti in un insieme di possibili energie caratteristiche, ciascuna con una sua probabilità di emissione. La rivelazione di raggi gamma di energie specifiche permette di discriminare la presenza del ^{116}In e di determinarne l'attività e quindi la quantità presente in un certo campione. Non tutti i gamma vengono emessi con la stessa probabilità, si definisce branching ratio (BR) la frazione di eventi in cui un determinato gamma è presente, ad es. un BR=25% significa che, mediamente, il raggio gamma in questione è presente in un decadimento su 4. Nella nostra misura abbiamo considerato i raggi gamma con il BR più elevato, cioè i picchi corrispondenti alle energie di 416.90 keV (BR=27.2%), 1097.28 keV (BR=58.5%) e 1293.56 keV (BR=84.8%), fig 1 . Nel decadimento radioattivo la probabilità che una particella decada in un tempo dt è proporzionale al tempo dt e al numero di nuclei presenti, la costante di proporzionalità viene indicata con λ, ovvero la *costante di decadimento*. Il numero di nuclei che decadono nel tempo dt è dato da $dN = -\lambda dt N$. Integrando l'equazione precedente e indicando con N_0 la popolazione di nuclei presente al tempo $t = 0$ si ottiene $N = N_0 e^{-\lambda t}$. Questa relazione può anche essere scritta come $N = N_0 e^{-\frac{t}{\tau}}$, dove $\tau = \frac{1}{\lambda}$ è la *vita media*. Un parametro facilmente interpretabile e proporzionale alla vita media è il tempo di dimezzamento $T_{1/2}$, definito come il tempo necessario affinché la metà della popolazione di nuclei di un certo elemento decada. La relazione tra vita media e tempo di dimezzamento si ricava risolvendo l'equazione $N_0 e^{-\frac{T_{1/2}}{\tau}} = \frac{N_0}{2}$, da cui si ricava $T_{1/2} = \tau ln2 = \frac{ln2}{\lambda}$ [5]. Un'altra grandezza molto importante nei decadimenti radioattivi è l'attività, definita come il numero di decadimenti per unità di tempo. Il numero di decadimenti dopo un tempo t è pari a $N_0 - N = N_0 - N_0 e^{-\frac{t}{\tau}} = N_0(1 - e^{-\frac{t}{\tau}})$, se il tempo t è piccolo rispetto a τ, $N_0 - N$ può essere approssimato a $N_0 \frac{t}{\tau}$ e quindi l'attività può essere calcolata come

$$A = \frac{(N_0 - N)}{t} = \frac{N_0 \frac{t}{\tau}}{t} = \frac{N_0}{\tau}. \qquad (1)$$

e quindi considerata costante nell'intervallo di tempo t.

2 Misura e analisi dati

L'isotopo ^{116}In è stato prodotto attraverso la reazione $^{115}In(n,\gamma)^{116}In$, irraggiando un dischetto ($\phi \sim$ 1mm) di

^{115}In con un flusso di neutroni emessi da una sorgente di ^{241}Am -^{9}Be. Per rivelare i gamma emessi in seguito al decadimento del ^{116}In è stato utilizzato un rivelatore al Germanio ad alta purezza HPGe di tipo p coassiale [4]. I rivelatori di gamma a semiconduttore funzionano come un diodo polarizzato in modo inverso, in questa maniera si ottiene una zona di svuotamento che è tanto più grande quanto è maggiore la tensione inversa. Gli elettroni prodotti dall'interazione dei raggi gamma, quando attraversano la zona di svuotamento creano coppie elettrone lacuna che vengono poi raccolte dagli elettrodi creando un segnale elettrico. La catena elettronica di amplificazione e digitalizzazione trasforma il segnale in un numero intero [2]. Sussiste una relazione lineare tra il numero (canale) e l'energia del gamma incidente, per determinare i coefficienti di tale relazione il rivelatore deve essere calibrato in energia, in pratica si misurano i canali relativi a picchi di raggi gamma a differenti energie, prodotti da sorgenti tarate e si calcolano i coefficienti mediante un fit lineare [6].

I rivelatori HPGe, come in genere i rivelatori a semiconduttori, hanno un'elevata risoluzione in energia. Il rivelatore utilizzato presenta una risoluzione di 2 keV [4]. Un parametro molto importante in tutti i rivelatori è l'efficienza, cioè il rapporto tra il numero di gamma effettivamente rivelati e quelli emessi dalla sorgente. L'efficienza dipende dalla geometria del sistema e dall'efficienza intrinseca del rivelatore. Per questo motivo il rivelatore viene calibrato in efficienza misurando la risposta in termini di conteggi a una serie di sorgenti che emettono gamma di energia e attività nota. Il risultato della calibrazione è una funzione (o tabella di valori) che esprimono il rapporto tra i gamma misurati e quelli emessi. La calibrazione dipende fortemente dalla geometria della sorgente, la quale deve essere molto simile a quella che si intenderà utilizzare per le misure vere e proprie. Nel nostro caso la calibrazione era stata effettuata per contenitori (beaker) di tipo Marinelli, mentre la sorgente utilizzata per la misura era un campione a forma di disco.
In fase di misura, il campione di ^{116}In è stato posizionato sopra il rivelatore e sono stati effettuati 12 cicli di misurazione di 5 minuti ciascuno. In ogni ciclo è stato misurato il numero di conteggi relativo a ciascuno dei tre picchi considerati. L'energia e i conteggi di ogni picco sono determinati in automatico dal software del rivelatore, ricostruendo lo spettro gamma e assegnando il valore dell'energia a ciascun canale. L'energia del picco viene individuata mediante il centro della gaussiana ottenuta con un best fit sul picco. Il numero di conteggi viene determinato sommando i conteggi dei canali all'interno del picco e sottraendo il fondo, determinato dalla media dei conteggi di 3-4 canali a destra e a sinistra della gaussiana. I risultati delle misure dei tre picchi per ciascun run sono riportati nella tabella 1, insieme agli errori, come valore di t è stato riportato il valore medio in ciascun intervallo. Con i dati in tabella sono stati determinati i parametri della legge di decadimento esponenziale utilizzando due differenti metodi. La funzione utilizzata per il fit è $f(x) = ae^{-bx}$, dove a rappresenta la popolazione iniziale e b è lambda. In laboratorio abbiamo eseguito una linearizzazione dell'equazione applicando il logaritmo ad ambo i membri: $lnf(x) = lna - bx$. Applicando il metodo dei minimi quadrati lineare considerando il logaritmo naturale dei conteggi in funzione del tempo, abbiamo ottenuto, i valori di lna, da cui abbiamo calcolato $a = e^{lna}$, e b. Abbiamo successivamente ripetuto l'analisi con un best fit non lineare per mezzo delle librerie python *numpy [3]* e *scipy [7]*. La differenza tra i due metodi è ampiamente entro l'errore sperimentale, tuttavia il fit non lineare fornisce una somma dei quadrati degli scarti inferiore. In figura sono mostrati i dati con le barre di errore e le due curve di fit.

Picco 413 keV			**Picco 1097.28 keV**			**Picco 1293.56 keV**		
t(min)	Cont.	Err.	t(min)	Cont.	Err.	t(min)	Cont.	Err.
2,5	246	20	2,5	324	22	2,5	341	21
7,5	263	19	7,5	267	21	7,5	331	19
12,5	234	20	12,5	266	16	12,5	334	19
17,5	240	19	17,5	248	19	17,5	275	18
22,5	199	18	22,5	251	17	22,5	258	18
27,5	209	18	27,5	243	17	27,5	253	20
32,5	191	17	32,5	236	15	32,5	247	17
37,5	180	15	37,5	190	17	37,5	214	18
42,5	198	15	42,5	170	17	42,5	226	16
47,5	178	15	47,5	171	19	47,5	231	15
52,5	154	12	52,5	147	16	52,5	193	15
57,5	151	13	57,5	153	18	57,5	211	14

Tabella 1: Dati relativi ai tre picchi in esame.

Picco 416.90 keV	
a = 265 ± 8	b = 0.0093 ±0.0010(min^{-1})
attività iniz.= (10000 ± 300)dec/min	$T_{1/2} = (76 \pm 8)min$
(167 ± 5) Bq	
Picco 1097.28 keV	
a = 322 ± 11	b = 0.0132±0.0012(min^{-1})
attività iniz.= (11600 ± 400)dec/min	$T_{1/2} = (54 \pm 5)min$
(193 ± 7) Bq	
Picco 1293.56 keV	
a = 350 ± 11	b = 0.0105±0.0011(min^{-1})
attività iniz.= (9900 ± 300)dec/min	$T_{1/2} = (67 \pm 7)min$
(164 ± 5) Bq	

Tabella 2: Risultati.

Per la determinazione del tempo di dimezzamento non è necessario tenere conto dell'efficienza di rivelazione del rivelatore, in quanto vengono confrontati conteggi alla stessa energia, quella del picco in esame. Differente il discorso per la misura dell'attività, la quale è determinata dalla relazione $A = \frac{C}{\epsilon b T}$, dove C sono i conteggi, T il tempo di misura, ϵ l'efficienza all'energia del γ, e b il branching ratio del γ. Questo calcolo può essere effettuato per ciascuno degli intervalli di presa dati, noi lo abbiamo calcolato per l'intervallo iniziale, utilizzando il valore dei conteggi ricavato dal best fit. Nella tabella 2 sono riportati i valori dei parametri a e b, ovvero il numero di conteggi iniziali e la costante di decadimento (min^{-1}) con i relativi errori e i valori dell'attività iniziale e del tempo di dimezzamento ottenuti dai risultati del fit.

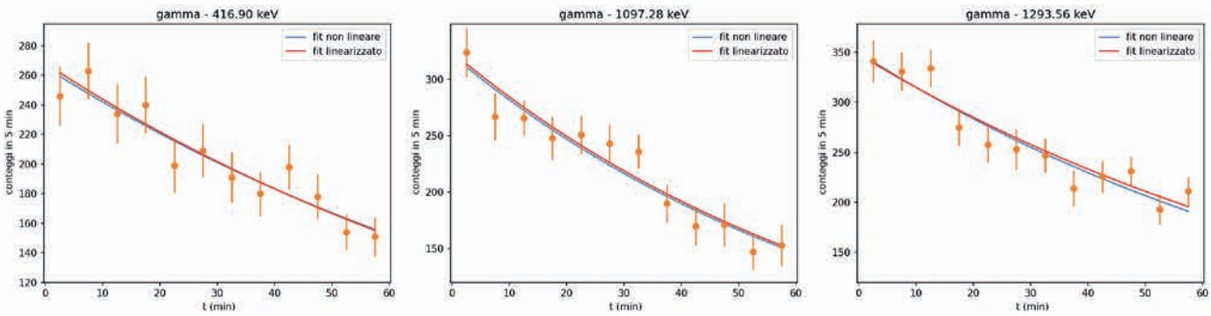

Figura 2: Grafici dei conteggi riferiti ai tre differenti raggi gamma con le curve di best fit.

3 Conclusioni

I dati relativi ai conteggi sono in buon accordo con la legge teorica del decadimento radioattivo. La misura del tempo di dimezzamento, pur essendo abbastanza accurata nei tre casi, è in accordo con i valori riportati in letteratura soltanto per il picco 1097.28 keV. Per quanto riguarda le misure dell'attività, quelle relative ai gamma da 416.90 keV e 1293.56 keV sono in accordo tra di loro e differiscono da quella calcolata dal gamma a 1097.28 keV; in questo caso il valore teorico è sconosciuto, a meno di conoscere l'attività iniziale del campione e il tempo trascorso dalla sua produzione, inoltre la misura è affetta da un errore sistematico dovuta alla differente geometria del campione misurato rispetto a quella della sorgente di calibrazione. Dato che i dati dei conteggi dei vari picchi dei gamma sono stati letti e trascritti manualmente si potrebbe pensare a un qualche errore di lettura/trascrizione. Si evidenzia come i dati relativi ai picchi che hanno un tempo di dimezzamento in disaccordo con quello aspettato (416.90 keV e 1293.56 keV) abbiano dato risultati consistenti tra loro, nei limiti degli errori statistici. Sarebbe interessante poter esaminare gli spettri in questione e ricalcolare i valori dei conteggi.

Riferimenti bibliografici

[1] IAEA. Livechart of nuclides - advanced version. "https://www.iaea.org/resources/databases/livechart-of-nuclides-advanced-version", 2024.

[2] G. F. Knoll. Radiation detection and measurement; 4th ed. Wiley, New York, NY, 2010.

[3] Numpy. The fundamental package for scientific computing with Python. "https://numpy.org", 2024.

[4] Ortec. Detective x: Ultra high resolution hpge radioisotope identification device. "https://www.ortec-online.com/-/media/ametekortec/brochures/d/detective-x.pdf".

[5] G. G. Rapisarda. Radioattività ambientale - seminario PID@LNS 6-10 nov 2023, 2023.

[6] G. G. Rapisarda and R. Leanza. Misure di radioattività - attività sperimentale PID@LNS 6-10 nov 2023, 2023.

[7] SciPy. Scipy: Fundamental algorithms for scientific computing in Python. "https://scipy.org", 2024.

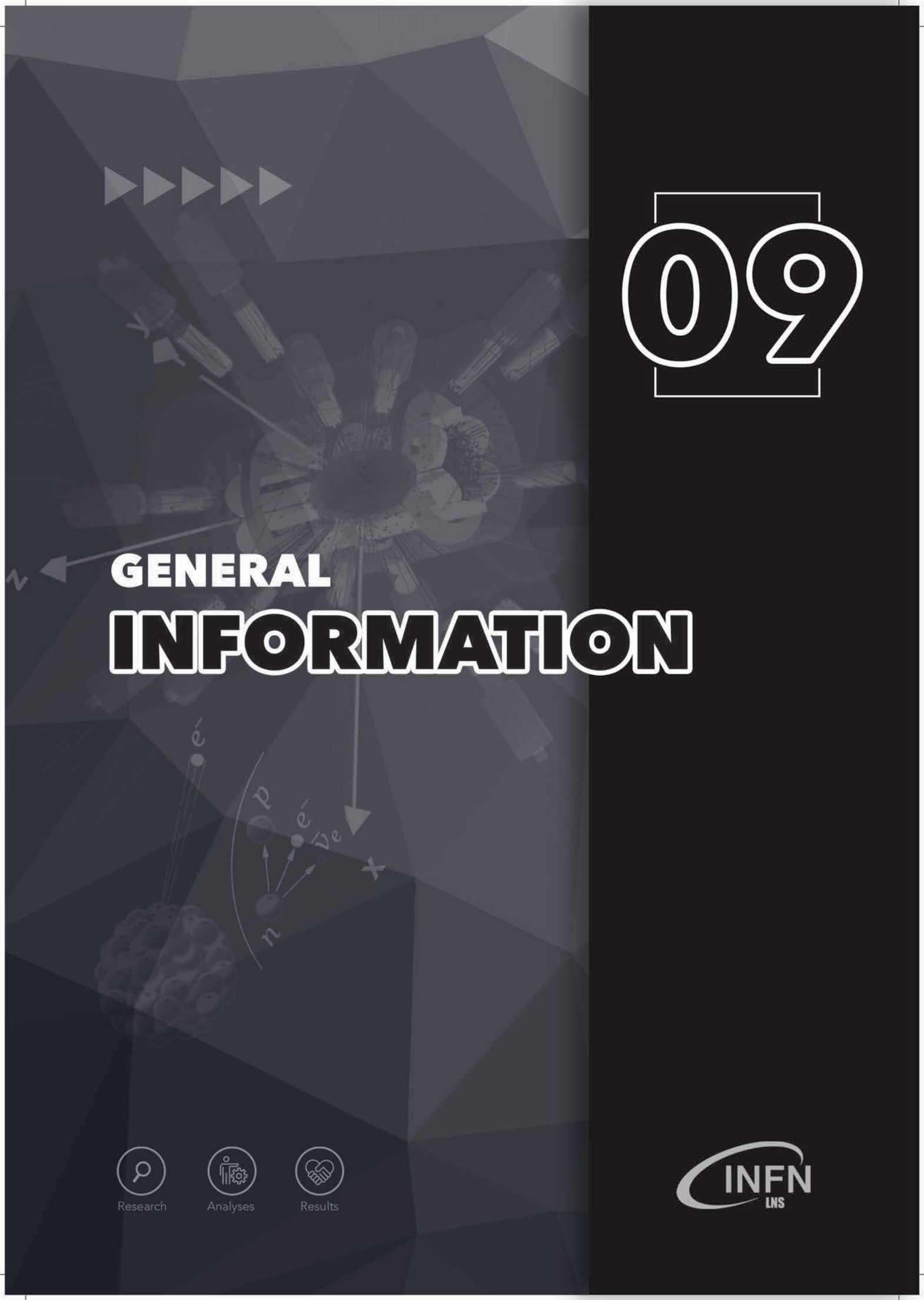

09

GENERAL INFORMATION

Research Analyses Results

INFN LNS

- Workshops, Meetings Outreach Events
- Schools and Institutional Visits
- Seminars and Espresso Seminars
- Photo Gallery
- Organization

Workshops Meetings 2023

BCT/I-LUCE meeting	03/01/23
InnovaTron: An innovative compact high-intensity proton cyclotron	10/02/23
Geant4-DNA for the flash radiotherapy: biological damage prediction	24/02/23
2nd workshop INFN ACCELERATORI	27/02/23
Towards a unified equation of state for astrophysical simulations	08/03/23
La Bellezza nella fisica	10/03/23
A new Thompson Parabola for p-11B experiments and high energy proton beams	24/03/23
Studies on Proton Boron Fusion Reactions and applications at INFN-LNS	30/03/23
Theoretical Modelling of ECR Plasmas for Application to PANDORA	05/04/23
Internal Seminar by a Engineering Student, working on numerical simulations on ECR plasmas.	27/04/23
Biological damage estimation with machine learning approach and Geant4-DNA: a comparison with experimental data	28/04/23
The p-11B fusion reaction in plasma: the experiments performed at PALS	28/04/23
Looking for Dark-Matter: the DarkSide of the Universe	09/05/23
Machine Learning in biological damage estimation with Geant4-DNA: a comparison with experimental data	26/05/23
PRAGUE detector prototype: experimental tests and future developments	30/06/23
Majorana come ponte tra materia e antimateria	04/07/23
La facility I-LUCE: nuove prospettive per la produzione di fasci e studi di plasmi ai LNS con laser di alta potenza	03/07/23
Multi-channel study of direct nuclear reactions: a tool to provide data driven information on neutrino-less double-beta decay	18/07/23
PIC simulation with SMILE code: the p-11B reaction as a case of study	28/07/23
Institute of Plasma Physics, Chinese Academy of Sciences, Research and development of the superconducting cyclotron for proton therapy in HFCAS.	08/09/23
Riunione CSN2 INFN	18/09/23
The biological damage with Geant4-DNA: the comparison with experimental data	29/09/23
Status and future perspective of ground-base Gravitational Waves measurements infrastructure in Europe	10/10/23
WPCF2023 - XVI Workshop on Particle Correlations and Femtoscopy	06/11/23
La SICILIA verso il GREEN – Le sei filiere da costruire	15/11/23
KM3NeT data processing and Monte Carlo simulations: the path to cosmic neutrino event	22/11/23
Theoretical modelling of Heavy Ion Double Charge Exchange reactions and calculations for the NUMEN project	06/12/23
Quantum Simulation of Collective Neutrino Oscillations	07/12/23

Outreach Events

Una schiacciata per la vita - in ricordo di Emilio Zappalà	**22/01/23**
Lab2Go - PCTO	01/02/23
PCTO LNS - IIS "Leonardo" - Giarre	01/02/23
Mostra interattiva AIF - Giarre	12/03/23
"Ale' Europe" : Vincenzo Nibali presenta IDMAR	03/04/23
Primavera della Scienza 2023	march-april-may 2023
Lab2go PCTO	13/04/23
Progetto "Laboratori Nazionali del Sud" di alternanza scuola-lavoro	18/04/23
Pint of Science	22/05/23
Premiazione Campionati di fisica 2023	26/05/23
Giornata del Mare - Città della Scienza	27/05/23
Etna Comics	01/06/23
Sharper Night "Notte Europea dei Ricercatori " 2023	29/09/23
Art&Science across Italy	02/10/23
Blue Challenges in the Mediterranean, evento Nazionale WestMED	04/10/23
Programma INFN per Docenti (PID@LNS)	06/10/23
Il progetto IDMAR alla 21 edizione della EURegionsWeek di Bruxelles	10/10/23
Congresso AIF "La fisica per la società futura"	18/10/23
Comunicare la scienza è comunicazione pubblica. Verso una relazione "Evidence based and data drive"	19/10/23
L'INFN: come realizzare a Catania un laboratorio scientifico di livello internazionale	06/11/23
International Cosmic Day 2023	21/11/23
"Hands-on Physics - HOP" progetto di formazione promosso dal CERN	04/12/23
Corso Nazionale "Tecniche di comunicazione scientifica"	15/12/23

Schools and Institutional Visits

giovedì 12 gennaio 2023	Studenti Corso di Laurea Triennale, Istituzioni di Fisica Nucleare e Subnucleare DFA-Università di Catania
giovedì 26 gennaio 2023	Liceo Scientifico "Leonardo da Vinci" - Niscemi
giovedì 23 febbraio 2023	I.C. "G.Parini" - Catania
martedì 28 febbraio 2023	Liceo Scientifico "Cannizzaro" - Palermo
giovedì 2 marzo 2023	Partecipanti al Workshop "2nd Workshop INFN Acceleratori "
giovedì 2 marzo 2023	I.C. "G.Parini" - Catania
martedì 7 marzo 2023	I.C. "G.Parini" - Catania
giovedì 9 marzo 2023	Liceo Scientifico "Ven. I. Capizzi"- Bronte
martedì 14 marzo 2023	Liceo Classico "M. Amari" - Giarre
giovedì 16 marzo 2023	I.C."G. Verga" - Scordia
martedì 21 marzo 2023	Liceo Classico "M. Amari "- Giarre
giovedì 23 marzo 2023	I.C. "G. Verga" - Scordia
venerdì 24 marzo 2023	Studenti Corso di Fisica degli Acceleratori, Laurea Magistrale in Fisica DFA, Università di Catania
martedì 28 marzo 2023	Liceo Scientifico "Archimede" - Messina
giovedì 30 marzo 2023	Liceo Scientifico "Archimede" - Messina
martedì 4 aprile 2023	I.I.S. "L. Einaudi"- Siracusa e Liceo "L. Pirandello" - Agrigento
martedì 4 aprile 2023	Visita organizzatori dell'evento "Alè Europe" visita di Vincenzo Nibali
giovedì 13 aprile 2023	Liceo Scientifico "G. Ferro" - Alcamo
martedì 18 aprile 2023	Liceo Scientifico "Principe Umberto" - Catania
martedì 18 aprile 2023	Liceo Scientifico "Principe Umberto" e Liceo Scientifico "Boggio Lera"- Catania
giovedì 20 aprile 2023	I.I.SS. "Benedetto Radice" - Adrano
giovedì 20 aprile 2023	Visita pubblico generico
venerdì 21 aprile 2023	Liceo Scientifico Statale "P. Farinato" - Enna
giovedì 27 aprile 2023	Liceo Scientifico "Principe Umberto" - Catania
giovedì 27 aprile 2023	Visita pubblico generico
martedì 2 maggio 2023	Liceo Polivalente "M.Quinitiliano" - Siracusa
mercoledì 3 maggio 2023	I.C. "Dante Alighieri" - Leonforte
giovedì 4 maggio 2023	Liceo Scientifico "Ettore Majorana" - Scordia

giovedì 4 maggio 2023	Liceo Scientifico "M. Amari" - Linguaglossa
giovedì 11 maggio 2023	Liceo Classico "Nicola Spedalieri" - Catania
giovedì 11 maggio 2023	Liceo Polivalente "M.Quintiliano" - Siracusa
martedì 16 maggio 2023	Liceo Scientifico "Gulli e Pennisi" - Acireale
martedì 16 maggio 2023	Visita pubblico generico
giovedì 18 maggio 2023	Visita pubblico generico Kids - Adrano
mercoledì 24 maggio 2023	Istituto Superiore “Lorenzo Rota” di Calolziocorte (LC)
giovedì 25 maggio 2023	I.I.S. "Leonardo" - Giarre
venerdì 22 settembre 2023	Visita pubblico generico
martedì 26 settembre 2023	Studenti Università Palermo- Dipartimento di Fisica e Chimica
martedì 26 settembre 2023	Studenti Università Palermo - Dipartimento di Fisica e Chimica
giovedì 28 settembre 2023	Visita pubblico generico
mercoledì 4 ottobre 2023	Visita Sindaco di Catania Avv. Enrico Trantino, DG INFN Nando Minnella
giovedì 5 ottobre 2023	Visita partecipanti evento nazionale WestMED European Partenership for Radiation Protection Research
venerdì 6 ottobre 2023	Visita partecipanti evento nazionale WestMED European Partenership for Radiation Protection Research
mercoledì 11 ottobre 2023	Visita personale amministrativo INFN- LNS
sabato 21 ottobre 2023	Visita partecipanti al congresso AIF
martedì 7 novembre 2023	Visita Laboratorio di Portopalo partecipanti corso PID@LNS
mercoledì 8 novembre 2023	Liceo Scientifico "A.Volta" - Reggio Calabria
giovedì 9 novembre 2023	I.I.S. "L.Einaudi" - Siracusa
venerdì 10 novembre 2023	Visita partecipanti corso PID@LNS
martedì 21 novembre 2023	Liceo Scientifico "E. Fermi "- Ragusa
giovedì 23 novembre 2023	Liceo Scientifico "E. Fermi" - Ragusa
giovedì 30 novembre 2023	Studenti del corso in " Ingegneria civile ed ambientale" Università Catania
martedì 12 dicembre 2023	I.C. "Carlo Alberto dalla Chiesa" -S.G.La Punta- III^ medie
giovedì 14 dicembre 2023	I.C. "Carlo Alberto dalla Chiesa" - S.G. La Punta- III^ medie
venerdì 15 dicembre 2023	Visita partecipanti corso nazionale di formazione sulla comunicazione
martedì 19 dicembre 2023	Liceo Scientifico "Vittorio Emanuele III" - Patti
mercoledì 20 dicembre 2023	I.I.S.S. "L. Pirandello di Bivona" - Agrigento

Seminars 2023

10-2-2023	Grazia D'Agostino,InnovaTron: An innovative compact high-intensity proton cyclotron
24-2-2023	Fateme Farokh, Geant4-DNA for the flash radiotherapy: biological damage prediction
24-3-2023	Alma Kurmanova, A new Thompson Parabola for p-11B experiments and high energy proton beams
30-3-2023	Giuseppe Cirrone, Studies on Proton Boron Fusion Reactions and applications at INFN-LNS
28-4-2023	Ferdinanda Consoli, The p-11B fusion reaction in plasma: the experiments performed at PALS
26-5-2023	Alberto Sciuto, Machine Learning in biological damage estimation with Geant4-DNA: a comparison with experimental data
30-6-2023	Cristina Guarrera, PRAGUE detector prototype: experimental tests and future developments
28-7-2023	Andrea Di Fini, PIC simulation with SMILE code: the p-11B reaction as a case of study
11-9-2023	Kaizhong Ding, Institute of Plasma Physics, Chinese Academy of Sciences, Research and development of the superconducting cyclotron for proton therapy in HFCAS.
29-9-2023	Ruhani Khanna, The biological damage with Geant4-DNA: the comparison with experimental data
10-10-2023	Massimo Carpinelli, Status and future perspective of ground-base Gravitational Waves measurements infrastructure in Europe
7-12-2023	Alessandro Roggero, Quantum Simulation of Collective Neutrino Oscillations

Espresso Seminars 2023@LNS

December 2023

06 Dec Jessica Bellone, "Theoretical modelling of Heavy Ion Double Charge Exchange reactions and calculations for the NUMEN project"

November 2023

22 Nov Anna Sinopoulou, "KM3NeT data processing and Monte Carlo simulations: the path to cosmic neutrino event"

July 2023

18 Jul Alessandro Spatafora, "multi-channel study of direct nuclear reactions: a tool to provide data driven information on neutrino-less double-beta decay"

May 2023

09 May Simone Sanfilippo, "Looking for Dark-Matter: the DarkSide of the Universe"

April 2023

05 Apr Bharat Mishra, "Theoretical Modelling of ECR Plasmas for Application to PANDORA"

March 2023

08 Mar Stefano Burrello, "TOWARDS A UNIFIED EQUATION OF STATE FOR ASTROPHYSICAL SIMULATIONS"

PHOTO GALLERY 2023

4/6-10-2023 BLUE CHALLENGES IN THE MEDITERRANEAN

4-4-2023 ALÈ EUROPE CON VINCENZO NIBALI

4-4-2023 POLITECNICO DEL MARE

4-4-2023 VINCENZO NIBALI AI LNS

4-4-2023 EUROPELOVESICILY

14-4-2023 PCTO LICEO SCIENTIFICO - G.FERRO - ALCAMO

1/4-6-2023 ETNA COMICS CON STAND INFN KIDS

6-11-2023 INCONTRO CULTURALE

25/27-10-2023 BORSA DELLA RICERCA

28-4-2023 AFTER FESTIVAL ARCHITETTURA

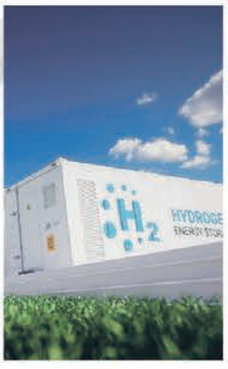

Nelle foto tre dei tavoli dell'intenso forum all'Infn promosso da "La Sicilia" e Dse Pubblicità; sotto l'intervento da remoto del vicepremier Matteo Salvini

TECNOLOGIA A IDROGENO

Cnr: l'elettrolisi di biomassa trasforma scarti agricoli

CATANIA. La transizione ecologica italiana ed europea passa anche attraverso la tecnologia legata all'idrogeno. Nel 2020 la Commissione Europea ha pubblicato la strategia sull'idrogeno e ha reso la produzione sostenibile una priorità di investimento nel piano Next Generation Europe. Il piano del ministero dello Sviluppo economico prevede una penetrazione del 2% negli usi dell'energia entro il 2030 e fino al 20% nel 2050. Nel Pnrr sono stati stanziati 3,2 miliardi di euro per la ricerca, la sperimentazione, la produzione e l'utilizzo di H2. La Sicilia con la creazione della Valle dell'idrogeno e i progetti per il trasporto ferroviario e stradale avrà un ruolo da protagonista.

In questo campo il Cnr è all'avanguardia avendo introdotto un ulteriore metodo rivoluzionario: l'elettrolisi di biomassa. «Questo metodo – ha spiegato ieri Alessandro Lavacchi, ricercatore dell'Istituto di chimica dei composti organometallici del Cnr - non si limita a produrre idrogeno verde, ma trasforma anche rifiuti organici, come, ad esempio, scarti agricoli, in composti chimici ad alto valore aggiunto». Un'innovazione che promette di ridurre l'impatto ambientale dell'industria chimica, riducendone la dipendenza da fonti fossili.

«Una sciocchezza solo l'elettrico»

Salvini. L'intervento in video del ministro: «Non c'è ancora un'energia totalmente a impatto zero. Ma l'importante è non avere ideologie quando si parla di energia e sostenibilità»

CATANIA. «La rivoluzione green sì, che deve essere compatibile con la sostenibilità economica e sociale perché è fondamentale decarbonizzare e avere sovranità energetica però tutelando la sopravvivenza di imprese e la Sicilia può diventare veramente una piattaforma da tanti punti di vista».

Così il vicepremier e ministro delle Infrastrutture e dei Trasporti Matteo Salvini ha esordito ieri intervenendo in videoconferenza a Catania durante un incontro sulle energie rinnovabili "La Sicilia verso il green" organizzato dal quotidiano "La Sicilia" e dalla società Domenico Sanfilippo Editore. Salvini non rinuncia al suo cliché di personaggio istrionico, dotato di pragmatismo con un pizzico di autocompiacimento. «Va benissimo che si investa sullo studio dell'idrogeno verde (quello che non inquina ndr) che si accelerino nuove procedure per l'autorizzazione di nuovi impianti per il fotovoltaico che aspettano solo di essere autorizzati.

TERNA ED ENEL IMPEGNATE ANCHE NELLA FORMAZIONE

Nel corso del panel pomeridiano che ha visto impegnati al tavolo dei relatori anche i rappresentanti di Terna e di Enel, è stato sottolineato come la transizione energetica debba necessariamente essere accompagnata anche da una formazione specifica che possa offrire ai giovani nuove opportunità occupazionali. A questo proposito, le due aziende hanno spiegato come siano già impegnate su questo versante. Proprio nei giorni scorsi, ad esempio, Terna ha presentato il progetto Tyrrhenian Lab che prevede un investimento complessivo di 100 milioni di euro dal 2022 al 2026.

Sul motore endotermico (quello alimentato con prodotti come diesel, benzina o gasolio ottenuti da fonti fossili ndr) stiamo facendo una battaglia per il biocarburante, per salvare la specificità del motore endotermico perché dire solo elettrico dal 2035 come mezzo di locomozione è assolutamente una sciocchezza che non ha un criterio né economico, né ambientale, né sociale».

Il ministro tiene a precisare che per quanto sforzi si stiano facendo, non esiste ancora al mondo una fonte energetica che possa garantire di essere totalmente esente da inquinamento. «Non c'è ancora un'energia totalmente pulita che ha impatto zero» dice. «Ma l'importante è non avere ideologie quando si parla di produzione energetica e sostenibilità. Servono i termovalorizzatori? Sì. La risposta da tutto il mondo è sì».

Non a caso, ieri il ministro dell'Energia, Gilberto Pichetto Fratin ha detto che se la Sicilia deciderà di farli, il ministero che lui dirige l'affiancherà.

Il ministro Salvini non ha perso l'occasione per ricordare che in Sicilia non ci si sta limitando a favorire gli investimenti nel campo delle energie rinnovabili, ma anche per ammodernare i sistemi di trasporto, cominciando dal Ponte sullo Stretto, per la cui realizzazione ha confermato il piano impegno del Governo che ha stanziato 11,6 miliardi di euro per la sua realizzazione nella manovra per la legge di Bilancio 2024.

«Il Ponte sullo Stretto - ha ricordato Salvini - sarà un moltiplicatore di valore aggiunto, un modello di sostenibilità al di là del miracolo di ingegneria italiana oltre a portare alcune decine di migliaia di posti di lavoro. Ribadisco la volontà di aprire i cantieri l'anno prossimo, nel 2024».

Non solo. «Penso che la Sicilia possa vivere nei prossimi anni, con la quantità di risorse già stanziate e progetti già approvati, una rivoluzione positiva come non si vive in Italia dal secondo dopoguerra. Oltre al Ponte vi sono 30 miliardi di euro in fase di investimento per strade e ferrovie».

G. P.

16-11-2023 - LA SICILIA

20-12-2023 ISTITUTO SUPERIORE "ENRICO MEDI - N.VACCALLUZZO" LEONFORTE

18-11-2023 ART&SCIENCE LICEO SCIENTIFICO-VOLTA-REGGIO CALABRIA

20-12-2023 SERVIZIO TELEVISIVO SU EURONEWS

30-11-2023 STUDENTI INGEGNERIA UNICT

23-11-2023 LICEO SCIENTIFICO-E.FERMI-DI RAGUSA

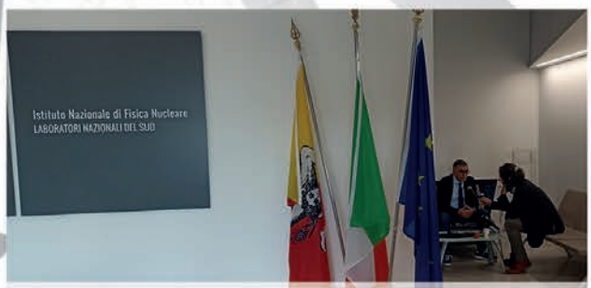

24-11-2024 INTERVISTA RADIO SVIZZERA

23-11-2023 KM3NET4RR MEETING

29-09-2023 SHARPER

INFN KIDS 2023

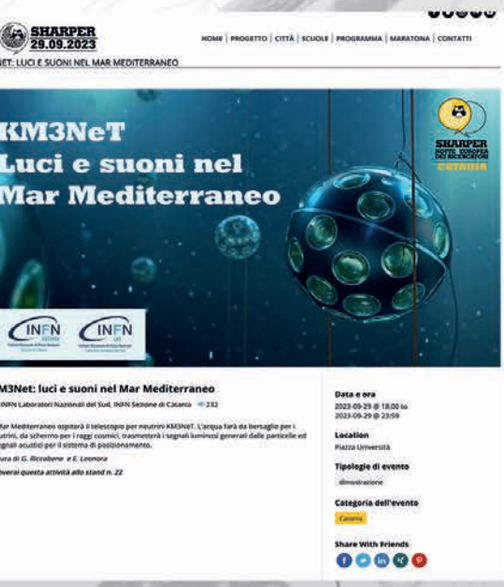

29-9-2023 SHARPER

LA PRIMAVERA DELLA SCIENZA

NOV 2023 PID

PREMI SIF 2023 MATTEO BEZMALINOVICH

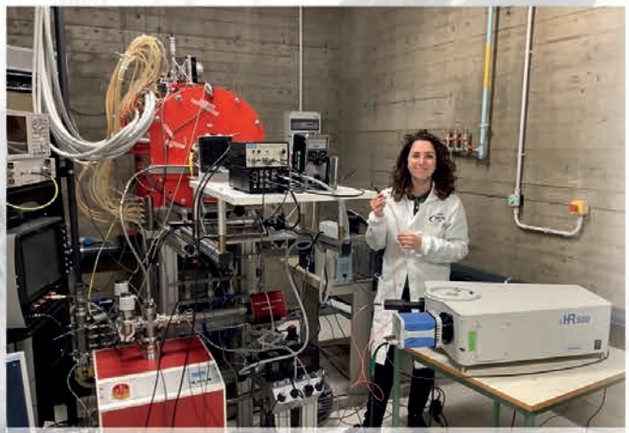

PREMI SIF 2023 GIULIA EMMA CAMPAGNA

PREMI SIF 2023 CLAUDIA SALVIA

10\12-10-2023 EUREGIONS WEEK BRUSSEL

20\24-3-2023 MOSTRA AIF SPERIMENTARE GIOCANDO

2\3-3-2023 GIORNATA ACCELERATORI CATANIA

5-6-2023 - 90 ANNI PROF. G. PAPPALARDO

5-6-2023 - 90 ANNI PROF. G. PAPPALARDO

10-5-2023 POSA STAZIONE IPANEMA FONDALI DI PANAREA

13-2-2023 SELEZIONE CAMPIONATI DI FISICA

14-3-2023 AIF - GIARRE (CATANIA)

17-5-2023 PREMIAZIONE CAMPIONATI DI FISICA

17-5-2023 STUDENTI 1 ANNO DI FISICA UNICT

INFN - Laboratori Nazionali del Sud
Pubblicato da Gaetano Agnello · 4 ottobre 2023 ·

Il sindaco di Catania Enrico Trantino, il direttore generale dell'INFN Nando Minnella e il direttore INFN LNS Santo Gammino porgono il saluto di benvenuto della città di #Catania alla delegazione maltese e ai rappresentanti di Algeria, Libia e Tunisia, in occasione dei lavori di apertura del meeting organizzato su iniziativa del #West MED #Blue Challenges in the #Mediterranean per discutere dell'ecosistema della blue economy del #Mediterraneo.




INFN - Laboratori Nazionali del Sud
Pubblicato da Gaetano Agnello · 25 ottobre 2023 ·


Fondazione Emblema
25 ottobre 2023 ·

🔴 Borsa della Ricerca 2023 🔴

Sessione Plenaria | Life after PNRR
..si comincia!

INFN - Laboratori Nazionali del Sud
Pubblicato da Gaetano Agnello · 23 ottobre 2023 ·

Grazie a tutti i partecipanti al LXI Congresso nazionale dell'Associazione per l'Insegnamento della Fisica #AIF

INFN - Laboratori Nazionali del Sud
Pubblicato da Gaetano Agnello · 29 settembre 2023 ·

🔴 LIVE NOW 📍 Catania

A piazza Università, cuore pulsante della edizione 2023 della notte #Europea dei ricercatori, nello stand dei Ins dedicato alle energie pulite grazie allo studio dei #plasmi per la fusione #termonucleare

#sharpernight #EuropeanResearchersNight #ern2023 #MSCAnight #ernitaly #MSCAction #HorizonEurope

INFN - Laboratori Nazionali del Sud
Pubblicato da Gaetano Agnello · 6 novembre 2023 ·

"Presente e futuro della Comunicazione Scientifica" è stato il tema dell'intervento del direttore INFN - LNS Santo Gammino che ha trattato davanti ai docenti che partecipano al Programma INFN per Docenti #PIDINFN. L'intervento è proseguito con la presentazione delle attività di ricerca e i futuri programmi di sviluppo dei LNS. Appuntamento domani, alla stazione di terra dell'infrastruttura di ricerca sottomarina #KM3NeT dei LNS, a #Portopalo di Capo #Passero.

INFN - Laboratori Nazionali del Sud
Pubblicato da Gaetano Agnello · 7 novembre 2023 ·

La seconda giornata di lavoro del #PID – Programma INFN per Docenti ai LNS, si è svolta nella stazione a mare infn lns di #Portopalo di Capo Passero, dove si trova il centro di acquisizione dei dati sperimentali, della grande infrastruttura europea di ricerca multidisciplinare #km3Net, in fase di costruzione a 3500 metri di profondità nel #Mediterraneo.

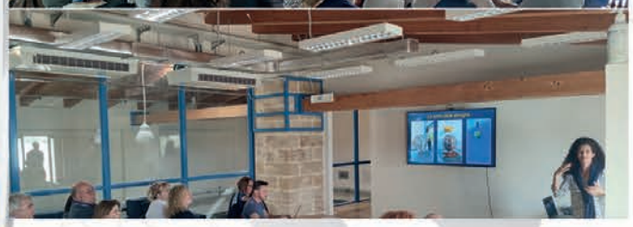

INFN - Laboratori Nazionali del Sud
Pubblicato da Gaetano Agnello · 10 novembre 2023 ·

Si è concluso oggi il corso di formazione Infn dedicato ai docenti #PID delle scuole superiori delle materie #STEM: cinque giorni intensi con lezioni frontali, seminari, laboratori, visite guidate nelle sale sperimentali, nel centro dei trattamenti di protonterapia, nella sala acceleratori, al visitor centre. Grazie ai nostri ricercatori perché sono stati sempre al loro fianco. Grazie soprattutto ai docenti, provenienti dalle diverse regioni italiane, che trasferiranno il valore della ricerca scientifica alle nuove generazioni di studenti.

INFN - Laboratori Nazionali del Sud
Pubblicato da Gaetano Agnello · 15 novembre 2023 ·

La Sicilia verso il green: le sei filiere da costruire.
Il direttore dei Lns Santo Gammino a colloquio con il sindaco di Catania Enrico Trantino.

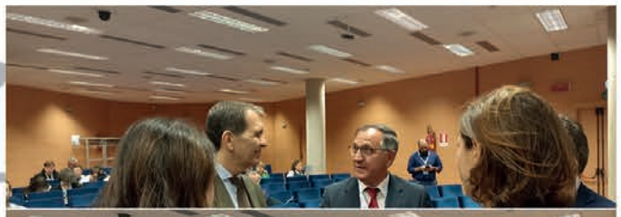

INFN - Laboratori Nazionali del Sud
Pubblicato da Gaetano Agnello · 15 novembre 2023 ·

C'è il tutto esaurito nella sala conferenza dei Lns durante lo svolgimento della terza tavola rotonda del convegno su La Sicilia verso il green : le sei filiere da costruire, insieme ai delegati di Terna, Enel, Confindustria Catania e rappresentanti di aziende nel settore del green per discutere di impianti di interconnessione e reti di trasporto di energia e razionalizzazione di risorse idriche. Molti sono anche i giovani studenti presenti in sala che lasciano ben sperare per le informazioni che oggi possono acquisire.

INFN - Laboratori Nazionali del Sud
Pubblicato da Gaetano Agnello · 24 novembre 2023 ·

Fabio Meliciani, giornalista scientifico della Radiotelevisione svizzera, curatore del programma Il Giardino di #Albert (#RSI Rete Due) per la realizzazione ai LNS di un audiodoc sul #Km3Net4RR.

INFN - Laboratori Nazionali del Sud
Pubblicato da Gaetano Agnello · 23 novembre 2023 ·

Due classi di studenti di quinto anno del Liceo Scientifico E. #Fermi di #Ragusa in visita ai LNS, insieme ai loro docenti Innocenza Rizzo e Concetto Gianino. A fare loro da guida i nostri due ricercatori Luciano Pandola e Alberto Sciuto.

INFN - Laboratori Nazionali del Sud
Pubblicato da Gaetano Agnello · 4 dicembre 2023 ·

Gli studenti del corso di #laurea in #Ingegneria civile, #ambientale e #gestionale dell'#Università di #Catania, guidati dal prof. Gianluca Pizzone, in visita ai LNS.

INFN - Laboratori Nazionali del Sud
Pubblicato da Gaetano Agnello · 4 dicembre 2023 ·

Un'intera giornata di formazione in presenza dedicata agli insegnanti della scuola secondaria di I grado di #Matematica e #Scienze e di #Tecnologia: è questo il progetto #HOP – Hands on #Physics che si svolge oggi ai LNS, per proporre e sviluppare strumenti e idee per l'insegnamento del metodo scientifico.
Sono circa 50 i docenti, provenienti da diverse scuole, che saranno impegnati, insieme ai ricercatori INFN LNS, in attività laboratoriali. HOP è una collaborazione di tre i... **Altro...**

INFN - Laboratori Nazionali del Sud
Pubblicato da Gaetano Agnello · 5 dicembre 2023 ·

In memoria di Giulia e di tutte le donne vittime di violenze.

INFN - Laboratori Nazionali del Sud
Pubblicato da Gaetano Agnello · 6 dicembre 2023 ·

Gli effetti collaterali che ci piacciono!
La giornata di formazione in presenza ai LNS, dedicata agli insegnanti della scuola secondaria di I grado di #Matematica #Scienze e #Tecnologia, che hanno partecipato al progetto #HOP – Hands on #Physics, ha incrementato la richiesta di visite ai LNS.

INFN - Laboratori Nazionali del Sud
Pubblicato da Gaetano Agnello · 11 dicembre 2023 ·

In occasione dell'ultimo Congresso SIF, tenutosi a Salerno nel settembre 2023, Claudia Salvia ha ottenuto il primo premio per la migliore presentazione nella sessione #Fisica Applicata, #Acceleratori e Beni #Culturali.
Claudia ha presentato una comunicazione orale che racchiudeva i temi, affrontati durante la sua tesi di laurea, relatore il prof. David Mascali, svolta presso i nostri laboratori, nell'ambito del progetto #DTT, incentrata sul tema della #Fusione Nucleare.
Sempre nello stesso congresso, le comunicazioni di Giulia Emma - sugli strumenti diagnostici per i plasmi da fusione e per le sorgenti, quali spettroscopia ottica e riflettometria - e di Matteo Bezmalinovich - sul modelling delle opacità dei plasmi nelle cosiddette #Kilonovae - sono state selezionate tra quelle migliori e meritorie di una pubblicazione sul Nuovo #Cimento.
Sia Giulia che Matteo hanno svolto la loro tesi presso i LNS nel 2021-22 nell'ambito del progetto #PANDORA (Giulia provenendo da #UniCT; Matteo dall'Università di #Camerino).
#PANDORA e #DTT, due importanti attività di ricerca dei LNS, stanno consentendo a molti giovani di cimentarsi in un ambito profondamente interdisciplinare, che spazia dalla fisica fondamentale e l'astronomia multimessaggera alla ricerca sulla produzione di energia da fusione #termonucleare controllata.

INFN - Laboratori Nazionali del Sud
Pubblicato da Gaetano Agnello · 12 dicembre 2023 ·

La squadra infn lns sempre più forte. Benvenuti colleghi!

INFN - Laboratori Nazionali del Sud
Pubblicato da Gaetano Agnello · 29 settembre 2023 ·

🔴 LIVE NOW 🏓 Catania il direttore INFN - LNS Santo Gammino, appena rientrato dal consiglio direttivo infn di Roma, si è unito al gruppo dei giovani ricercatori impegnati con INFN Kids

#sharpernight #EuropeanResearchersNight #ern2023 #MSCAnight #ernitaly #MSCAction #HorizonEurope

INFN - Laboratori Nazionali del Sud
Pubblicato da Gaetano Agnello · 22 dicembre 2022 ·

Dal primo gennaio 2023 Luca Guardo sarà il nuovo coordinatore del Public Engagement (PE) dei LNS. Succede a Carla Distefano che lo ha guidato per due mandati (2016-17 e 2020-2022) e a Cettina Maiolino (2018-2019). L'attuale composizione del gruppo, di nomina direttoriale, comprende Giovanna Ferrara, Nancy Martorana, Angelo Pidatella e Alessandro Spatafora. Nel corso di questi sette anni si sono avvicendati altri giovani ricercatori nella composizione del gruppo . Il PE si occupa "della organizzazione e realizzazione di eventi di vario genere promossi da questi Laboratori, come giornate di studio o iniziative per la divulgazione di informazioni sulle attività, l'orientamento di studenti e l'interazione con il pubblico". La passione per la divulgazione della scienza e la promozione della cultura scientifica, l'impegno per il coinvolgimento delle scuole, delle istituzioni, delle famiglie e di tutto il pubblico rappresentano per i LNS una missione nata come patto solidale per lo sviluppo della nostra società.

Il Consiglio dell'#Unione #Europea, visto il il trattato della Comunità Europea dell'#energia #atomica #EURATOM, ha nominato i membri del comitato scientifico e tecnico per il prossimo quinquennio. La decisione del Consiglio è stata pubblicata sulla Gazzetta Ufficiale #UE del 26.10.2023. Il dott. Giacomo Cuttone, dirigente di ricerca INFN LNS, entra a far parte del comitato che avrà il compito di coadiuvare le scelte delle politiche europee nell'ambito della #radioprotezione per apportare miglioramenti nelle tecnologie mediche, nell'industria, l'#agricoltura, #ambiente e sicurezza.

INFN - Laboratori Nazionali del Sud
Pubblicato da Gaetano Agnello · 15 dicembre 2023 ·

Il direttore infn Ins Santo Gammino porge il suo saluto ai partecipanti al III Corso di Formazione Nazionale sulla #Comunicazione che si svolge a #Catania.

INFN - Laboratori Nazionali del Sud
Pubblicato da Gaetano Agnello · 12 gennaio 2023 ·

Gli studenti del terzo anno del corso di Laurea in Fisica #unict accompagnati dalla prof.ssa Francesca Rizzo, oggi ai lns-infn. Una preziosa occasione per conoscere le attività di ricerca nei vari settori della fisica, dall'#astrofisica nucleare, a quella #astroparticellare per finire alle applicazioni in altri ambiti disciplinari #adroterapia # biomedica # cultural #heritage.

INFN - Laboratori Nazionali del Sud
Pubblicato da Gaetano Agnello · 10 febbraio 2023 ·

INFN - Istituto Nazionale di Fisica Nucleare
8 febbraio 2023 ·

#WomenInScience: l'INFN partecipa con tanti eventi in tutta Italia all'International Day of Women and Girls in Science che si celebra l'11 febbraio.
Sui nostri canali social, vi racconteremo le storie e le esperienze di tante scienziate, in fasi diverse della loro carriera, con immagini e brevi video.
Per scoprire tutti gli eventi: https://home.infn.it/.../5531-l-infn-celebra-la-giornata...

INFN - Laboratori Nazionali del Sud
Pubblicato da Gaetano Agnello · 1 marzo 2023 ·

Il forum del Quotidiano di Sicilia #QdS del mese di marzo è dedicato all'intervista a Santo Gammino, direttore INFN - Laboratori Nazionali del Sud, che interviene sui temi della ricerca e delle attività dell'#INFN e dei LNS, sulle collaborazioni con #Università - #Enti di ricerca e sulla necessità di una riforma della #scuola.
https://qds.it/santo-gammino-infn-ndispensabile-fare.../...

orum con Santo Gammino, direttore dei Laboratori Nazionali del Sud-Istituto nazionale i fisica Nucleare di Catania

INFN - Laboratori Nazionali del Sud
Pubblicato da Gaetano Agnello · 6 febbraio ·

Su #EURONEWS il canale televisivo della #EC è andato in onda il servizio realizzato da Aurora Velez ai LNS e a #Portopalo di Capo Passero, al coordinatore scientifico del laboratorio multidisciplinare #IDMAR Giacomo Cuttone.

IT.EURONEWS.COM
Idmar, il laboratorio sottomarino che raccoglie dati 24 ore su 24
Giacomo Cuttone, coordinatore scientifico del laboratorio multidisciplinare, ha spiegato a E...

INFN - Laboratori Nazionali del Sud
Pubblicato da Gaetano Agnello · 13 febbraio 2023 ·

Gli studenti vincitori delle gare di Istituto dei #Campionati Italiani di #Fisica 2023 del polo CT1, organizzati dall'Associazione per l'Insegnamento della Fisica #AIF su mandato del Ministero dell'Istruzione, sono stati impegnati oggi ai LNS nello svolgimento della gara di secondo livello per la partecipazione alla gara nazionale di #Senigallia. Contemporaneamente presso il dipartimento di Fisica e Astronomia #DFA erano impegnati gli studenti del polo 2 CT. Complimenti a tutti gli studenti e ai loro docenti per il notevole impegno messo in campo per arrivare fin qui.

INFN - Laboratori Nazionali del Sud
Pubblicato da Gaetano Agnello · 8 marzo 2023 ·

Continua la collaborazione con l'Istituto Comprensivo G. Parini di Catania. Dopo le due recenti visita ai LNS di alcune classi di terza media, oggi in occasione della Giornata internazionale della donna saremo presenti con alcune nostre ricercatrici.

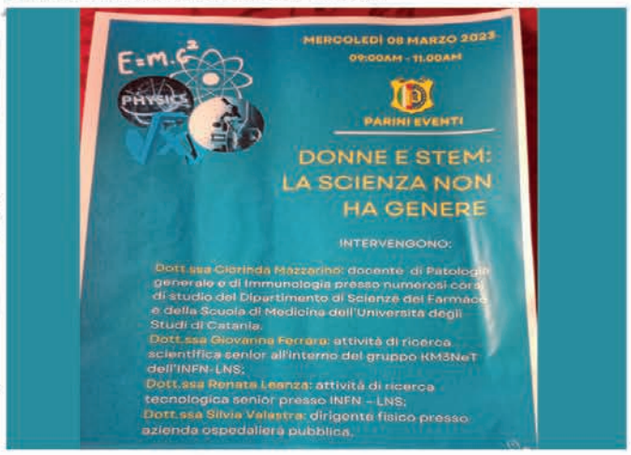

INFN - Laboratori Nazionali del Sud
Pubblicato da Gaetano Agnello · 6 aprile 2023 ·

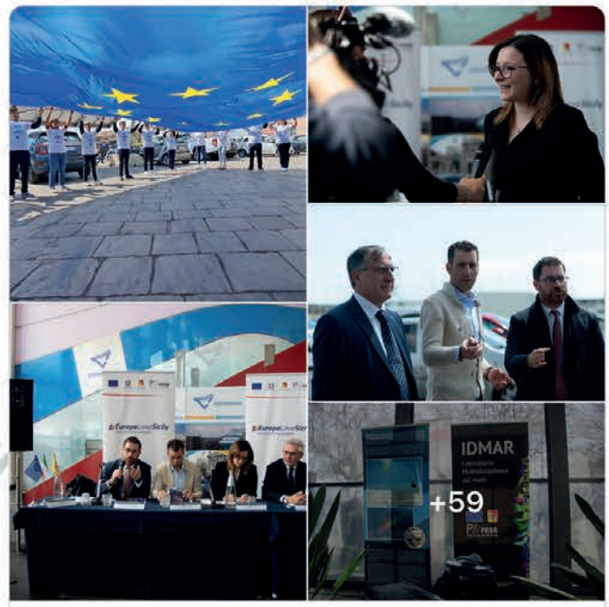

Europe Love Sicily ha aggiunto 63 nuove foto all'album: **Presentazione progetto #IDMAR - Alè Europe con Vincenzo Nibali**.
aprile 2023 ·

Il campione di ciclismo Vincenzo Nibali e l'Assessore al Territorio e Ambiente Elena Pagana hanno presentato il 4 aprile 2023 al porto di Catania il progetto IDMAR e la serie Alè Europe, finanziati con i fondi UE

Europe Love Sicily
6 aprile 2023 ·

Gli scatti di presentazione, a Catania, del progetto #IDMAR che prevede la realizzazione del laboratorio marino più grande d'Europa.

L'intervento, finanziato con le risorse del #POFESRSicilia1420, è stato illustrato nell'ambito dell'iniziativa Alè Europe, sostenuta dalla #CommissioneEuropea, che racconta, attraverso i campioni dello sport, 12 progetti di successo realizzati con le risorse Ue.

All'evento ha partecipato il campione di ciclismo Vincenzo Nibali, tra i protago... **Altro...**

INFN - Laboratori Nazionali del Sud
Pubblicato da Gaetano Agnello · 6 aprile 2023 ·

INFN - Istituto Nazionale di Fisica Nucleare è con **KM3NeT4RR**.
5 aprile 2023 ·

Realizzare in Sicilia un laboratorio subacqueo multidisciplinare distribuito per la ricerca scientifica e tecnologica in ambiente marino: è questo l'obiettivo del progetto IDMAR, che la Regione Siciliana ha presentato ieri nel corso di un evento a cui ha partecipato il ciclista Vincenzo Nibali.
Dopo la presentazione, Vincenzo ha visitato i INFN - Laboratori Nazionali del Sud dove gli è stato presentato il telescopio sottomarino KM3NeT, parte trainante del progetto IDMAR, in fase avanzata di realizzazione con il fondamentale contrubito INFN al largo di Capo Passero.
Per saperne di più: https://www.regione.sicilia.it/.../fondi-ue-pagana-nibali...

INFN - Istituto Nazionale di Fisica Nucleare
15 aprile ·

Docenti a scuola di fisica: si è chiusa lo scorso venerdì, 12 aprile, l'edizione 2023-2024 del Programma INFN per i Docenti. Insegnanti provenienti da tutta Italia sono stati impegnati in 5 giorni di visite ai laboratori, seminari e attività sperimentali in cui hanno potuto scoprire le ultime frontiere della fisica, grazie ai corsi organizzati in autunno ai INFN-Laboratori Nazionali di Legnaro e ai INFN - Laboratori Nazionali del Sud e ora ai Laboratori Nazionali Del Gran Sasso - INFN.

INFN - Laboratori Nazionali del Sud
Pubblicato da Gaetano Agnello · 13 marzo 2023 ·

Inaugurata l'ottava edizione della Mostra Interattiva di #Scienza, organizzata dall'#AIF della Sezione di #Giarre-#Riposto, all'Istituto d'Istruzione Superiore Michele Amari. I LNS partecipano con uno stand dedicato all'accoglienza degli studenti.

INFN - Laboratori Nazionali del Sud
Pubblicato da Gaetano Agnello · 13 marzo 2023 ·

Maria Cristina Guarrera con Emanuele Pagano, nello stand INFN LNS, impegnati nella Mostra Interattiva di Scienza, che apre ufficialmente oggi il ciclo di visite dedicate agli studenti.

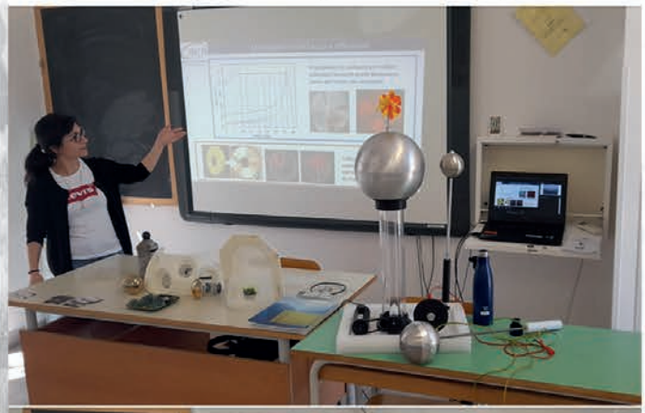

INFN - Laboratori Nazionali del Sud
Pubblicato da Gaetano Agnello · 15 marzo 2023 ·

Maria Cristina Guarrera con Emanuele Pagano anche ieri nello stand INFN LNS impegnati nella Mostra Interattiva di Scienza ,in corso fino a venerdì 17 marzo, al Liceo "Michele #Amari" di Giarre
#aif

INFN - Laboratori Nazionali del Sud
Pubblicato da Gaetano Agnello · 16 marzo 2023 ·

La prima uscita, dopo la fase pandemia, per i bambini della scuola primaria "G. #Verga" di #Scordia è dedicata alla visita a Catania dei nostri laboratori. Grazie al progetto #INFNKids i bambini sono stati guidati alla scoperta del mondo delle #particelle, alle applicazioni nel settore dei beni artistici e culturali e della medicina. Il viaggio è proseguito nelle sale del visitor centre per per guardare l'evoluzione del ciclo delle stelle e nelle profondità sottomarine il fun... Altro...

INFN - Laboratori Nazionali del Sud
Pubblicato da Gaetano Agnello · 17 marzo 2023 ·

Chiude oggi la prima tappa della ottava edizione della mostra interattiva di scienze, svoltasi presso il Liceo "Michele Amari" di #Giarre. Giuseppe Castro e Antonio Massara sono stati i ricercatori impegnati in questa ultima giornata che ha registrato una forte affluenza di studenti. La mostra si sposta a Catania dove sarà ospitata presso il Liceo Scientifico "Principe Umberto" dal 20 al 24 marzo. Vi aspettiamo

#aif

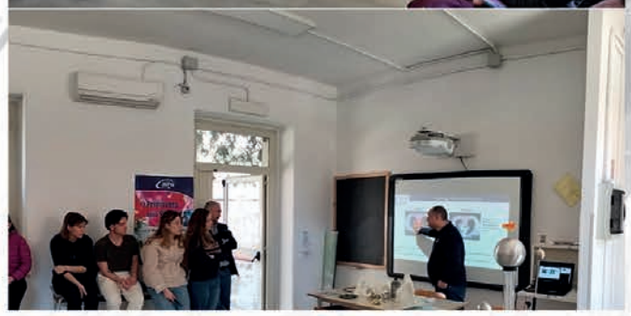

INFN - Laboratori Nazionali del Sud
Pubblicato da Gaetano Agnello · 20 marzo 2023 ·

Parte oggi la seconda tappa della Mostra Interattiva di # Scienze organizzata dall'#AIF. Lo stand dei LNS sarà presente per tutta la durata dell'evento in programma fino al 24 marzo. Il direttore INFN LNS Santo Gammino, insieme alle nostre due giovani ricercatrici e ai rappresentanti dell'AIF, è stato presente alla giornata inaugurale.

INFN - Laboratori Nazionali del Sud
Pubblicato da Gaetano Agnello · 23 marzo 2023 ·

Oggi in visita ai LNS i bambini della primaria della G.Verga di Scordia. La stagione primaverile appena iniziata ben si coniuga con il sorriso e l'entusiasmo che portano sempre i bambini.
#infnkids

società & cultura

Una donna regista per il nuovo film di James Bond

ALESSANDRA BALDINI pagina 14

TECNOLOGIA E PROTEZIONE CIVILE IN MARE

Un sensore per terremoti e tsunami

Presentato a Catania il progetto Idmar per studiare le condizioni e i movimenti dei fondali

MARIA ELENA QUAROTTI

CATANIA. Il mare ci parla, da sempre. Ora attraverso il progetto "Idmar" (Infrastruttura distrettuale Marina), unico siciliano e unico nel suo genere in Europa, riesce a farlo anche dalle profondità più inaccessibili. La presentazione ufficiale, e in corso d'opera, si è tenuta ieri mattina nella sede dell'Autorità di sistema portuale del mare di Sicilia Orientale al porto di Catania.

"Testimonial" del progetto, e attenzione, Vincenzo Nibali, il campione di ciclismo noto come lo "squalo di Messina".

Cos'è "Idmar"? Non si tratta solo di conoscere e studiare le condizioni del mare e dei fondali marini dal punto di vista geofisico, vulcanologico e della biologia marina, ma anche, attraverso l'integrazione con un sistema di monitoraggio comunque già operativo insieme alla protezione civile, riuscire a rilasciare informazioni sempre più sensibili, ad esempio, in merito a rilevazioni d'onde d'urto di terremoti, e di tsunami, per generare ancora più tempestivamente gli opportuni "allerti".

Dotato macchina di "Idmar" sono l'Istituto nazionale di fisica nucleare (Infn), Consiglio nazionale delle ricerche (Cnr) e istituto nazionale di geofisica e vulcanologia (Ingv).

Fondamentale è stato, ed è, il supporto della Regione Siciliana, che ha inserito "Idmar" nelle iniziative finanziate con i fondi del Po-Fesr (fondi europei di sviluppo regionale) Asse "Ricerca, sviluppo tecnologico e innovazione", per un importo di 19 milioni di euro (su 40 totali) nel ciclo 2014-2020, con "proseguimento nella programmazione 2021-2027", ha garantito Elena Pagana, assessore regionale al Territorio e Ambiente.

È vero, si è ancora agli inizi e "Idmar" per ora "copre" la costa orientale dall'Isola - a Portopalo di Capopassero (Siracusa), dove a circa 100 km dalla costa e a 3mila e 500 metri di profondità, si trova il più grande telescopio sottomarino mai realizzato in grado di monitorare un'area fino a 100 km, mentre a Catania è presente un sito di integrazione con strumentazioni poste a 20 Km dal porto e a 2mila metri di profondità – ma altri poli principali si trovano a Milazzo, Capo Granitola (Trapani) e Palermo, osservatori fisici mobili sono presenti alle Isole Eolie ed Agrigento.

Detto così ai lettori sembrerà tutto molto astratto, ma sarà un "docu-film" che vede come testimonial proprio il campione di ciclismo Vincenzo Nibali e la cui realizzazione è stata promossa nell'ambito di "Alè Europe" (prodotto da "Bed Carpet", dal 27 aprile sulla piattaforma streaming Chili) a rendere tutto più chiaro al grande pubblico. Una proiezione ufficiale è stata prevista a fine giugno anche a Bruxelles, alla Commissione Europea.

Il progetto siciliano è uno dei dodici selezionati dall'Unione Europea e ritenuti rappresentativi di un connubio di successo fra interventi finanziati con fondi europei e associati ad altrettanti investimenti sportivi.

"Sport e ricerca scientifica" insieme non è un caso, hanno in comune il sacrificio e la capacità nella ricerca dei risultati, e l'esempio più concreto per l'isola è proprio Nibali.

Non dovrà più sembrare strano che sia la Sicilia ora ad attrarre ogni anno ricercatori da tutta Italia ed Europa, che qui trovano un'opportunità sicura – ha sottolineato Giacomo Cuttone, referente scientifico del progetto "Idmar" – a Portopalo, dove con il Pierr abbiamo istituito ulteriori 87 milioni di euro per il telescopio sommerso, studiamo i neutrini ad altissima energia, pochi e sfuggenti da rilevare, per capire come si sta evolvendo l'universo, ma anche le profondità del mare dove si incontrano la grande faglia nordafricana e quella sud europea che hanno generato i grandi vulcani, Etna, Stromboli e Vulcano, o da dove sono iniziati i grandi terremoti. È un osservatorio unico in Europa e nel Mediterraneo.

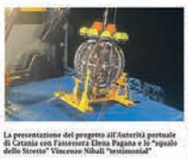

La presentazione del progetto all'Autorità portuale di Catania con l'assessora Elena Pagana e lo "squalo dello Stretto" Vincenzo Nibali "testimonial"

INFN - Laboratori Nazionali del Sud
Pubblicato da Giovanni Luca Guardo · 1 giugno 2023 ·

Lo stand INFN Kids dei LNS è pronto per accogliere i più piccoli nell'area family dell'edizione 2023 di Etna Comics
Il nuovo episodio delle avventure di Leo&Alice verrà svelato oggi!
Vi aspettiamo numerosi!!!
Gadget per tutti

INFN - Laboratori Nazionali del Sud
Pubblicato da Gaetano Agnello · 4 giugno 2023 ·

L'edizione 2023 di #etnacomics si è chiusa stasera con un enorme successo e partecipazione di pubblico. Anche lo stand #infnkids è stato un punto di incontro per le famiglie grazie ai laboratori come electrolab, ai giochi e ai piccoli esperimenti sull'elettricità dedicati ai bambini. Stasera è stato con noi anche il direttore INFN LNS Santo Gammino. Grazie ai nostri giovani ricercatori che hanno saputo trasmettere con il sorriso e la fantasia la passione per la ricerca scientifica.

INFN - Laboratori Nazionali del Sud
Pubblicato da Gaetano Agnello · 19 giugno 2023 ·

Argomento: Seminario I-LUCE
Ora: 3 lug 2023 02:30 PM Roma

Entra nella riunione in Zoom
https://infn-it.zoom.us/j/87188744740..... **Altro...**

INFN - Laboratori Nazionali del Sud
Pubblicato da Gaetano Agnello · 2 giugno 2023 ·

Tanti visitatori nello stand INFN Kids nell'edizione 2023 di #Etna #Comics

INFN - Laboratori Nazionali del Sud
Pubblicato da Gaetano Agnello · 6 giugno 2023 ·

Alla presenza di tantissimi colleghi e amici, riuniti nella Sala Conferenza "E.Migneco", si è svo
unedì 5 giugno, l'incontro per festeggiare i 90 anni del prof. Giuseppe Pappalardo. Dopo
'introduzione del rettore dell'#università di Catania prof. Francesco e del direttore INFN-LNS
dr Santo Gammino, il prof. Emilio Migneco e il dr. Giacomo Cuttone (Past Directors) hanno
ipercorso alcuni dei momenti più significativi della lunga carriera accademica del prof.
Pappalardo. L'attività scientifica è stata ricordata da Giuseppe Cardella, Massimo Papa, Salv
Tudisco, Alessia Di Pietro, Paolo Romano, Ninni Rizzo suoi allievi, oggi docenti e ricercatori.
Delle passioni del prof. Pappalardo, legate al mondo musicale e teatrale, ne hanno parlato i
colleghi INFN LNS Carmelo Marchetta e Nino D'Agata. Tantissima emozione e gratitudine ne
confronti del prof. Pappalardo, per una giornata indimenticabile nel segno di un grande fisico
nucleare che tanto ha dato alla comunità scientifica catanese e internazionale.

INFN - Laboratori Nazionali del Sud
Pubblicato da Gaetano Agnello · 4 maggio 2023 ·

Oggi in visita gli studenti del "Liceo Scientifico Ettore Majorana" di #Scordia. Dopo la partecipazione alla "Masterclass "Masterclass #DARK/Darkside" sulla ricerca di materia oscura dello scorso mese di dicembre, i ragazzi hanno pienamente riconfermato la loro attenzione alle tematiche legate alle attività di ricerca dei LNS. Vi aspettiamo per altri appuntamenti e formuliamo per gli studenti di quinto anno i migliori auguri per il proseguimento della loro carriera, sperando che l'incontro di oggi possa avere fornito spunti di riflessione.

INFN - Laboratori Nazionali del Sud
Pubblicato da Gaetano Agnello · 16 maggio 2023 ·

Pomeriggio di festa nella sala Conferenza dei LNS per gli studenti di scuola superiore del polo Catania1 (9 scuole e 43 alunni) e Catania2 (10 scuole e 42 alunni) che si sono distinti nelle prove di secondo livello e nelle fasi nazionali dei Campionati Italiani di #Fisica. Accompagnati dai loro genitori e dai docenti che li hanno seguiti in questo lungo percorso iniziato nel mese di Ottobre.
Il tributo speciale per questi fantastici studenti è stata la presenza di Francesco Priolo (Rettore dell'Università di Catania),Santo Gammino (Direttore INFN-LNS), Maria Grazia Grimaldi (Direttore Dipartimento di Fisica e Astronomia) Alessia Tricomi (Direttore INFN Sezione di Catania), Giuseppe Angilella (vice Direttore #DFA e Coordinatore della Classe di Scienze Sperimentali della Scuola Superiore di Catania, in rappresentanza del Presidente #SSC, Prof. Daniele Malfitana), Alessandro Pluchino (coordinatore PLS Fisica), Elena Geraci (Terza Missione del DFA). Dal Senato è intervenuto Francesco Giacobbe che insieme ai familiari ha voluto istituire un premio speciale dedicato alla memoria del giovane Riccardo Giacobbe, scomparso tre anni addietro all'età di diciotto anni. E'stato questo uno dei momenti più toccanti dell'incontro. Colonne portanti di questo evento sono le prof.sse Maria Luisa Lizzio polo CT1 e Lina Lo Presti polo CT2 responsabili delle gare di 2 livello. Le immagini più belle che rimangono al termine della premiazione sono l'impegno e la dedizione allo studio e i volti puliti di queste ragazze e ragazzi.

INFN - Laboratori Nazionali del Sud
Pubblicato da Gaetano Agnello · 24 maggio 2023 ·

Proseguono le visite ai LNS degli studenti universitari in occasione della "#Primavera della #Scienza" iniziata nel mese di marzo. Lieti di aver accolto gli studenti d laurea #magistrale in #Fisica, insegnamento Nuclear Astrophysics(la magistrale è internazionale), accompagnati dal prof. Lamia. I LNS rappresentano una solida realtà in campo europeo ed internazionale nel campo dell'Astrofisica Nucleare. Con cadenza biennale organizzano una scuola estiva, denominata " European Summer School on Experimental Nuclear Astrophysics", fucina di tantissimi affermati ricercatori, la cui XII edizione è in programma nel 2024.

INFN - Laboratori Nazionali del Sud
Pubblicato da Gaetano Agnello · 9 maggio 2023 ·

È stata completata con successo la fase di posa della stazione acustica sottomarina, nell'edificio vulcanico subacqueo caratterizzato da faglie tettoniche, a 25 metri di profondità, al largo di Panarea. L'attività del progetto europeo #IPANEMA è il monitoraggio acustico delle emissioni di #CO2. Grazie a questa operazione, l'infrastruttura di ricerca paneuropea (#ECCSEL-ERIC) distribuita che collega i principali laboratori esistenti in #Europa per la cattura e stoccaggio dell'anidride carbonica si arricchisce di nuova strumentazione.Le attività sono state condotte in collaborazione con i colleghi dell'#INGV di #Palermo.

INFN - Laboratori Nazionali del Sud
Pubblicato da Gaetano Agnello · 17 maggio 2023 ·

Il forte legame tra l'#Università di #Catania e gli Enti di #Ricerca, presenti nel campus universitario e nell'area catanese, è riconfermato dalla visita degli studenti del 1° anno del Corso di Laurea in Fisica del Dipartimento di #Fisica e #Astronomia. Accompagnati dai proff. Stefano Romano, Luca Guardo e Giuseppe Rapisarda gli studenti, dopo il seminario iniziale, hanno visto l'acceleratore Tandem, la sala dei trattamenti di #adroterapia e il Visitor Centre.

INFN - Laboratori Nazionali del Sud
Pubblicato da Gaetano Agnello · 14 aprile 2023 ·

Avvicinare gli studenti di scuola secondaria superiore alla scienza sperimentale è l'obiettivo della VII edizione di #lab2Go, un progetto #PCTO (Percorsi per le Competenze Trasversali e l'Orientamento) dell'Istituto Nazionale di Fisica Nucleare, nato in collaborazione con La #Sapienza Università di Roma al quale hanno aderito i LNS con diverse iniziative. Ieri abbiamo ospitato circa 50 studenti insieme ai loro docenti del Liceo Scientifico "G. Ferro" di #Alcamo. E' stata una giornata molto intensa con diverse iniziative e attività nei laboratori di #elettronica, tecniche chimico fisiche e di #radioprotezione, tutto grazie all'impegno dei nostri ricercatori, tecnologi e tecnici che hanno svolto le lezioni e hanno seguito gli studenti. Precedentemente lo scorso febbraio le attività di laboratorio si sono svolte direttamente nella scuola di Alcamo.



INFN - Laboratori Nazionali del Sud
Pubblicato da Gaetano Agnello · 28 aprile 2023 ·

#AFTER Festival diffuso di #architettura in Sicilia fa tappa a #Catania per parlare delle architetture di Giacomo Leone attraverso le parole di Giovanni Leone, tra le quali i LNS che hanno ospitato l'incontro con i numerosi giovani architetti per indagare alcuni temi di ricerca scientifica all'interno di questo
spazio architettonico.

#FOA #Genia #Italianostra #ortigia #



INFN - Laboratori Nazionali del Sud
Pubblicato da Gaetano Agnello · 17 aprile 2023 ·

Si è svolta oggi, nella Sala Conferenza dei LNS, la presentazione delle candidature per la direzione dei nostri Laboratori 2023-2027. Moderatore della presentazione il prof. Stefano Romano a sinistra nella foto, al centro la dott.ssa Piera Sapienza accanto al direttore in carica il dott. Santo Gammino.


INFN - Laboratori Nazionali del Sud
Pubblicato da Gaetano Agnello · 28 aprile 2023 ·

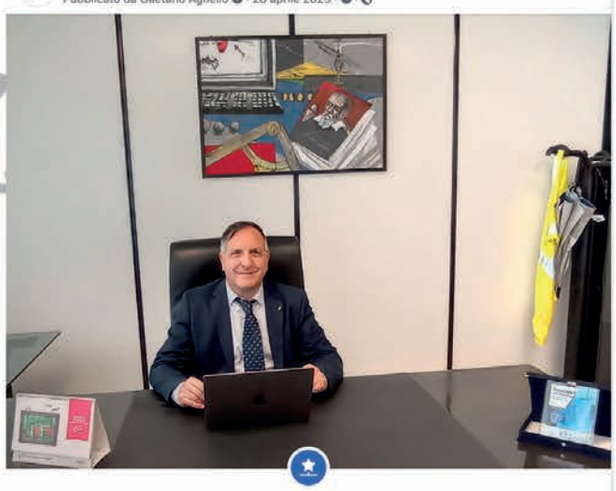

Il Consiglio Direttivo dell'INFN, nella riunione del 28 aprile, ha nuovamente affidato al dott. Santo Gammino la Direzione dei Laboratori Nazionali del Sud per il quadriennio 2023-2027

28 aprile 2023

Il Consiglio Direttivo dell'INFN, nella riunione del 28 aprile, ha nuovamente affidato al dott. Santo Gammino la Direzione dei Laboratori Nazionali del Sud per il quadriennio 2023-2027

INFN - Laboratori Nazionali del Sud
Pubblicato da Gaetano Agnello · 5 luglio 2023 ·

Alcuni momenti della serata inaugurale al Teatro Garibaldi di Modica, della MAYORANA (Multi-Aspect Young ORiented Advanced #Neutrino Academy) alla presenza del Rettore dell'#Università di #Catania Francesco Priolo, del Direttore INFN LNS Santo Gammino, delle autorità locali e del Ministro Nello Musumeci.
Contributi musicali di Giovanni Caccamo e dei Drums Together, Ensemble di Percussioni del Liceo Musicale «G. Verga» di Modica.

INFN - Laboratori Nazionali del Sud
Pubblicato da Gaetano Agnello · 7 luglio 2023 ·

Come tradizione si rinnova l'appuntamento con gli studenti magistrali del dipartimento di #fisica e astronomia dell'università di #Catania. Nella sede a mare INFN LNS di #Portopalo di Capo una full immersion con docenti unict e ricercatori INFN LNS, dedicata alla fisica #astroparticellare. Una occasione speciale per studiare da vicino e con i diretti interessati, le nuove frontiere della ricerca grazie alla grande infrastruttura di ricerca multidisciplinare europea #Km3NeT ... **Altro...**

INFN - Laboratori Nazionali del Sud
Pubblicato da Gaetano Agnello · 1 Agosto 2023 ·

Il direttore INFN LNS Santo Gammino insieme al capo divisione ricerca Aurora Tumino per fare il punto della situazione, in vista della imminente campagna marina #Km3net a settembre, nella sede distaccata a #Portopalo di Capo Passero, centro di acquisizione dei dati provenienti dai rivelatori sottomarini della grande infrastruttura di ricerca europea Km3net posto a 3500 metri di profondità , e collegati a terra tramite un cavo elettro ottico.

INFN - Laboratori Nazionali del Sud
Pubblicato da Gaetano Agnello · 30 Agosto 2023 ·

Il Congresso #AIF Associazione per l'Insegnamento della #Fisica 2023 si svolgerà a Catania dal 18 ottobre al 21 ottobre. Sabato 21 ottobre 12.30, dopo la relazione su invito del direttore INFN LNS Santo Gammino sul tema dell'impatto sociale della ricerca fondamentale, è in programma la visita guidata ai Laboratori Nazionali del Sud.

INFN - Laboratori Nazionali del Sud
Pubblicato da Gaetano Agnello · 26 settembre 2023 ·

Oggi in visita ai LNS un gruppo di studenti del Dipartimento di #Fisica e #Chimica "E. #Segrè" Università degli Studi di #Palermo. Un secondo gruppo dello stesso Dipartimento è atteso nel pomeriggio. Ringraziamo il prof. Giovanni Marsella per il rinnovato interesse nel coinvolgimento dei suoi studenti nella visita al nostro centro.

RICERCATORI E TECNOLOGI

AGODI Clementina	
ALTANA Carmen	(31/05/2025)
AMADUCCI Simone	(25/06/2025)
BIAGI Simone	
BONANNO Danilo Luigi	(31/05/2025)
BONANNO Vincenza Piera	
BURRELLO Stefano	
CARBONE Diana	
CASTRO Giuseppe	
CATALANO Roberto	
CAVALLARO Manuela	
CELONA Luigi	
CIANCIO Sebastiano	(02/03/2026)
CIRRONE Giuseppe	
CITTADINO Daniele	
COCIMANO Rosanna	
COLONNA Maria	
CONIGLIONE Rosa	
COSENTINO Luigi Giovanni	
COSTA Michele	
CUTTONE Giacomo	
D'AGOSTINO Grazia	
DI PIETRO Alessia	
DISTEFANO Carla	
FATTORI Serena	(14/05/2025)
FIGUERA Pierpaolo	
FINOCCHIARO Paolo	
GAMBACURTA Danilo	
GAMMINO Santo	
GIORGIO Emidio Maria	
GUARDO Giovanni Luca	
LA COGNATA Marco Salvatore Maria	
LAROSA Giuseppina	
LEANZA Renata	
LEONARDI Ornella	
LICCIARDELLO Elena Cristina	(02/04/2025)
MAIOLINO Concettina	
MASCALI David	
MAURO Giorgio Sebastiano	
MIRAGLIA Andrea	
MUSUMECI Mario Salvatore	
NASELLI Eugenia	(14/05/2025)
NERI Lorenzo	
NOTO Francesco	
OLIVA Alessandro	(14/05/2025)
ORLANDO Angelo	
PAESANI Daniele	(02/07/2025
PAGANO Emanuele Vincenzo	
PANDOLA Luciano	
PAPPALARDO Alfio Domenico	(31/05/2025)
PIDATELLA Angelo	(14/05/2025)
PETRINGA Giada	(09/07/2025)
PIATTELLI Paolo	
PULVIRENTI Sara Rita	
RICCOBENE Giorgio	
RIFUGGIATO Danilo	
ROVELLI Alberto	
RUSSO Antonio Domenico	
RUSSOTTO Paolo	
SANFILIPPO Simone	(14/05/2025)
SANTONOCITO Domenico	
SAPIENZA Piera	
SCHILLACI Gaetano	
SUAREZ VARGAS Jose Juan	(31/08/2025)
TORRESI Domenico	
TORRISI Giuseppe	
TUDISCO Salvatore	
VECCHIO Gianfranco	
VIOLA Salvatore	
ZITO Daniele	(14/05/2025)

DIRETTORE	**GAMMINO Santo**	
	GRECO Vincenzo	**(Supporto al Direttore)**
	Costa Michele	**(Incident Coordinator e Mobility Manager)**
	Schillaci Gaetano	**(Facility Manager)**
	Cosentino Luigi G.	**(Beam Coordinator)**
DIVISIONE RICERCA	**Tumino Aurora**	**(Responsabile)**
	Traina Irene	
Servizio utenti	**Di Pietro Alessia**	**(Responsabile)**
	Litrico Francesco	
Reparto tecnologie marine	**Grmek Antonio**	**(Responsabile)**
	Cacopardo Giorgio	
	D'Amato Carmelo	
	Felice Fabiano	(20/06/2025)
	Tangorra Cascione Riccardo	(16/07/2025)
Reparto gestione e manutenzione apparati sperimentali	**Rizzo Daniele**	**(Responsabile)**
	Passarello Davide	
Reparto laboratorio di tecniche chimico fisiche	**Massara Antonio**	**(Responsabile)**
	Ursino Martina	(13/09/2024)
Reparto elettronica e rivelatori	**Litrico Pietro**	**(Responsabile)**
	Calì Claudio	
	Cammarata Francesco	(14/05/2025)
	Caruso Fortunato Giuseppe	
	Cavallaro Bernadette M.C.	(14/05/2025)
	Passaro Giuseppe	
	Platania Luca	(14/05/2025)
	Sciuto Davide	(30/11/2024)
Servizio informazione scientifica	**Agnello Gaetano**	**(Responsabile)**
	Cardillo Salvatore	
	Di Mauro Rosalia Paola Camilla	
Servizio sviluppo apparati sperimentali	**Tudisco Salvatore**	**(Responsabile)**
	Bonanno Danilo Luigi	(aspettativa)
	Caruso Antonino (dal 15-4-24)	
	Passarello Santi Maria	
	Sapienza Giuseppe	
	Vinciguerra Francesco	(18/06/2025)
Servizio calcolo e tecnologie informatiche	**GIORGIO Emidio Maria**	**(Responsabile)**
	Coppolino Lucio Mirko	(15/05/2025)
	Ricceri Rita Domenica	(14/05/2025)
Reparto reti, trasmissione dati ed acquisizione dati	**Cannizzaro Stefano**	**(Responsabile)**
	Passaro Gianluca	(22/09/2024)
	Piazza Daniele Carmelo	
	Sclafani Matteo	
LABORATORIO LANDIS	**Gammino Santo**	**(Responsabile)**
LABORATORIO CATANA	**Cirrone Giuseppe**	**(Responsabile)**
LABORATORIO LARA	**Romano Stefano**	**(Responsabile)**

DIVISIONE ACCELERATORI

	Rifuggiato Danilo	**(Responsabile)**
	Caruso Antonino	(fino al 14-4-24)
Servizio tecnologie per gli acceleratori	**Russo Antonio Domenico**	**(Responsabile)**
Reparto vuoto	**Vinciguerra Salvatore** Battiato Giuseppe	**(Responsabile)**
Reparto criogenia	**Speziale Fabrizio**	**(Responsabile)**
Reparto radiofrequenza	**Longhitano Alberto** Spartà Antonino	**(Responsabile)**
Reparto elettronica, convertitori di potenza, diagnostica ed automazioni	**Amato Antonino** Avolio Renato De Luca Giovanni Manna Carmelo Oliva Demetrio Tudisco Daniele	**(Responsabile)** (30/11/2024)
Servizio operazioni e controllo	**Vecchio Gianfranco**	**(Responsabile)**
Reparto sistemi informatici	**Pulvirenti Salvatore** Cavallaro Salvo Rita Diana Benedetto Furia Enrico	**(Responsabile)**
Reparto operazione e conduzione degli acceleratori	**Reina Paolo** Calabrese Giuseppe Marletta Rosario	**(Responsabile)**
Servizio progettazione e manutenzioni	**Costa Michele**	**(Responsabile)**
Reparto progettazione meccanica	**Gallo Giuseppe** Allegra Luciano Russo Filippo	**(Responsabile)**
Reparto dispositivi meccanici	**Messina Esteban G.** Pastore Giuseppe	**(Responsabile)**
Reparto metrologia, linee di fascio e allineamenti	**Maugeri Antonio** Seminara Angelo	**(Responsabile)**
Servizio iniettori	**Leonardi Ornella** Siliato Davide Costanzo Giacomo	**(Responsabile)**

DIVISIONE TECNICA E DEI SERV. GEN.	**Musumeci Mario Salvatore**	**(Responsabile)**
Servizio impianti elettrici, operazioni e Manutenzioni	**Musumeci Mario Salvatore** Castro Fabrizio Mirabella Alfio Platania Fabio	**(Responsabile ad interim)**
Servizio impianti a fluido, operazioni e manutenzioni	**Miraglia Andrea** Friscia Francesco Giuseppe Romeo Rosario	**(Responsabile)** dal 01/02/2024
Servizio edilizia	**Bandieramonte Davide** Anastasi Massimo D'Antoni Agatino Alfio Luca	**(Responsabile)**
Servizio attività generali e tecniche	**Piscopo Massimo**	**(Responsabile)**
Reparto progettazione e costruzioni meccaniche	**Piscopo Massimo**	**(Responsabile ad interim)**
Reparto logistica e magazzino	**Piscopo Massimo** Fichera Massimo	**(Responsabile ad interim)** dal 01/02/2024
Reparto officina meccanica e saldatura	**Vasta Giovanni** Tringale Matteo	**(Responsabile)**
Servizio di amministrazione	**Cesare Sarah** Consoli Olga	**(Responsabile)**
Ufficio contratti, approvvigionamenti e procedure di gara	**Marchese Letizia** Caruso Carmelo Caruso Fausta Spinali Rossella	**(Responsabile)**
Ufficio pagamenti e incassi	**Di Nunzio Dorotea** Allegra Antonino Salvatore Scandurra Anna Maria Toscano Lucio	**(Responsabile)**
Ufficio Missioni	**Mancuso Margherita** Platania Chiara	**(Responsabile)**
Servizio di direzione	**Schilirò Nunzia** Di Stefano Marco	**(Responsabile)**
Ufficio utenti e foresteria	**Potenza Virginia** Gallo Filippo	**(Responsabile)** dal 14/02/2024
Servizio del personale	**Saitta Nunzio** Gallo Filippo Garraffo Rosa Privitera Patrizia	**(Responsabile)** fino al 13/02/2024
** **Servizio Fondi Esterni**	**Rapicavoli Carolina Rita** Torrisi Daniela Vittorio Viviana	**(Responsabile)**

** Il Servizio svolge l'attività anche per la sezione di Catania e la Responsabile è stata nominata di concerto con il direttore della Sezione di Catania.

Servizio di Project Management	**Musumeci Mario Salvatore** Falcomatà Alessandra	**(Responsabile ad interim)**
Servizio di Radioprotezione	**Russo Salvatore**	**(Responsabile)**
Servizio di Prevenzione e Protezione	**Noto Francesco**	**(Responsabile)**

INFN • LNS

LABORATORI NAZIONALI DEL SUD

Istituto Nazionale di Fisica Nucleare

Via Santa Sofia, 62 • Catania • Italy
www.lns.infn.it
www.facebook.com/infn.lns
@LNS_INFN
@lns_infn
ISSN 1827-1561